Woods Hole Oceanographic Institution **WHOI-96-10**

Technical Report
August 1996

Meteorological and Oceanographic Data during the ASREX III Field Experiment: Cruise and Data Report

by

Nancy R. Galbraith
Anand Gnanadesikan
William M. Ostrom
Eugene A. Terray
Bryan S. Way
Upper Ocean Processes Group
Woods Hole Oceanographic Institution

Neil J. Williams
Rosenstiel School of Marine and Atmospheric Sciences
University of Miami

Steven H. Hill
Ocean Acoustics Group
Institute for Ocean Sciences

Eric Terrill
Scripps Institution of Oceanography

19970630 114

DISTRIBUTION STATEMENT A
Approved for public release
Distribution Unlimited

Upper Ocean Processes Group
Woods Hole Oceanographic Institution
Woods Hole, Massachusetts 02543
UOP Technical Report 96-1

DTIC QUALITY INSPECTED 1

WHOI-96-10
UOP 96-01

Meteorological and Oceanographic Measurements during the ASREX III Field Experiment: Cruise and Data Report

by

Nancy R. Galbraith
Anand Gnanadesikan
William M. Ostrom
Eugene A. Terray
Bryan S. Way
Upper Ocean Processes Group
Woods Hole Oceanographic Institution

Neil J. Williams
Rosenstiel School of Marine and Atmospheric Sciences
University of Miami

Steven H. Hill
Ocean Acoustics Group
Institute for Ocean Sciences

Eric Terrill
Scripps Institution of Oceanography

Technical Report

Woods Hole Oceanographic Institution
Woods Hole, Massachusetts 02543

September 1996

Funding was provided by the Office of Naval Research through
Grant No. N00014-91-J-1891.

Reproduction in whole or in part is permitted for any purpose of the United States Government. This report should be cited as Woods Hole Oceanog. Inst. Tech. Rept., WHOI-96-10.

Approved for public release; distribution unlimited.

Approved for Distribution:

James F Price for
Philip L. Richardson, Chair
Department of Physical Oceanography

Abstract

The Third Acoustic Surface Reverberation Experiment (ASREX III) took place from December 1993 to March 1994 at Site L (34°N, 70°W) in the mid-Atlantic. As part of this experiment, two moorings were deployed to measure the environmental background. A meteorological and oceanographic mooring was deployed to characterize the surface wind stress, buoyancy flux, and the current and temperature structure over the top 500 meters. A Seatex Wavescan™ buoy was deployed to characterize the directional wave spectrum. This report presents results from these moorings. Wind speeds up to 25 m/s were seen, with significant heat losses (up to 1050 W/m^2) when cold continental air moved out over the warm Atlantic. The wave heights ranged up to 8 m, with significant wave heights of several meters persisting for relatively long periods. Wave height and period, nondirectional spectra, directional spectra and a typology of wave events are presented and related to surface forcing.

Table of Contents

List of Figures

List of Tables

1. Introduction

The Third Acoustic Surface Reverberation Experiment, (ASREX III) was designed to study processes causing degraded acoustic transmission in high sea states (see McDaniel, 1993, for a review of the state of the scientific understanding before this experiment). The experiment took place in late 1993 and early 1994 at Site L (34N 70W) over the Hatteras Abyssal Plain. In support of this experiment, a total of five moorings were deployed. Section 2 of this report describes the mooring array in order to provide the overall context for the experiment. Section 3 then describes the environmental background during the experiment, including the temperature, salinity, and current structure in the upper 500 m, surface meteorology, and wave conditions. The bulk of this data is taken from two moorings, a meteorological/oceanographic mooring and a wave mooring deployed by the Upper Ocean Processes (UOP) group at the Woods Hole Oceanographic Institution.

2. Mooring Information

2.1 Introduction

The moorings were deployed from the R/V *Knorr* of Woods Hole Oceanographic Institution, sailing from Woods Hole on 8 December 1993. The moorings were recovered by the R/V *Edwin Link* of Harbor Branch Oceanographic Institution, sailing from Jacksonville on 18 March 1994. Figure 2.1 shows a bathymetric map of the area surrounding the experiment site. Recovery and deployment were directed by John Kemp of WHOI's Ocean Acoustics Laboratory (OAL). A list of cruise participants appears in Appendix 1 and the chronology of the cruises is described in Appendix 2.

A total of five moorings were deployed during ASREX III. These were:

1. A near-surface soundspeed mooring, instrumented by Dr. W. K. Melville's group at Scripps Institution of Oceanography (SIO).
2. A Seatex wave mooring instrumented by the UOP and OAL groups at WHOI.
3. A meteorological/oceanographic discus mooring instrumented by the UOP group at WHOI.
4. An acoustics mooring instrumented by Dr. H. DeFerrari's group at the University of Miami and Dr. D. M. Farmer's group at the Institute for Ocean Sciences (IOS), Sidney, BC, Canada.
5. An ELSI B sonar mooring instrumented by D. Farmer's group at IOS.

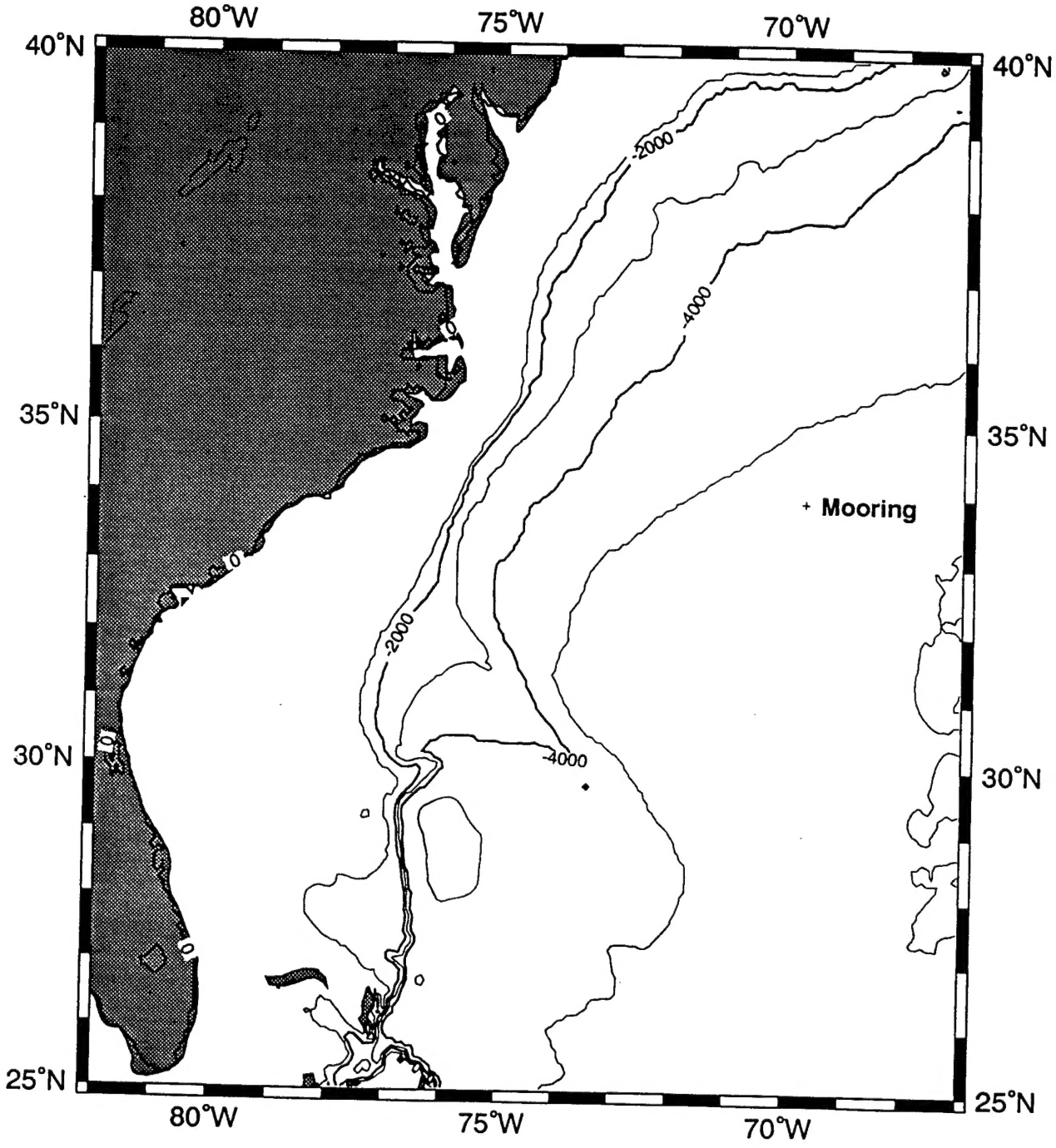

Figure 2.1: Bathymetric map of experiment site.

Table 2.1 lists the locations and durations of the five moorings and Figure 2.2 shows their locations and watch circles. The planned duration for the array was 12 weeks. The actual deployment was longer than this because the ship scheduled for the pickup cruise, the R/V *Endeavor*, was unable to get clearance to sail as planned.

Buoy	**Deployed**	**Recovered**	**Latitude**	**Longitude**
SIO Spar (WHOI 957)	2041 10 Dec 93	2213 24 Mar 94	33°56.62N	70°06.34W
WHOI Seatex (WHOI 958)	2216 13 Dec 93	1324 23 Mar 94	34°03.89N	70°05.10W
WHOI Discus (WHOI 959)	0613 15 Dec 93	1143 24 Mar 94	33°52.70N	69°44.83W
Miami Acoustics (WHOI 960)	2140 18 Dec 93	1416 21 Mar 94	33°49.05N	70°00.25W
ISO ELSI B (WHOI 961)	0631 19 Dec 93	1234 22 Mar 94	33°54.52N	69°56.20W

Table 2.1: Locations and durations of the five moorings. Deployment time is anchor splash, recovery time is when release is fired. Position is for the anchor.

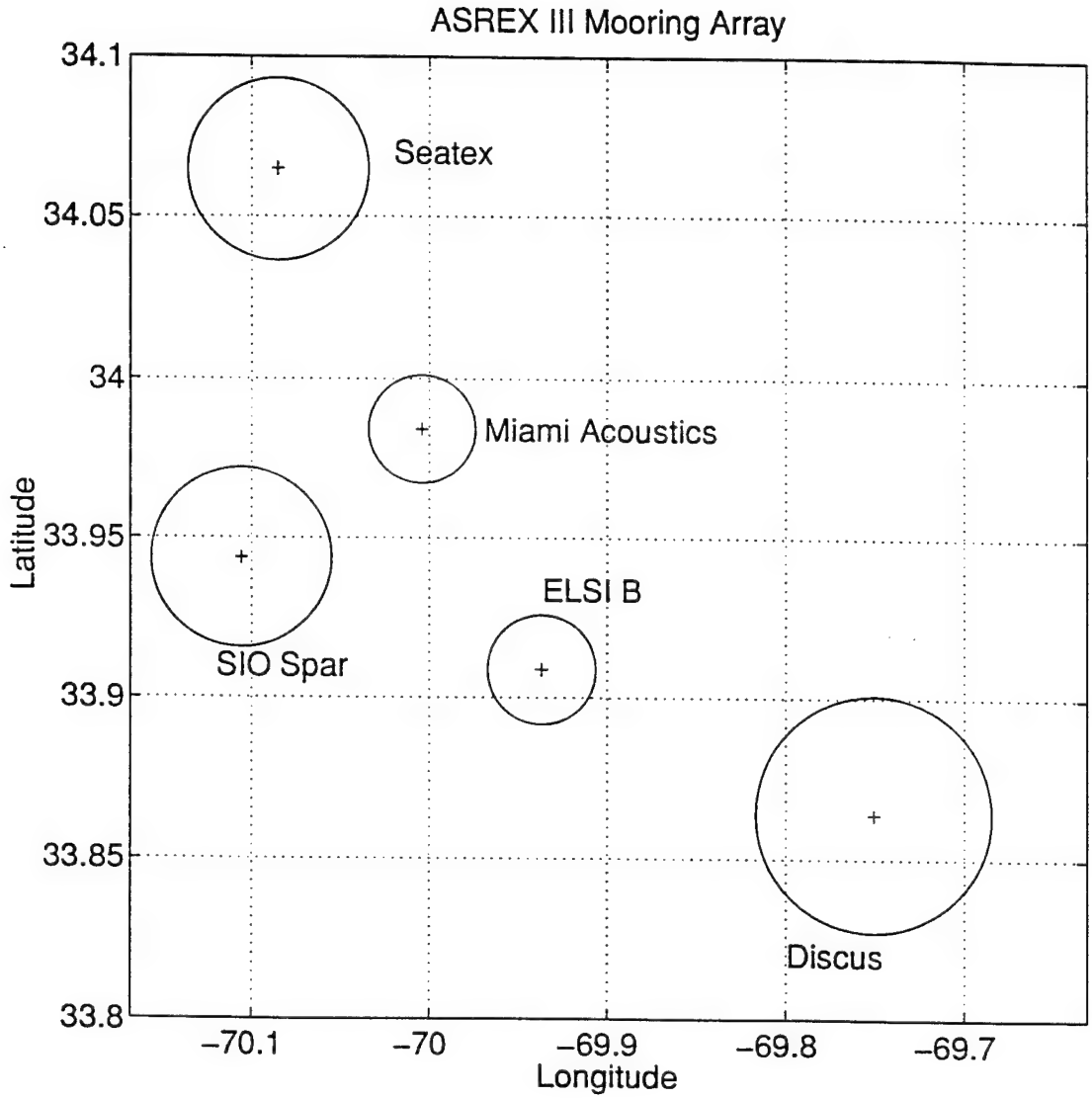

Figure 2.2: Locations and watch circles of the moorings in the array.

2.2 SIO Soundspeed Mooring

A spar buoy was deployed by SIO to measure acoustic properties of bubble clouds in the upper 7 meters. The buoy had an overall length of 10.66 m and a maximum diameter of 2.43 m. It was composed of three pieces:

a. A stainless steel tower above the surface holding solar panels, Argos PTTs, the data acquisition system and associated electronics.
b. A Seward International donut-shaped float with 6400 lb total buoyancy. The central well of this float was filled with a battery pack which was recharged by the solar panels.
c. A 7 m spar made of 20.31 cm (8 in) outer diameter Aluminum 6061 tubing, extending below the float. All environmental sensors were connected to this spar.

The buoy made measurements of four environmental parameters. Soundspeed was measured by recording the travel times of acoustic pulses between hydrophone pairs at approximately 1 m spacing. The duty cycle was 40 minutes on, 2 Hz pulse rate/pair and 50 minutes off. The frequency of the pulses transmitted during each acquisition period cycled though 3, 5 and 10 kHz, so that 40 minute time series for individual frequencies occur at 4.5 hour intervals. Measurements were made at 0.69, 1.02, 1.58, 1.96, 2.96 4.44, and 6.94 m depth. The acoustic data was logged to hard disk on a Compaq 486 notebook computer.

Temperature was measured using a sensor manufactured by Falmouth Scientific Inc. (F.S.I.) at depths of 0.71, 1.33, 1.97, 3.03, 4.49 and 7.00 m. Conductivity was measured using a sensor manufactured by F.S.I. at depths of 0.71 3.03 and 7.00 m. Dissolved oxygen was measured using a sensor by Royce at 0.65, 3.18, and 7.19 m. The environmental data was logged to disk on an Onset Tattletale 6.

Data was successfully sampled from 10 December 1993 until 22 January 1994. On 22 January, the system unexpectedly shut down due to low power. It is suspected that a seawater ground/short developed and quickly drained the batteries faster than the solar panels could recharge them. Evidence of this has been seen in the time series of battery voltage saved on the Tattletale.

In order to allow the buoy to be attached to the mooring at one side, it was important to limit the tension on the mooring line. This presented a difficulty given the high currents known to be associated with cold-core rings seen at the site during previous deployments. The problem was solved by linking the surface and subsurface floats with an S-tether with a scope of 2.5 consisting of a negatively buoyant upper section and a positively buoyant lower section. This design allowed the mooring to tilt over in high current regimes without greatly increasing the surface tension. A surface tether made of 3/8" trawler chain covered with Tygon tubing was connected to the center of gravity of the buoy. Buoyancy for the surface tether was

provided via 45 Panther-Plast Type 629 floats equally spaced on the top 21 meters. It was presumed that the Tygon tubing would provide sufficient stiffness to prevent the tether from fouling on the spar. This appears to have been the case. The mooring diagram for this instrument is shown in Figure 2.3, and a summary of the instrumentation is presented in Table 2.2.

2.3 The Seatex Mooring

This mooring was instrumented with a Seatex Wavescan™ buoy manufactured by Seatex A/S of Trondheim, Norway. Like the SIO Spar, the Wavescan buoy was tethered to a subsurface float via an S-tether which was designed to decouple the dynamics of the mooring from the motion of the surface float. Like the SIO Spar mooring, the Seatex mooring tether also lost most of the surface floats on the tether due to working in rough seas. The data collected from the buoy is summarized in Table 2.3 and the mooring diagram is shown in Figure 2.4.

2.4 The UOP Discus Mooring

The surface float on this mooring was a 3 m discus buoy outfitted with two meteorological packages, a Vector Averaging Wind Recorder (VAWR) with a full sensor suite, and an Improved Meteorological (IMET) package with a reduced sensor suite. The mooring line was instrumented with 8 Vector Measuring Current Meters (VMCMs), 12 temperature pods (T-POD) made by Brancker Inc. of Toronto, Ontario, Canada, 2 Seacat conductivity/ temperature packages, and an inverted Echo-sounder. Details of the instrumentation and sampling are given in Table 2.4. The mooring diagram is shown in Figure 2.5.

2.5 The Miami Acoustics Mooring

The Miami Acoustic Mooring for ASREX III was designed to produce high level acoustic transmissions at frequencies ranging from 100 Hz to 800 Hz and record the acoustic energy backscattered from the ocean surface via a 64 element hydrophone array and a pair of electronic receivers over the course of the 3 month long experiment. The mooring diagram is shown in Figure 2.6, and specifications of the instrumentation and acoustics packages are given in Tables 2.5 and 2.6. From top to bottom the mooring consisted of the following major components:

Instrument	Parameters Measured	Sample Rate	Duty Cycle	Depth
Dissolved Oxygen sensor	Dissolved oxygen	0.5 Hz	Continuous	0.65 m
Acoustic transducer	Soundspeed @ 3, 5 and 10 kHz	2Hz pulse rate	40 min. on, 50 min off cycling through all 3 frequencies	0.69 m
Conductivity/ Temperature sensor	Conductivity, temperature	0.5 Hz (Cond) 2 Hz (Temp)	Continuous	0.71 m
Acoustic transducer	Soundspeed @ 3, 5 and 10 kHz.	2Hz pulse rate	40 min. on, 50 min off cycling through all 3 frequencies	1.02 m
Temperature sensor	Temperature	2 Hz	Continuous	1.33 m
Acoustic transducer	Soundspeed @ 3, 5 and 10 kHz.	2Hz pulse rate	40 min. on, 50 min occ cycling through all 3 frequencies	1.69 m
Temperature sensor	Temperature	2 Hz	Continuous	1.97 m
Acoustic transducer	Soundspeed @ 3, 5 and 10 kHz	2 Hz pulse rate	40 min on, 50 min off cycling through all 3 frequencies	2.96 m
Conductivity/ Temperature sensor	Conductivity, temperature	0.5 Hz (Cond) 2 Hz (Temp)	Continuous	3.03 m
Dissolved Oxygen sensor	Dissolved oxygen	0.5Hz	Continuous	3.18 m
Acoustic transducer	Soundspeed @ 3, 5 and 10 kHz.	2 Hz pulse rate	40 min. on, 50 min off cycling through all 3 frequencies	4.44 m
Temperature sensor	Temperature	2 Hz	Continuous	4.49 m
Acoustic transducer	Soundspeed @ 3, 5 and 10 kHz.	2 Hz pulse rate	40 min. on, 50 min off cycling through all 3 frequencies	6.94 m
Conductivity/ Temperature sensor	Conductivity, temperature	0.5 Hz (Cond) 2 Hz (Temp)	Continuous	7.00 m
Dissolved Oxygen sensor	Dissolved oxygen	0.5 Hz	Continuous	7.18 m

Table 2.2: Instrumentation, sampling strategy, and days good data for the SIO soundspeed mooring.

Instrument	Fields Measured	Sample Interval	Sample Rate	Days Good Data
Motion Package	Heave Tilts	1 sec	2048 samples every 3 hours	98
	Wave Spectrum	2048 sec	Every 3 hours	

Table 2.3: Seatex Wave Mooring. All instrumentation is at surface.

Istrument Type	Fields Measured	Sample Interval	Sample Rate (sec)	Days of Good Data	Depth (meters)
VAWR	WS, WD, AT, SST, RH, BP, SW, LW	450	450	99 except WD	Surface
IMET	WS,WD, AT, RH, SW	450	450	99	Surface
T-POD	T	450	450	99	1
T-POD	T	450	450	99	1
Seacat	S,T	225	225	99	1
VMCM	U,V,T	120	120	90	5
VMCM	U,V,T	120	120	89	10
VMCM	U,V,T	120	120	90	15
VMCM	U,V,T	120	120	90	20
T-POD	T	450	450	99	37.5
VMCM	U,V,T	120	120	89	50
T-POD	T	450	450	99	75
T-POD	T	450	450	99	100
T-POD	T	450	450	99	125
VMCM	U,V,T	120	120	90	150
T-POD	T	450	450	99	175
T-POD	T	450	450	99	200
T-POD	T	450	450	99	230
T-POD	T	450	450	99	260
VMCM	U,V,T	120	120	89	300
T-POD	T	450	450	99	350
T-POD	T	450	450	99	400
Seacat	T,C	225	225	87	450
VMCM	U,V,T	120	120	89	500

WS: Wind speed
WD: Wind Direction
RH: Relative Humidity
BP: Barometric Pressure
AT: Air Temperature
SST: Sea Surface Temp.
SW: Short wave Radiation
LW: Long wave Radiation
U,V: East, North Velocity
T: Temperature
C: Conductivity

Table 2.4: Instrumentation and data return from the UOP meteorological/oceanographic mooring. Total deployment time for this mooring was 99 days. An inverted Echo-sounder package was also deployed at 30 meters, but did not record any data.

Instrument	Fields Measured	Sample Rate	Sample Interval	Depths relative to top plate	Days Good Data
Conical Beam Sonars (4)	Backscatter @55, 110, 200 and 300 Khz	2 Hz	27 minutes every 12 hours	Surface	10
Water Structure Profiler (WASP)	Backscatter @200 kHz	1/6 sec	Continuous	0.25m bins, 10–50m above instrument	10
Sidescan sonars (4)	Backscatter, doppler velocity @ 100 kHz	2 Hz	27 minutes every 12 hours	Surface	10
Wide-band, omnidirectional hydrophone	Ambient noise spectrum		Every 1 hour	At instrument	10
Temperature sensor	Temp,		Every 1 hour	At instrument	10
Conductivity sensor	Cond.		Every 1 hour	At instrument	10
Pressure sensor	Pressure		Every 1 hour	At instrument	10
Motion Package	Tilt, Orientation		Every 1 hour	At instrument	10
SeaData TDR	Temp, Pressure	1/450 sec			84
Hydrophone array (see Table 2.6 for details)	Sound level at 100, 200, 400 and 800 Hz				84

Table 2.5: Miami Acoustics Mooring, Instrumentation and Data Return. One TDR, located on the disk buoy, was inadvertently turned off when the endcap was placed on the instrument. This instrument functioned normally during post-cruise calibrations and the data loss, while unfortunate, was apparently due to human error and/or a design flaw (twisting of the end cap to line up the securing latches apparently caught the switch and turned it off).

University of Miami Low Frequency Source and Receiver Arrays

The UM source and receiver arrays are autonomous and general purpose instruments that can be moored at sea for periods of months and transmit and receive complex acoustical signals under computer control. The source is constructed with four arrays of air-backed, pressure-compensated transducers with center frequencies of 100, 200, 400 and 800 Hz. that transmit at a level of ~200 dB//µPa @ 1 m. The two receiver packages each handle a 32 element hydrophone array with 20 gigabytes of storage capacity. The packages can be moored separately or on the same mooring to form a 64 element array.

Source

•Frequencies	100	200	400	800	Hz
•Source Levels	196	197	196	198	dB//µPa @ 1 m
•Bandwidth	25	66	133	266	Hz
•Pulse period	.040	.015	.0075	.0038	sec
•Operating depth	300 m				
•Duration	12 week, 20% Duty cycle, (full complement alkaline batteries)				
•Signal types	Fm, M-sequences, CW pulses, Golay codes, anything programmable within bandwidth				
•Size	size: ~5 ft dia x 18 ft long (~1.5 m dia x 5.5 m long)				
•Weight	-6218 lbf (27.7 kN) -- in air -550 lbf (2.4 kN) -- in sea water, bladders evacuated -187 lbf (832 N) -- in sea water, bladders full of air				

Receivers

•Reception	4 x Fc sample and store or phase coherent demodulation with coherent circular averaging
•Storage	5 gigabytes expandable to 20 in each receiver
•Hydrophone spacing	2 x 16 element and 1 x 32 element arrays with .94 m spacing (3.1 ft) (half wavelength for 800 Hz) 2 x 16 element and 1 x 32 element arrays with 1.88 m spacing (6.2 ft) (half wavelength for 400 Hz)
•Sensitivity	178 db//1V/µPa @1m
•Size	~4 ft dia x 9 ft long (~1.2 m dia x 2.7 m long)/ea receiver
•Weight	-3743 lbf (16.7 kN) in air +670 lbf (3.0 kN) buoyant in s.w.

Table 2.6: Specifications of the U. Miami Acoustic Array.

Extended Life Sonar Instrument (ELSI) - IOS/Canada

This instrument used high frequency acoustics to measure the content and nature of bubble plumes that were generated by breaking surface gravity waves at high sea states. Parameters of the ELSI deployed from this mooring are described in Table 2.5.

Disk Buoy

A disk shaped syntactic foam buoy package provided most of the buoyancy required to maintain high tension in the subsurface taut mooring. It provided approximately 3100 lbs of positive buoyancy at depths up to 2000 m. A pair of Argos satellite Platform Terminal Transmitters (PTTs), one oriented up and the other down, were mounted on the side of the buoy to provide location information to a shore station should the mooring have surfaced prematurely. A Sea Data/Pacer/WHIS temperature-depth recorder (TDR) was mounted on the top of the disk buoy and recorded the temperature and pressure every 7.5 minutes over the course of the experiment.

Acoustic Transmitter ("Miami Sound Machine")

A 5.3 meter long, 6100 lb (in air) package contained an electronic signal generating system powered by alkaline batteries, a syntactic foam flotation module that reduced its weight in water to under 750 lbs, and an array of acoustic transducers mounted in an aluminum framework that could broadcast acoustic signals at levels on the order of 200 dB//1 μPa @ 1 m at four frequencies (100 Hz, 200 Hz, 400 Hz, and 800 Hz). This instrument transmits a series of acoustic pulses and coded signals that are listened for by the receiver packages/acoustic array described below. The transmitter also provided a clock signal that was transmitted down a 20 meter long electro-mechanical cable to the uppermost receiver system. This technique assured that the source and receivers were always "in synch" with one another.

Acoustic Receivers/Hydrophone Array

There were two receiving packages on the Miami mooring each of which recorded signals received by 32 of the 64 total hydrophones distributed between them. The receiver packages contain electronics and tape recording systems capable of recording 25 gigabytes of data each. The electronics are powered by a series of alkaline battery packs mounted in cylindrical aluminum pressure housings. The pressure housings are recess mounted in custom built syntactic foam buoyancy modules, and bolted to an aluminum framework. Each receiver package weighs about 4000 lbs in air and is 3.1 meters long. In seawater, however, the packages provide over 650 lbs of positive buoyancy. In addition to recording acoustic signals, the receivers also monitor and record tilt and ambient pressure. TDR's were mounted on each

end of each receiver to provide additional records of pressure and ambient temperature. A Benthos XT-6000 acoustic beacon, modified to include a pressure sensor, was mounted on the uppermost receiver and was used to telemeter its pressure (depth) back to a DS7000 deck unit when interrogated at the proper frequency. This was useful during the deployment operation as it gave a real time indication that the instrument was moored at its proper depth.

The hydrophone array consisted of 64 HT1 hydrophones spaced to provide beam-forming capabilities at all of the frequencies output by the transmitter. The hydrophones were mounted in aluminum pipes that were whipped to a Kevlar-based electromechanical cable that has a breaking strength in excess of 12,000 lb. In addition, a 3/8" diameter 3x19 jacketed wire rope ran in parallel to provide backup protection, should the Kevlar strength member be severed (i.e., by fish bite). The array also featured a 3-strand fairing to reduce cable strumming. Just below the lower receiver system was a 200 meter length of SAIC Quiet Cable® which was also used to reduce cable strumming which can interfere with acoustic measurements.

The remainder of the mooring consisted of 3/8" wire rope, 1/2" chain, glass buoyant spheres, and a pair of Benthos 865A acoustic releases mounted in parallel, all of which were chained to a 7000 lb cast iron anchor (Figure 2.6).

2.6 The ELSI B Mooring

This mooring included an ELSI B instrument platform which included a number of sonar instruments as shown on Figure 2.7. These were:

a. 6 upward looking conical beam sonars operating at frequencies of 28, 50, 88, 100, 200, and 400 kHz.
b. A fixed 100 kHz sidescan sonar identical to that deployed on the Miami acoustics mooring.
c. A 100 kHz sidescan sonar mounted on a rotating base allowing it to scan 360 degrees in azimuth every 77 seconds. Because of the extra time required to move the sonar, the overall ping rate was reduced to 1.67 Hz.
d. Instruments to measure ambient sound and environmental parameters. The sonars collected data for 27 minutes every 6 hours.

Additional instrumentation on the mooring included an Anderaa temperature chain with thermistors every 5 meters below the top plate of ELSI B, an S4 current meter at 7.5 m below the top plate of ELSI B and a 12 channel WOTAN (wind observation through ambient noise) instrument 70 m below the top plate of ELSI B. Table 2.7 lists the ELSI B mooring instrumentation.

Figures 2.8 and 2.9 show the positions of the Discus and Seatex buoys from System Argos. Both buoys show a consistent pattern, lying to the northeast of the moorings during December, shifting around to the east during January, and then more to the southeast during February, and finally to the south during March. These positions reflect the prevailing currents over the course of the deployment.

Instrument	Parameters Measured	Sample Rate	Sample Frequency	Depths relative to top plate	Days Good Data
Conical beam sonars	Backscatter at 28, 50, 88, 100, 200, and 400 kHz	1557 sec (2600 pings @ 1.67 Hz)	12 hours	Ocean Surface	90
Fixed 100 kHz Sidescan	Backscatter, Doppler velocities out to ~300 m	1557 sec. (2600 pings @ 1.67 Hz)	12 hours	Ocean Surface	90
Rotating 100 kHz Sidescan	Backscatter, Doppler velocities out to ~300 m	1557 sec. (2600 pings @ 1.67 Hz	12 hours	Ocean Surface	90
Environmental Sensor Pack	Temperature, conducitivity, depth			1	90
Thermistor String	Temperature	1200 sec	1200 sec	10, 15, 20, 25, 30, 35, 40, 45, 50, 55, 60	82
WOTAN	Ambient noise in 12 channels	15 sec	180 sec	70	90

Table 2.7: IOS ELSI B Mooring, Instrumentation and Data Return. This mooring was deployed for a total of 90 days. An S4 current meter was also deployed on this mooring but was severely damaged on recovery with consequent loss of data.

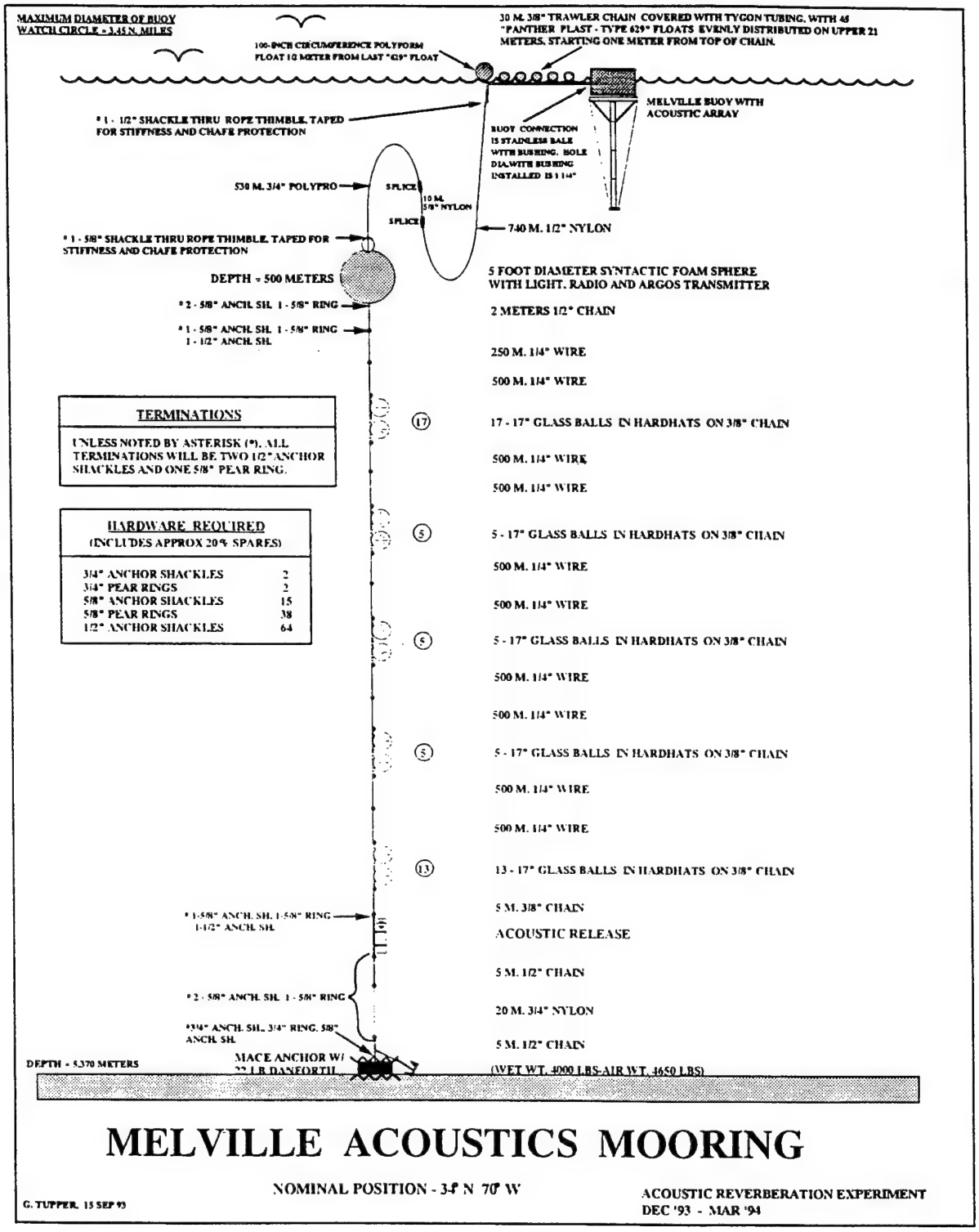

Figure 2.3: Diagram of SIO Soundspeed Mooring.

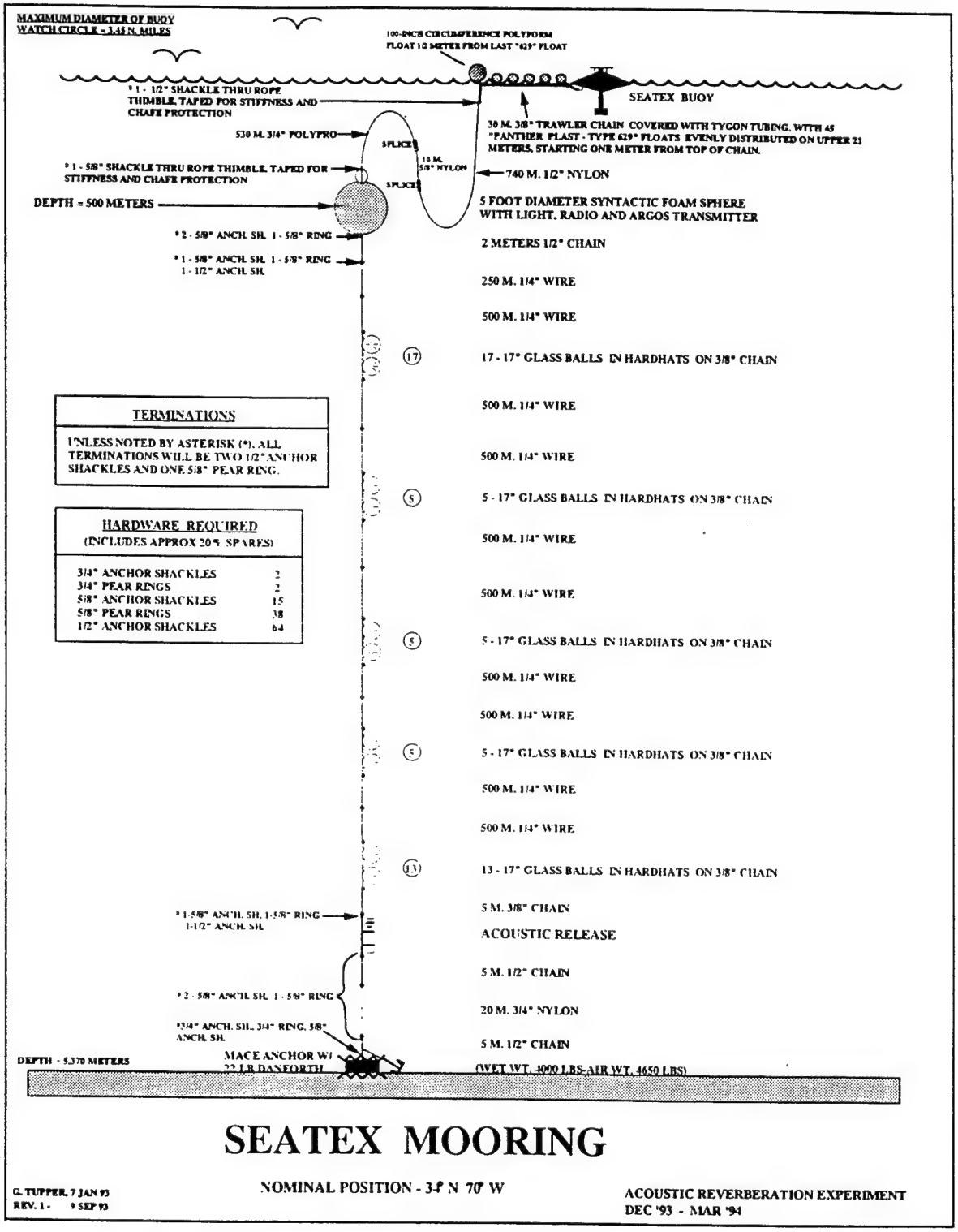

Figure 2.4: Diagram of WHOI Seatex Mooring.

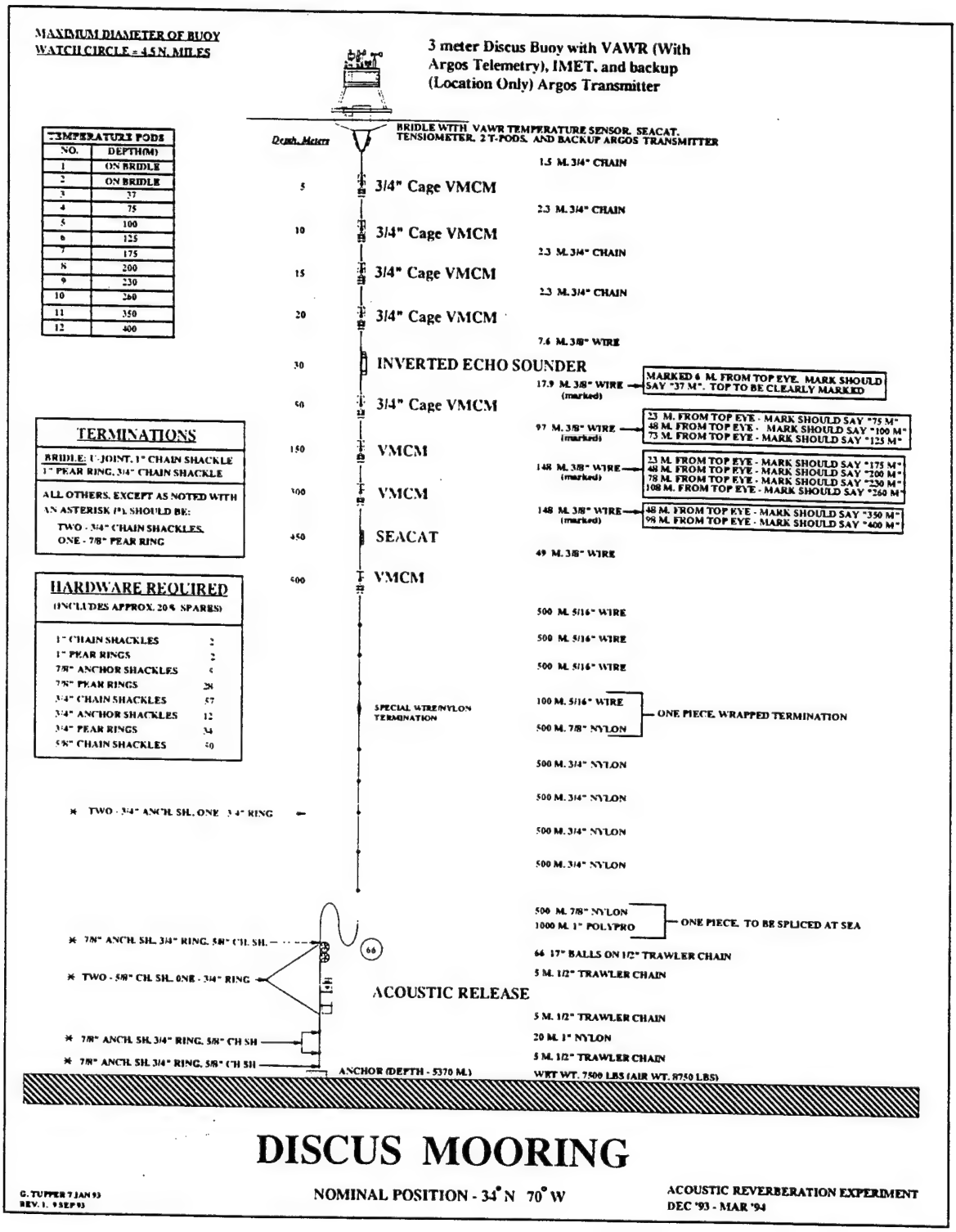

Figure 2.5: Diagram of WHOI Discus Mooring.

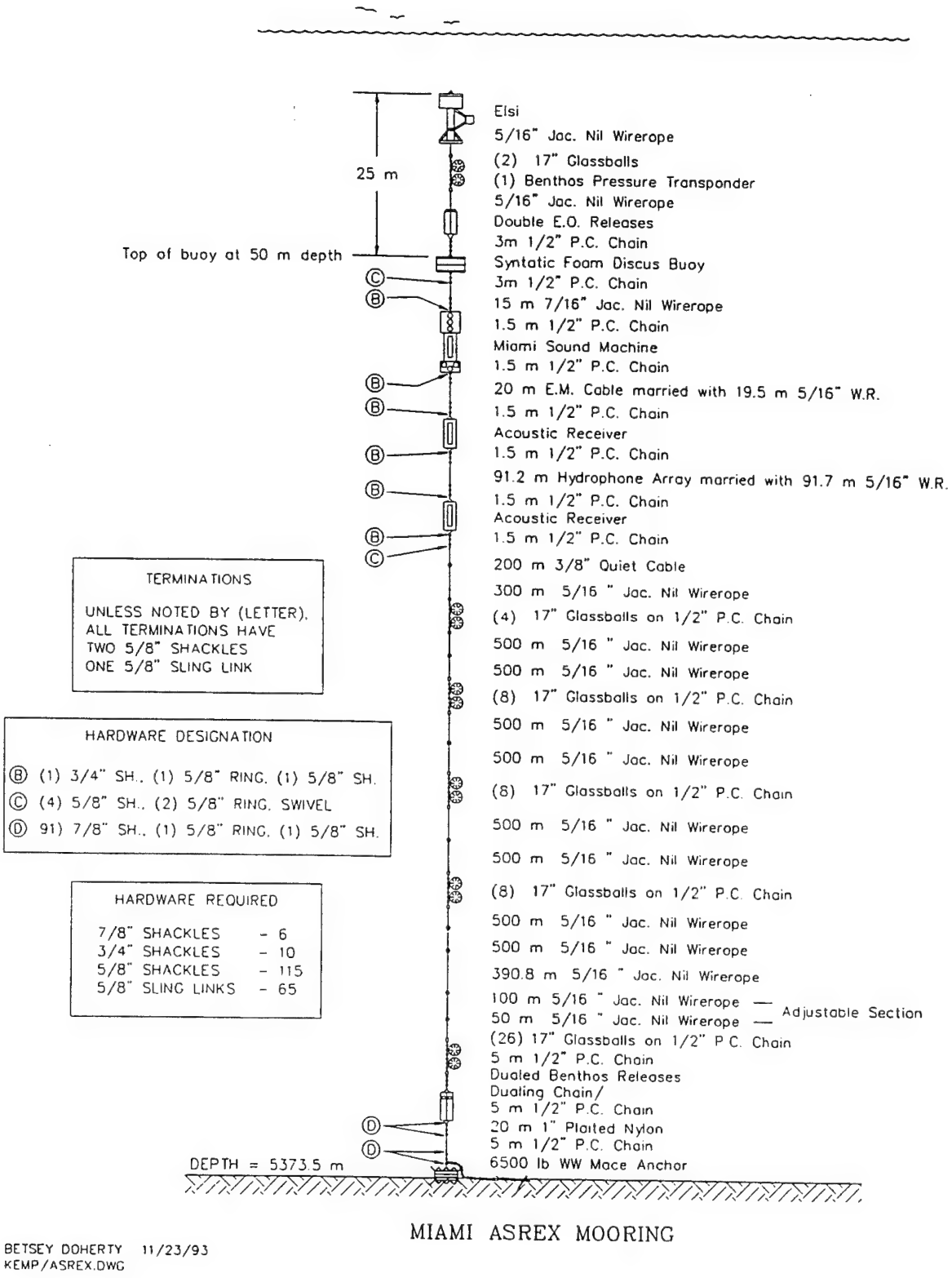

Figure 2.6: Diagram of Miami Acoustics Mooring.

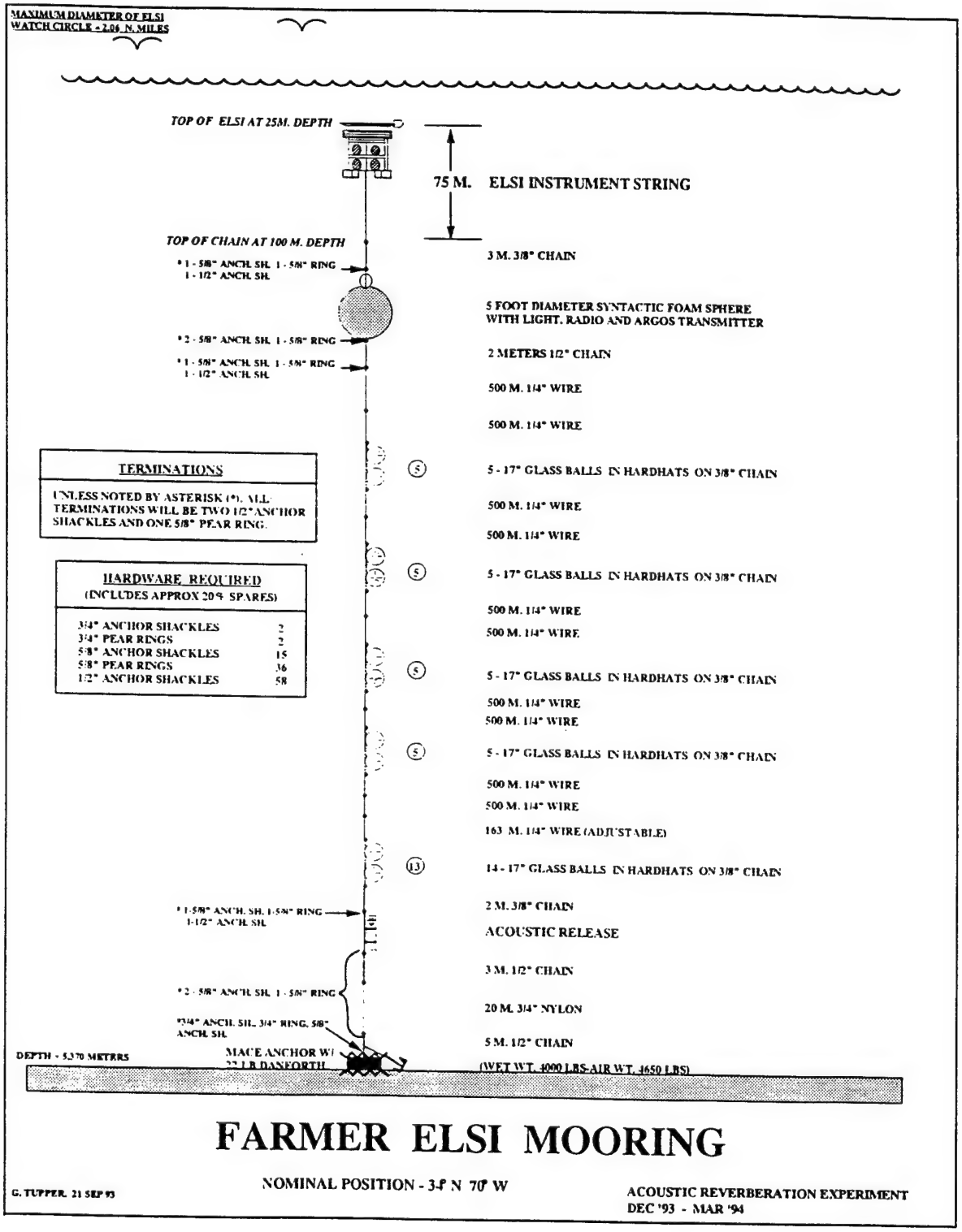

Figure 2.7: Diagram of IOS ELSI B Mooring.

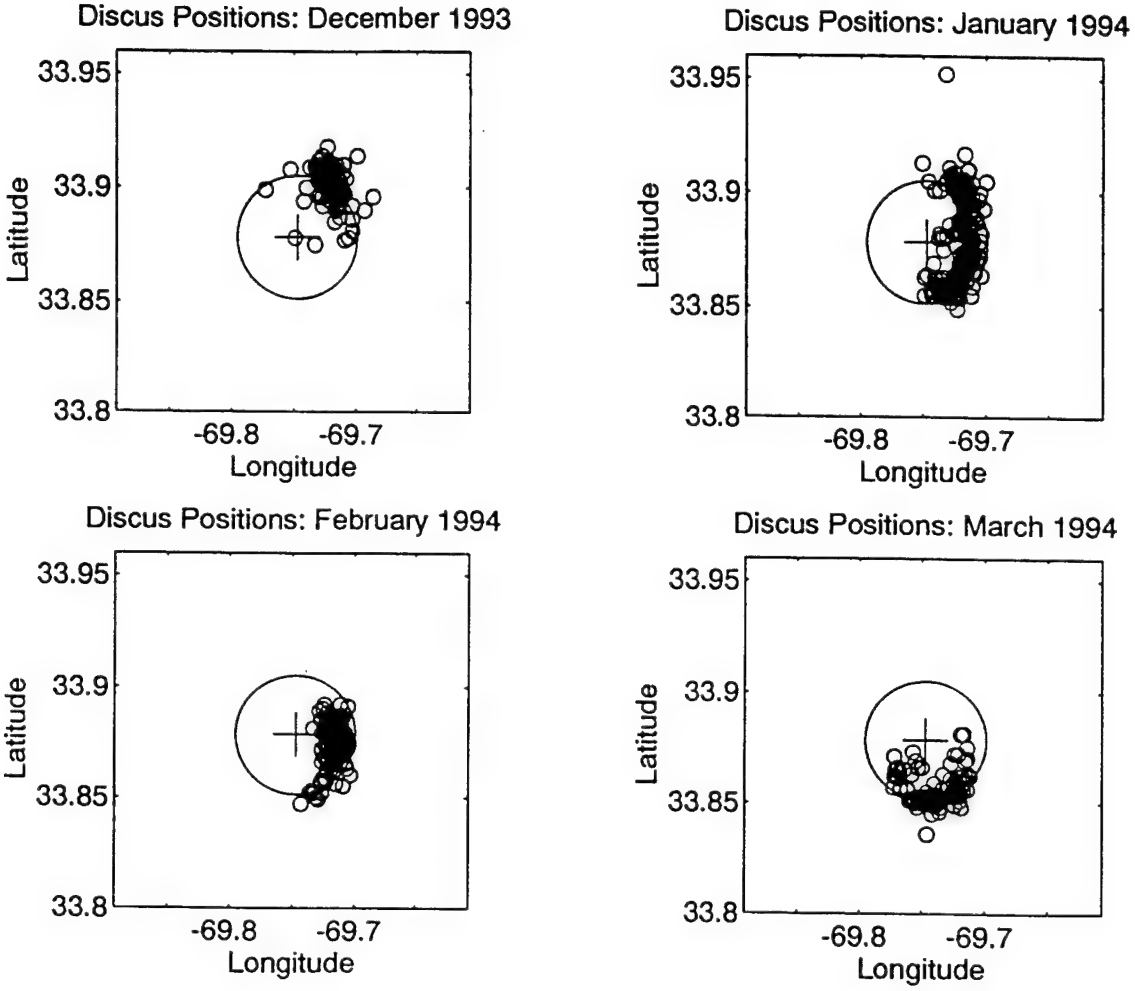

Figure 2.8: Argos positions of Discus buoy.

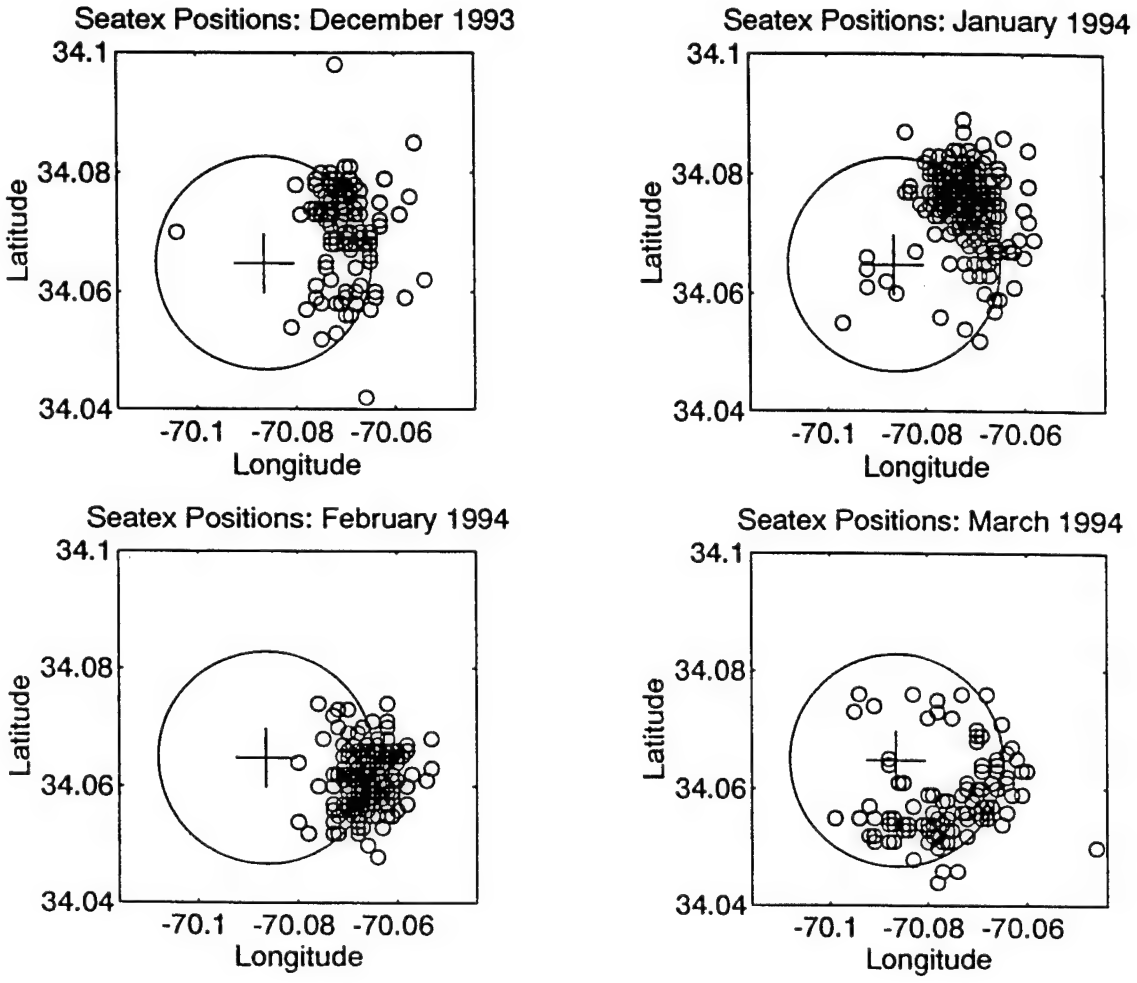

Figure 2.9: Argos positions of Seatex buoy.

3. Data Presentation

3.1 Meteorology during ASREX III

Meteorological Observations

Meteorological data was recorded using a VAWR with a 7.5 minute record rate. A second meteorological instrument package, an IMET system, also recorded a reduced set of data (short wave radiation, wind speed and direction, relative humidity and air temperature).

Tables 3.1.1-3.1.2 summarize the sensors, their accuracy, and the sampling strategy for each of the packages. Table 3.1.1 shows a schematic of how the VAWR sampled each sensor during the 7.5 minute recording interval. Note that while the wind and radiation sensors recorded over the entire interval, the relative humidity and barometric pressure are sampled for a very short period of time in the middle of the recording interval.

Figures 3.1.1-3.1.7 show time series of meteorological variables from the composite data set. From top to bottom, the wind east and north, sea surface and air temperature, barometric pressure, relative humidity, and short wave and long wave radiation are shown.

A check of the time base for the VAWR found 99 missing or incorrect clock counts. The data was interpolated over these gaps. The final processed data file had a total of 19099 records at 7.5 minute intervals between 15 December 1993 00:18 and 24 March 1994 11:33. A magnetic variation of 15.9° was applied to the data from both instruments.

The IMET data were found to agree very well with the VAWR data in general, although several small, systematic differences were found. The VAWR recorded wind speeds about 9% higher than the IMET. The IMET and VAWR air temperatures exhibited a systematic difference with the IMET showing lower air temperatures than the VAWR when the surface air temperatures were low. Both sensors showed a consistent diurnal cycle, with the VAWR exhibiting a mean diurnal cycle of about 0.5°C, while the IMET showed a mean diurnal cycle of about half that amplitude. Because this is most likely due to radiative heating of the sensor, the IMET temperature was used in the composite meteorological file.

Like the air temperature, the long wave radiation exhibited a diurnal cycle which had an averaged amplitude of about 13 W/m^2. Alados-Arboledas *et al.* (1988) showed that such an effect could arise from solar heating of the pyrgeometer dome. They suggested that the long wave radiation be reduced by 3.6% of the incoming short wave radiation. When this correction was applied to the data, the diurnal cycle of long wave radiation disappeared. The corrected long wave radiation was used in the composite meteorological file.

On 15 January 1994, the wind vane on the VAWR broke at the height of a strong storm. Thereafter wind direction was not available from the VAWR. This would not have been serious had not the IMET wind sensor experienced significant interference, which contaminated

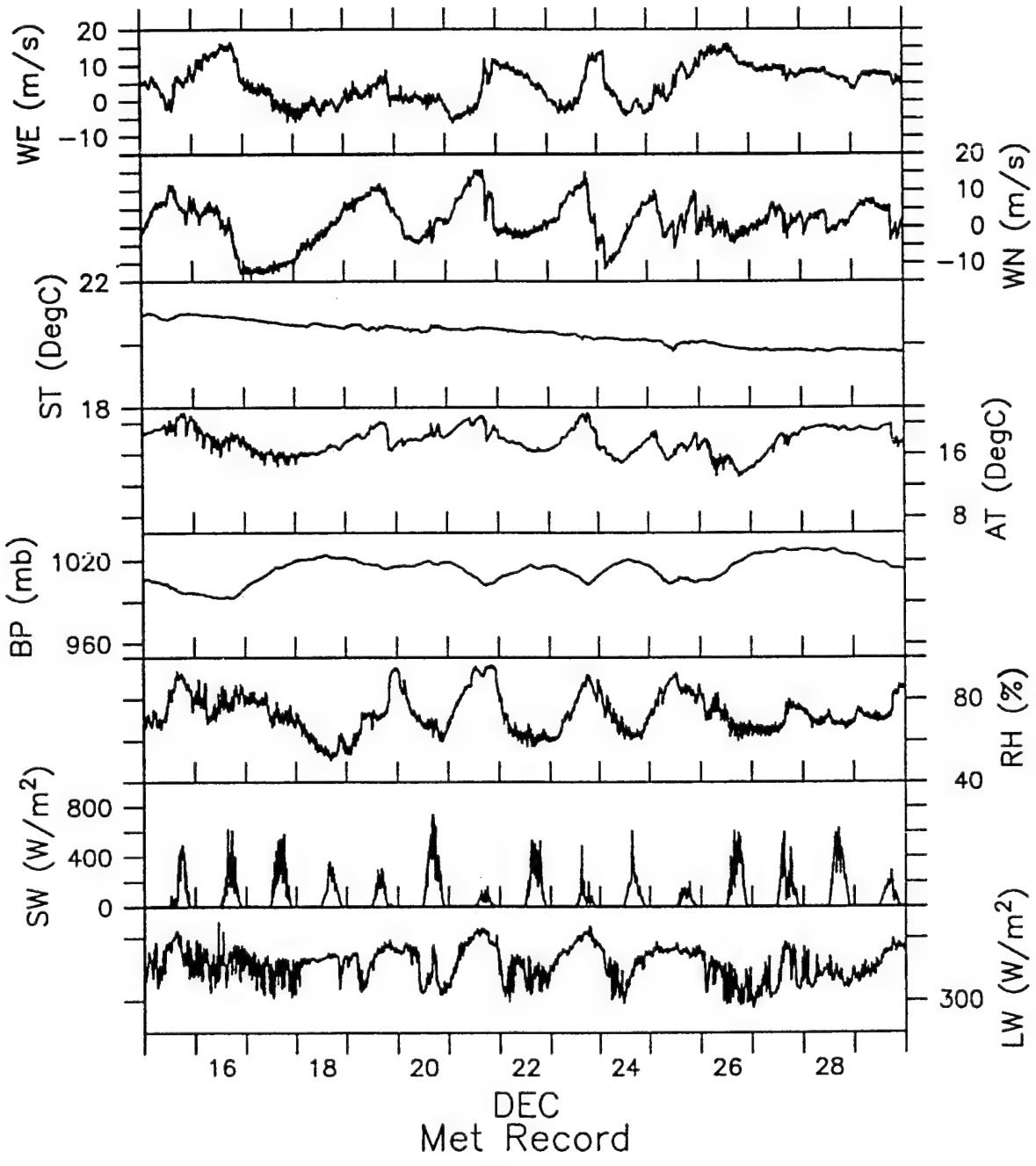

Figure 3.1.1: Meteorological Variables from the Composite Data Set.

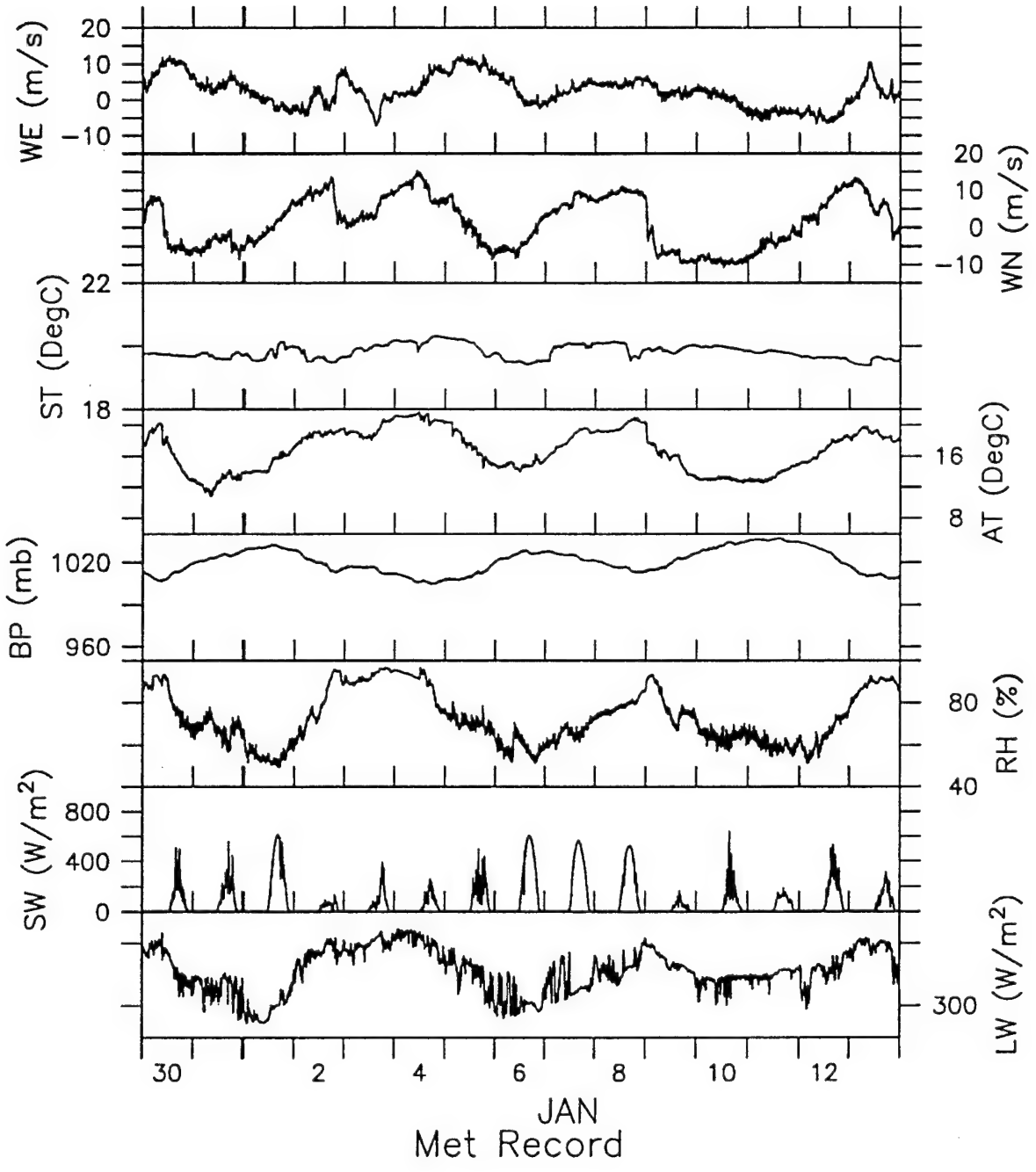

Figure 3.1.2: Meteorological Variables from the Composite Data Set.

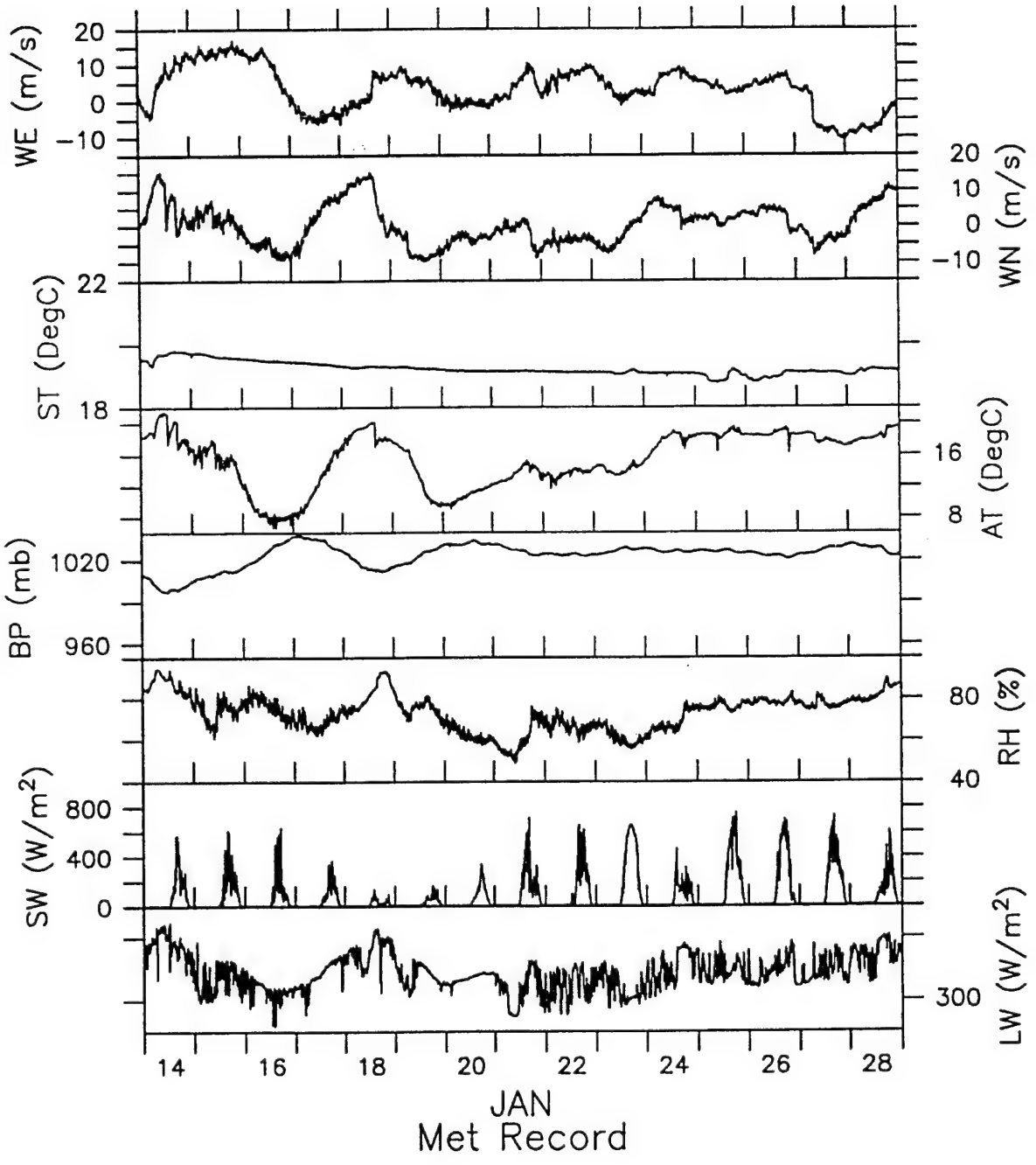

Figure 3.1.3: Meteorological Variables from the Composite Data Set.

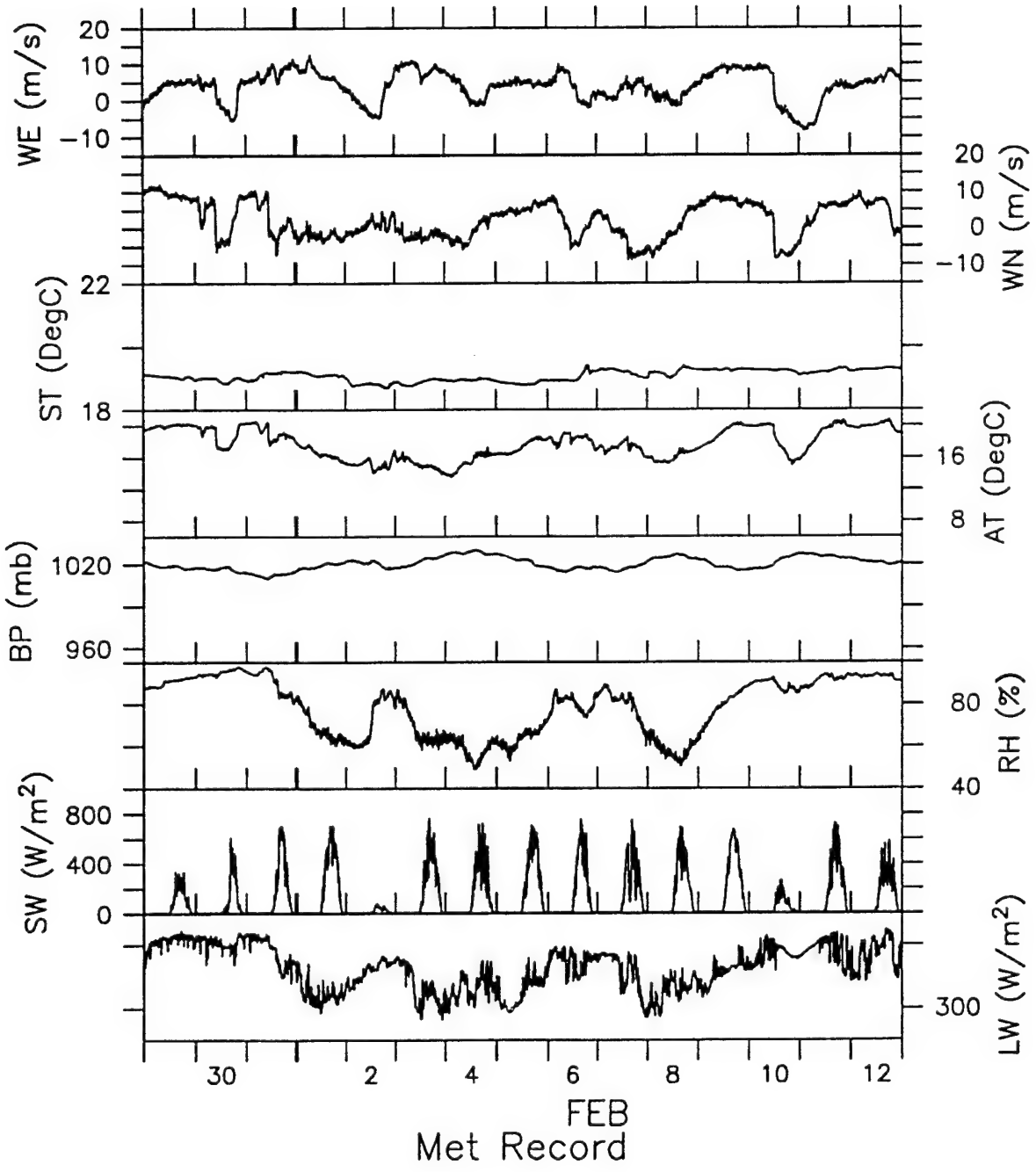

Figure 3.1.4: Meteorological Variables from the Composite Data Set.

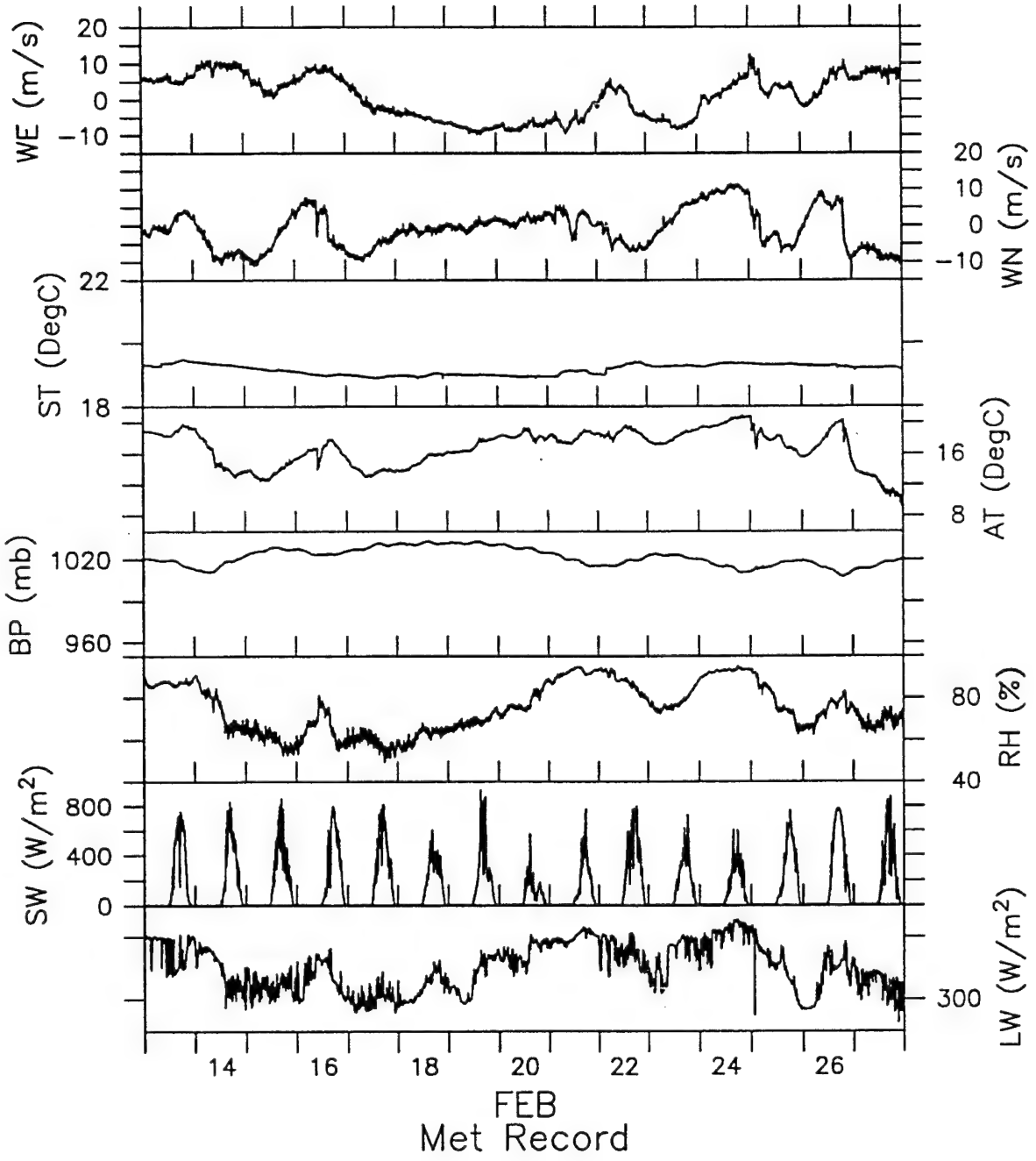

Figure 3.1.5: Meteorological Variables from the Composite Data Set.

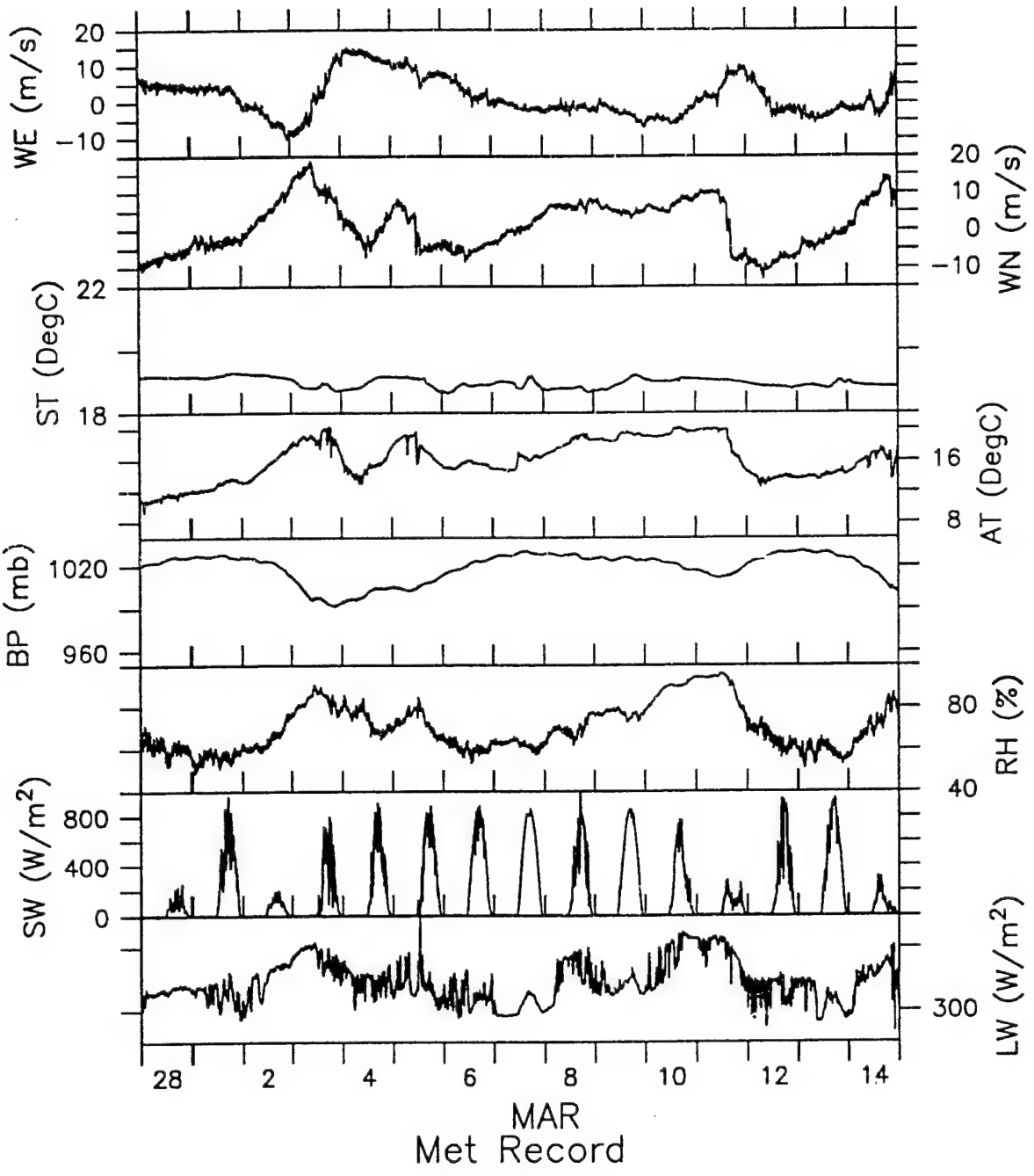

Figure 3.1.6: Meteorological Variables from the Composite Data Set.

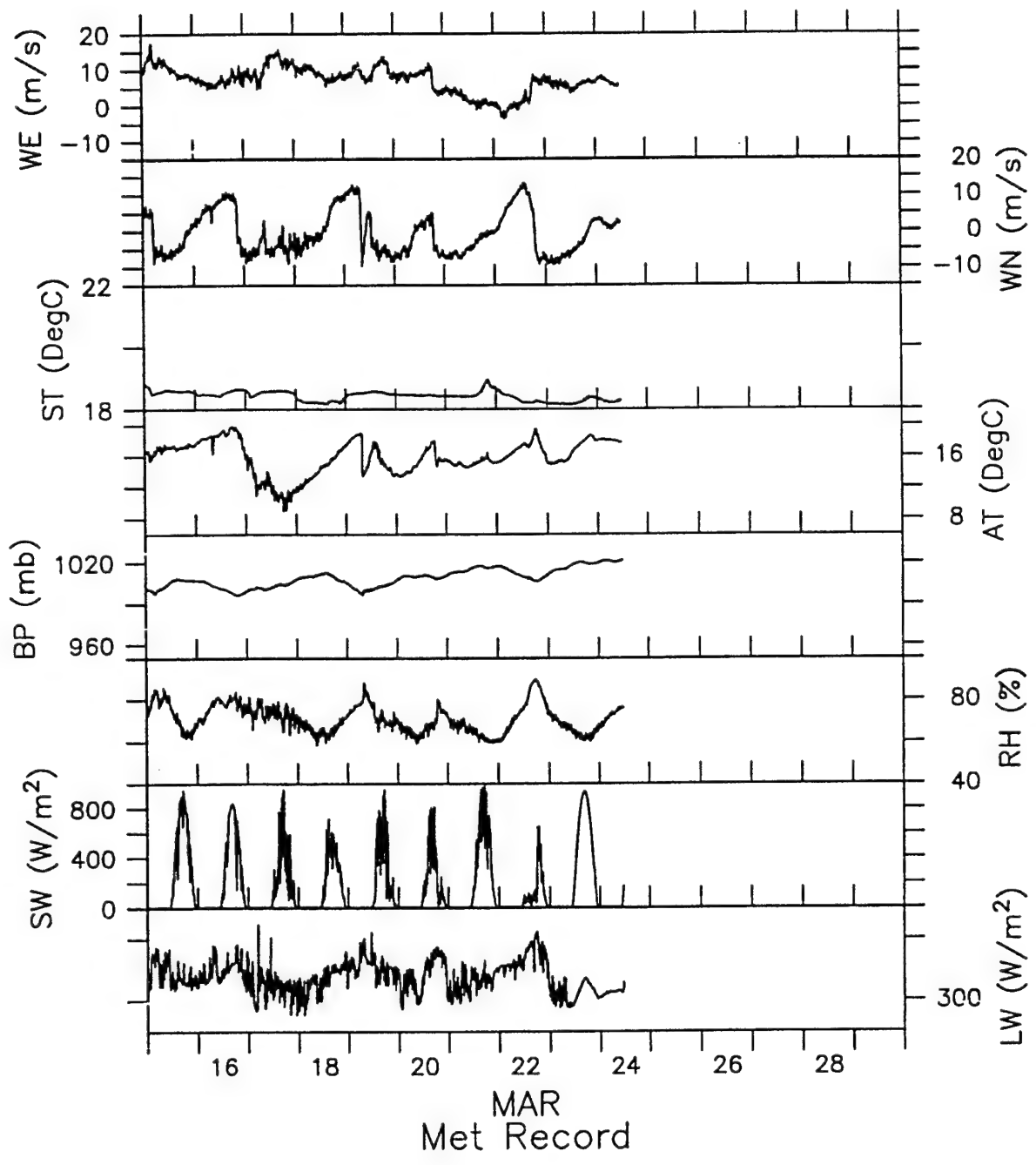

Figure 3.1.7: Meteorological Variables from the Composite Data Set.

WHOI VAWR Sensor Averaging Periods

Record Interval		----------
North		----------
East		----------
Rotor		----------
Vane	*	-
Compass	*	-
Short wave		----------
Relative Humidity	**	--
Barometric Pressure	***	-
Sea Temperature	****	----------
Air Temperature	****	----------
Long wave		----------

* Vane and Compass data recorded is the last sample taken in the record interval.
** Relative Humidity sensor is on for 7 seconds and counted for 3.515 seconds
*** Barometric Pressure sensor is on for 4.39 seconds and counted for 2.636 seconds
**** Air and Sea Temperature sensors are counted for 1/2 the record interval. Actual averaging interval is half the record rate minus 1.7578125 seconds (delay and settle time between sensors)

Table 3.1.1: Schematic of VAWR sensor averaging periods.

Parameter	Sensor Type	Accuracy	Record Time
Wind Speed	R.M.Young 3 cup anemometer	+/- 2% above 0.7 m/s	Vector Averaged
Wind Direction	Integral vane WHOI/EG&G	+/- 1 bit 5.6 degrees	Vector Averaged
Short Wave Radiation	Pyranometer Eppley 8-48	+/- 3%	Averaged over record interval
Long Wave Radiation	Pyrgeometer Eppley PIR	+/- 10%	Averaged over record interval
Relative Humidity	Vaisala umicap 0062HMP	+/- 2%	3.515 Seconds Average Note 1
Barometric Pressure	Paroscientific 216-B-101	+/- 0.2mbar wind < 2.m/s	2.636 Seconds Average Note 1
Sea Temperature	Thermistor Thermometrics	+/- 0.005 degrees C	Averaged over record time Note 2
Air Temperature	Thermistor Yellow Springs #44034	+/- 0.2 degrees C wind > 5 m/s	Averaged over 1/2 record time Note 3

Table 3.1.2: Meteorological Sensor Specifications, VAWR

approximately 20% of the records. In order to reconstruct the wind direction during the remainder of the experiment, the following procedure was applied:

1. A "first guess" based on the VAWR wind speed and the orientation of the buoy was calculated.
2. Points where the IMET wind direction deviated from the first guess by more than 90 degrees, or the IMET wind speed differed from 0.91 of the VAWR wind speed by more than 2 m/s, were interpolated.
3. Any remaining "spikes" (defined as a 1-point deviation in the east or north IMET wind by more than 2 m/s) were interpolated over.

The resulting time series of wind direction was found to agree extremely well with the observed wind direction from the VAWR (rms difference of ~2 degrees) during the time period when this parameter was available. Additionally, the synthetic wind direction agreed very well with the high frequency (3-4 sec) wave direction over the course of the experiment. This gives us strong confidence that the synthetic time series accurately represents the real wind.

Air-Sea Fluxes

Fluxes of momentum, sensible heat, and latent heat for the site were computed from the meteorological variables using the stability-dependent bulk aerodynamic formulae of Large and Pond (1981; 1982). The net short wave radiation is computed using an albedo of 0.06. The net long wave radiation is estimated using sea surface temperature assuming a sea-surface which radiates with an emissivity of 0.98.

Time series of the heat fluxes computed from the composite meteorological data set are shown in Figures 3.1.8-3.1.14. From top to bottom, the sensible, latent, net short wave, net long wave and total heat flux in W/m^2 are shown. Figures 3.1.15-3.1.21 show the wind stress time series computed from the composite meteorological data set. Shown from top to bottom are the eastward wind stress, northward wind stress, wind stress magnitude, wind stress direction (towards), and the nondimensional stability parameter z/L. (L is the Monin-Obhukhov length $-c_p T u^3_* / kgQ$, where c_p is the specific heat, T is the temperature, u^* the friction velocity, g is gravity, k is the Von Karman constant, and Q is the heat gained by the atmosphere from the ocean). Large negative values of L mean that the atmospheric boundary layer is convectively unstable, so that the shear of the velocity is reduced from a logarithmic profile.

Figure 3.1.22 shows the rotary spectrum of the wind stress (solid represents clockwise rotation, dashed counterclockwise rotation), and the spectrum of the sea-surface temperature, air temperature, short wave radiation, barometric pressure and relative humidity. Other than the short wave radiation, which shows a distinct set of peaks at the first, second, and third harmonics of the diurnal frequency, there are no significant peaks.

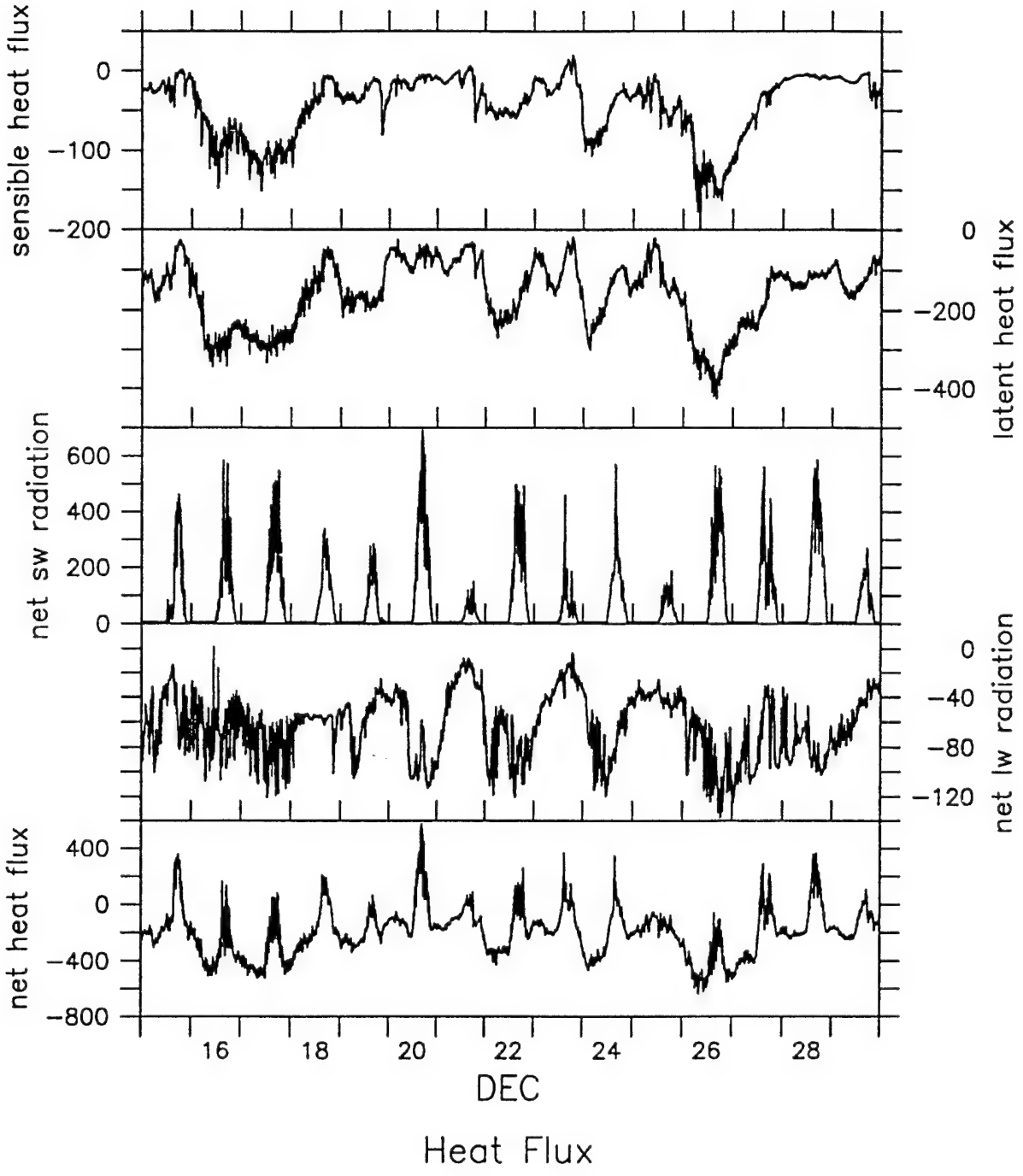

Figure 3.1.8: Heat Flux Time Series from the Composite Data Set.

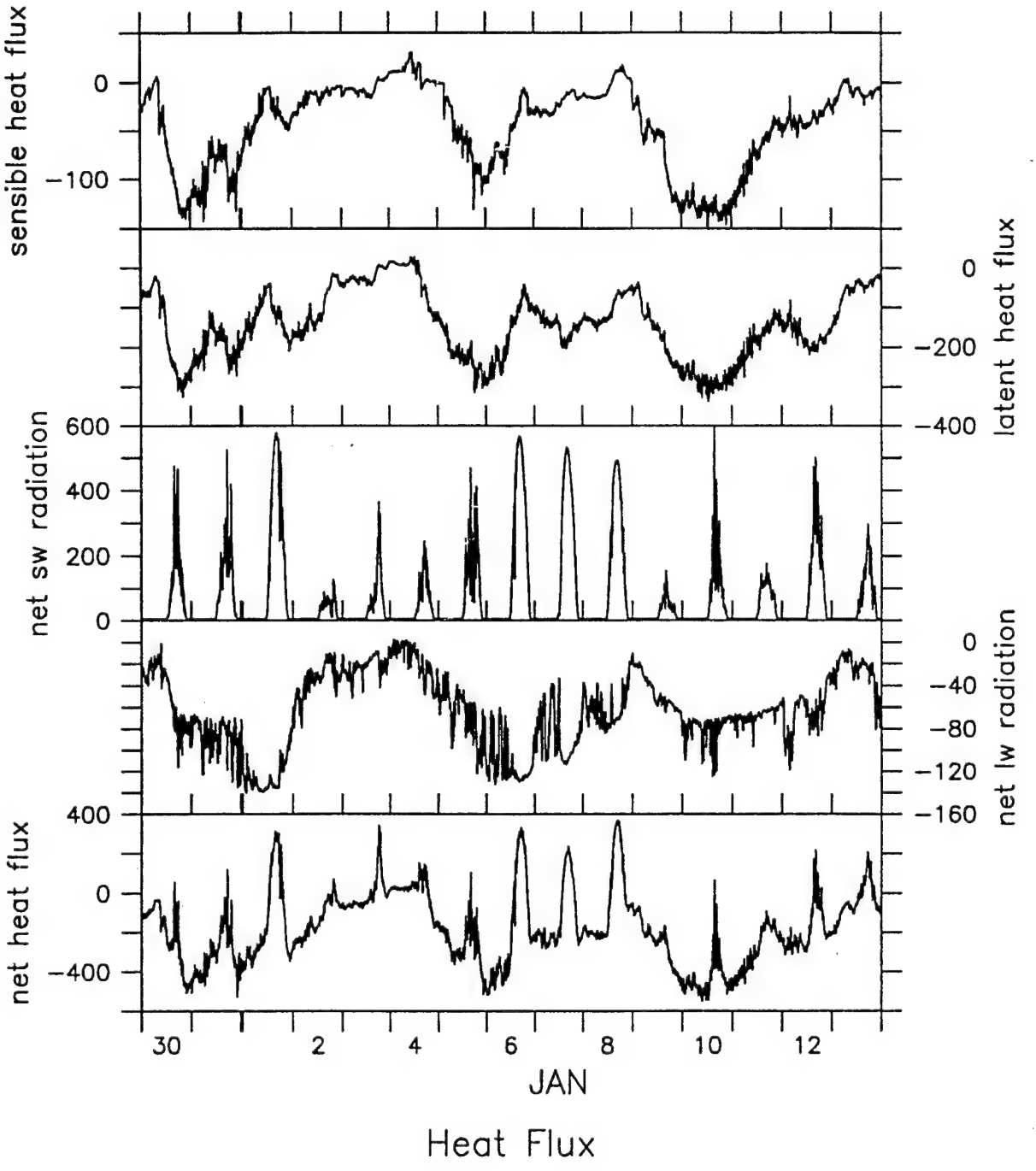

Figure 3.1.9: Heat Flux Time Series from the Composite Data Set.

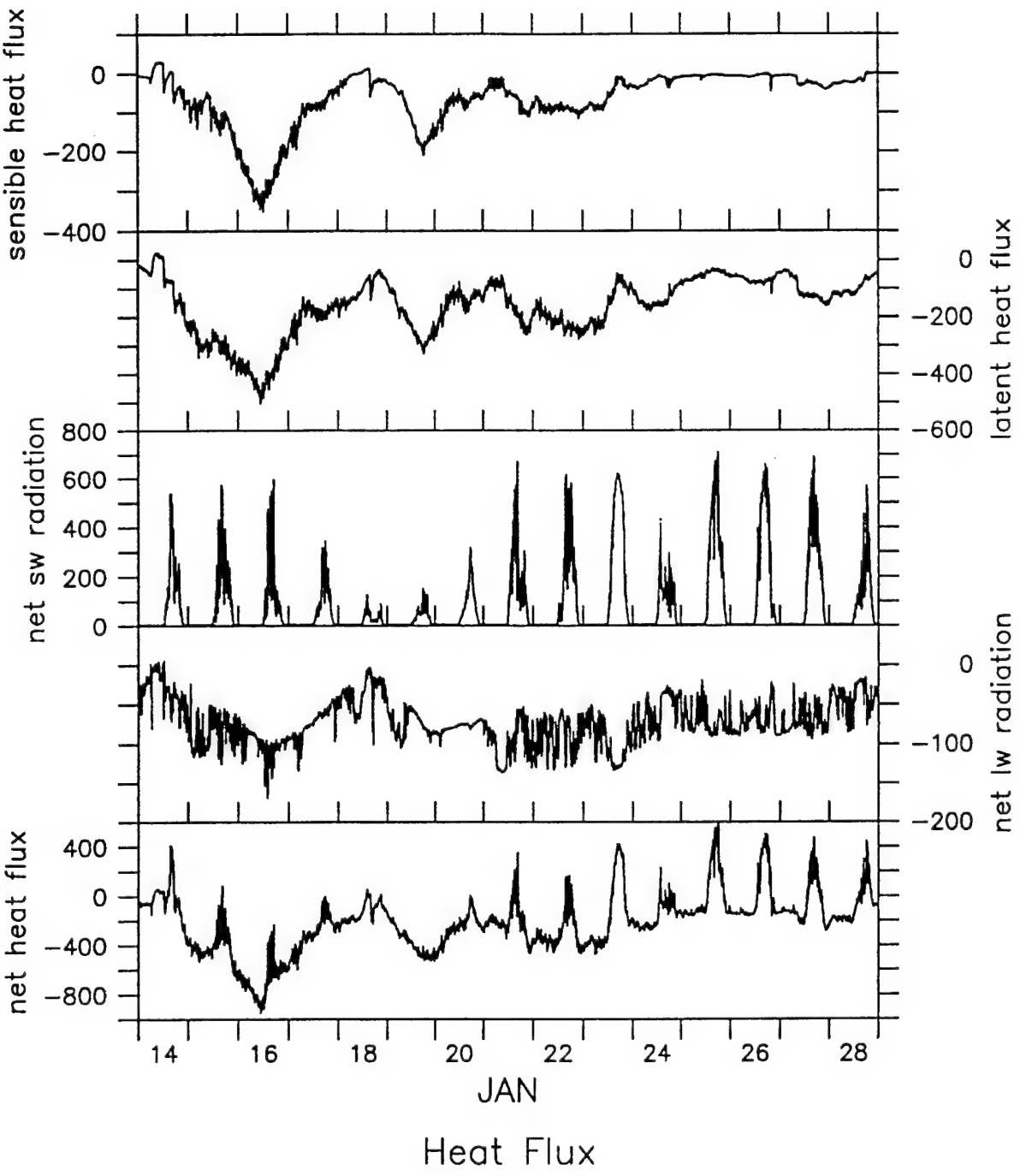

Figure 3.1.10: Heat Flux Time Series from the Composite Data Set.

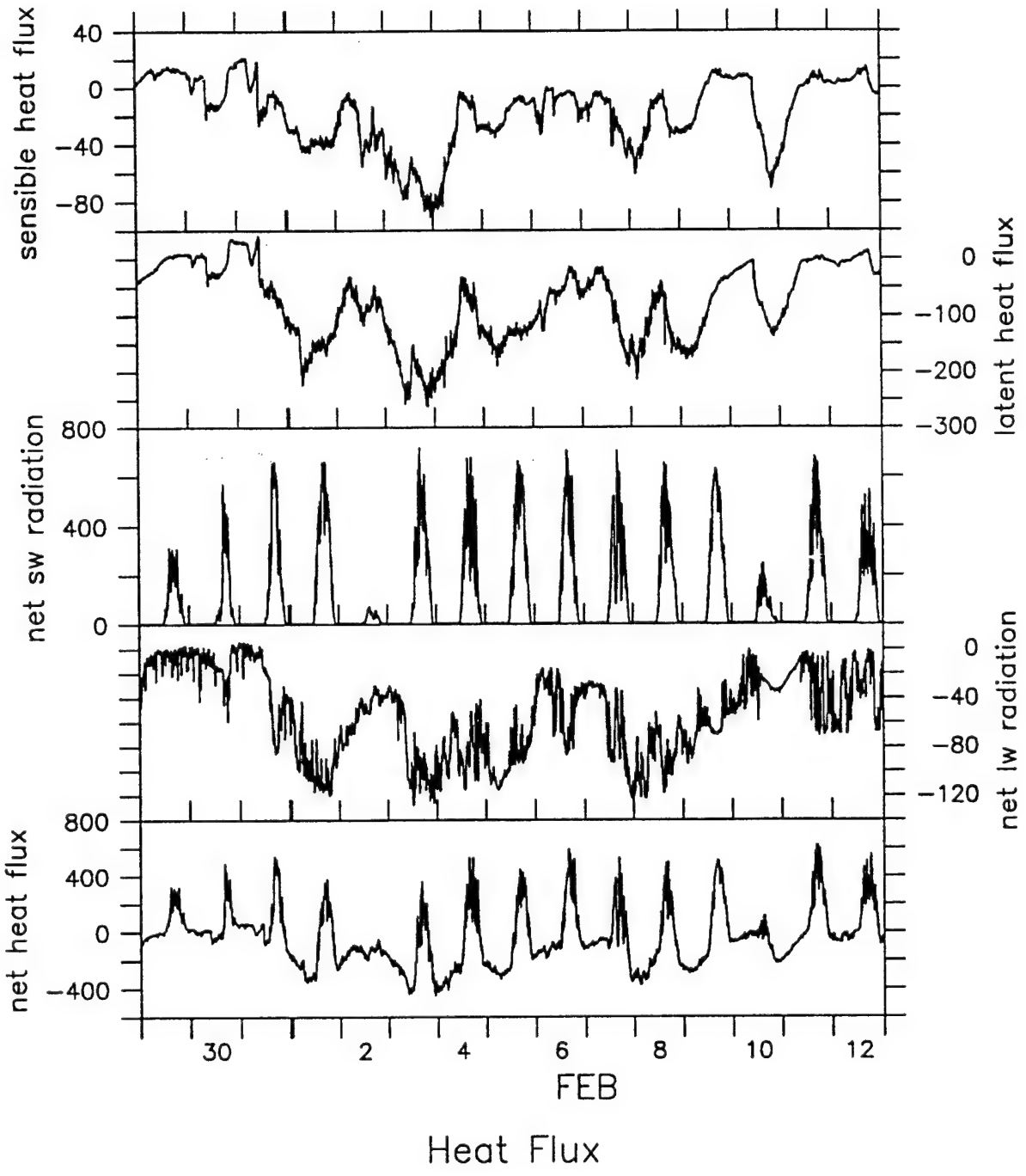

Figure 3.1.11: Heat Flux Time Series from the Composite Data Set.

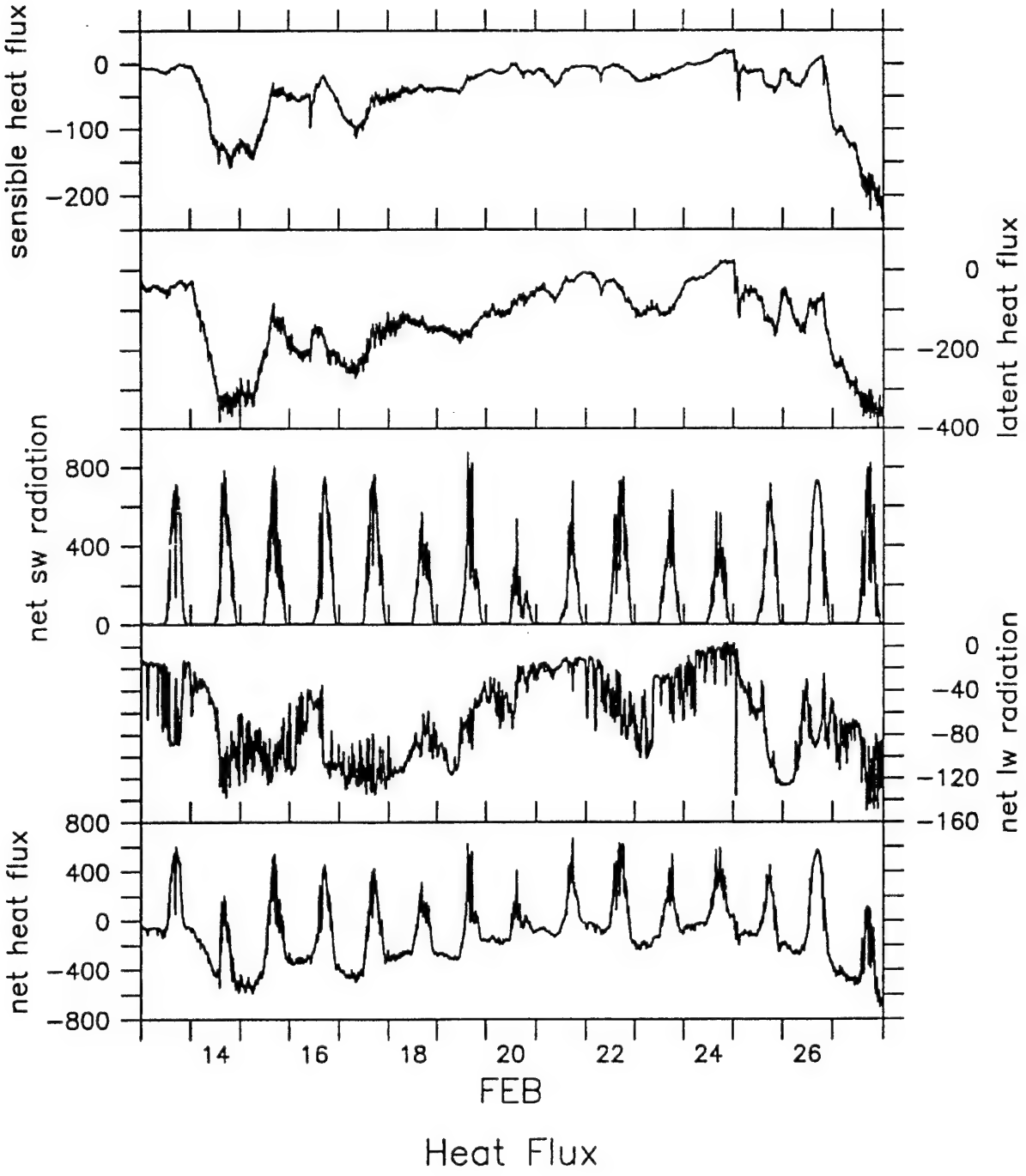

Figure 3.1.12: Heat Flux Time Series from the Composite Data Set.

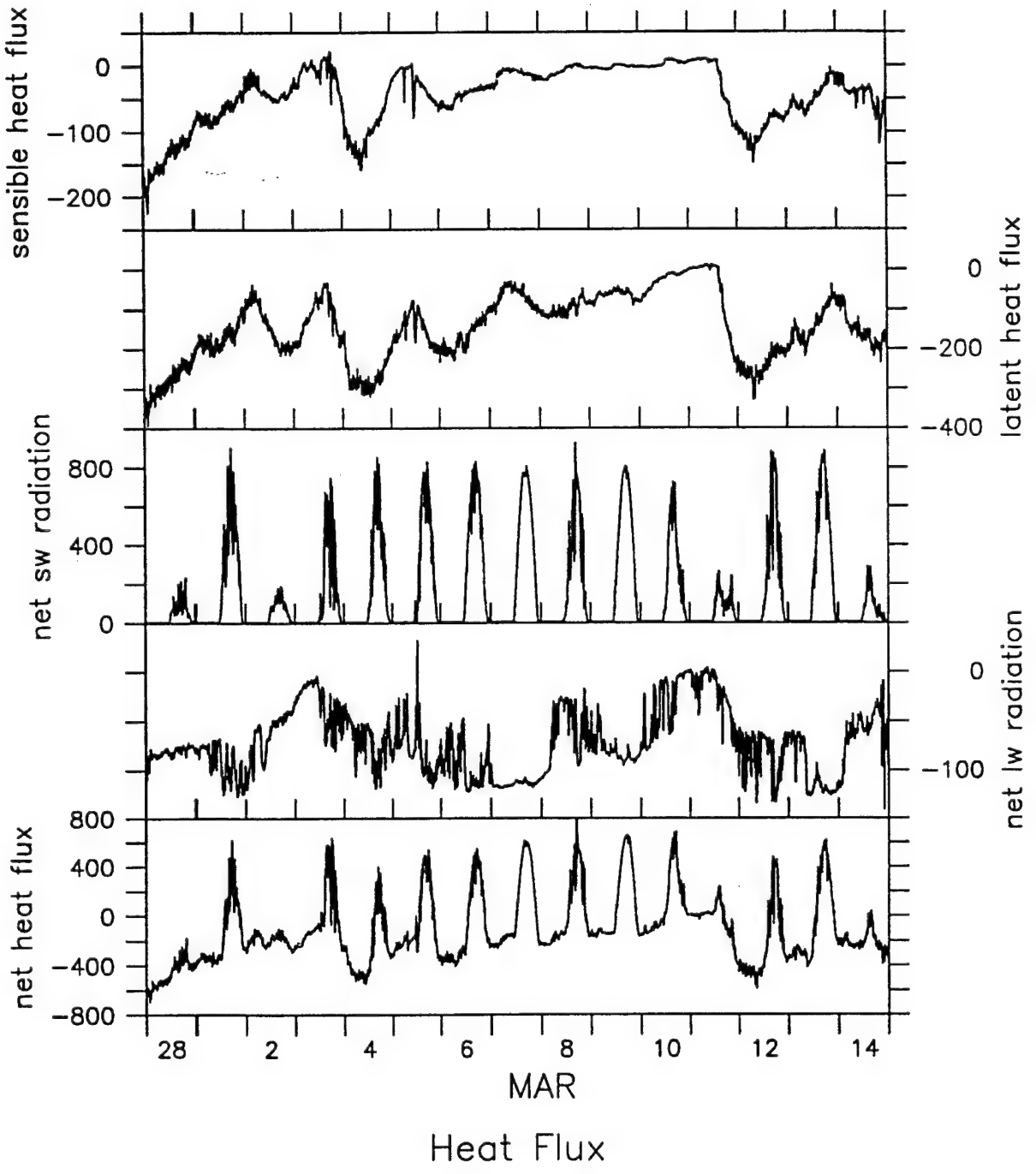

Figure 3.1.13: Heat Flux Time Series from the Composite Data Set.

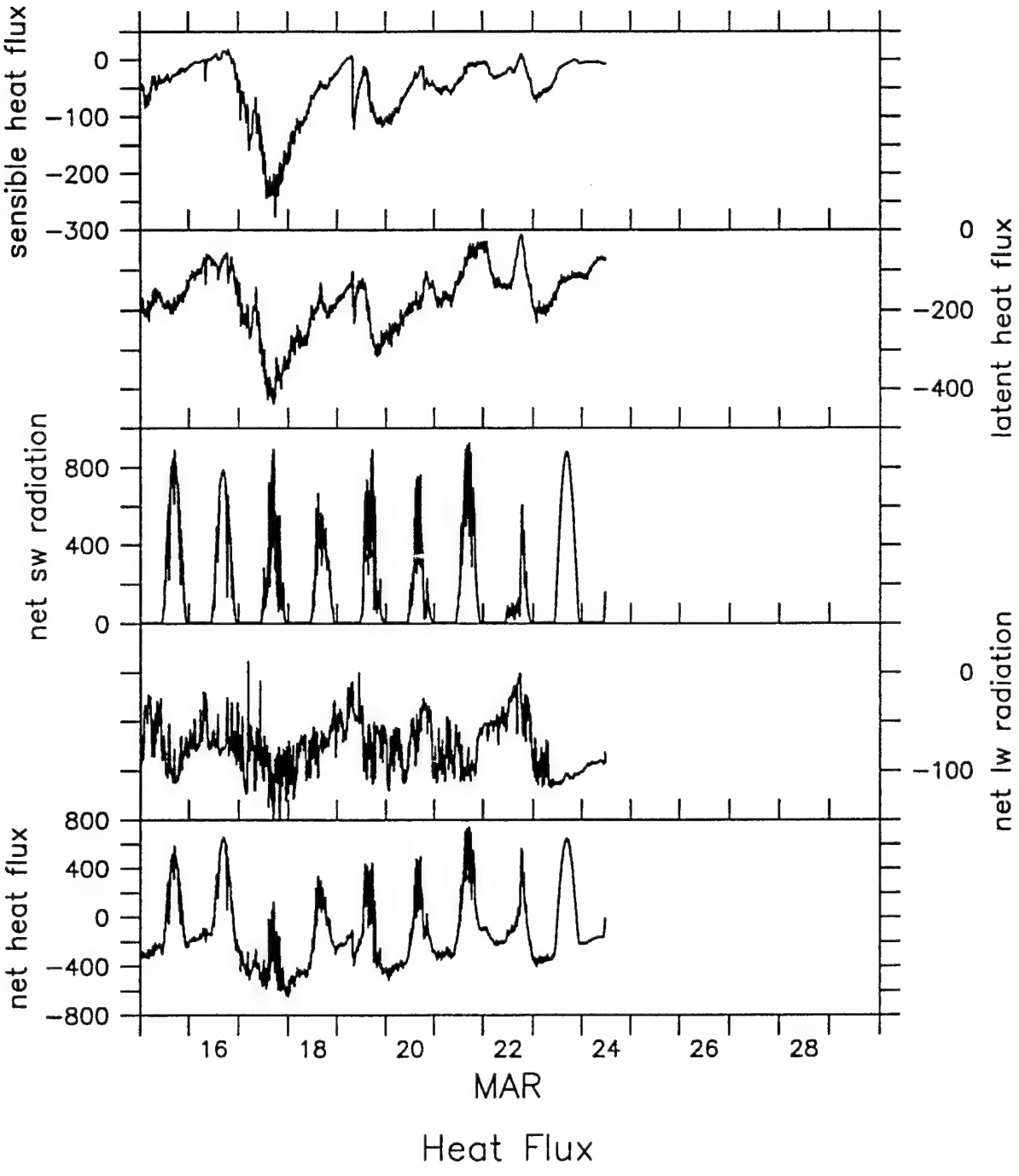

Figure 3.1.14: Heat Flux Time Series from the Composite Data Set.

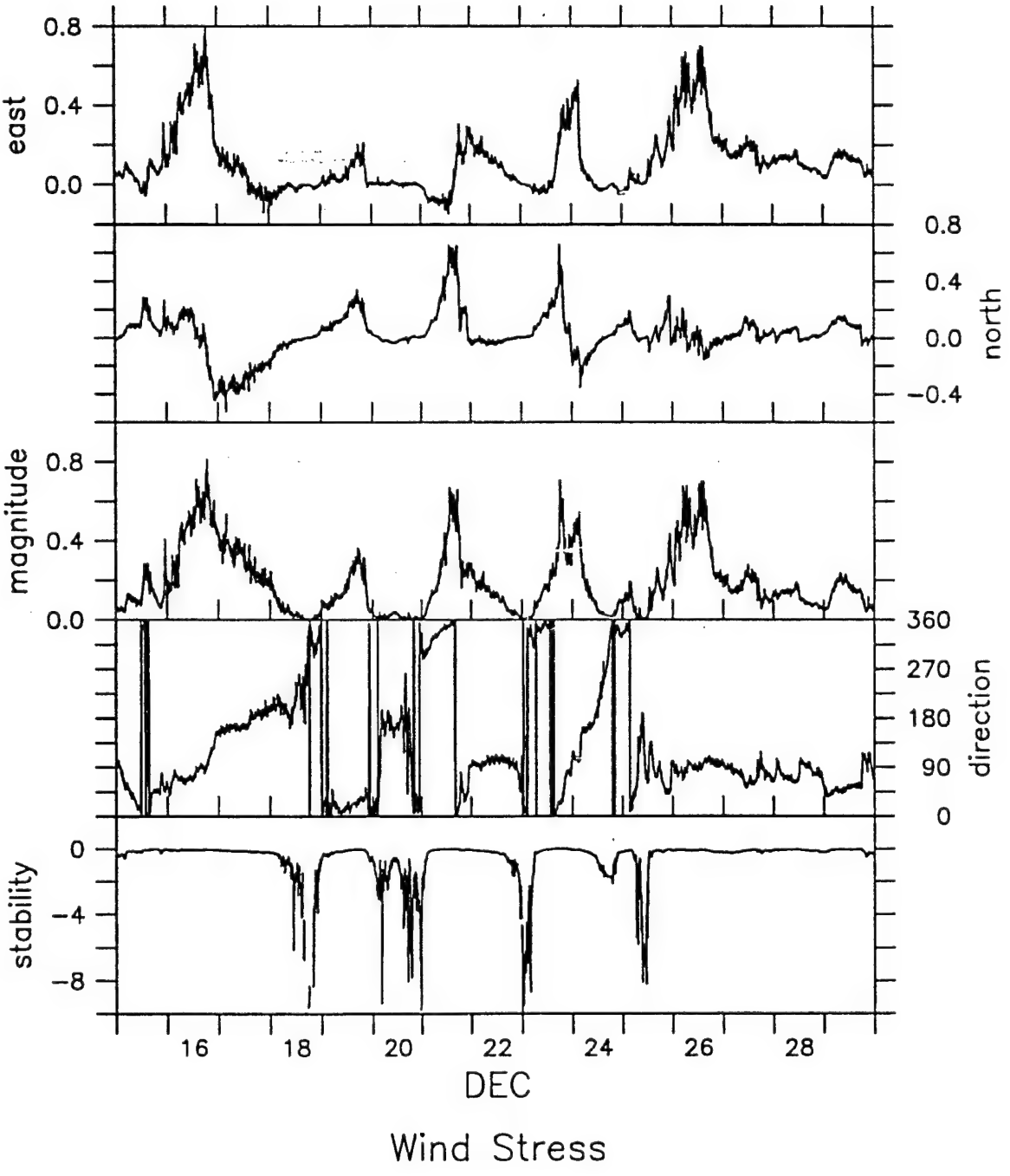

Figure 3.1.15: Wind Stress Time Series from the Composite Data Set.

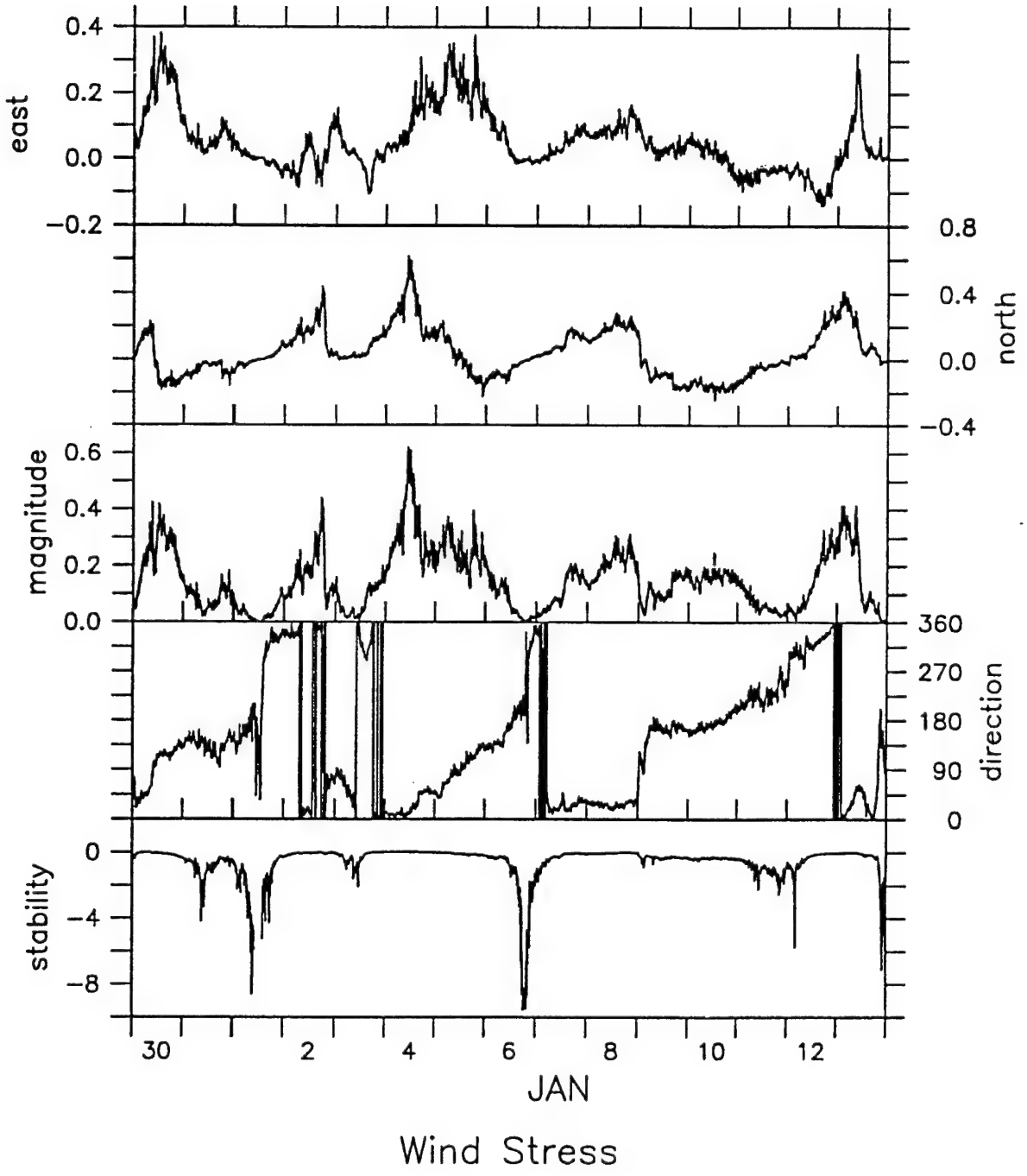

Figure 3.1.16: Wind Stress Time Series from the Composite Data Set.

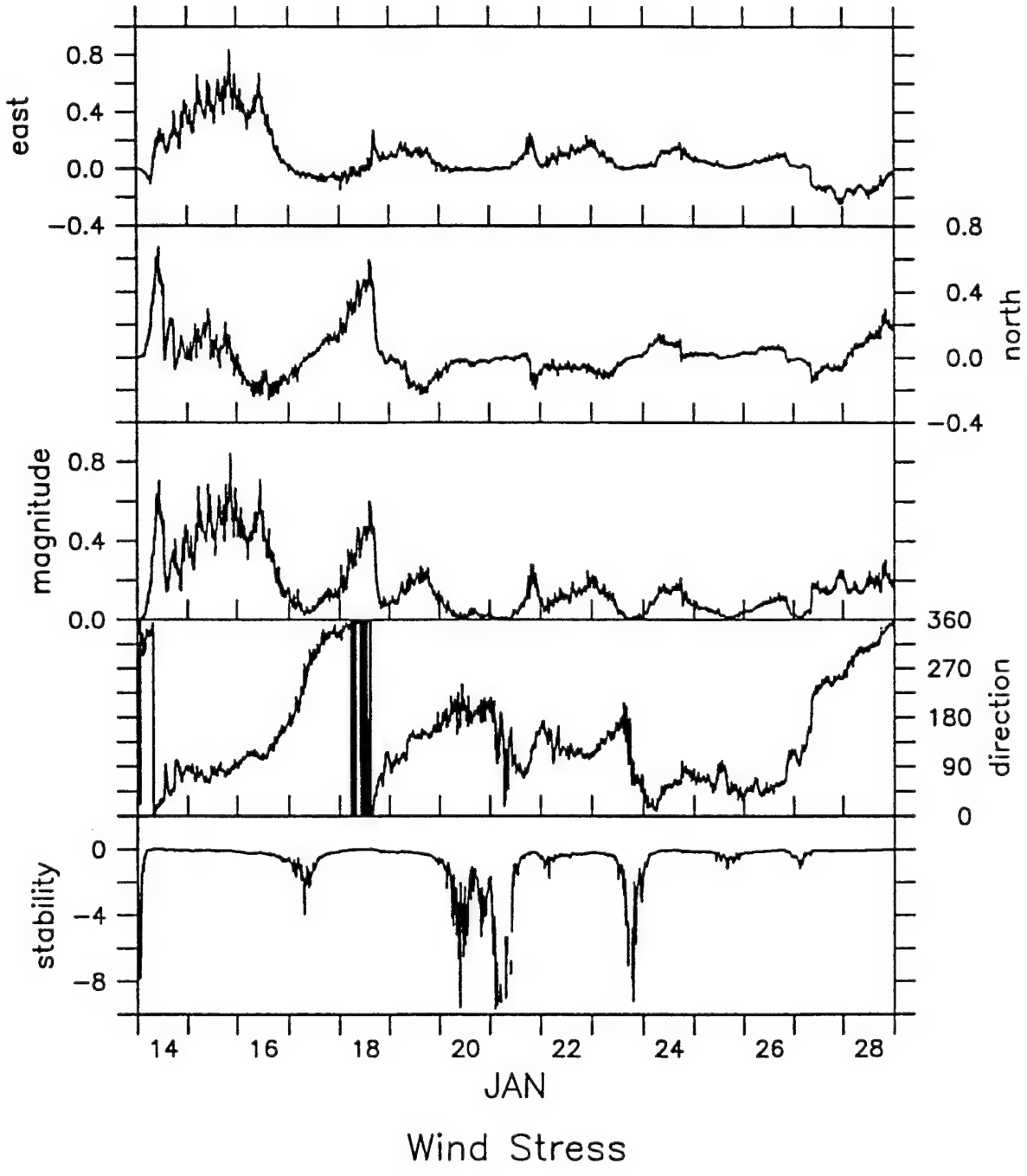

Figure 3.1.17 Wind Stress Time Series from the Composite Data Set.

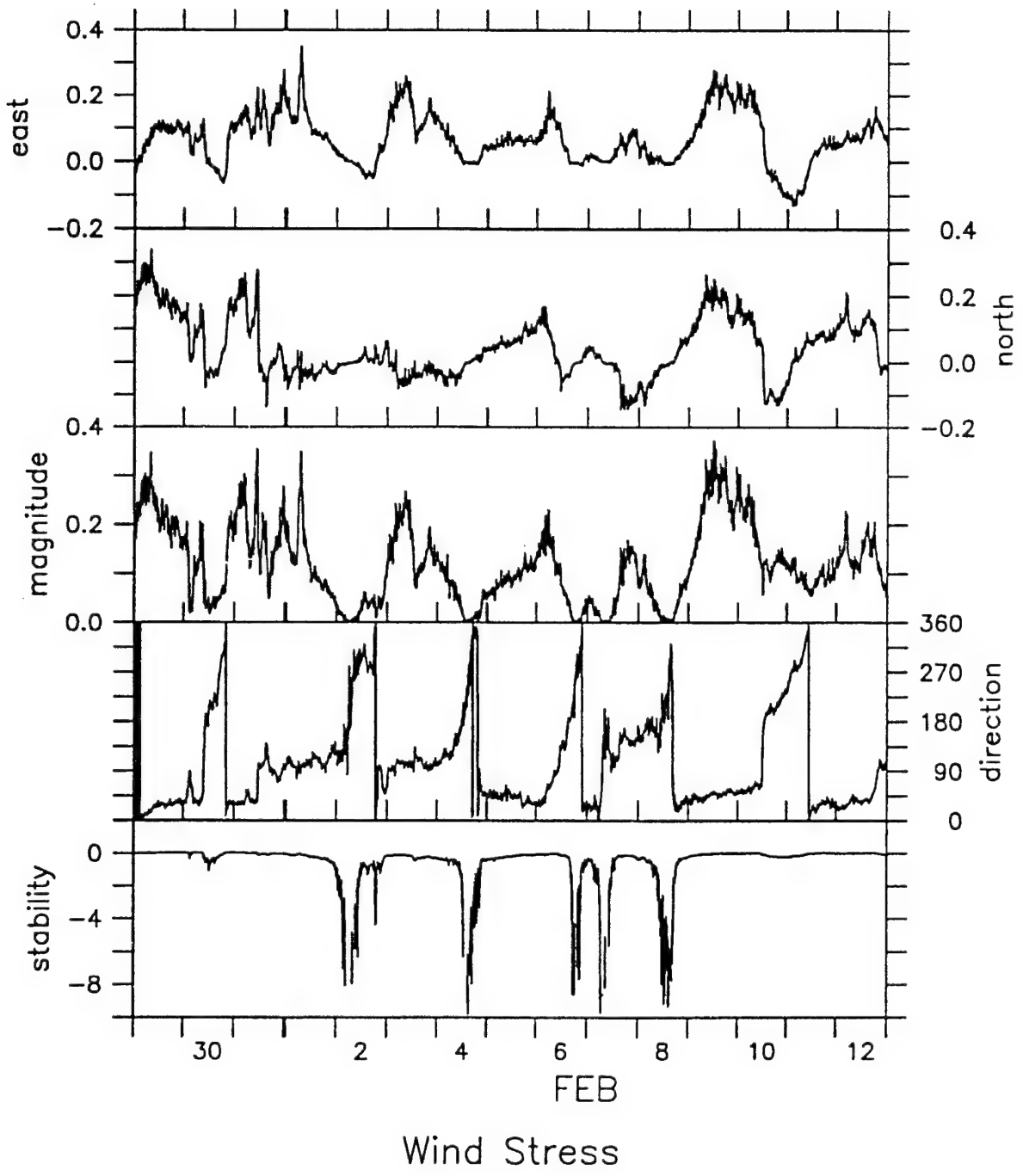

Figure 3.1.18 Wind Stress Time Series from the Composite Data Set.

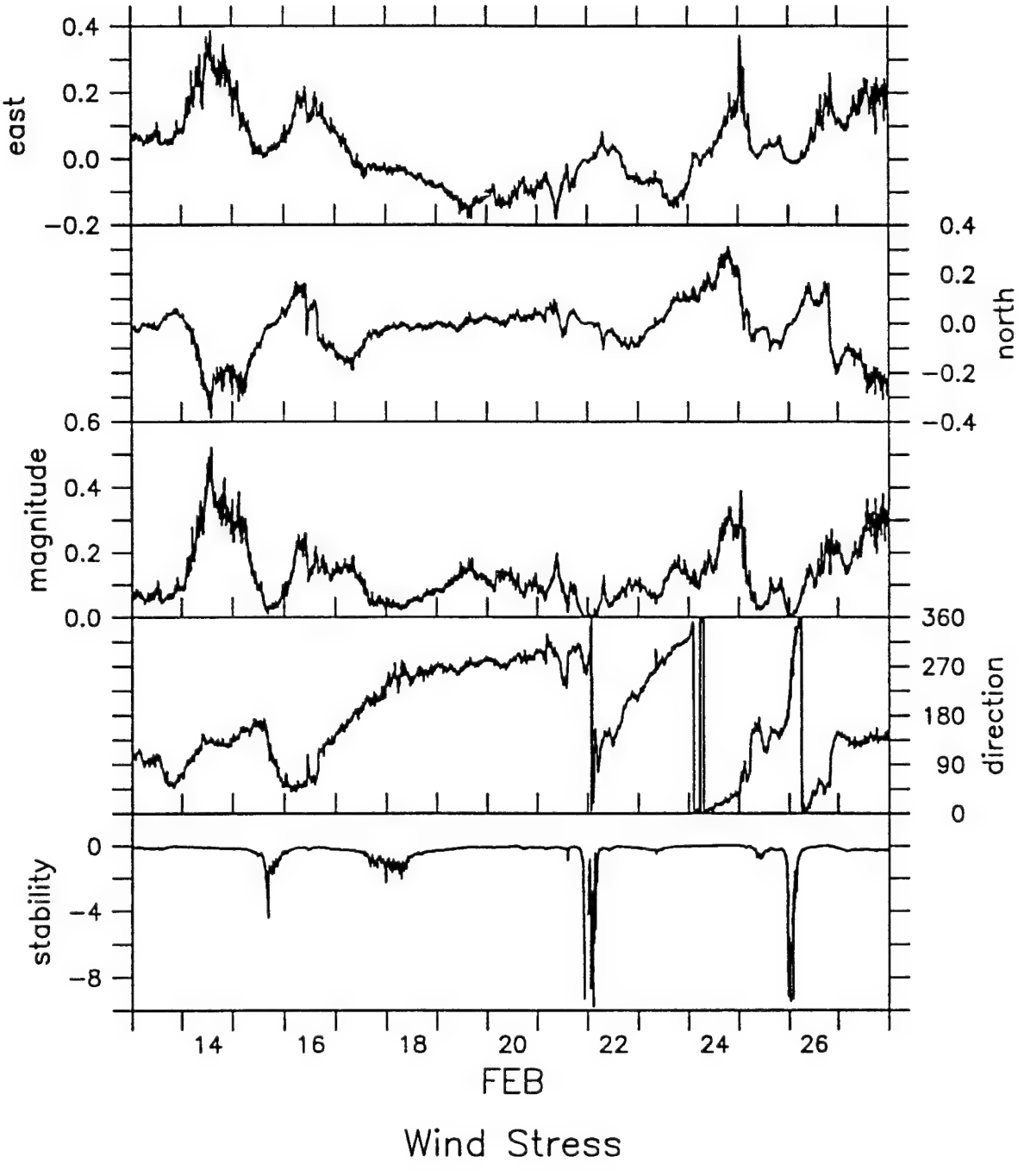

Figure 3.1.19 Wind Stress Time Series from the Composite Data Set.

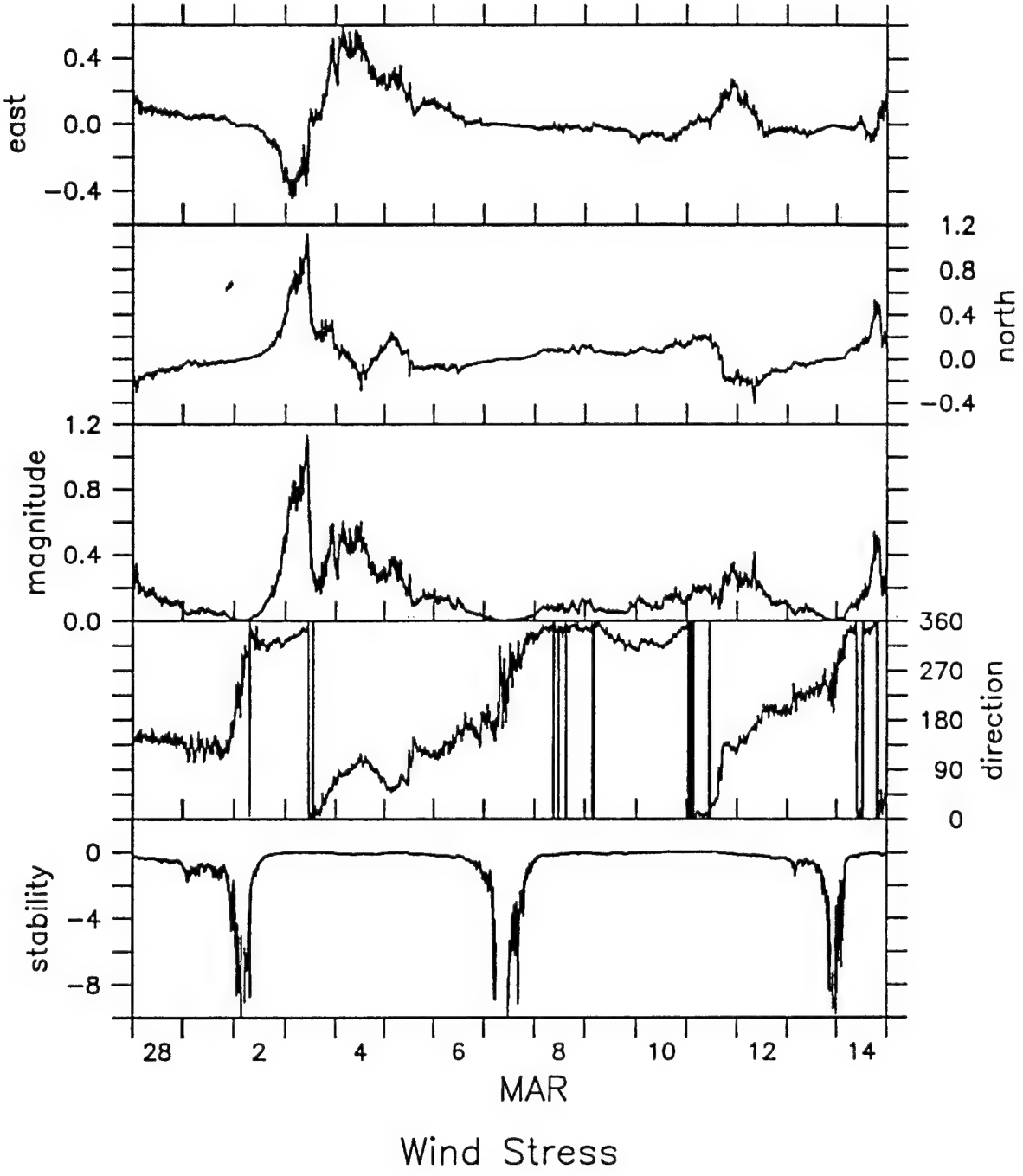

Figure 3.1.20 Wind Stress Time Series from the Composite Data Set.

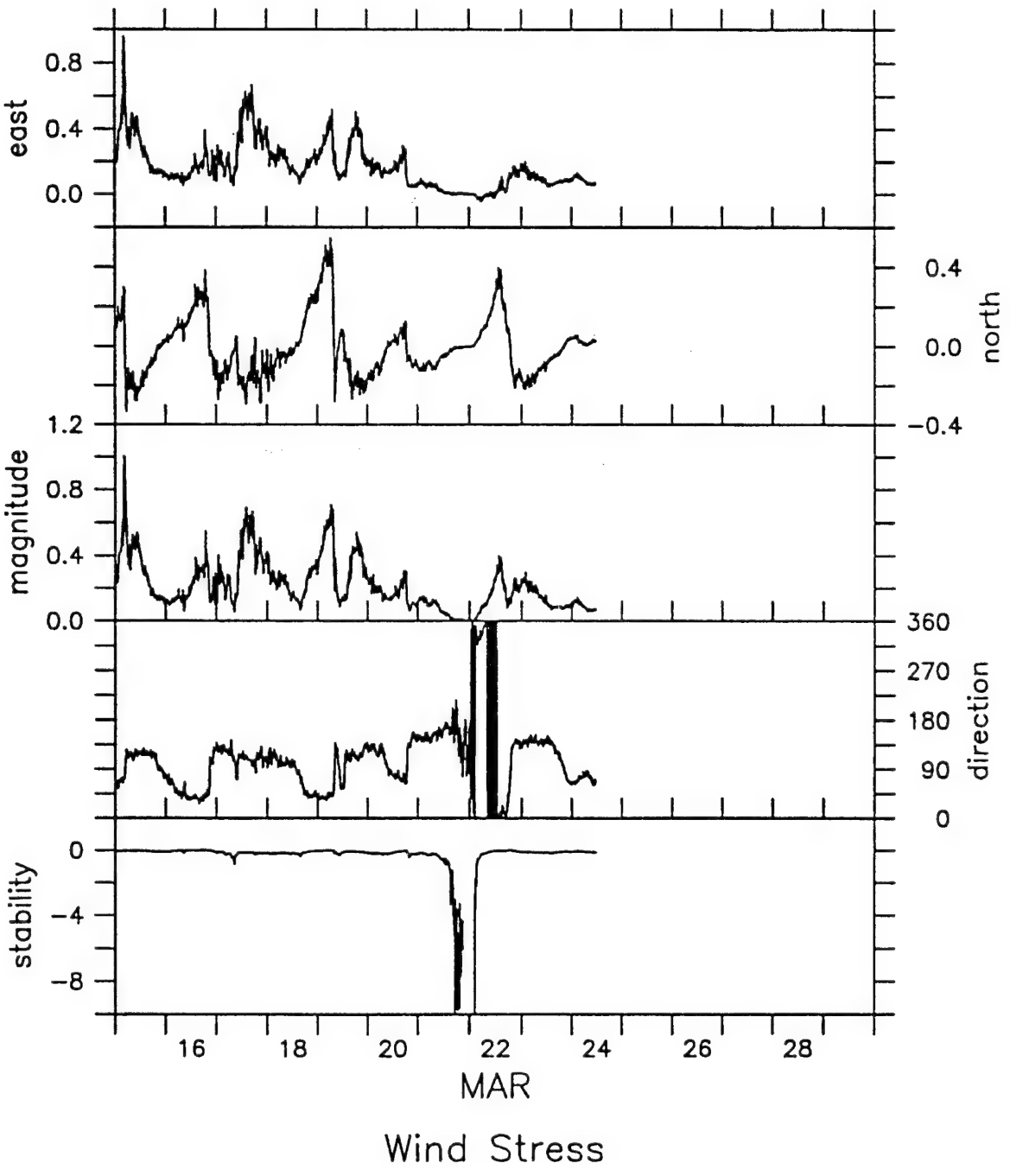

Figure 3.1.21 Wind Stress Time Series from the Composite Data Set.

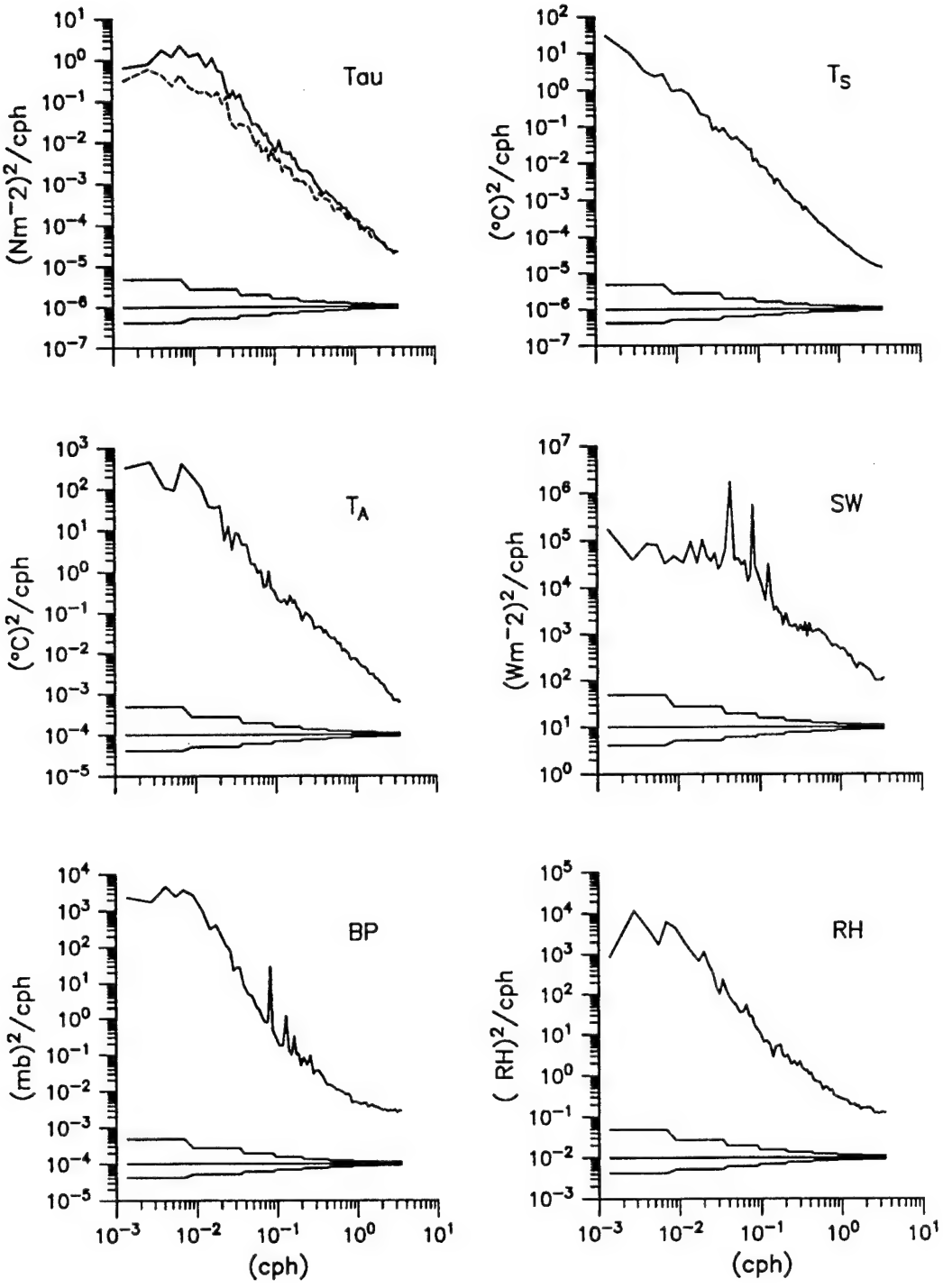

Figure 3.1.22: Autospectra of wind stress, air temperature, barometric pressure, sea surface temperature, insolation, and relative humidity from the composite data set. Rotary autospectra are shown for wind stress; solid curves show the clockwise component, and dashed curves show the counter-clockwise

3.2 Temperature and Density Structure during ASREX III

Sea temperatures were measured by the VAWR, by twelve Brancker temperature recorders (TPODs) two of which were on the bridle at a depth of 1m, the remainder on the mooring line at depths of 37, 75, 125, 175, 200, 230, 260, 300, 350, and 400 m, by two Seabird Seacats at depths of 1 and 450m, and by eight Vector Measuring Current Meters (VMCMs) at 5, 10, 15, 20, 50, 150, 300 and 500 m. VMCMs recorded data every 120 seconds, Seacats every 225 seconds, and TPODs recorded every 7.5 minutes.

Each temperature was calibrated in the lab before and after the experiment. There was an improvement made to the calibration procedure for the TPODs during this experiment, and therefore the post-cruise calibrations for those instruments was used in the final processing. Both VMCM and Seacat temperatures calculated with pre-deployment calibrations matched surrounding instrument data, so pre-deployment calibrations were used for those instruments.

Figure 3.2.1 is a contour plot of all the temperature data from the moored array instruments. Data was filtered using a 24-hour running mean to remove the semidiurnal tide signal, and subsampled at 2-hour intervals to produce a uniform time-series for the contour plot.

Time-series and spectra of temperature at each depth are presented in Figures 3.2.2 through 3.2.23. In the upper frame of each of these plots, temperature is represented along the y axis and time (UTC) along the x axis. The lower frame contains the spectra. The long arrows on the lower frames indicate the frequency of the semidiurnal tidal peak and the short arrows show the frequency of the Coriolis peak. Confidence limits are displayed at the bottom of the frame. Captions indicate instrument type and depth. Unlike the previous plot, the data here is not smoothed, so that the strong signals associated with the semidiurnal tides are readily visible.

A Seacat with a pressure sensor was used to collect profile data shortly before deployment and shortly after recovery of the moored array. There were 4 pre-deployment casts, one to 400 m and 3 to about 150 m. The post-recovery cast was to a depth of 475 m. Although the Seacat recorded temperature, salinity, and density, the salinity and density records were too noisy to be of use. Temperature profiles from these casts are shown in Figure 3.2.24. Salinity and density values recorded by the instrument are not included because the data quality was poor due to different sensors' time-constants.

The moored instrument temperature records in the upper 75 meters of the water column show relatively little short-time variability. The temperature records between depths of 100 and 260 meters exhibit rapid changes as the instruments move in and out of the mixed layer as the result of tidal and inertial motions.

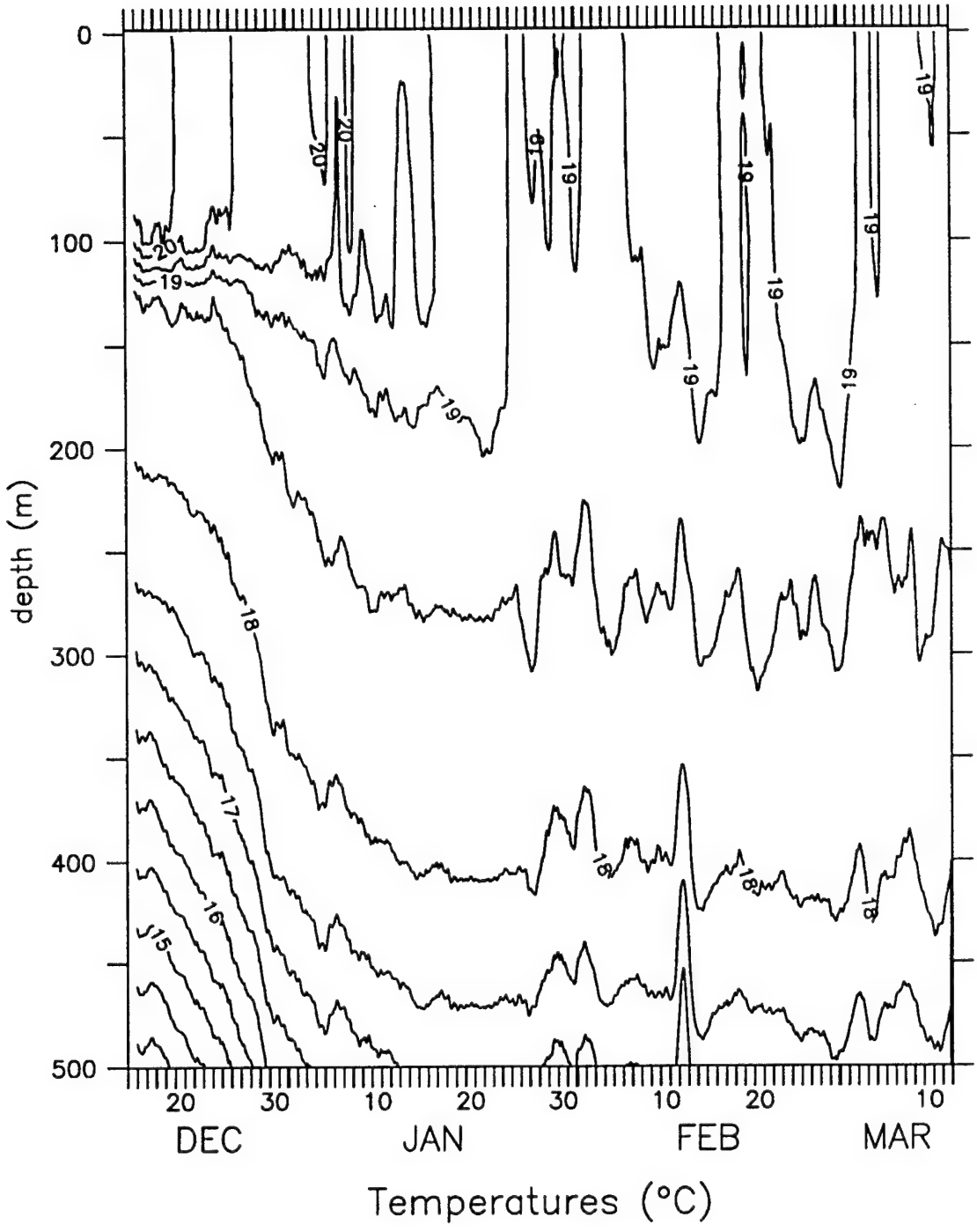

Figure 3.2.1: Temperature Contours from instruments at 1, 5, 10, 15, 20, 37, 50, 75, 100, 125, 150, 175, 200, 230, 260, 300, 350, 400, 450, and 500m.

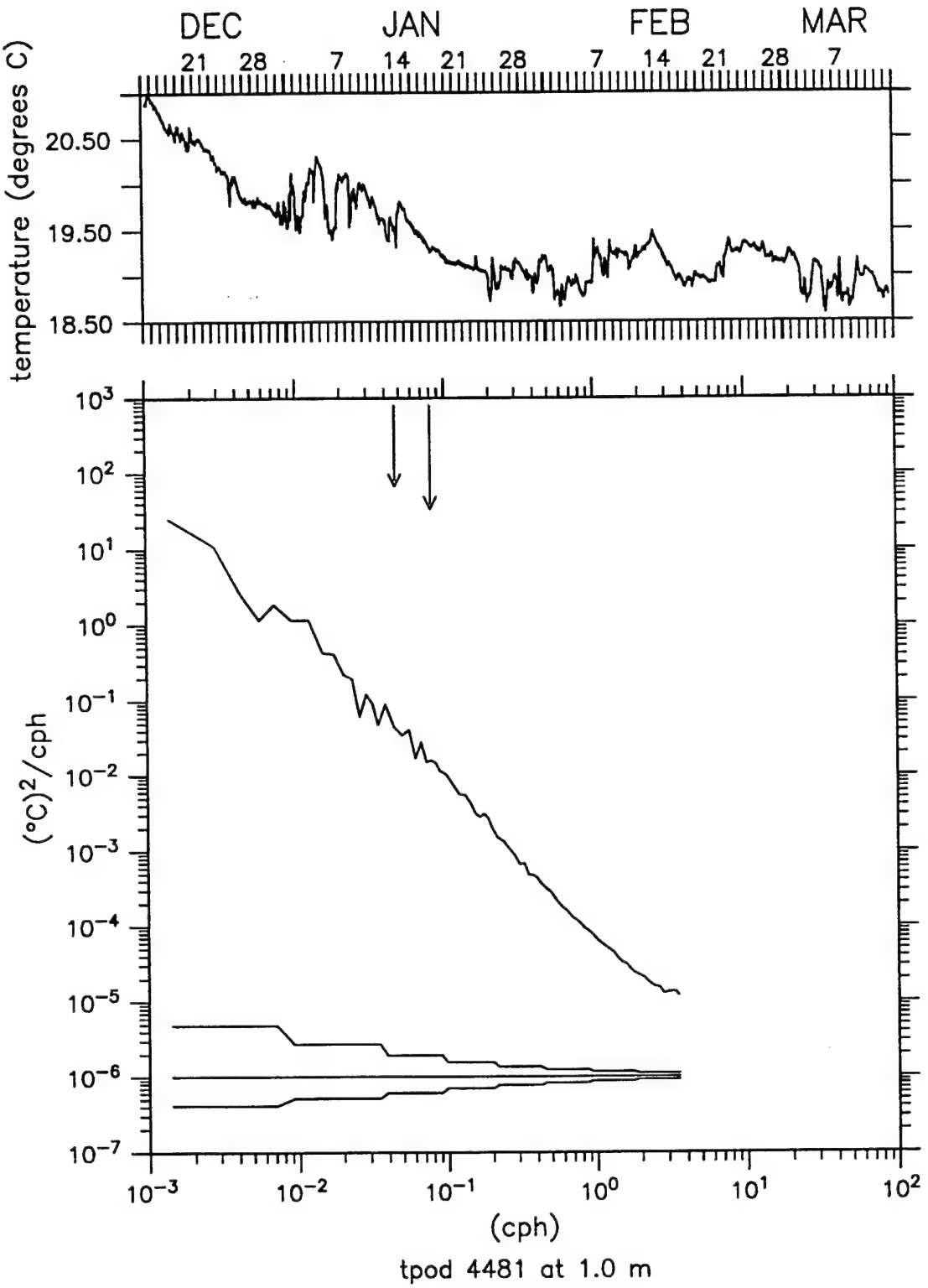

Figure 3.2.2: Temperature Time Series and Spectra at 1m. Long arrow indicates semi-diurnal tidal frequency, short arrow indicates Coriolis frequency.

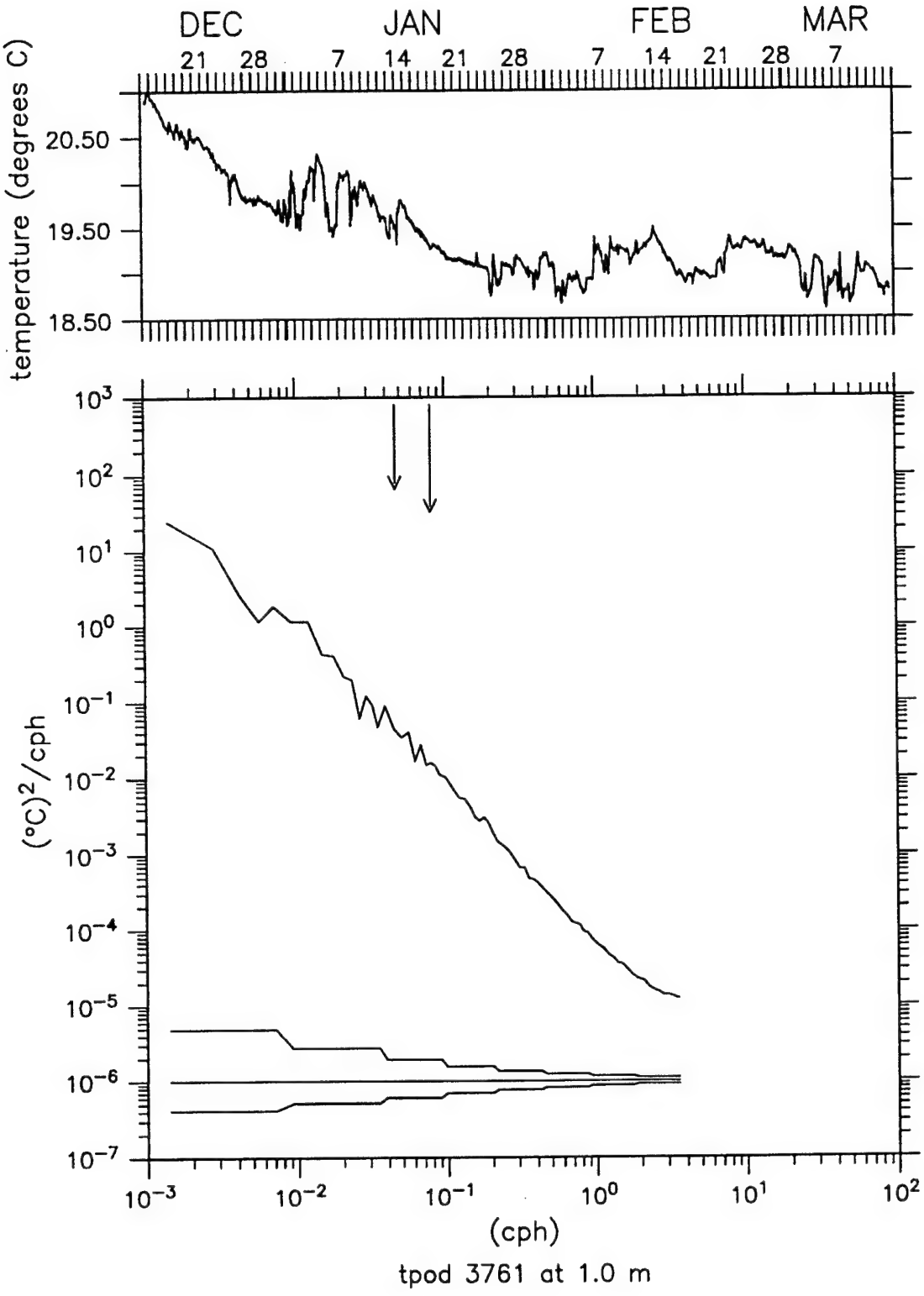

Figure 3.2.3: Temperature Time Series and Spectra at 1m. Long arrow indicates semi-diurnal tidal frequency, short arrow indicates Coriolis frequency.

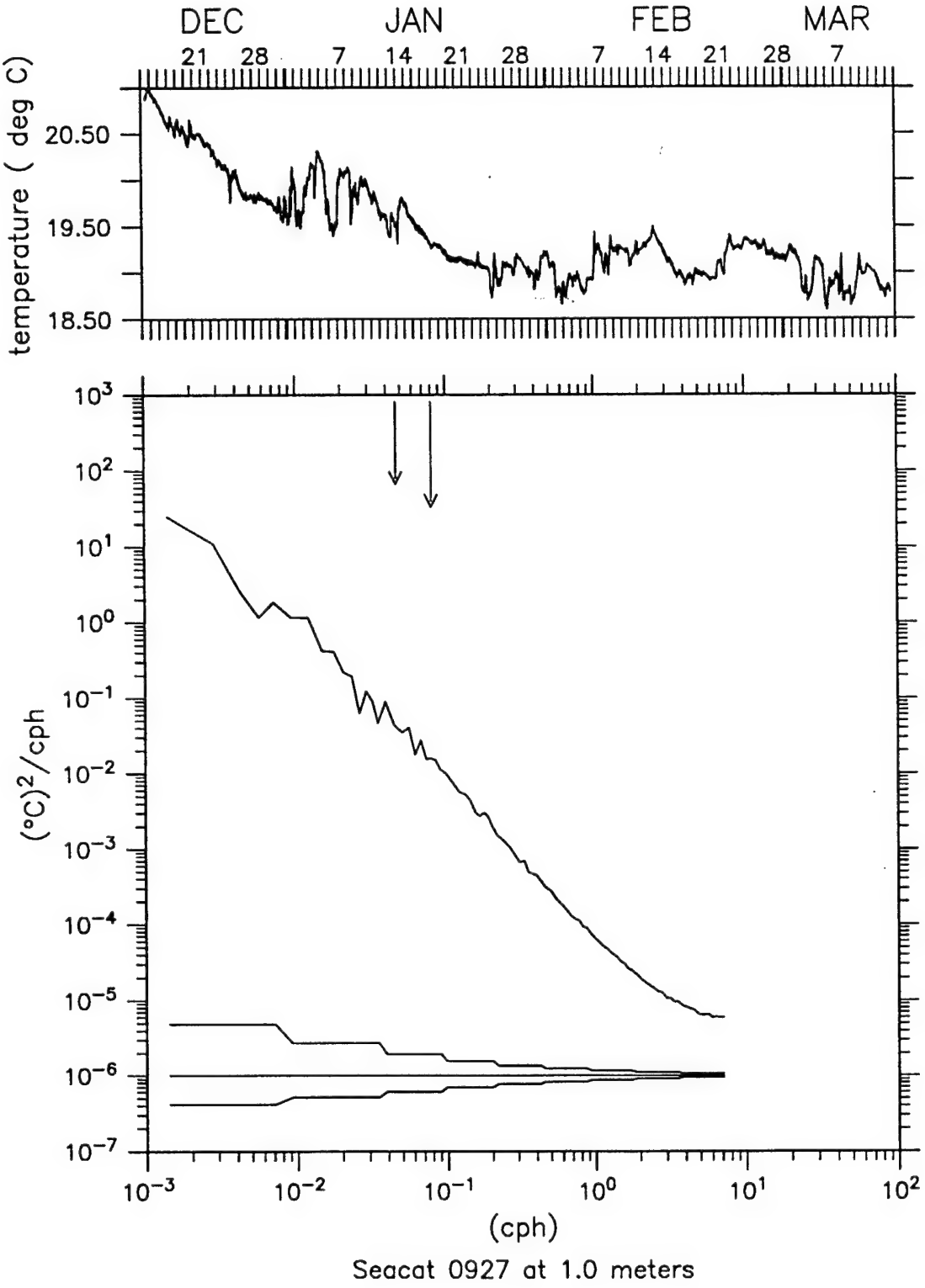

Figure 3.2.4: Temperature Time Series and Spectra at 1m. Long arrow indicates semi-diurnal tidal frequency, short arrow indicates Coriolis frequency.

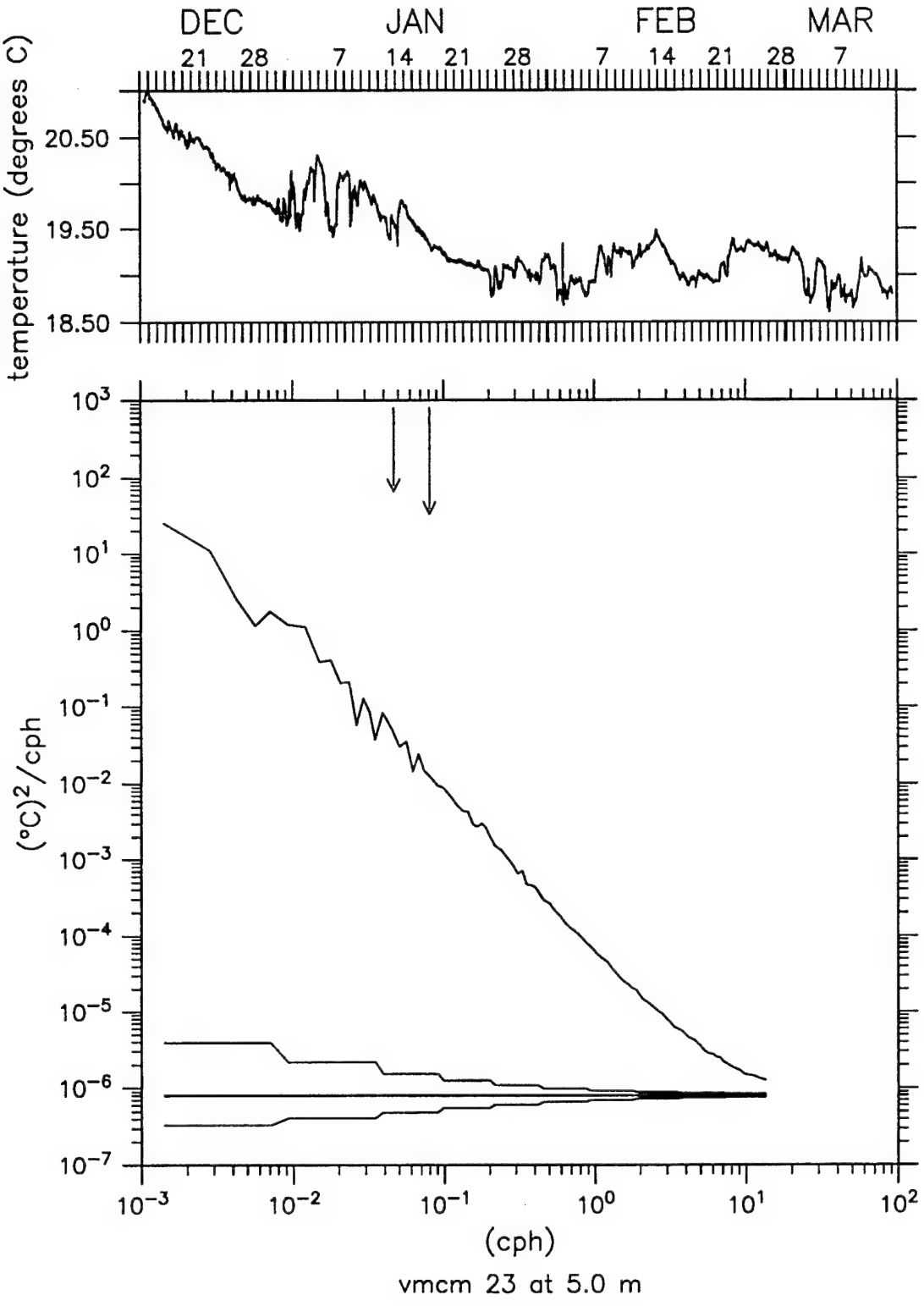

Figure 3.2.5: Temperature Time Series and Spectra at 5m. Long arrow indicates semi-diurnal tidal frequency, short arrow indicates Coriolis frequency.

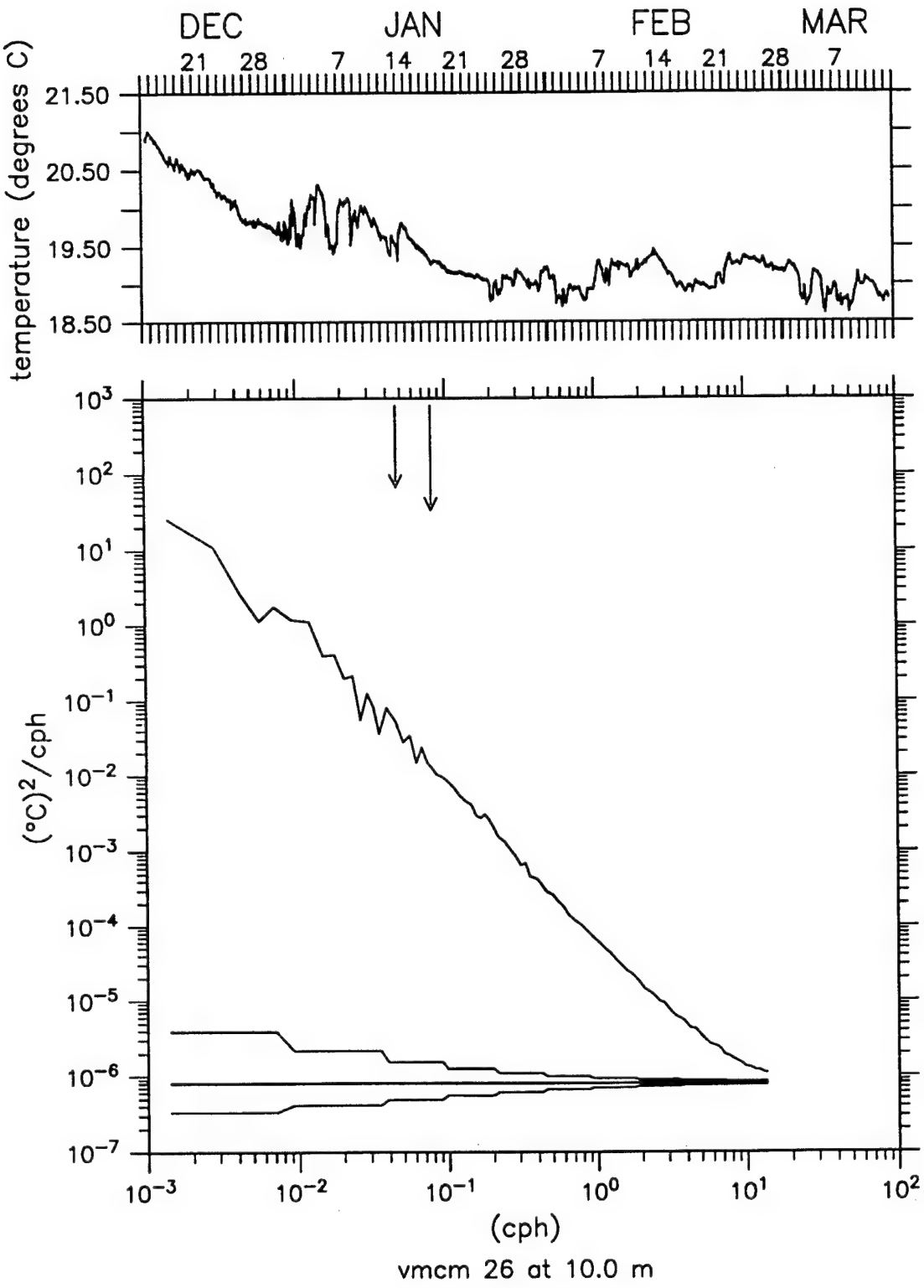

Figure 3.2.6: Temperature Time Series and Spectra at 10m. Long arrow indicates semi-diurnal tidal frequency, short arrow indicates Coriolis frequency.

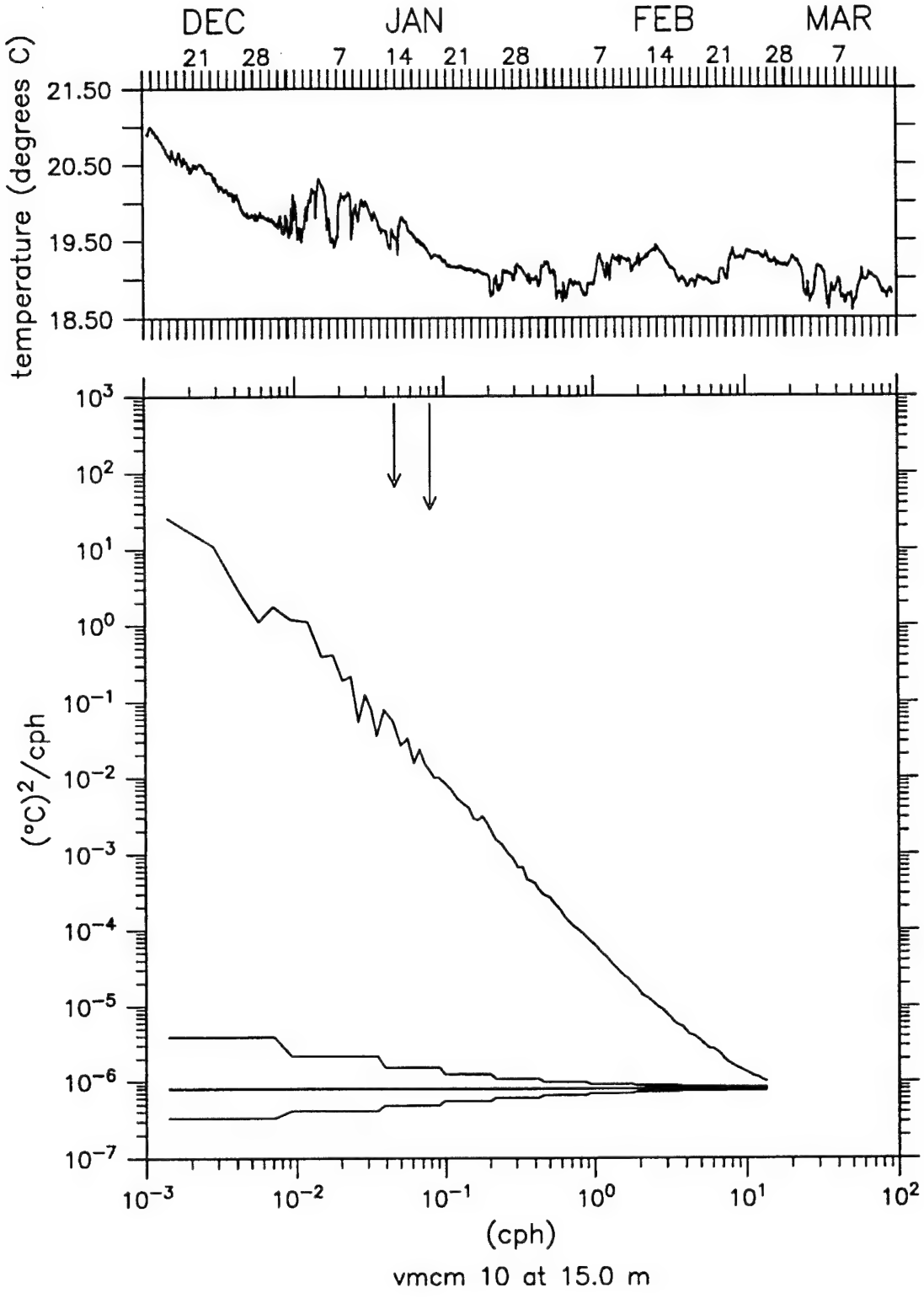

Figure 3.2.7: Temperature Time Series and Spectra at 15m. Long arrow indicates semi-diurnal tidal frequency, short arrow indicates Coriolis frequency.

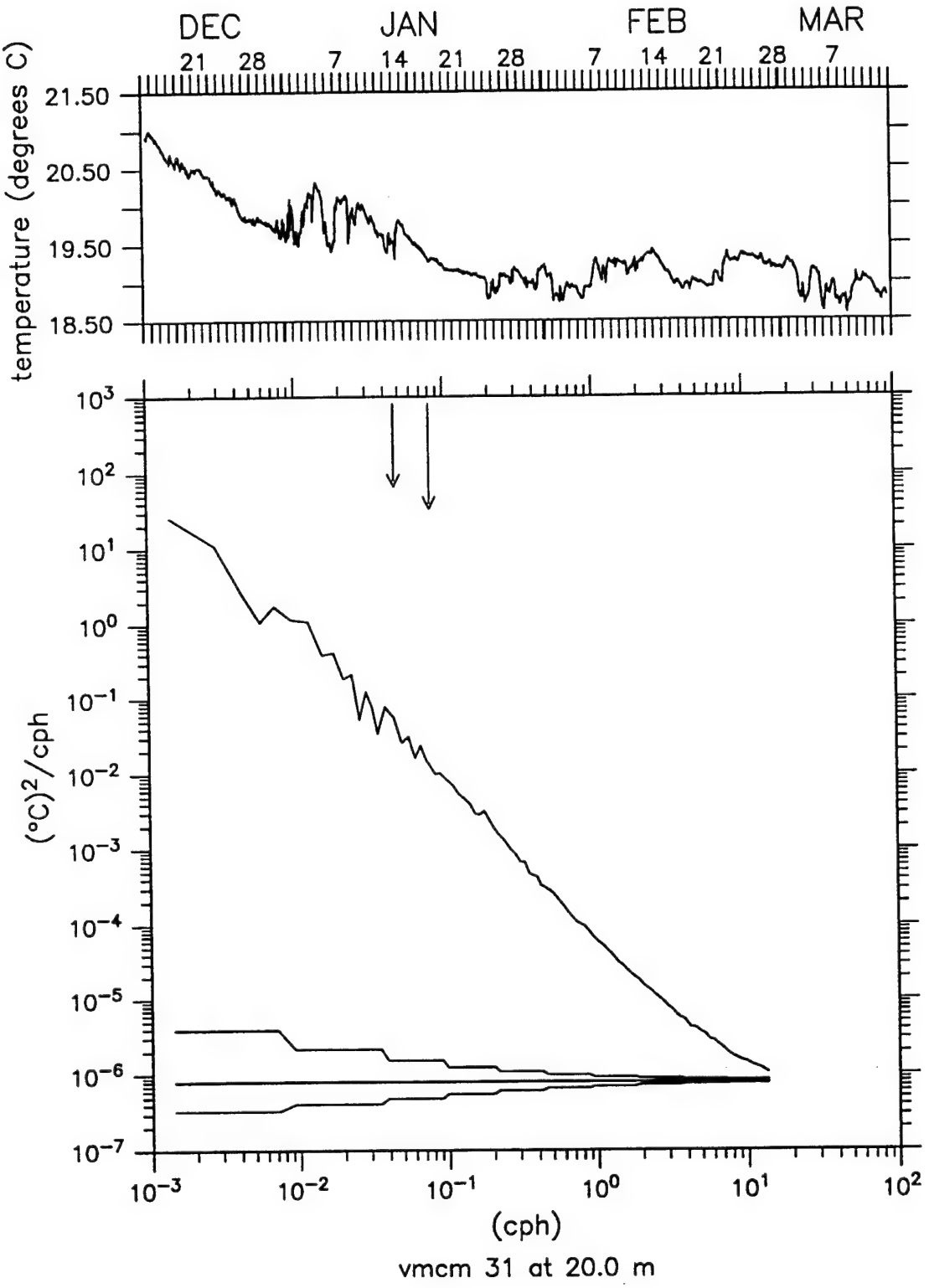

Figure 3.2.8: Temperature Time Series and Spectra at 20m. Long arrow indicates semi-diurnal tidal frequency, short arrow indicates Coriolis frequency.

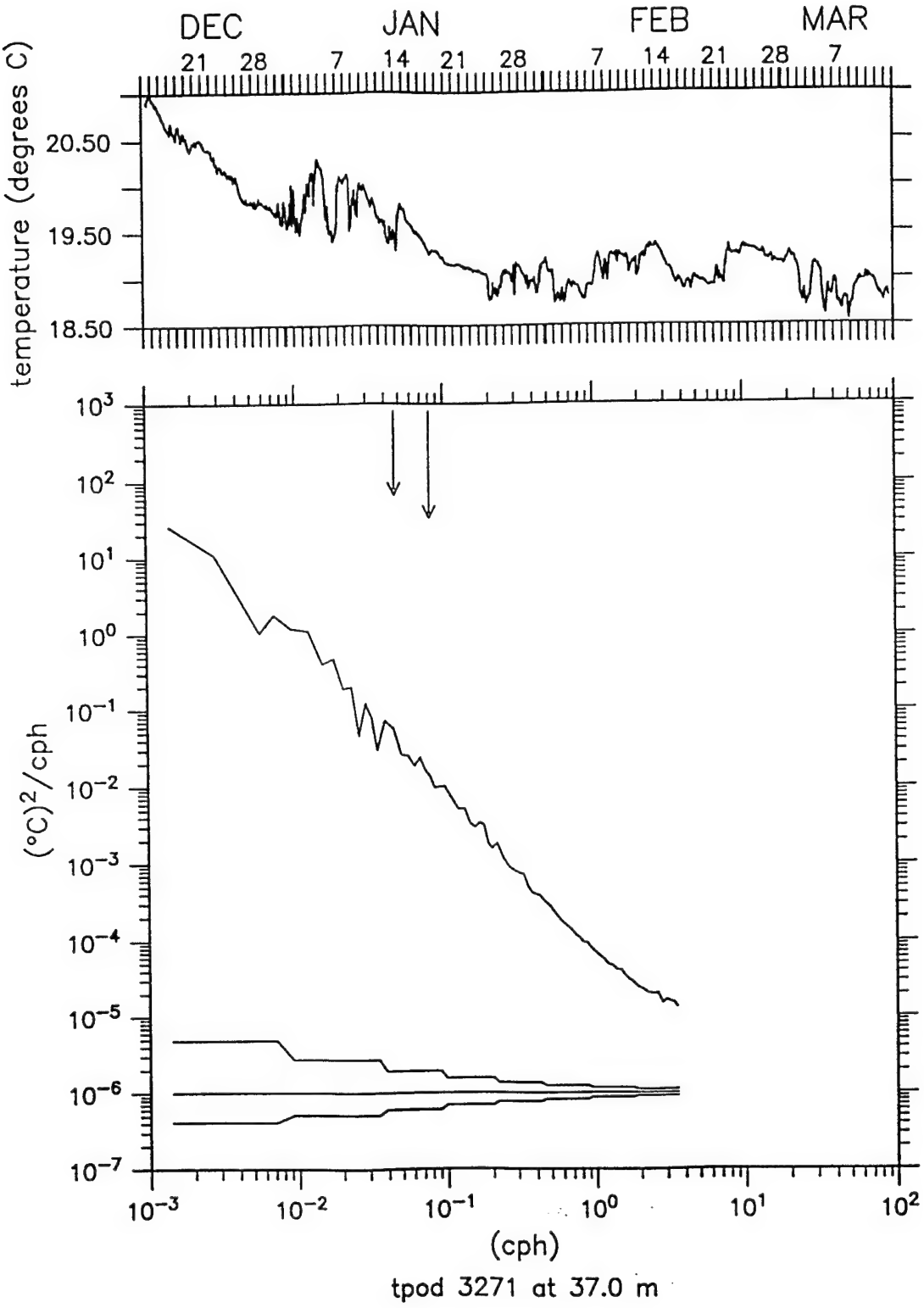

Figure 3.2.9: Temperature Time Series and Spectra at 37m. Long arrow indicates semi-diurnal tidal frequency, short arrow indicates Coriolis frequency.

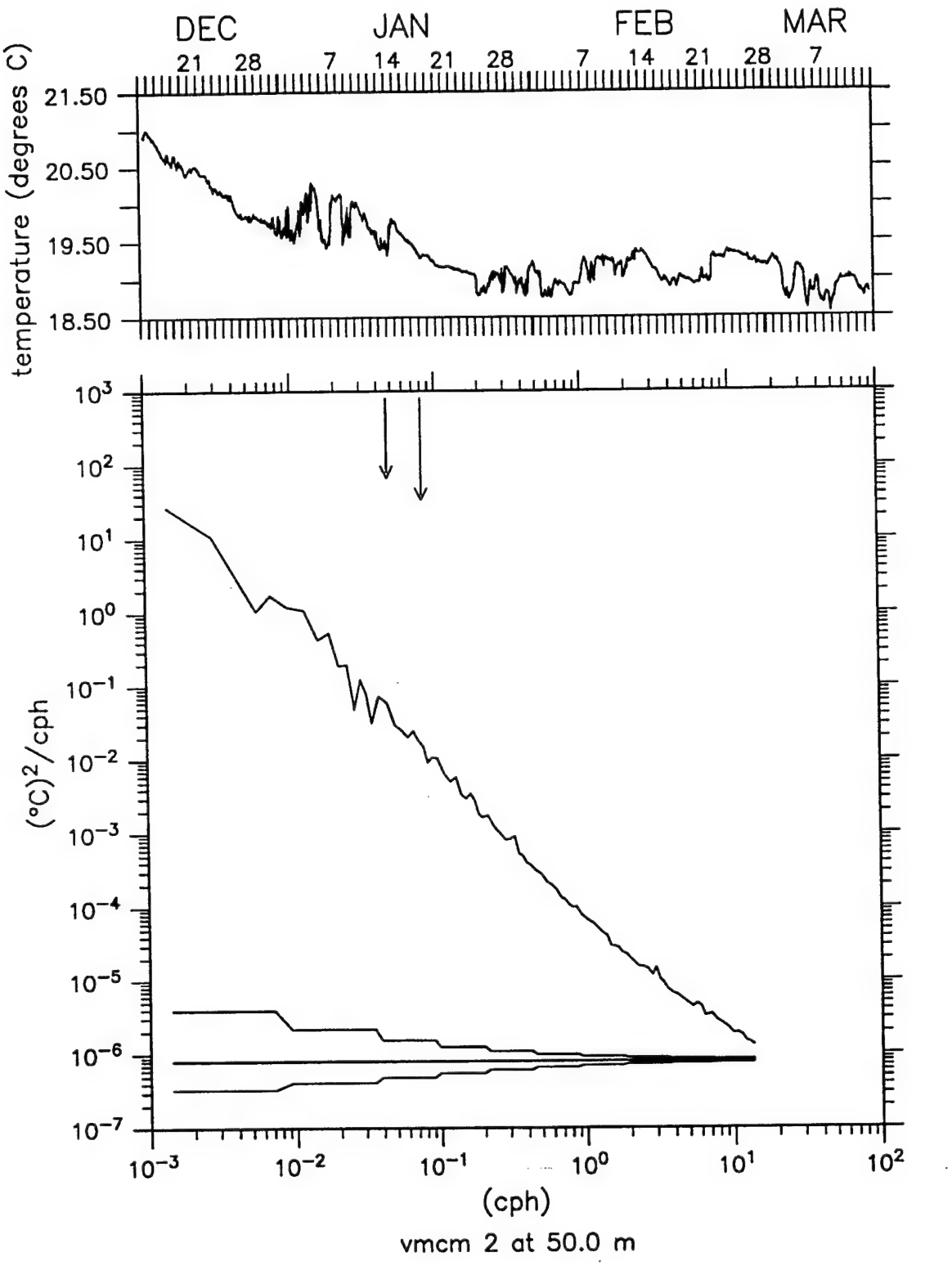

Figure 3.2.10: Temperature Time Series and Spectra at 50m. Long arrow indicates semi-diurnal tidal frequency, short arrow indicates Coriolis frequency.

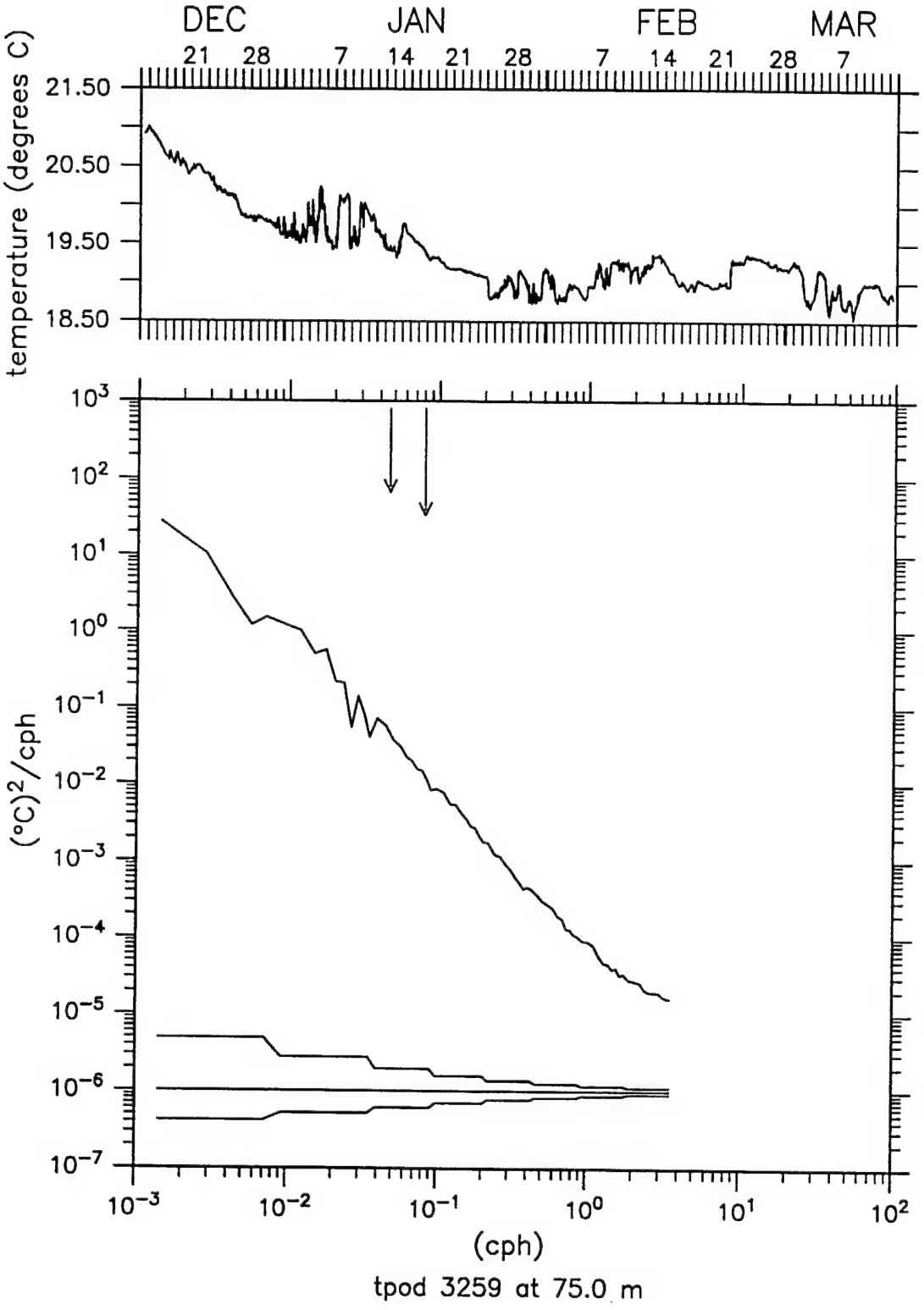

Figure 3.2.11: Temperature Time Series and Spectra at 75m. Long arrow indicates semi-diurnal tidal frequency, short arrow indicates Coriolis frequency.

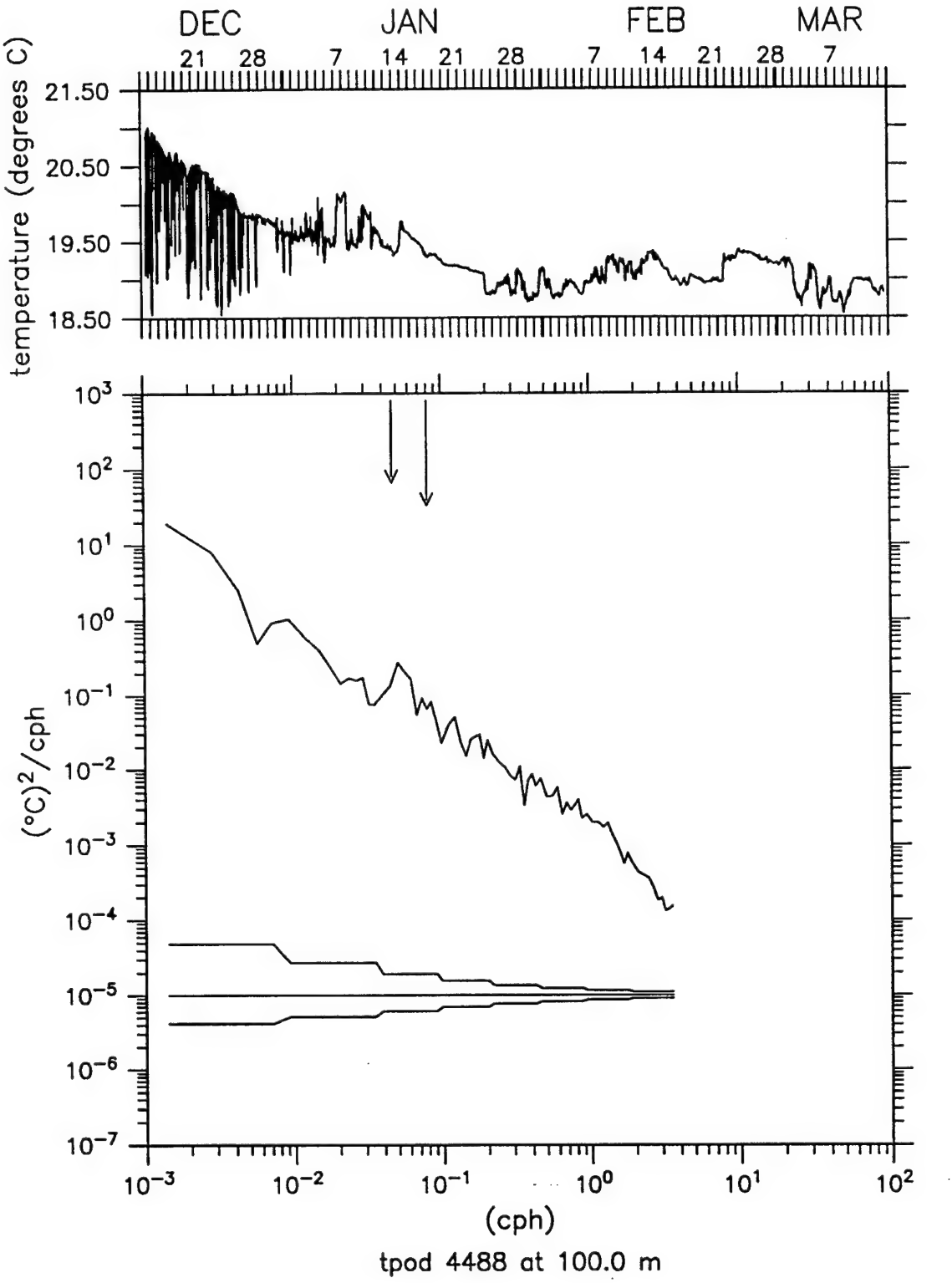

Figure 3.2.12: Temperature Time Series and Spectra at 100m. Long arrow indicates semi-diurnal tidal frequency, short arrow indicates Coriolis frequency.

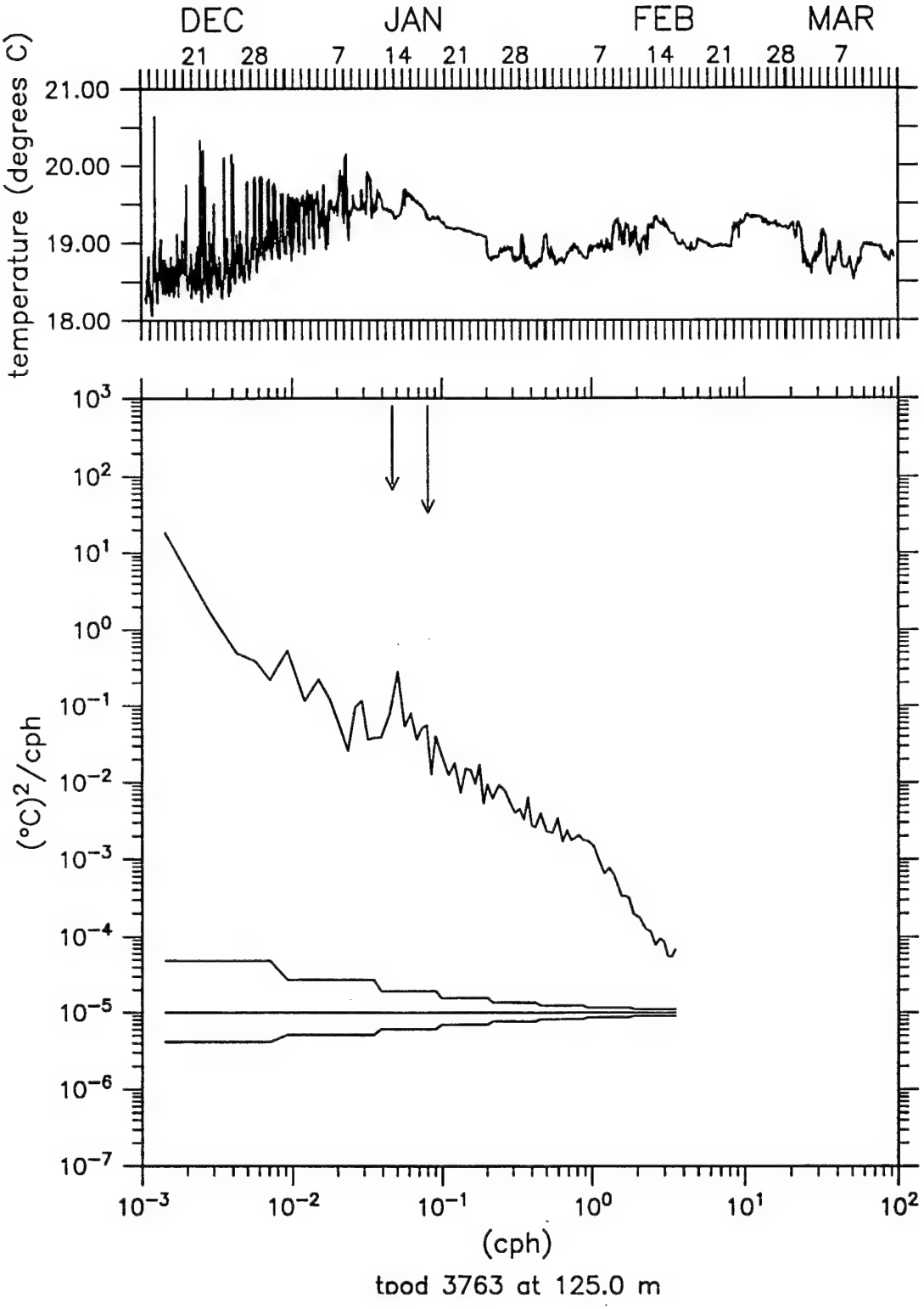

Figure 3.2.13: Temperature Time Series and Spectra at 125m. Long arrow indicates semi-diurnal tidal frequency, short arrow indicates Coriolis frequency.

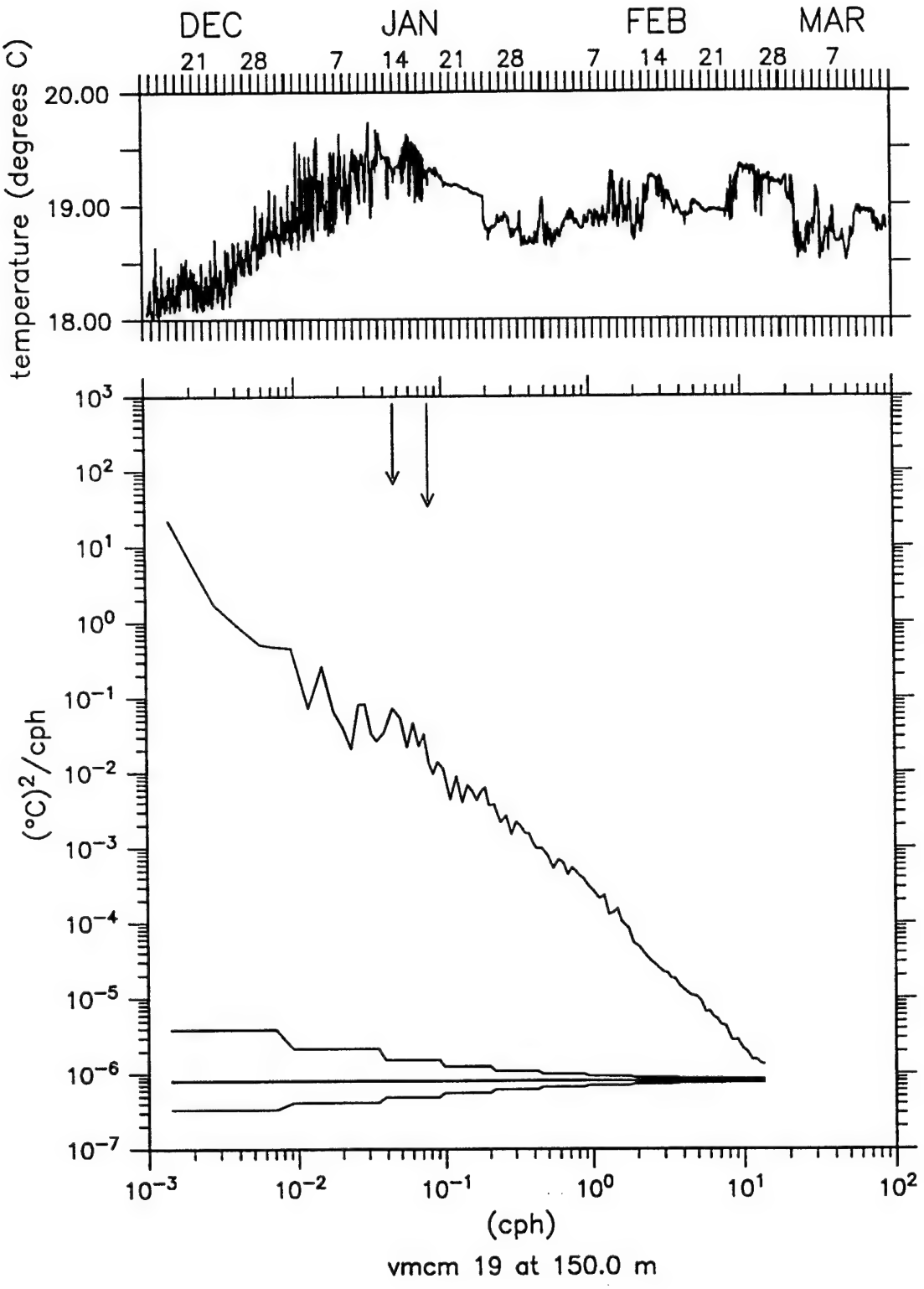

Figure 3.2.14: Temperature Time Series and Spectra at 150m. Long arrow indicates semi-diurnal tidal frequency, short arrow indicates Coriolis frequency.

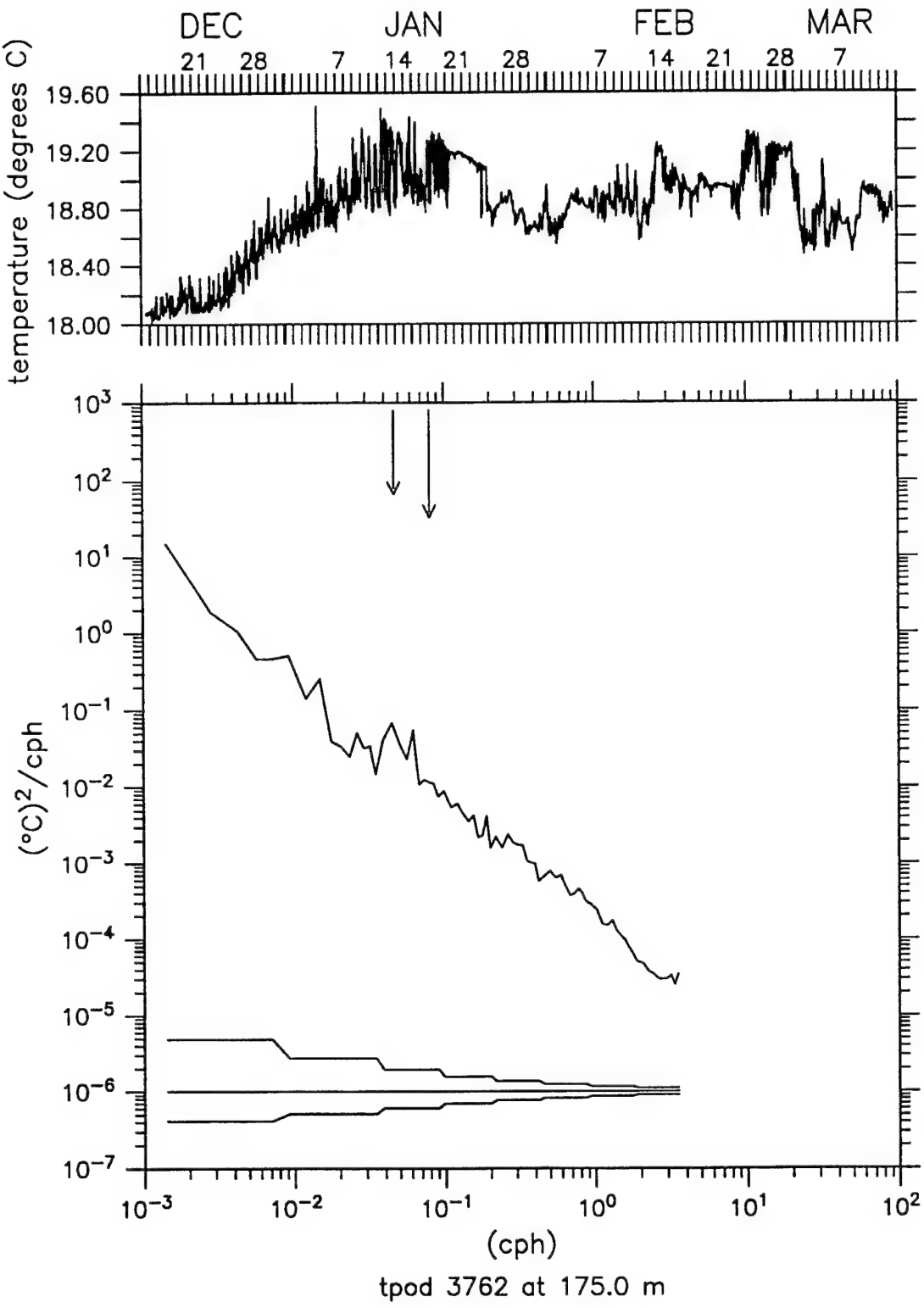

Figure 3.2.15: Temperature Time Series and Spectra at 175m. Long arrow indicates semi-diurnal tidal frequency, short arrow indicates Coriolis frequency.

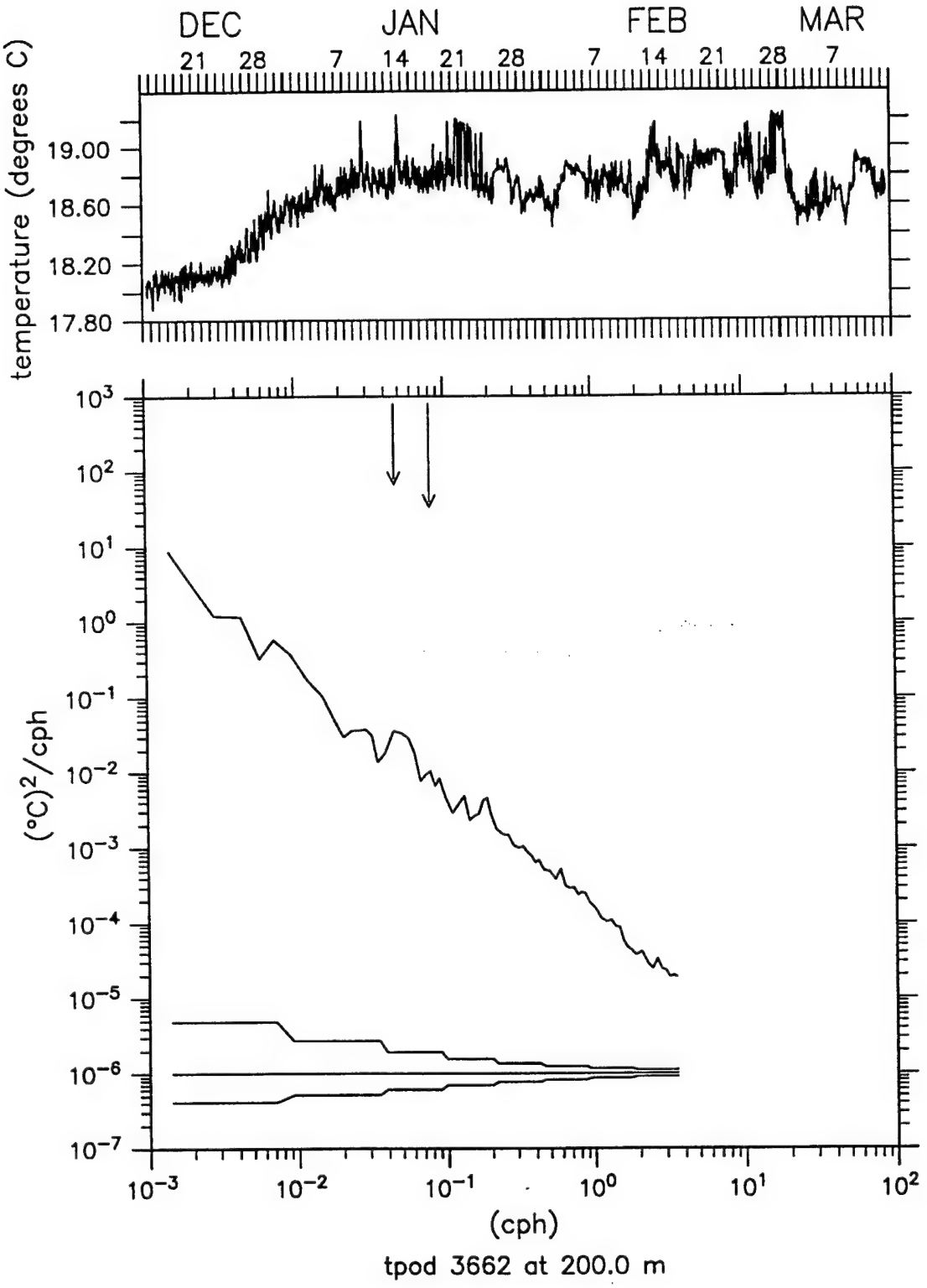

Figure 3.2.16: Temperature Time Series and Spectra at 200m. Long arrow indicates semi-diurnal tidal frequency, short arrow indicates Coriolis frequency.

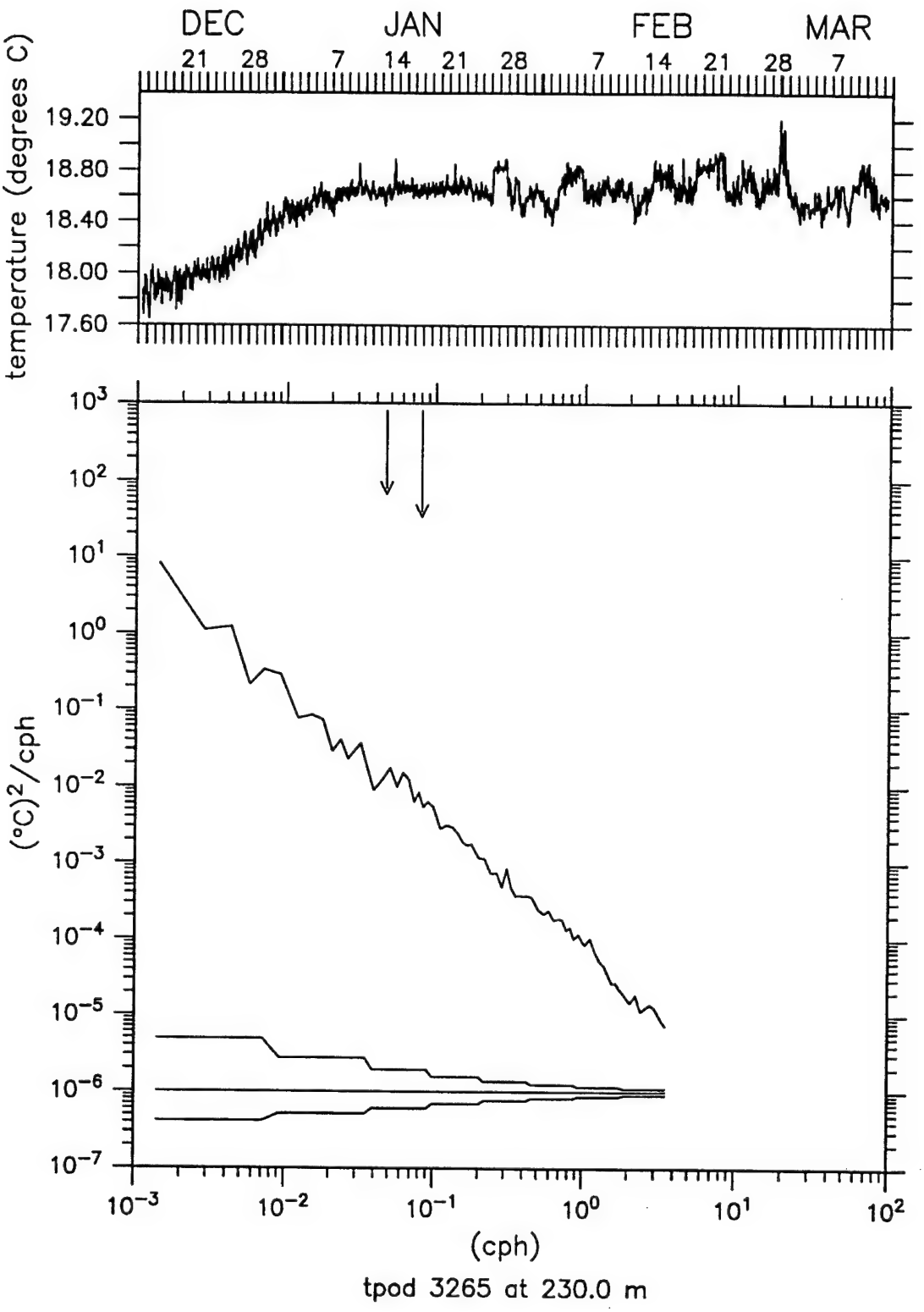

Figure 3.2.17: Temperature Time Series and Spectra at 230m. Long arrow indicates semi-diurnal tidal frequency, short arrow indicates Coriolis frequency.

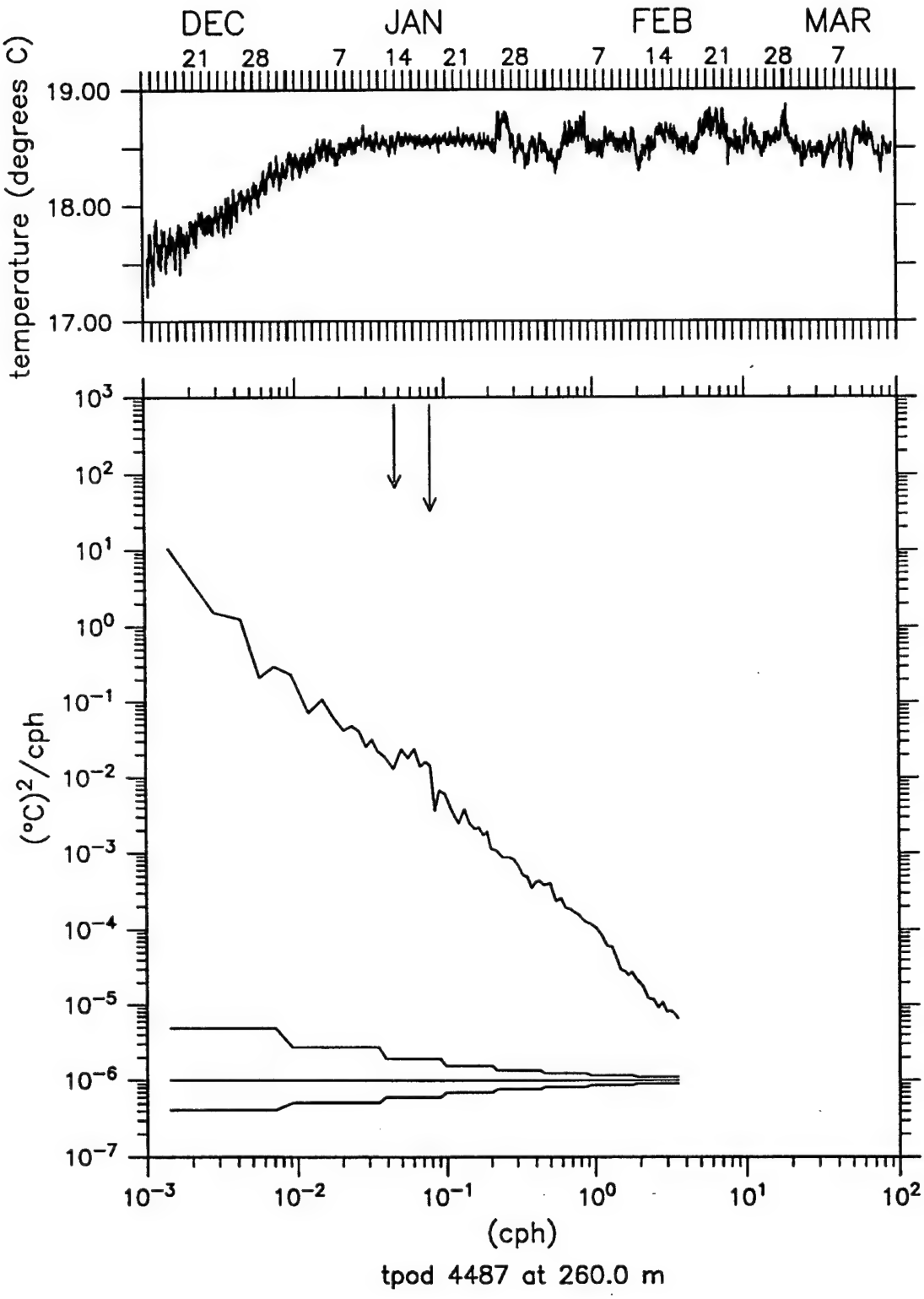

Figure 3.2.18: Temperature Time Series and Spectra at 260m. Long arrow indicates semi-diurnal tidal frequency, short arrow indicates Coriolis frequency.

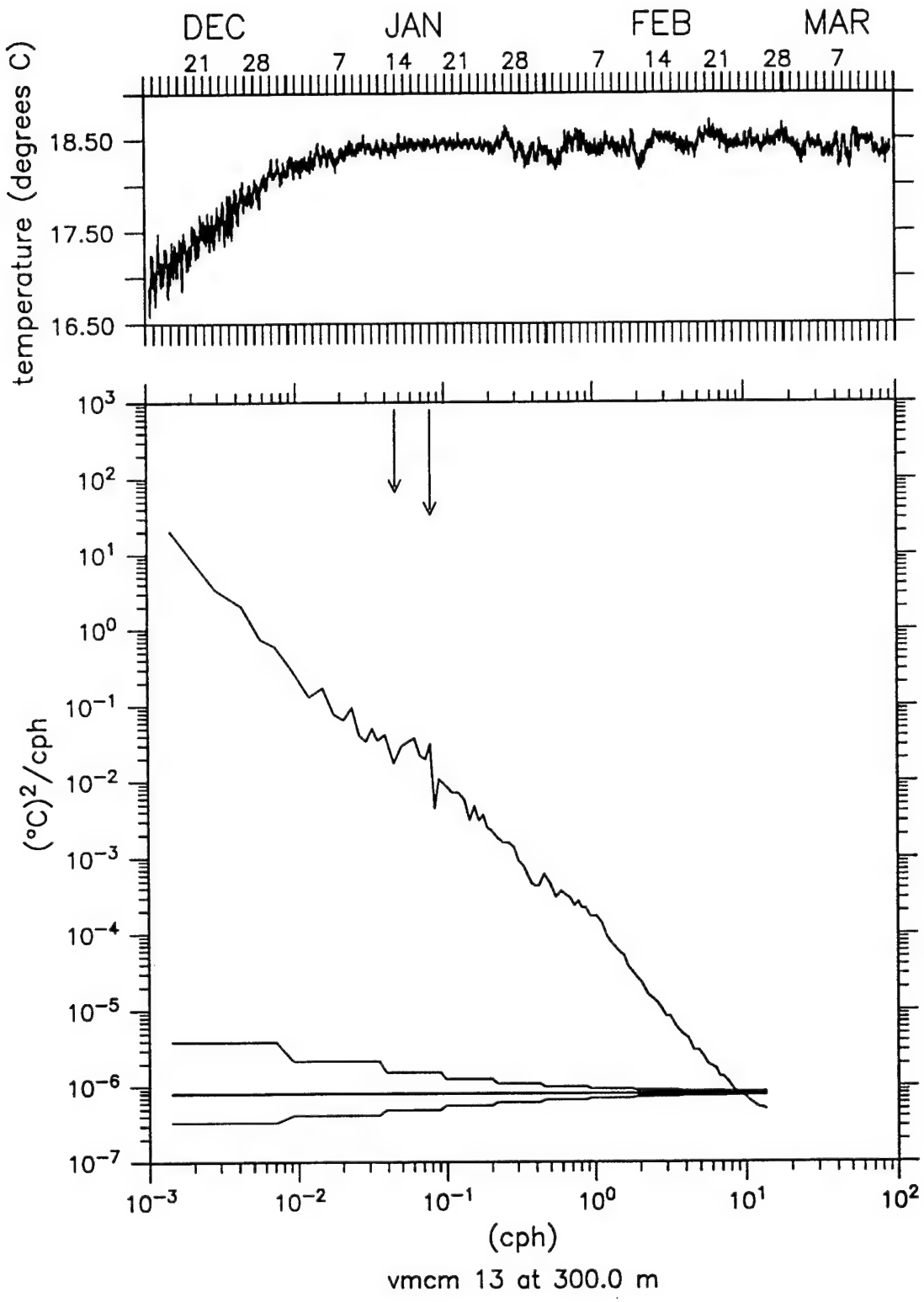

Figure 3.2.19: Temperature Time Series and Spectra at 300m. Long arrow indicates semi-diurnal tidal frequency, short arrow indicates Coriolis frequency.

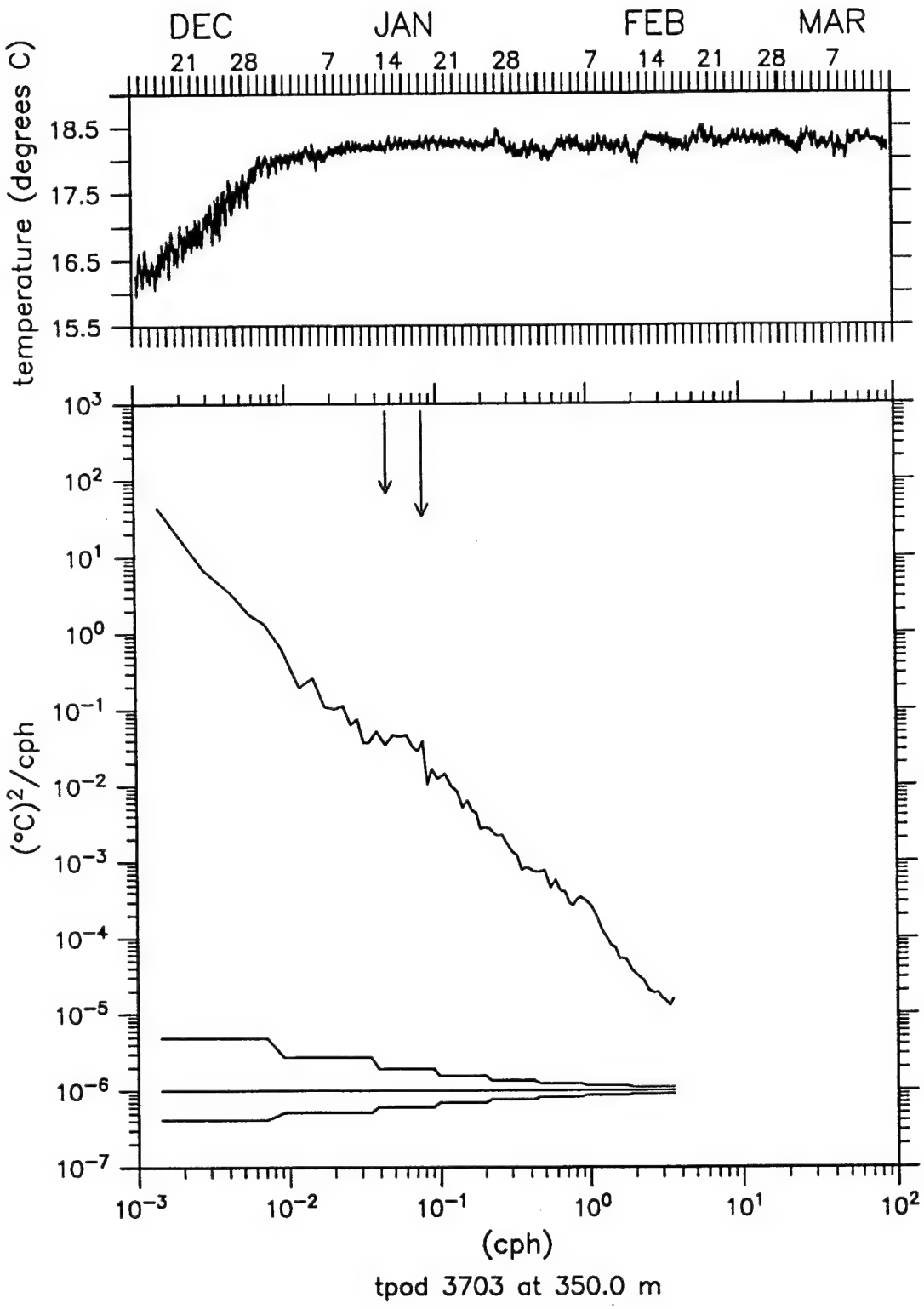

Figure 3.2.20: Temperature Time Series and Spectra at 350m. Long arrow indicates semi-diurnal tidal frequency, short arrow indicates Coriolis frequency.

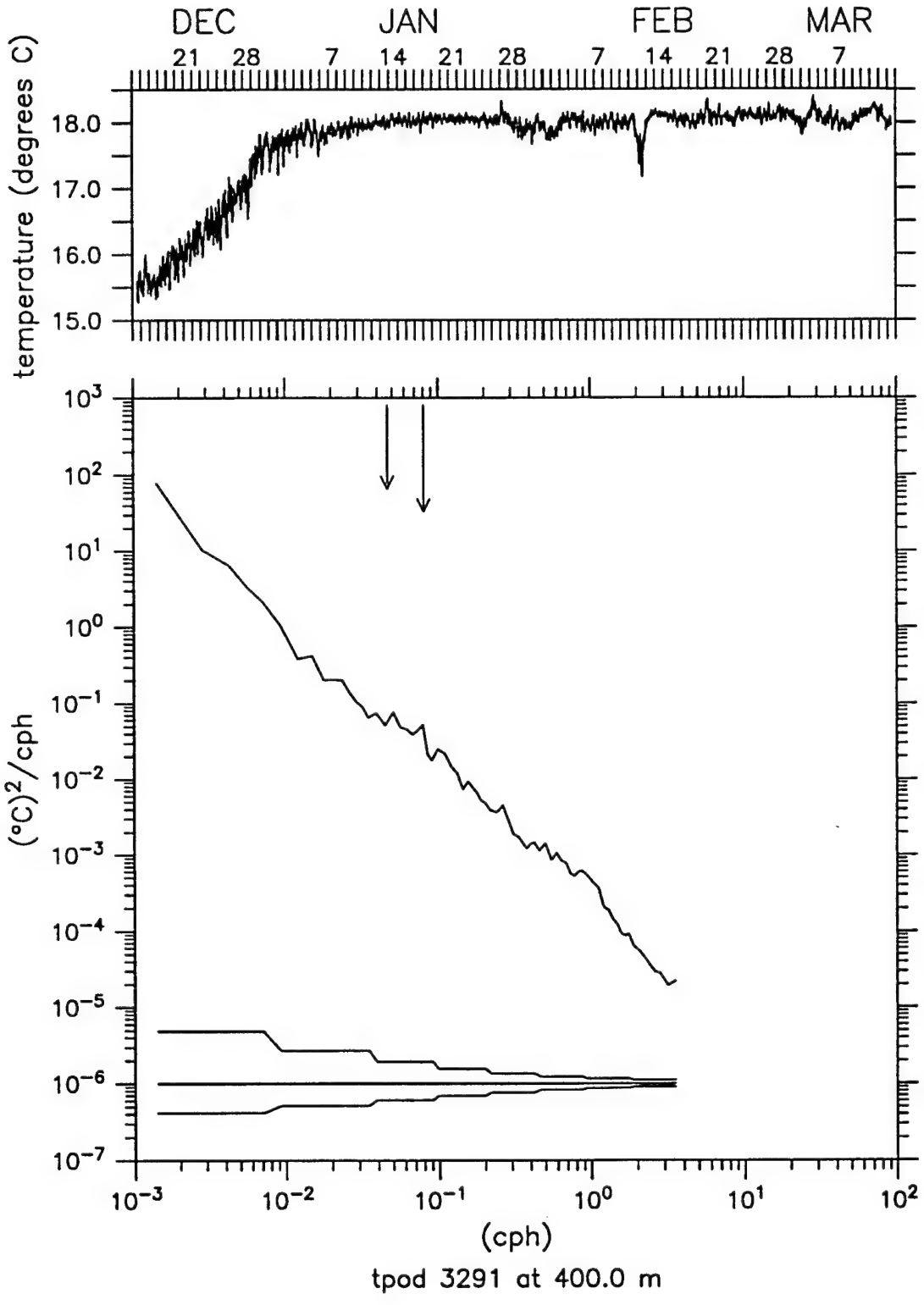

Figure 3.2.21: Temperature Time Series and Spectra at 400m. Long arrow indicates semi-diurnal tidal frequency, short arrow indicates Coriolis frequency.

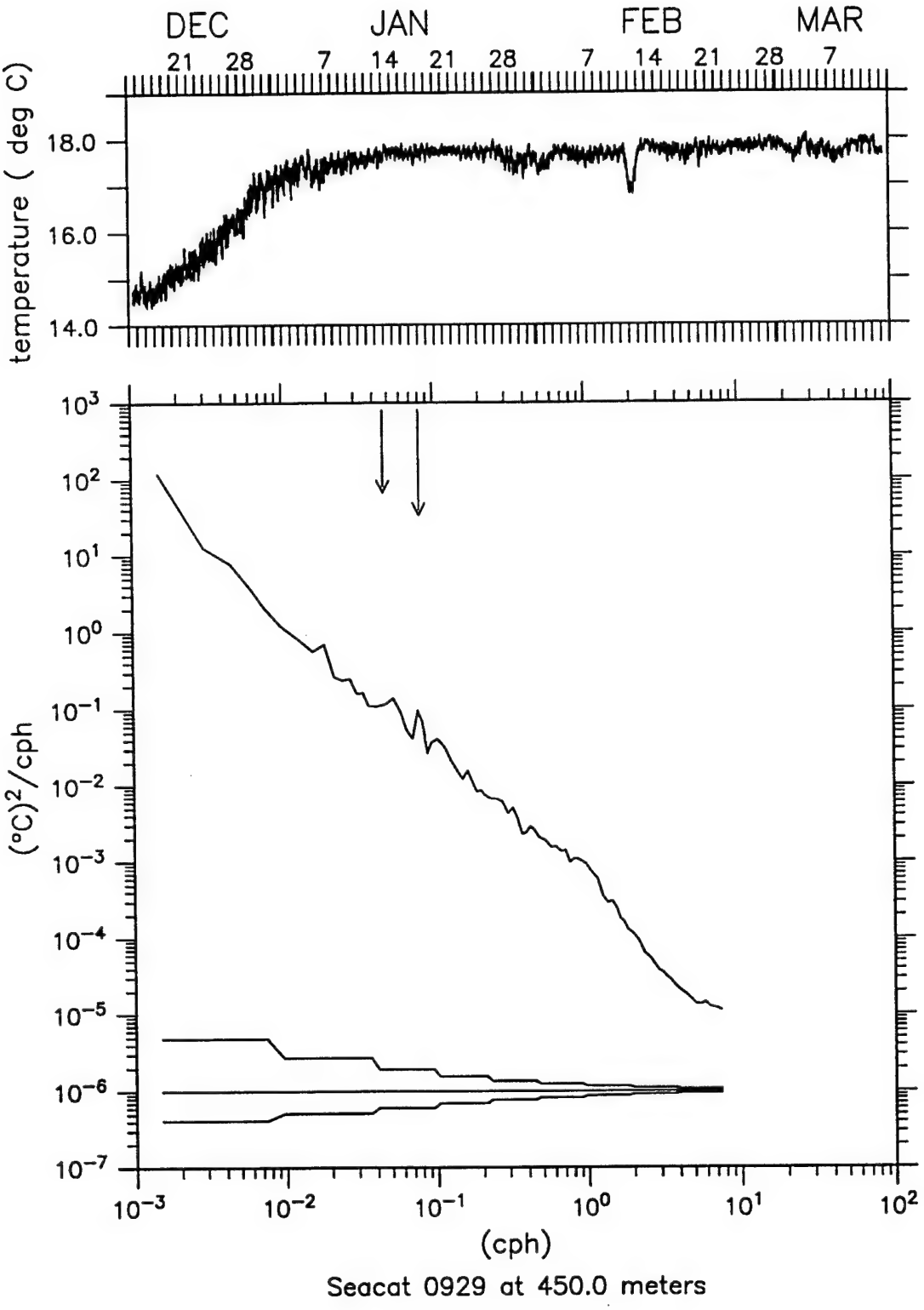

Figure 3.2.22: Temperature Time Series and Spectra at 450m. Long arrow indicates semi-diurnal tidal frequency, short arrow indicates Coriolis frequency.

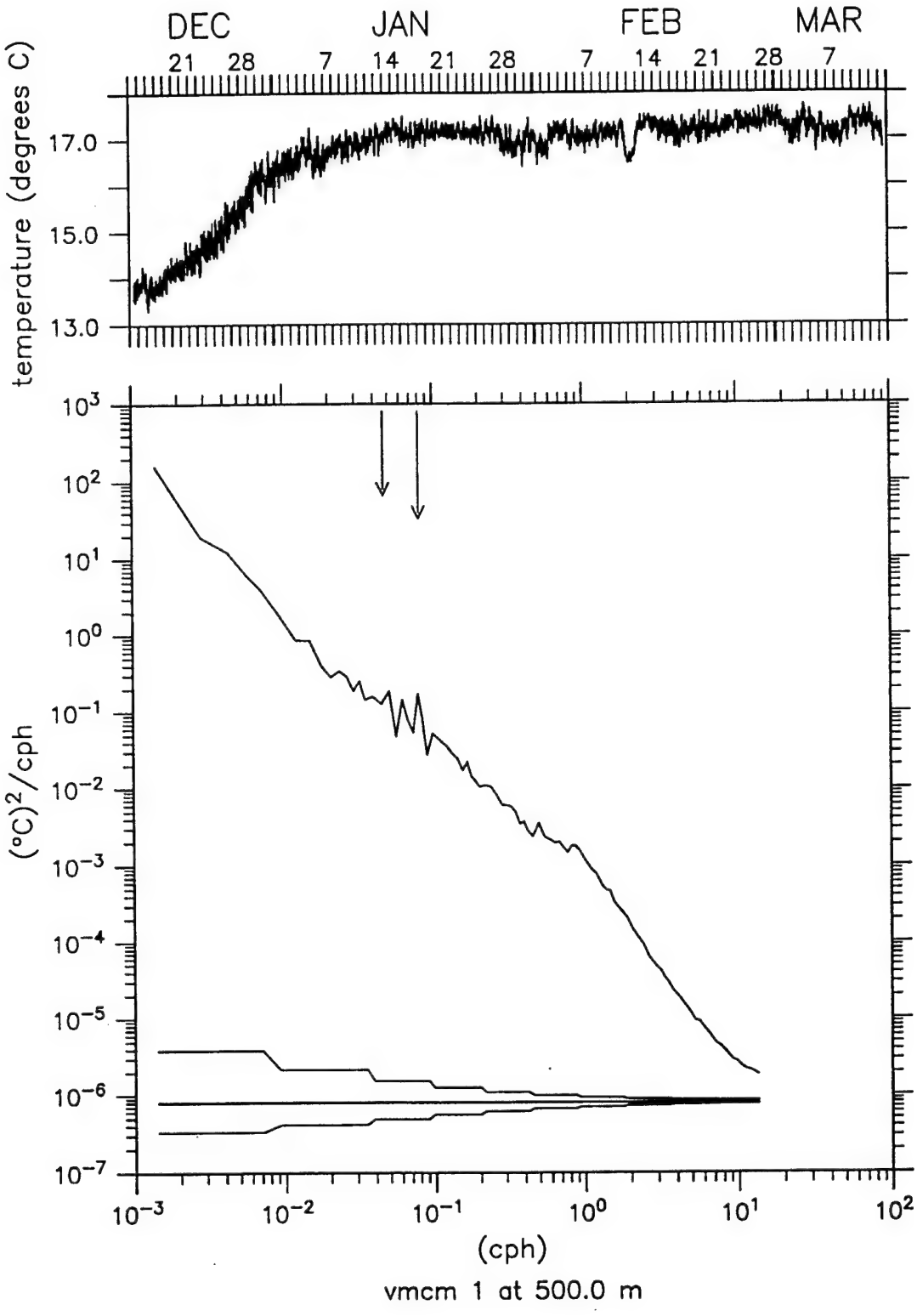

Figure 3.2.23: Temperature Time Series and Spectra at 500m. Long arrow indicates semi-diurnal tidal frequency, short arrow indicates Coriolis frequency.

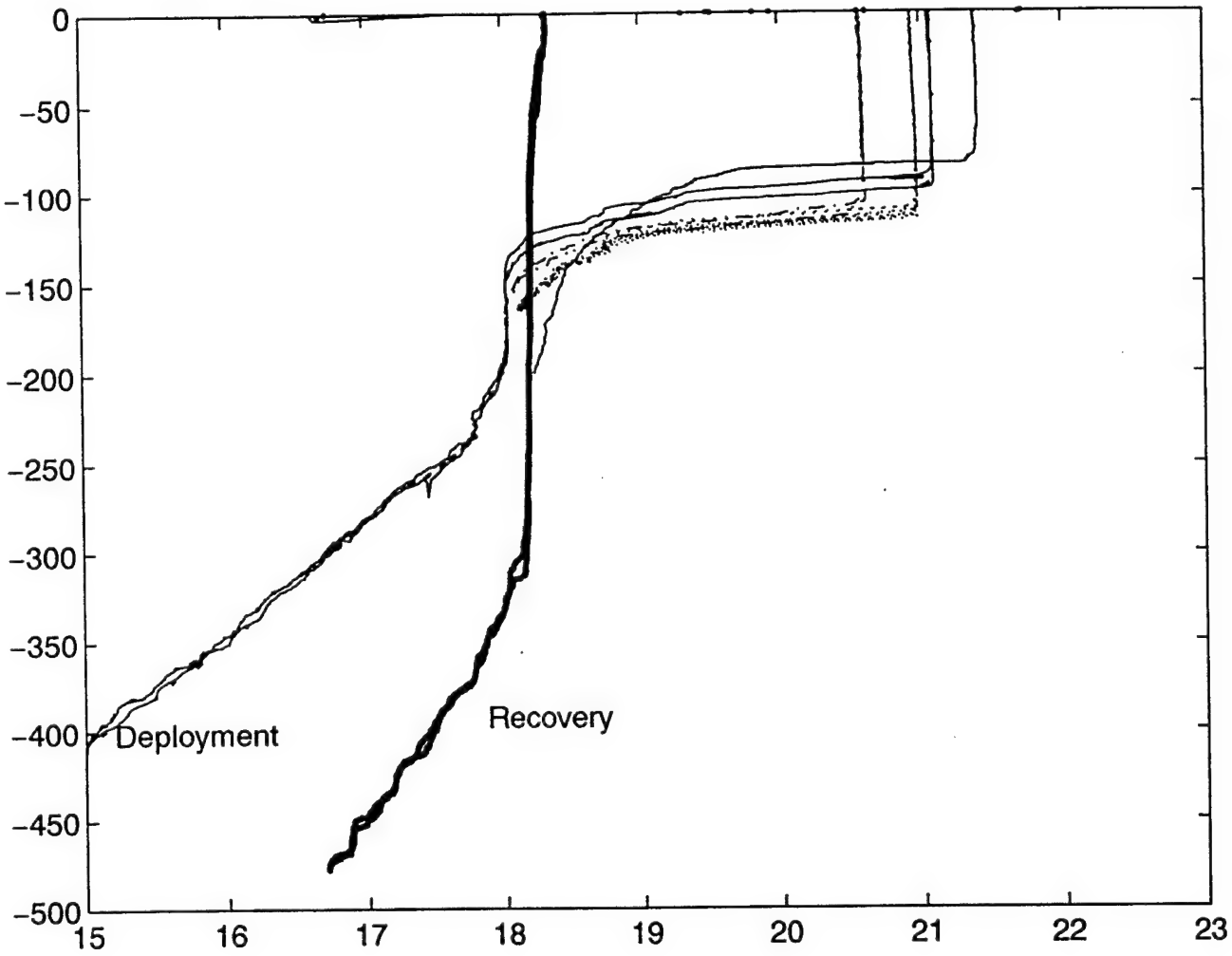

Figure 3.2.24: Temperature profiles from Seacat casts.

3.3 Current Velocities During ASREX III

Currents were measured by VMCMs at 5, 10, 15, 20, 50, 150, 300 and 500 m. The current meters recorded at a rate of once every 120 seconds. A time-base checking program was used to correct missing data and data with invalid time-words before any further processing was carried out.

Time series stick-plots of the water vectors at each depth are in Figures 3.3.1 through 3.3.6. Data was filtered over a 48-hour period and decimated to 2 hours for the vector plots. Northerly velocities are represented by vectors pointing toward the top of the page.

Progressive vector plots for the eight VMCMs are shown in Figures 3.3.7 and 3.3.8. Velocity data was filtered and decimated to 4 hour values before plotting. Relative speed is indicated by the square symbols, which mark months.

Figures 3.3.9 through 3.3.16 are combined time-series and spectra for currents at each depth. These plots show unfiltered data. The upper frame for each plot represents the north and east velocities along the vertical axes and time (UTC) along the horizontal axis. The lower frame contains the spectra, with a solid line indicating the clockwise component and a dashed line indicating the counterclockwise component. As for temperature plots, the frequency of the Coriolis parameter and the semidiurnal tide are shown on the plots, and confidence limits are displayed. There are significant peaks associated with both the tide and Coriolis frequency.

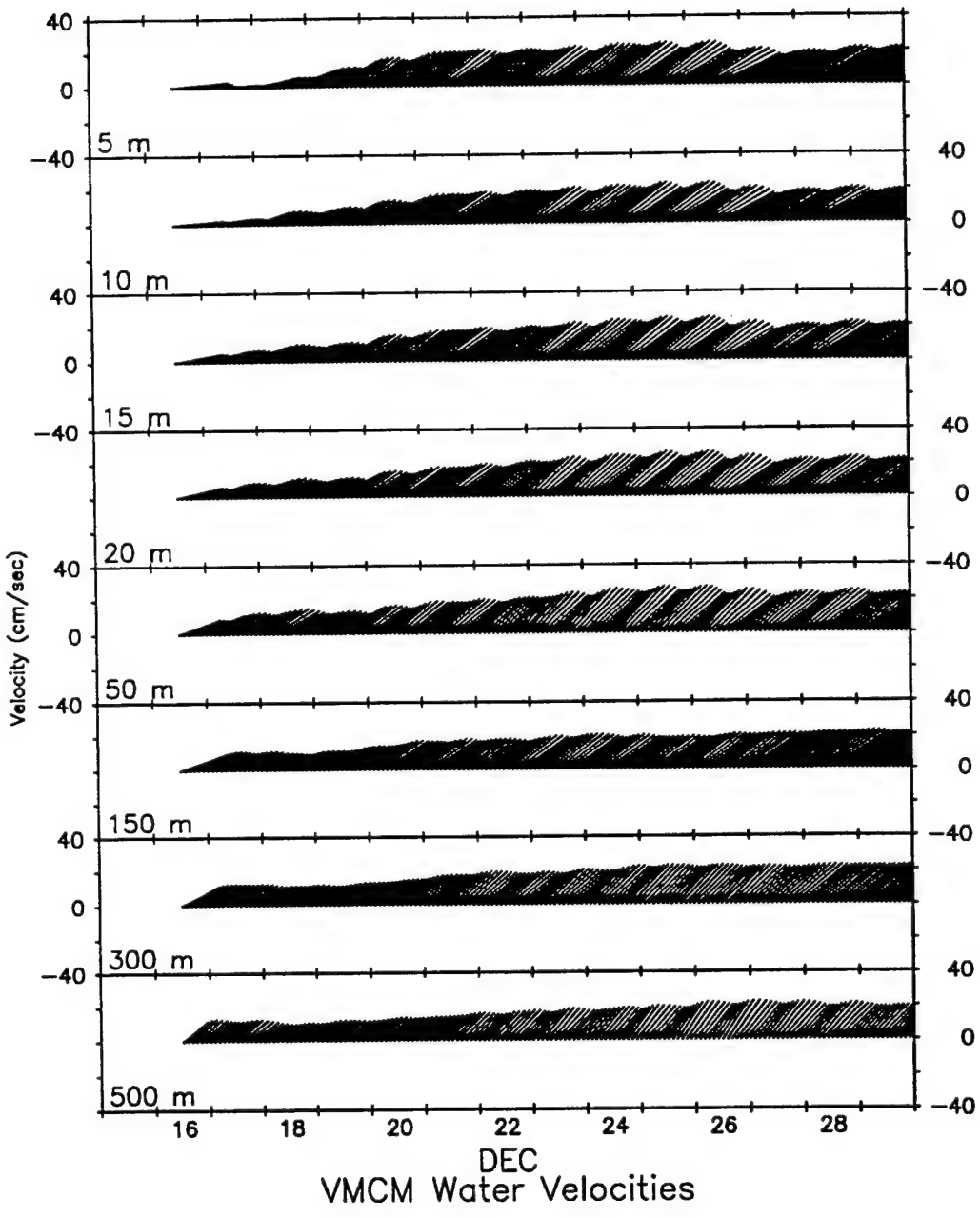

Figure 3.3.1: Sub-surface velocity vectors at 8 depths. Northerly component is towards top of page. Data is filtered over 48 hours and subsampled at 2 hours before plotting.

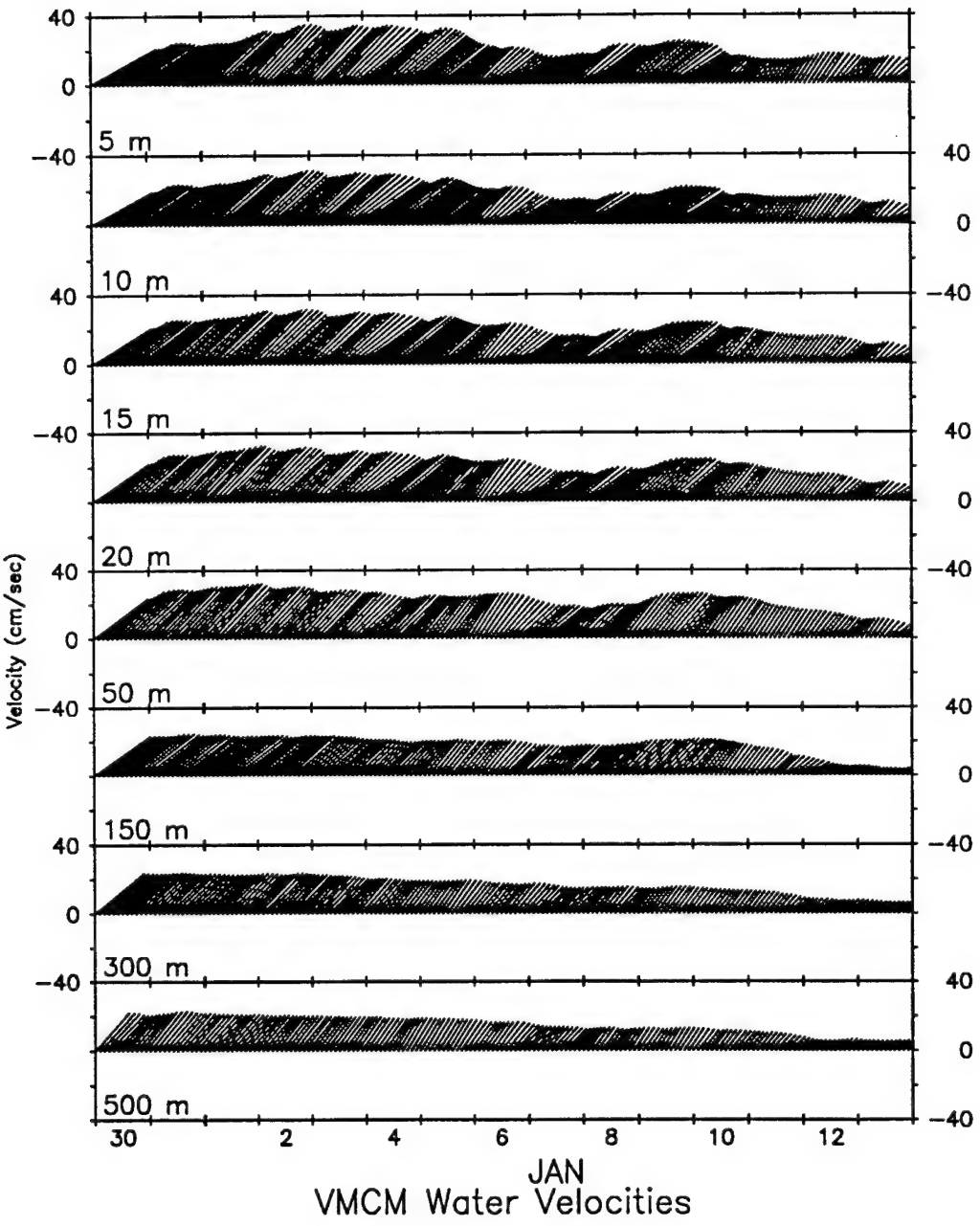

Figure 3.3.2: Sub-surface velocity vectors at 8 depths. Northerly component is towards top of page. Data is filtered over 48 hours and subsampled at 2 hours before plotting.

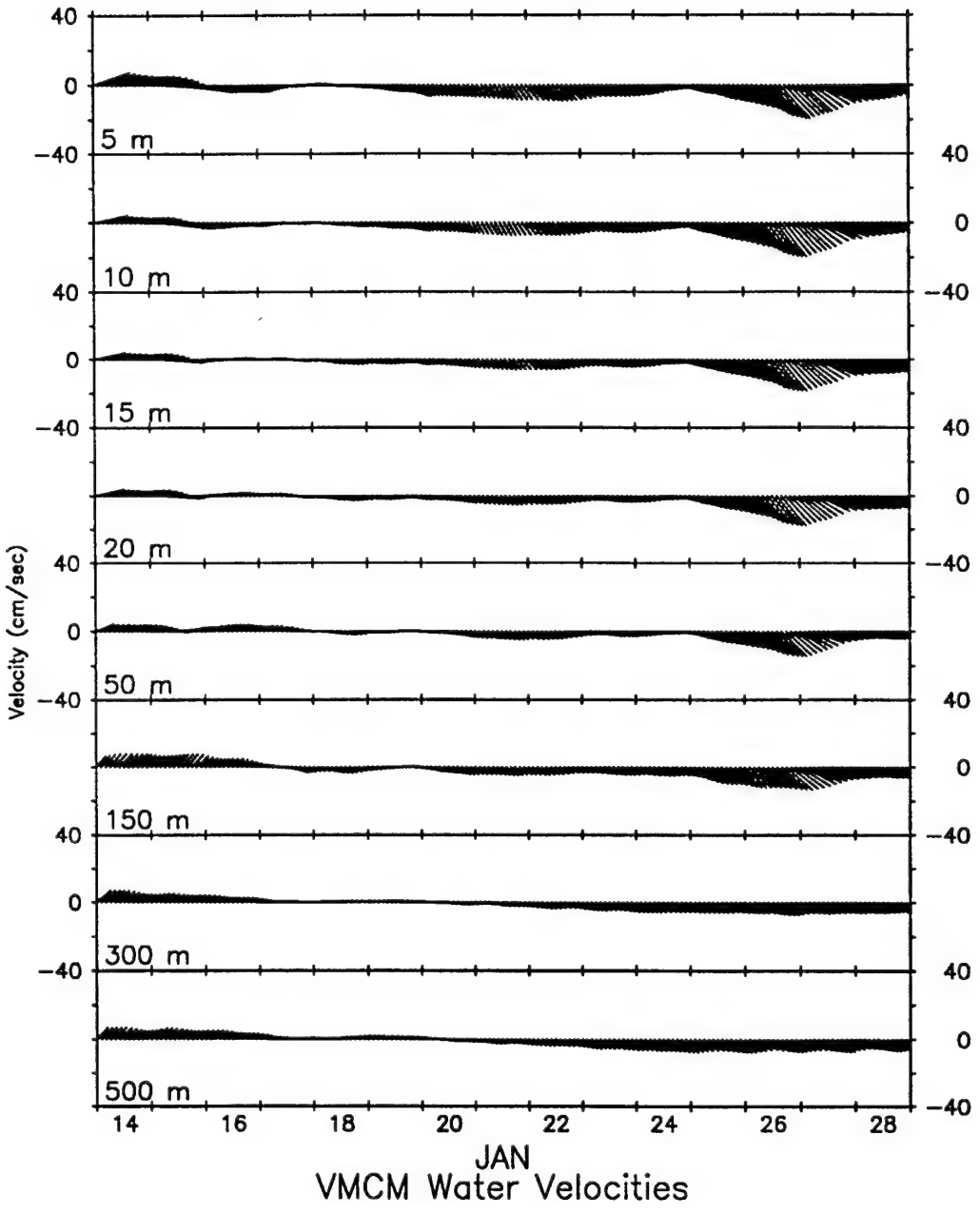

Figure 3.3.3: Sub-surface velocity vectors at 8 depths. Northerly component is towards top of page. Data is filtered over 48 hours and subsampled at 2 hours before plotting.

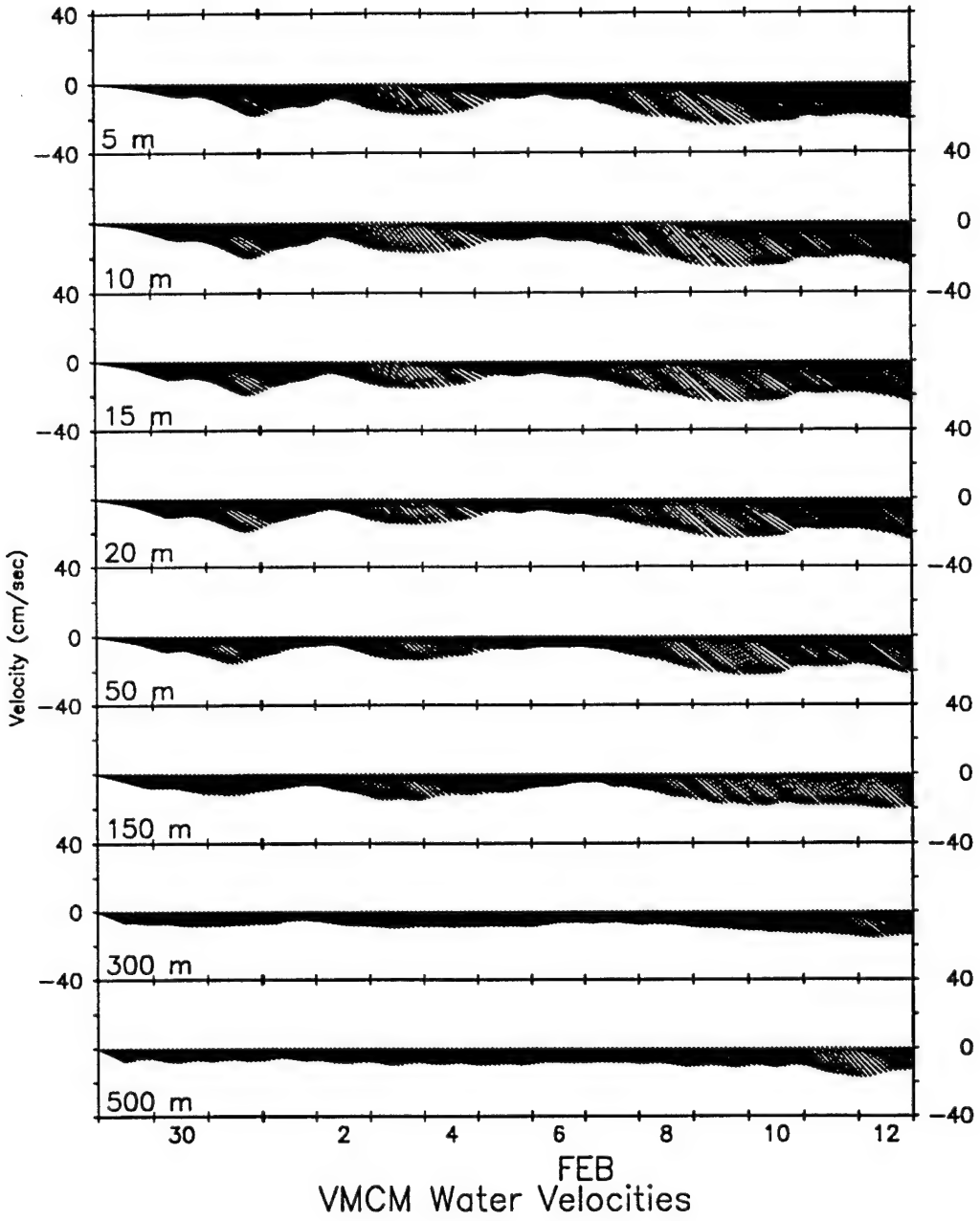

Figure 3.3.4: Sub-surface velocity vectors at 8 depths. Northerly component is towards top of page. Data is filtered over 48 hours and subsampled at 2 hours before plotting.

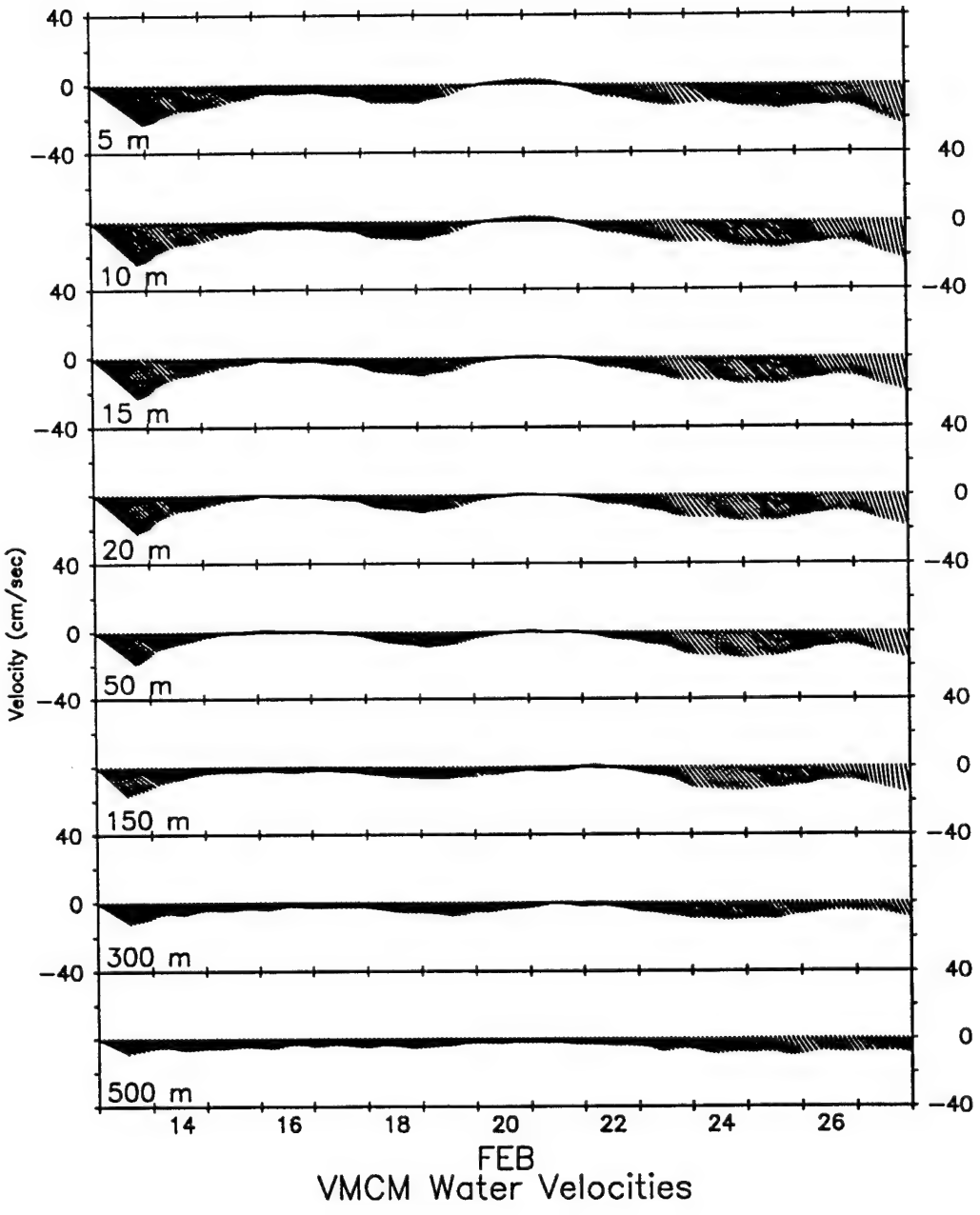

Figure 3.3.5: Sub-surface velocity vectors at 8 depths. Northerly component is towards top of page. Data is filtered over 48 hours and subsampled at 2 hours before plotting.

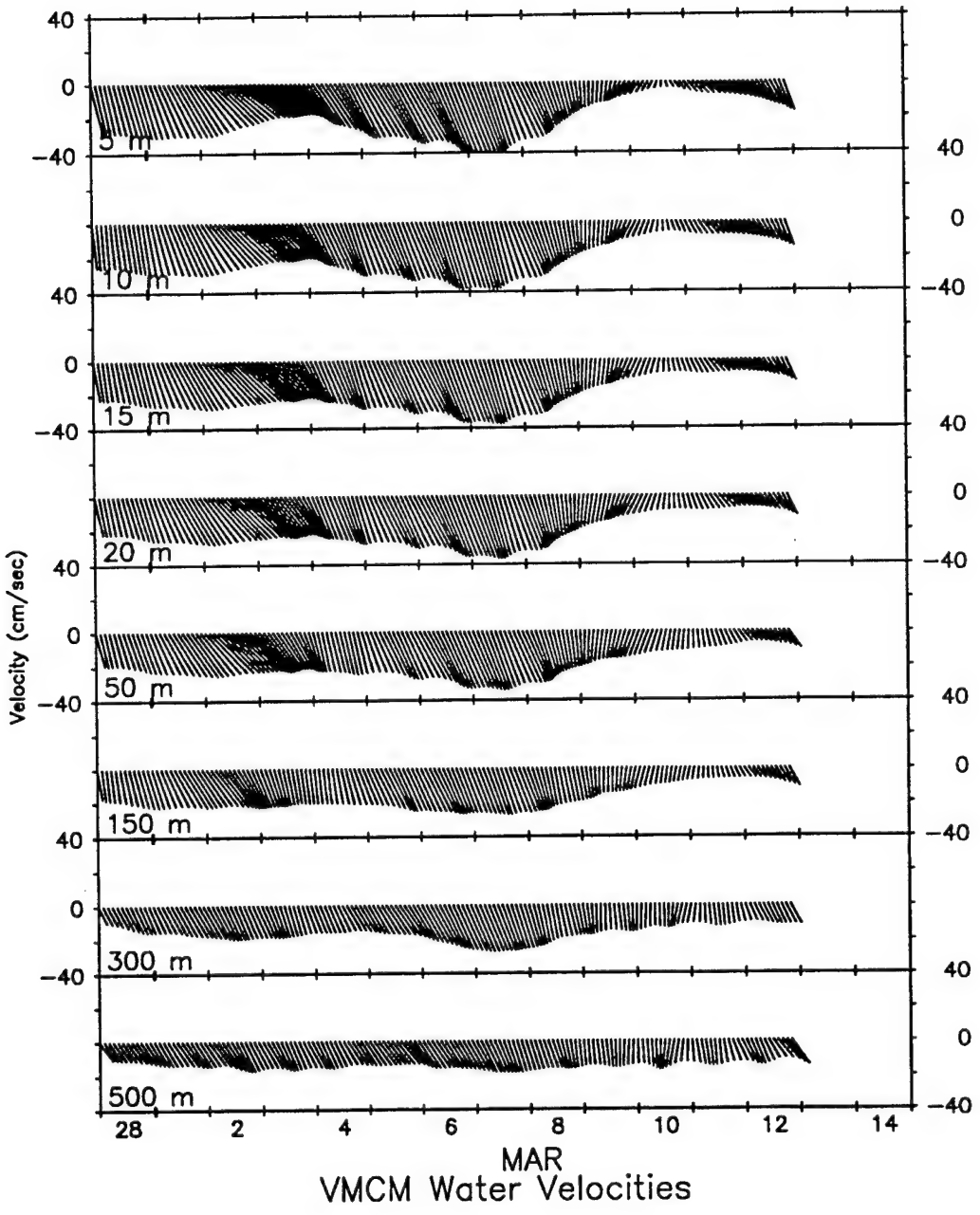

Figure 3.3.6: Sub-surface velocity vectors at 8 depths. Northerly component is towards top of page. Data is filtered over 48 hours and subsampled at 2 hours before plotting.

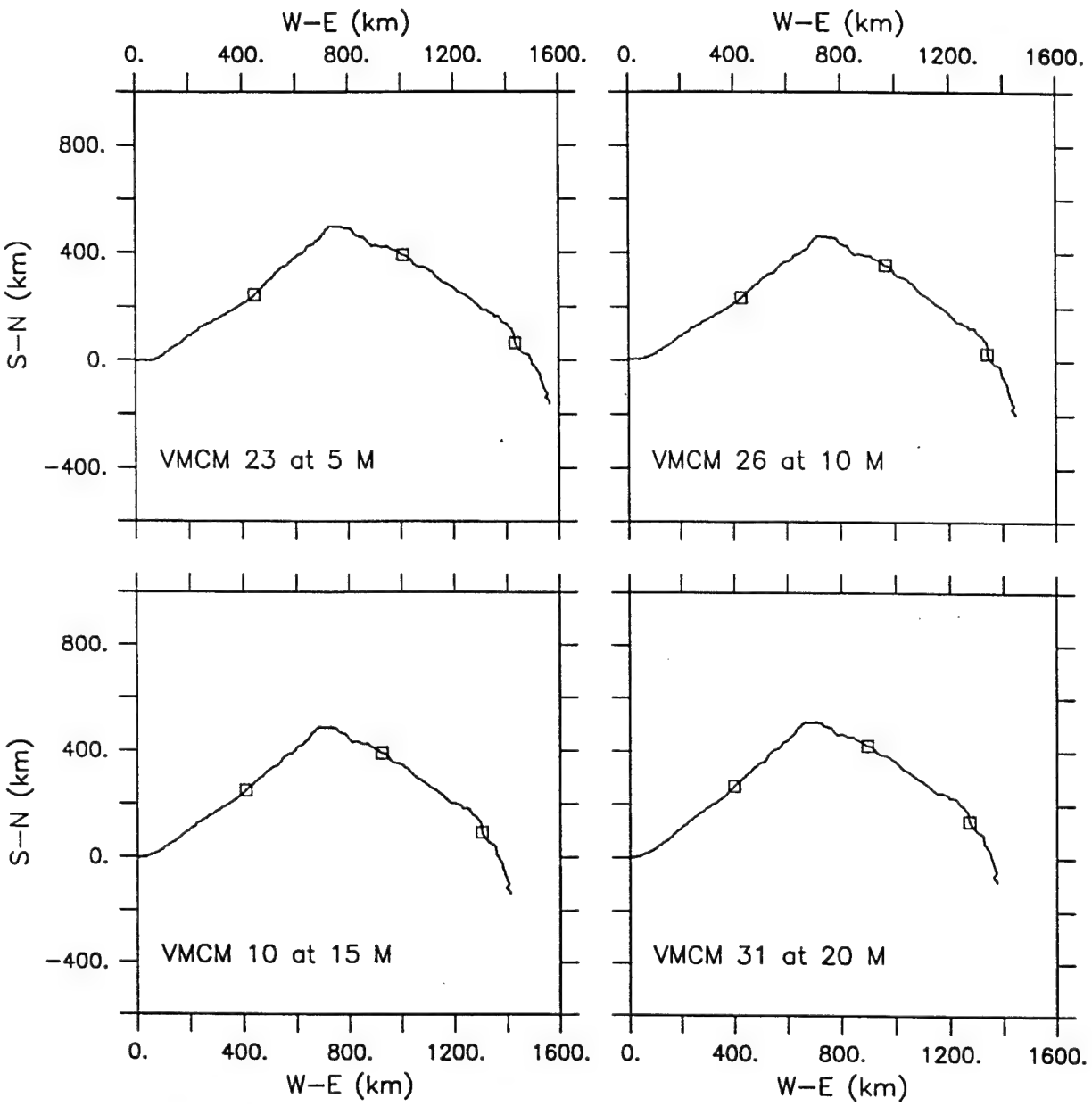

Start date 93/12/15 12:00

End date 94/03/13 12:00

Square symbols at new month

Figure 3.3.7: Progressive water velocity vectors at 4 depths, constructed from velocity data averaged over 4 hours.

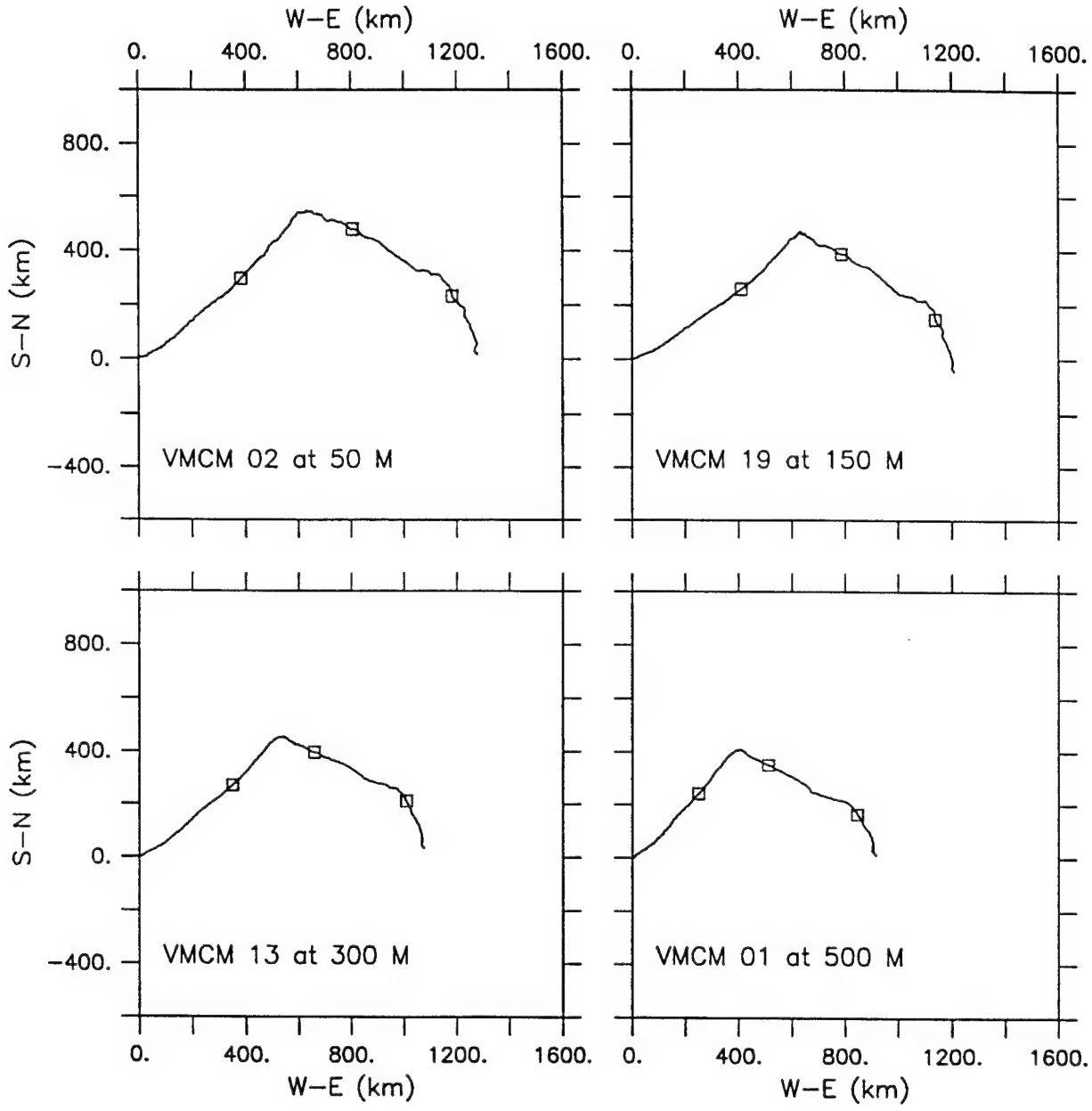

Figure 3.3.8: Progressive water velocity vectors at 4 depths, constructed from velocity data averaged over 4 hours.

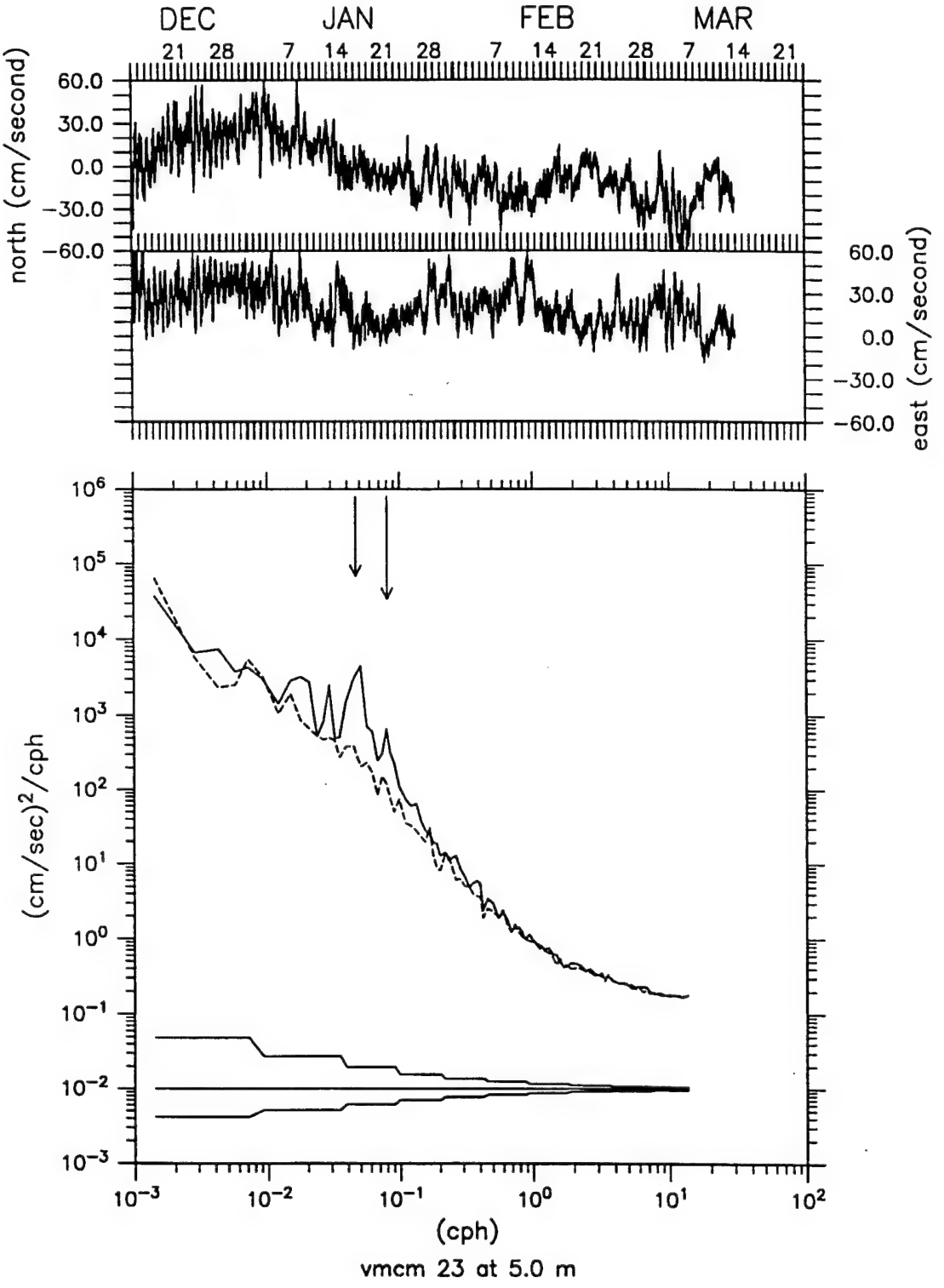

Figure 3.3.9: Velocity Time Series and Spectra at 5m. Solid curves show the clockwise component, and dashed curves show the counter-clockwise component. Long arrow indicates semi-diurnal tidal frequency, short arrow indicates Coriolis frequency.

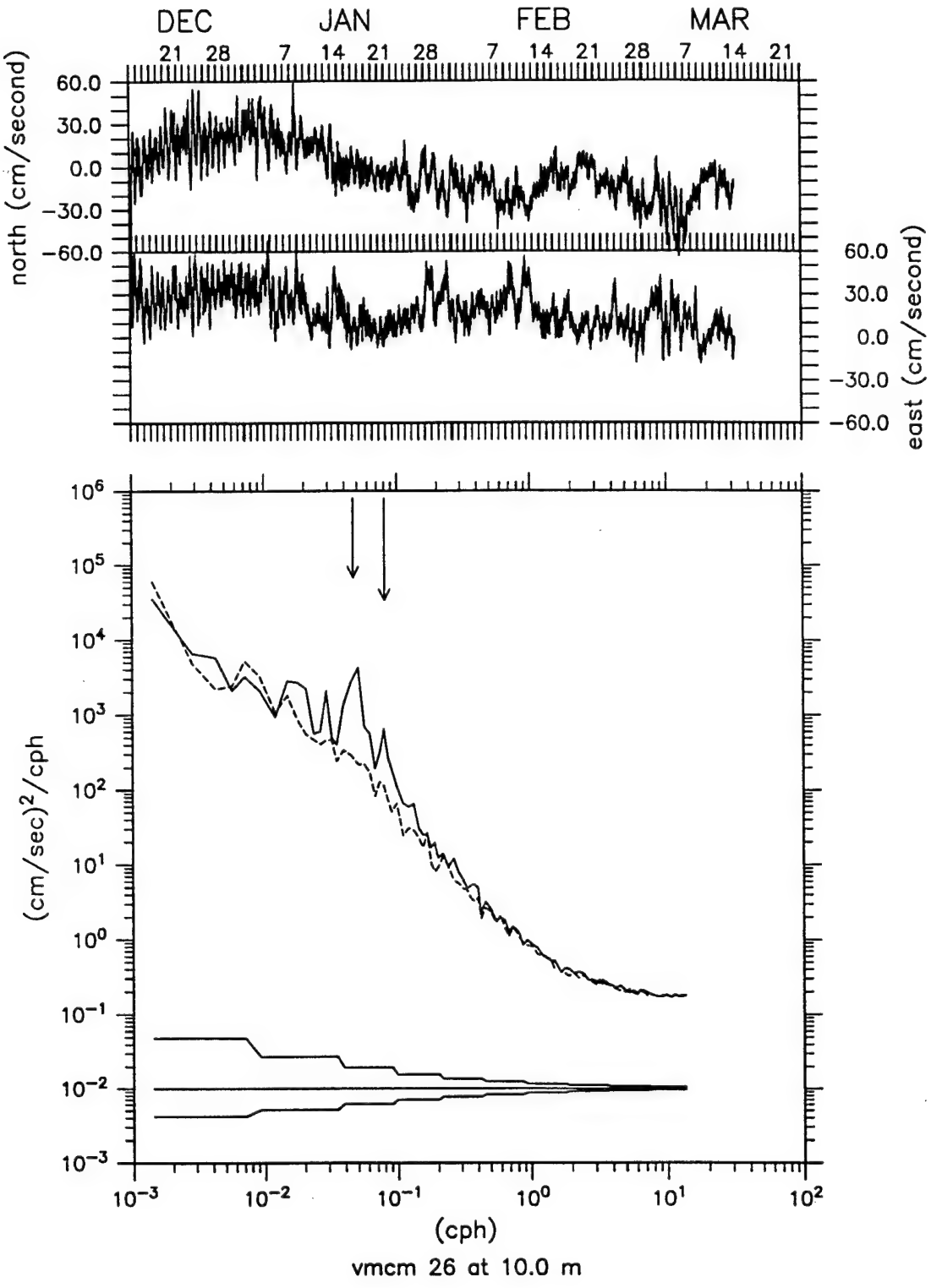

Figure 3.3.10: Velocity Time Series and Spectra at 10m. Solid curves show the clockwise component, and dashed curves show the counter-clockwise component. Long arrow indicates semi-diurnal tidal frequency, short arrow indicates Coriolis frequency.

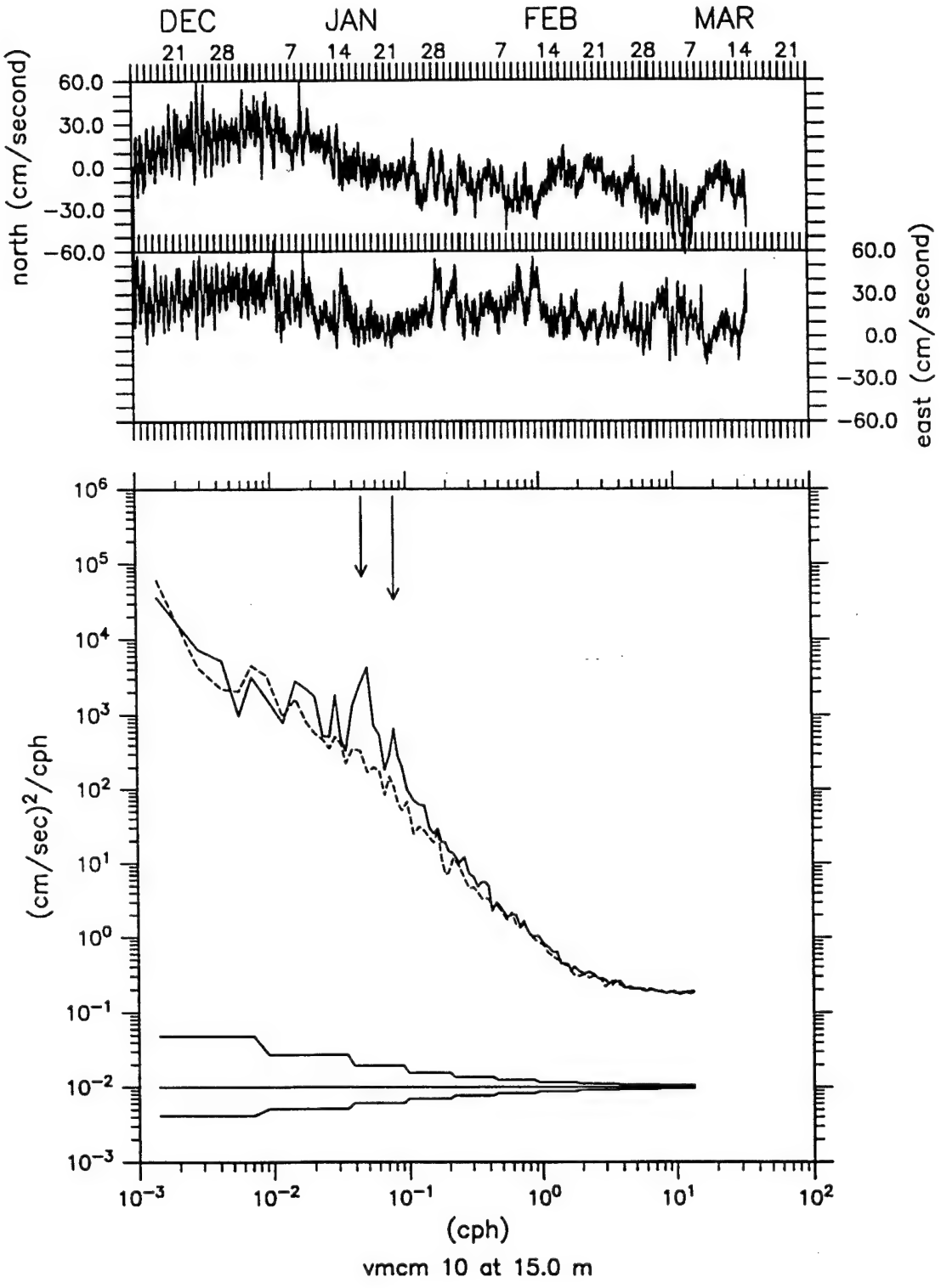

Figure 3.3.11: Velocity Time Series and Spectra at 15m. Solid curves show the clockwise component, and dashed curves show the counter-clockwise component. Long arrow indicates semi-diurnal tidal frequency, short arrow indicates Coriolis frequency.

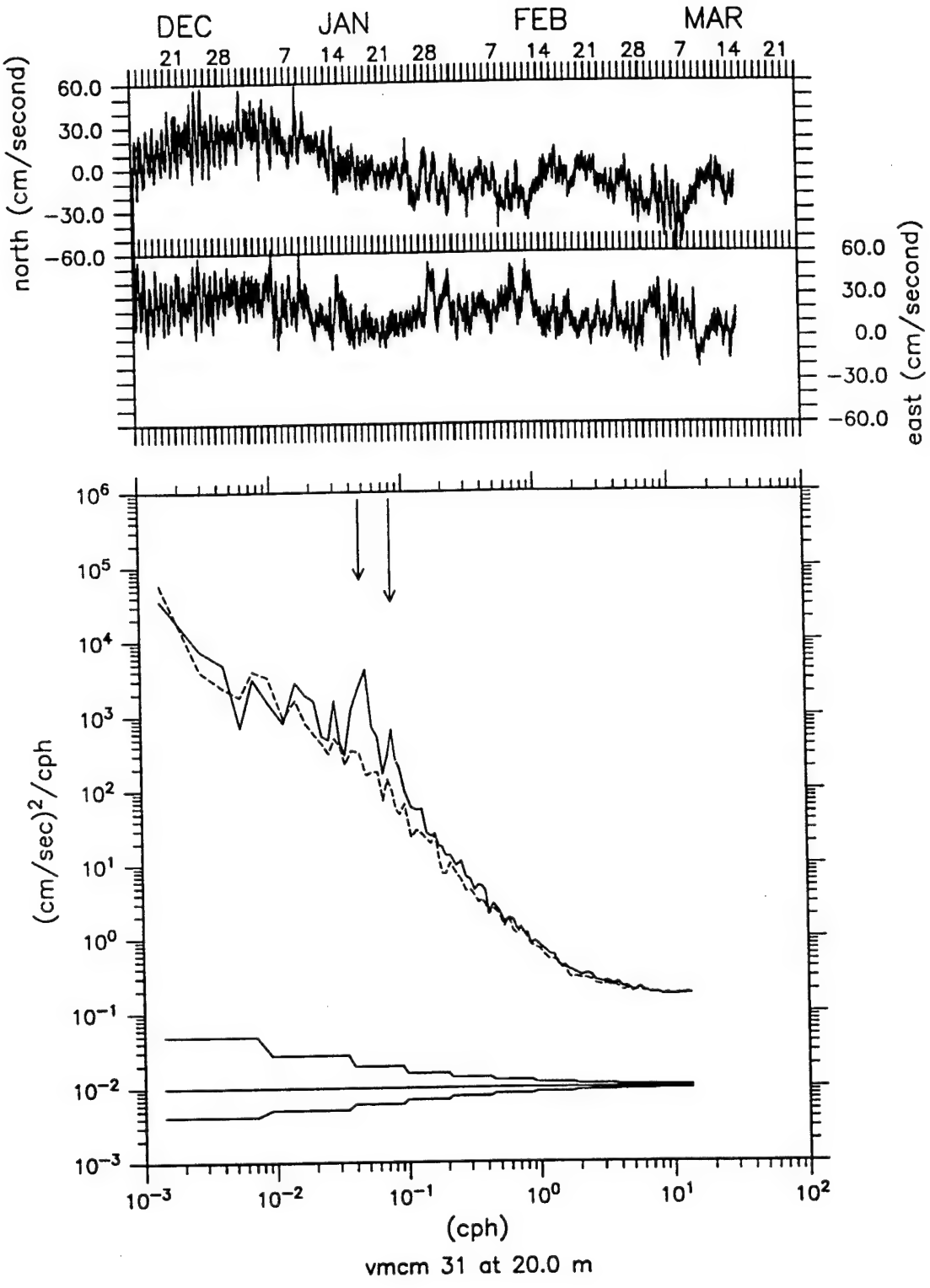

Figure 3.3.12: Velocity Time Series and Spectra at 20m. Solid curves show the clockwise component, and dashed curves show the counter-clockwise component. Long arrow indicates semi-diurnal tidal frequency, short arrow indicates Coriolis frequency.

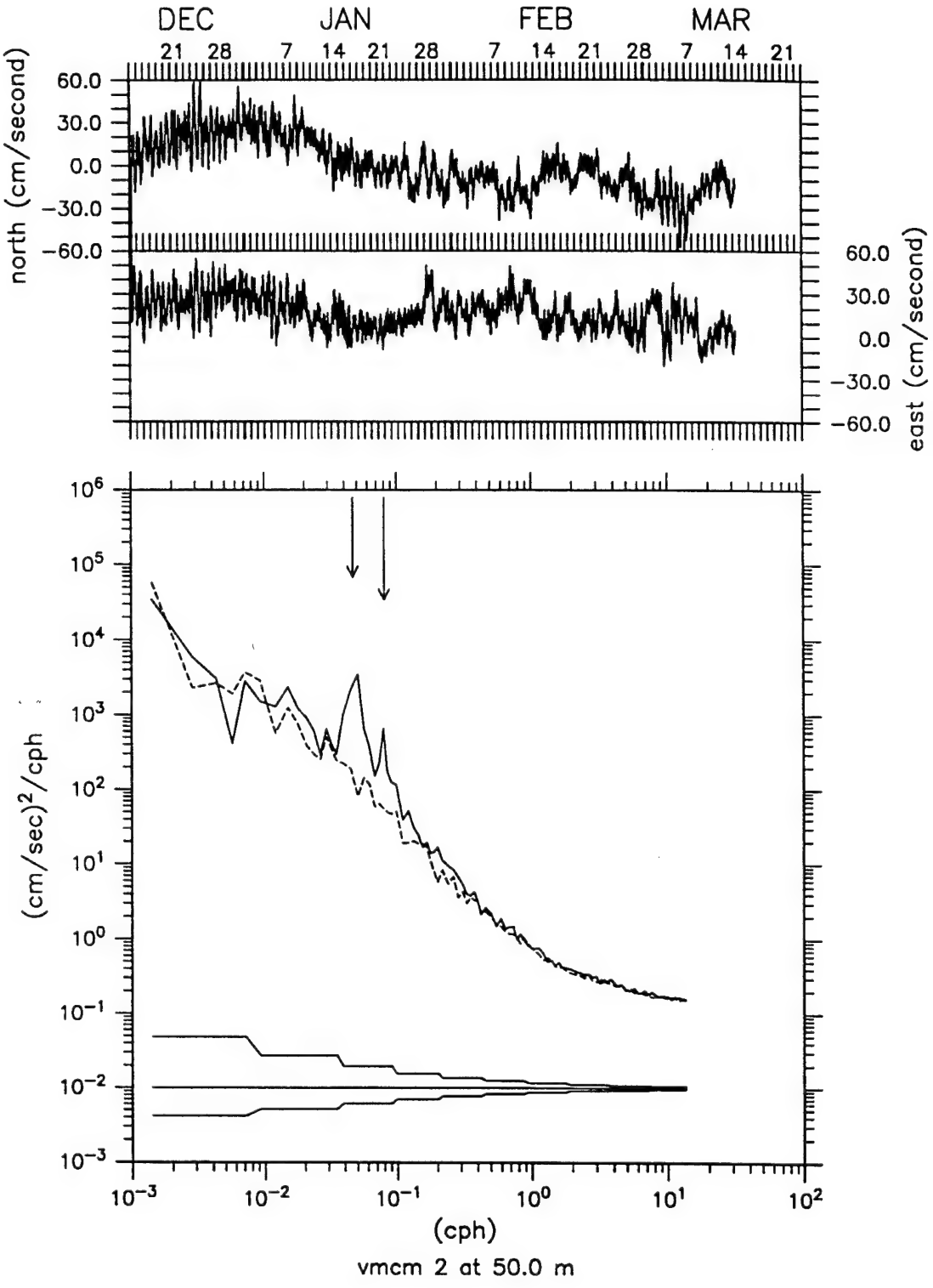

Figure 3.3.13: Velocity Time Series and Spectra at 50m. Solid curves show the clockwise component, and dashed curves show the counter-clockwise component. Long arrow indicates semi-diurnal tidal frequency, short arrow indicates Coriolis frequency.

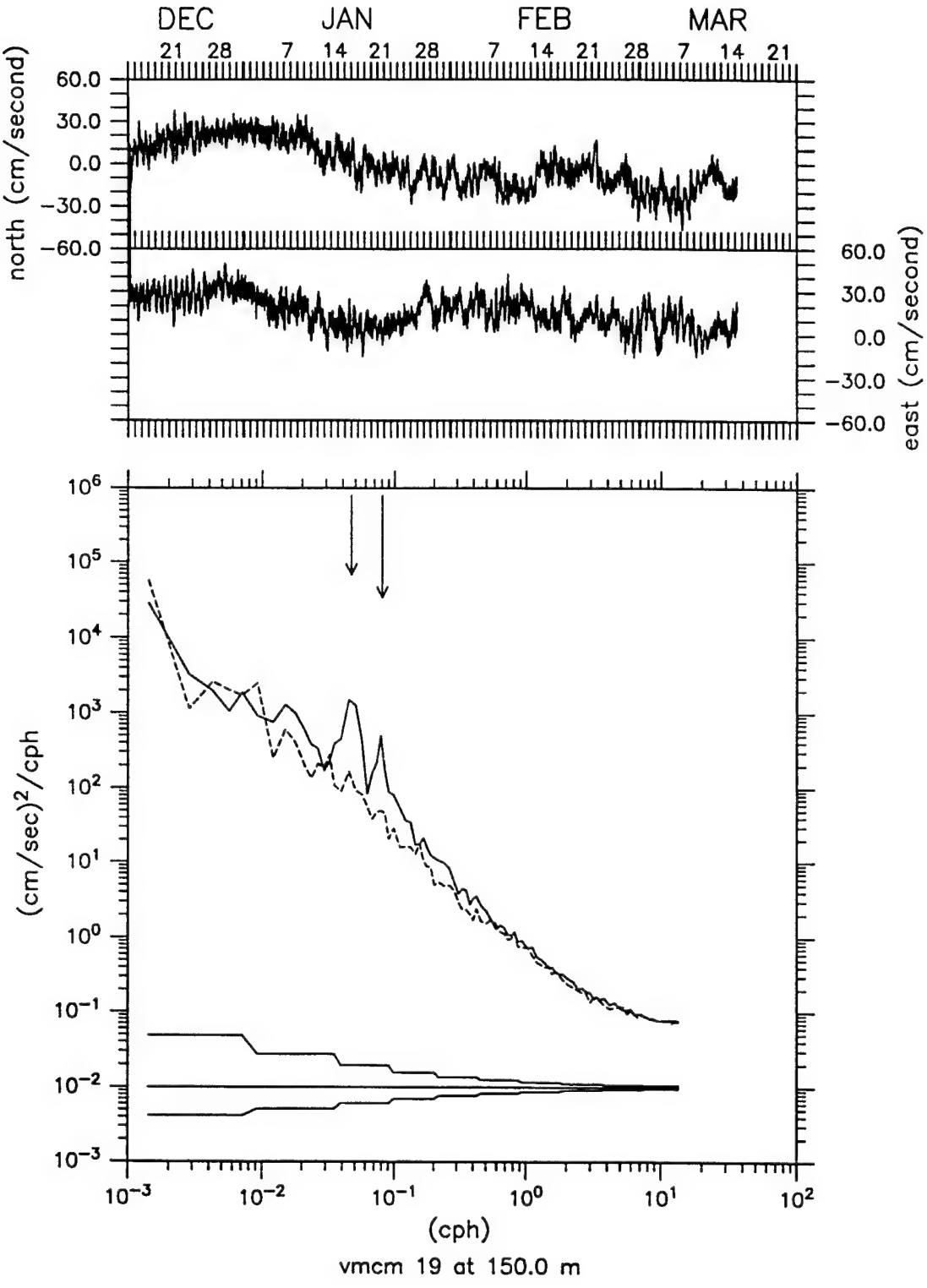

Figure 3.3.14: Velocity Time Series and Spectra at 150m. Solid curves show the clockwise component, and dashed curves show the counter-clockwise component. Long arrow indicates semi-diurnal tidal frequency, short arrow indicates Coriolis frequency.

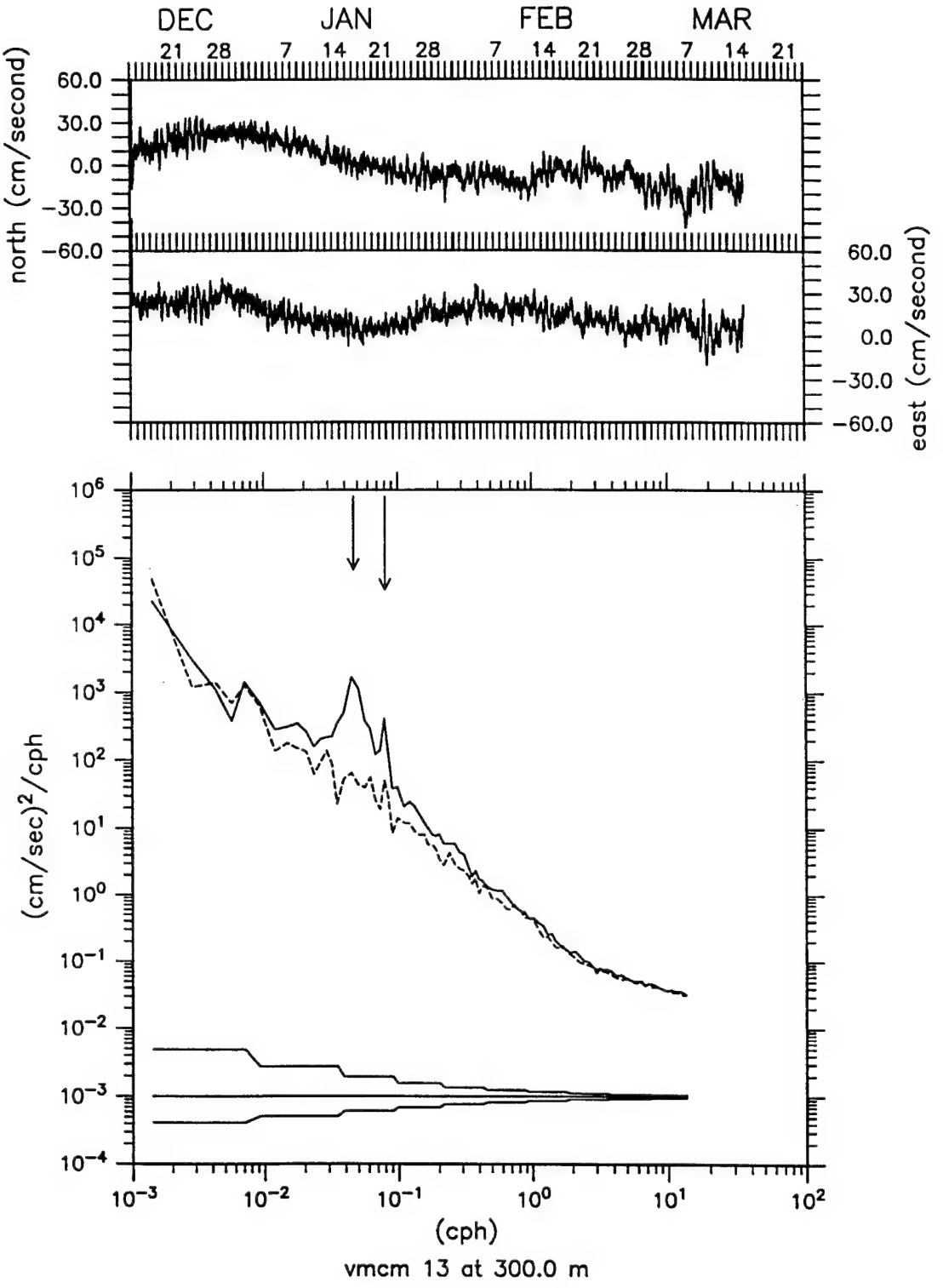

Figure 3.3.15: Velocity Time Series and Spectra at 300m. Solid curves show the clockwise component, and dashed curves show the counter-clockwise component. Long arrow indicates semi-diurnal tidal frequency, short arrow indicates Coriolis frequency.

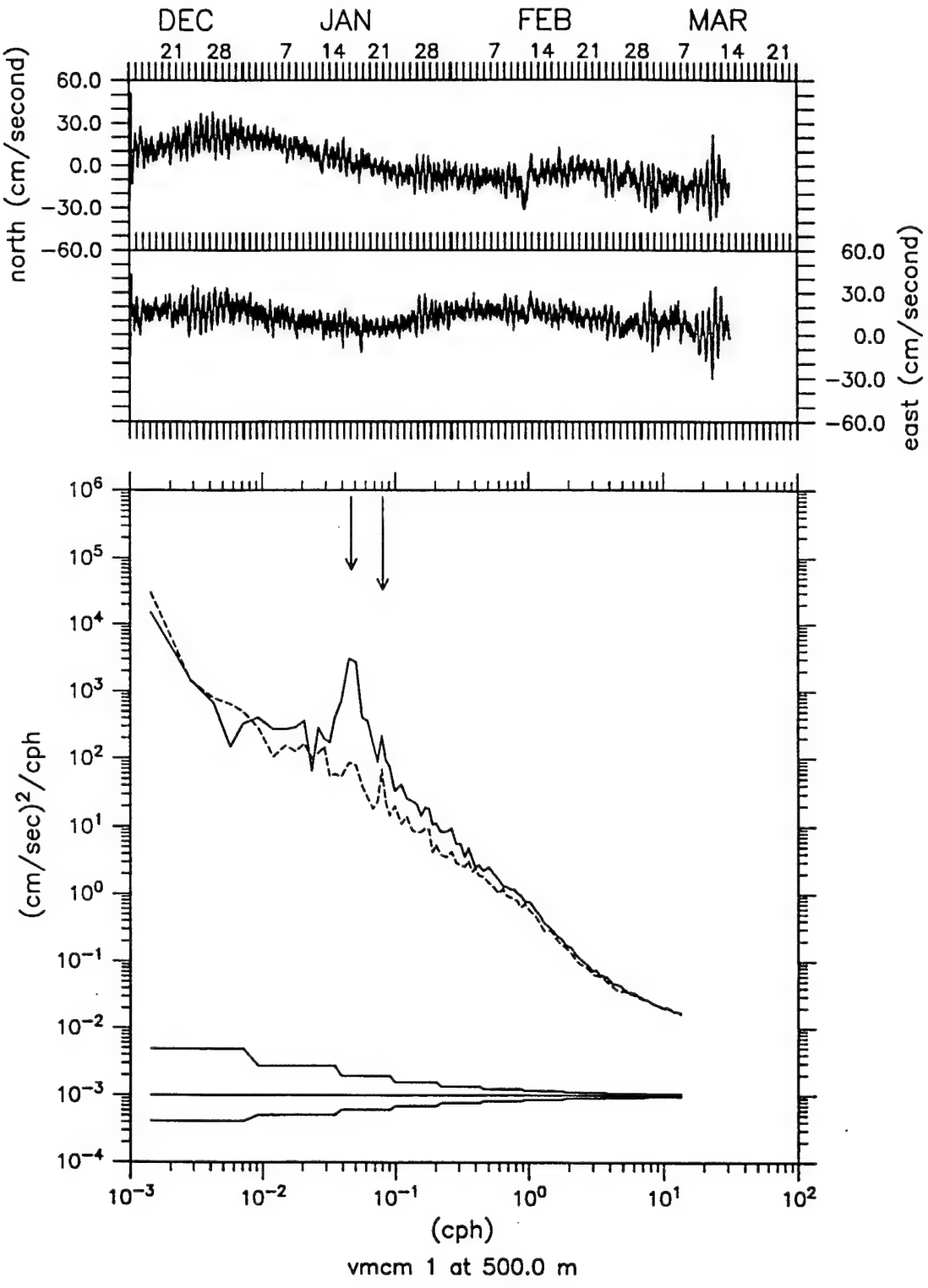

Figure 3.3.16: Velocity Time Series and Spectra at 500m. Solid curves show the clockwise component, and dashed curves show the counter-clockwise component. Long arrow indicates semi-diurnal tidal frequency, short arrow indicates Coriolis frequency.

3.4 Wave Measurements

3.4.1 Nondirectional Wave Parameters

Figures 3.4.1-3.4.3 shows time series of wave parameters measured from the Seatex buoy. The significant wave height and period were computed as follows. The interval between successive zero-up crossings of the sea-surface height was defined as corresponding to a single wave. The height of this wave was defined as the difference between the maximum and minimum surface heights. The period of the wave was defined as the time interval between the successive zero-up-crossings. The significant wave is defined as the height of the highest 1/3 of the waves. The significant wave period is the mean period of the highest 1/3 of the waves. The height of the largest wave seen during the 34 minute observing period is shown in the lower panel of each figure. During the deployment we see that the waves were in general quite large, with a peak significant height of 8.34 meters at 12Z on 2 March 94 . The largest wave seen during the entire deployment (12.7 meters in height) was seen earlier in the experiment (12Z on 26 Dec 93).

3.4.2 Spectral Evolution

Figures 3.4.4-3.4.6 show the evolution of the energy in the surface wave field as a function of frequency over the course of the ASREX III experiment. Contours are log10 spectral density. The heavy dashed lines show some of the clearly identifiable events corresponding to locally generated wind sea for which the frequency of the peak of the spectrum increases with time. The straight heavy solid lines show identifiable swell propagation events for which the frequency of the peak of the spectrum decreases with time.

Directional wave spectra were calculated using the Maximum Entropy Method of Lygre and Krogstad (1986). Corrections to the measured direction of orientation due to buoy tilt were calculated and applied. The tilts were then rotated into geographic coordinates. The spectra and cross-spectra of the heave and tilt were calculated with corrections being made for sensor response and buoy transfer function. The resulting heave and tilt spectra, quadrature spectrum of heave and north and east tilt, and cospectrum of north and east tilt were input to the Maximum Entropy routine of Lygre and Krogstad, and directional spectra were produced. The MATLAB code used to produce these spectra is given in Appendix 4. If the resulting spectra are integrated over frequency, one may get a sense of how the wave energy depends on direction. Figures 3.4.7-3.4.9 show contour plots of the wave energy as a function of direction. The plot shows the direction towards which the waves were propagating, with the wind direction superimposed. The directional distribution of wave energy in general reflects the wind direction, though there are some cases where there are differences. Figures 3.4.10–3.4.139 show the Seatex directional wave spectra. The wind direction is superimposed on each contour plot. No data was obtained from 03Z 8 February until 00Z 9 February or from 03Z 14 March to 00Z 15 March, due to tape write errors.

Acknowledgments

The Seatex moorings were designed by George Tupper. The moorings were fabricated in the WHOI rigging shop by David Simoneau. John Kemp of the Ocean Acoustics Laboratory supervised the mooring deployment and recovery, which was carried out with expert help from the crews of the R/V *Knorr* and R/V *Edwin Link*. We would like to acknowledge assistance from Seatex A/S during the course of the experiment. This work was supported by the Ocean Acoustics Program (Code 324OA) of the Office of Naval Research under contract N00014–91–J-1891.

References

Alados-Arboledas, L., J. Vida, and J. I. Jimenez, 1988. Effects of solar qradiation on the performance of pyrgeometers with silicon domes, *J. Atmos. Oceanic Tech.*, **5**:666-670.

Large, W. G. and S. Pond, 1981. Open ocean momentum flux measurements in moderate to strong winds. *J. Phys. Oceanogr.*, **11**:324–336.

Large, W. G. and S. Pond, 1982. Sensible and latent heat flux measurements over the ocean. *J. Phys. Oceanogr.*, **12**:464-482.

Lygre A., and H. E. Krogstad, 1986. Maximum Entropy Estimation of the Directional Distribution in Ocean Wave Spectra, *J. Phys. Oceanogr.*, **16**:2052-2060.

McDaniel, S. T., 1993. Sea surface reverberation: A review, *J. Acous. Soc. Am.*, **94**:1905-1922.

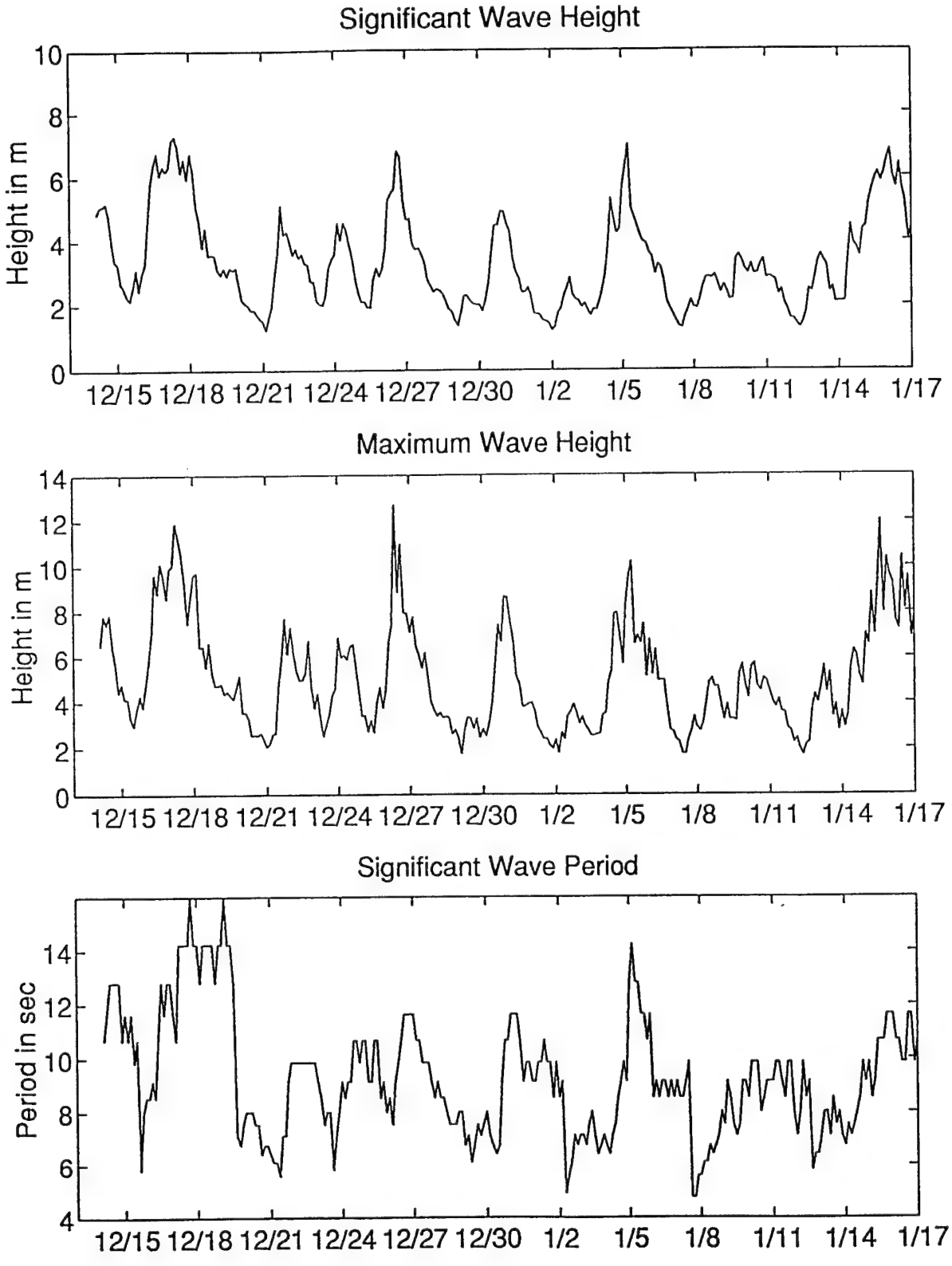

Figure 3.4.1: Nondirectional wave parameters. Significant wave height, maximum wave height, and significant wave period.

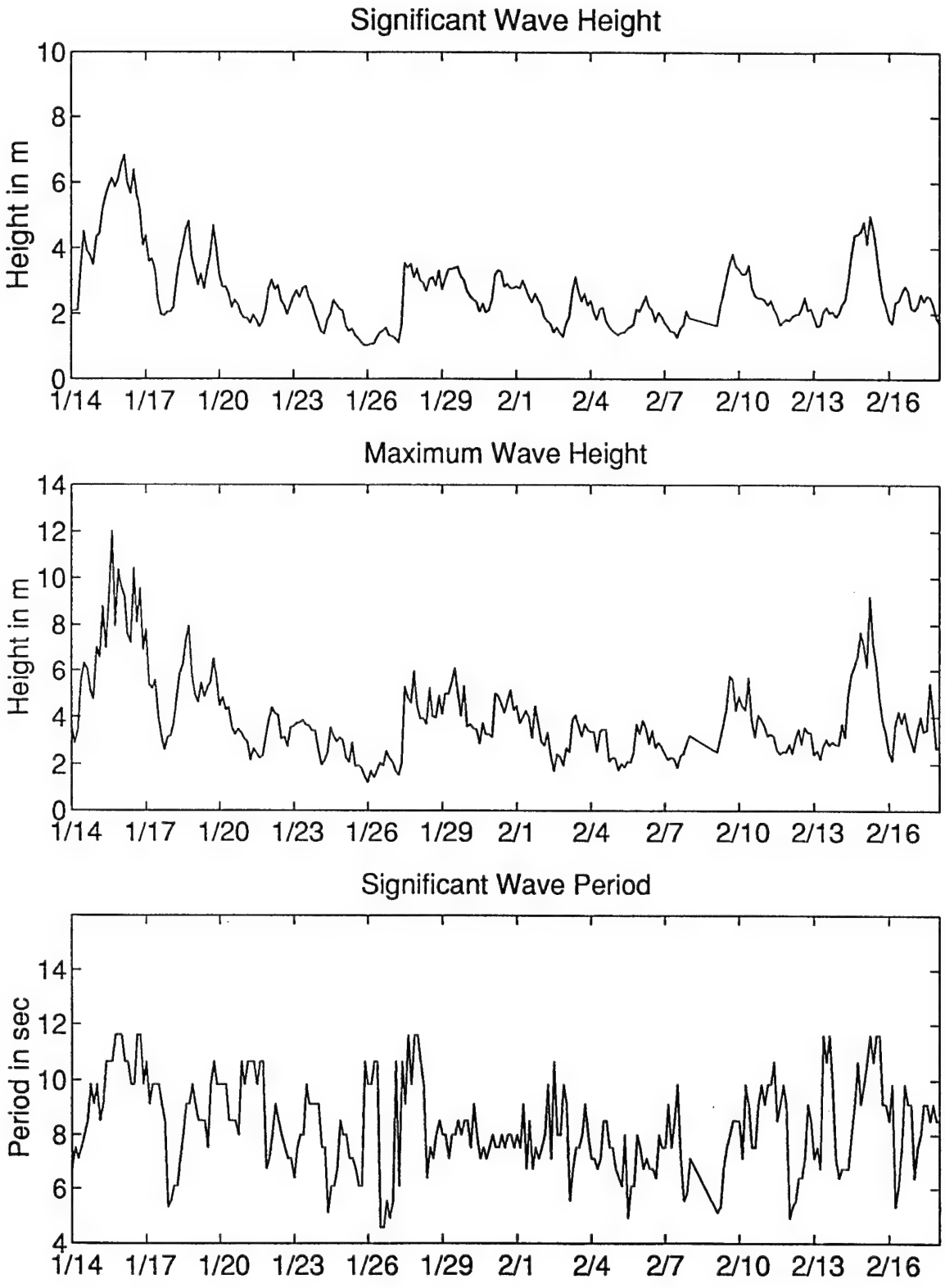

Figure 3.4.2: Nondirectional wave parameters. Significant wave height, maximum wave height, and significant wave period.

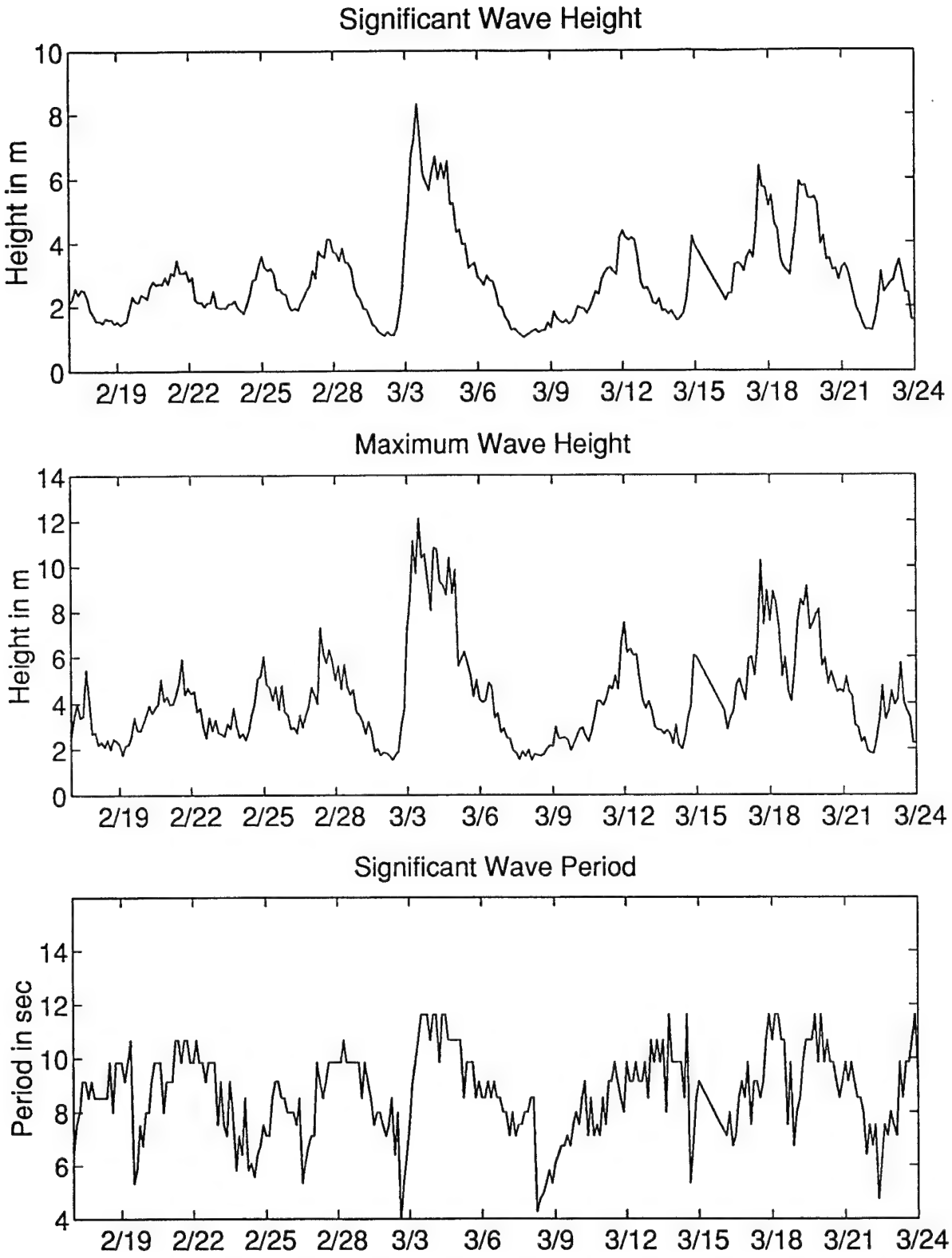

Figure 3.4.3: Nondirectional wave parameters. Significant wave height, maximum wave height, and significant wave period.

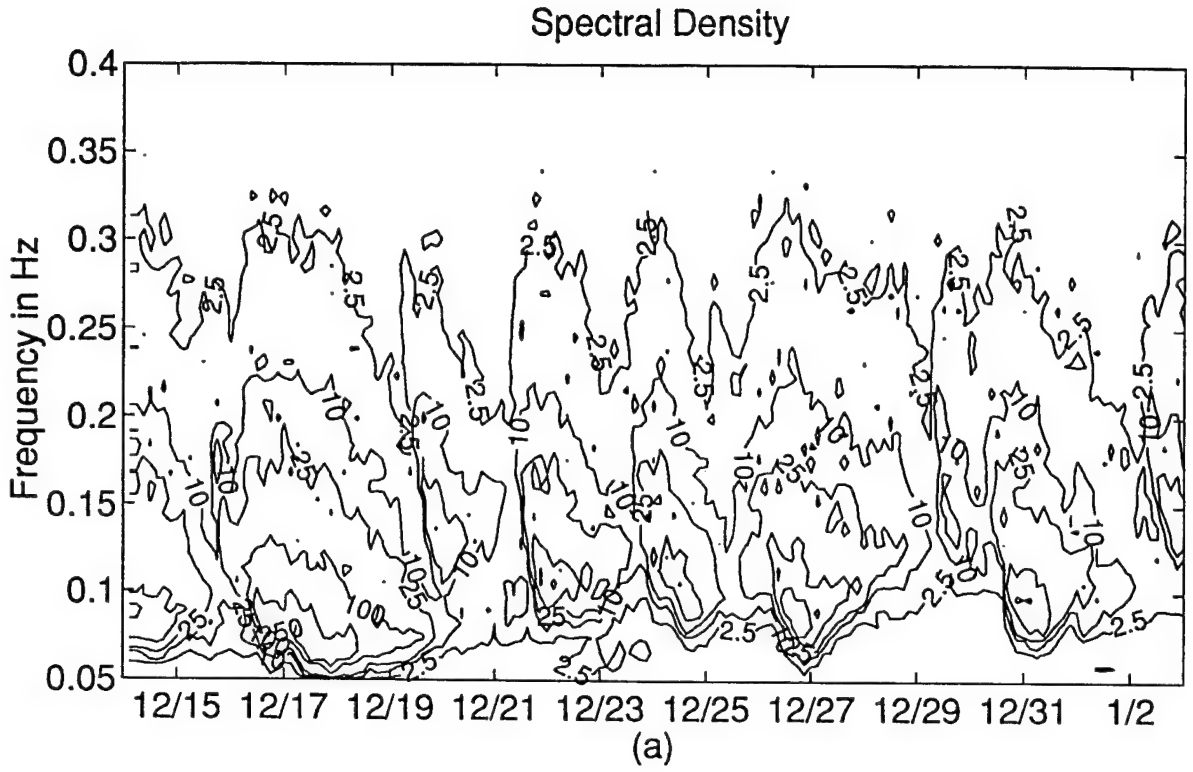

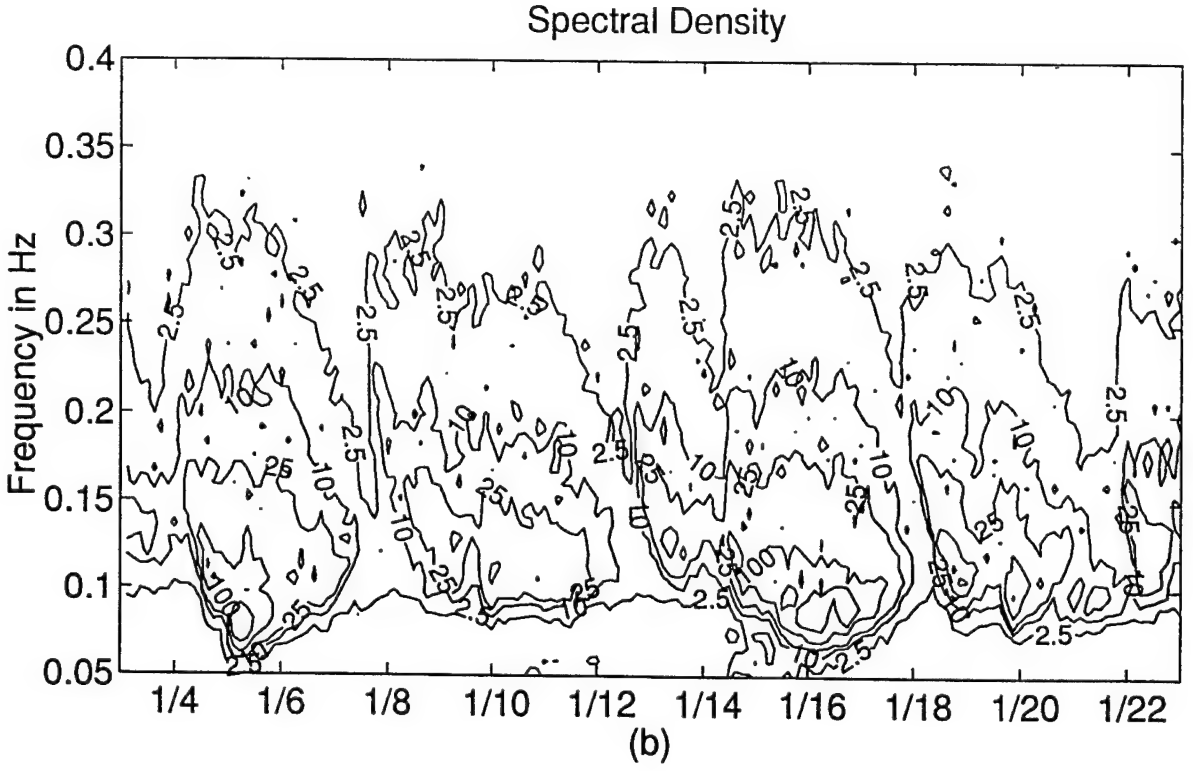

Figure 3.4.4: Spectral evolution of the surface waves. Contours of spectral density as a function of frequency over time. Contours are 2.5, 10, 25, 100, 250.

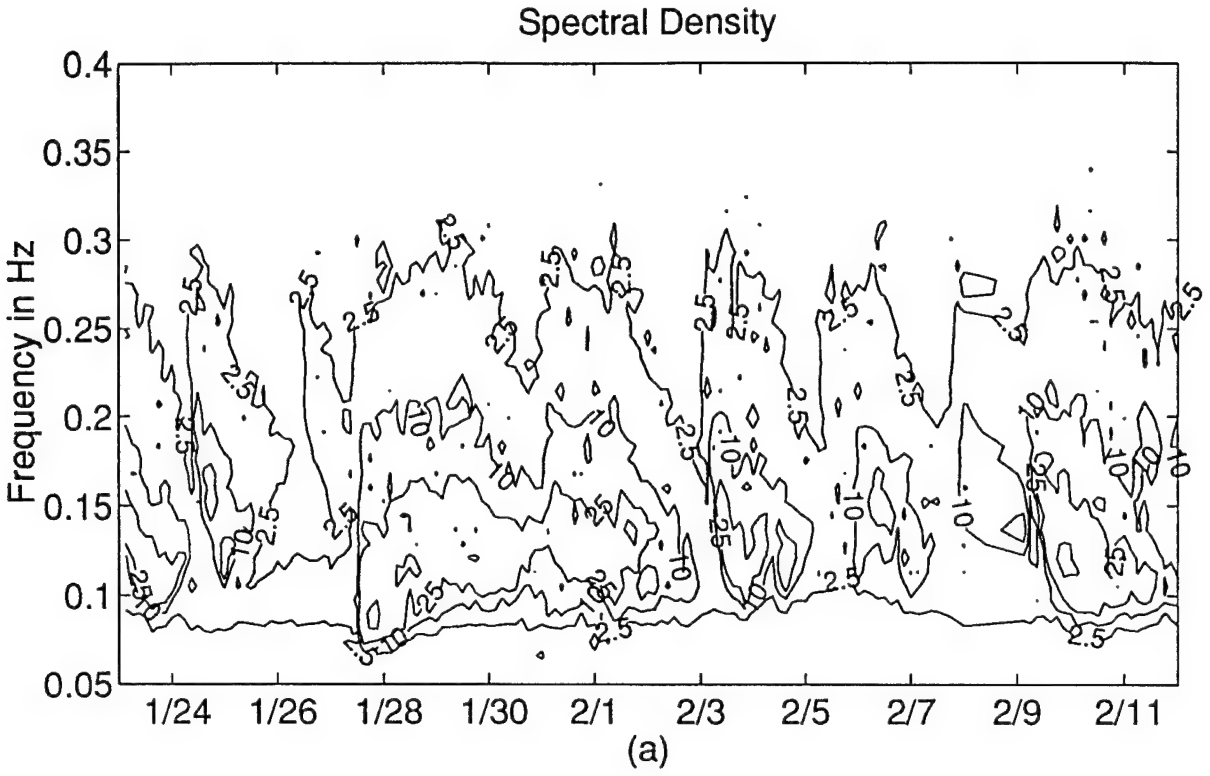

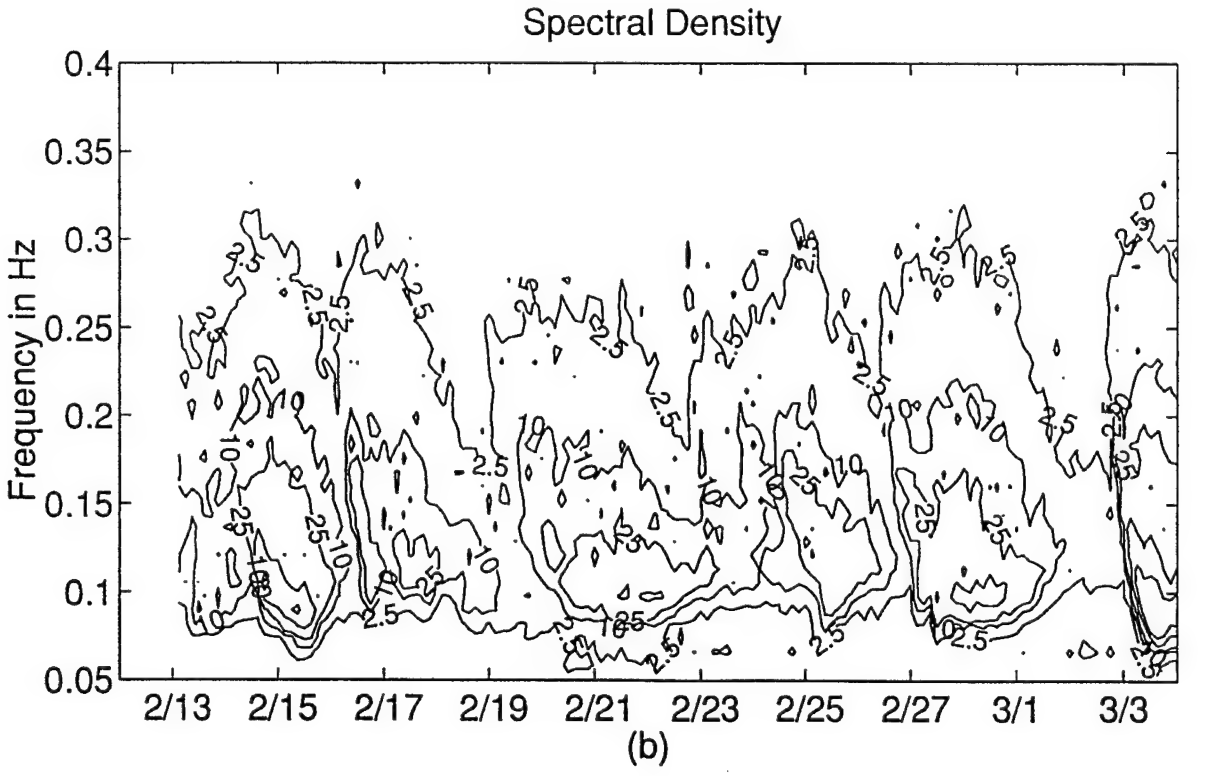

Figure 3.4.5: Spectral evolution of the surface waves. Contours of spectral density as a function of frequency over time. Contours ar 2.5, 10, 25, 100, 250.

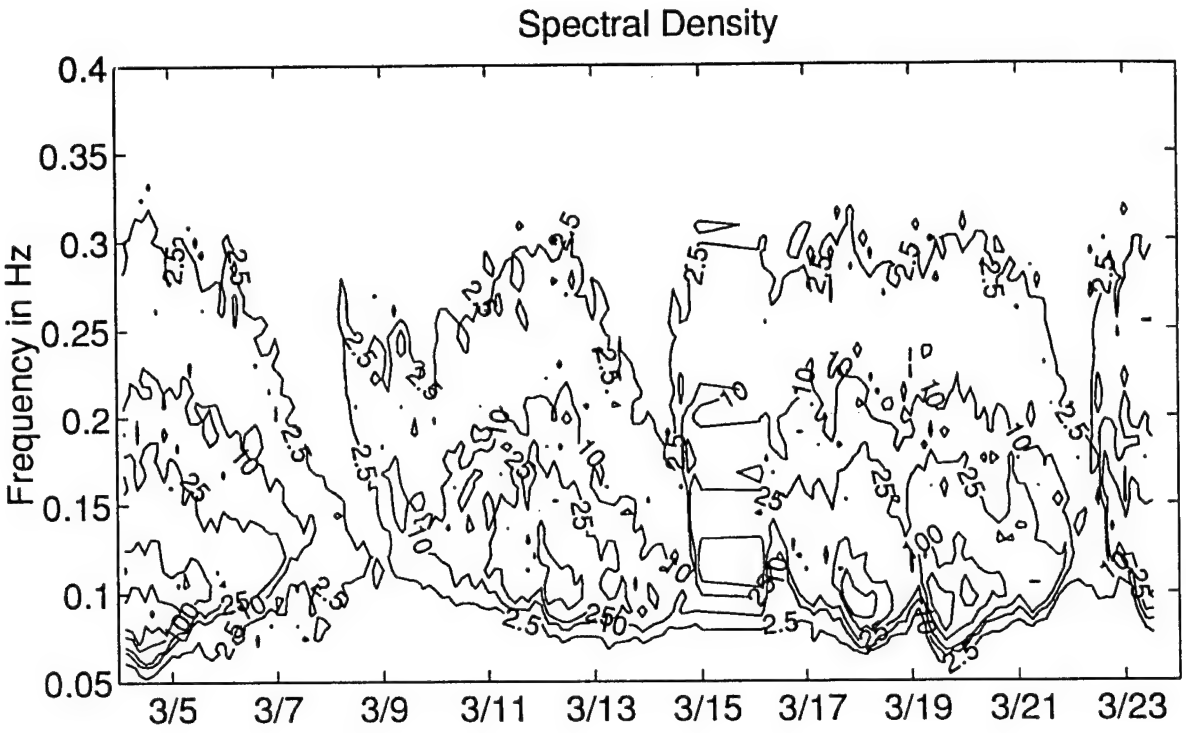

Figure 3.4.6: Spectral evolution of the surface waves. Contours of spectral density as a function of frequency over time. Contours are 2.5, 10, 25, 100, 250.

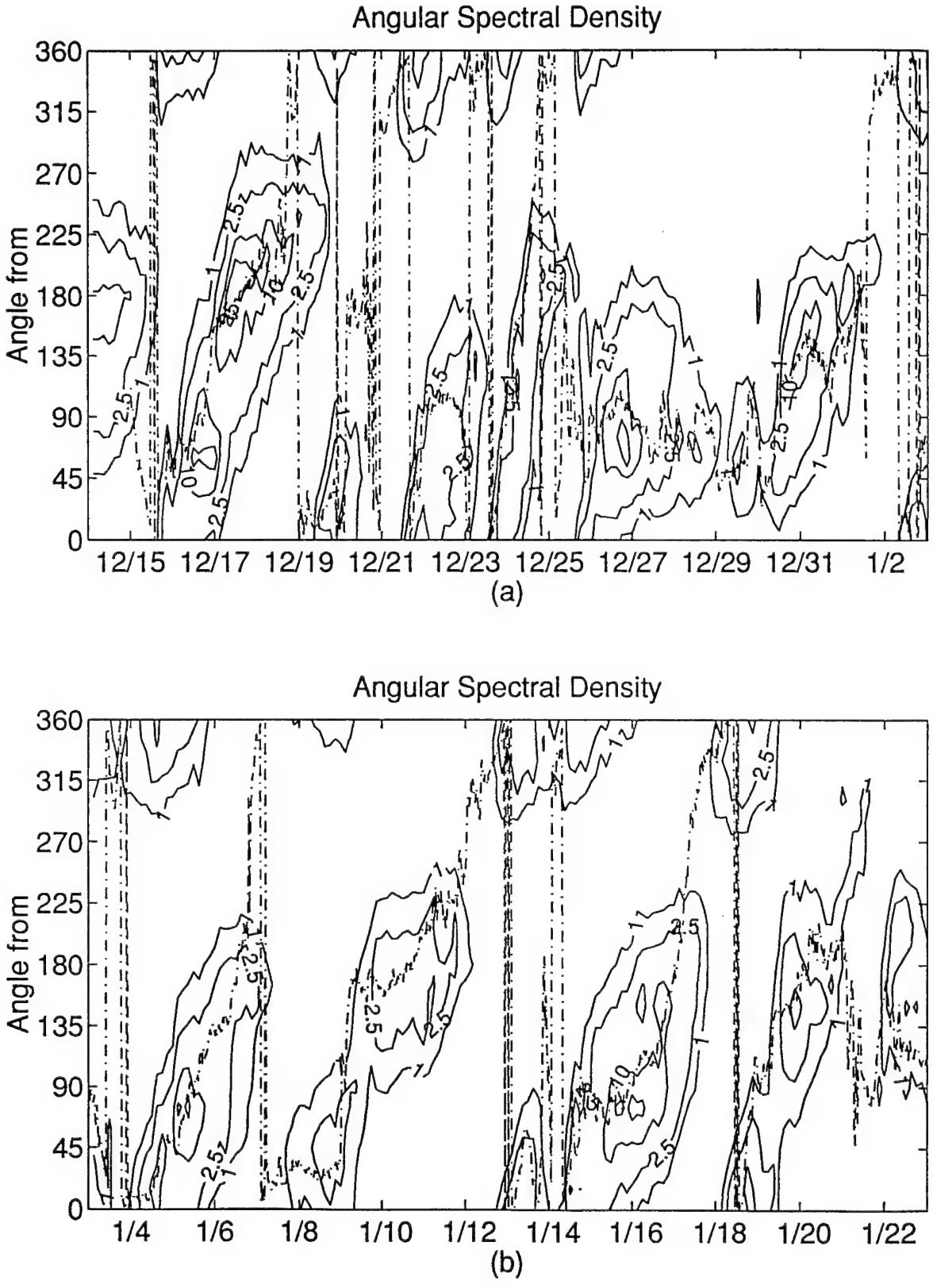

Figure 3.4.7: Directional evolution of the surface waves. Contours of spectral density as a function of direction. Contours are 1, 2.5, 10, 25, 100, and 250. Wind direction is shown by chain-dot line.

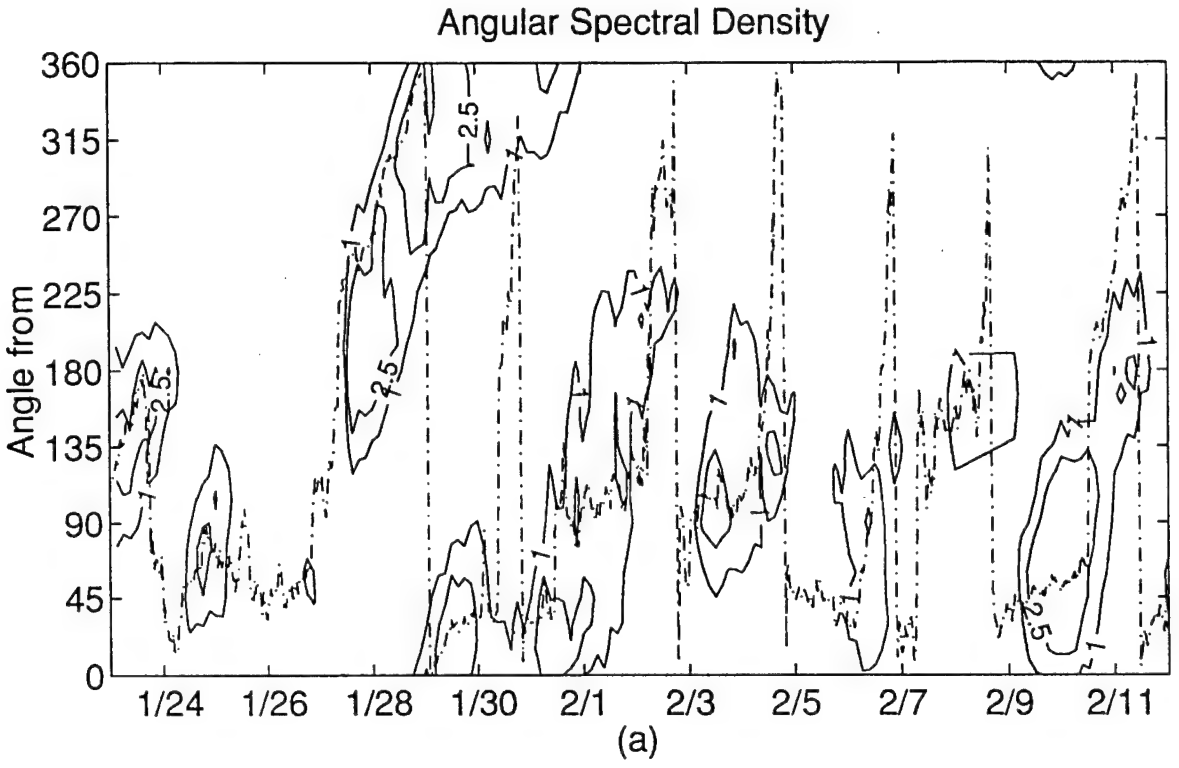

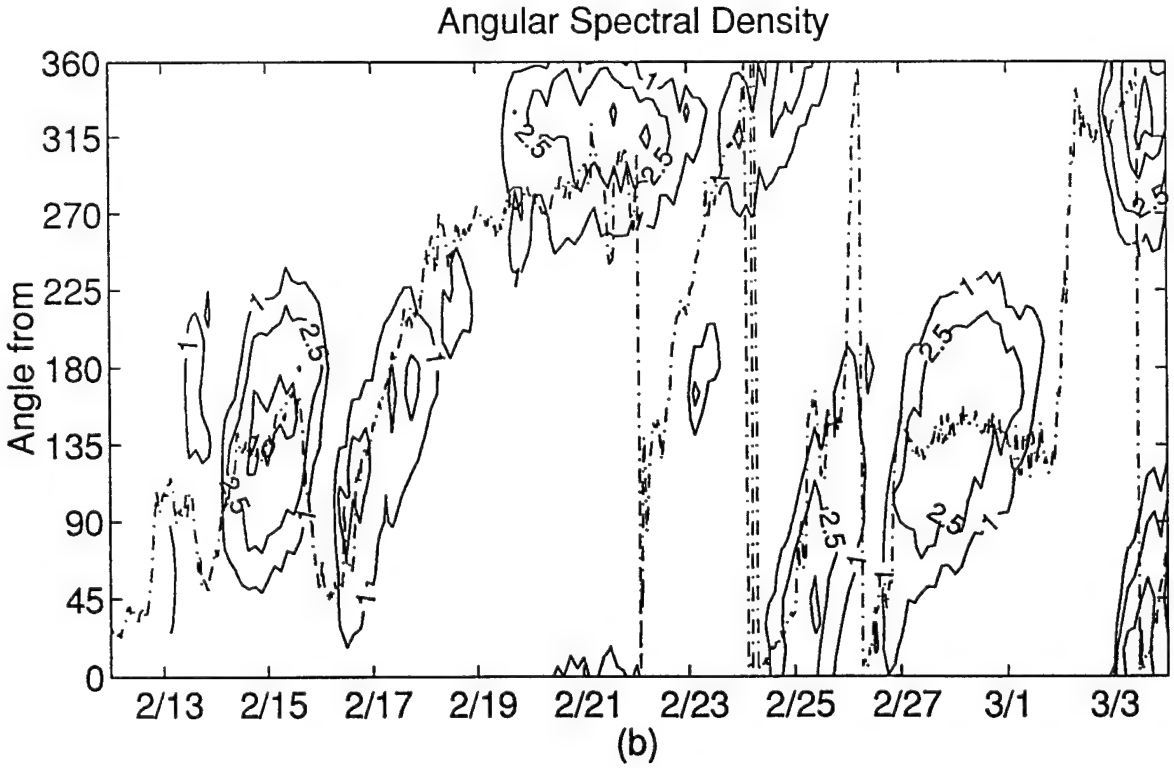

Figure 3.4.8: Directional evolution of the surface waves. Contours of spectral density as a function of direction. Contours are 1, 2.5, 10, 25, 100, and 250. Wind direction is shown by chain-dot line.

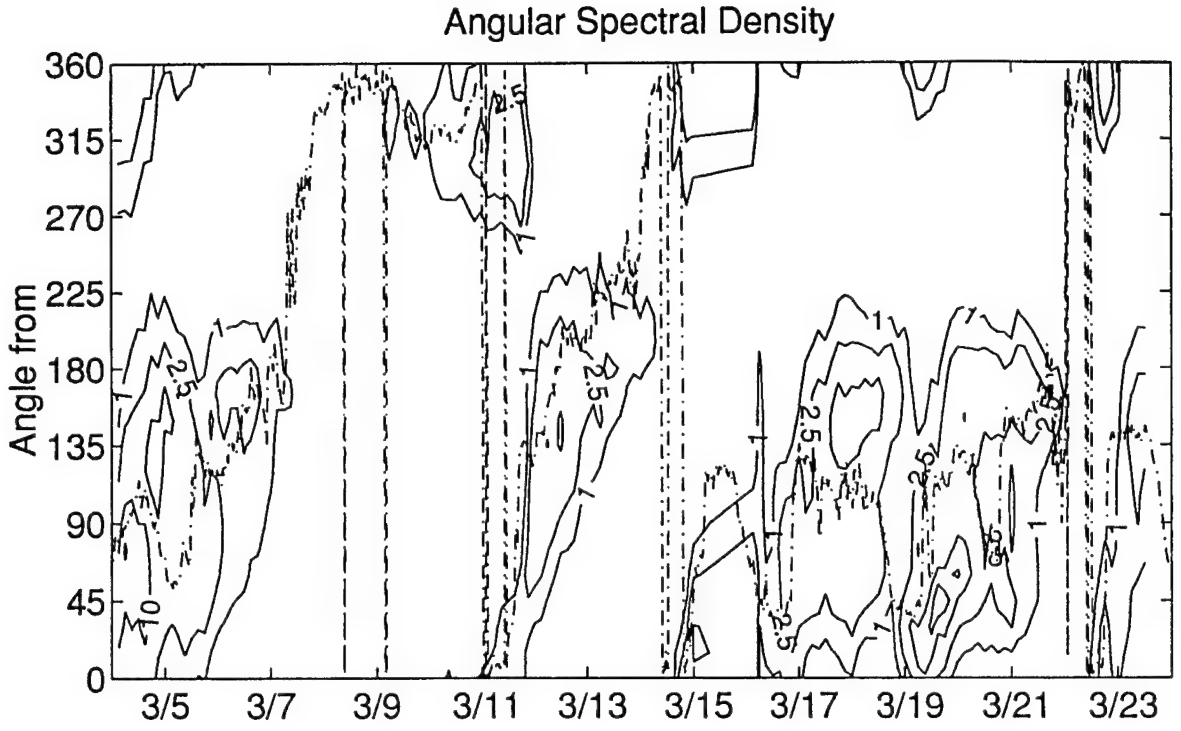

Figure 3.4.9: Directional evolution of the surface waves. Contours of spectral density as a function of direction. Contours are 1, 2.5, 10, 25, 100, and 250. Wind direction is shown by chain-dot line.

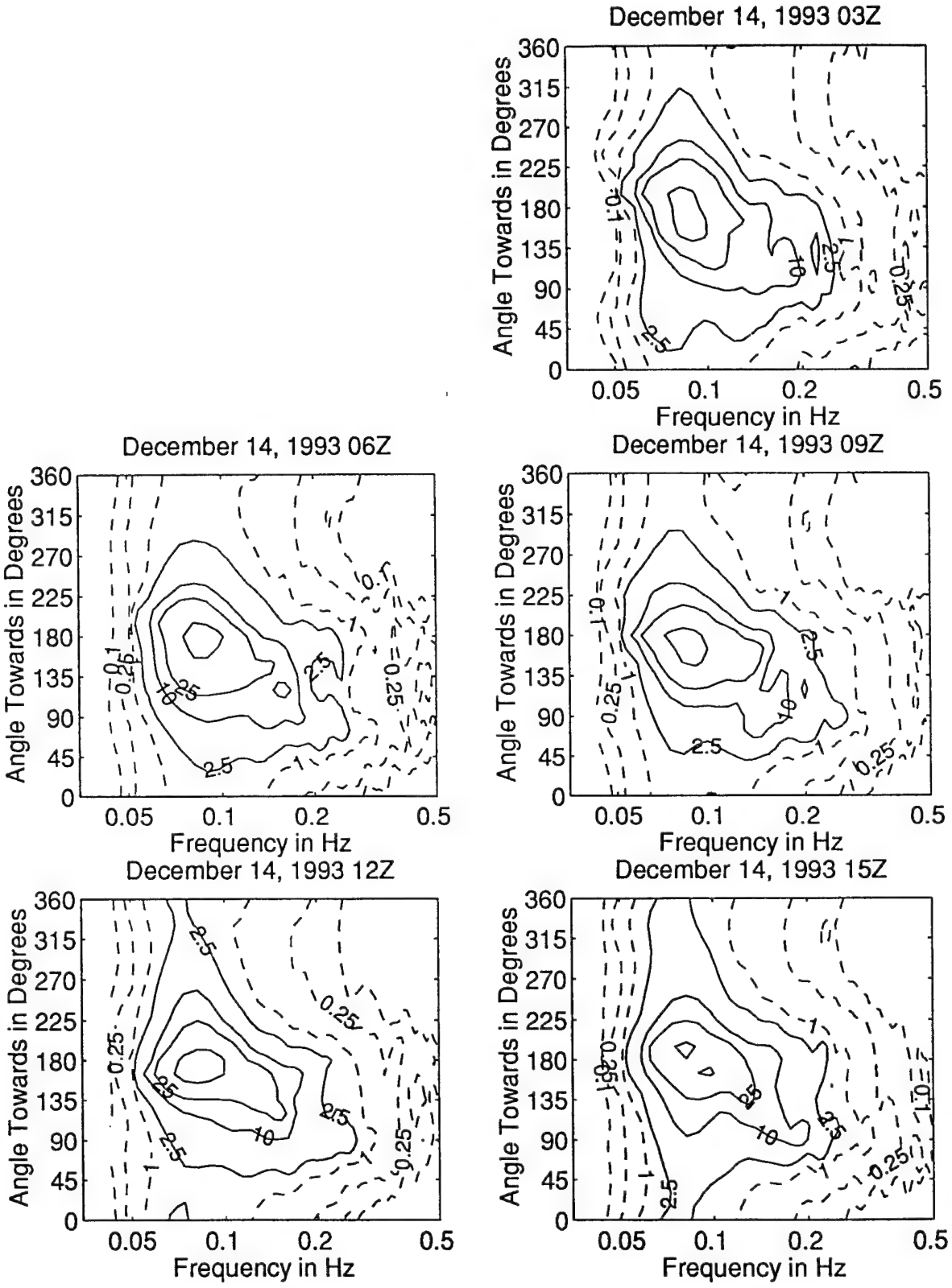

Figure 3.4.10: Directional wave spectra, computed using maximum entropy method. Contours of spectral density as a function of direction. Contours are 0.1, 0.25, 1 (dashed), 2.5, 10, 25, 100, and 250 (solid). Wind direction is shown by thick dashed line.

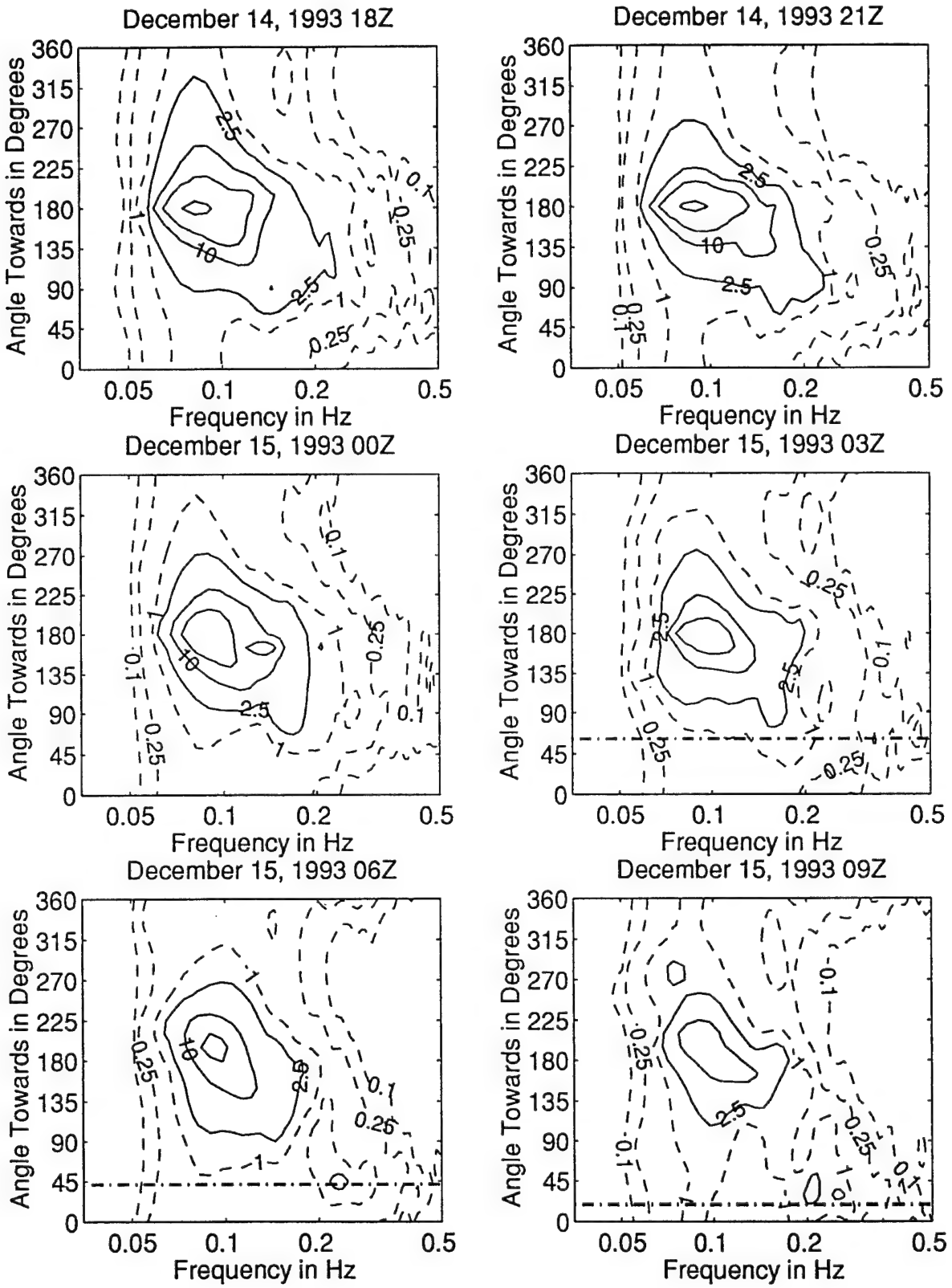

Figure 3.4.11: Directional wave spectra, computed using maximum entropy method. Contours of spectral density as a function of direction. Contours are 0.1, 0.25, 1 (dashed), 2.5, 10, 25, 100, and 250 (solid). Wind direction is shown by thick dashed line.

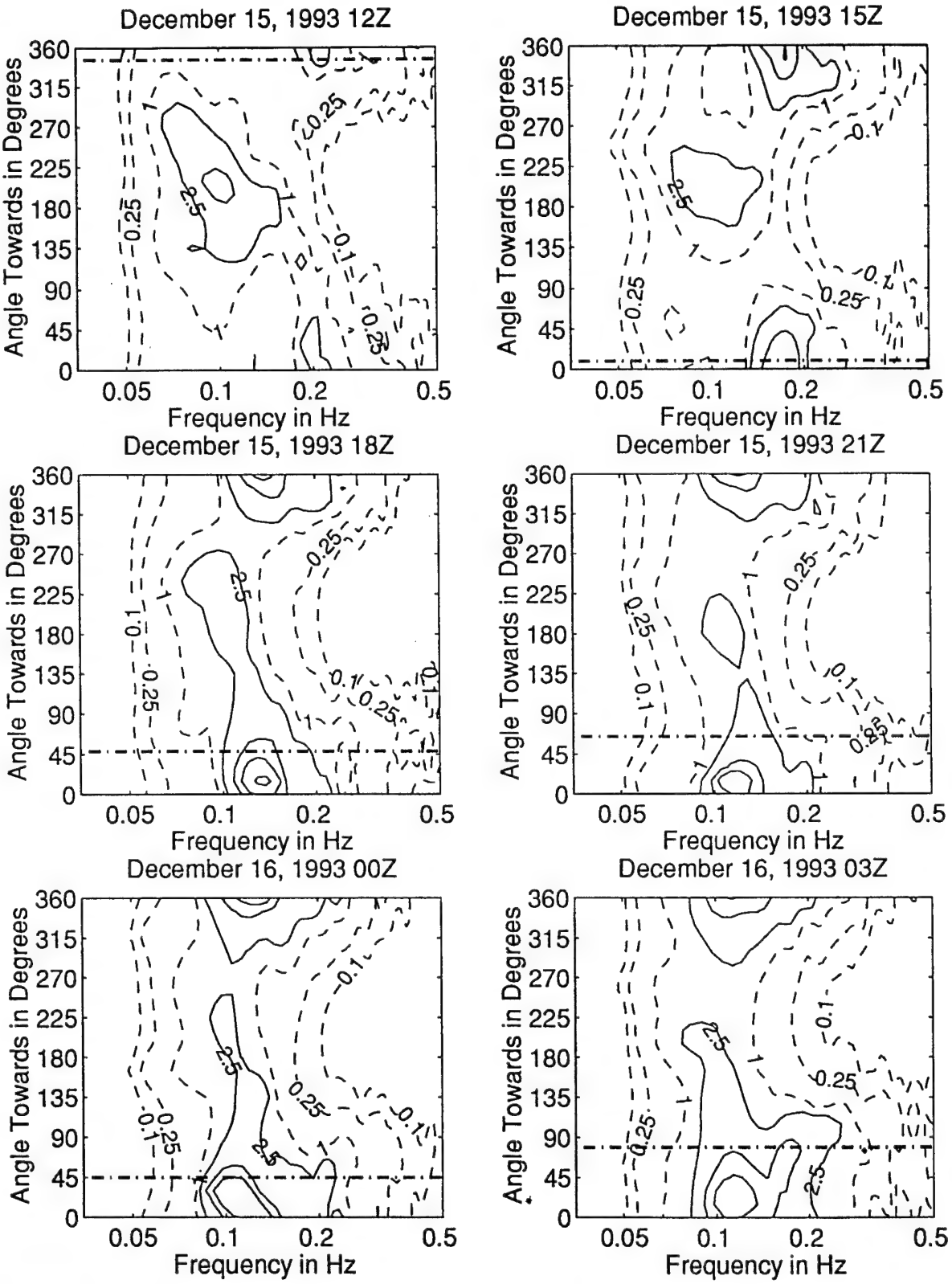

Figure 3.4.12: Directional wave spectra, computed using maximum entropy method. Contours of spectral density as a function of direction. Contours are 0.1, 0.25, 1 (dashed), 2.5, 10, 25, 100, and 250 (solid). Wind direction is shown by thick dashed line.

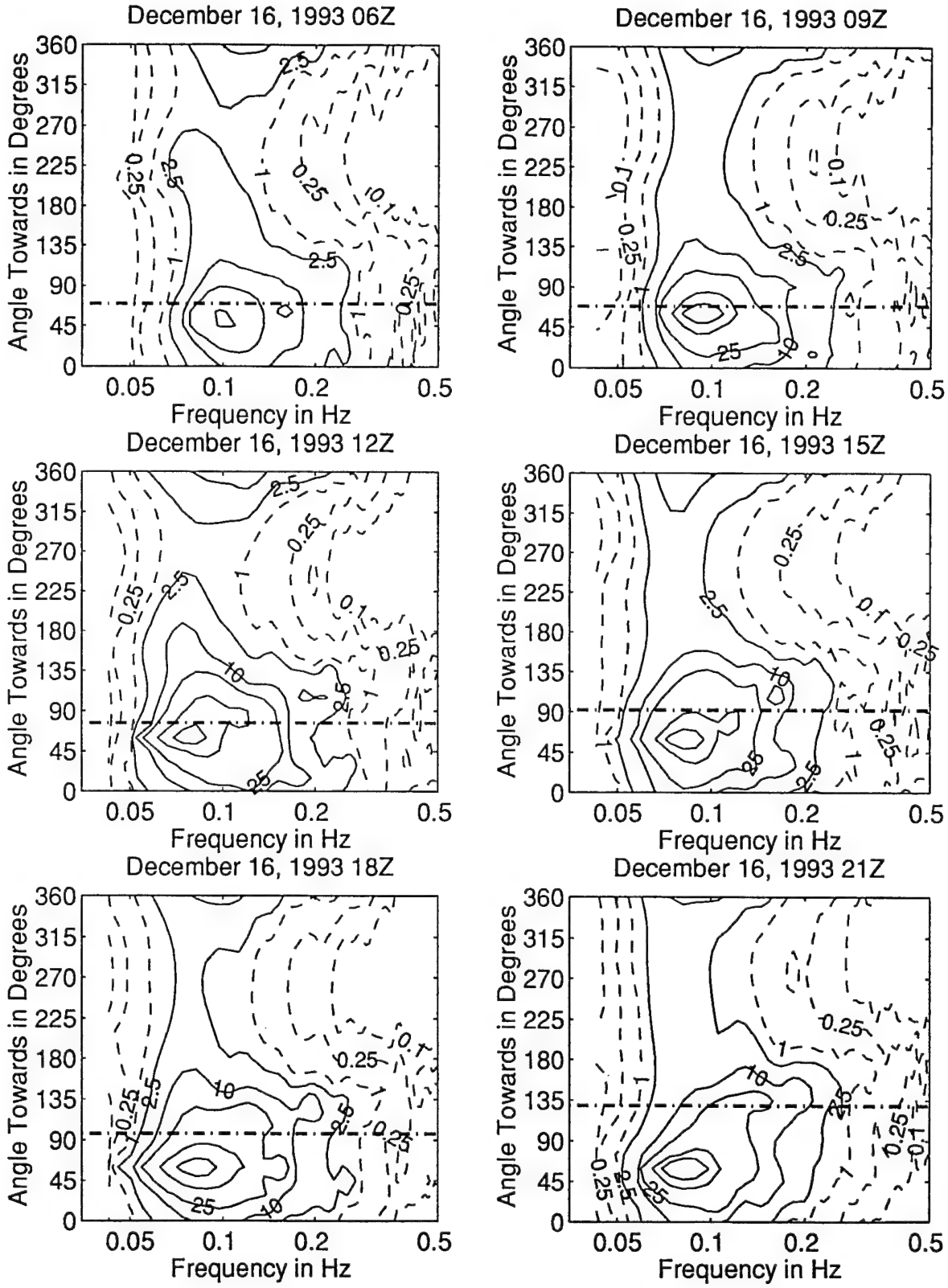

Figure 3.4.13: Directional wave spectra, computed using maximum entropy method. Contours of spectral density as a function of direction. Contours are 0.1, 0.25, 1 (dashed), 2.5, 10, 25, 100, and 250 (solid). Wind direction is shown by thick dashed line.

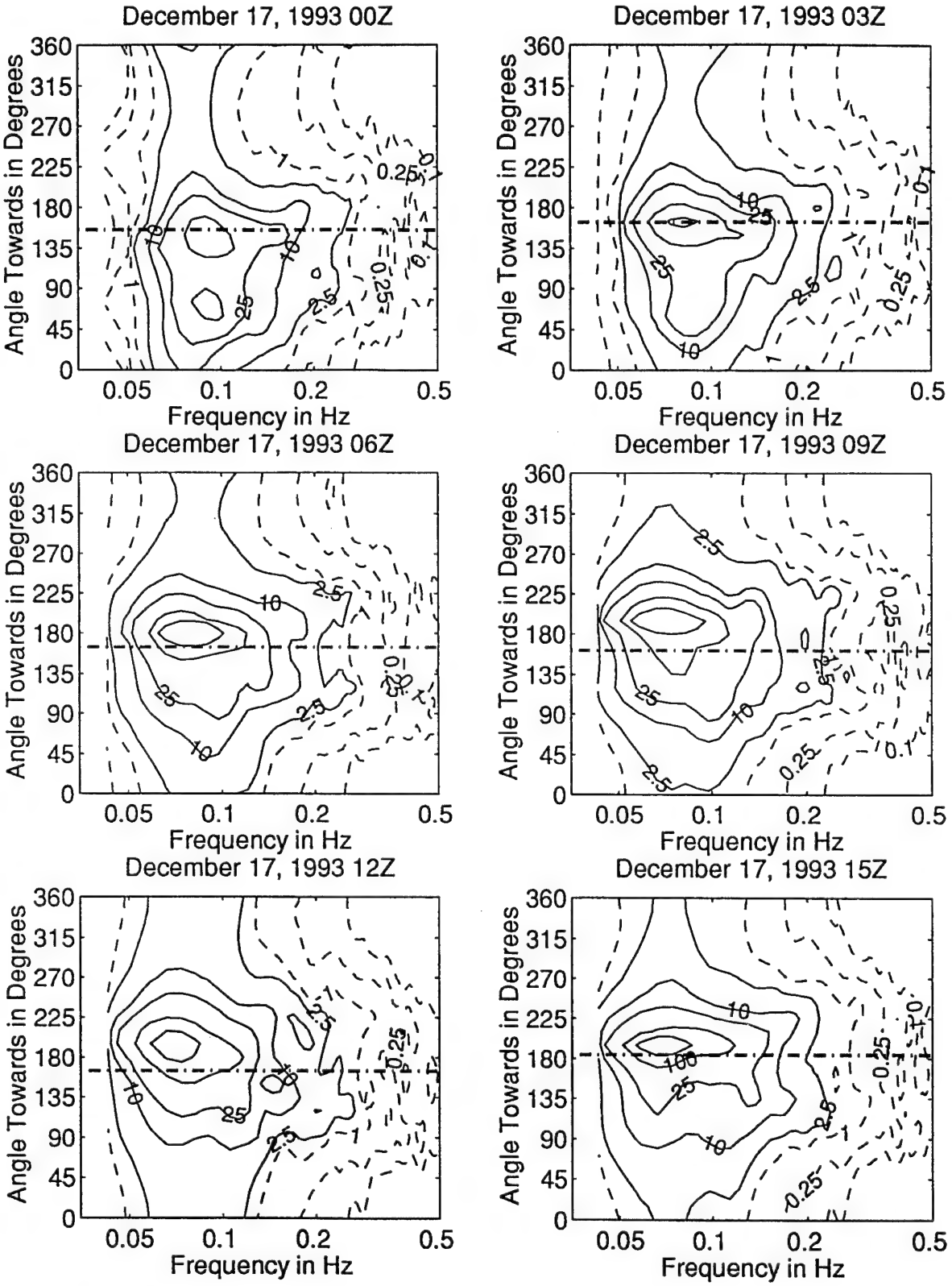

Figure 3.4.14: Directional wave spectra, computed using maximum entropy method. Contours of spectral density as a function of direction. Contours are 0.1, 0.25, 1 (dashed), 2.5, 10, 25, 100, and 250 (solid). Wind direction is shown by thick dashed line.

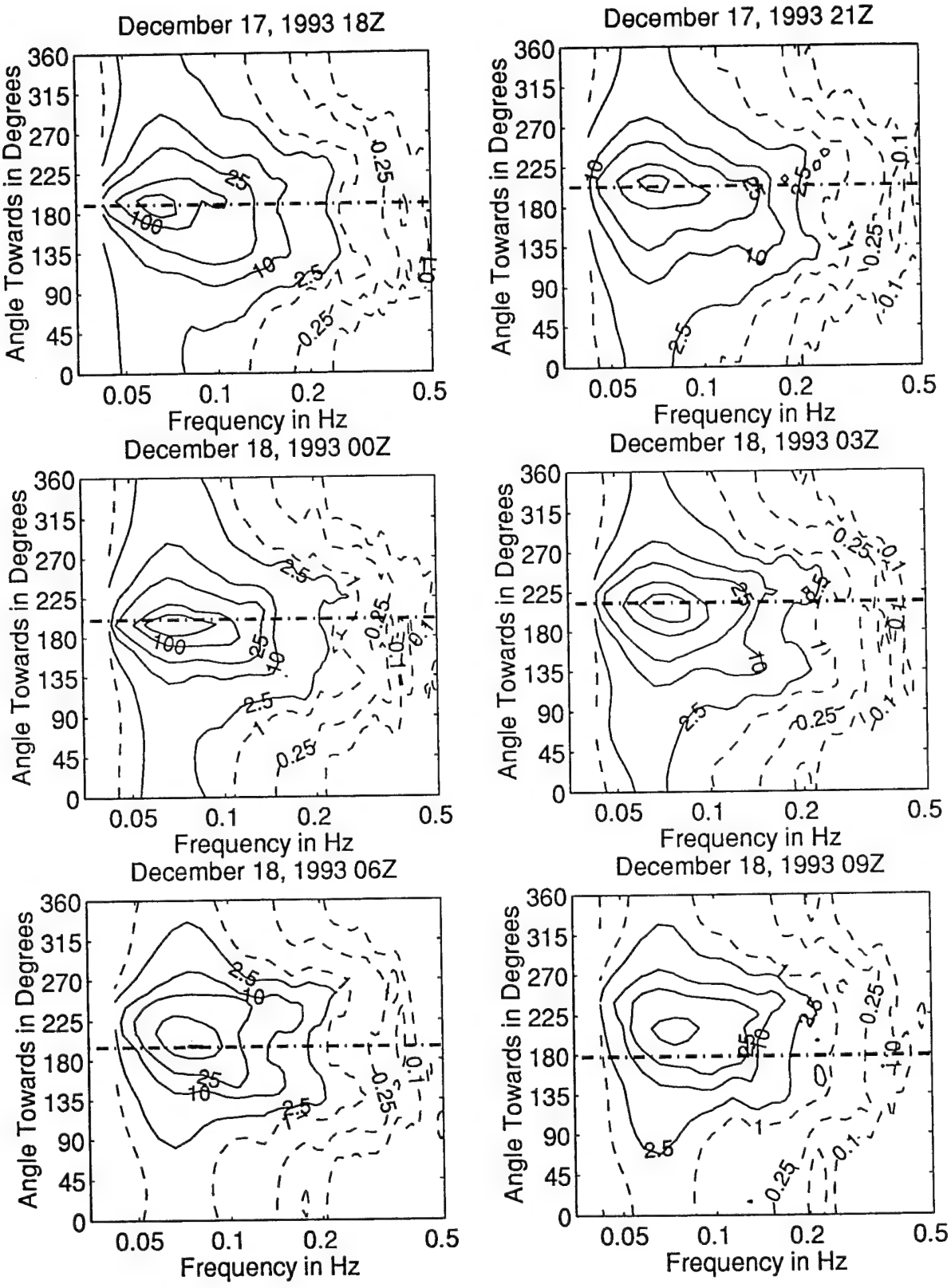

Figure 3.4.15: Directional wave spectra, computed using maximum entropy method. Contours of spectral density as a function of direction. Contours are 0.1, 0.25, 1 (dashed), 2.5, 10, 25, 100, and 250 (solid). Wind direction is shown by thick dashed line.

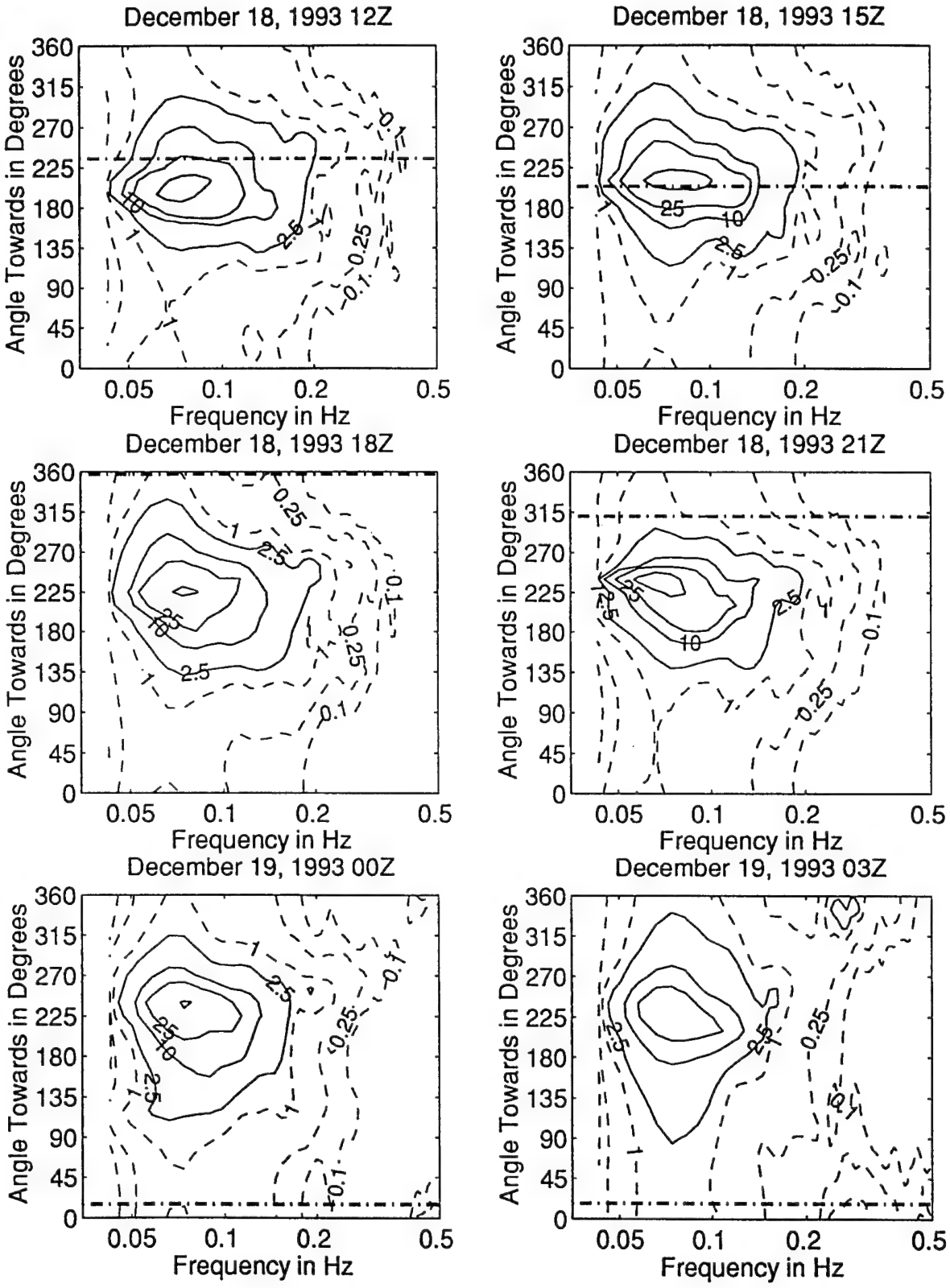

Figure 3.4.16: Directional wave spectra, computed using maximum entropy method. Contours of spectral density as a function of direction. Contours are 0.1, 0.25, 1 (dashed), 2.5, 10, 25, 100, and 250 (solid). Wind direction is shown by thick dashed line.

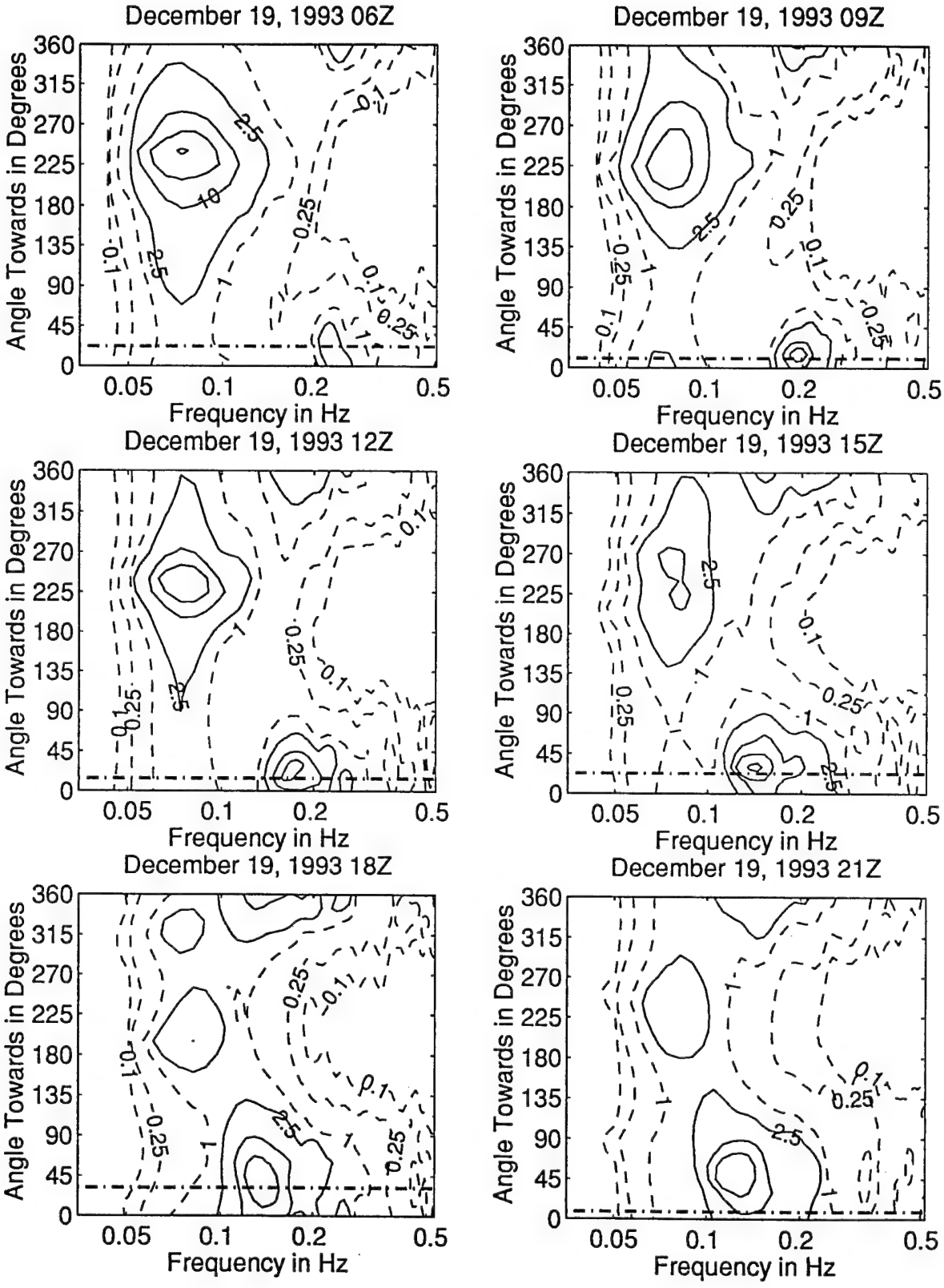

Figure 3.4.17: Directional wave spectra, computed using maximum entropy method. Contours of spectral density as a function of direction. Contours are 0.1, 0.25, 1 (dashed), 2.5, 10, 25, 100, and 250 (solid). Wind direction is shown by thick dashed line.

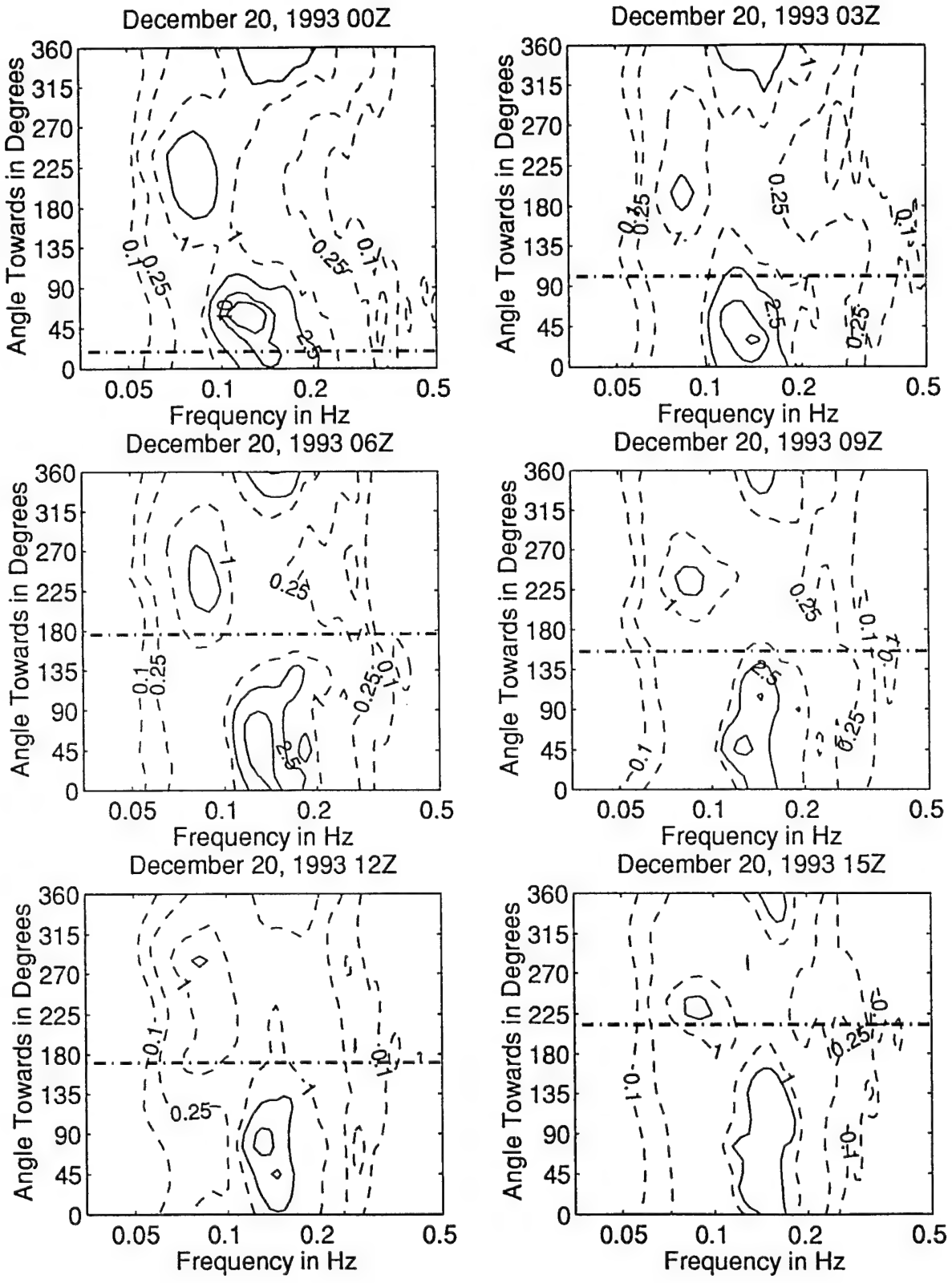

Figure 3.4.18: Directional wave spectra, computed using maximum entropy method. Contours of spectral density as a function of direction. Contours are 0.1, 0.25, 1 (dashed), 2.5, 10, 25, 100, and 250 (solid). Wind direction is shown by thick dashed line.

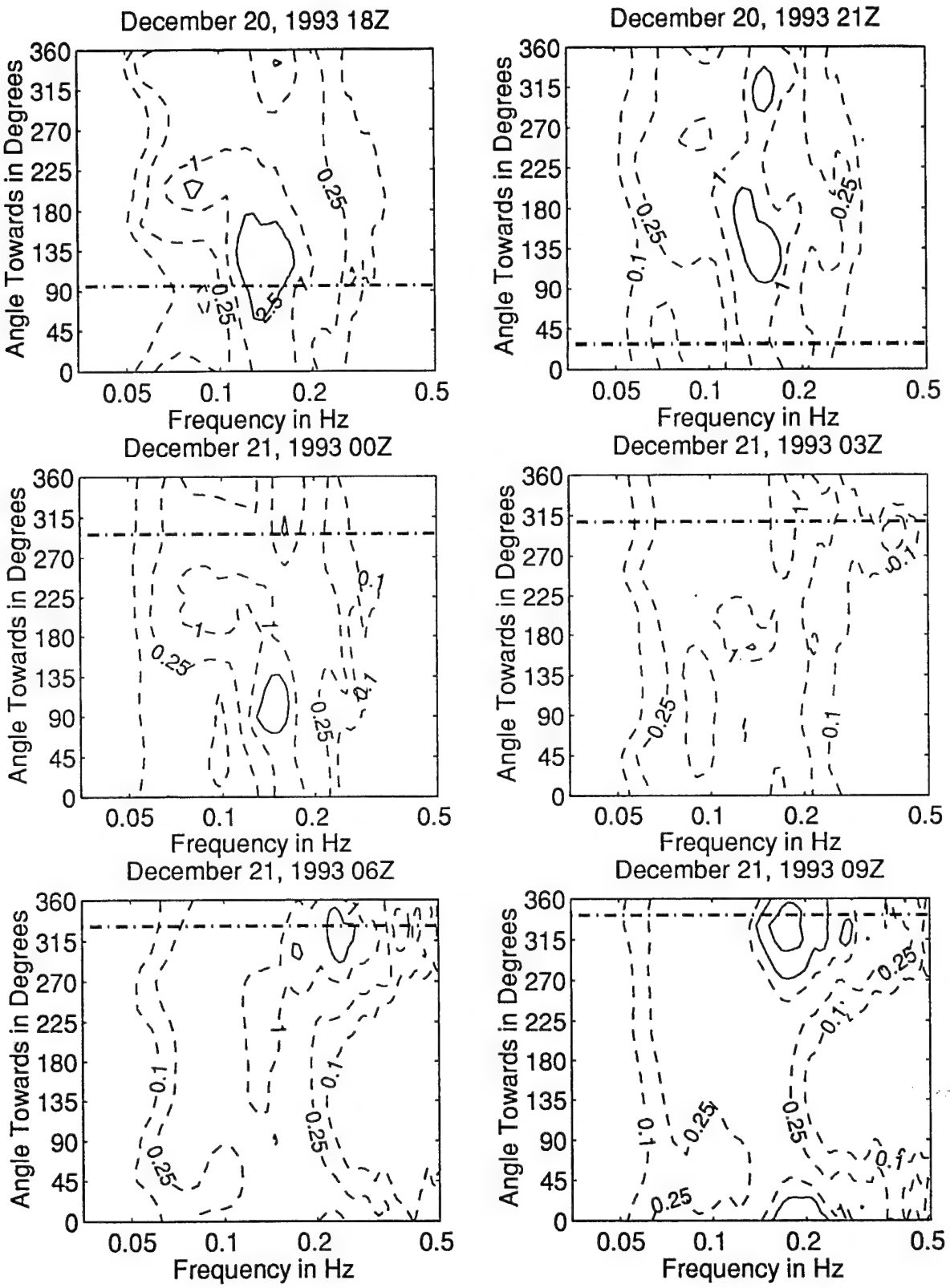

Figure 3.4.19: Directional wave spectra, computed using maximum entropy method. Contours of spectral density as a function of direction. Contours are 0.1, 0.25, 1 (dashed), 2.5, 10, 25, 100, and 250 (solid). Wind direction is shown by thick dashed line.

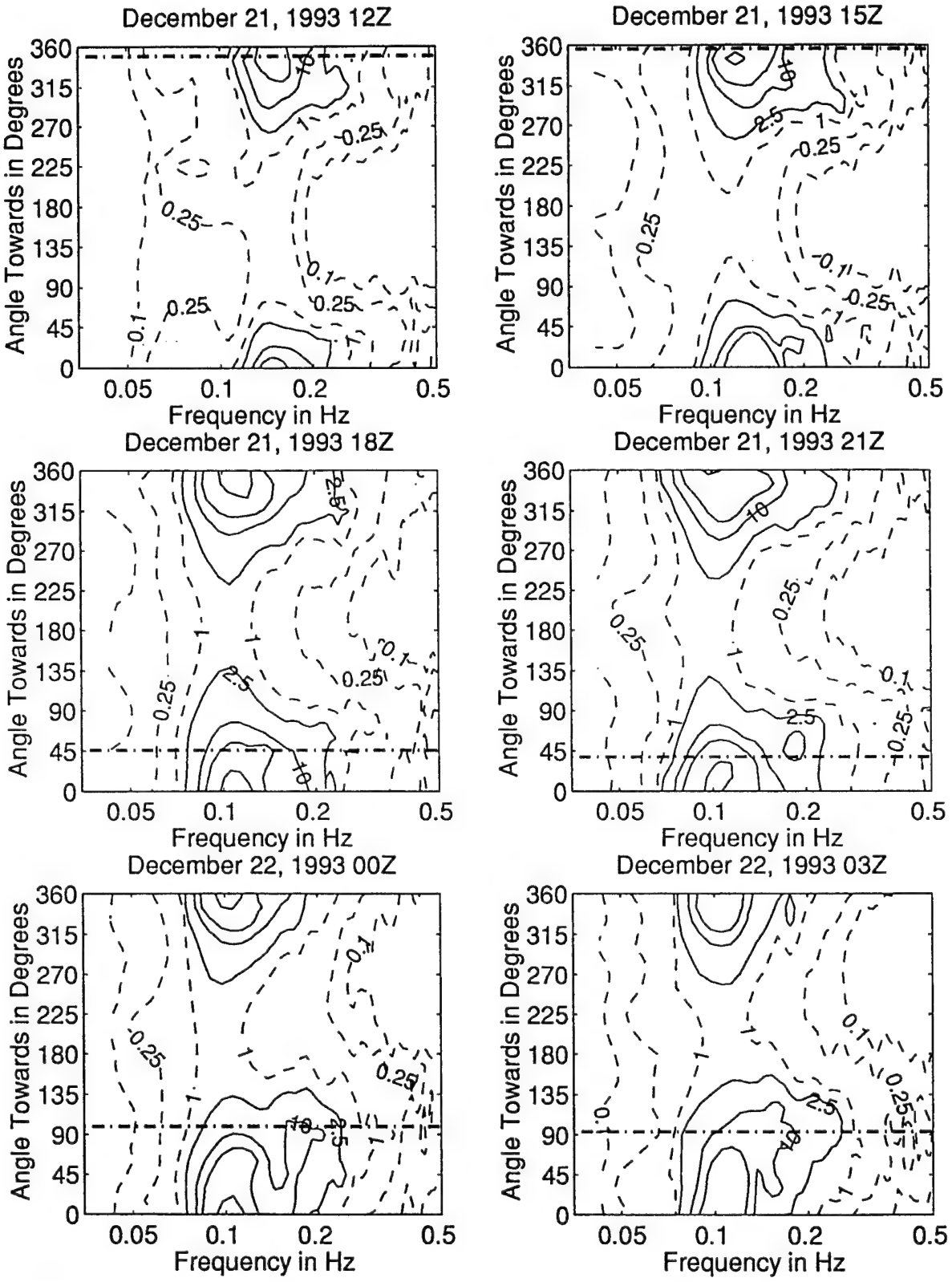

Figure 3.4.20: Directional wave spectra, computed using maximum entropy method. Contours of spectral density as a function of direction. Contours are 0.1, 0.25, 1 (dashed), 2.5, 10, 25, 100, and 250 (solid). Wind direction is shown by thick dashed line.

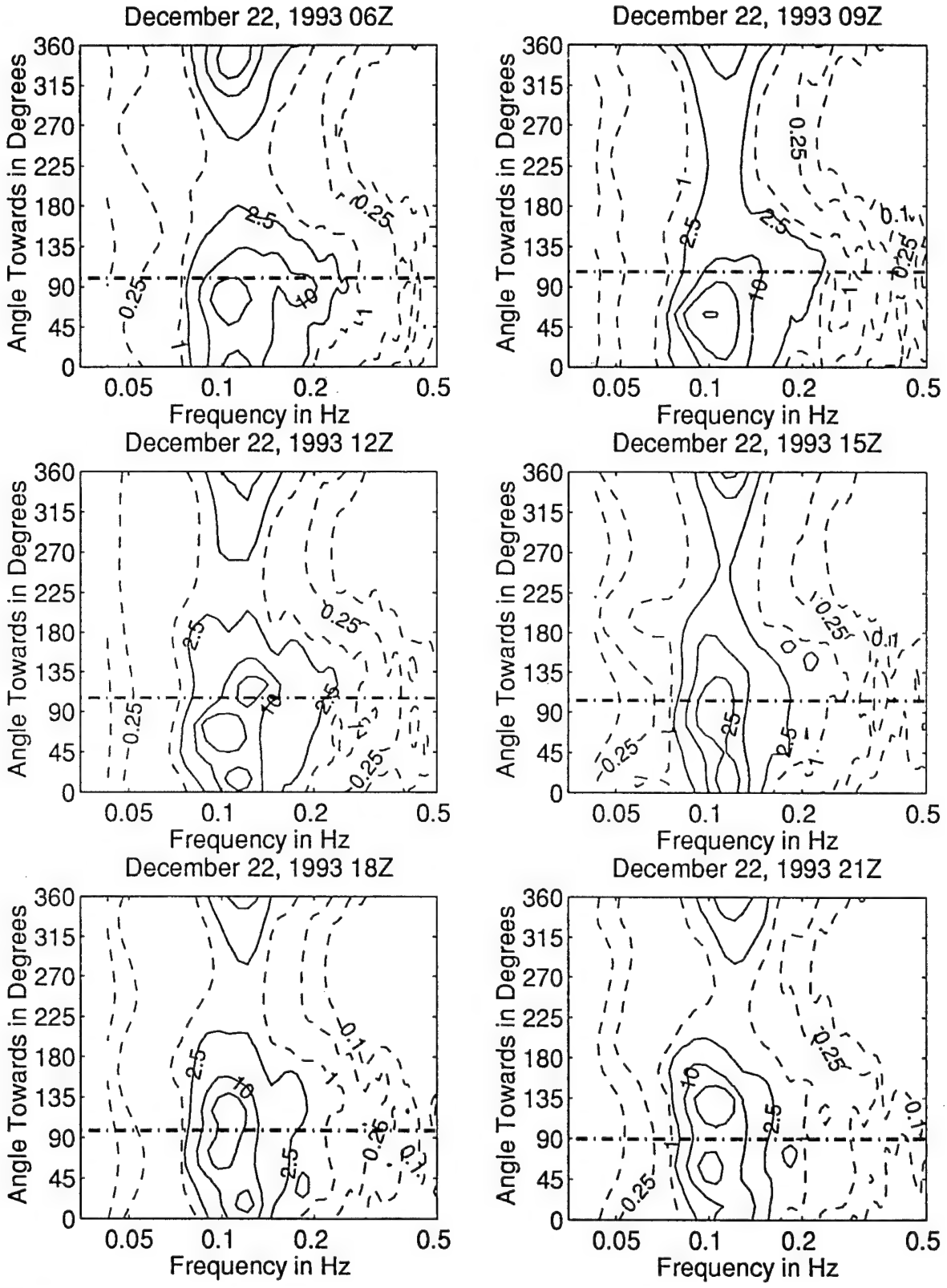

Figure 3.4.21: Directional wave spectra, computed using maximum entropy method. Contours of spectral density as a function of direction. Contours are 0.1, 0.25, 1 (dashed), 2.5, 10, 25, 100, and 250 (solid). Wind direction is shown by thick dashed line.

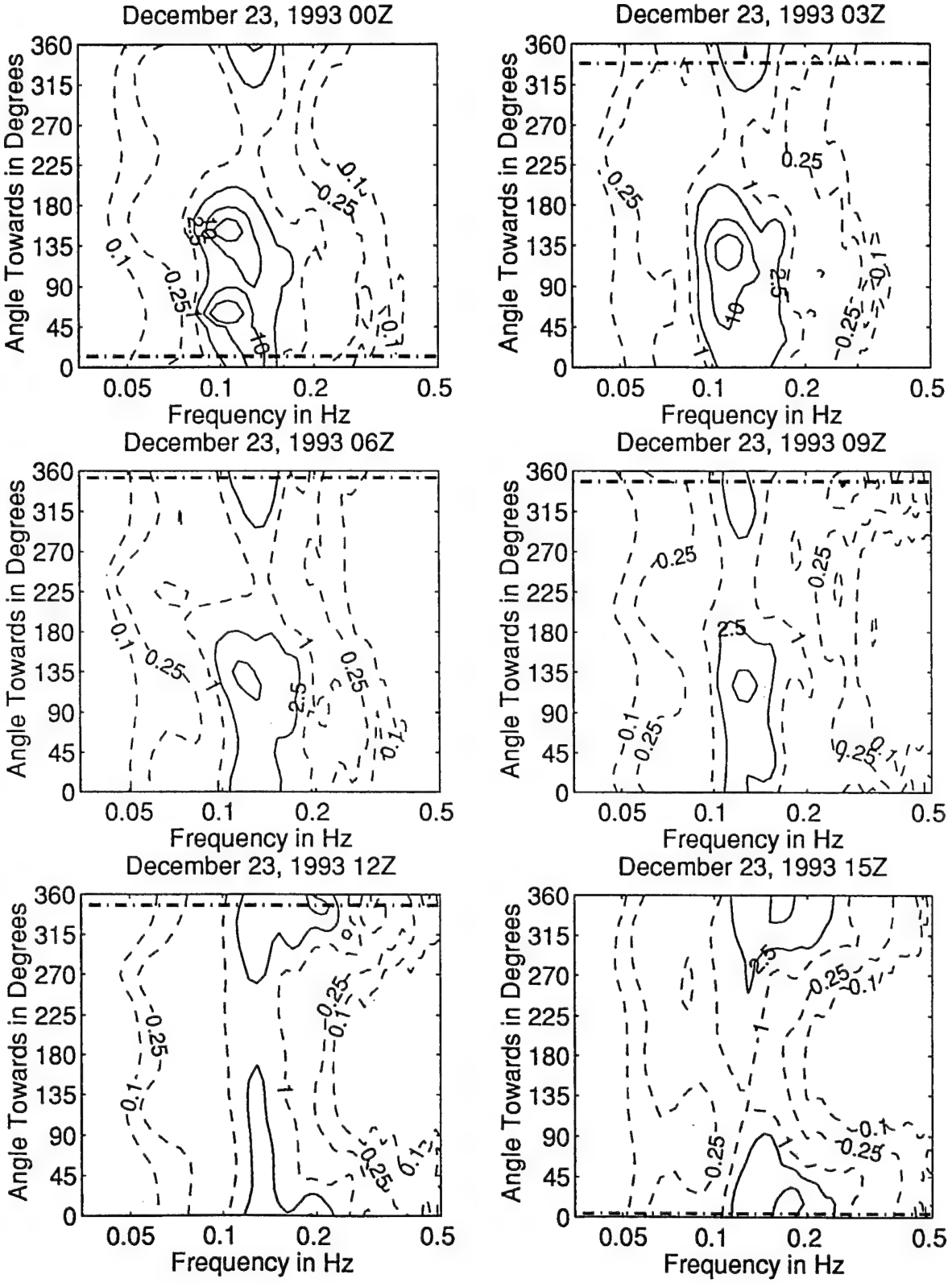

Figure 3.4.22: Directional wave spectra, computed using maximum entropy method. Contours of spectral density as a function of direction. Contours are 0.1, 0.25, 1 (dashed), 2.5, 10, 25, 100, and 250 (solid). Wind direction is shown by thick dashed line.

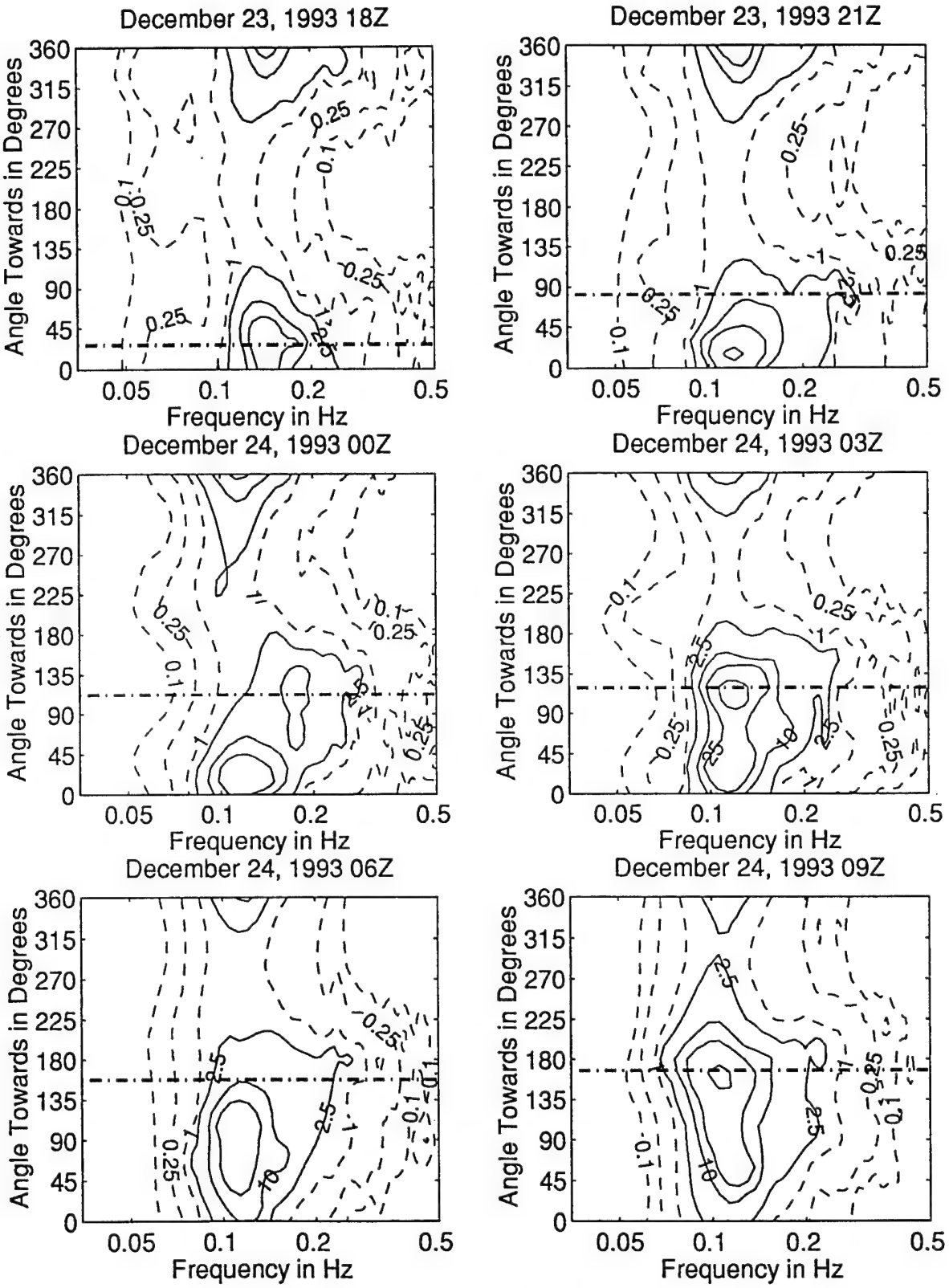

Figure 3.4.23: Directional wave spectra, computed using maximum entropy method. Contours of spectral density as a function of direction. Contours are 0.1, 0.25, 1 (dashed), 2.5, 10, 25, 100, and 250 (solid). Wind direction is shown by thick dashed line.

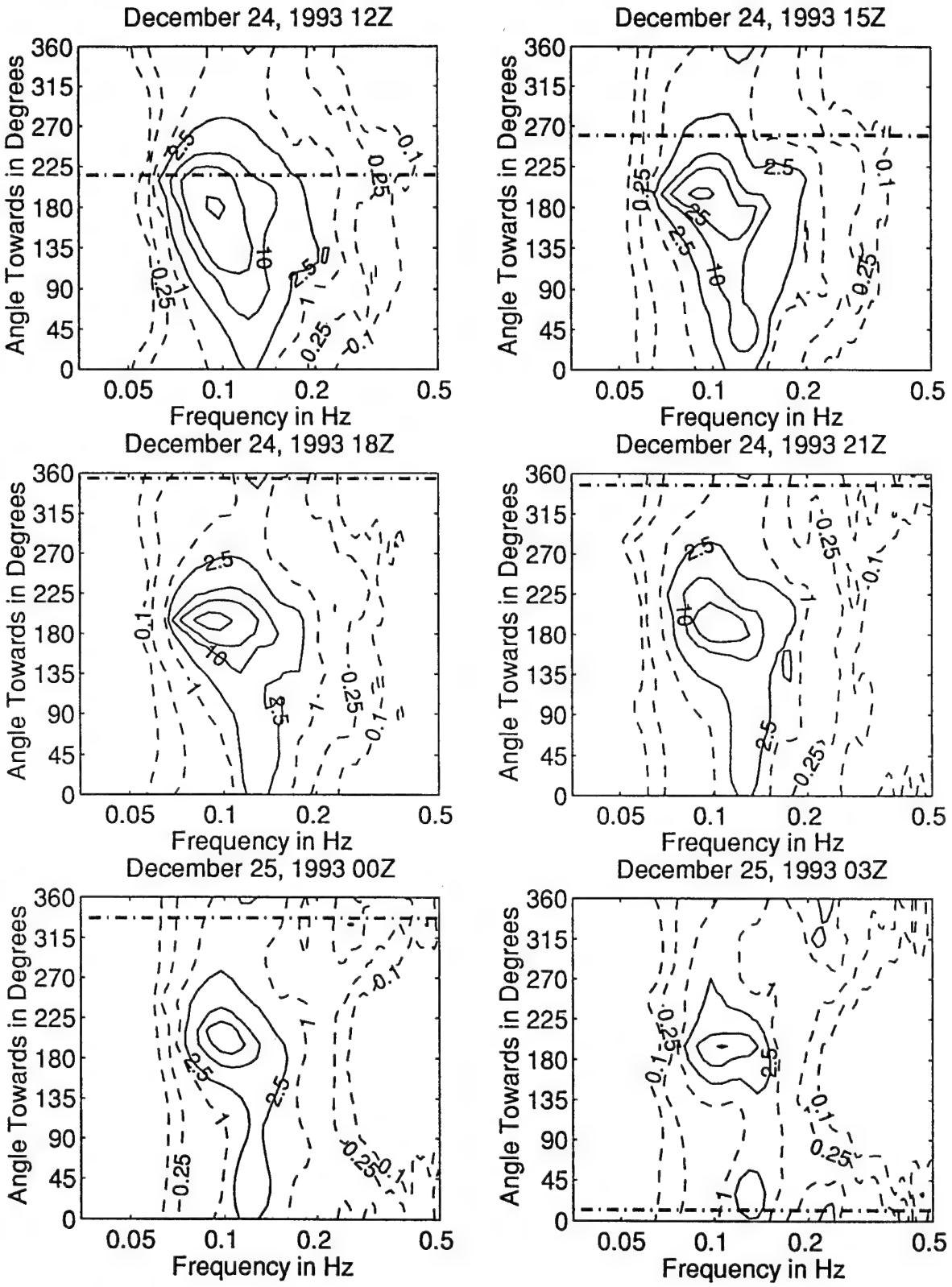

Figure 3.4.24: Directional wave spectra, computed using maximum entropy method. Contours of spectral density as a function of direction. Contours are 0.1, 0.25, 1 (dashed), 2.5, 10, 25, 100, and 250 (solid). Wind direction is shown by thick dashed line.

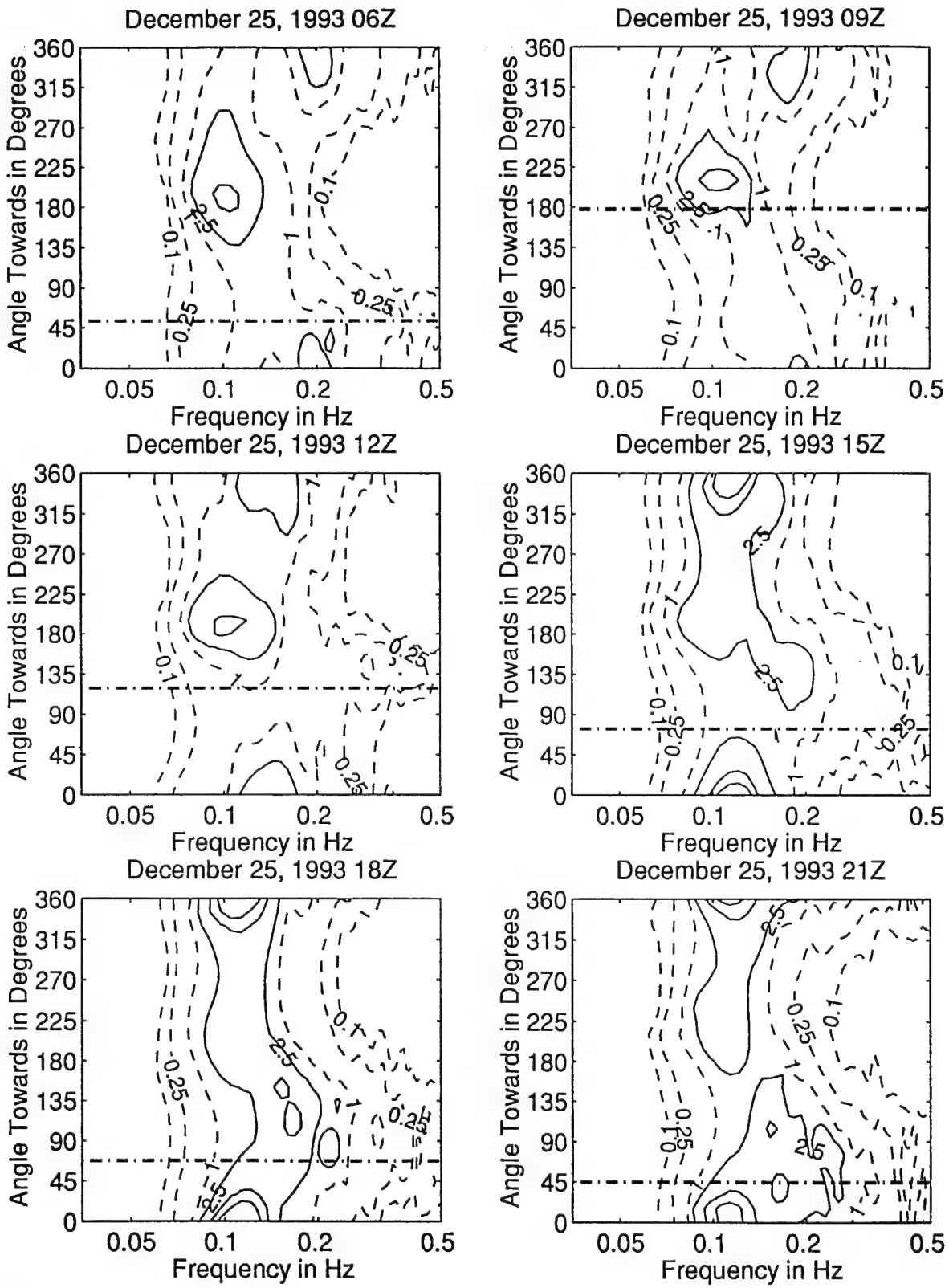

Figure 3.4.25: Directional wave spectra, computed using maximum entropy method. Contours of spectral density as a function of direction. Contours are 0.1, 0.25, 1 (dashed), 2.5, 10, 25, 100, and 250 (solid). Wind direction is shown by thick dashed line.

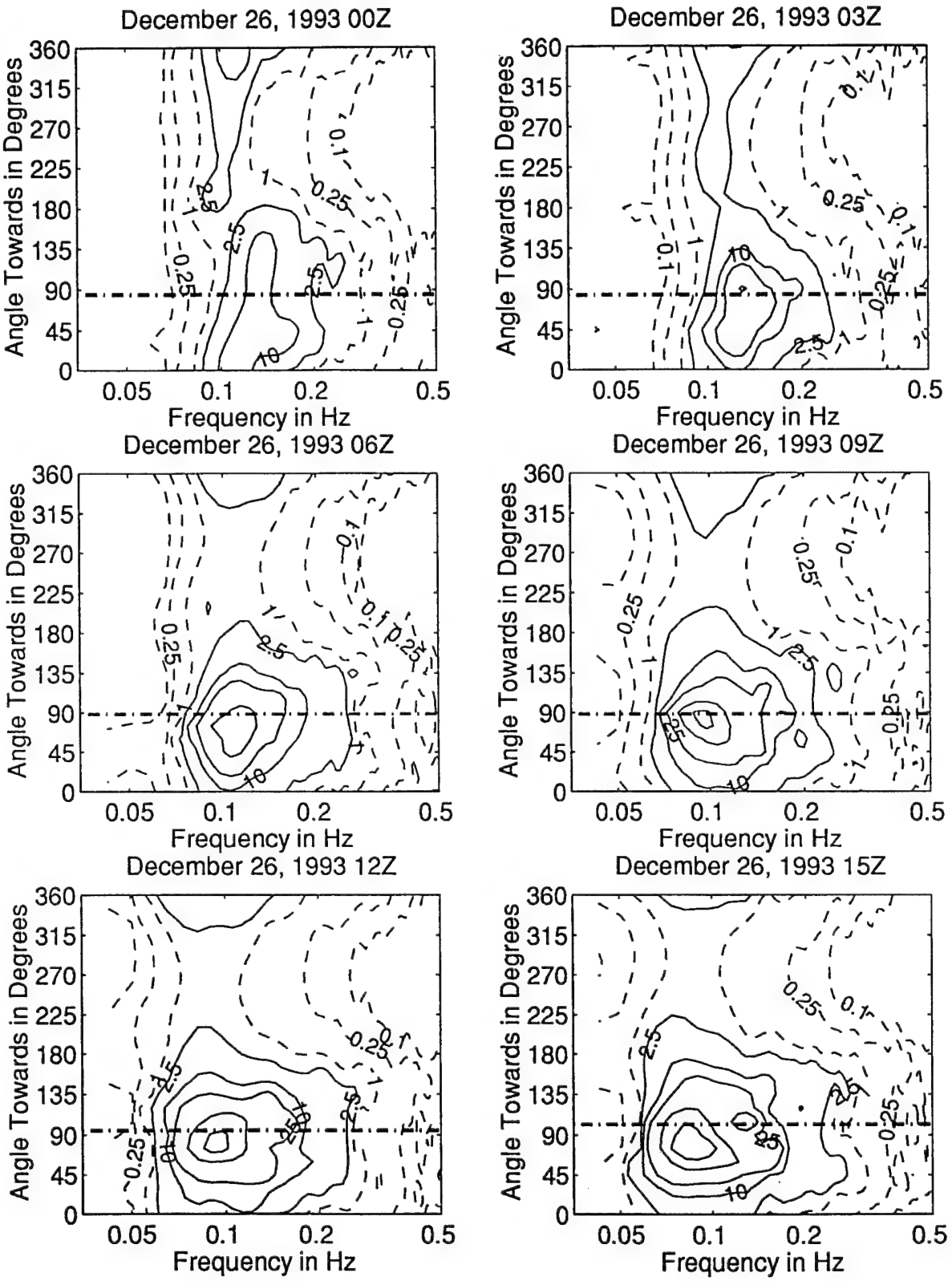

Figure 3.4.26: Directional wave spectra, computed using maximum entropy method. Contours of spectral density as a function of direction. Contours are 0.1, 0.25, 1 (dashed), 2.5, 10, 25, 100, and 250 (solid). Wind direction is shown by thick dashed line.

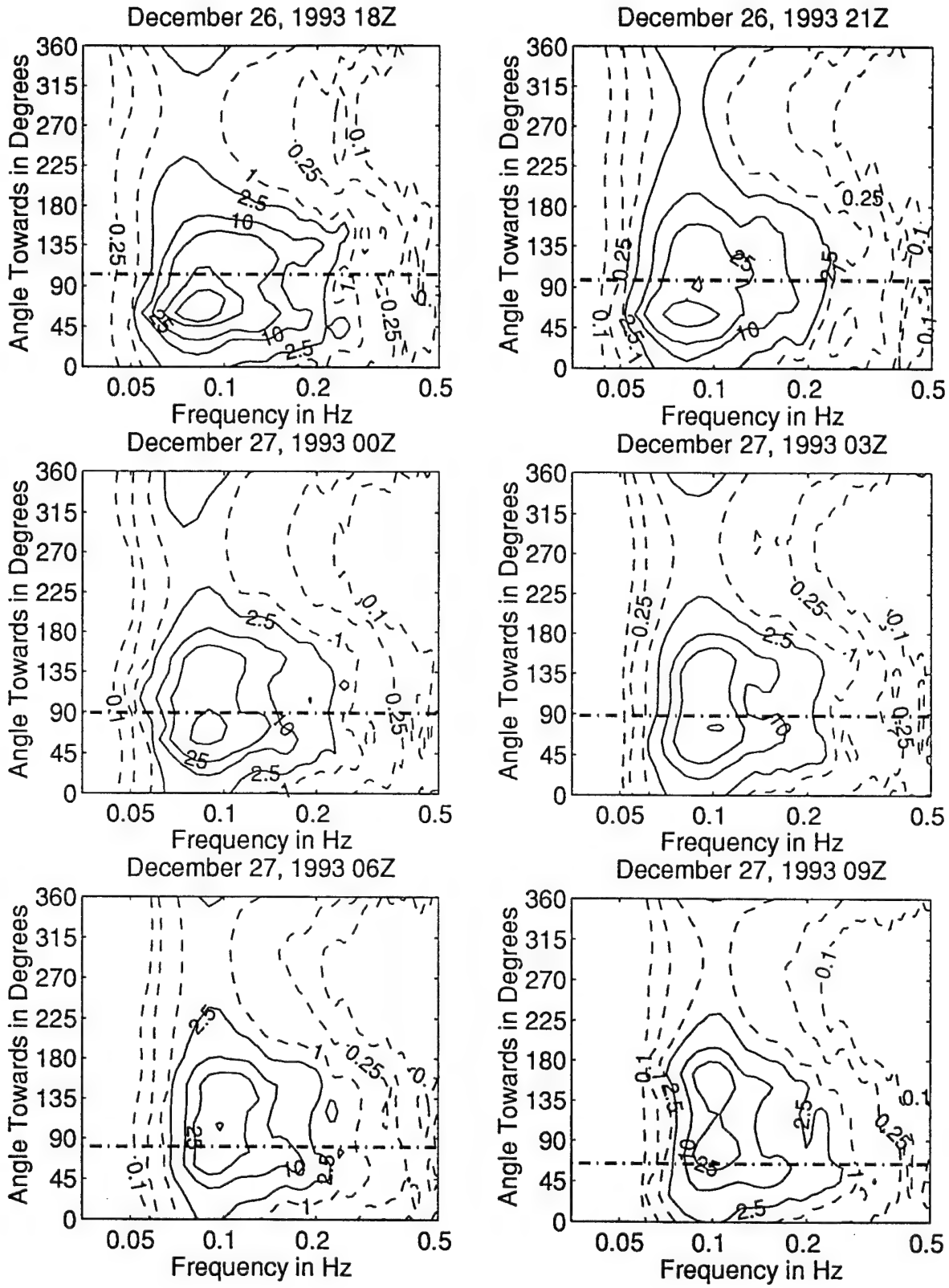

Figure 3.4.27: Directional wave spectra, computed using maximum entropy method. Contours of spectral density as a function of direction. Contours are 0.1, 0.25, 1 (dashed), 2.5, 10, 25, 100, and 250 (solid). Wind direction is shown by thick dashed line.

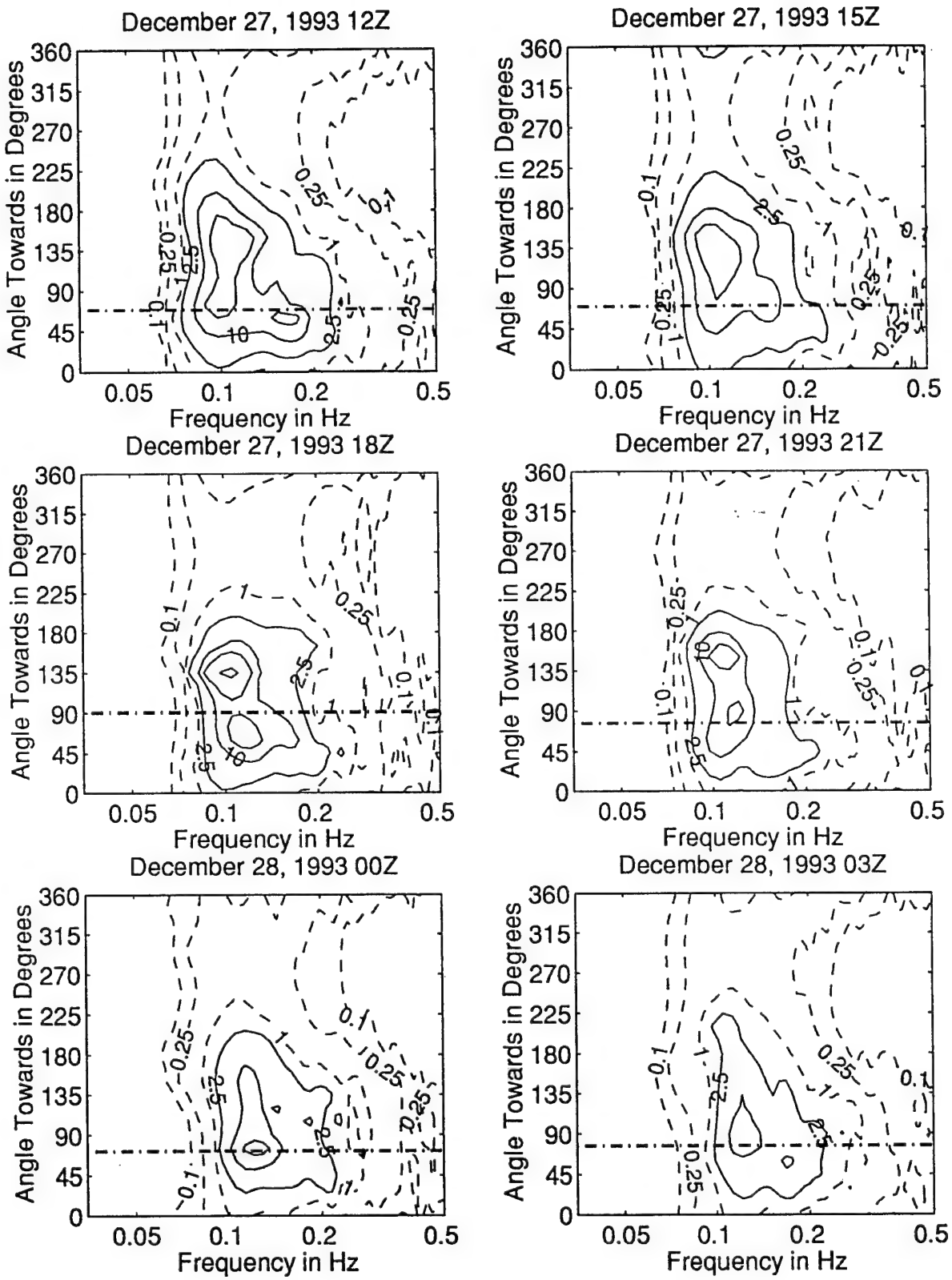

Figure 3.4.28: Directional wave spectra, computed using maximum entropy method. Contours of spectral density as a function of direction. Contours are 0.1, 0.25, 1 (dashed), 2.5, 10, 25, 100, and 250 (solid). Wind direction is shown by thick dashed line.

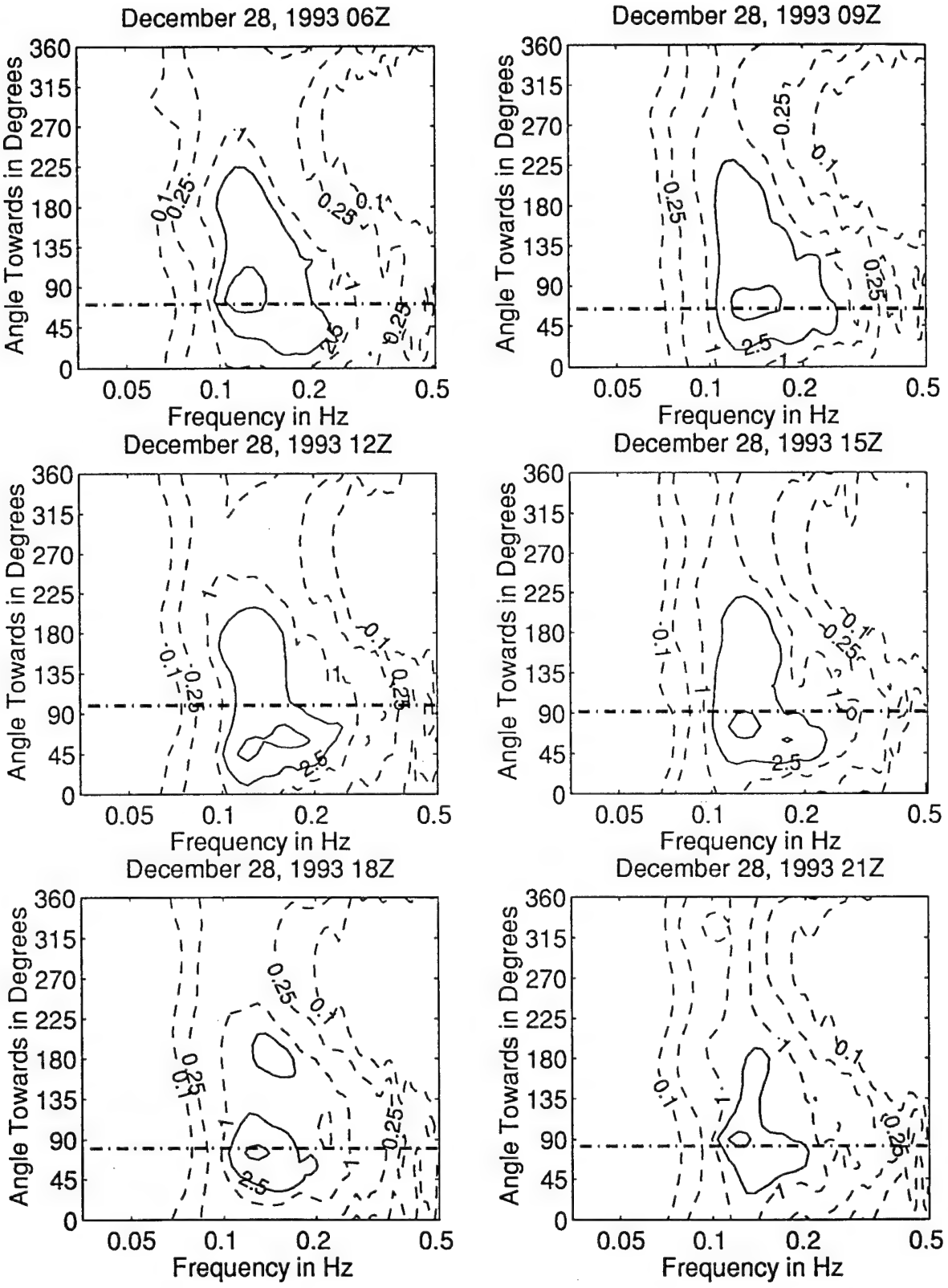

Figure 3.4.29: Directional wave spectra, computed using maximum entropy method. Contours of spectral density as a function of direction. Contours are 0.1, 0.25, 1 (dashed), 2.5, 10, 25, 100, and 250 (solid). Wind direction is shown by thick dashed line.

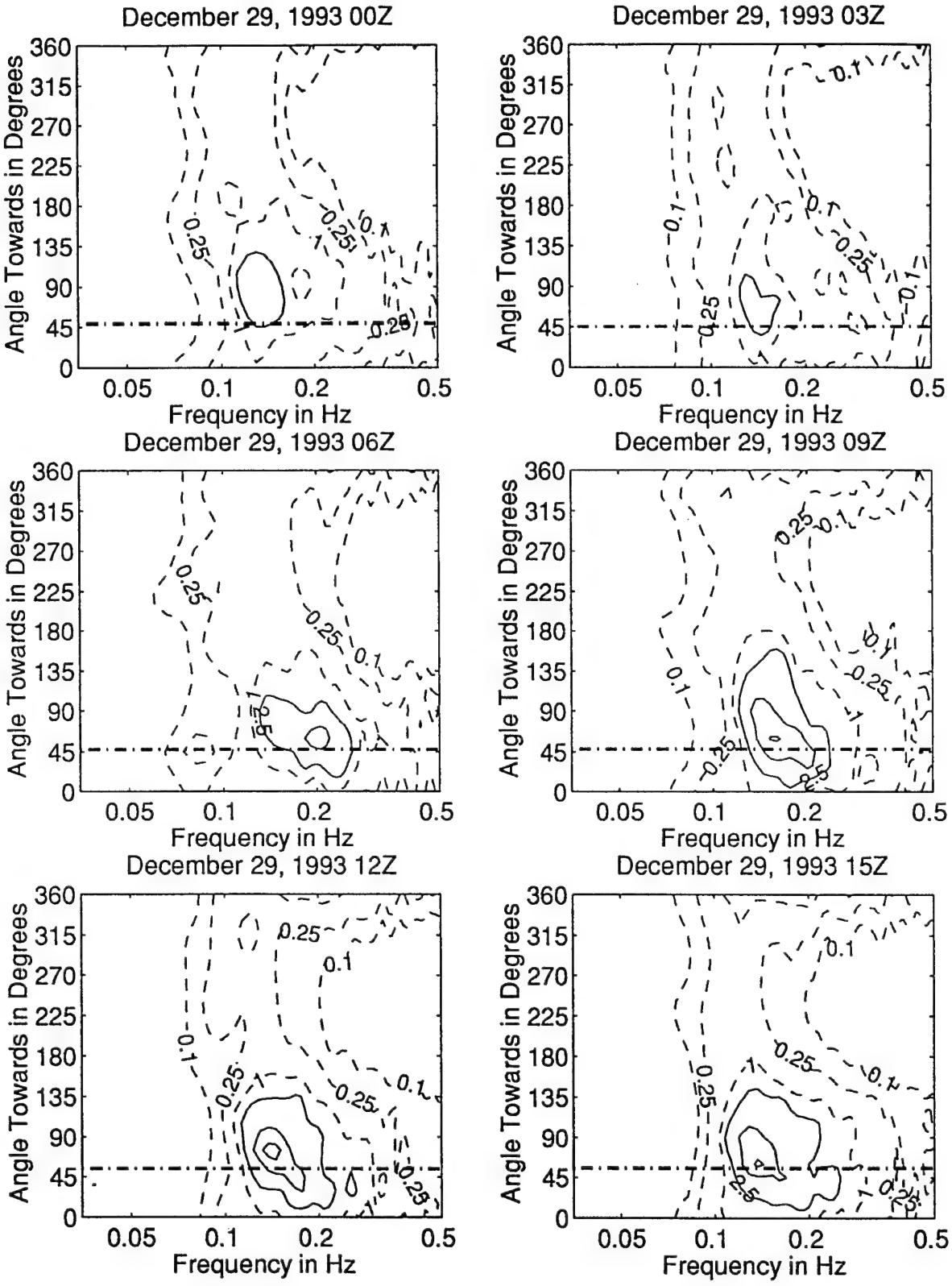

Figure 3.4.30: Directional wave spectra, computed using maximum entropy method. Contours of spectral density as a function of direction. Contours are 0.1, 0.25, 1 (dashed), 2.5, 10, 25, 100, and 250 (solid). Wind direction is shown by thick dashed line.

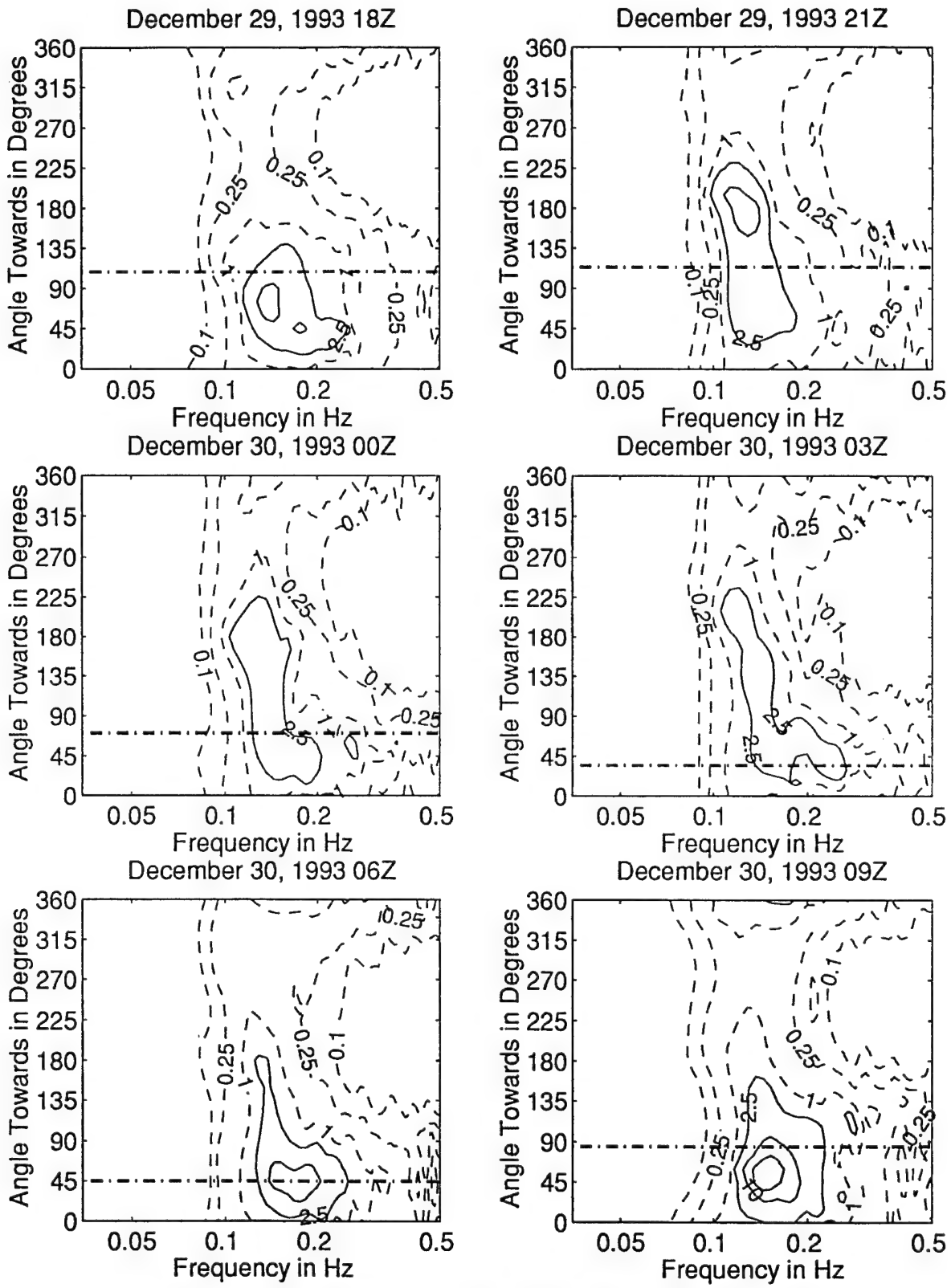

Figure 3.4.31: Directional wave spectra, computed using maximum entropy method. Contours of spectral density as a function of direction. Contours are 0.1, 0.25, 1 (dashed), 2.5, 10, 25, 100, and 250 (solid). Wind direction is shown by thick dashed line.

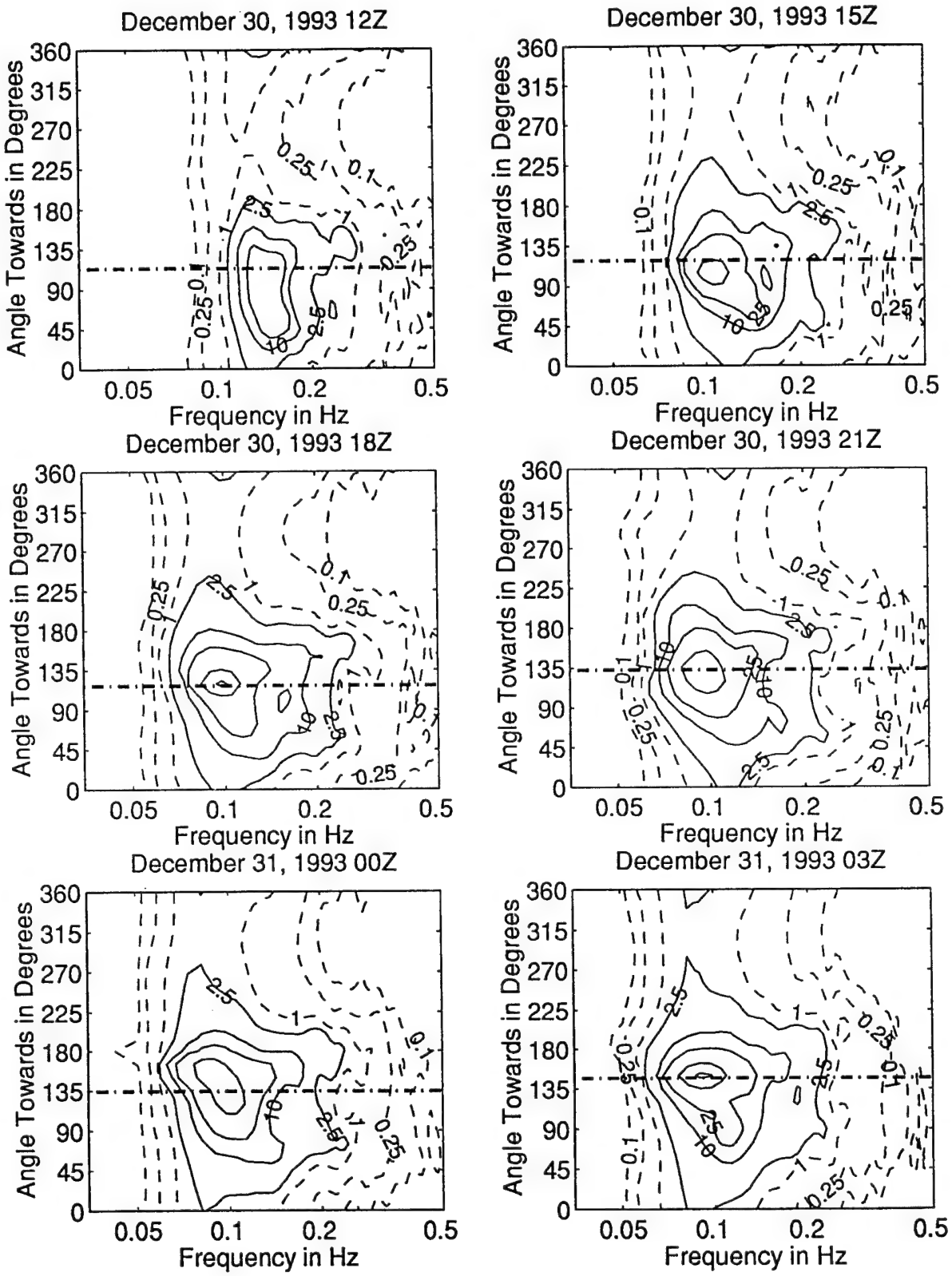

Figure 3.4.32: Directional wave spectra, computed using maximum entropy method. Contours of spectral density as a function of direction. Contours are 0.1, 0.25, 1 (dashed), 2.5, 10, 25, 100, and 250 (solid). Wind direction is shown by thick dashed line.

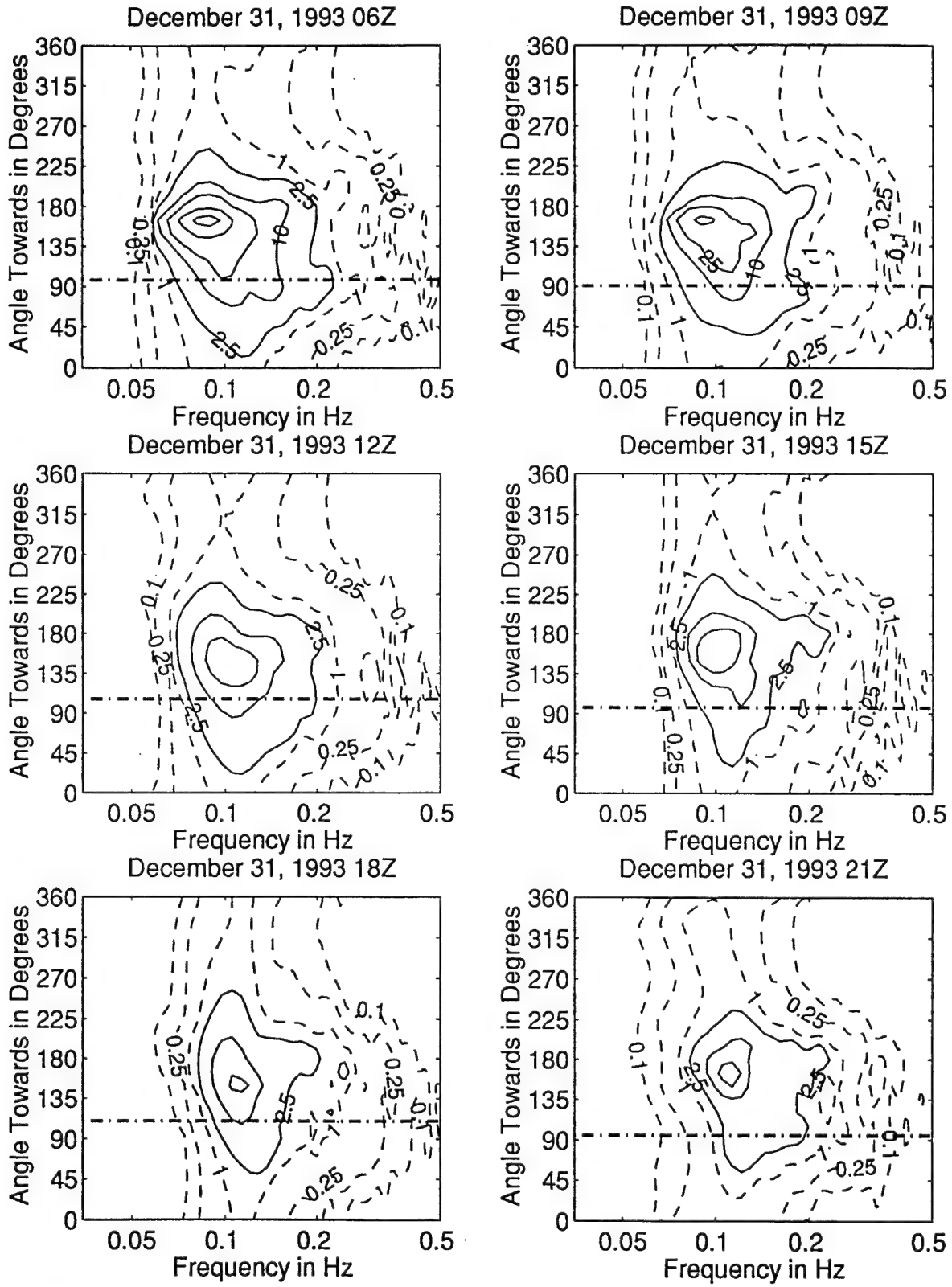

Figure 3.4.33: Directional wave spectra, computed using maximum entropy method. Contours of spectral density as a function of direction. Contours are 0.1, 0.25, 1 (dashed), 2.5, 10, 25, 100, and 250 (solid). Wind direction is shown by thick dashed line.

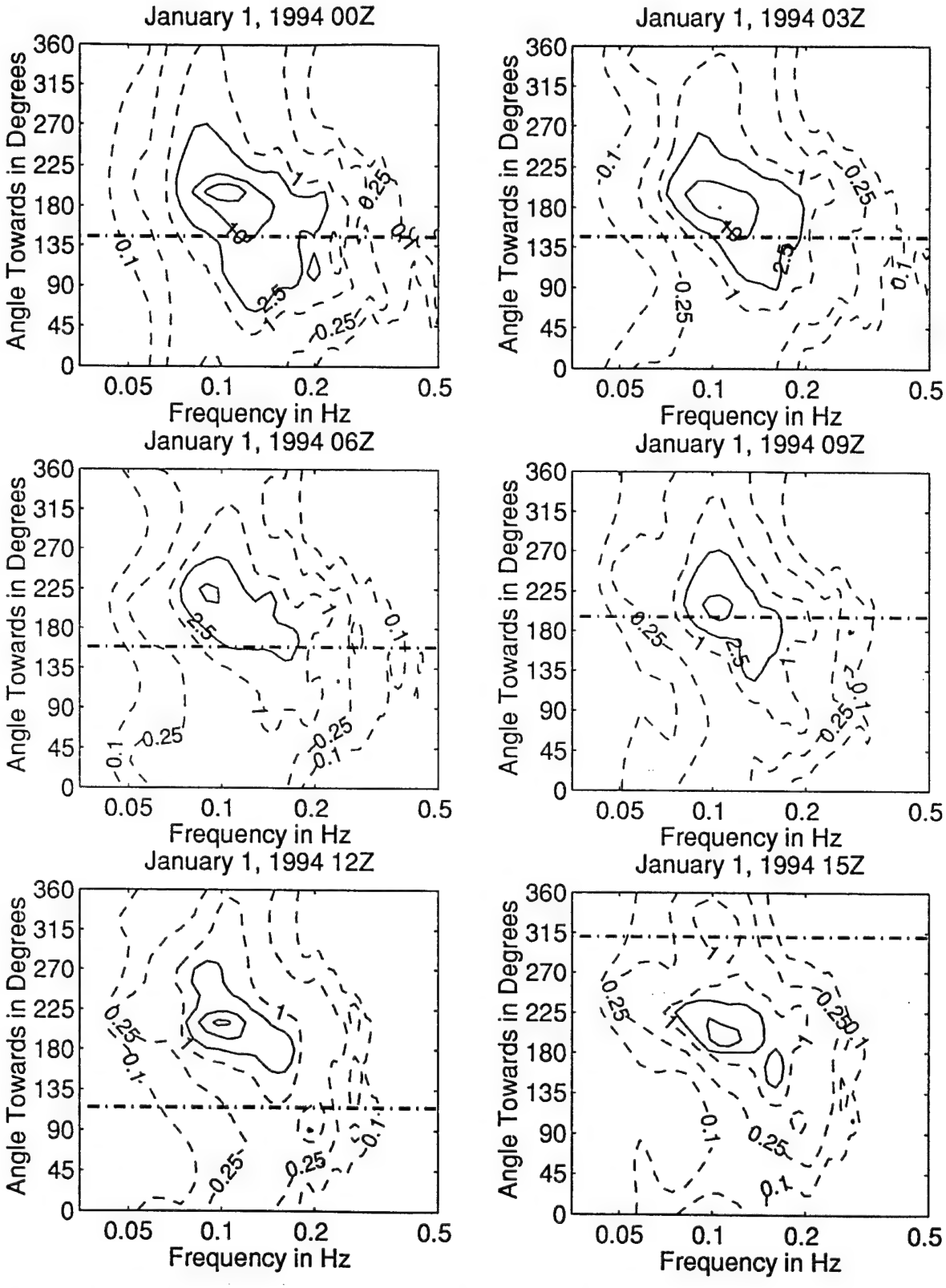

Figure 3.4.34: Directional wave spectra, computed using maximum entropy method. Contours of spectral density as a function of direction. Contours are 0.1, 0.25, 1 (dashed), 2.5, 10, 25, 100, and 250 (solid). Wind direction is shown by thick dashed line.

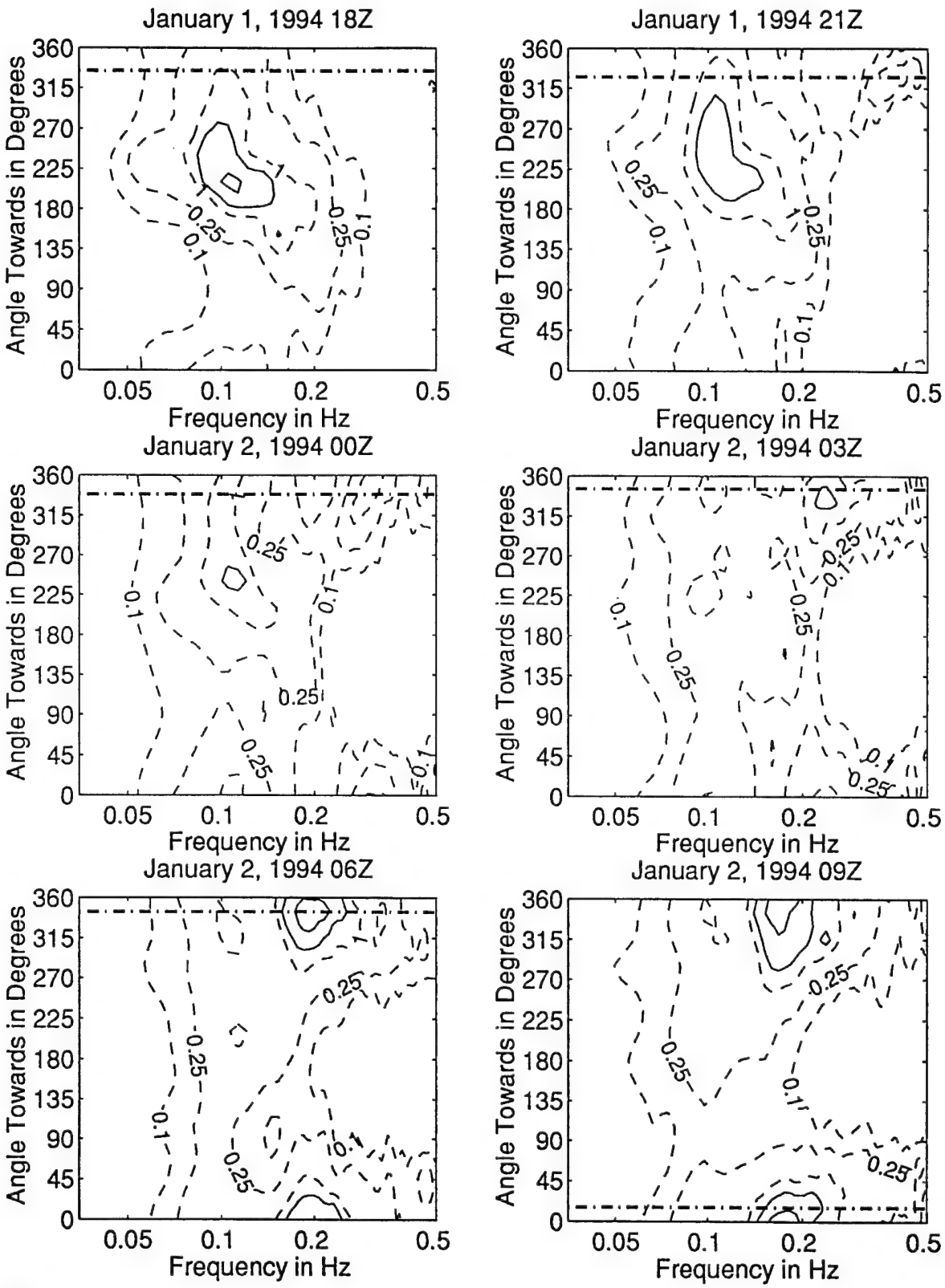

Figure 3.4.35: Directional wave spectra, computed using maximum entropy method. Contours of spectral density as a function of direction. Contours are 0.1, 0.25, 1 (dashed), 2.5, 10, 25, 100, and 250 (solid). Wind direction is shown by thick dashed line.

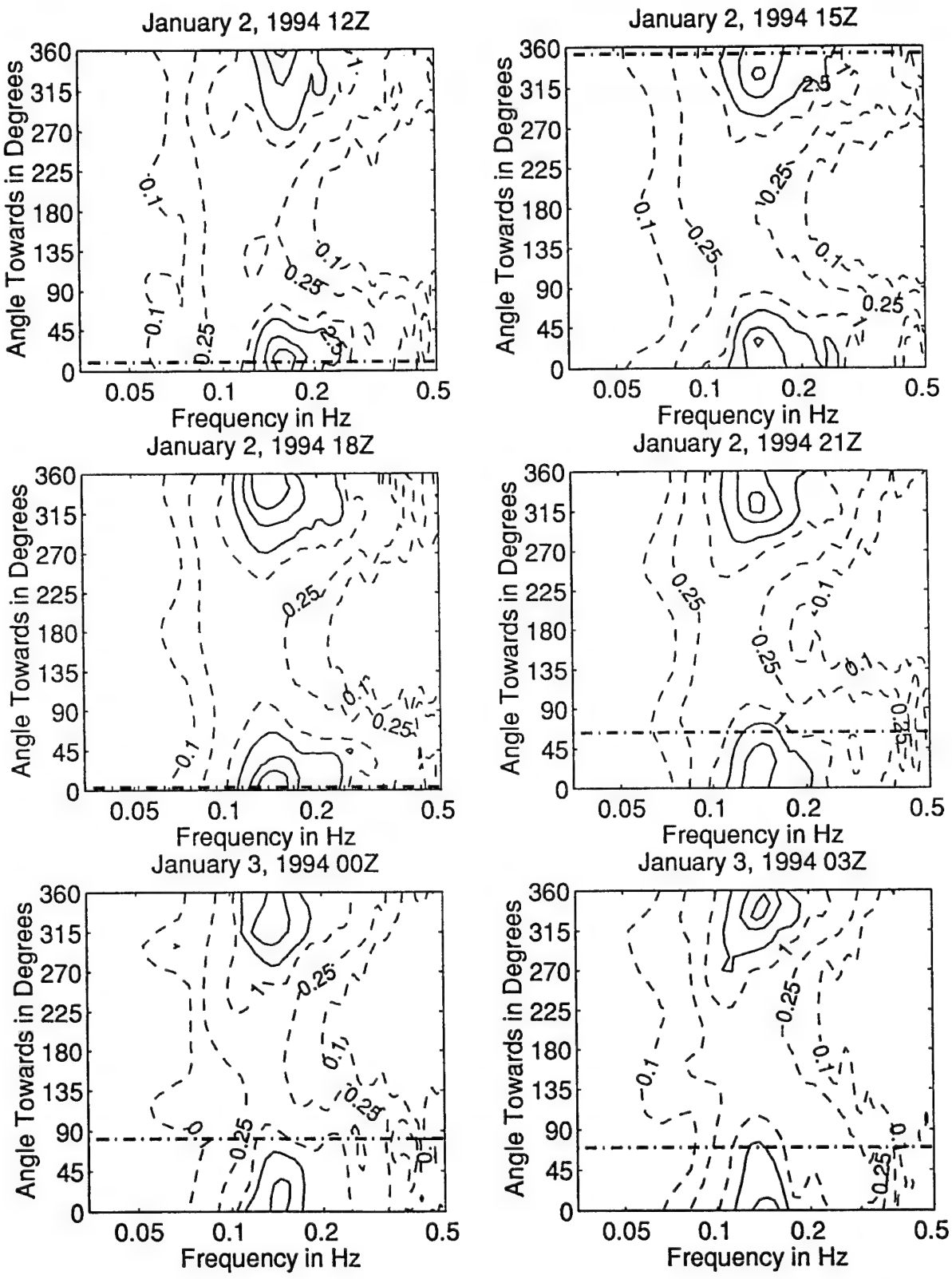

Figure 3.4.36: Directional wave spectra, computed using maximum entropy method. Contours of spectral density as a function of direction. Contours are 0.1, 0.25, 1 (dashed), 2.5, 10, 25, 100, and 250 (solid). Wind direction is shown by thick dashed line.

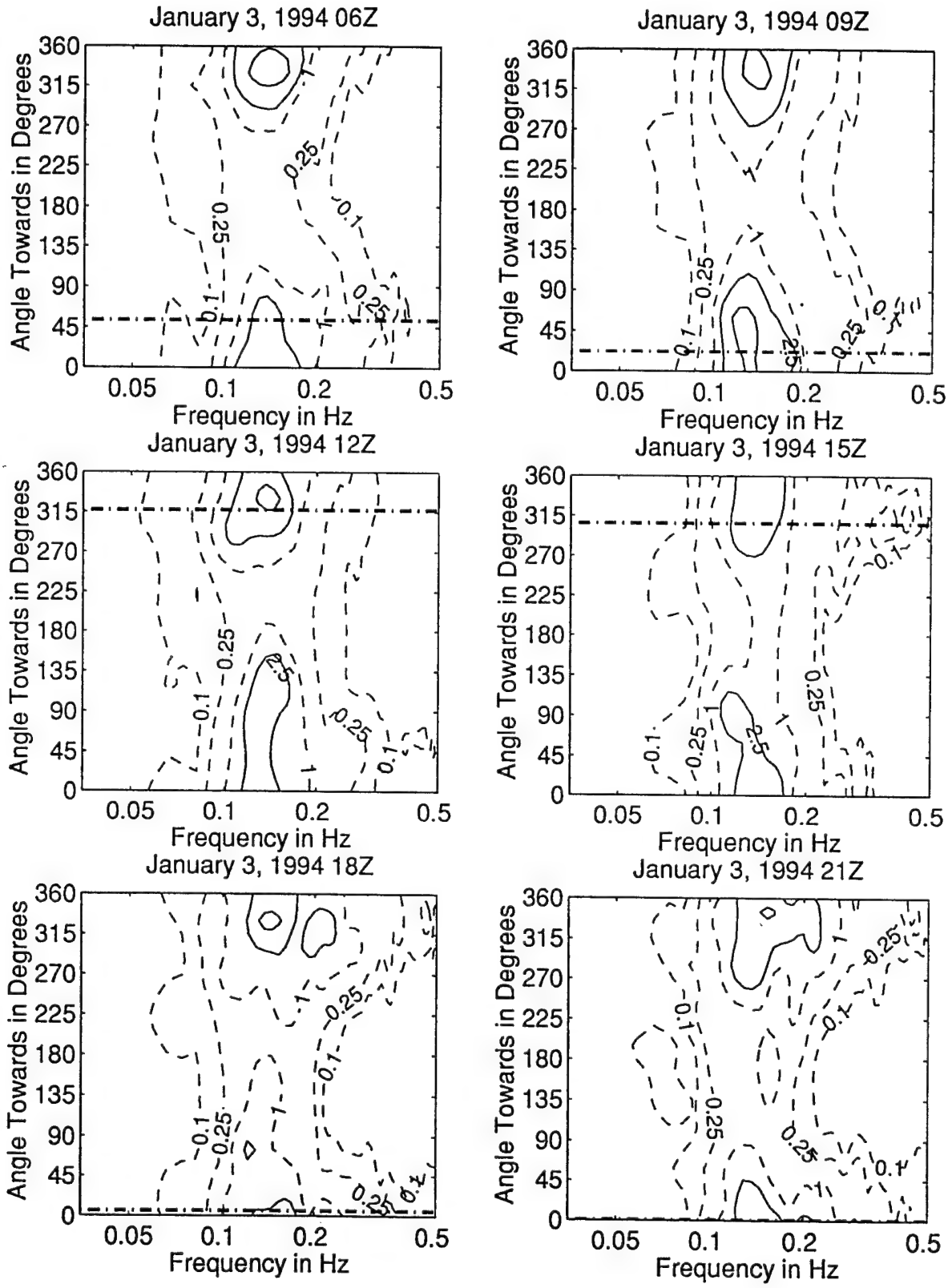

Figure 3.4.37: Directional wave spectra, computed using maximum entropy method. Contours of spectral density as a function of direction. Contours are 0.1, 0.25, 1 (dashed), 2.5, 10, 25, 100, and 250 (solid). Wind direction is shown by thick dashed line.

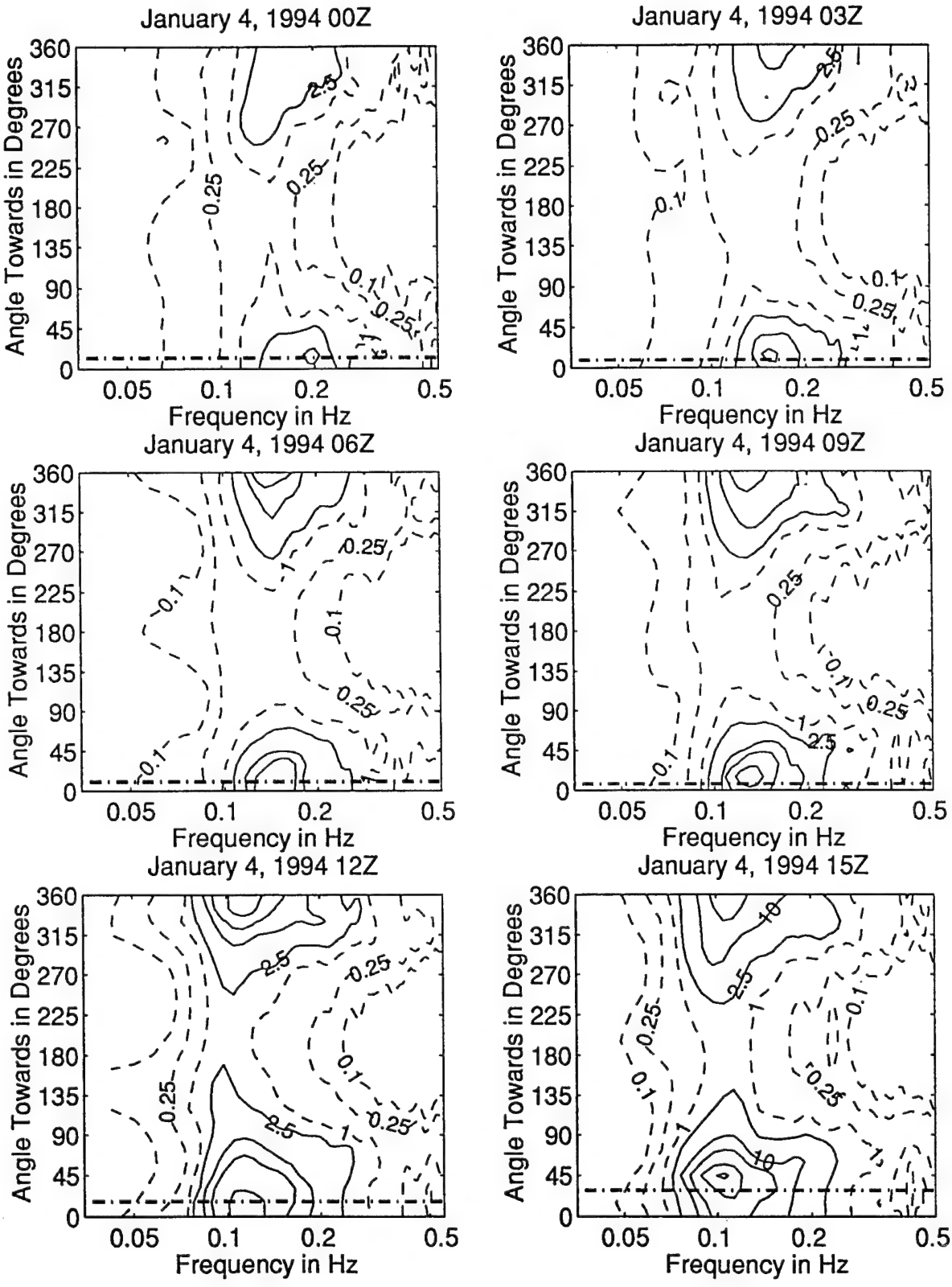

Figure 3.4.38: Directional wave spectra, computed using maximum entropy method. Contours of spectral density as a function of direction. Contours are 0.1, 0.25, 1 (dashed), 2.5, 10, 25, 100, and 250 (solid). Wind direction is shown by thick dashed line.

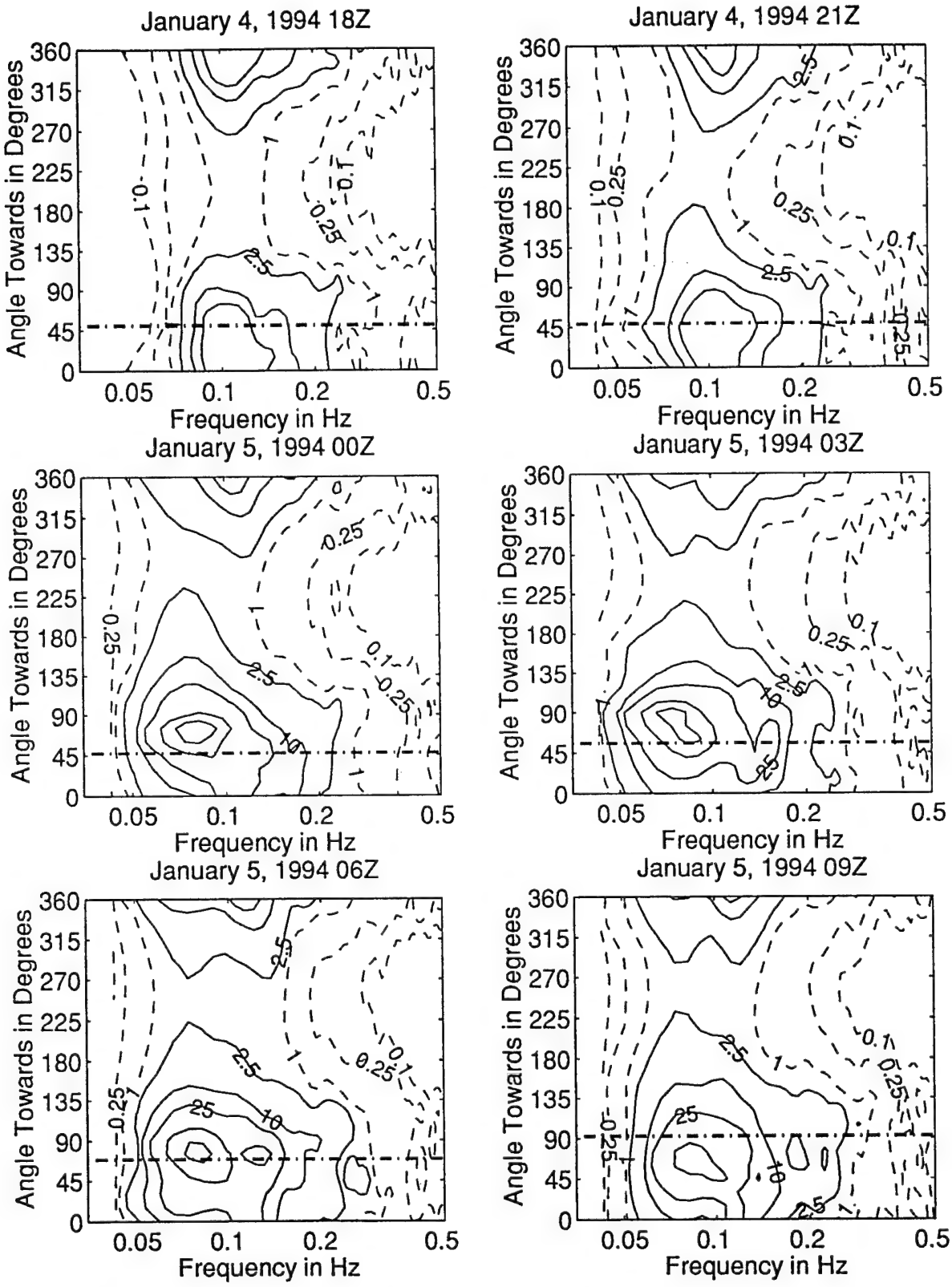

Figure 3.4.39: Directional wave spectra, computed using maximum entropy method. Contours of spectral density as a function of direction. Contours are 0.1, 0.25, 1 (dashed), 2.5, 10, 25, 100, and 250 (solid). Wind direction is shown by thick dashed line.

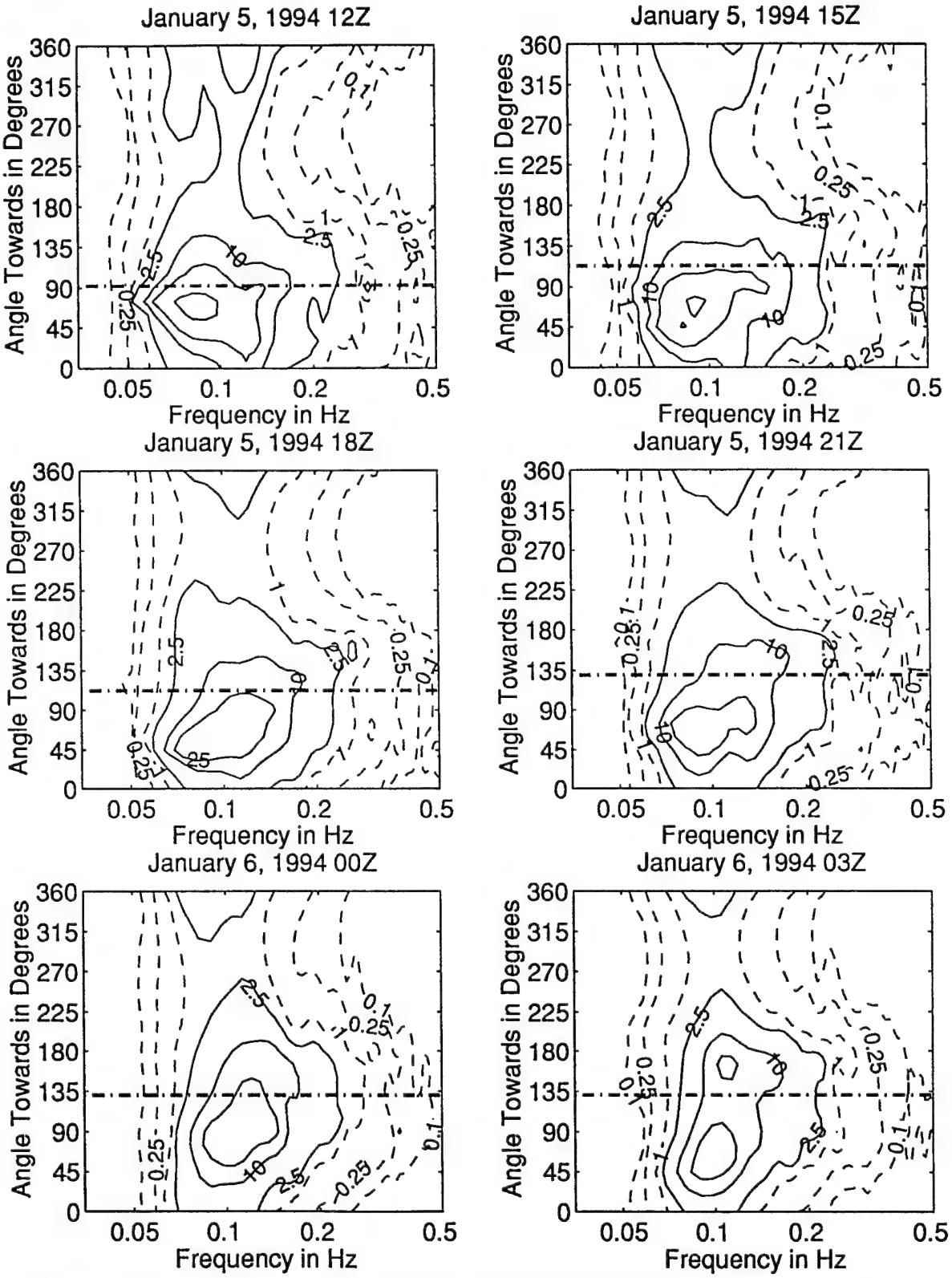

Figure 3.4.40: Directional wave spectra, computed using maximum entropy method. Contours of spectral density as a function of direction. Contours are 0.1, 0.25, 1 (dashed), 2.5, 10, 25, 100, and 250 (solid). Wind direction is shown by thick dashed line.

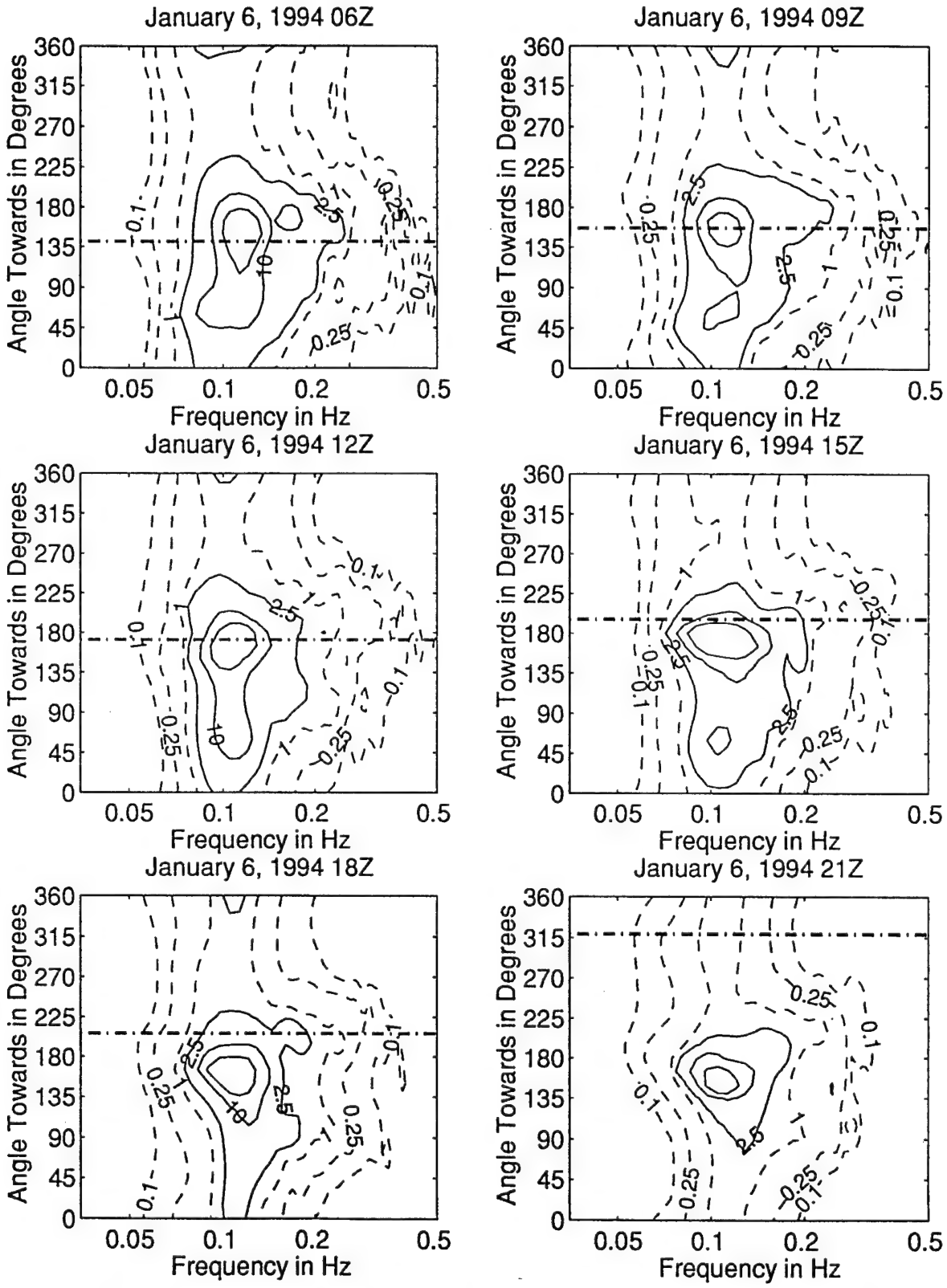

Figure 3.4.41: Directional wave spectra, computed using maximum entropy method. Contours of spectral density as a function of direction. Contours are 0.1, 0.25, 1 (dashed), 2.5, 10, 25, 100, and 250 (solid). Wind direction is shown by thick dashed line.

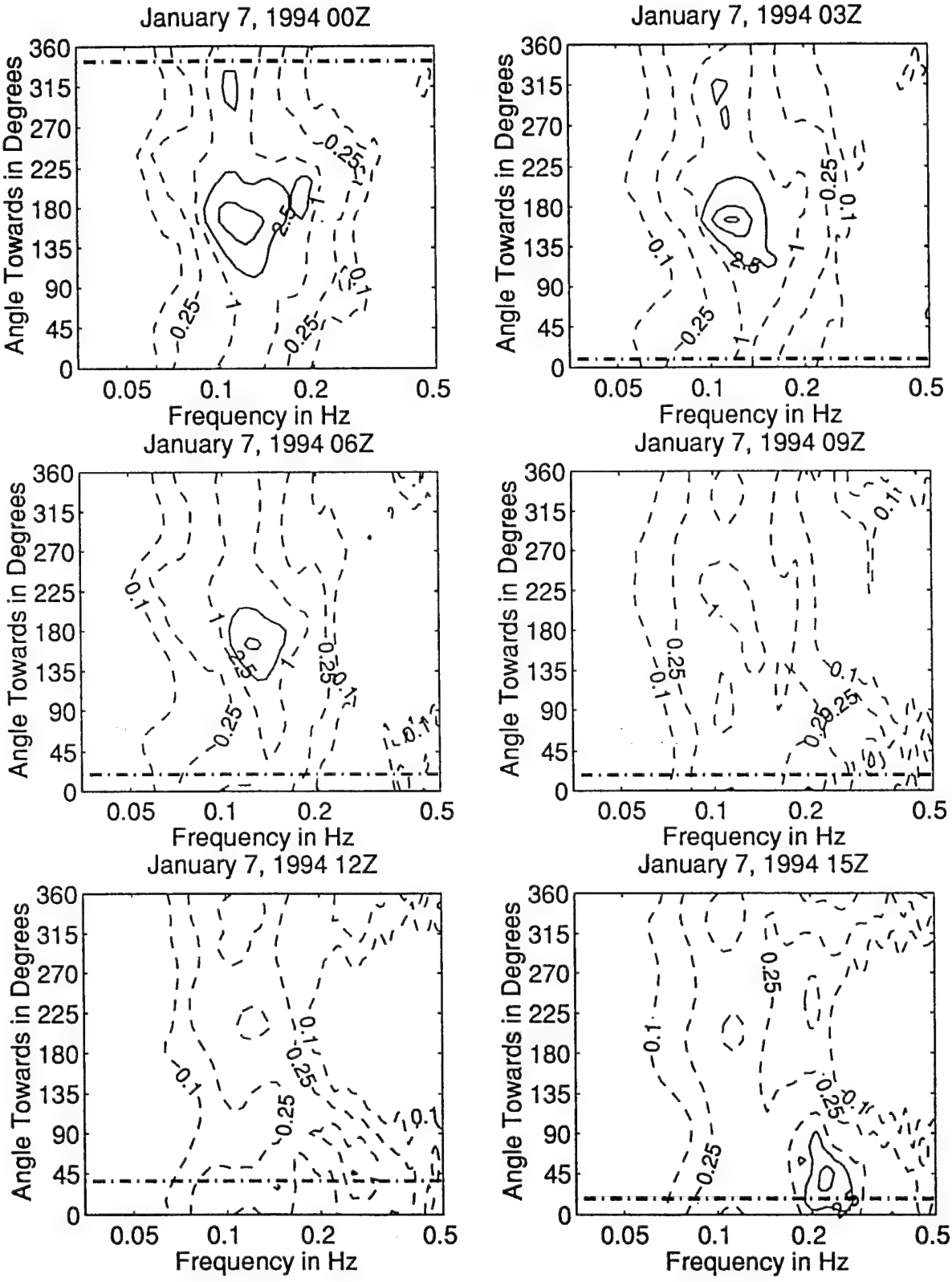

Figure 3.4.42: Directional wave spectra, computed using maximum entropy method. Contours of spectral density as a function of direction. Contours are 0.1, 0.25, 1 (dashed), 2.5, 10, 25, 100, and 250 (solid). Wind direction is shown by thick dashed line.

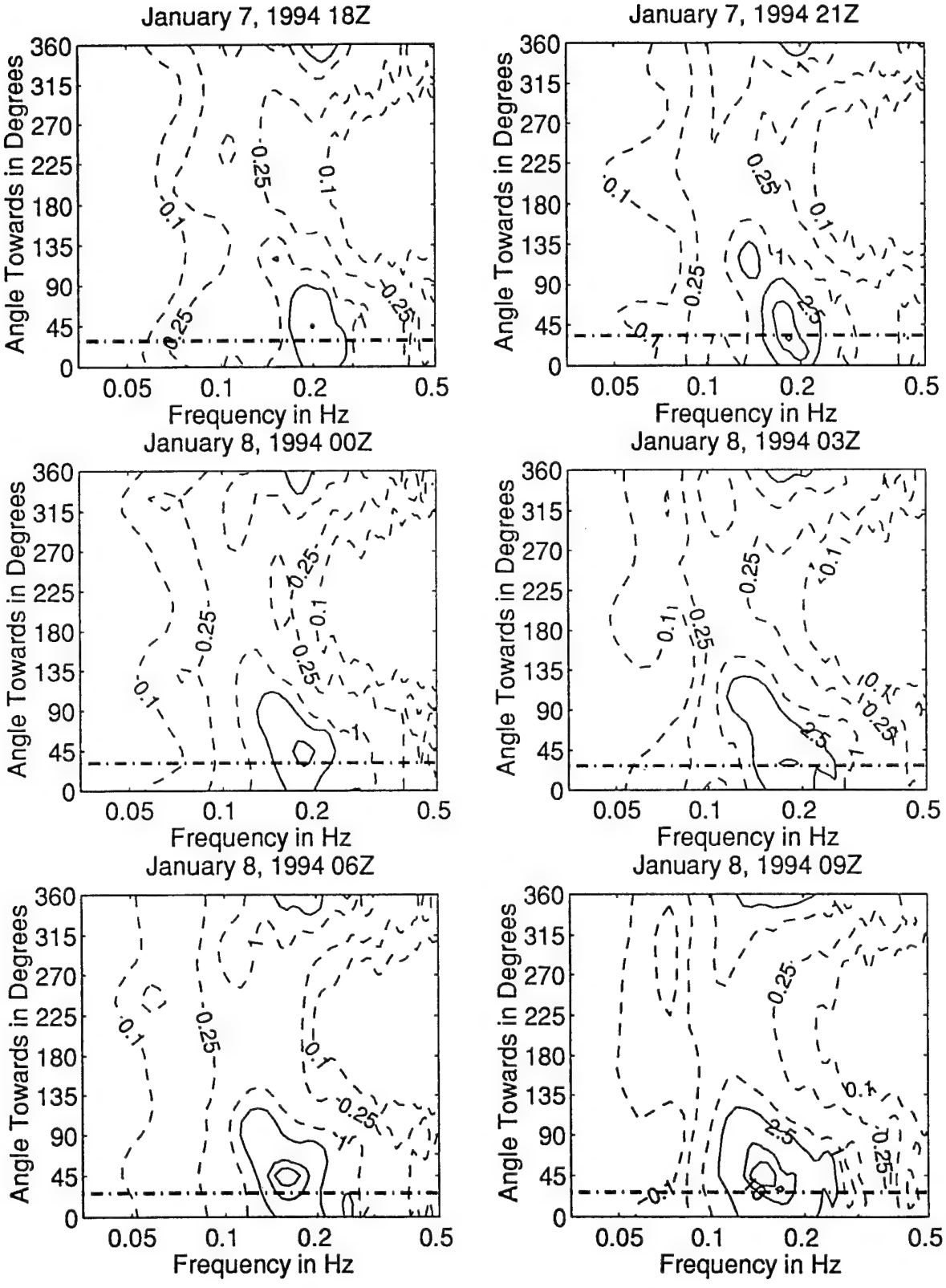

Figure 3.4.43: Directional wave spectra, computed using maximum entropy method. Contours of spectral density as a function of direction. Contours are 0.1, 0.25, 1 (dashed), 2.5, 10, 25, 100, and 250 (solid). Wind direction is shown by thick dashed line.

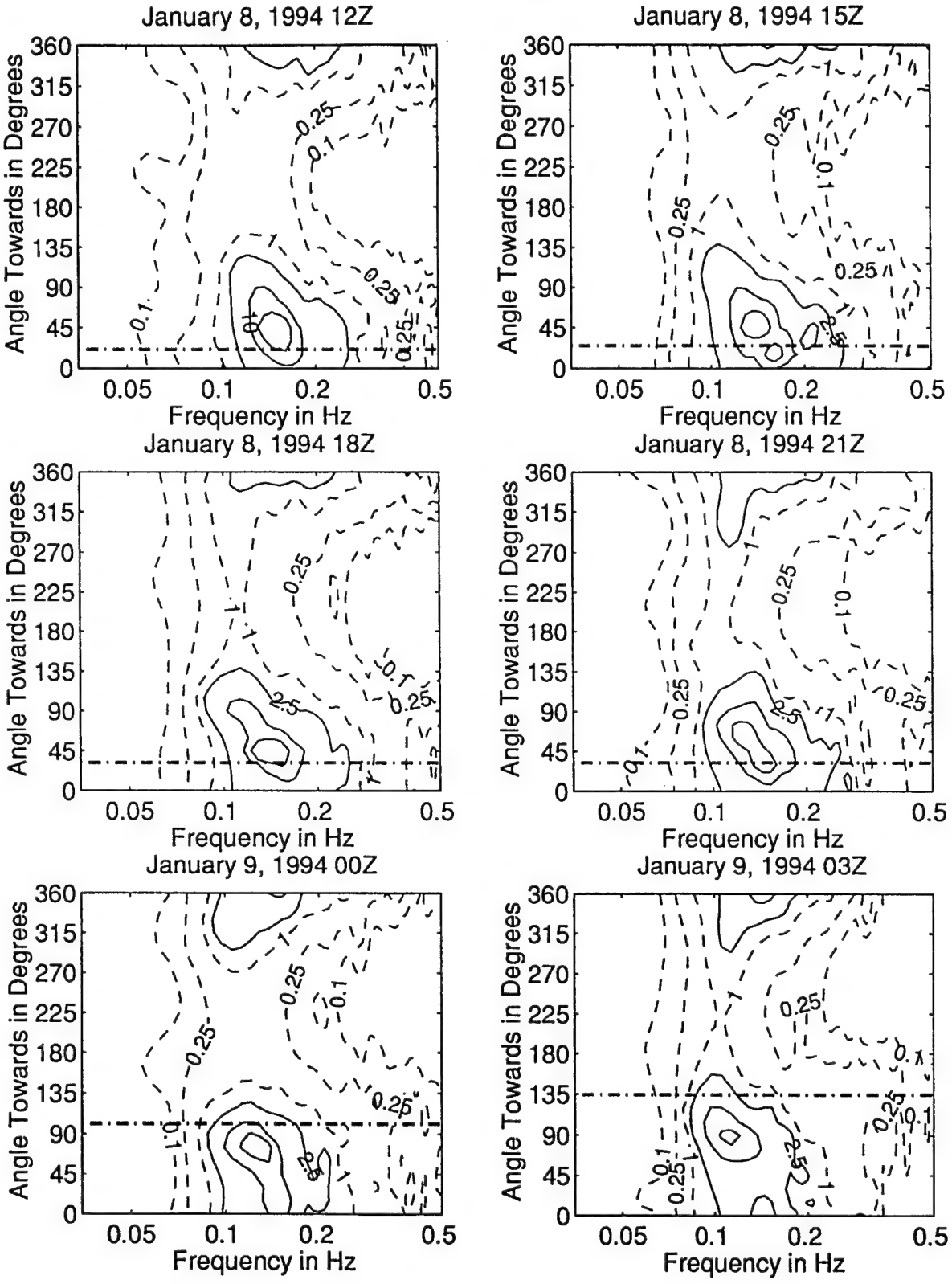

Figure 3.4.44: Directional wave spectra, computed using maximum entropy method. Contours of spectral density as a function of direction. Contours are 0.1, 0.25, 1 (dashed), 2.5, 10, 25, 100, and 250 (solid). Wind direction is shown by thick dashed line.

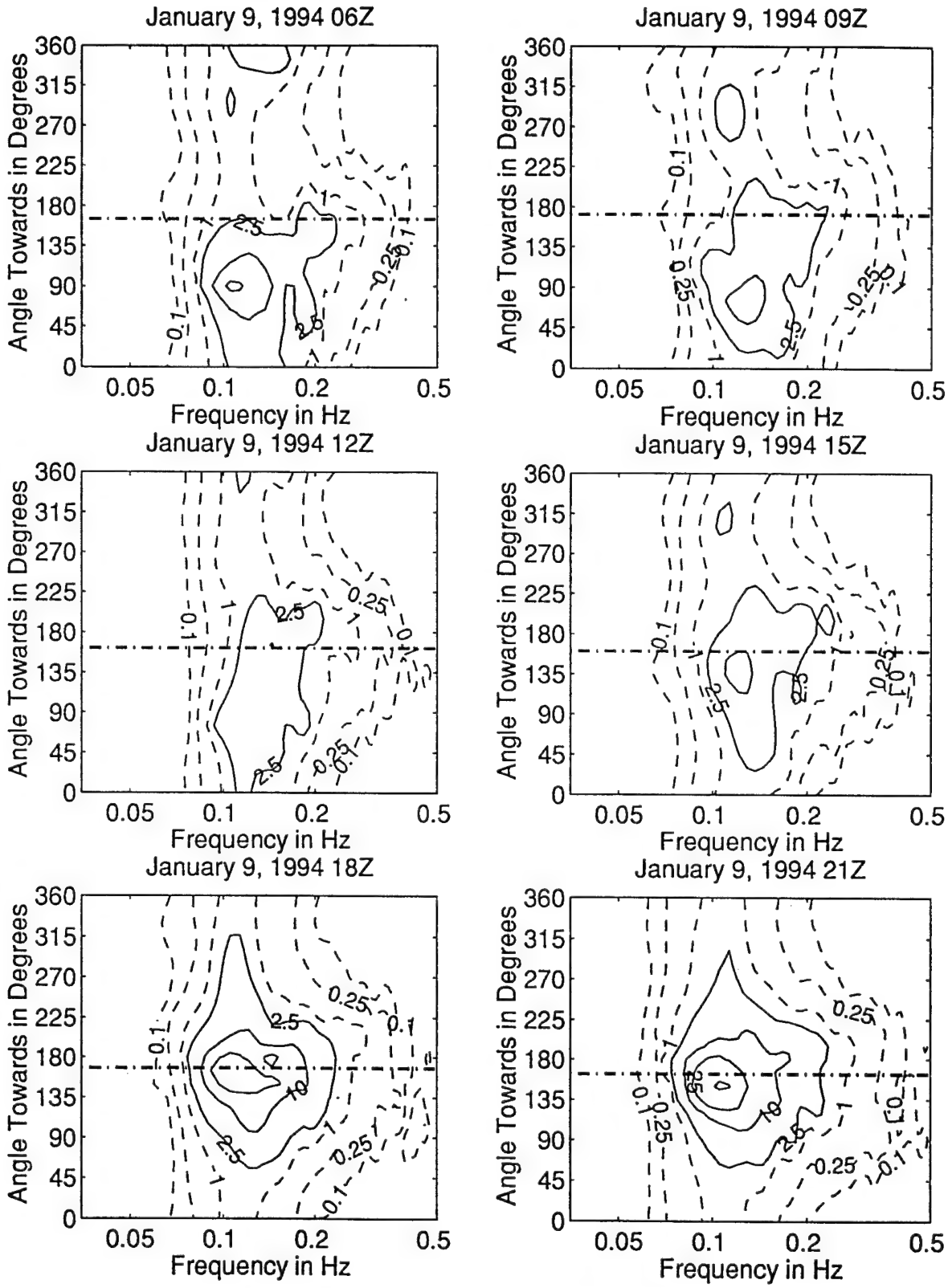

Figure 3.4.45: Directional wave spectra, computed using maximum entropy method. Contours of spectral density as a function of direction. Contours are 0.1, 0.25, 1 (dashed), 2.5, 10, 25, 100, and 250 (solid). Wind direction is shown by thick dashed line.

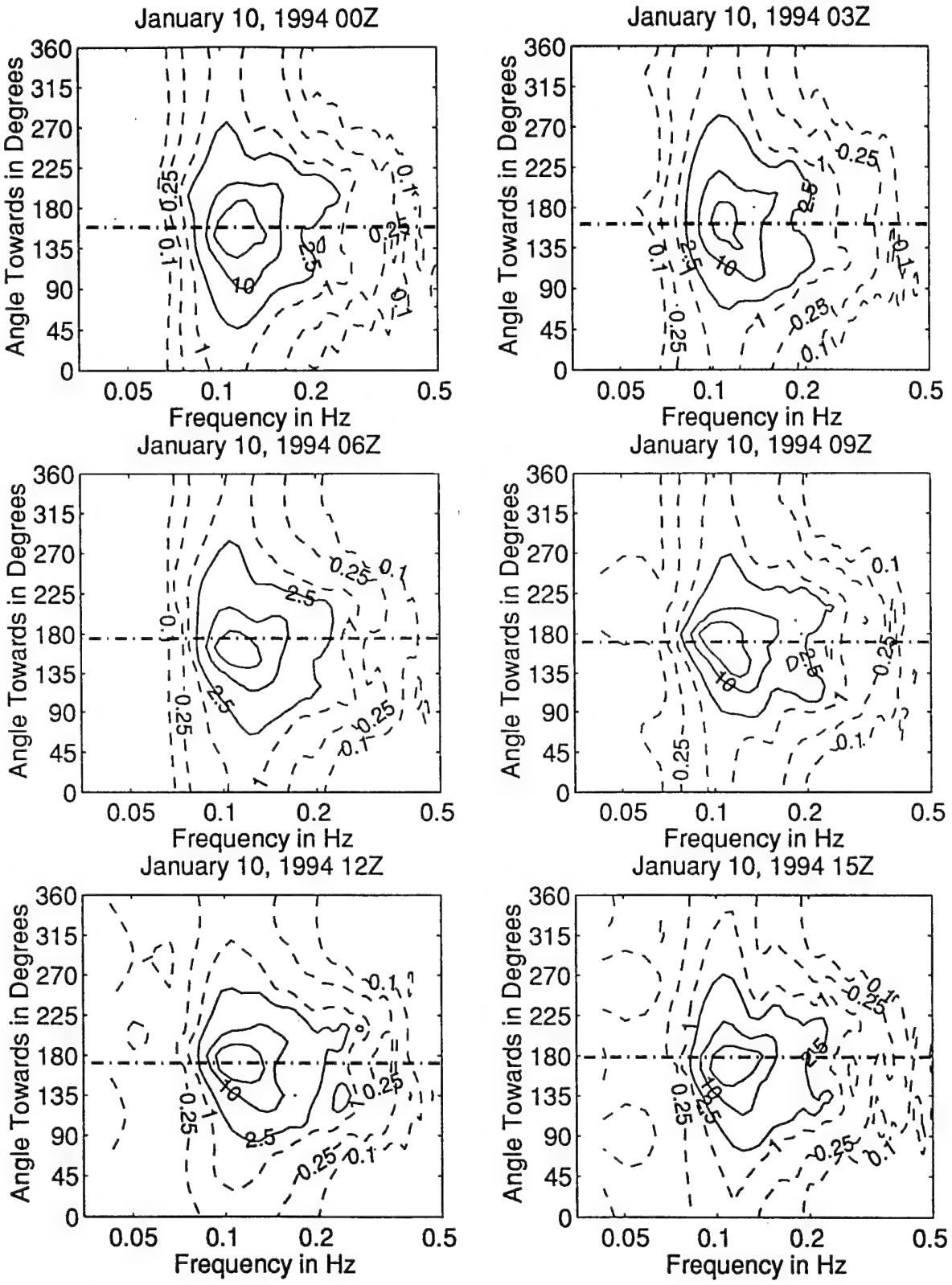

Figure 3.4.46: Directional wave spectra, computed using maximum entropy method. Contours of spectral density as a function of direction. Contours are 0.1, 0.25, 1 (dashed), 2.5, 10, 25, 100, and 250 (solid). Wind direction is shown by thick dashed line.

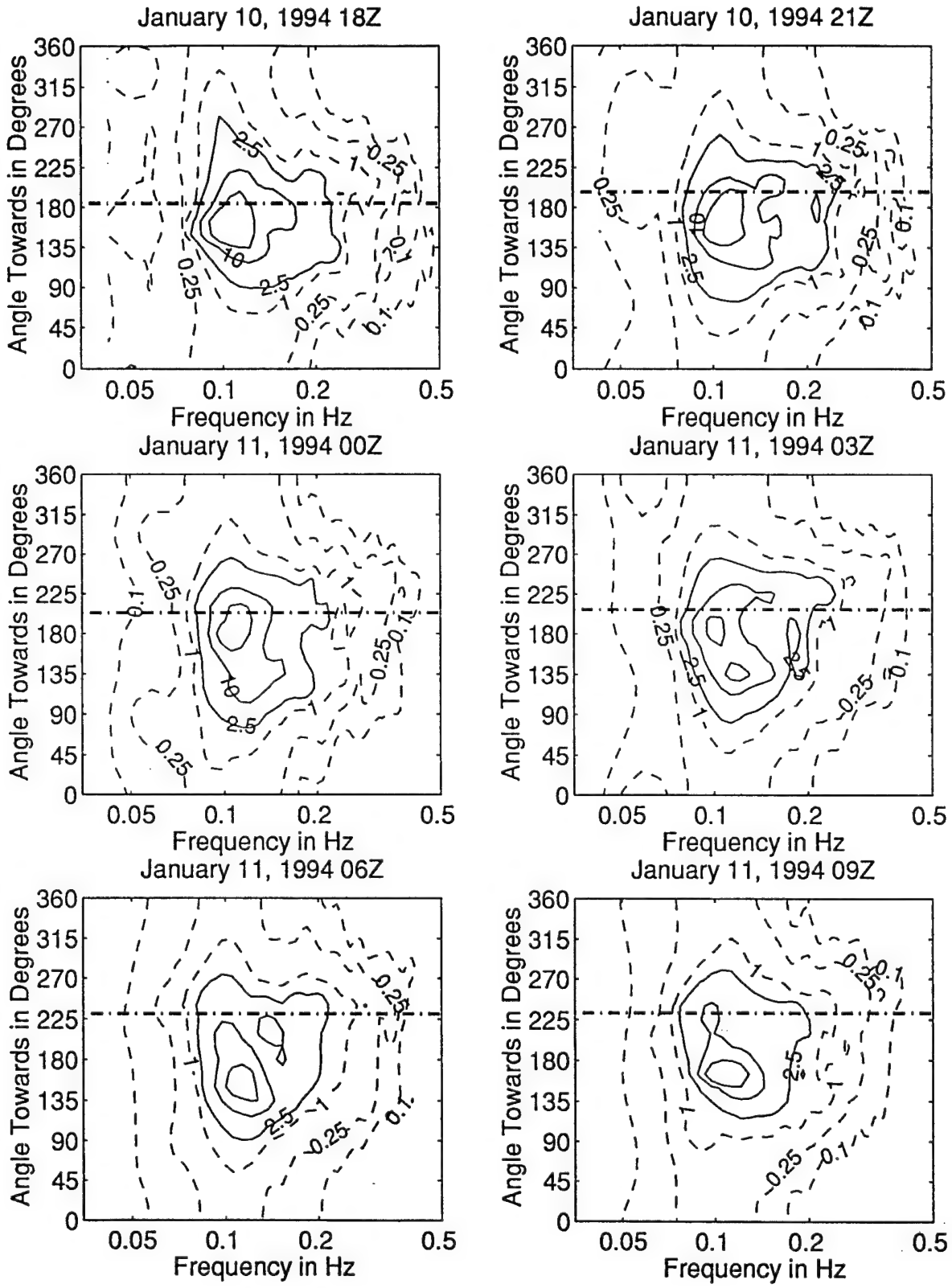

Figure 3.4.47: Directional wave spectra, computed using maximum entropy method. Contours of spectral density as a function of direction. Contours are 0.1, 0.25, 1 (dashed), 2.5, 10, 25, 100, and 250 (solid). Wind direction is shown by thick dashed line.

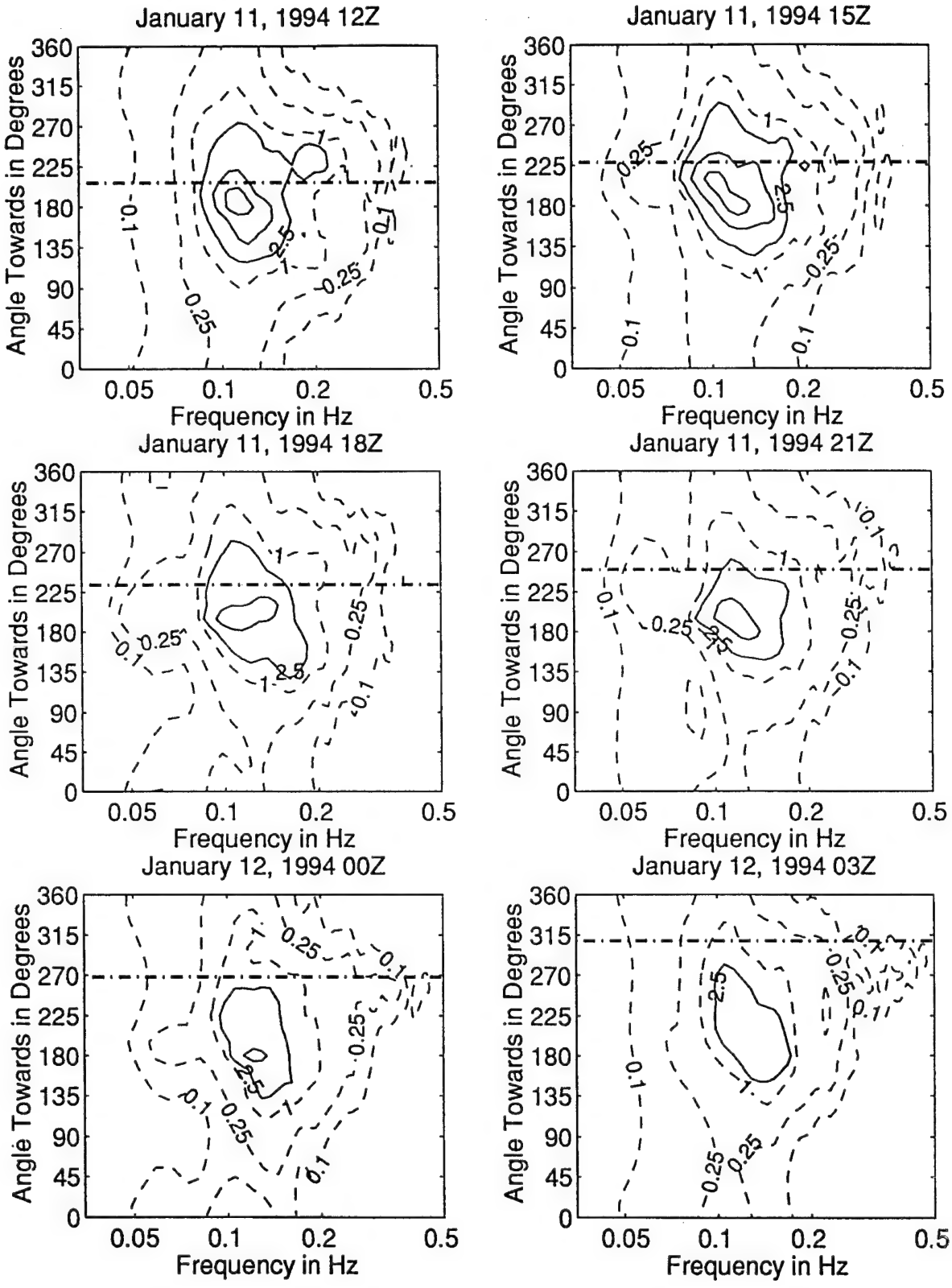

Figure 3.4.48: Directional wave spectra, computed using maximum entropy method. Contours of spectral density as a function of direction. Contours are 0.1, 0.25, 1 (dashed), 2.5, 10, 25, 100, and 250 (solid). Wind direction is shown by thick dashed line.

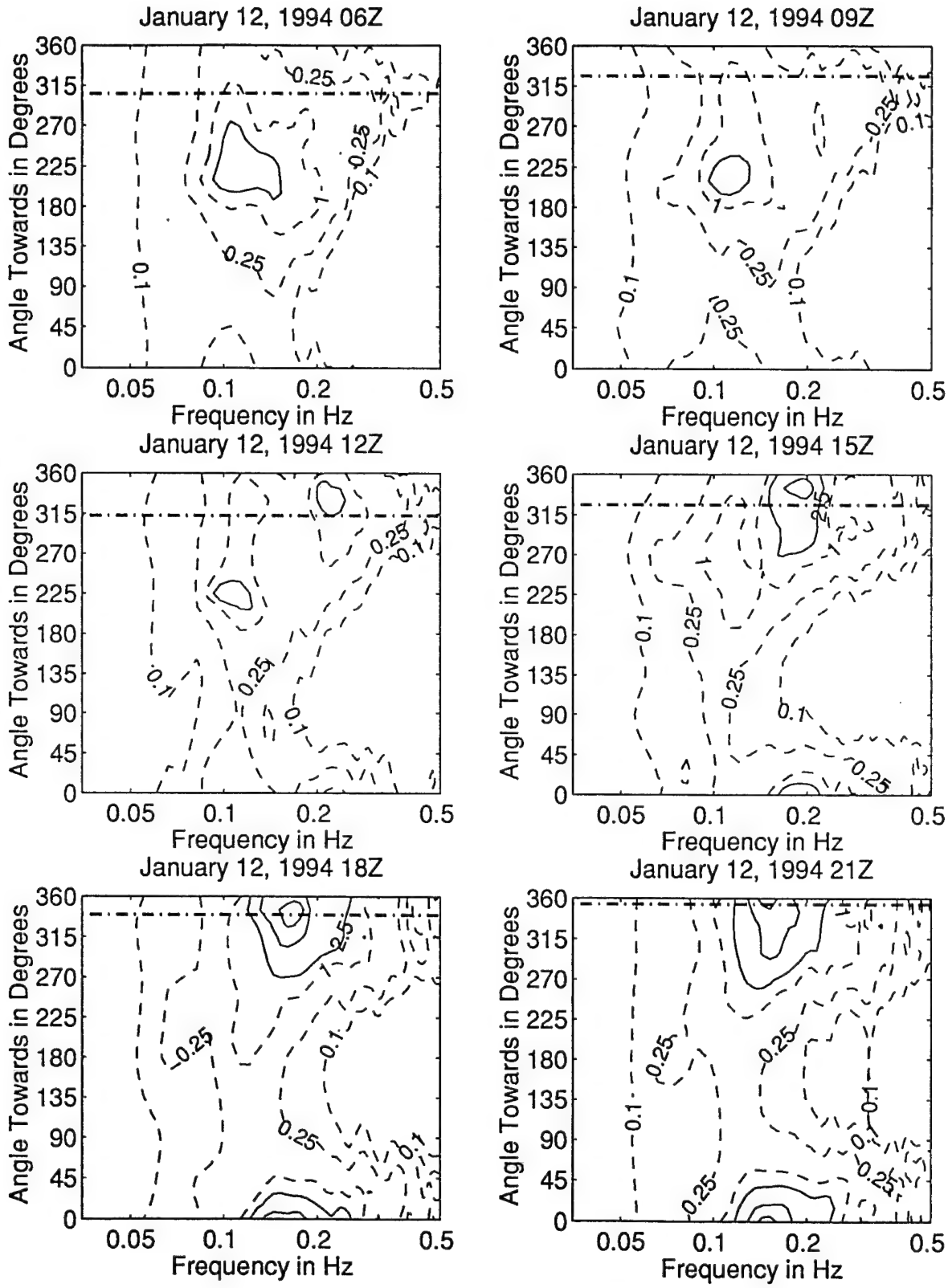

Figure 3.4.49: Directional wave spectra, computed using maximum entropy method. Contours of spectral density as a function of direction. Contours are 0.1, 0.25, 1 (dashed), 2.5, 10, 25, 100, and 250 (solid). Wind direction is shown by thick dashed line.

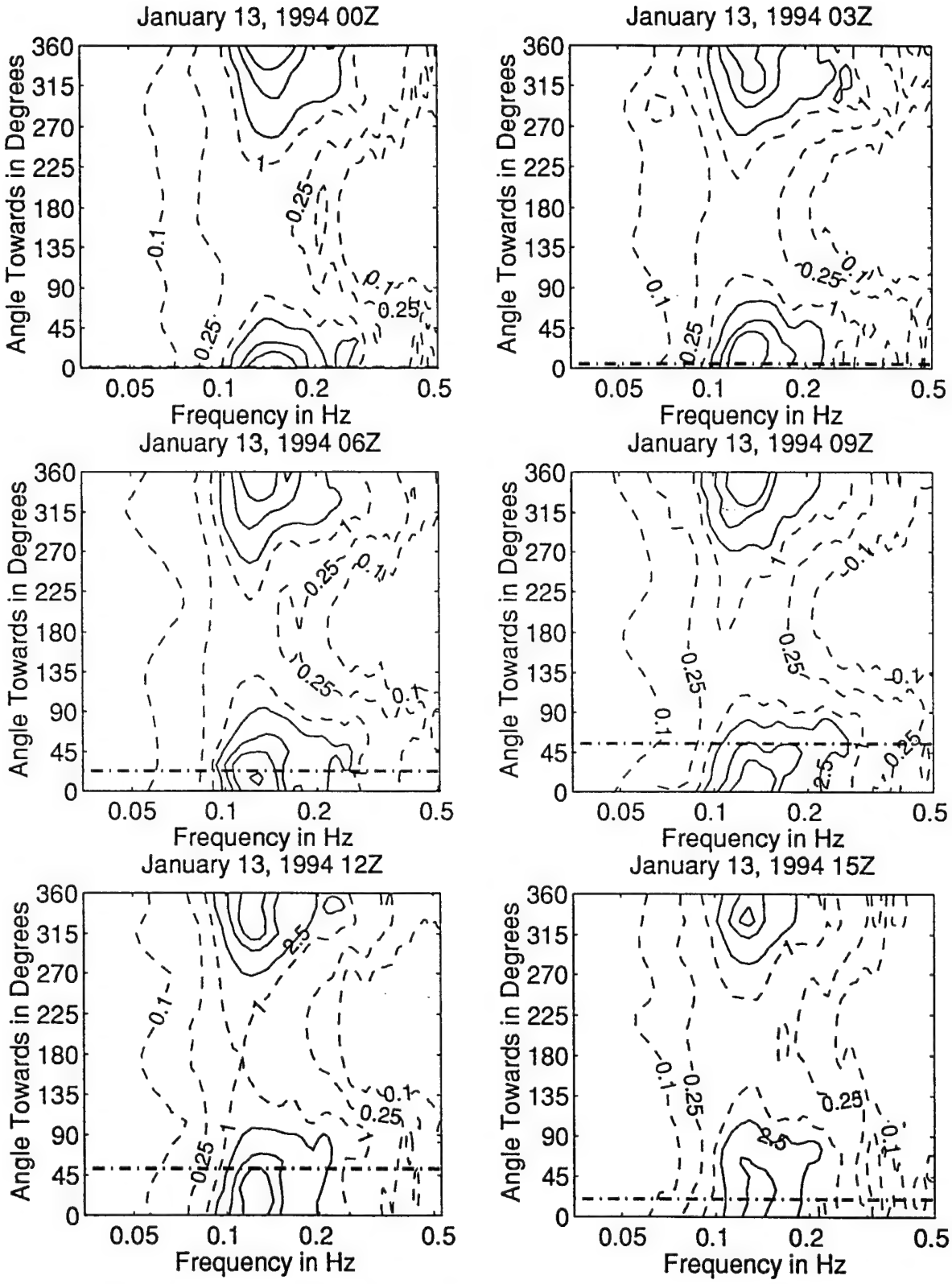

Figure 3.4.50: Directional wave spectra, computed using maximum entropy method. Contours of spectral density as a function of direction. Contours are 0.1, 0.25, 1 (dashed), 2.5, 10, 25, 100, and 250 (solid). Wind direction is shown by thick dashed line.

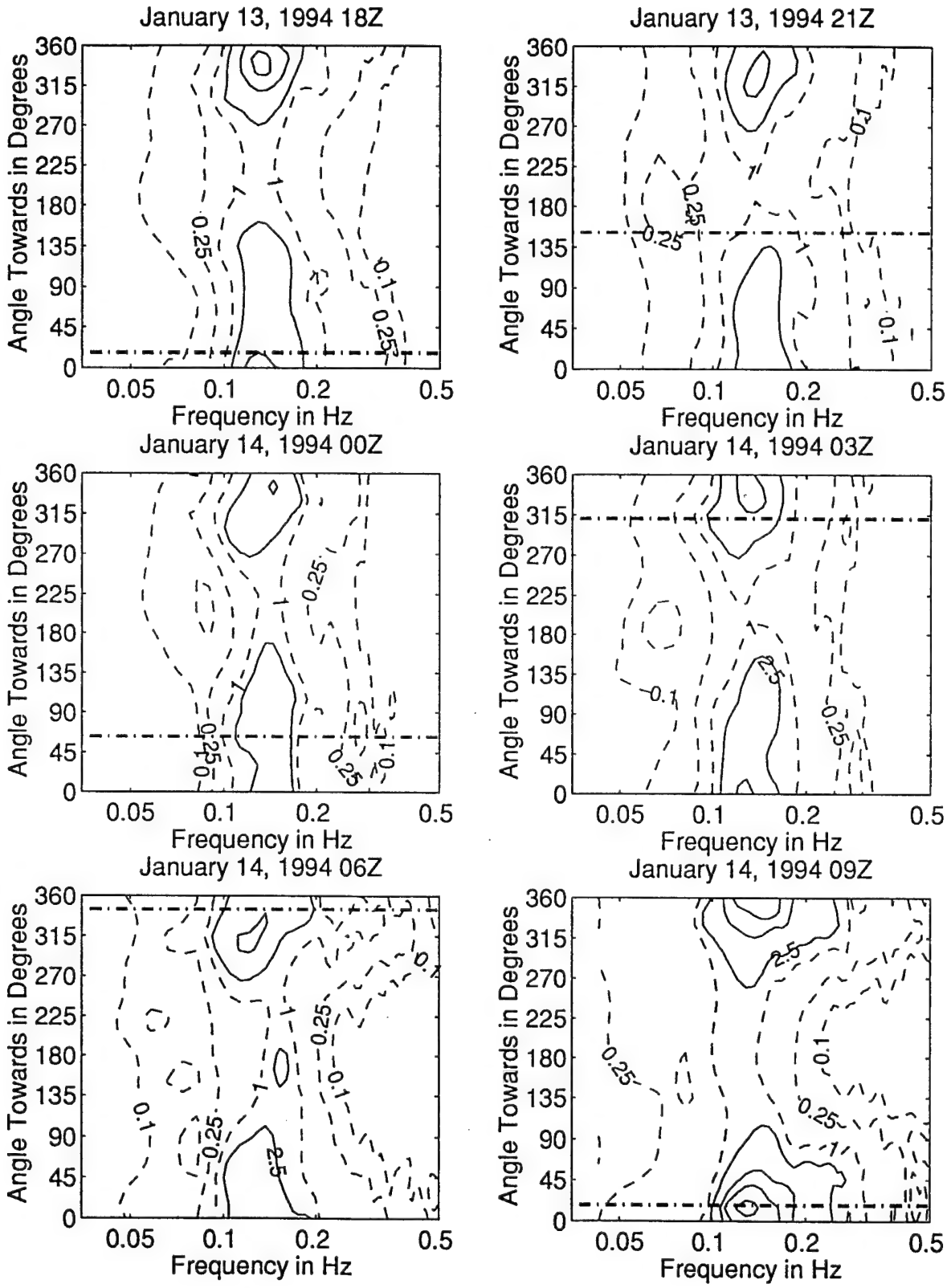

Figure 3.4.51: Directional wave spectra, computed using maximum entropy method. Contours of spectral density as a function of direction. Contours are 0.1, 0.25, 1 (dashed), 2.5, 10, 25, 100, and 250 (solid). Wind direction is shown by thick dashed line.

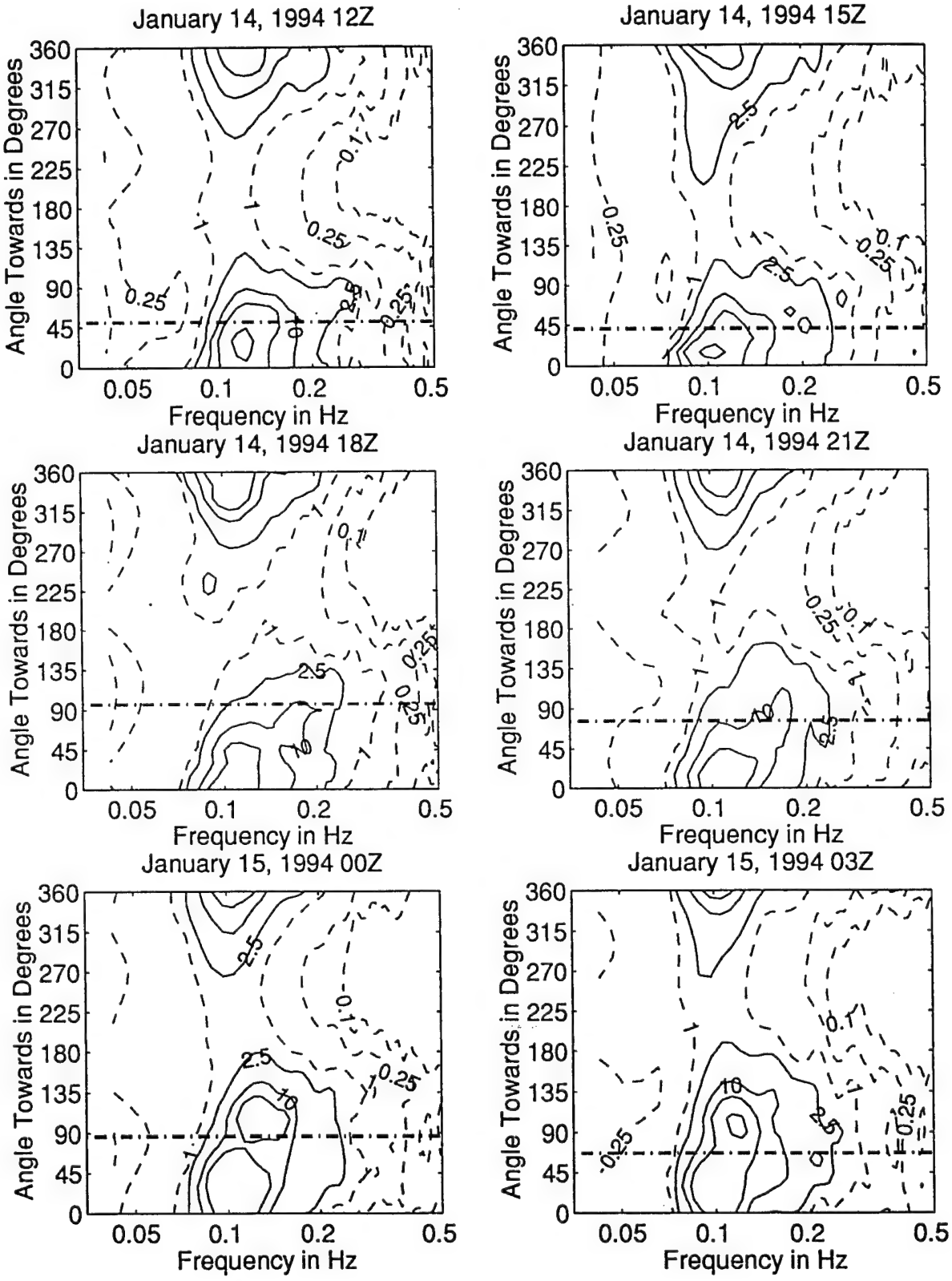

Figure 3.4.52: Directional wave spectra, computed using maximum entropy method. Contours of spectral density as a function of direction. Contours are 0.1, 0.25, 1 (dashed), 2.5, 10, 25, 100, and 250 (solid). Wind direction is shown by thick dashed line.

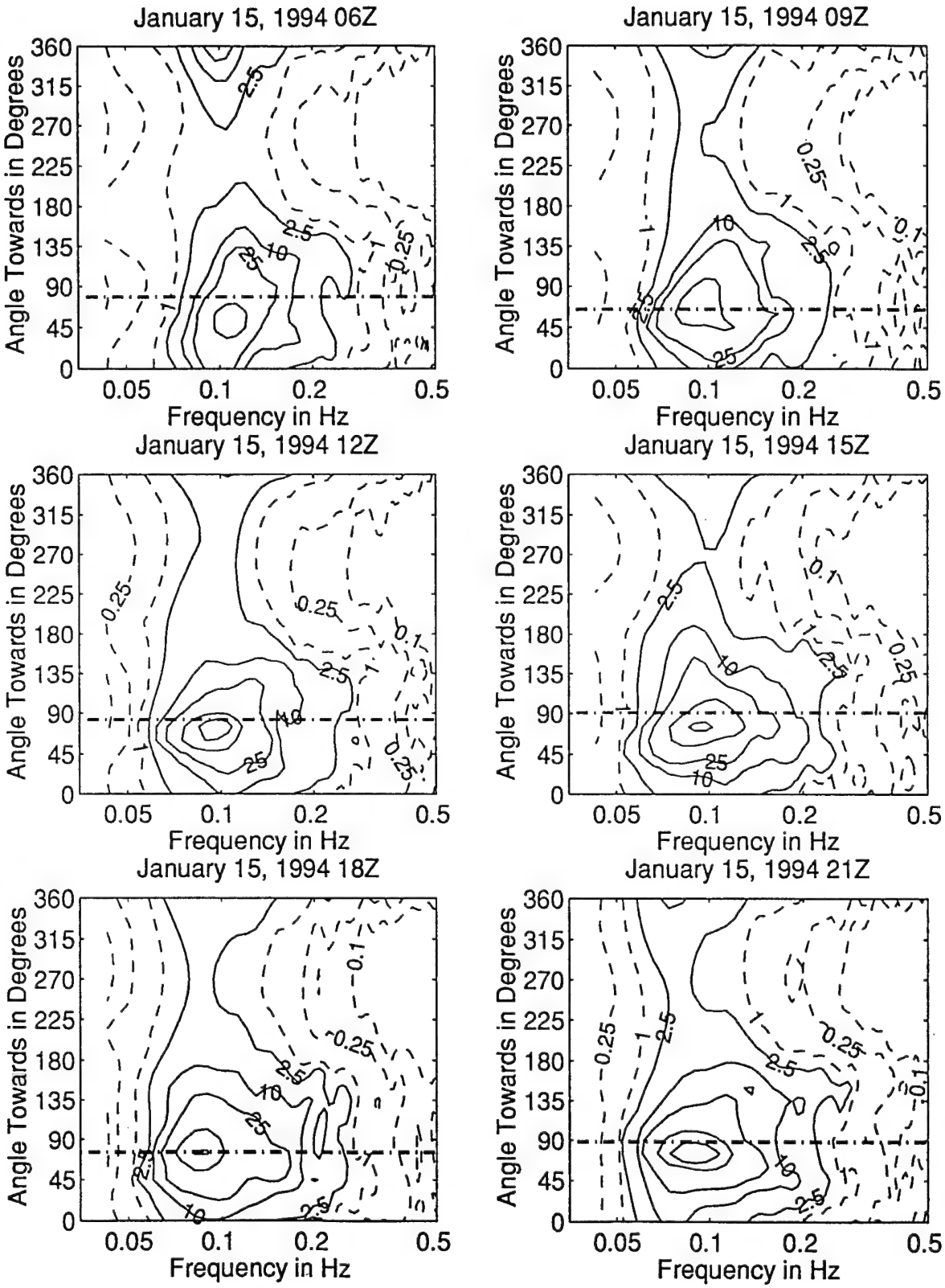

Figure 3.4.53: Directional wave spectra, computed using maximum entropy method. Contours of spectral density as a function of direction. Contours are 0.1, 0.25, 1 (dashed), 2.5, 10, 25, 100, and 250 (solid). Wind direction is shown by thick dashed line.

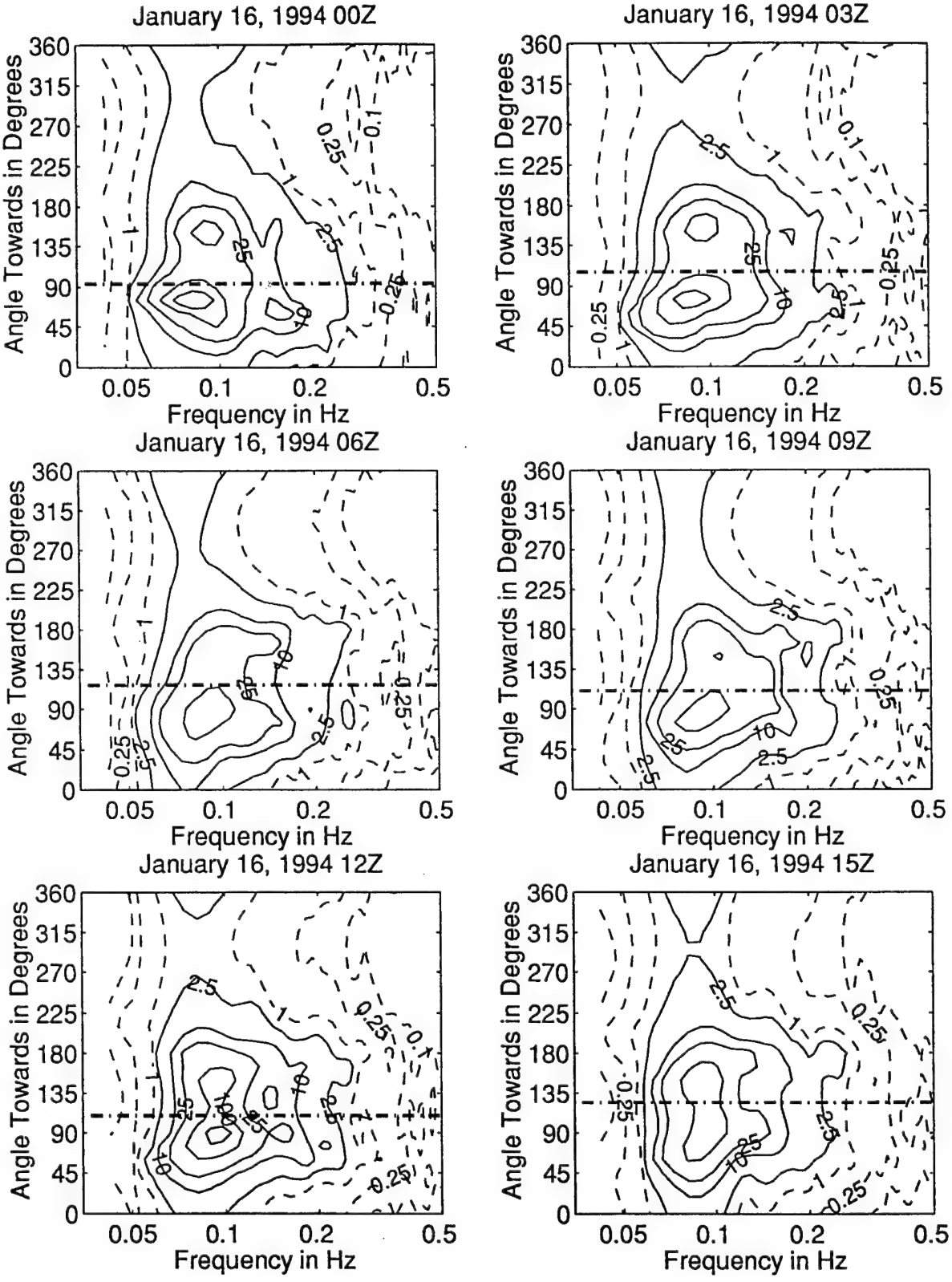

Figure 3.4.54: Directional wave spectra, computed using maximum entropy method. Contours of spectral density as a function of direction. Contours are 0.1, 0.25, 1 (dashed), 2.5, 10, 25, 100, and 250 (solid). Wind direction is shown by thick dashed line.

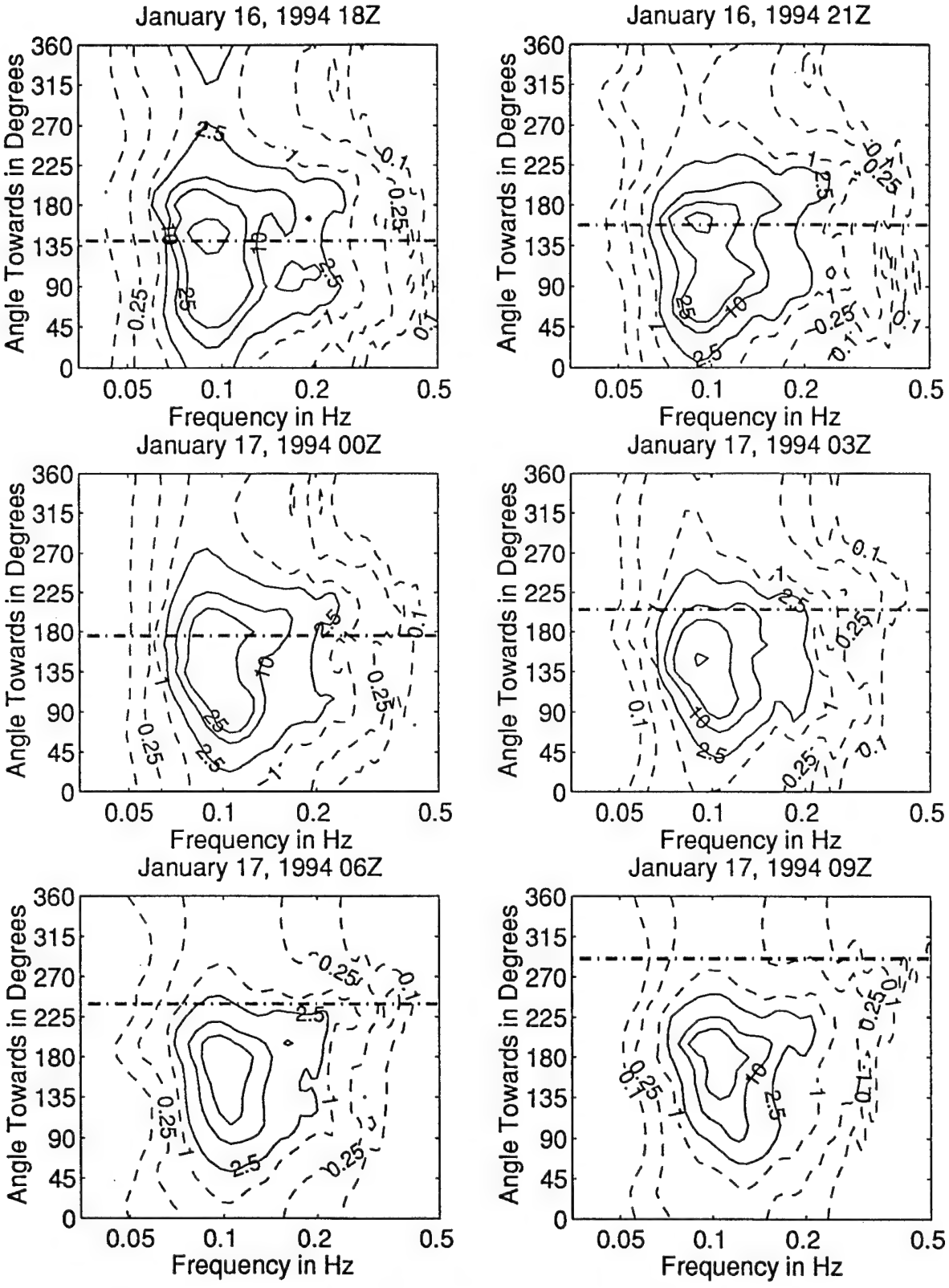

Figure 3.4.55: Directional wave spectra, computed using maximum entropy method. Contours of spectral density as a function of direction. Contours are 0.1, 0.25, 1 (dashed), 2.5, 10, 25, 100, and 250 (solid). Wind direction is shown by thick dashed line.

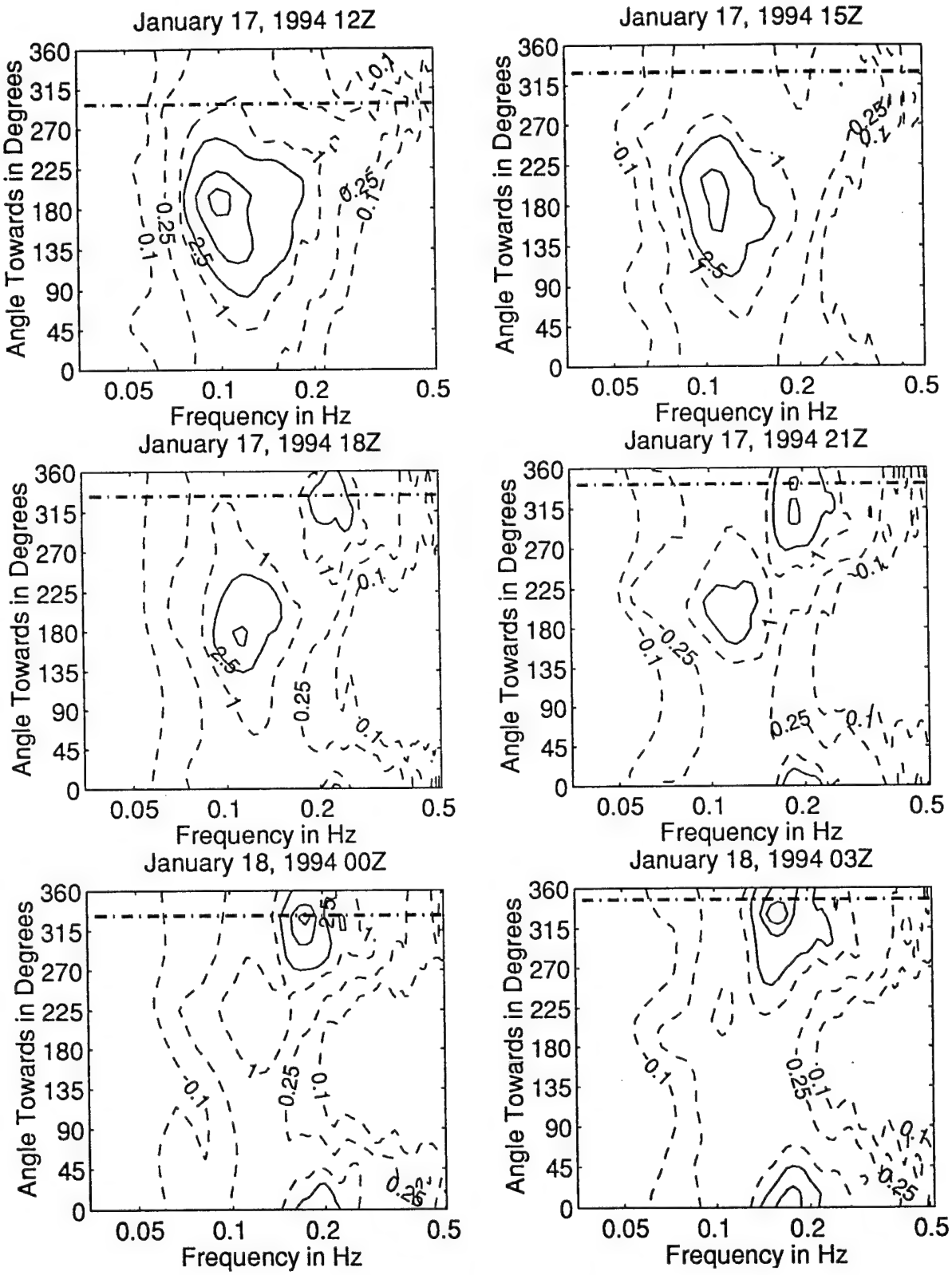

Figure 3.4.56: Directional wave spectra, computed using maximum entropy method. Contours of spectral density as a function of direction. Contours are 0.1, 0.25, 1 (dashed), 2.5, 10, 25, 100, and 250 (solid). Wind direction is shown by thick dashed line.

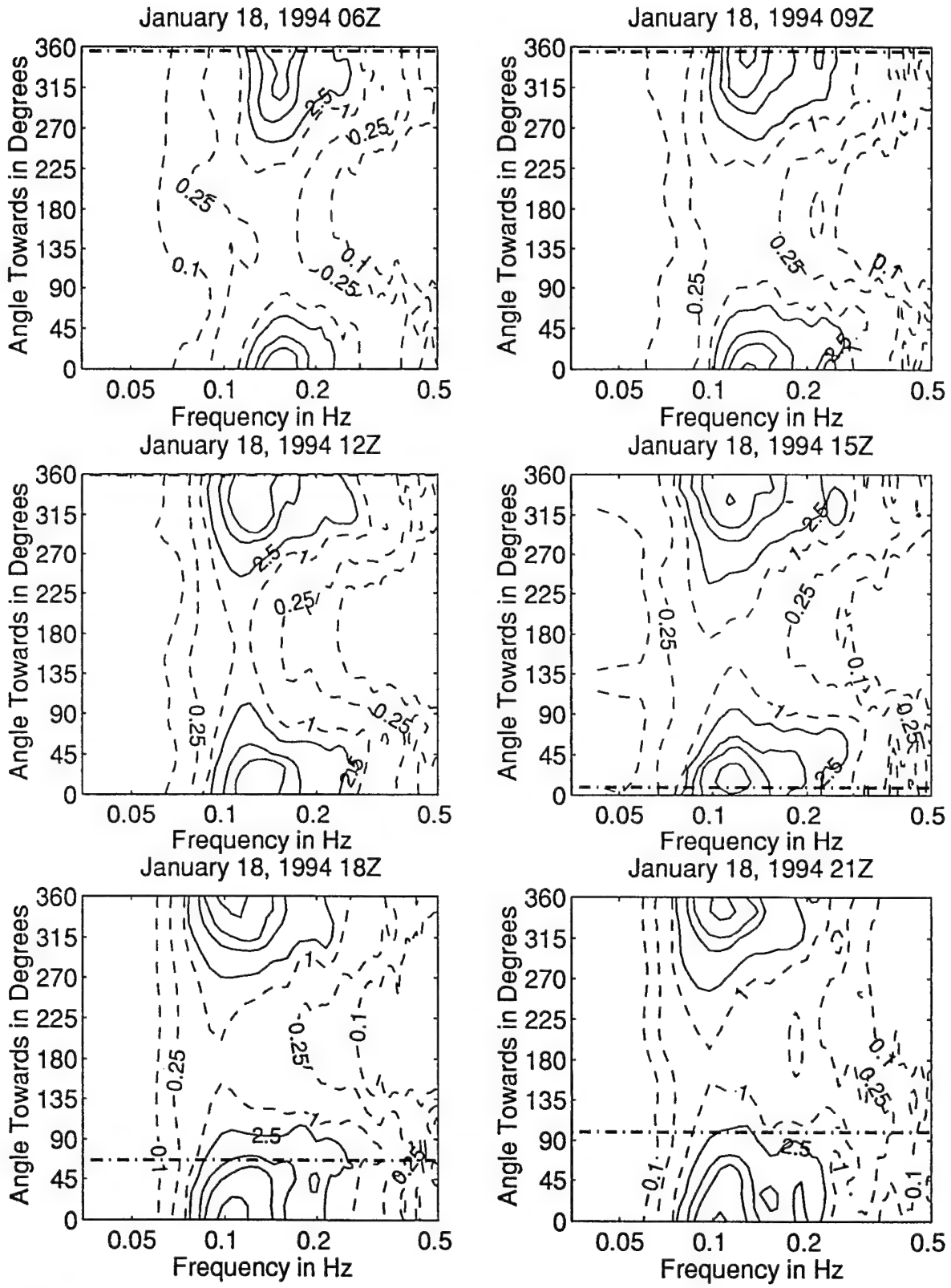

Figure 3.4.57: Directional wave spectra, computed using maximum entropy method. Contours of spectral density as a function of direction. Contours are 0.1, 0.25, 1 (dashed), 2.5, 10, 25, 100, and 250 (solid). Wind direction is shown by thick dashed line.

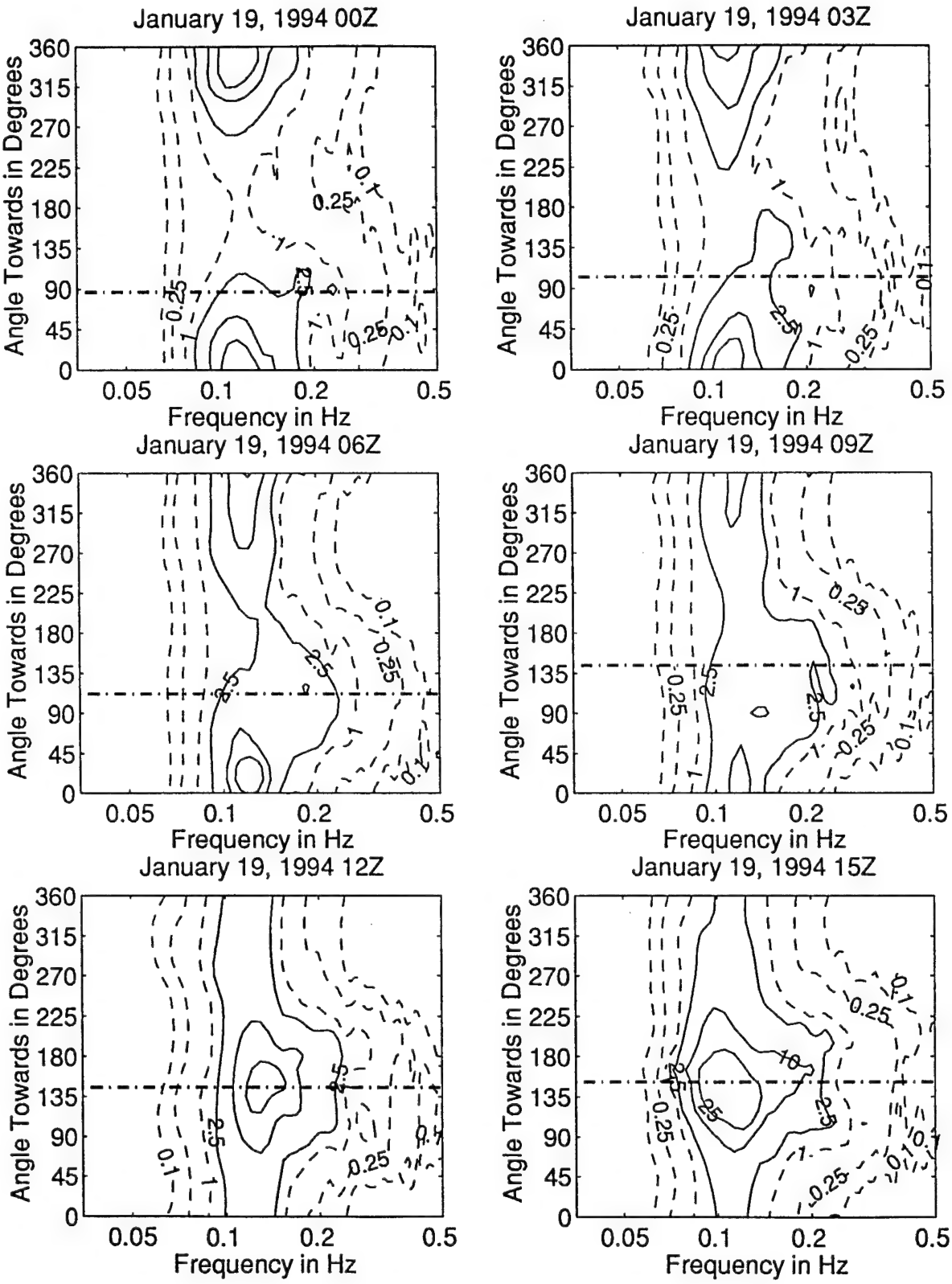

Figure 3.4.58: Directional wave spectra, computed using maximum entropy method. Contours of spectral density as a function of direction. Contours are 0.1, 0.25, 1 (dashed), 2.5, 10, 25, 100, and 250 (solid). Wind direction is shown by thick dashed line.

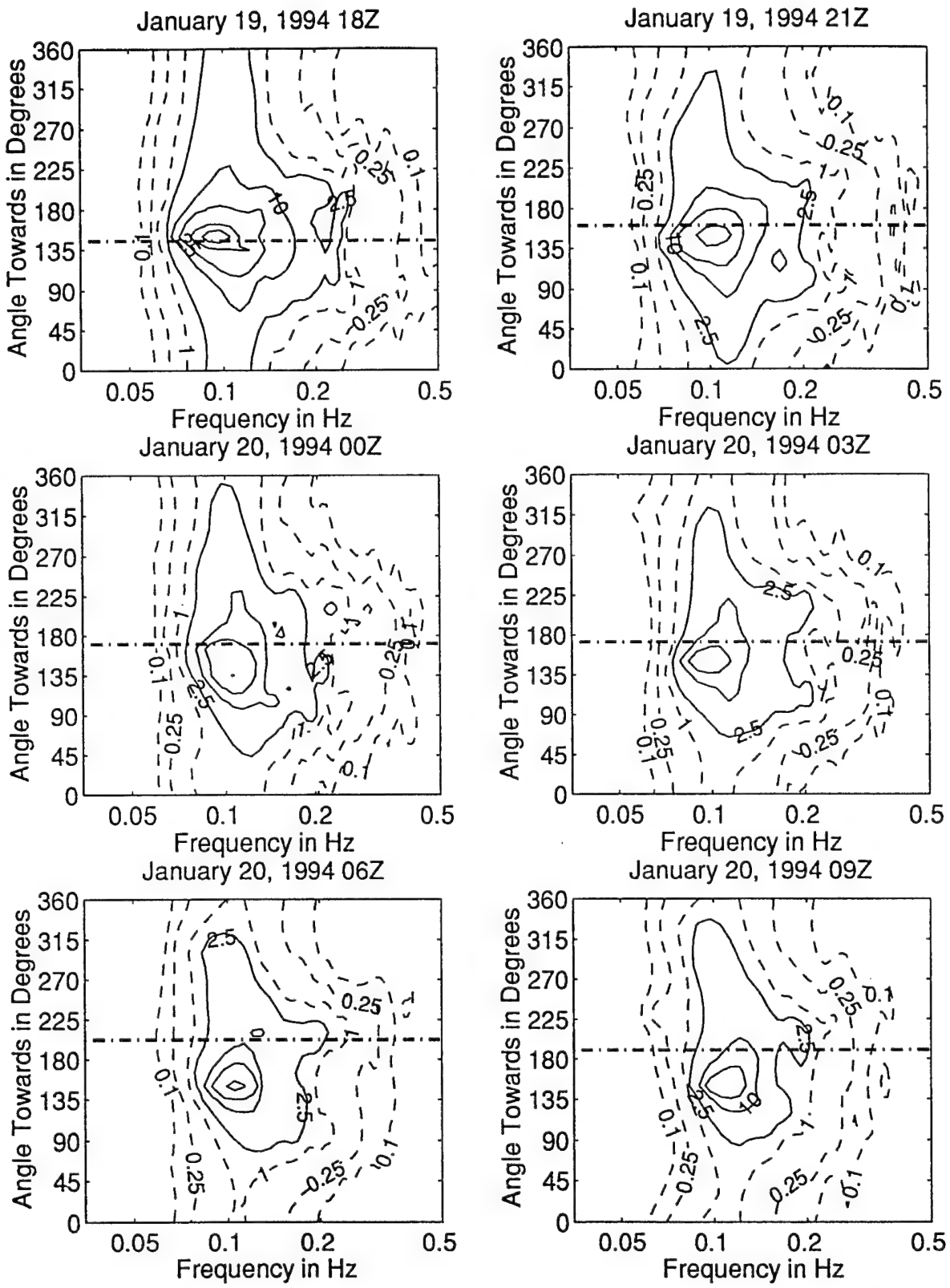

Figure 3.4.59: Directional wave spectra, computed using maximum entropy method. Contours of spectral density as a function of direction. Contours are 0.1, 0.25, 1 (dashed), 2.5, 10, 25, 100, and 250 (solid). Wind direction is shown by thick dashed line.

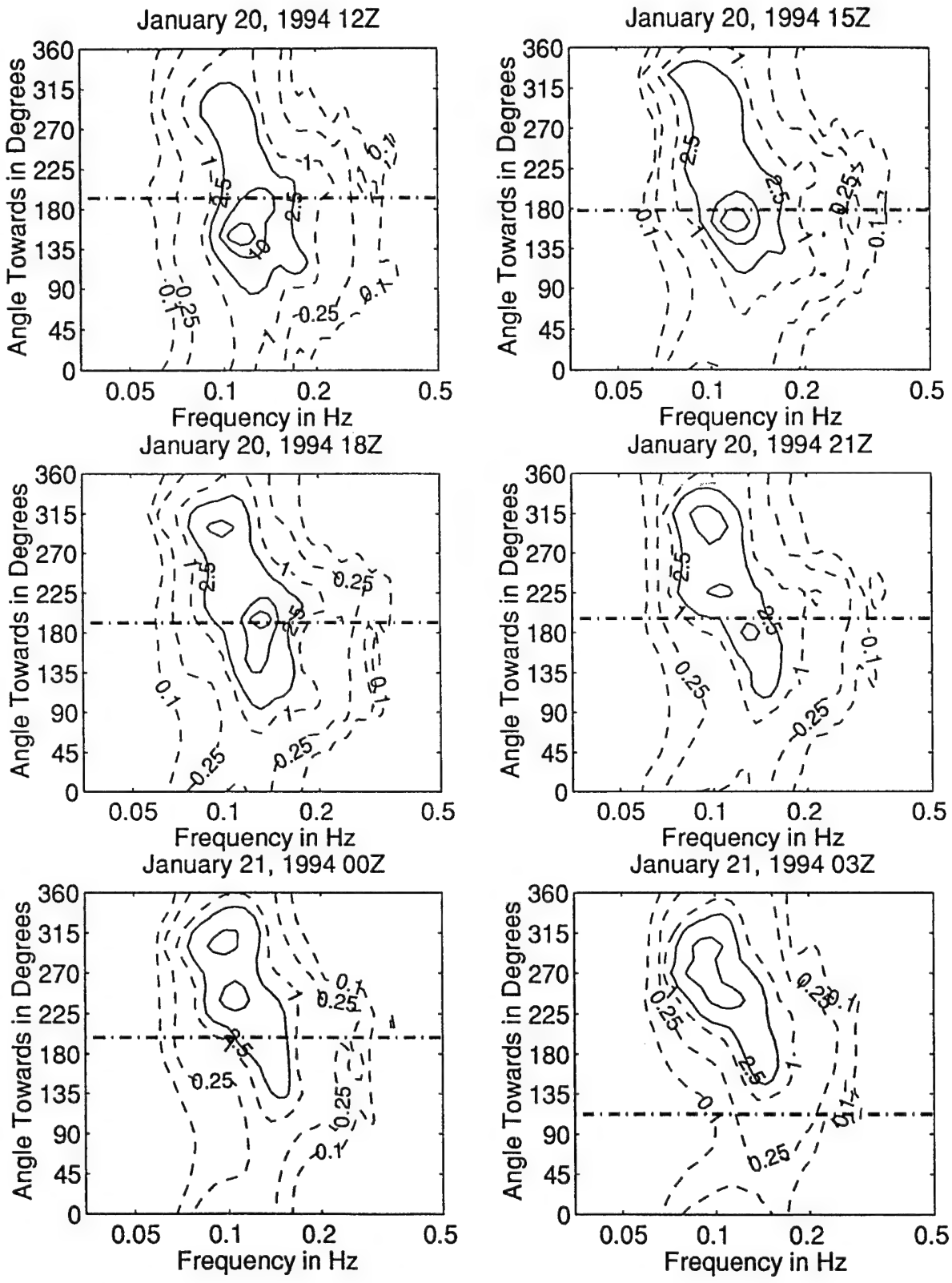

Figure 3.4.60: Directional wave spectra, computed using maximum entropy method. Contours of spectral density as a function of direction. Contours are 0.1, 0.25, 1 (dashed), 2.5, 10, 25, 100, and 250 (solid). Wind direction is shown by thick dashed line.

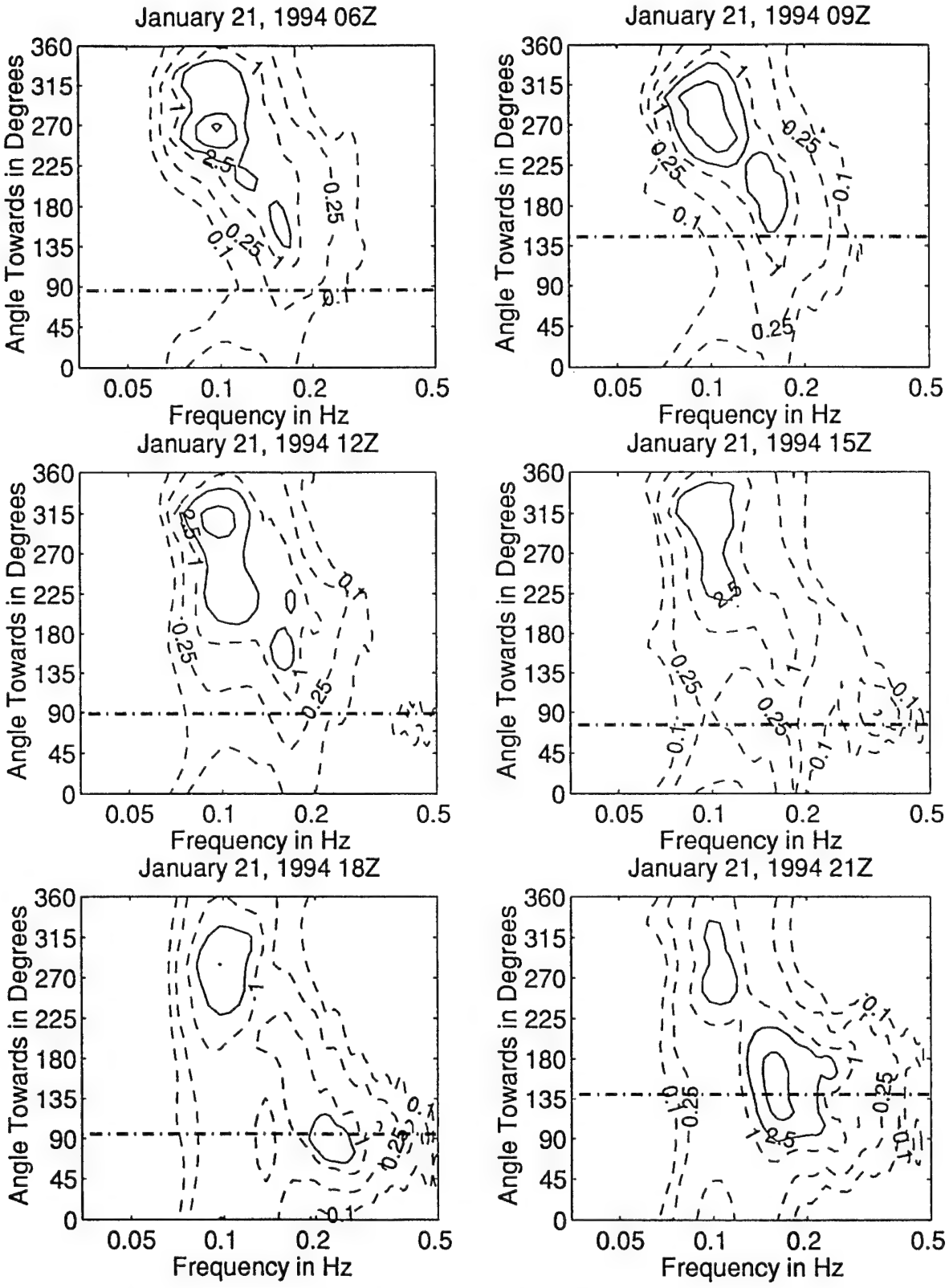

Figure 3.4.61: Directional wave spectra, computed using maximum entropy method. Contours of spectral density as a function of direction. Contours are 0.1, 0.25, 1 (dashed), 2.5, 10, 25, 100, and 250 (solid). Wind direction is shown by thick dashed line.

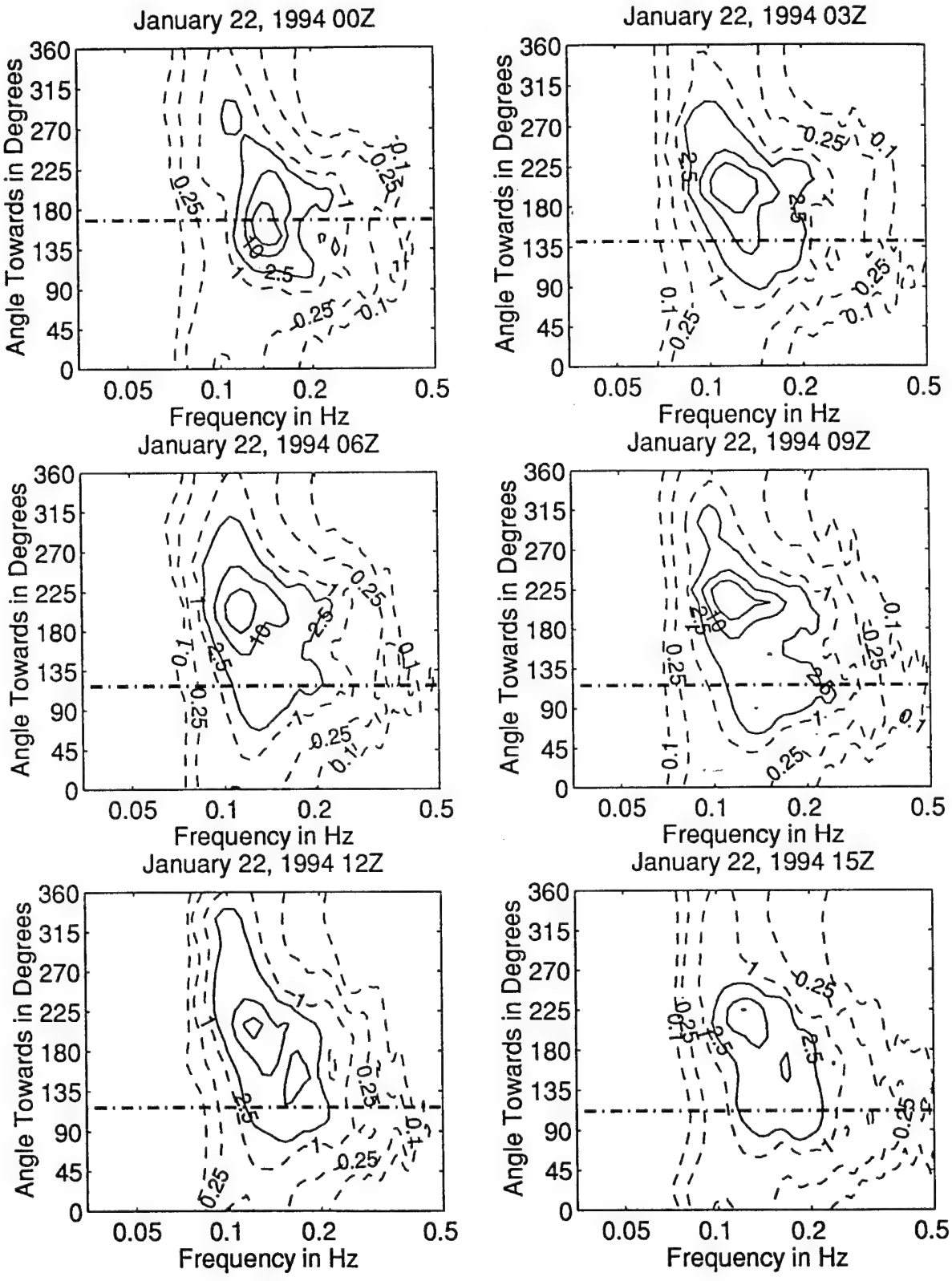

Figure 3.4.62: Directional wave spectra, computed using maximum entropy method. Contours of spectral density as a function of direction. Contours are 0.1, 0.25, 1 (dashed), 2.5, 10, 25, 100, and 250 (solid). Wind direction is shown by thick dashed line.

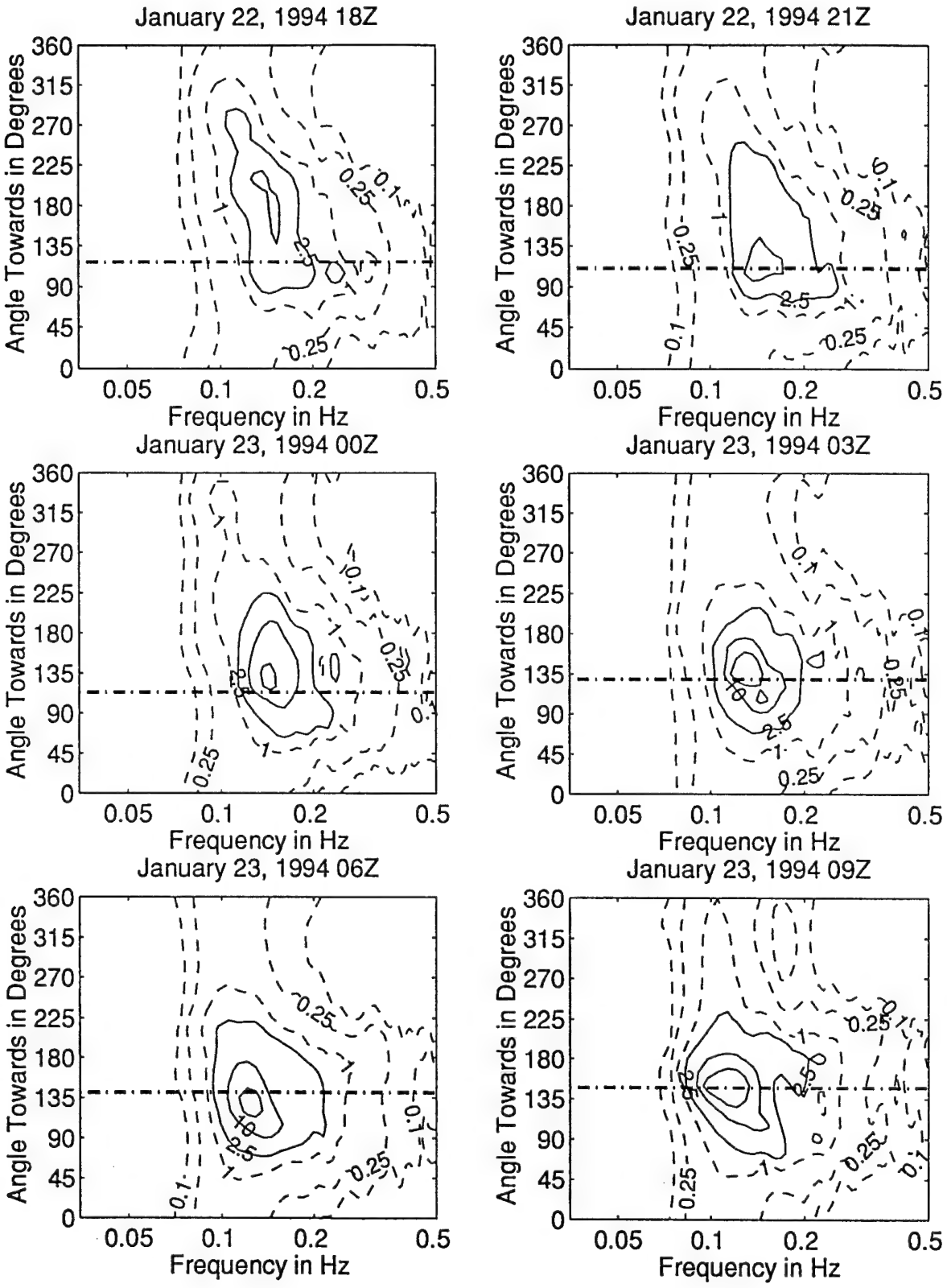

Figure 3.4.63: Directional wave spectra, computed using maximum entropy method. Contours of spectral density as a function of direction. Contours are 0.1, 0.25, 1 (dashed), 2.5, 10, 25, 100, and 250 (solid). Wind direction is shown by thick dashed line.

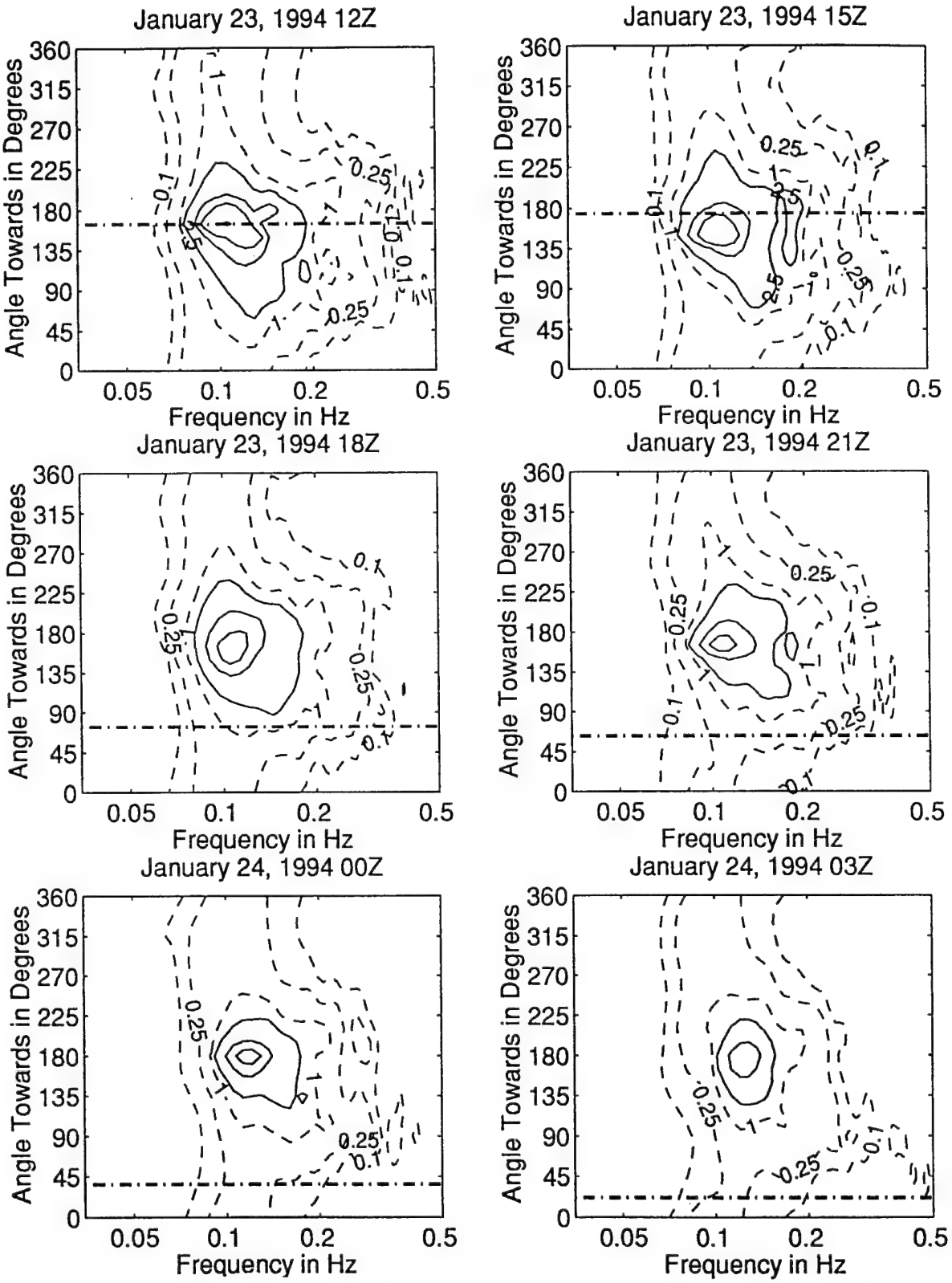

Figure 3.4.64: Directional wave spectra, computed using maximum entropy method. Contours of spectral density as a function of direction. Contours are 0.1, 0.25, 1 (dashed), 2.5, 10, 25, 100, and 250 (solid). Wind direction is shown by thick dashed line.

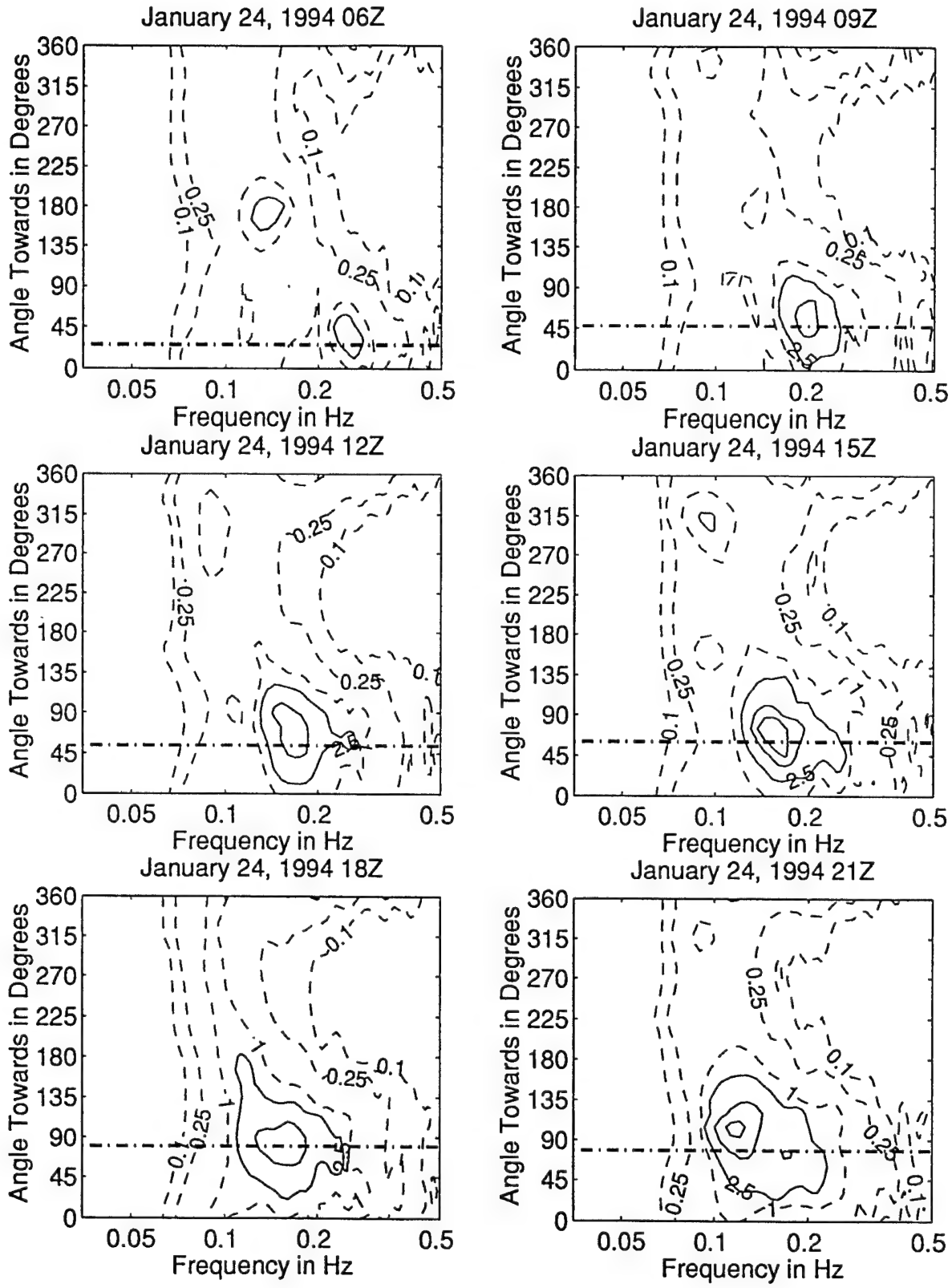

Figure 3.4.65: Directional wave spectra, computed using maximum entropy method. Contours of spectral density as a function of direction. Contours are 0.1, 0.25, 1 (dashed), 2.5, 10, 25, 100, and 250 (solid). Wind direction is shown by thick dashed line.

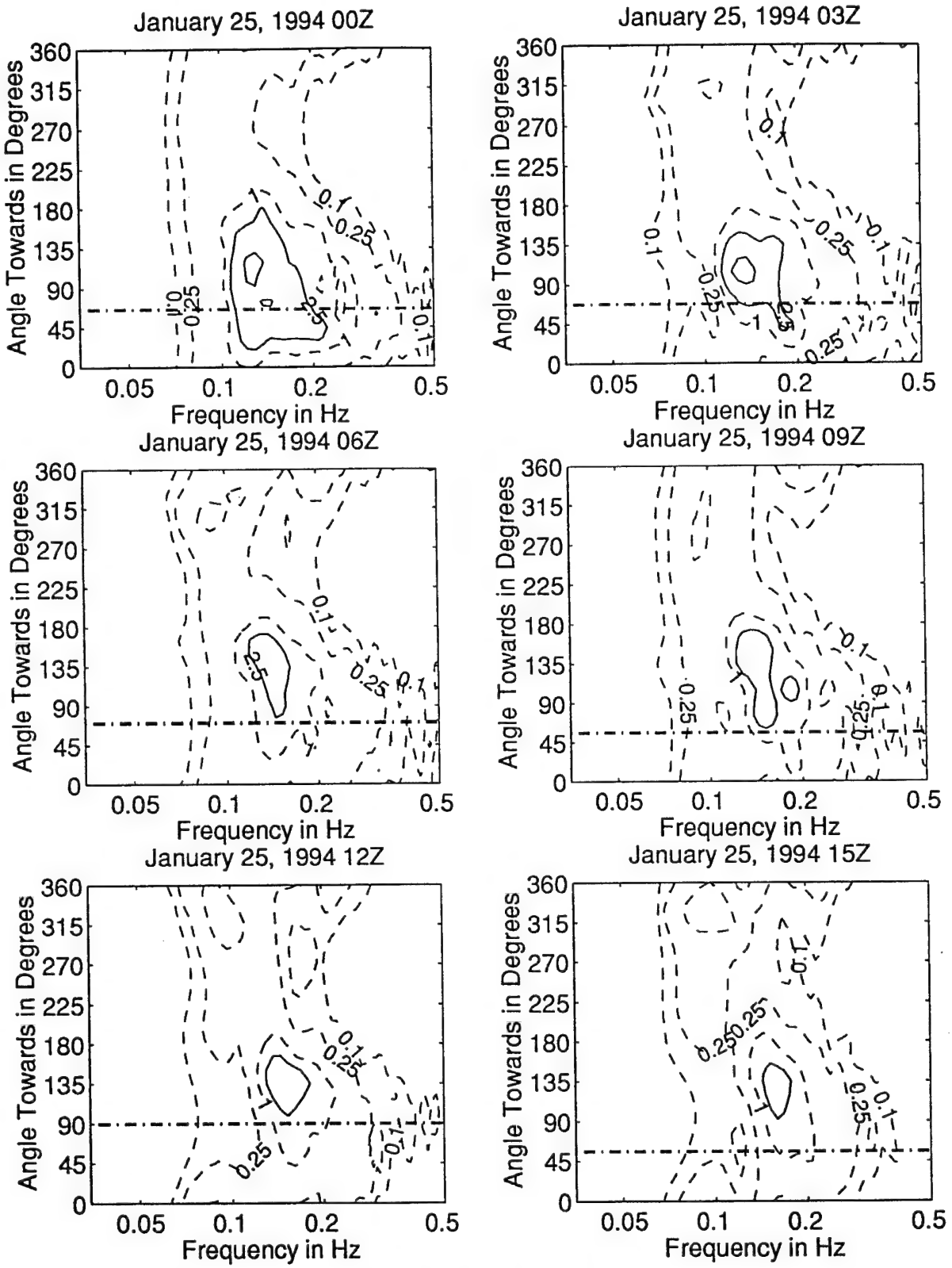

Figure 3.4.66: Directional wave spectra, computed using maximum entropy method. Contours of spectral density as a function of direction. Contours are 0.1, 0.25, 1 (dashed), 2.5, 10, 25, 100, and 250 (solid). Wind direction is shown by thick dashed line.

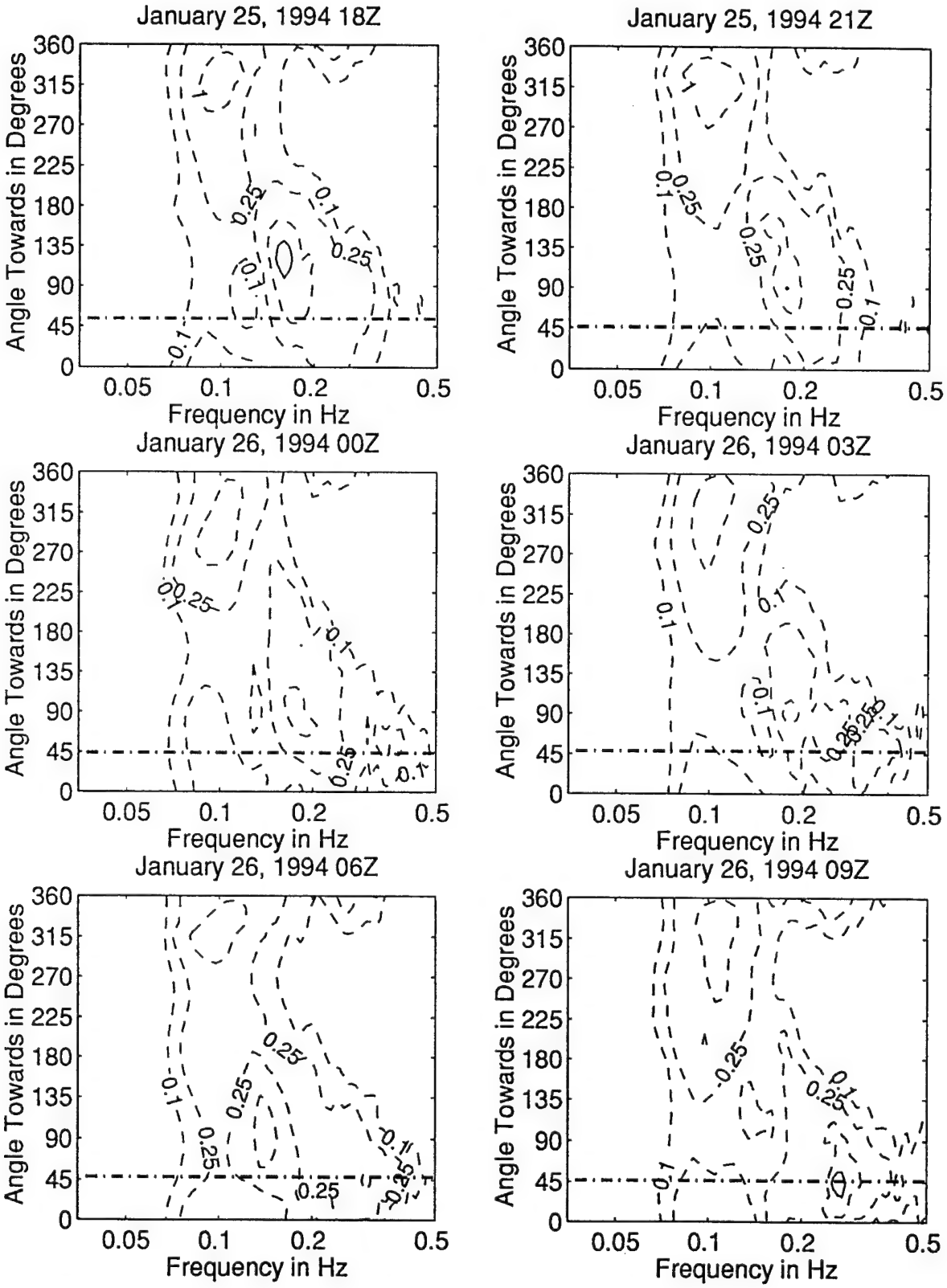

Figure 3.4.67: Directional wave spectra, computed using maximum entropy method. Contours of spectral density as a function of direction. Contours are 0.1, 0.25, 1 (dashed), 2.5, 10, 25, 100, and 250 (solid). Wind direction is shown by thick dashed line.

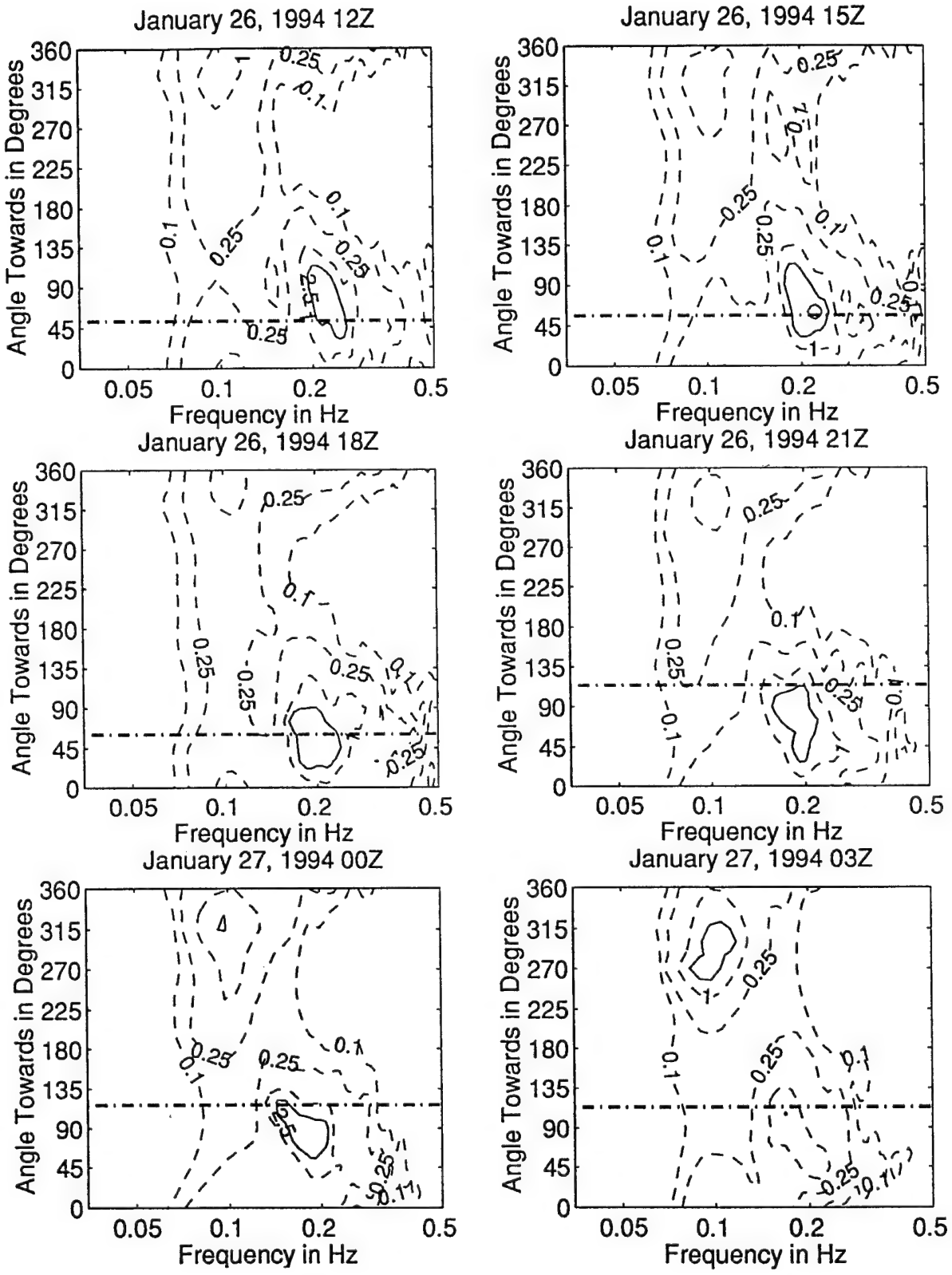

Figure 3.4.68: Directional wave spectra, computed using maximum entropy method. Contours of spectral density as a function of direction. Contours are 0.1, 0.25, 1 (dashed), 2.5, 10, 25, 100, and 250 (solid). Wind direction is shown by thick dashed line.

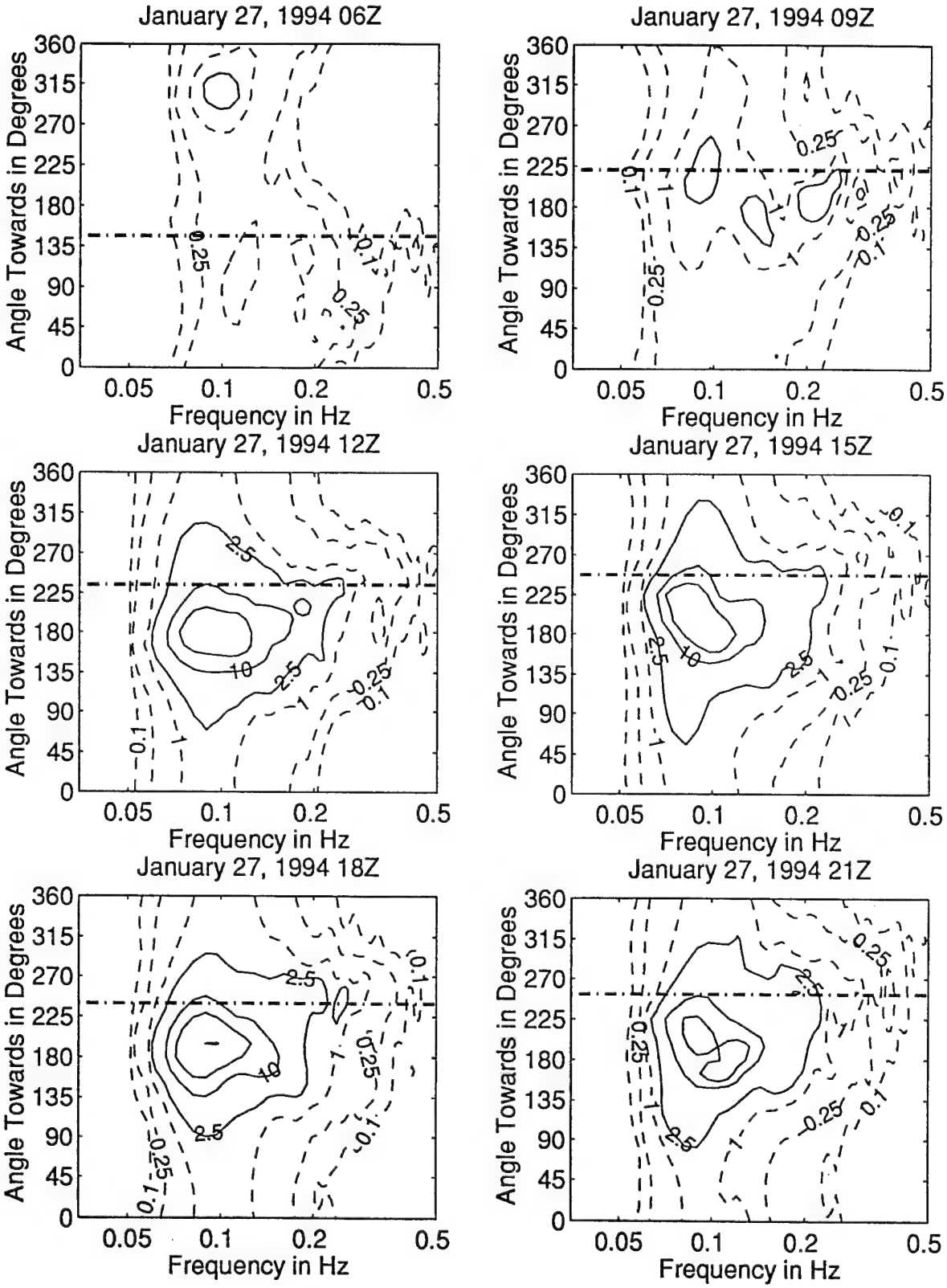

Figure 3.4.69: Directional wave spectra, computed using maximum entropy method. Contours of spectral density as a function of direction. Contours are 0.1, 0.25, 1 (dashed), 2.5, 10, 25, 100, and 250 (solid). Wind direction is shown by thick dashed line.

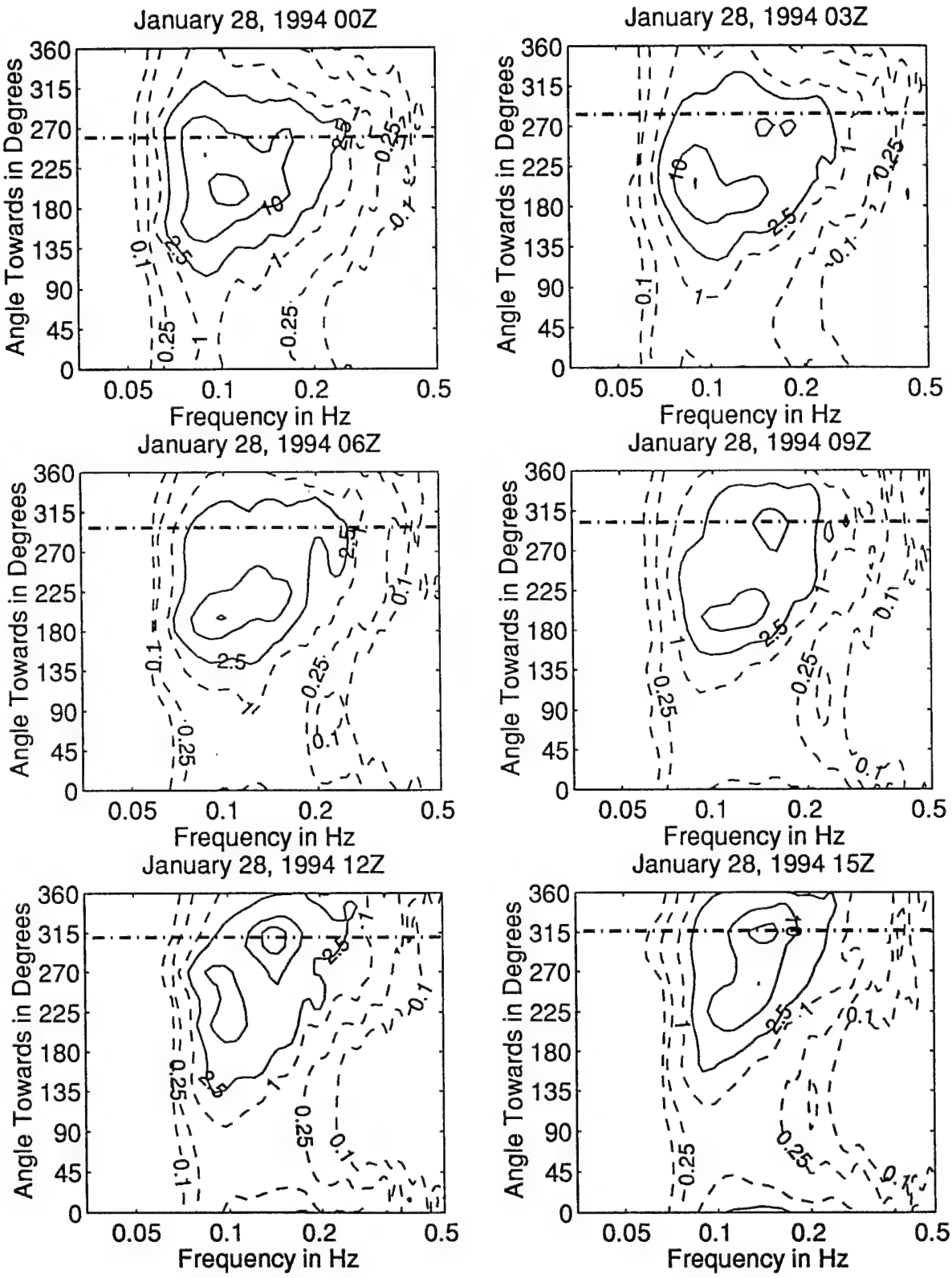

Figure 3.4.70: Directional wave spectra, computed using maximum entropy method. Contours of spectral density as a function of direction. Contours are 0.1, 0.25, 1 (dashed), 2.5, 10, 25, 100, and 250 (solid). Wind direction is shown by thick dashed line.

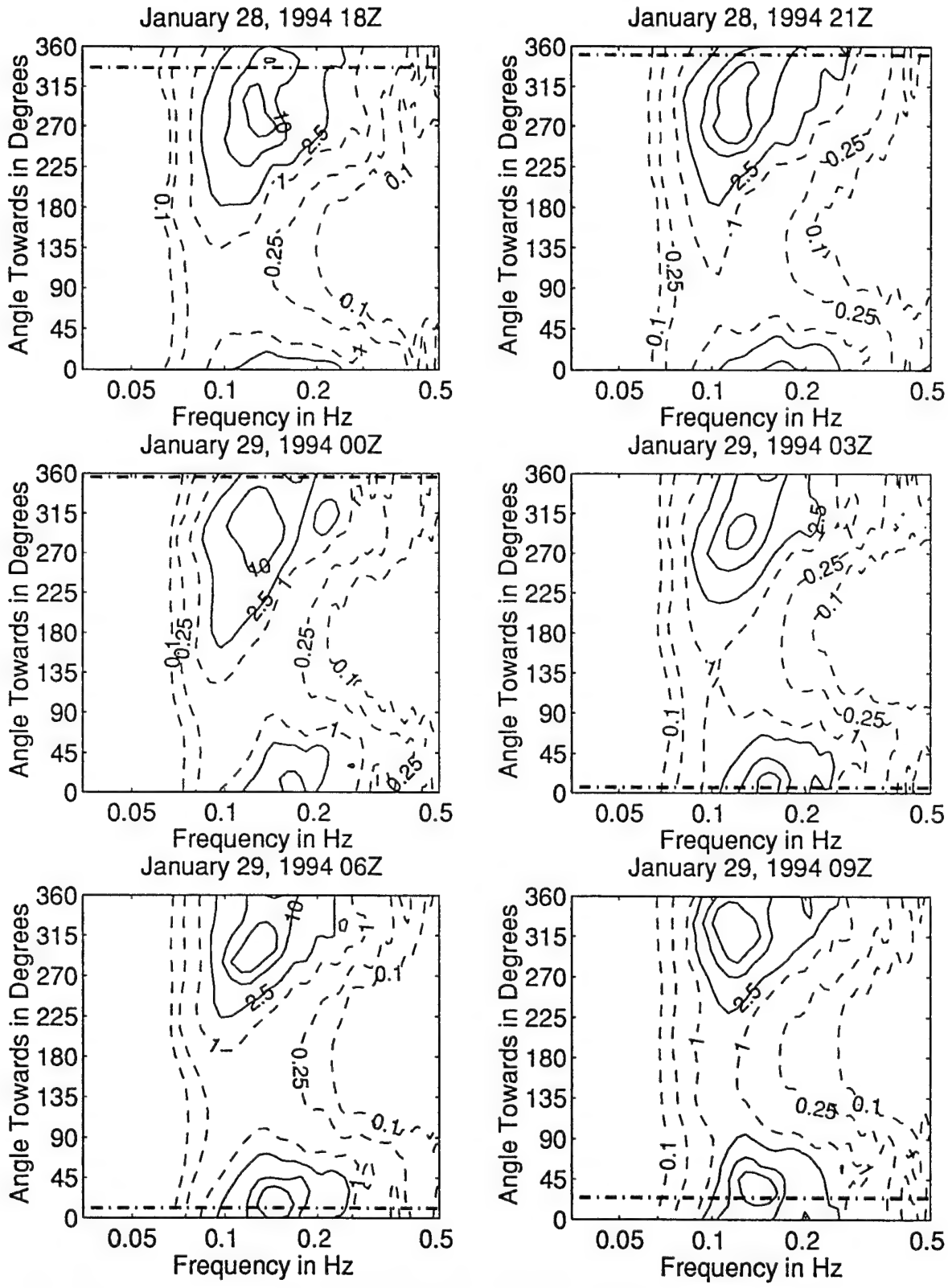

Figure 3.4.71: Directional wave spectra, computed using maximum entropy method. Contours of spectral density as a function of direction. Contours are 0.1, 0.25, 1 (dashed), 2.5, 10, 25, 100, and 250 (solid). Wind direction is shown by thick dashed line.

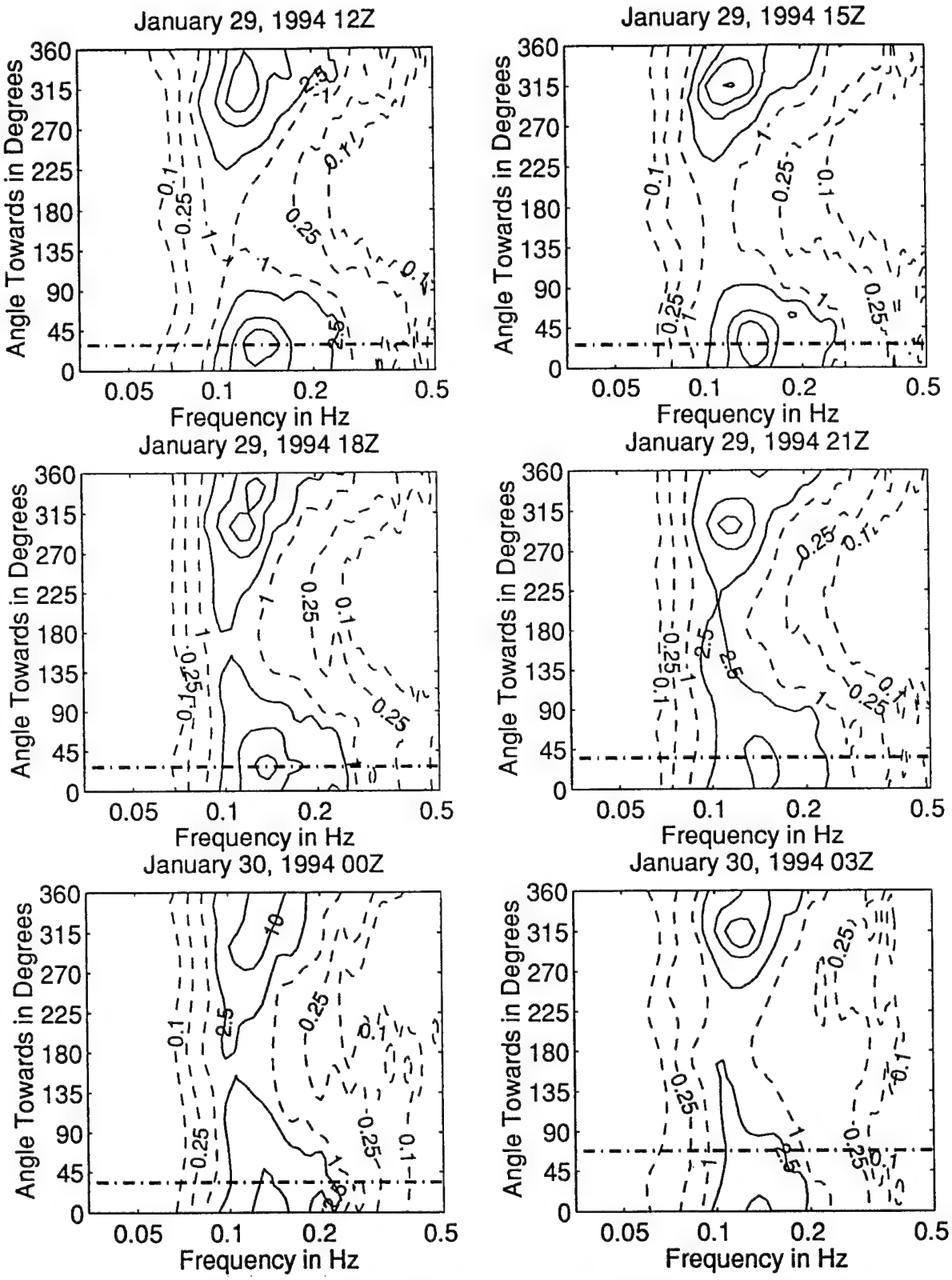

Figure 3.4.72: Directional wave spectra, computed using maximum entropy method. Contours of spectral density as a function of direction. Contours are 0.1, 0.25, 1 (dashed), 2.5, 10, 25, 100, and 250 (solid). Wind direction is shown by thick dashed line.

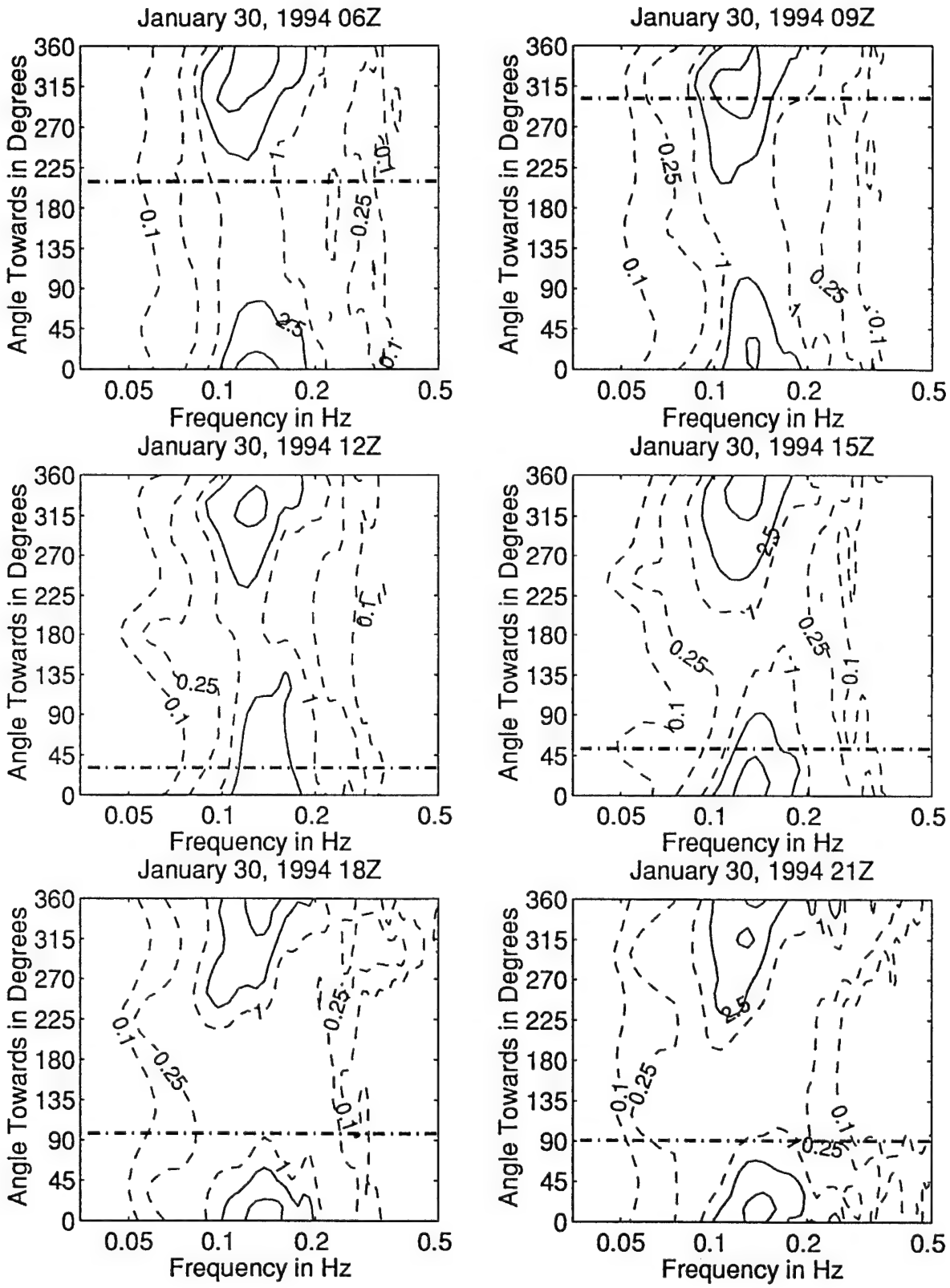

Figure 3.4.73: Directional wave spectra, computed using maximum entropy method. Contours of spectral density as a function of direction. Contours are 0.1, 0.25, 1 (dashed), 2.5, 10, 25, 100, and 250 (solid). Wind direction is shown by thick dashed line.

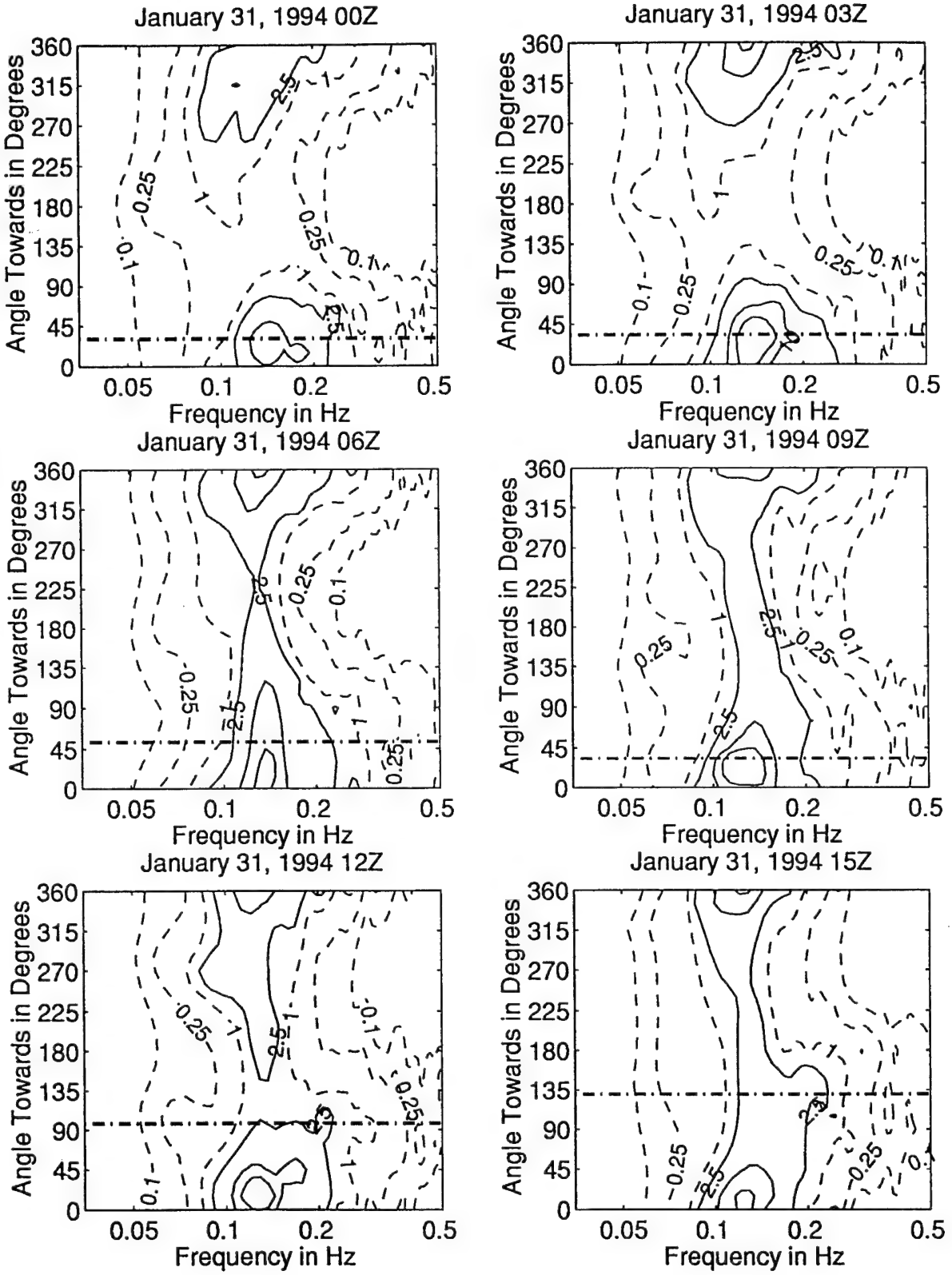

Figure 3.4.74: Directional wave spectra, computed using maximum entropy method. Contours of spectral density as a function of direction. Contours are 0.1, 0.25, 1 (dashed), 2.5, 10, 25, 100, and 250 (solid). Wind direction is shown by thick dashed line.

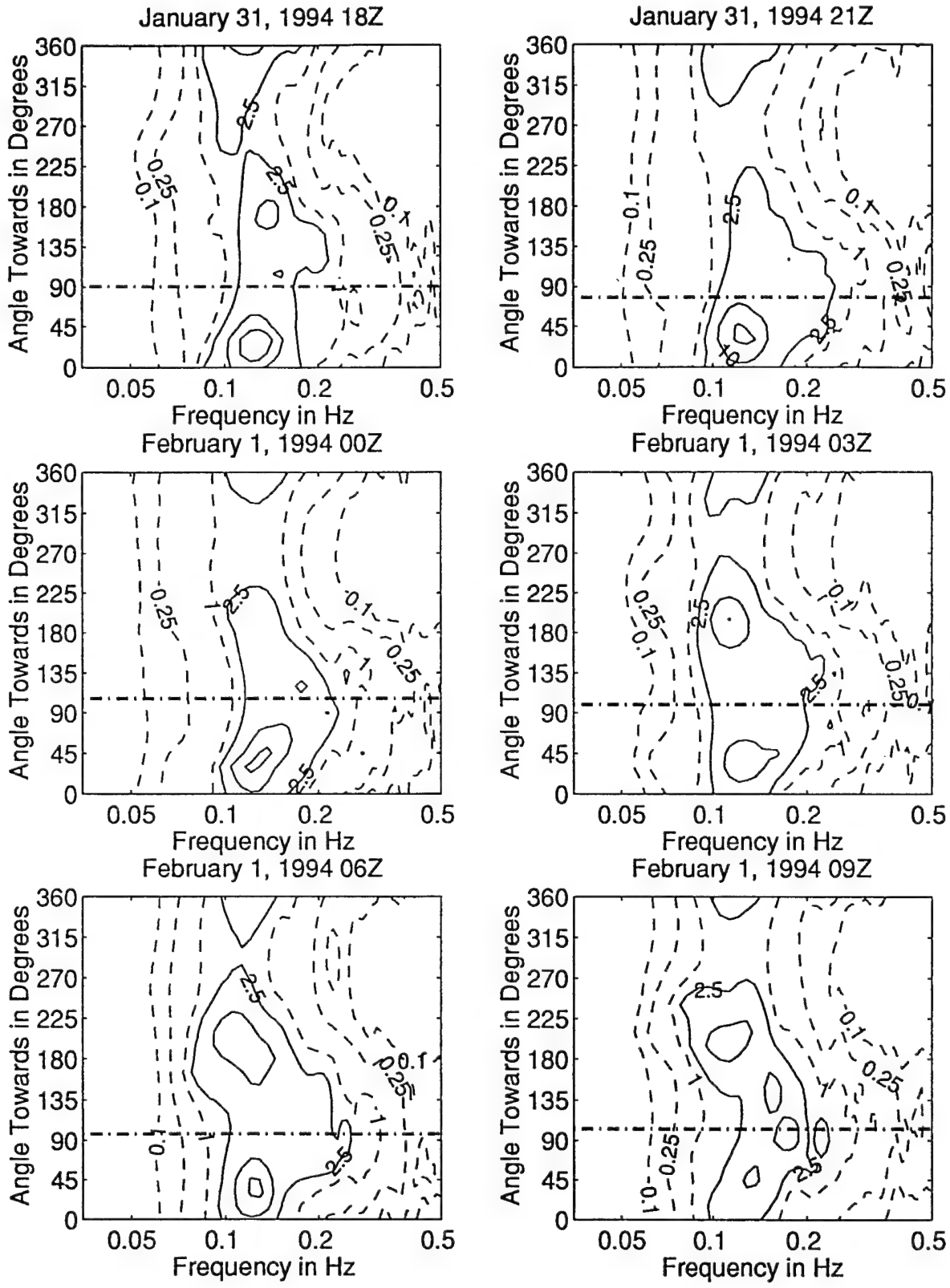

Figure 3.4.75: Directional wave spectra, computed using maximum entropy method. Contours of spectral density as a function of direction. Contours are 0.1, 0.25, 1 (dashed), 2.5, 10, 25, 100, and 250 (solid). Wind direction is shown by thick dashed line.

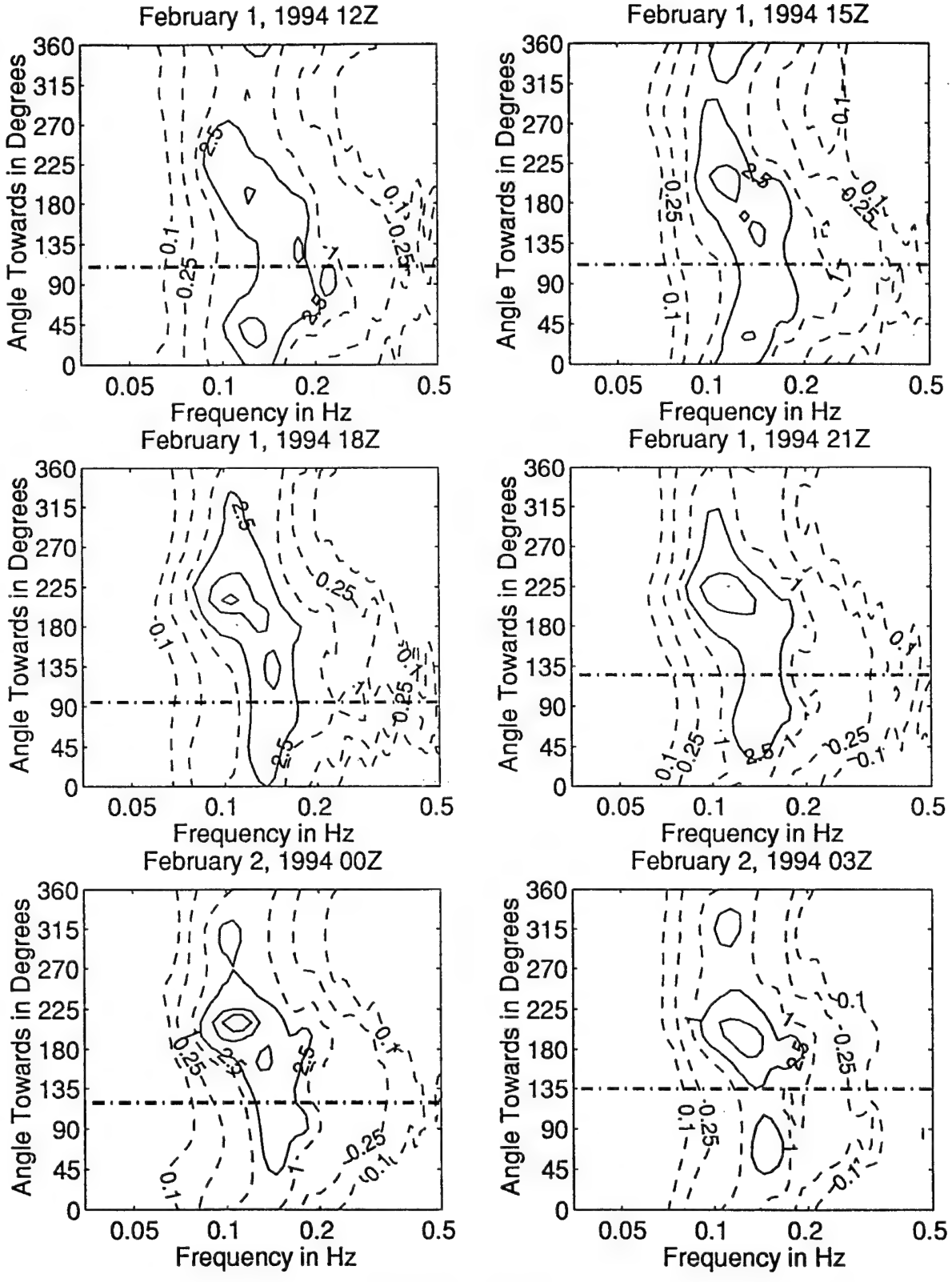

Figure 3.4.76: Directional wave spectra, computed using maximum entropy method. Contours of spectral density as a function of direction. Contours are 0.1, 0.25, 1 (dashed), 2.5, 10, 25, 100, and 250 (solid). Wind direction is shown by thick dashed line.

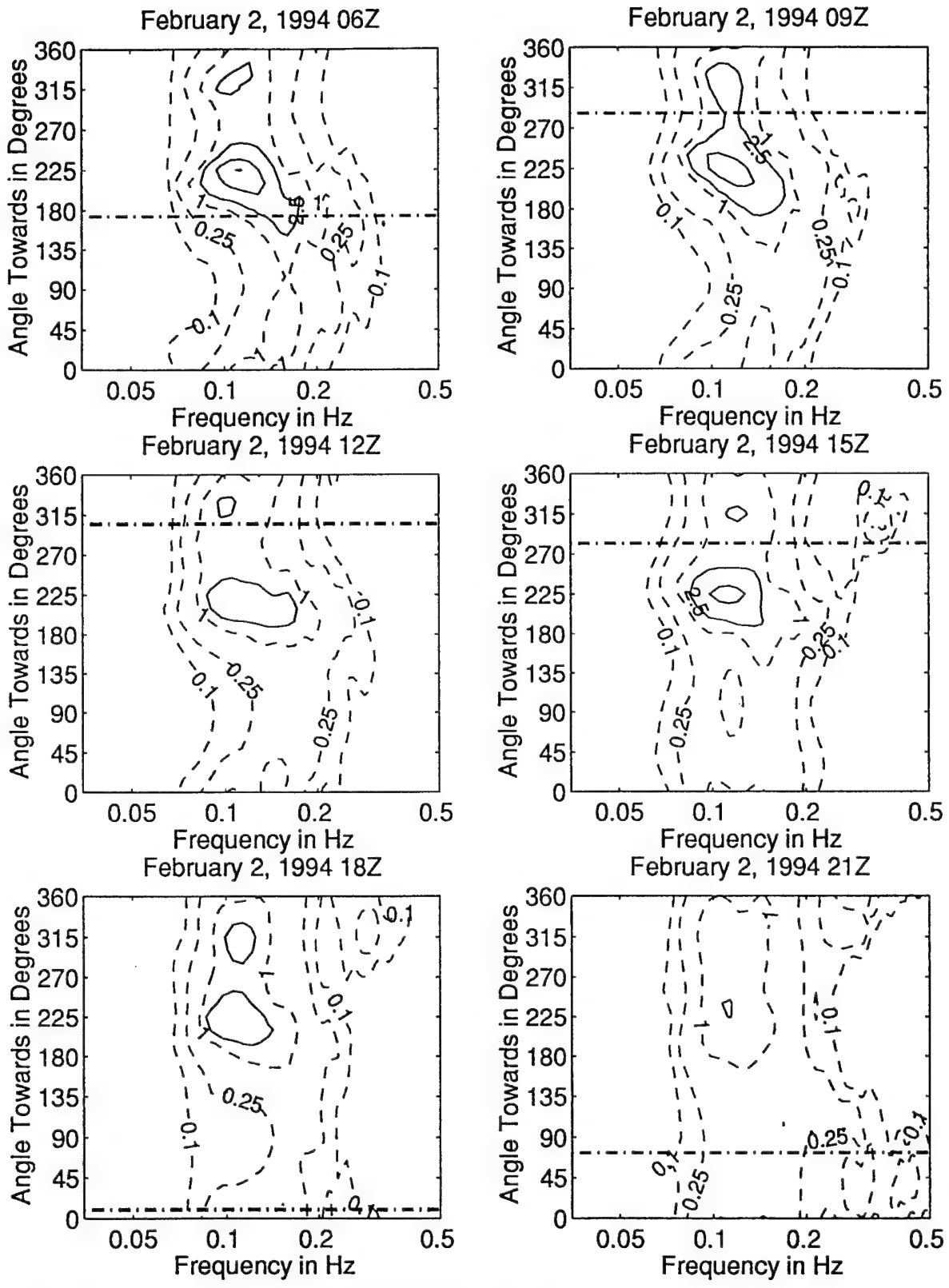

Figure 3.4.77: Directional wave spectra, computed using maximum entropy method. Contours of spectral density as a function of direction. Contours are 0.1, 0.25, 1 (dashed), 2.5, 10, 25, 100, and 250 (solid). Wind direction is shown by thick dashed line.

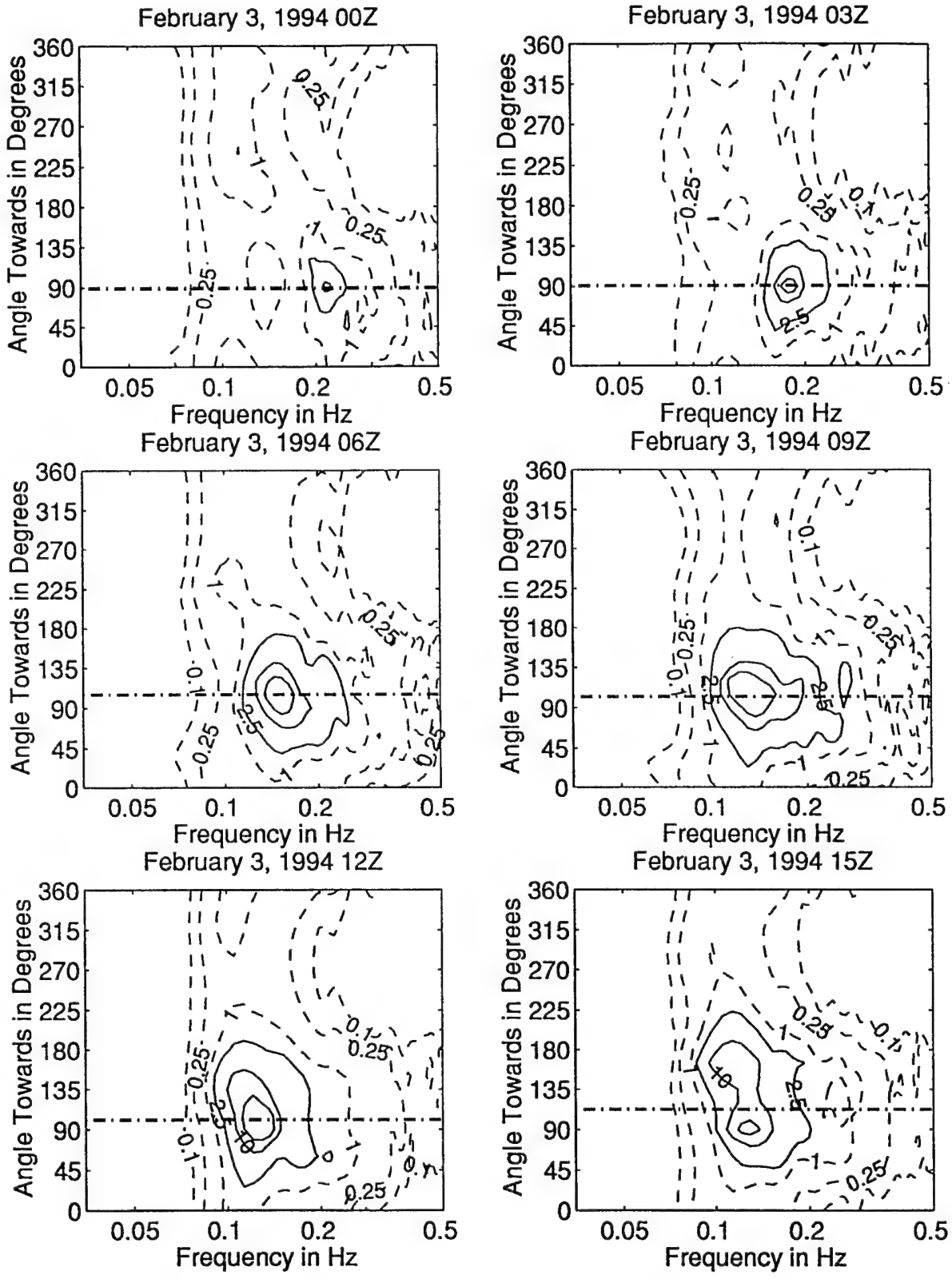

Figure 3.4.78: Directional wave spectra, computed using maximum entropy method. Contours of spectral density as a function of direction. Contours are 0.1, 0.25, 1 (dashed), 2.5, 10, 25, 100, and 250 (solid). Wind direction is shown by thick dashed line.

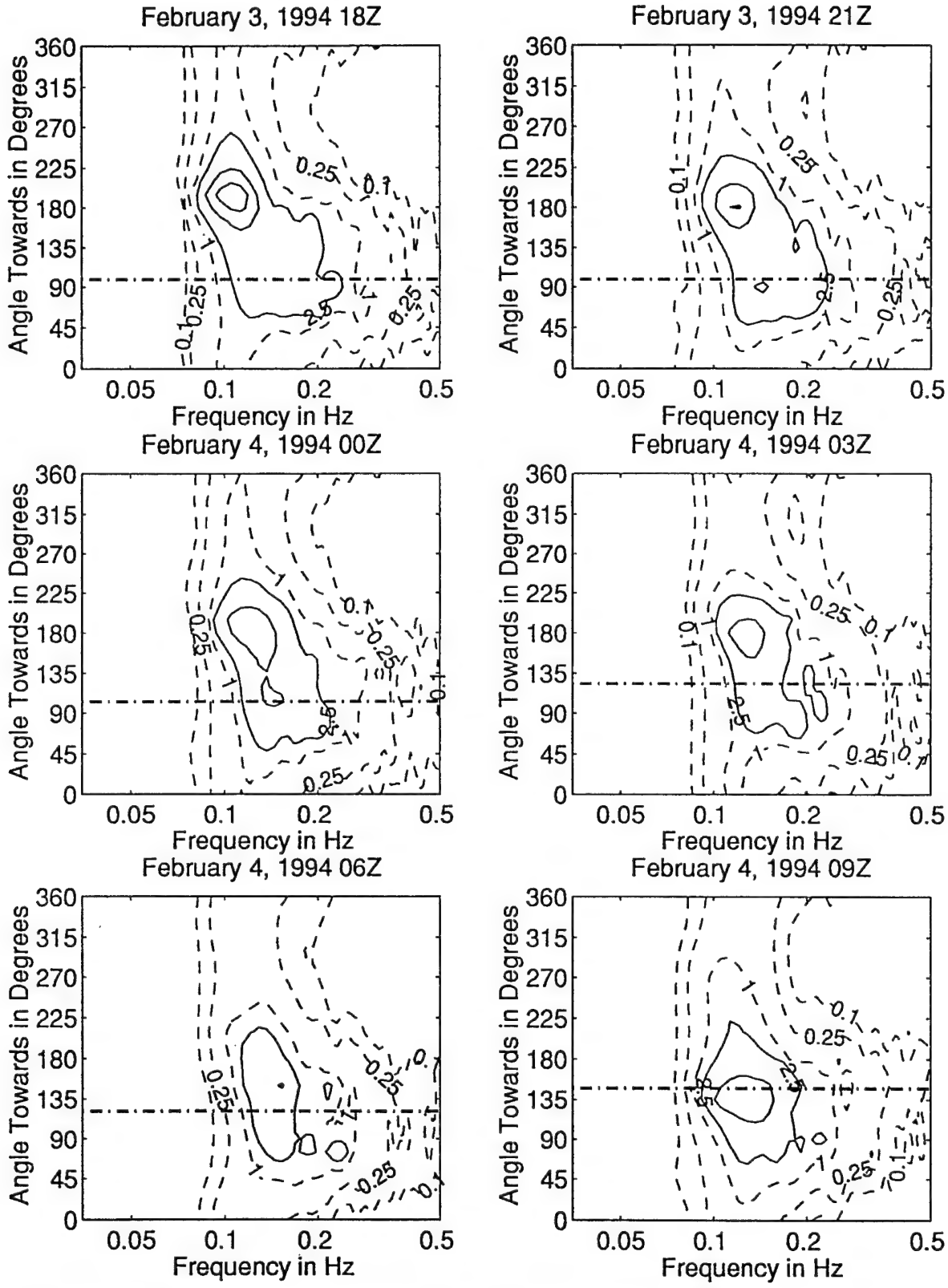

Figure 3.4.79: Directional wave spectra, computed using maximum entropy method. Contours of spectral density as a function of direction. Contours are 0.1, 0.25, 1 (dashed), 2.5, 10, 25, 100, and 250 (solid). Wind direction is shown by thick dashed line.

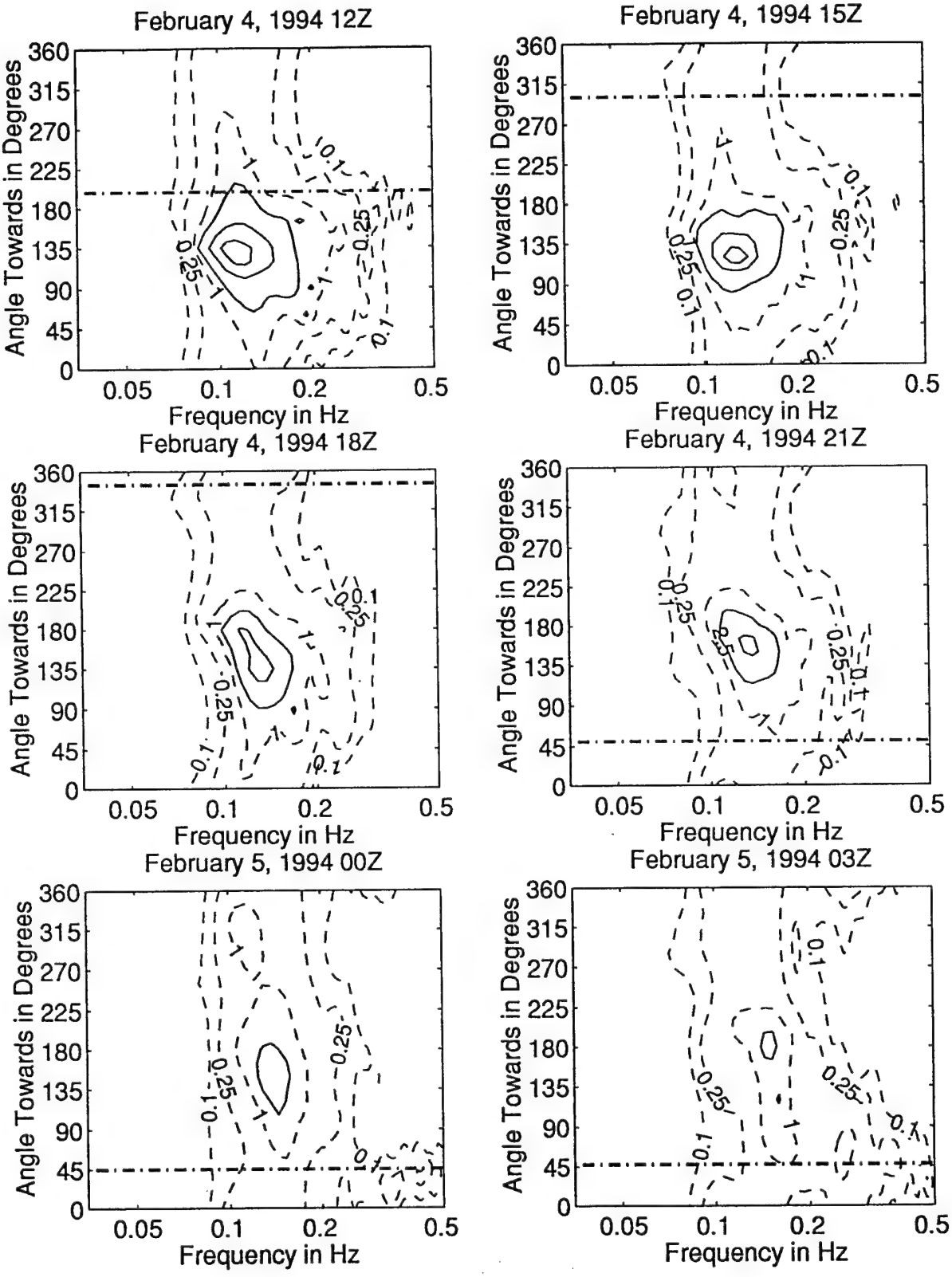

Figure 3.4.80: Directional wave spectra, computed using maximum entropy method. Contours of spectral density as a function of direction. Contours are 0.1, 0.25, 1 (dashed), 2.5, 10, 25, 100, and 250 (solid). Wind direction is shown by thick dashed line.

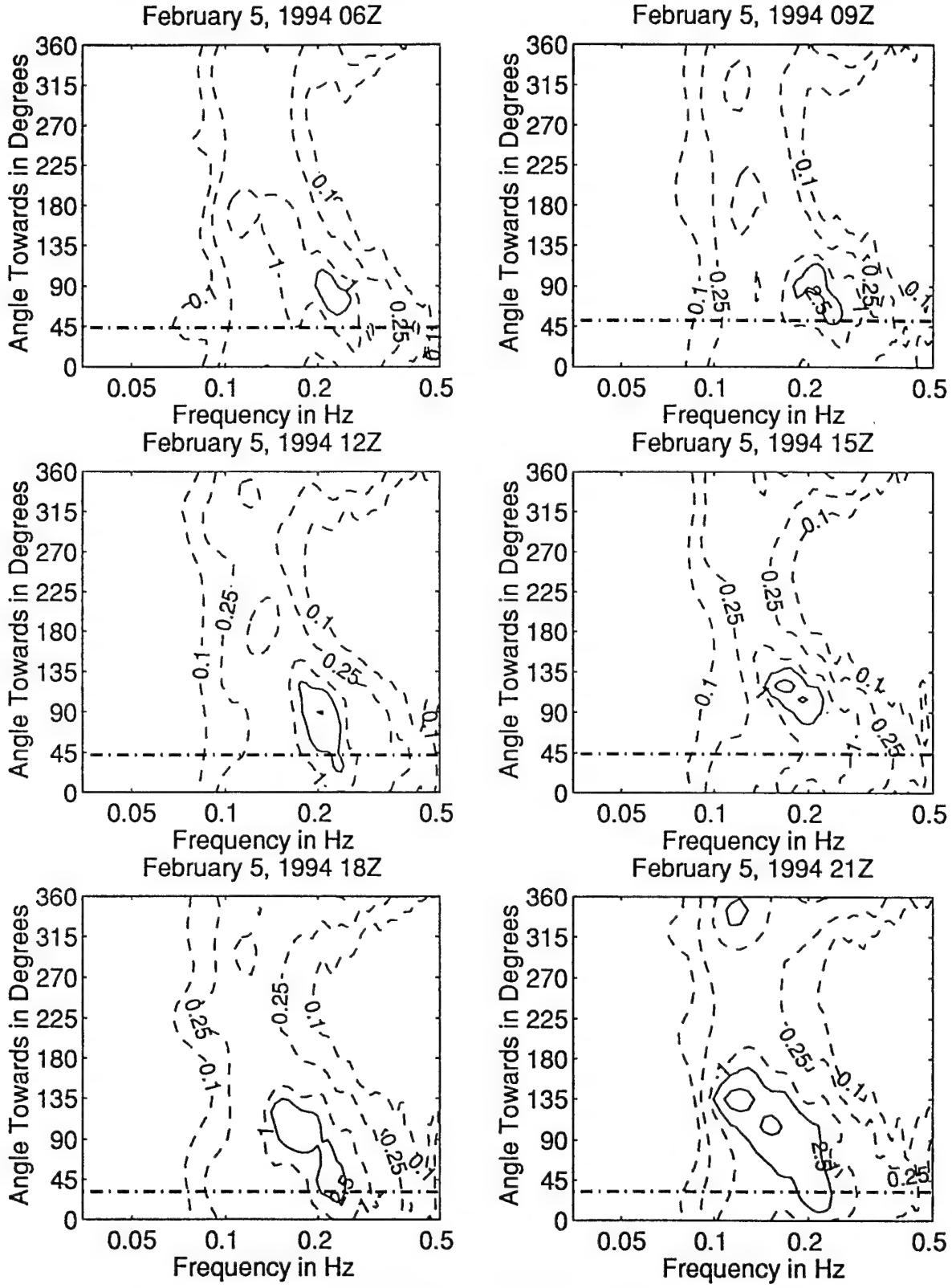

Figure 3.4.81: Directional wave spectra, computed using maximum entropy method. Contours of spectral density as a function of direction. Contours are 0.1, 0.25, 1 (dashed), 2.5, 10, 25, 100, and 250 (solid). Wind direction is shown by thick dashed line.

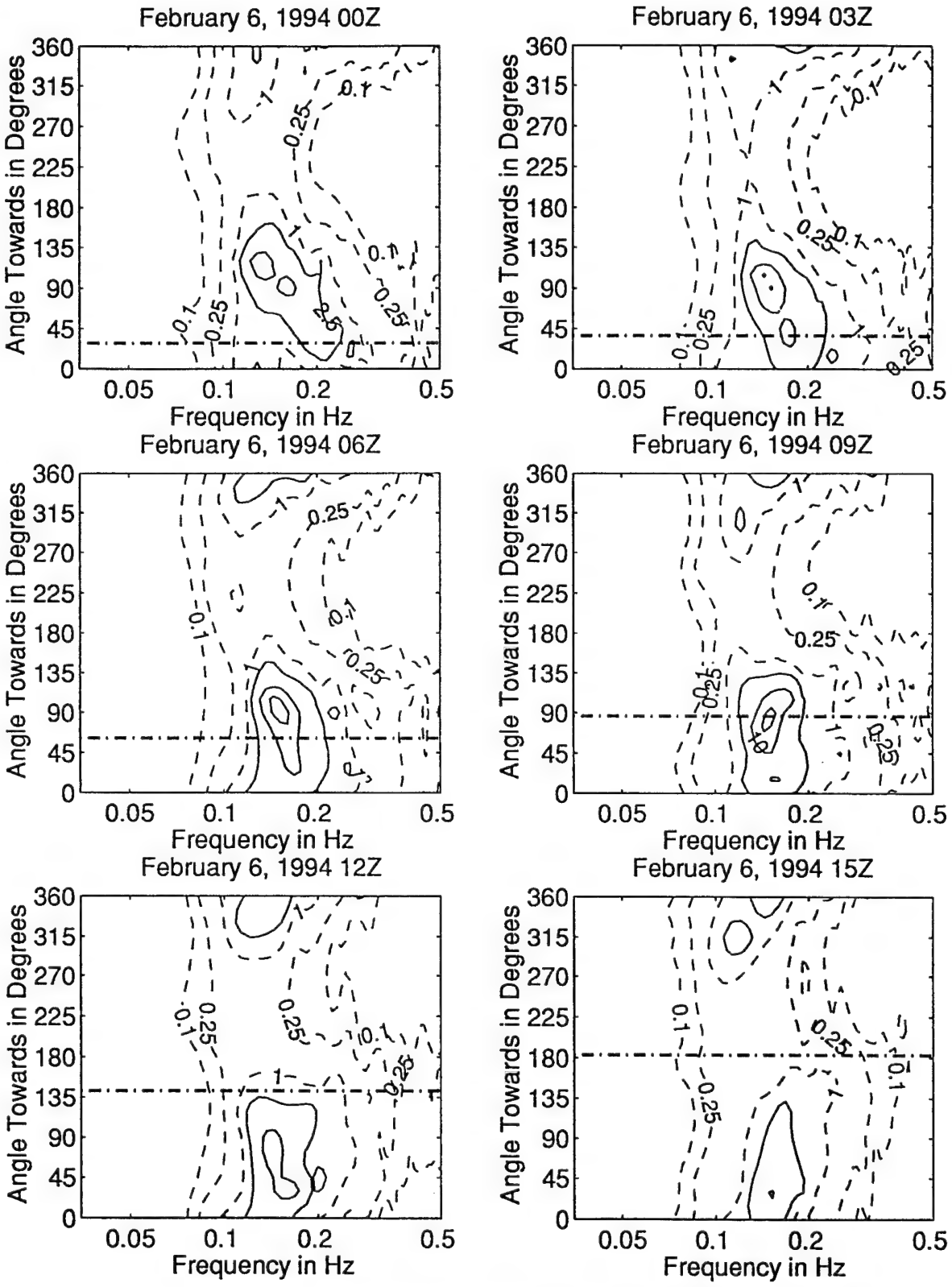

Figure 3.4.82: Directional wave spectra, computed using maximum entropy method. Contours of spectral density as a function of direction. Contours are 0.1, 0.25, 1 (dashed), 2.5, 10, 25, 100, and 250 (solid). Wind direction is shown by thick dashed line.

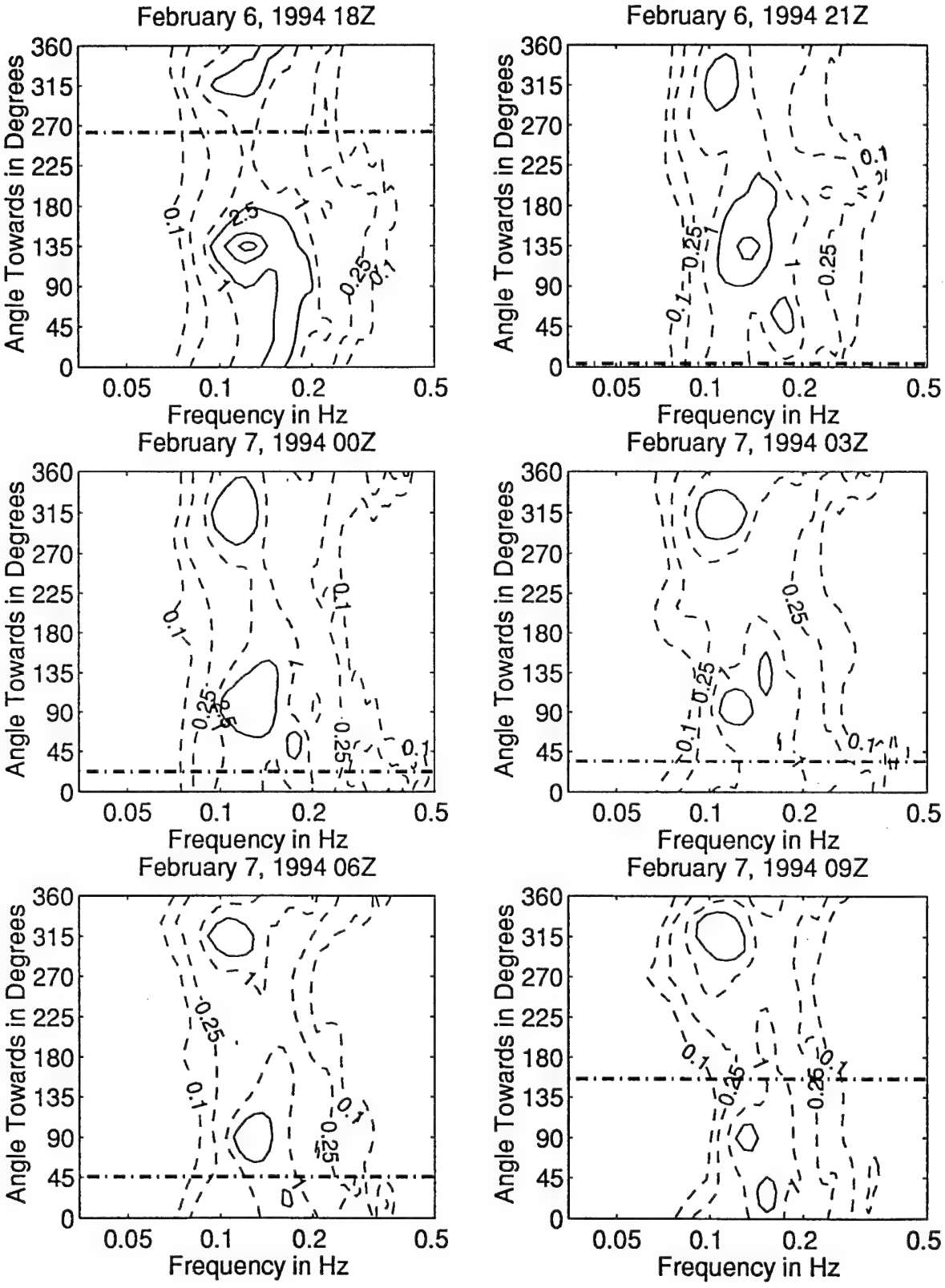

Figure 3.4.83: Directional wave spectra, computed using maximum entropy method. Contours of spectral density as a function of direction. Contours are 0.1, 0.25, 1 (dashed), 2.5, 10, 25, 100, and 250 (solid). Wind direction is shown by thick dashed line.

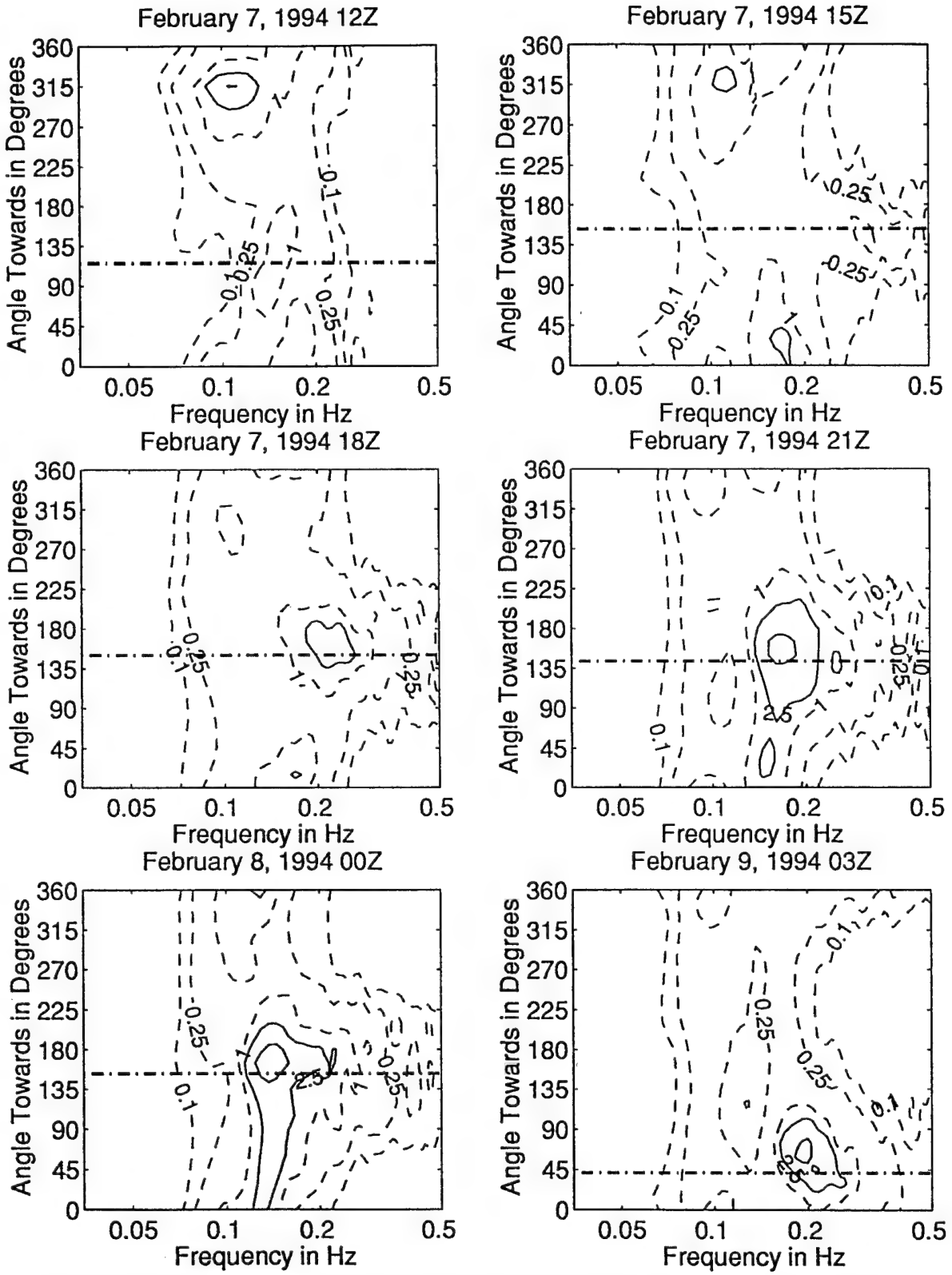

Figure 3.4.84: Directional wave spectra, computed using maximum entropy method. Contours of spectral density as a function of direction. Contours are 0.1, 0.25, 1 (dashed), 2.5, 10, 25, 100, and 250 (solid). Wind direction is shown by thick dashed line.

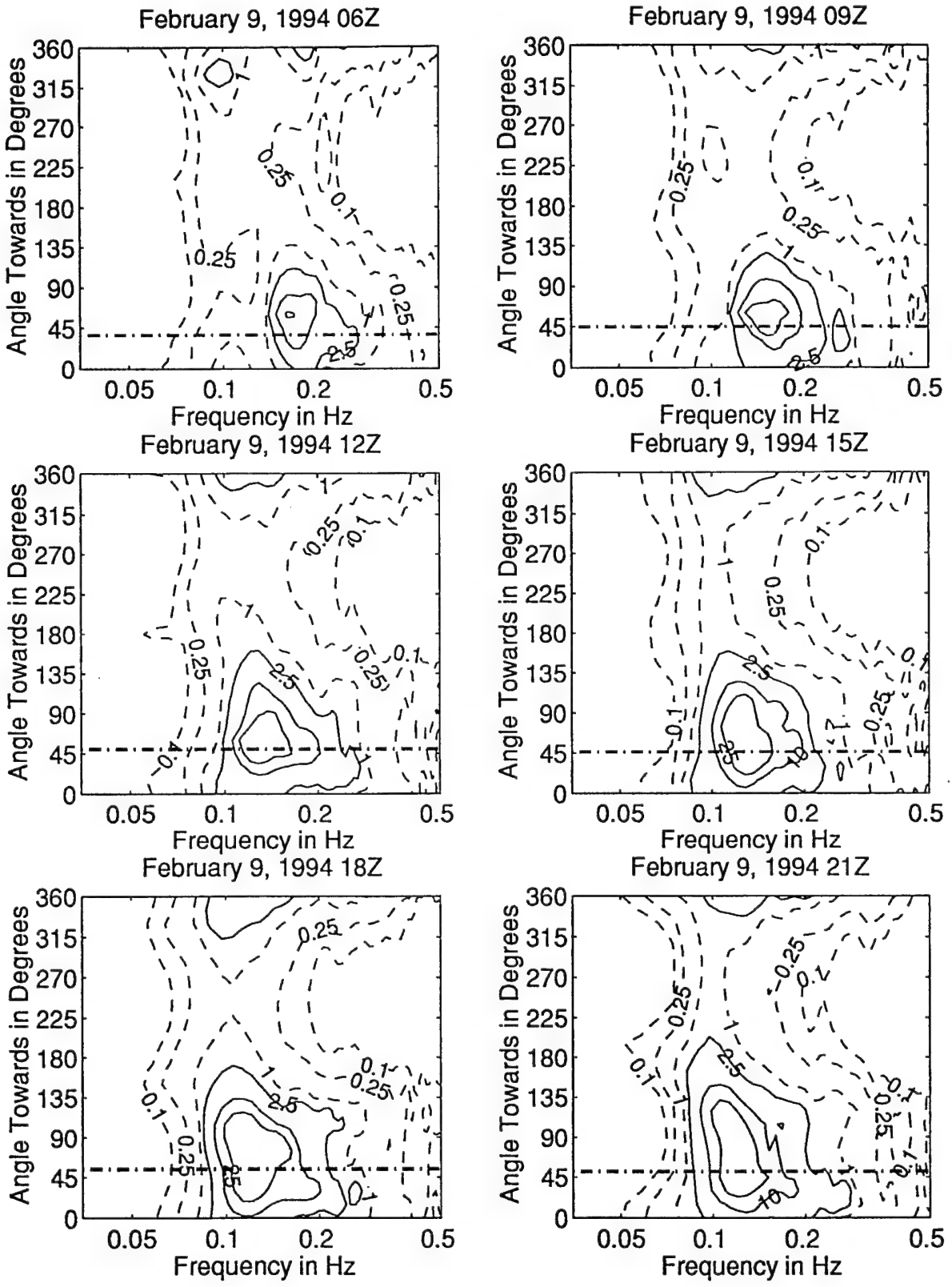

Figure 3.4.85: Directional wave spectra, computed using maximum entropy method. Contours of spectral density as a function of direction. Contours are 0.1, 0.25, 1 (dashed), 2.5, 10, 25, 100, and 250 (solid). Wind direction is shown by thick dashed line.

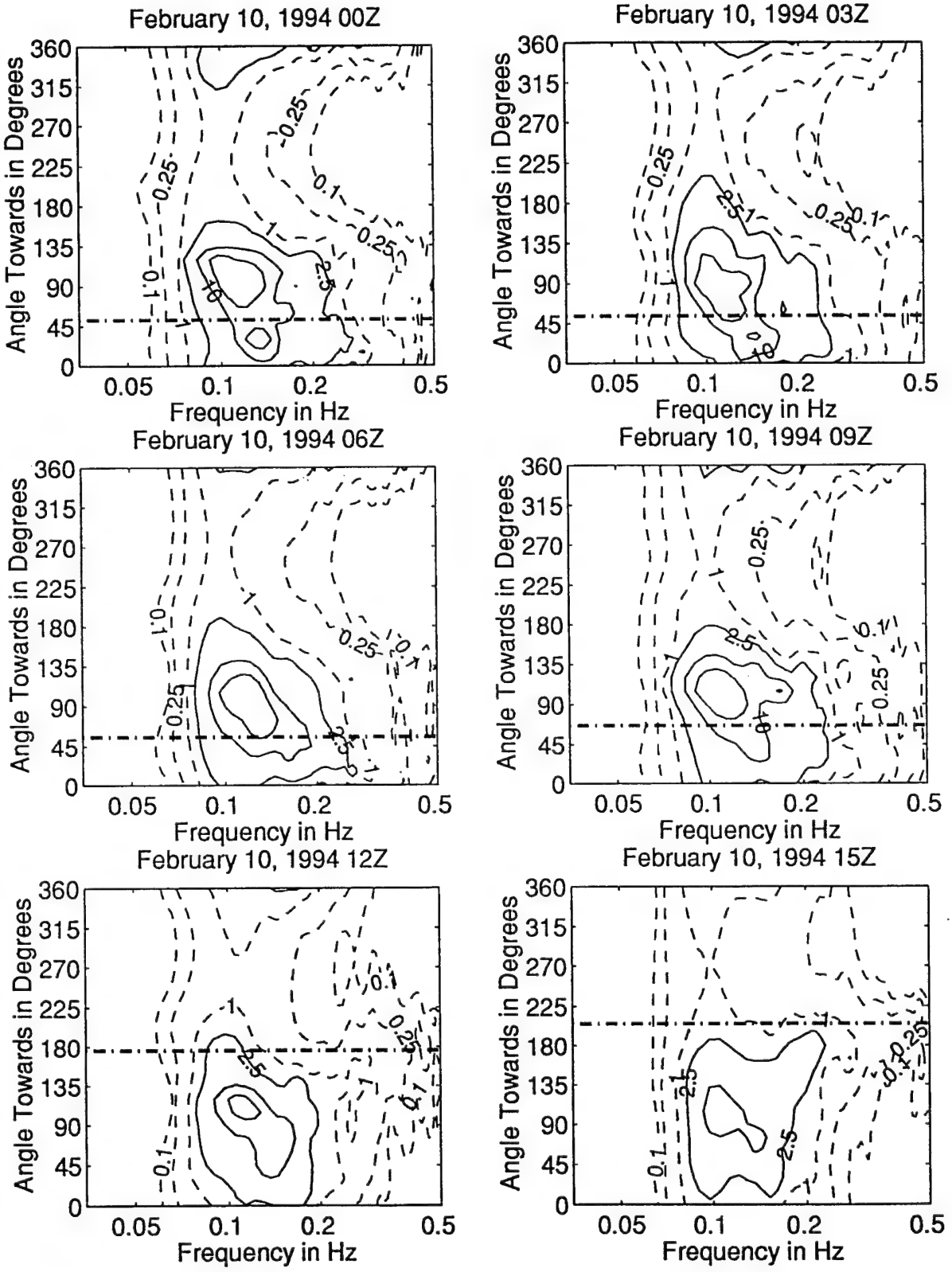

Figure 3.4.86: Directional wave spectra, computed using maximum entropy method. Contours of spectral density as a function of direction. Contours are 0.1, 0.25, 1 (dashed), 2.5, 10, 25, 100, and 250 (solid). Wind direction is shown by thick dashed line.

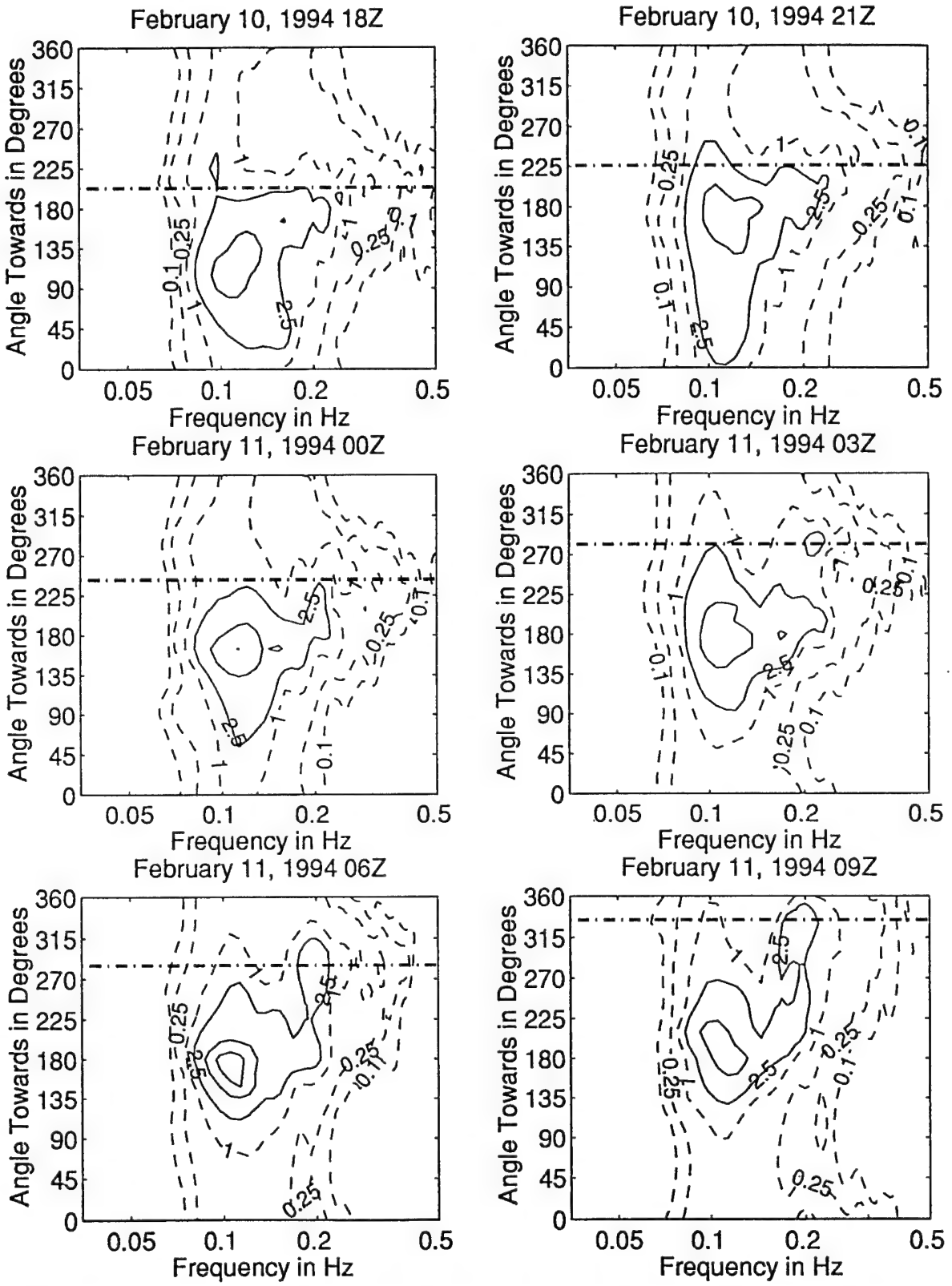

Figure 3.4.87: Directional wave spectra, computed using maximum entropy method. Contours of spectral density as a function of direction. Contours are 0.1, 0.25, 1 (dashed), 2.5, 10, 25, 100, and 250 (solid). Wind direction is shown by thick dashed line.

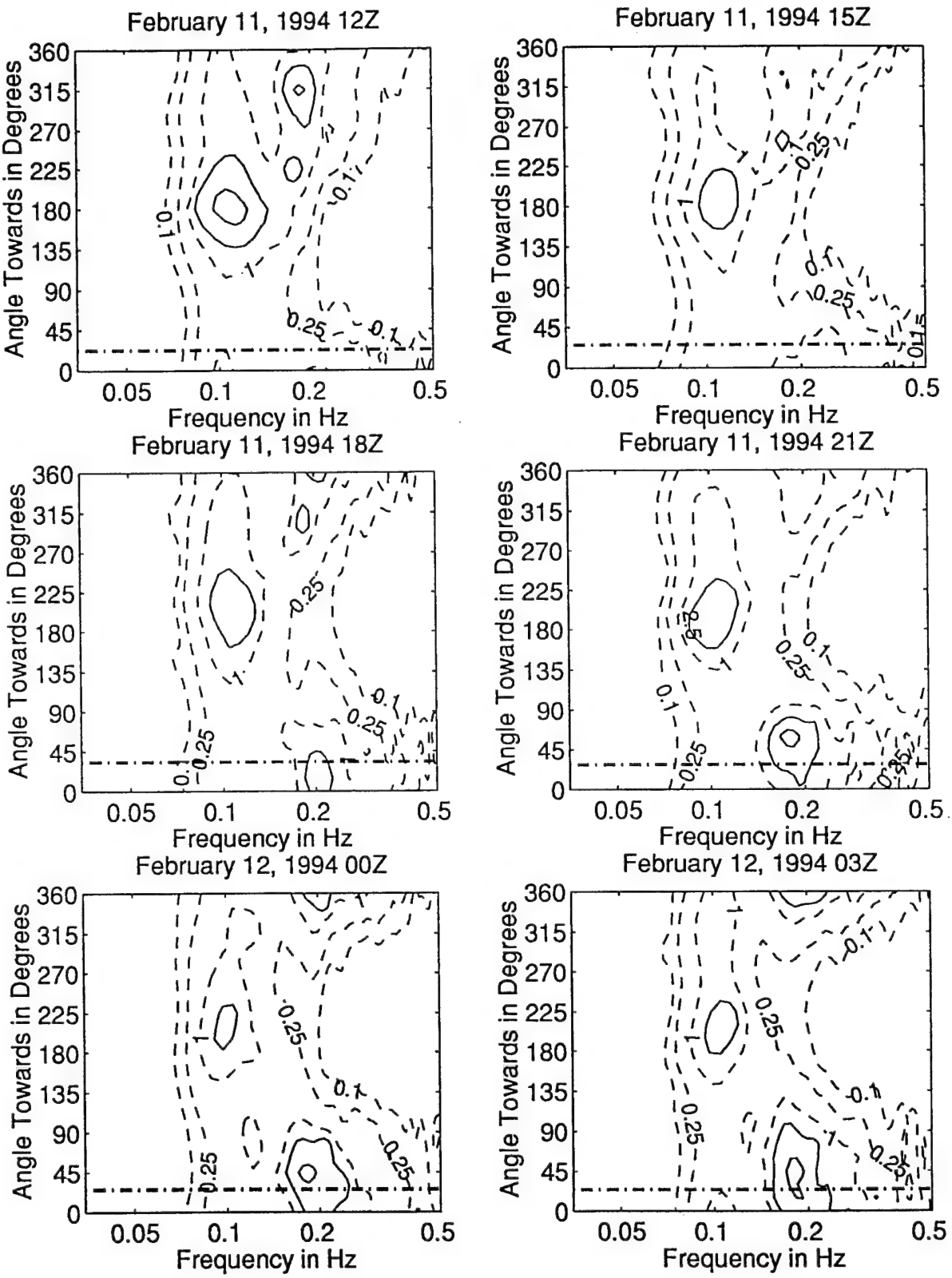

Figure 3.4.88: Directional wave spectra, computed using maximum entropy method. Contours of spectral density as a function of direction. Contours are 0.1, 0.25, 1 (dashed), 2.5, 10, 25, 100, and 250 (solid). Wind direction is shown by thick dashed line.

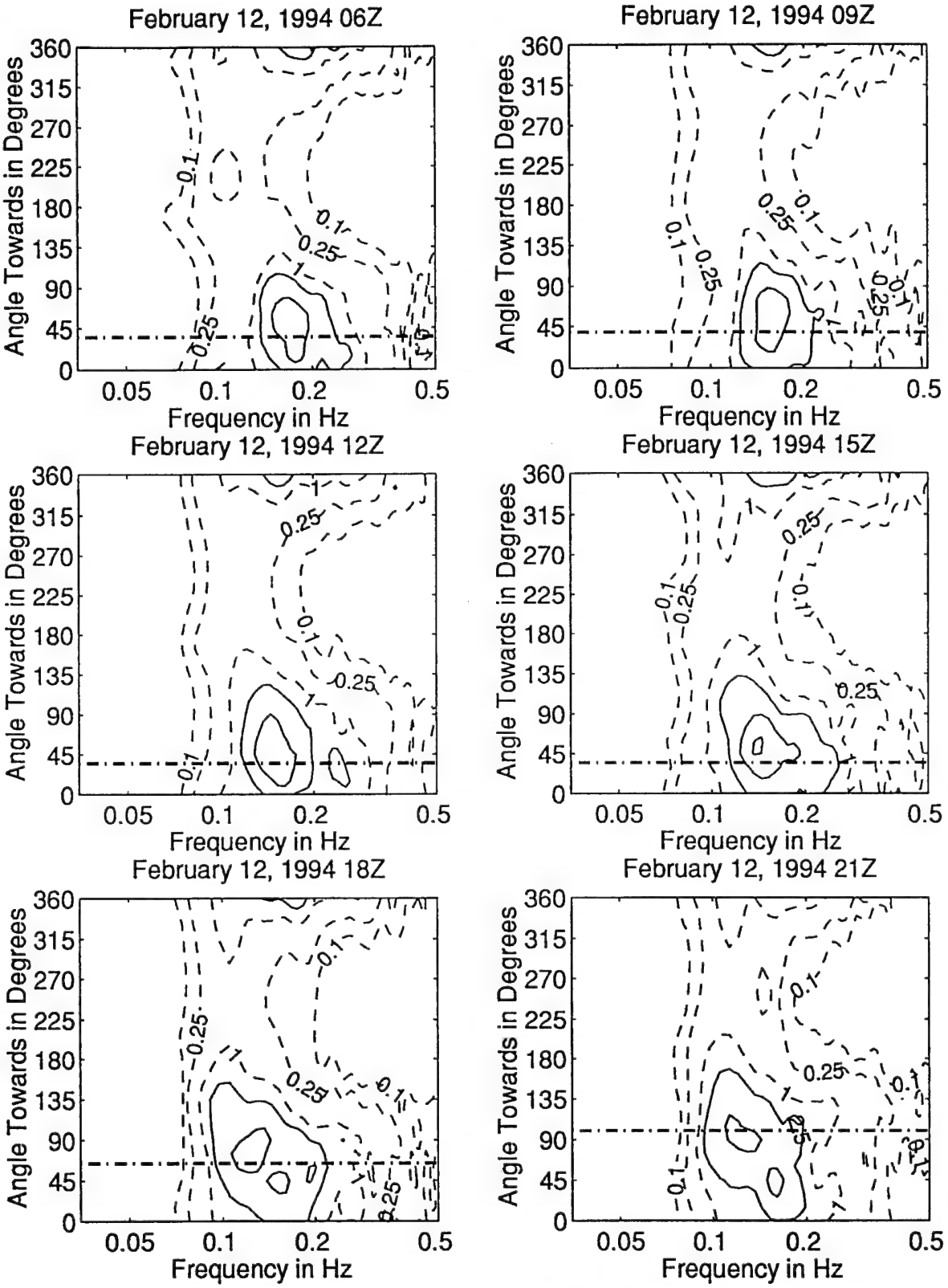

Figure 3.4.89: Directional wave spectra, computed using maximum entropy method. Contours of spectral density as a function of direction. Contours are 0.1, 0.25, 1 (dashed), 2.5, 10, 25, 100, and 250 (solid). Wind direction is shown by thick dashed line.

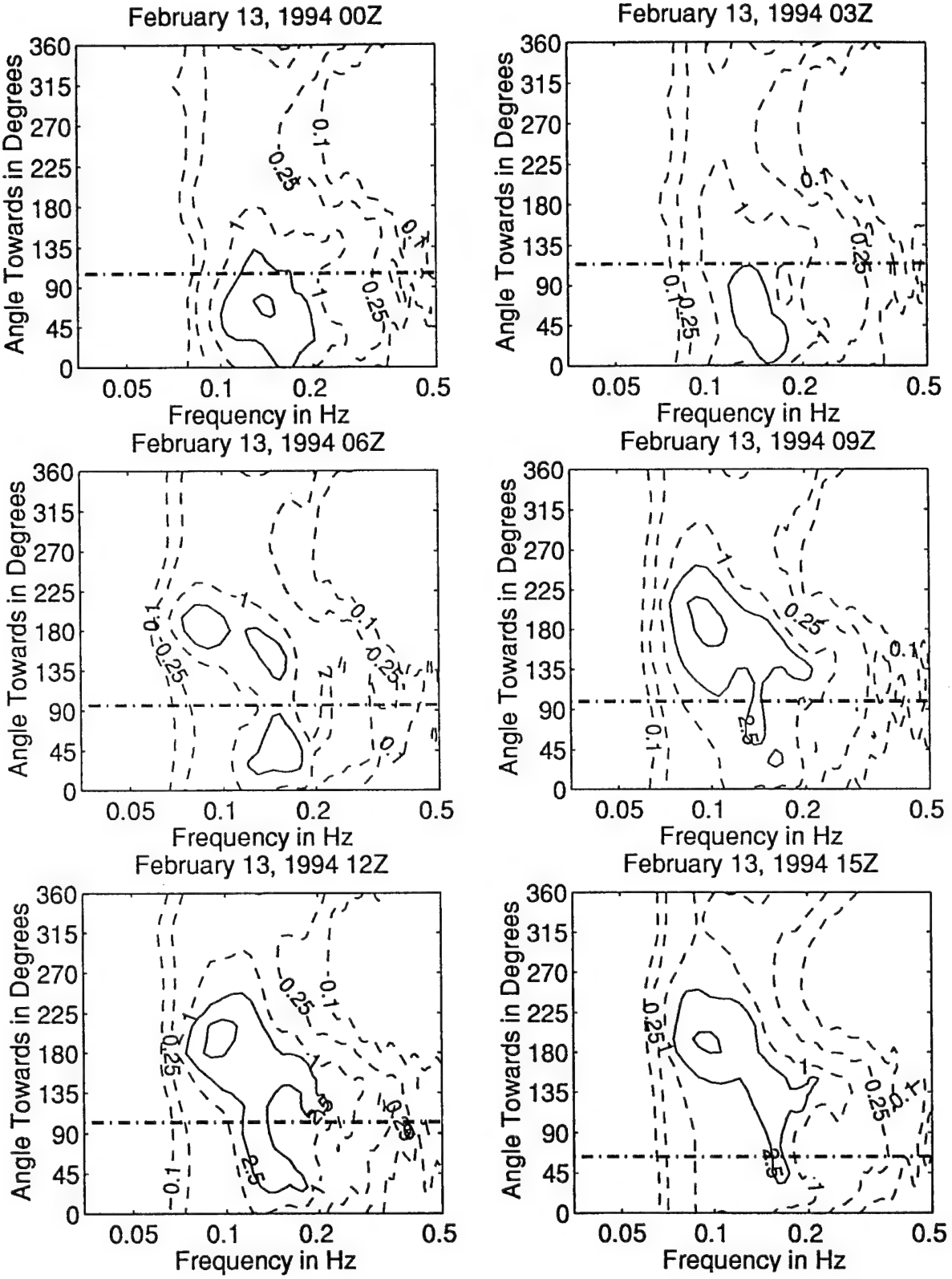

Figure 3.4.90: Directional wave spectra, computed using maximum entropy method. Contours of spectral density as a function of direction. Contours are 0.1, 0.25, 1 (dashed), 2.5, 10, 25, 100, and 250 (solid). Wind direction is shown by thick dashed line.

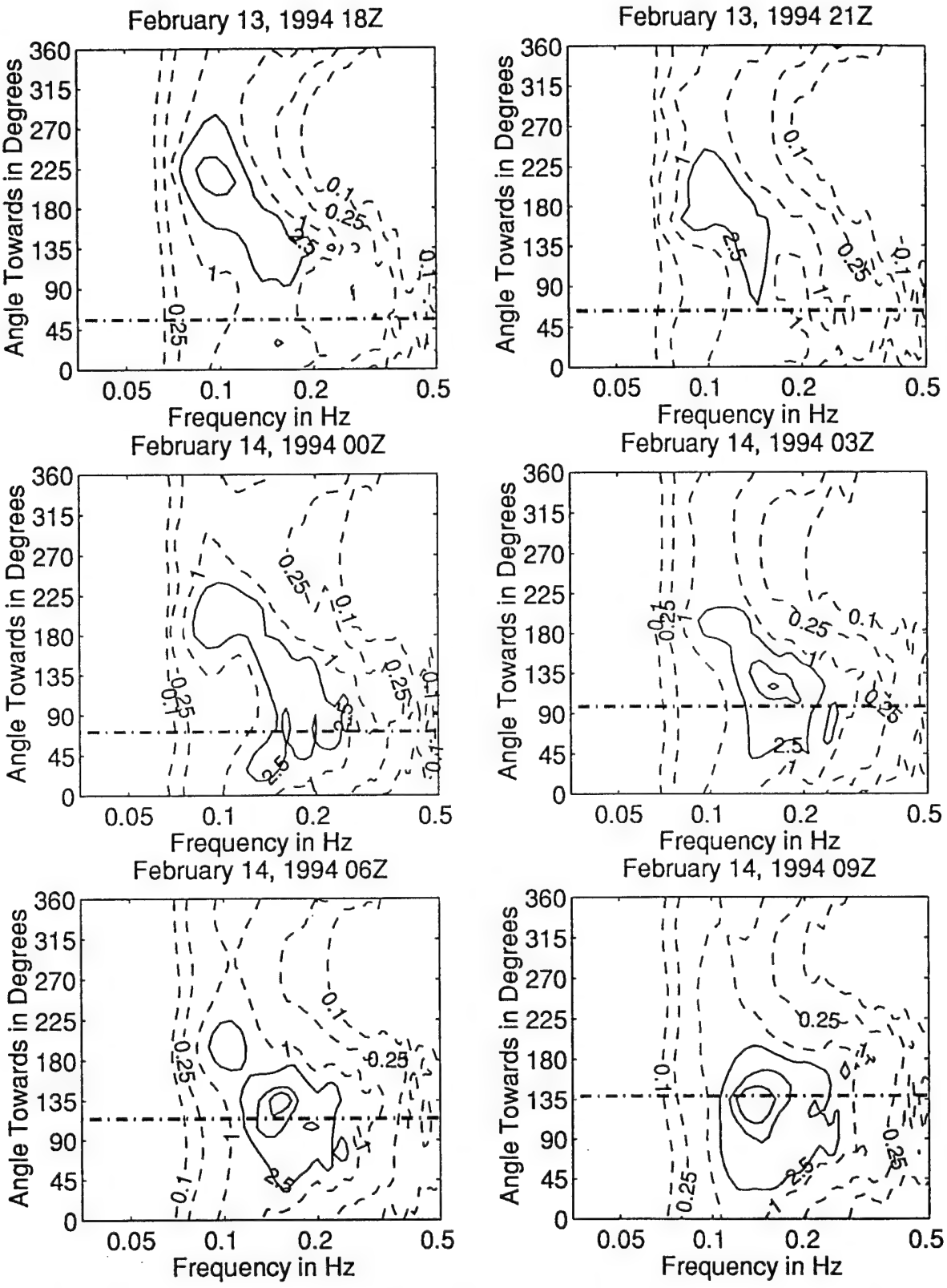

Figure 3.4.91: Directional wave spectra, computed using maximum entropy method. Contours of spectral density as a function of direction. Contours are 0.1, 0.25, 1 (dashed), 2.5, 10, 25, 100, and 250 (solid). Wind direction is shown by thick dashed line.

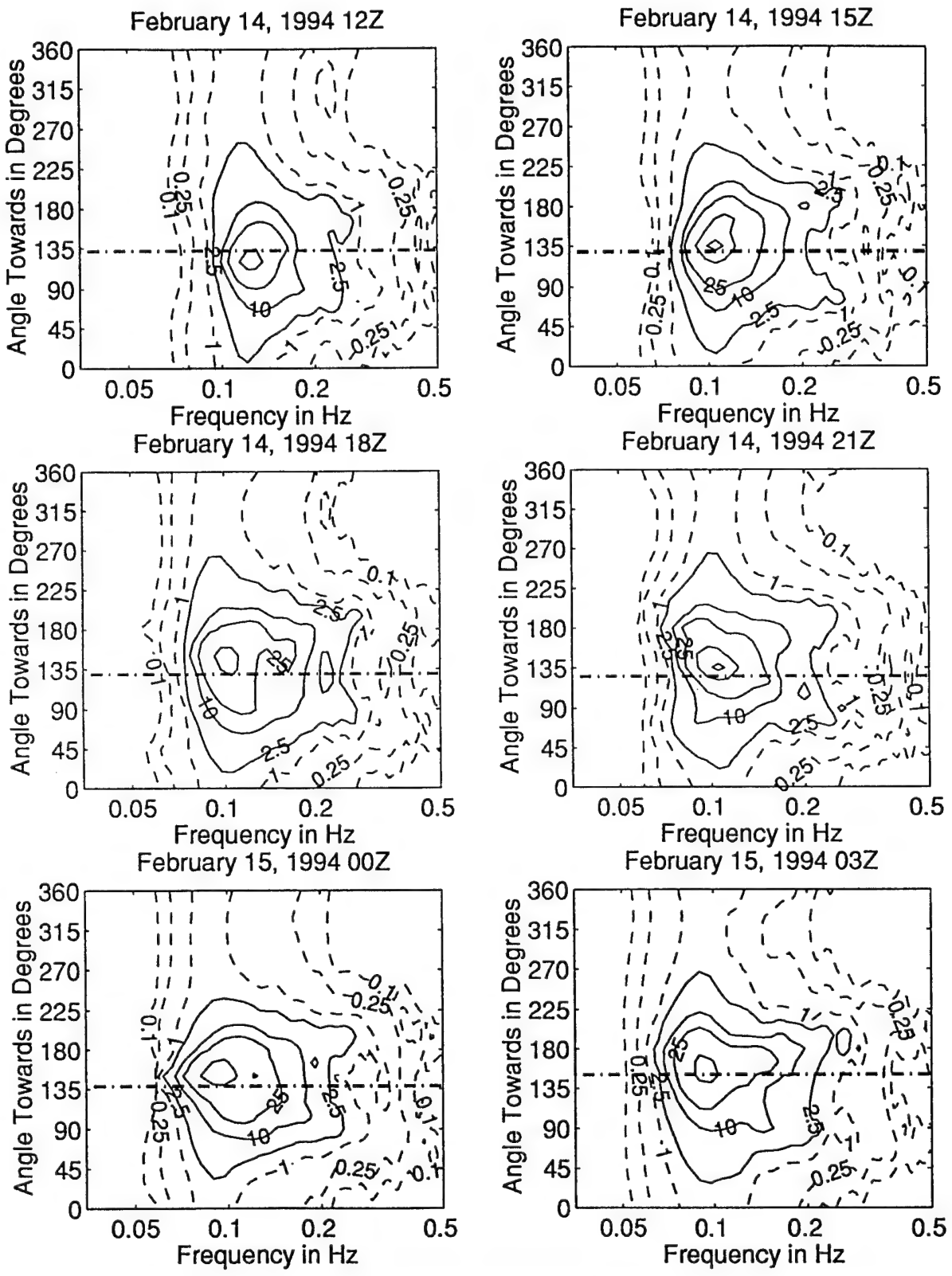

Figure 3.4.92: Directional wave spectra, computed using maximum entropy method. Contours of spectral density as a function of direction. Contours are 0.1, 0.25, 1 (dashed), 2.5, 10, 25, 100, and 250 (solid). Wind direction is shown by thick dashed line.

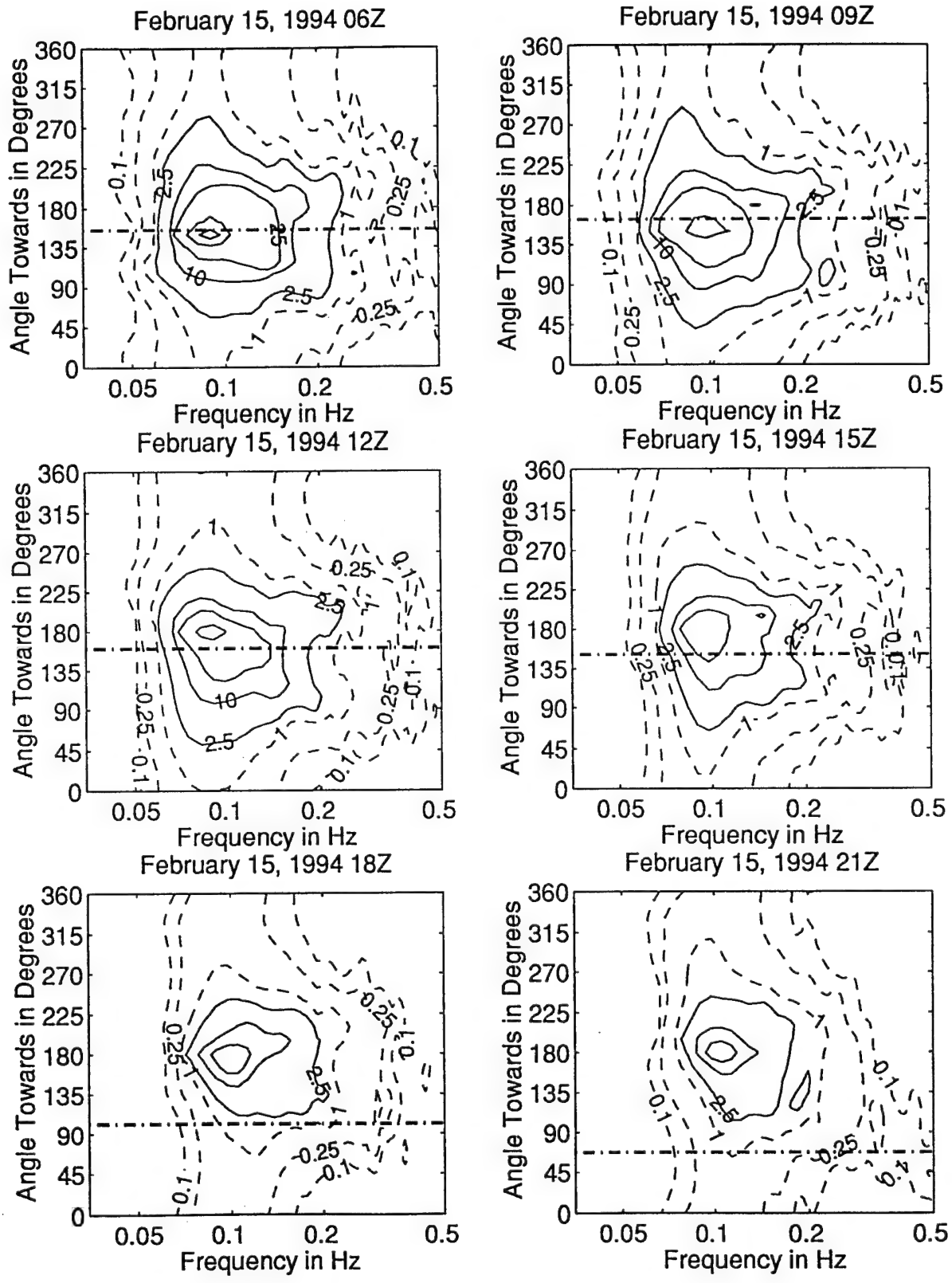

Figure 3.4.93: Directional wave spectra, computed using maximum entropy method. Contours of spectral density as a function of direction. Contours are 0.1, 0.25, 1 (dashed), 2.5, 10, 25, 100, and 250 (solid). Wind direction is shown by thick dashed line.

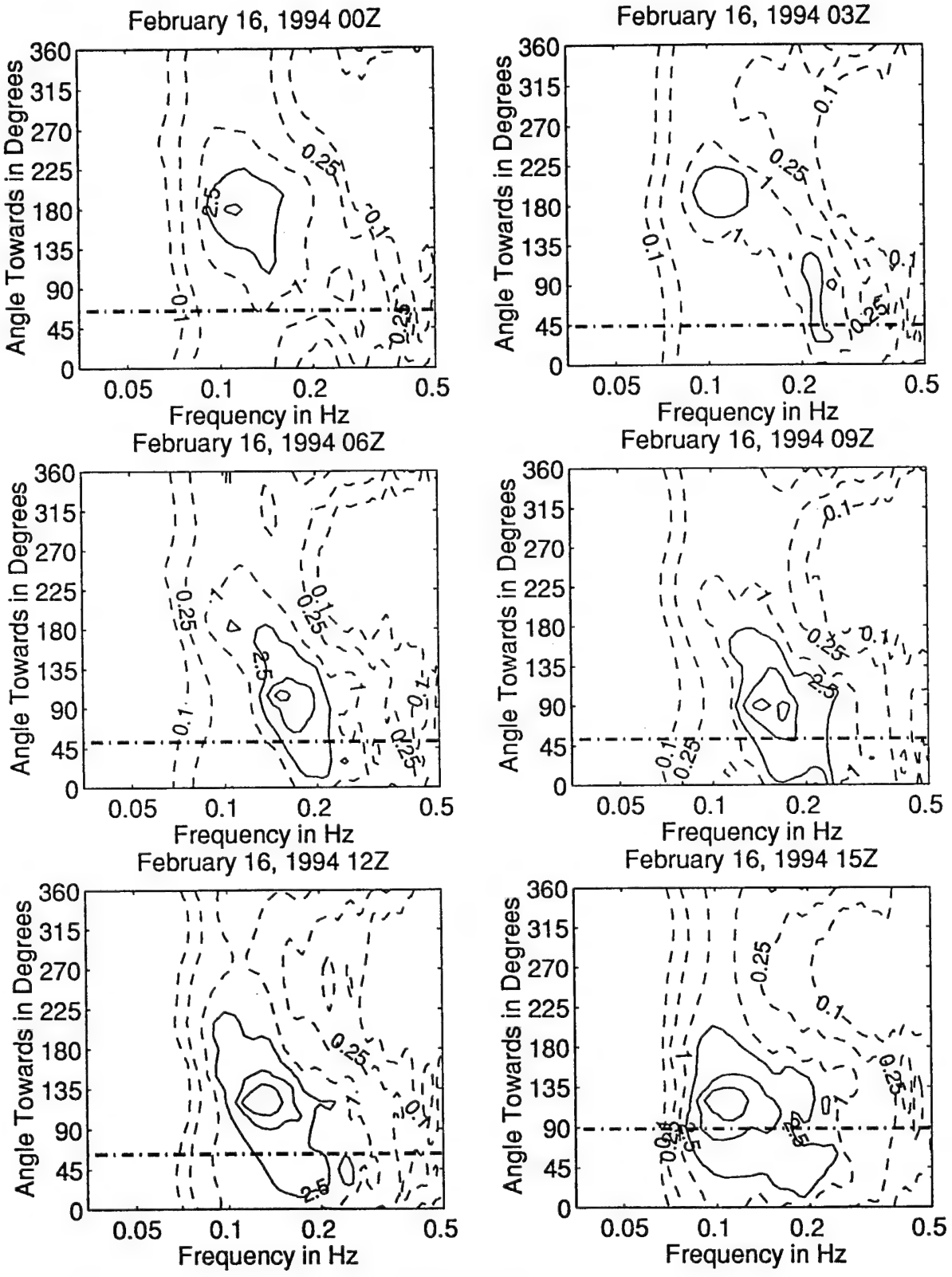

Figure 3.4.94: Directional wave spectra, computed using maximum entropy method. Contours of spectral density as a function of direction. Contours are 0.1, 0.25, 1 (dashed), 2.5, 10, 25, 100, and 250 (solid). Wind direction is shown by thick dashed line.

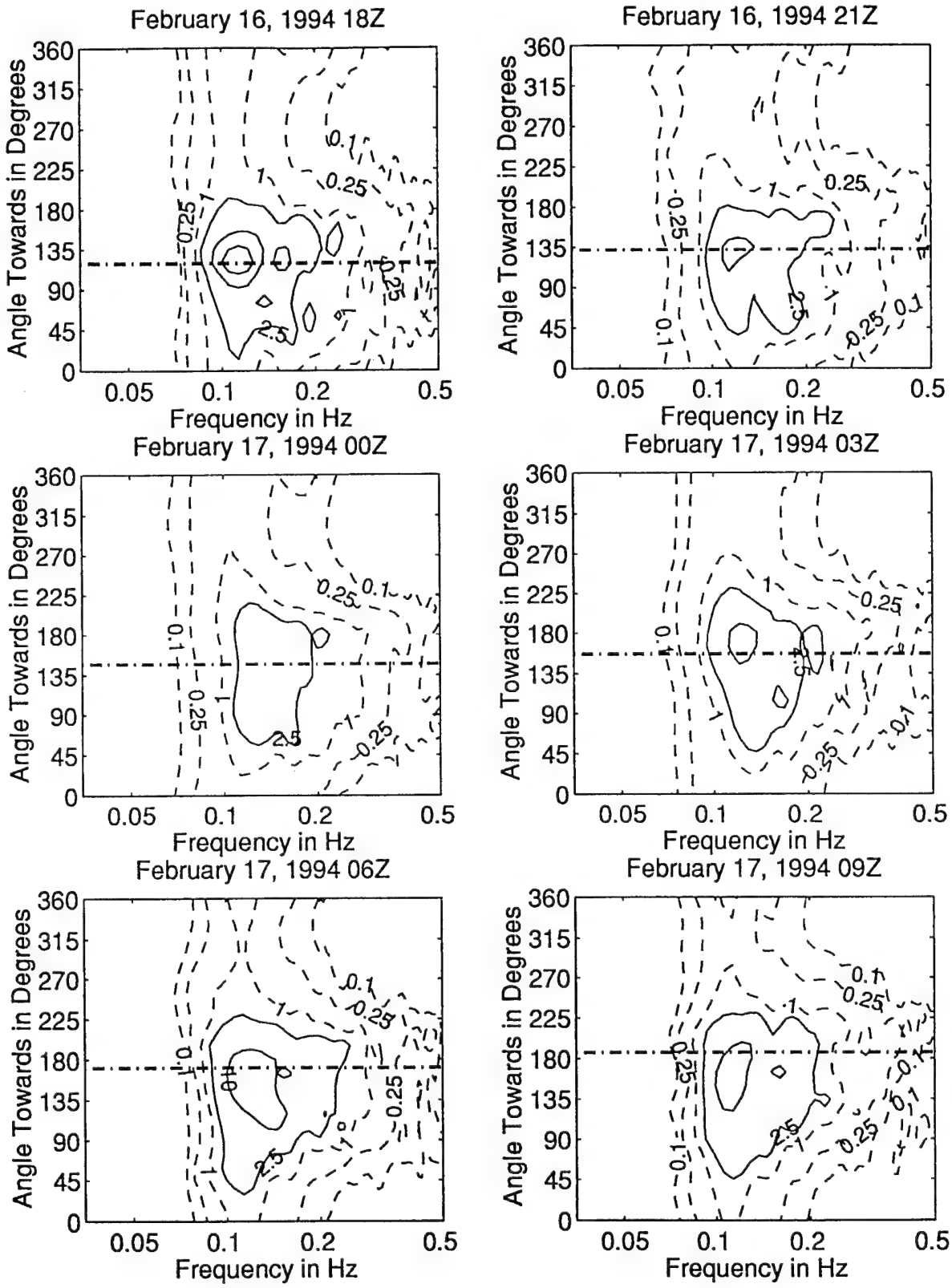

Figure 3.4.95: Directional wave spectra, computed using maximum entropy method. Contours of spectral density as a function of direction. Contours are 0.1, 0.25, 1 (dashed), 2.5, 10, 25, 100, and 250 (solid). Wind direction is shown by thick dashed line.

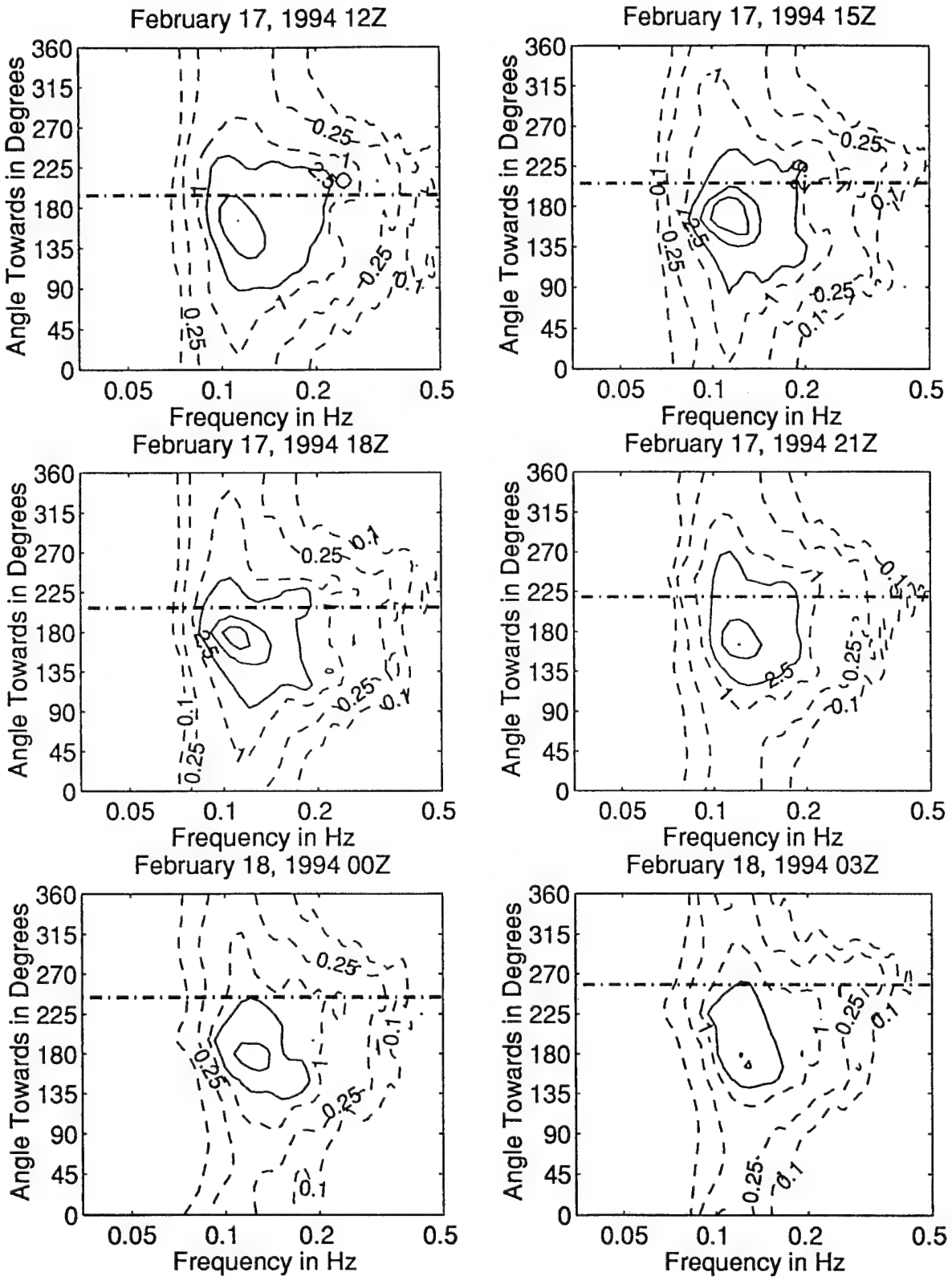

Figure 3.4.96: Directional wave spectra, computed using maximum entropy method. Contours of spectral density as a function of direction. Contours are 0.1, 0.25, 1 (dashed), 2.5, 10, 25, 100, and 250 (solid). Wind direction is shown by thick dashed line.

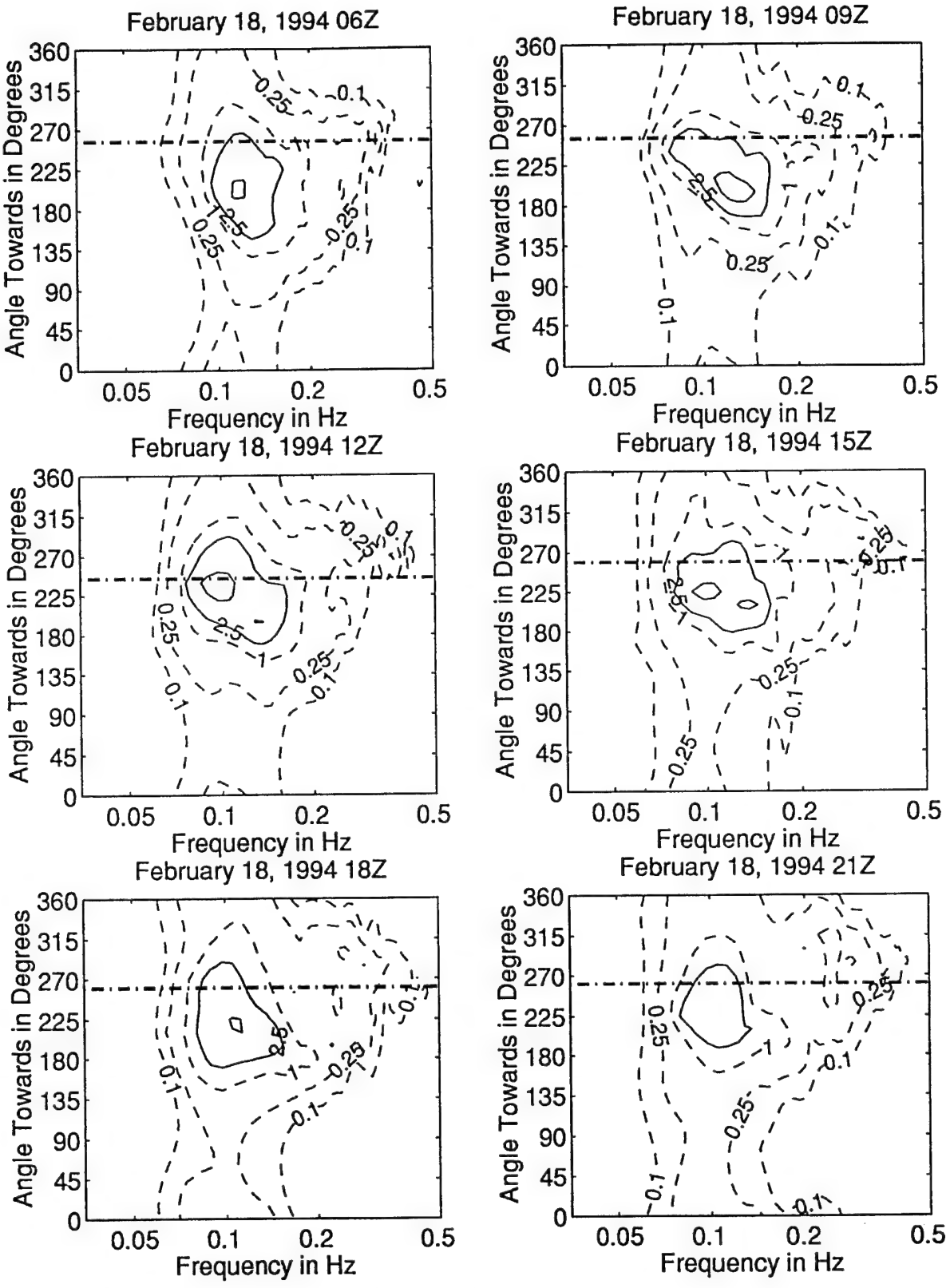

Figure 3.4.97: Directional wave spectra, computed using maximum entropy method. Contours of spectral density as a function of direction. Contours are 0.1, 0.25, 1 (dashed), 2.5, 10, 25, 100, and 250 (solid). Wind direction is shown by thick dashed line.

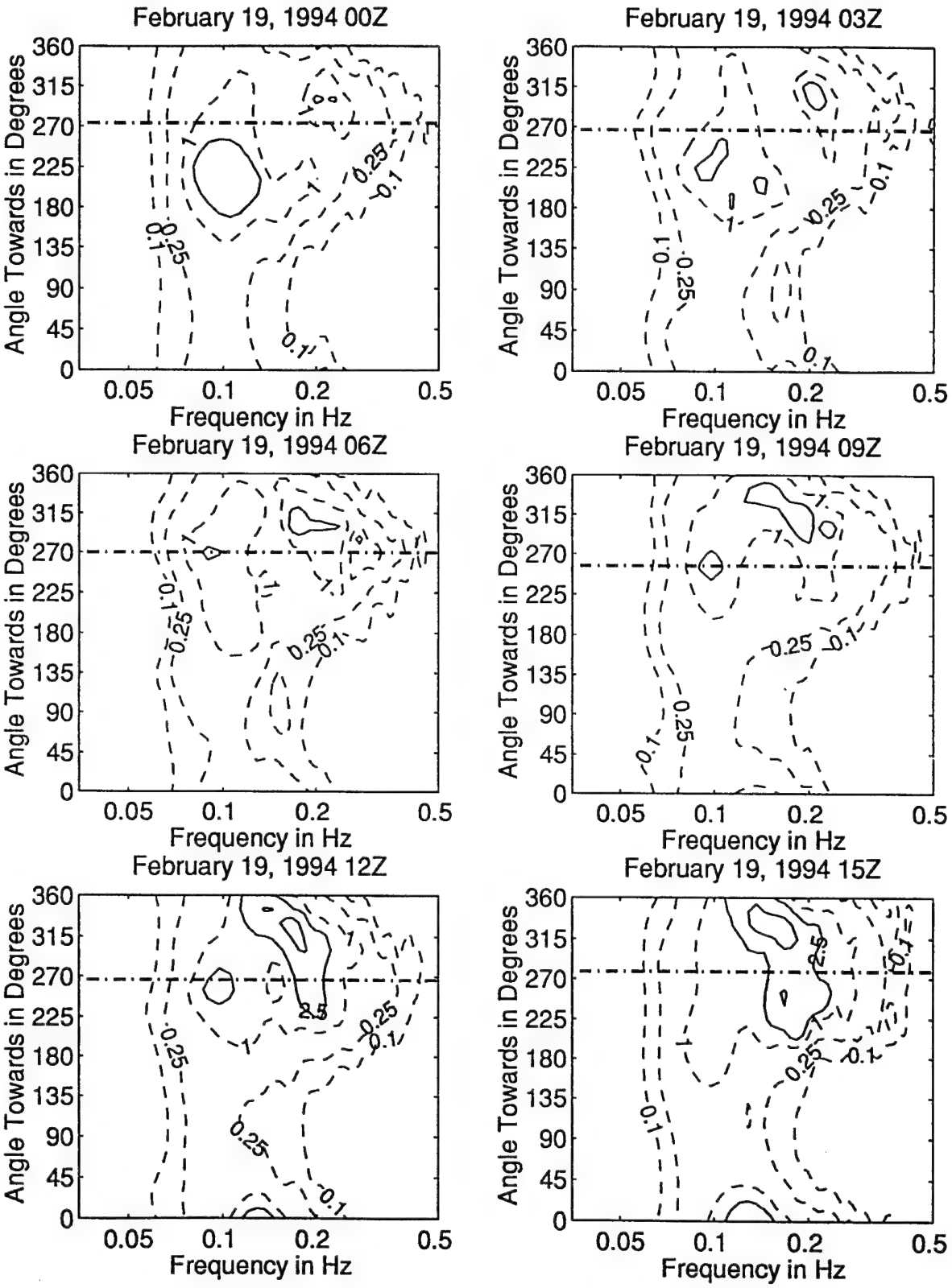

Figure 3.4.98: Directional wave spectra, computed using maximum entropy method. Contours of spectral density as a function of direction. Contours are 0.1, 0.25, 1 (dashed), 2.5, 10, 25, 100, and 250 (solid). Wind direction is shown by thick dashed line.

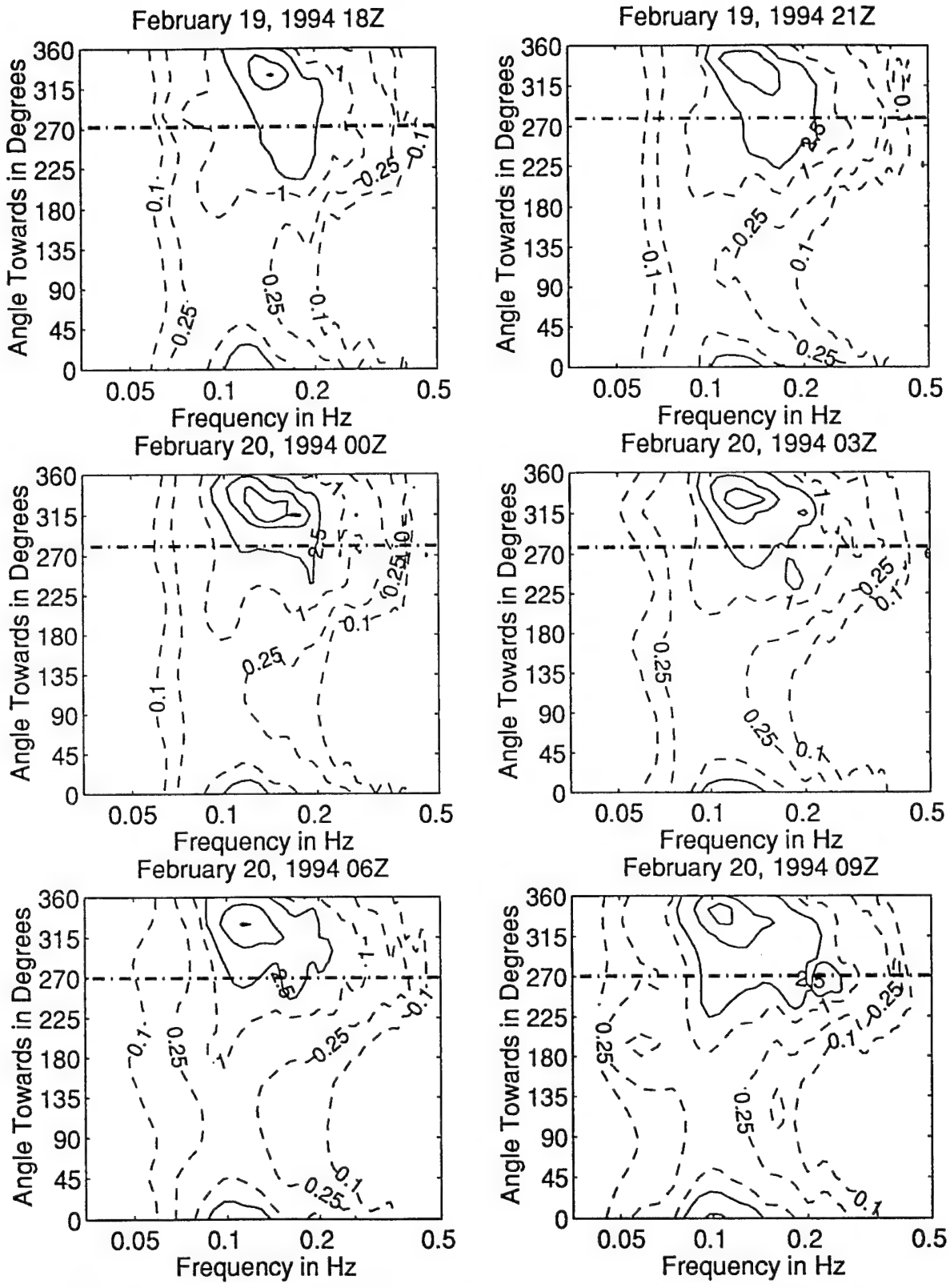

Figure 3.4.99: Directional wave spectra, computed using maximum entropy method. Contours of spectral density as a function of direction. Contours are 0.1, 0.25, 1 (dashed), 2.5, 10, 25, 100, and 250 (solid). Wind direction is shown by thick dashed line.

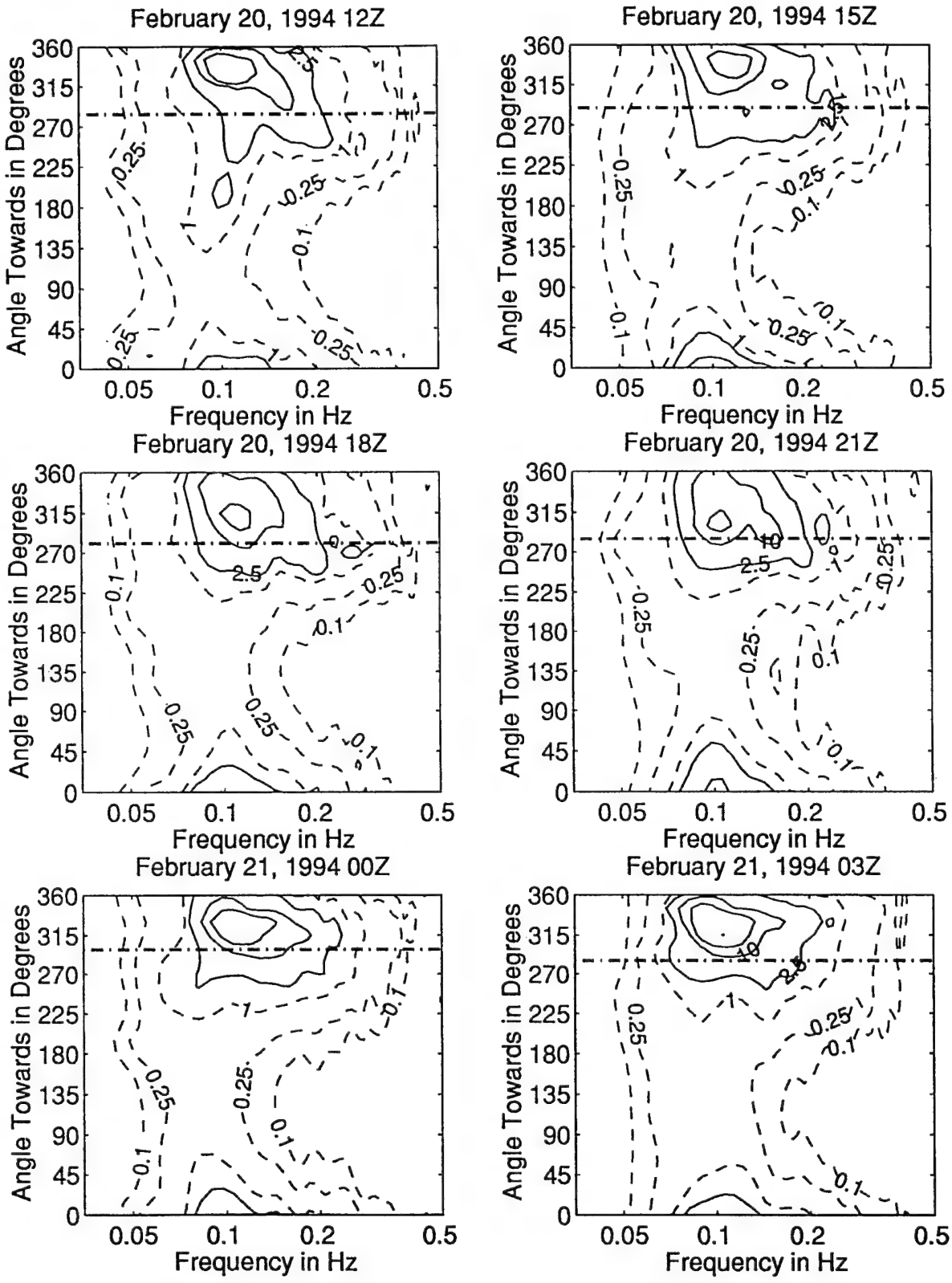

Figure 3.4.100: Directional wave spectra, computed using maximum entropy method. Contours of spectral density as a function of direction. Contours are 0.1, 0.25, 1 (dashed), 2.5, 10, 25, 100, and 250 (solid). Wind direction is shown by thick dashed line.

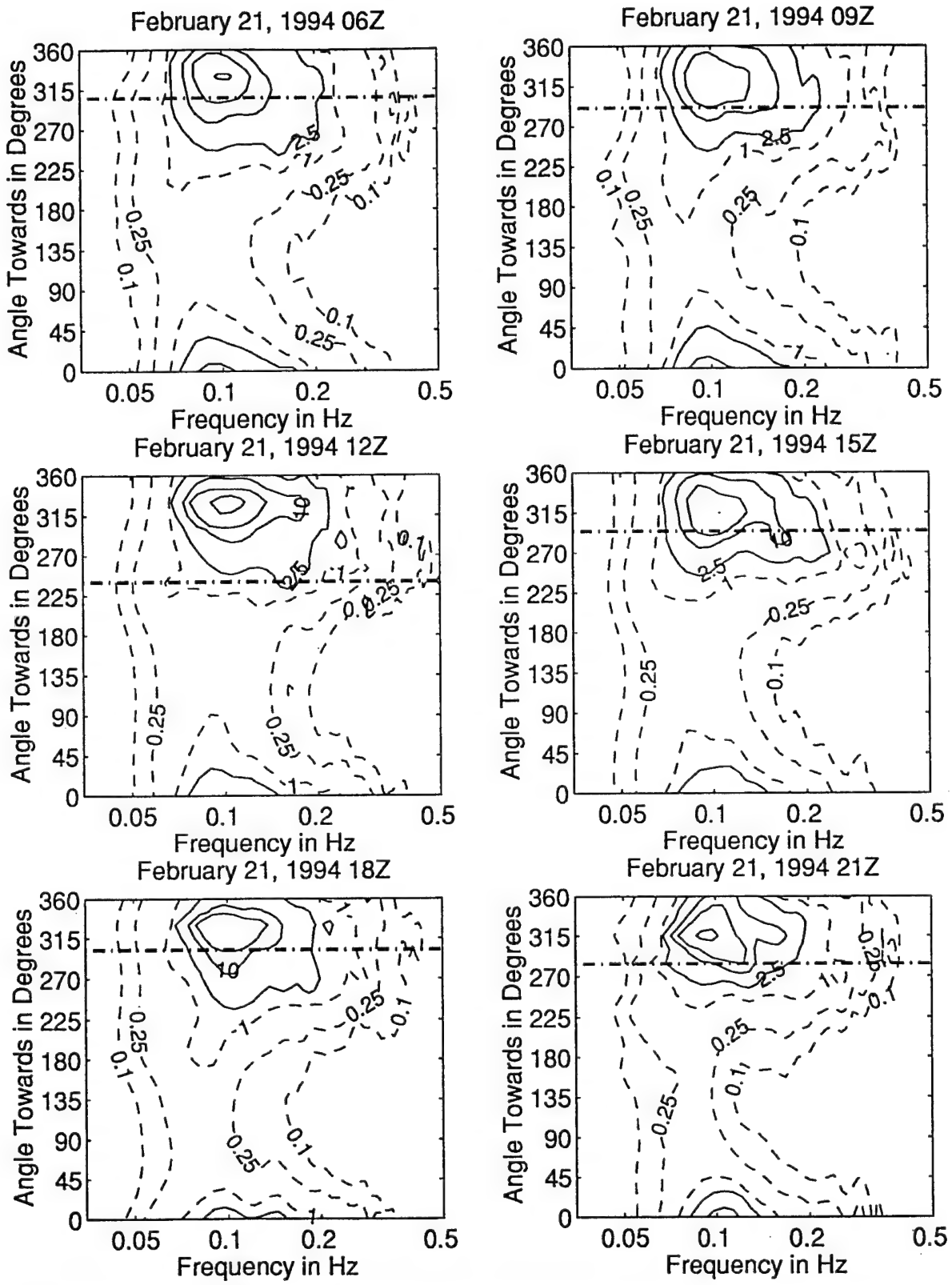

Figure 3.4.101: Directional wave spectra, computed using maximum entropy method. Contours of spectral density as a function of direction. Contours are 0.1, 0.25, 1 (dashed), 2.5, 10, 25, 100, and 250 (solid). Wind direction is shown by thick dashed line.

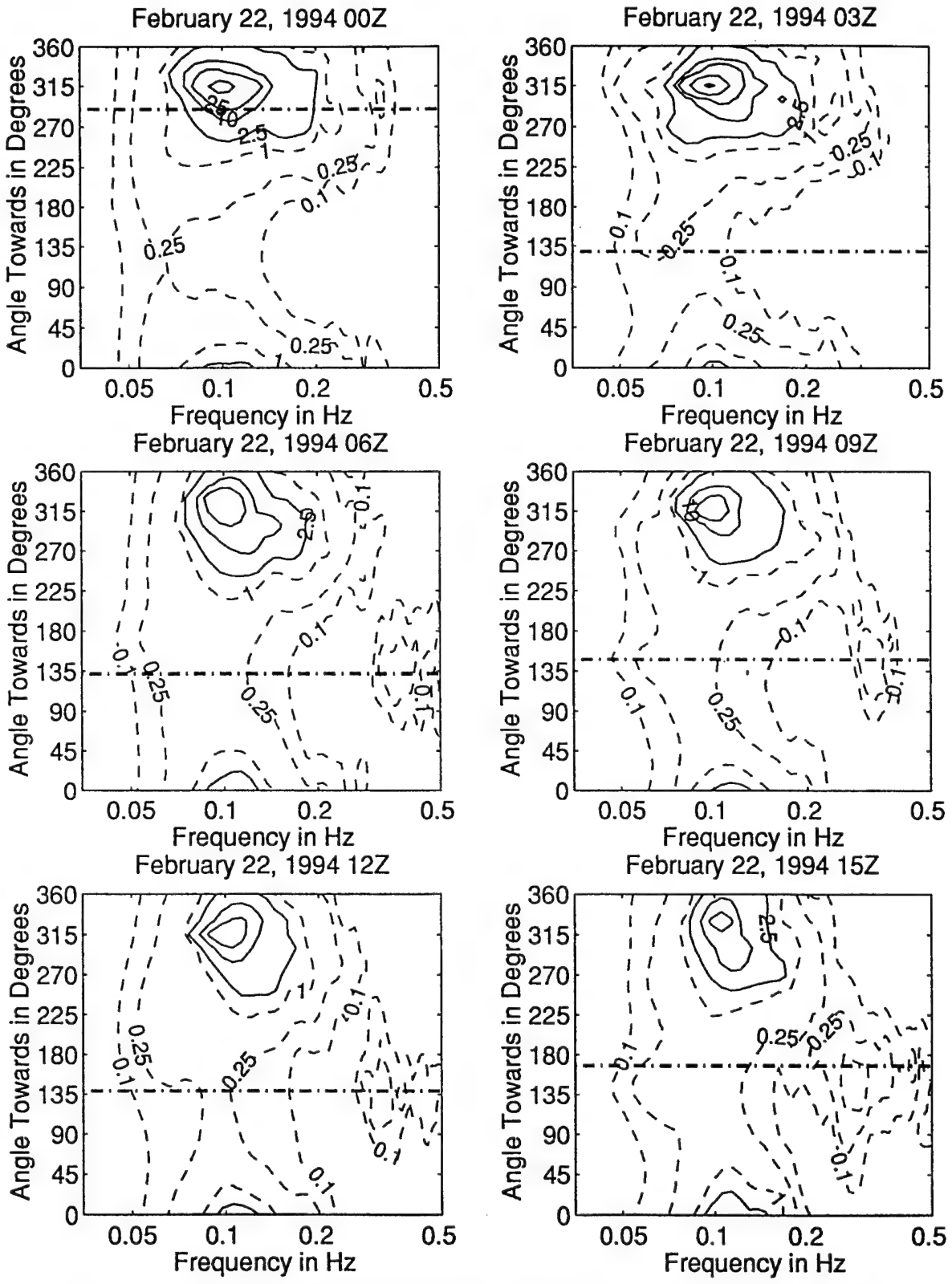

Figure 3.4.102: Directional wave spectra, computed using maximum entropy method. Contours of spectral density as a function of direction. Contours are 0.1, 0.25, 1 (dashed), 2.5, 10, 25, 100, and 250 (solid). Wind direction is shown by thick dashed line.

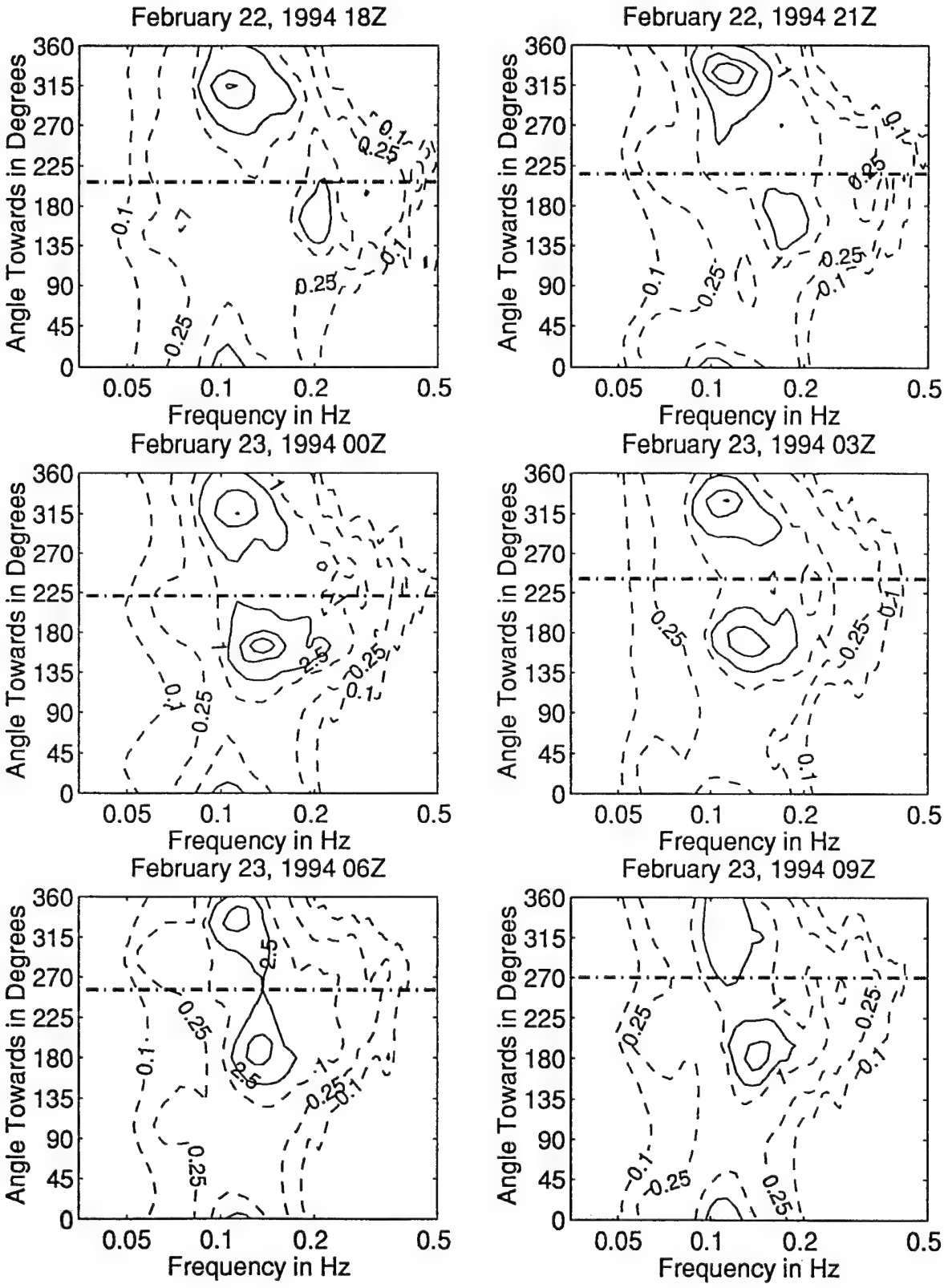

Figure 3.4.103: Directional wave spectra, computed using maximum entropy method. Contours of spectral density as a function of direction. Contours are 0.1, 0.25, 1 (dashed), 2.5, 10, 25, 100, and 250 (solid). Wind direction is shown by thick dashed line.

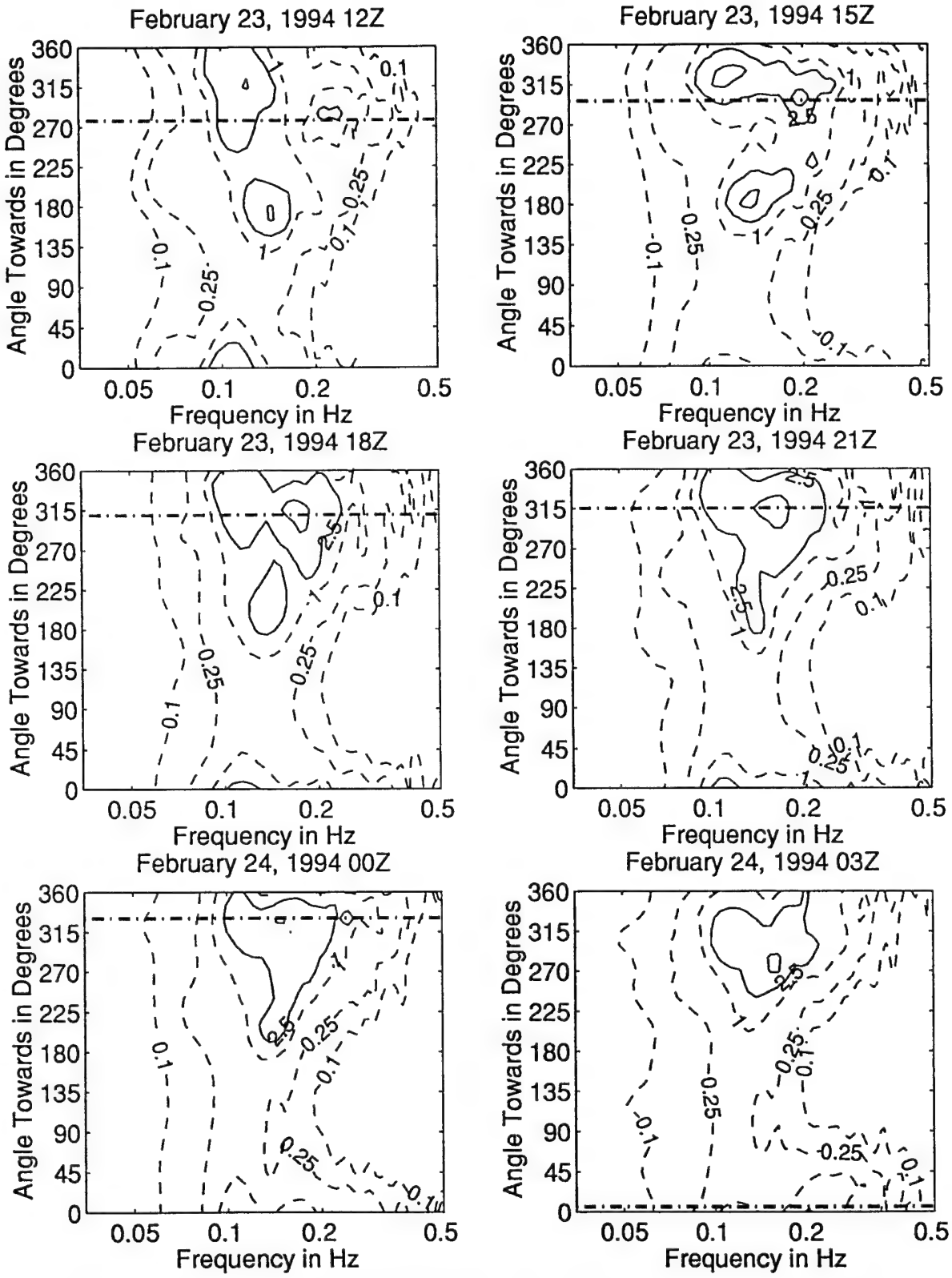

Figure 3.4.104: Directional wave spectra, computed using maximum entropy method. Contours of spectral density as a function of direction. Contours are 0.1, 0.25, 1 (dashed), 2.5, 10, 25, 100, and 250 (solid). Wind direction is shown by thick dashed line.

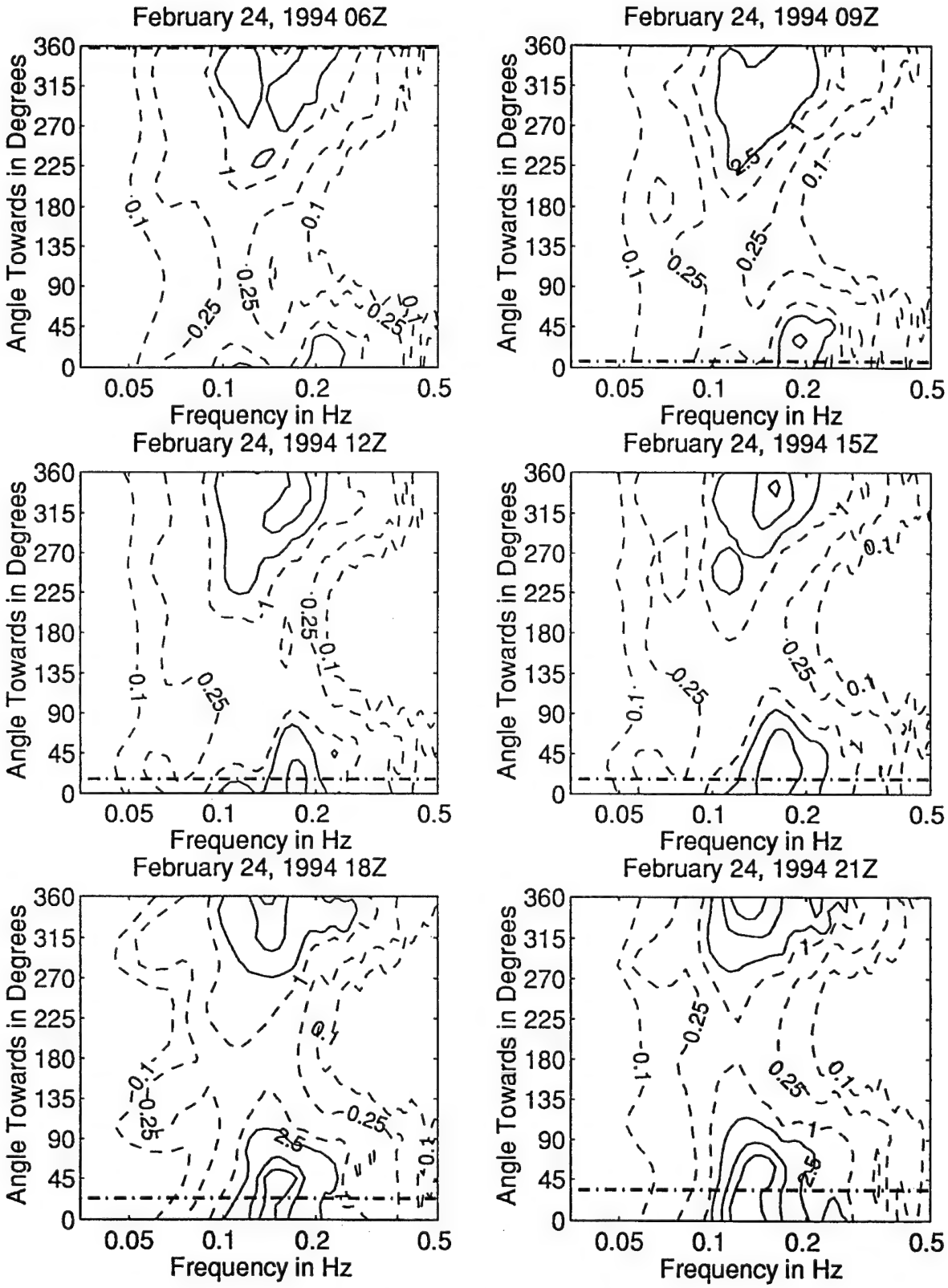

Figure 3.4.105: Directional wave spectra, computed using maximum entropy method. Contours of spectral density as a function of direction. Contours are 0.1, 0.25, 1 (dashed), 2.5, 10, 25, 100, and 250 (solid). Wind direction is shown by thick dashed line.

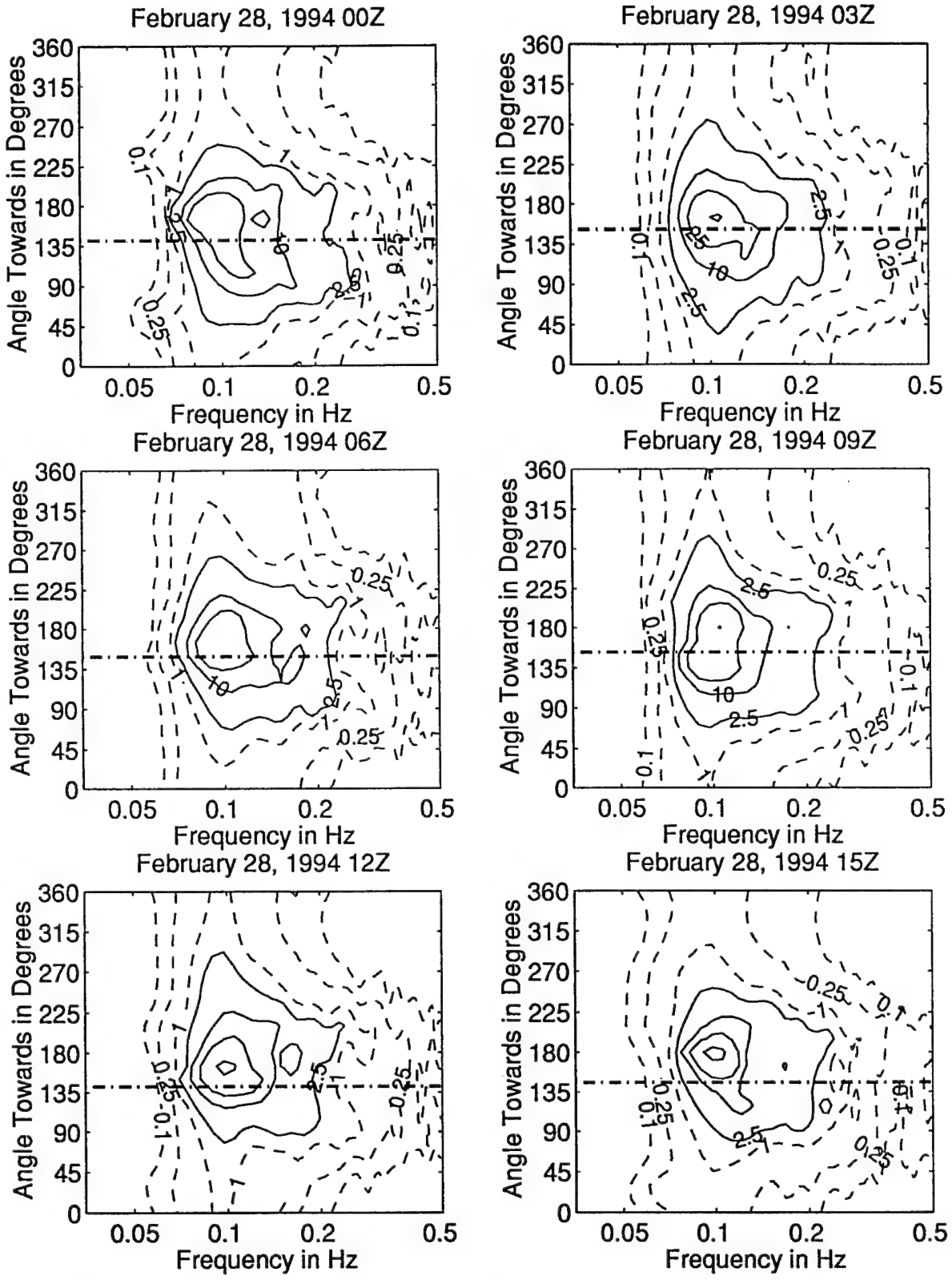

Figure 3.4.110: Directional wave spectra, computed using maximum entropy method. Contours of spectral density as a function of direction. Contours are 0.1, 0.25, 1 (dashed), 2.5, 10, 25, 100, and 250 (solid). Wind direction is shown by thick dashed line.

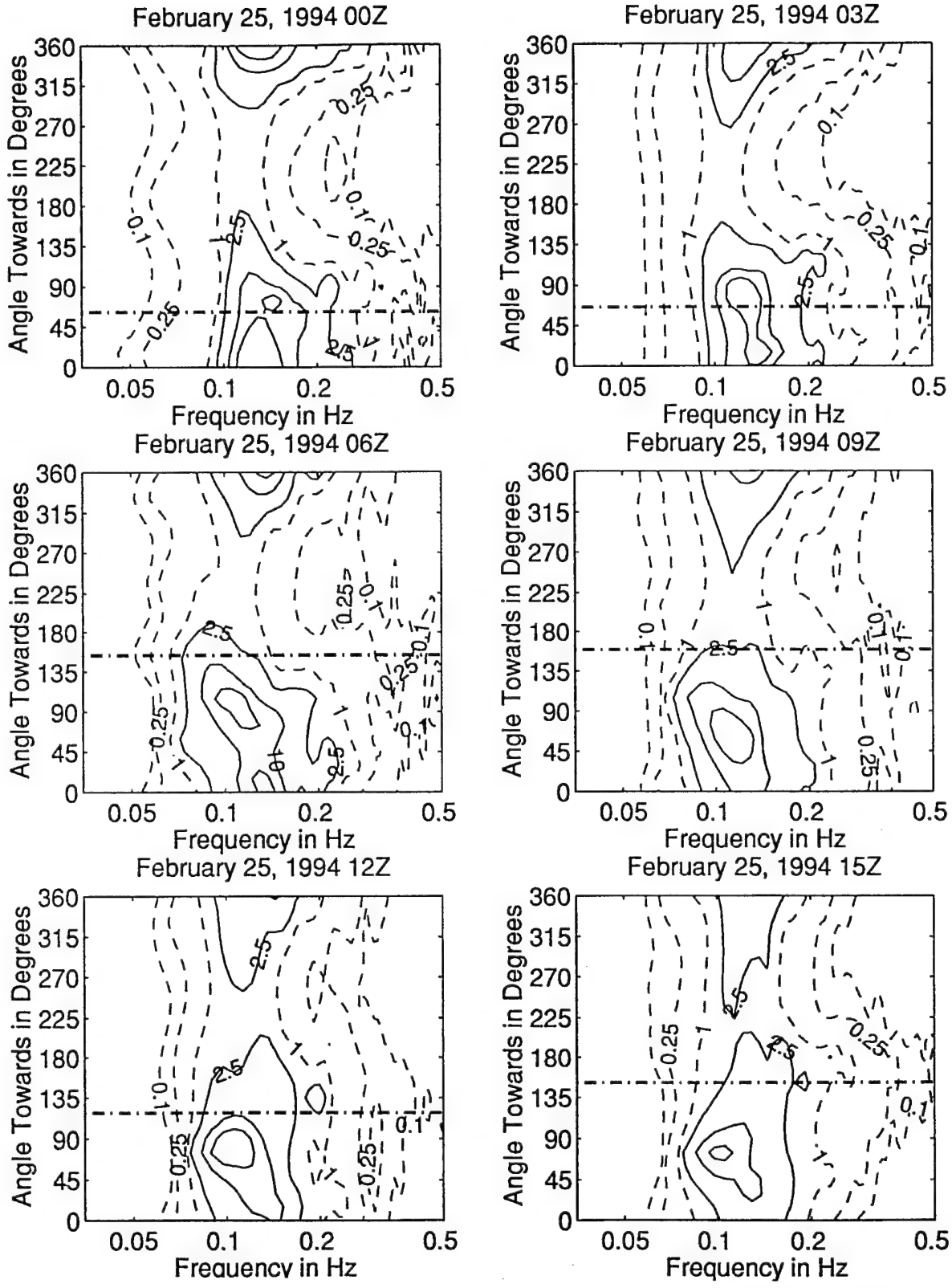

Figure 3.4.106: Directional wave spectra, computed using maximum entropy method. Contours of spectral density as a function of direction. Contours are 0.1, 0.25, 1 (dashed), 2.5, 10, 25, 100, and 250 (solid). Wind direction is shown by thick dashed line.

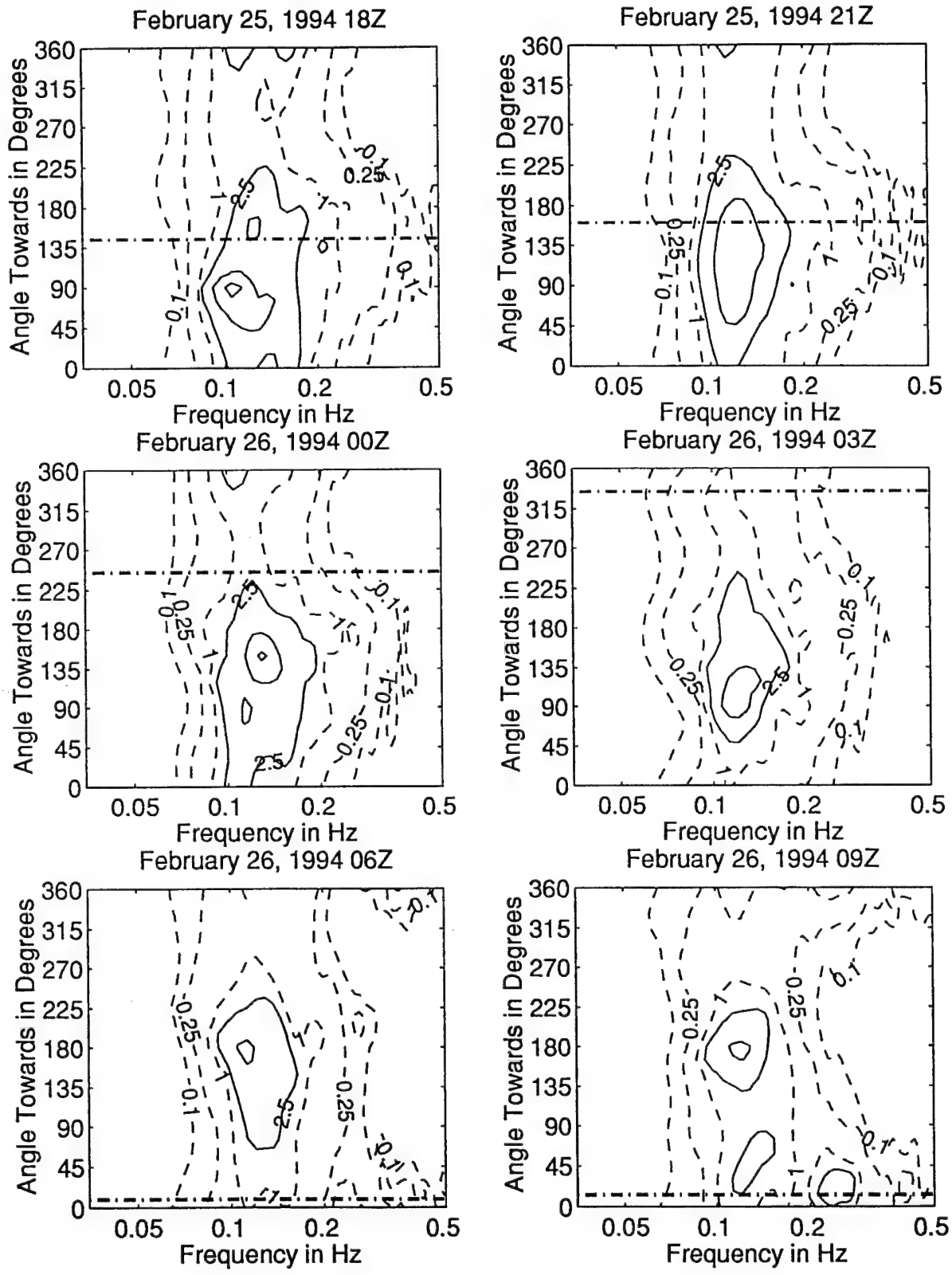

Figure 3.4.107: Directional wave spectra, computed using maximum entropy method. Contours of spectral density as a function of direction. Contours are 0.1, 0.25, 1 (dashed), 2.5, 10, 25, 100, and 250 (solid). Wind direction is shown by thick dashed line.

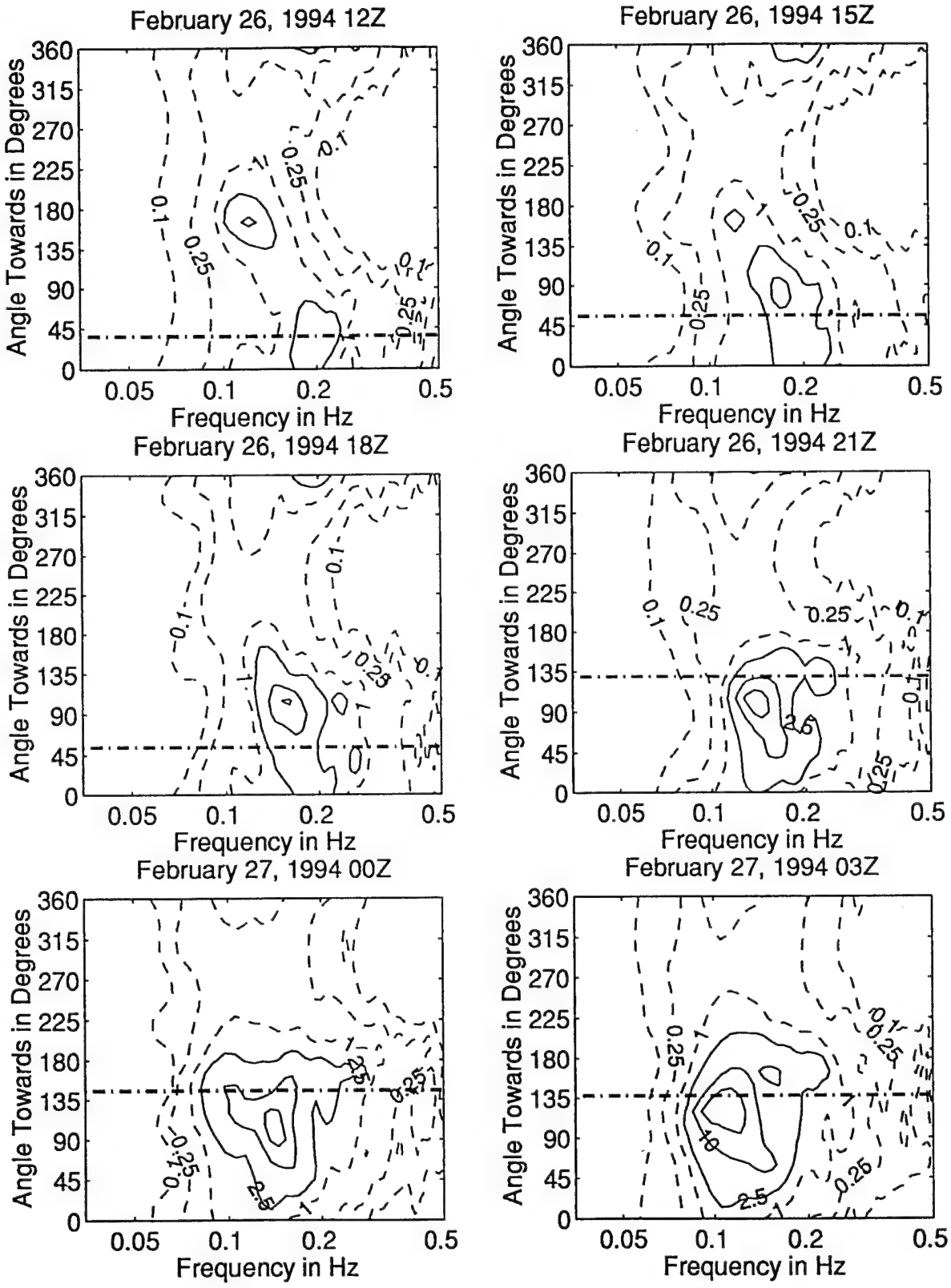

Figure 3.4.108: Directional wave spectra, computed using maximum entropy method. Contours of spectral density as a function of direction. Contours are 0.1, 0.25, 1 (dashed), 2.5, 10, 25, 100, and 250 (solid). Wind direction is shown by thick dashed line.

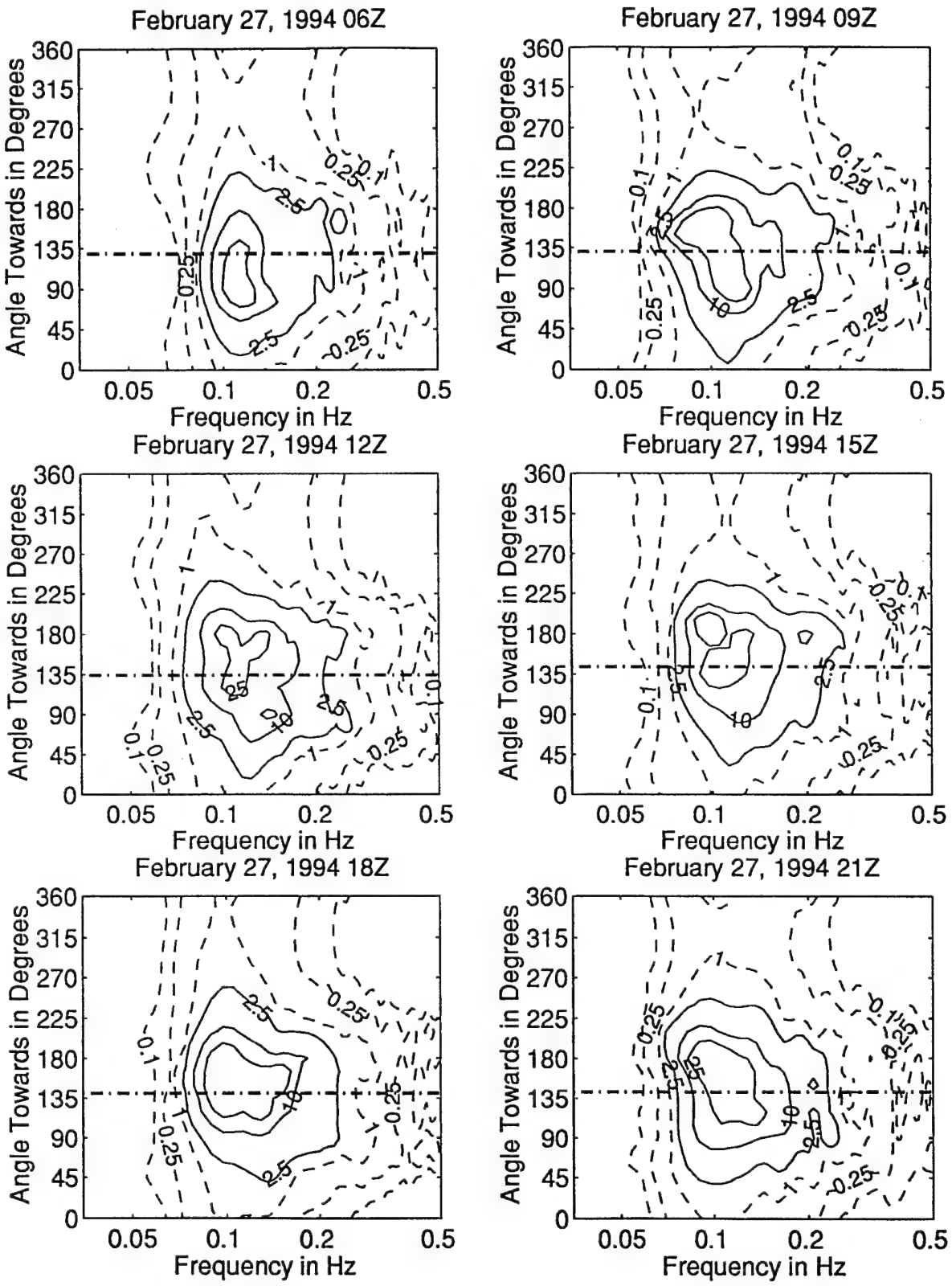

Figure 3.4.109: Directional wave spectra, computed using maximum entropy method. Contours of spectral density as a function of direction. Contours are 0.1, 0.25, 1 (dashed), 2.5, 10, 25, 100, and 250 (solid). Wind direction is shown by thick dashed line.

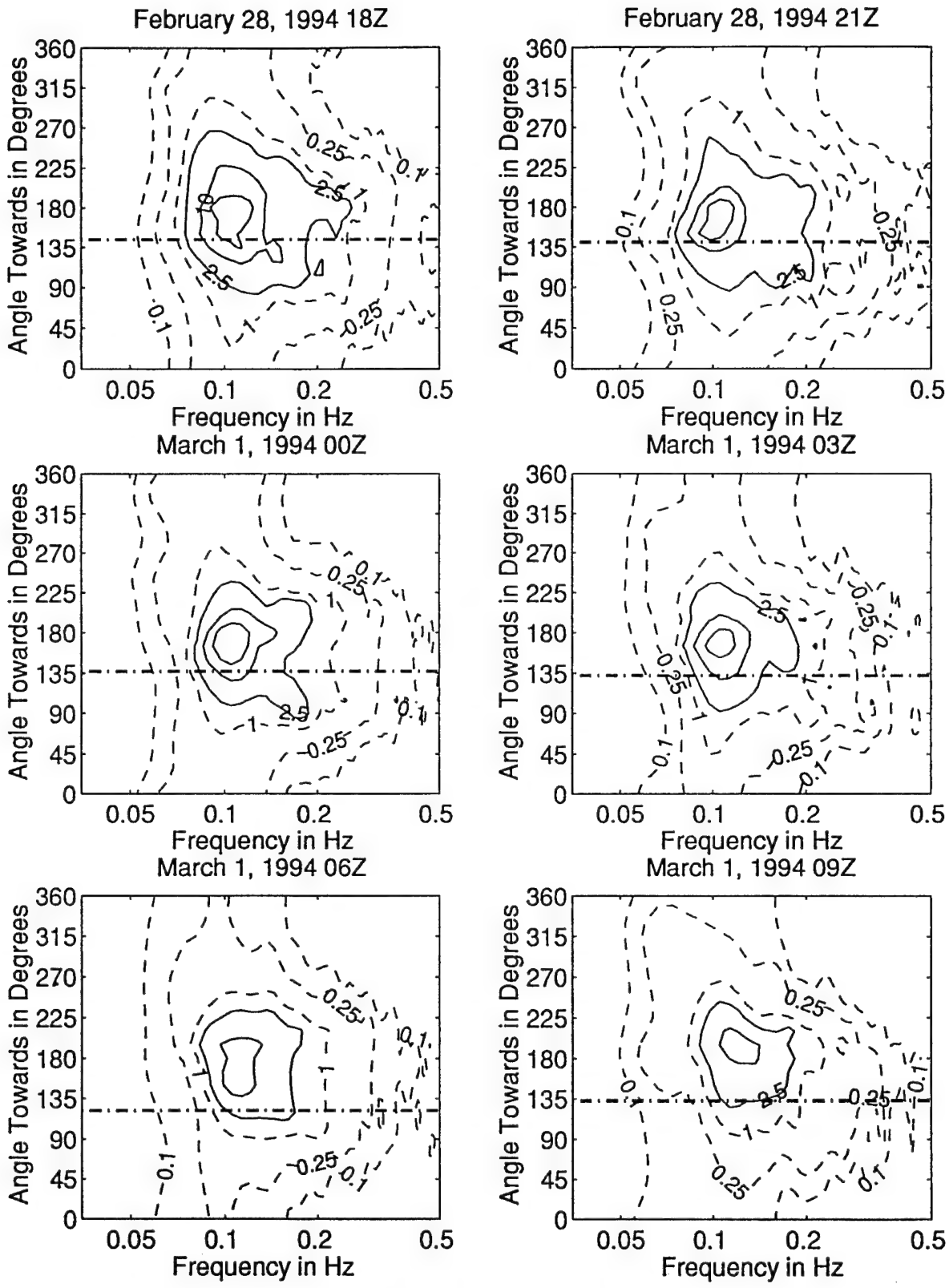

Figure 3.4.111: Directional wave spectra, computed using maximum entropy method. Contours of spectral density as a function of direction. Contours are 0.1, 0.25, 1 (dashed), 2.5, 10, 25, 100, and 250 (solid). Wind direction is shown by thick dashed line.

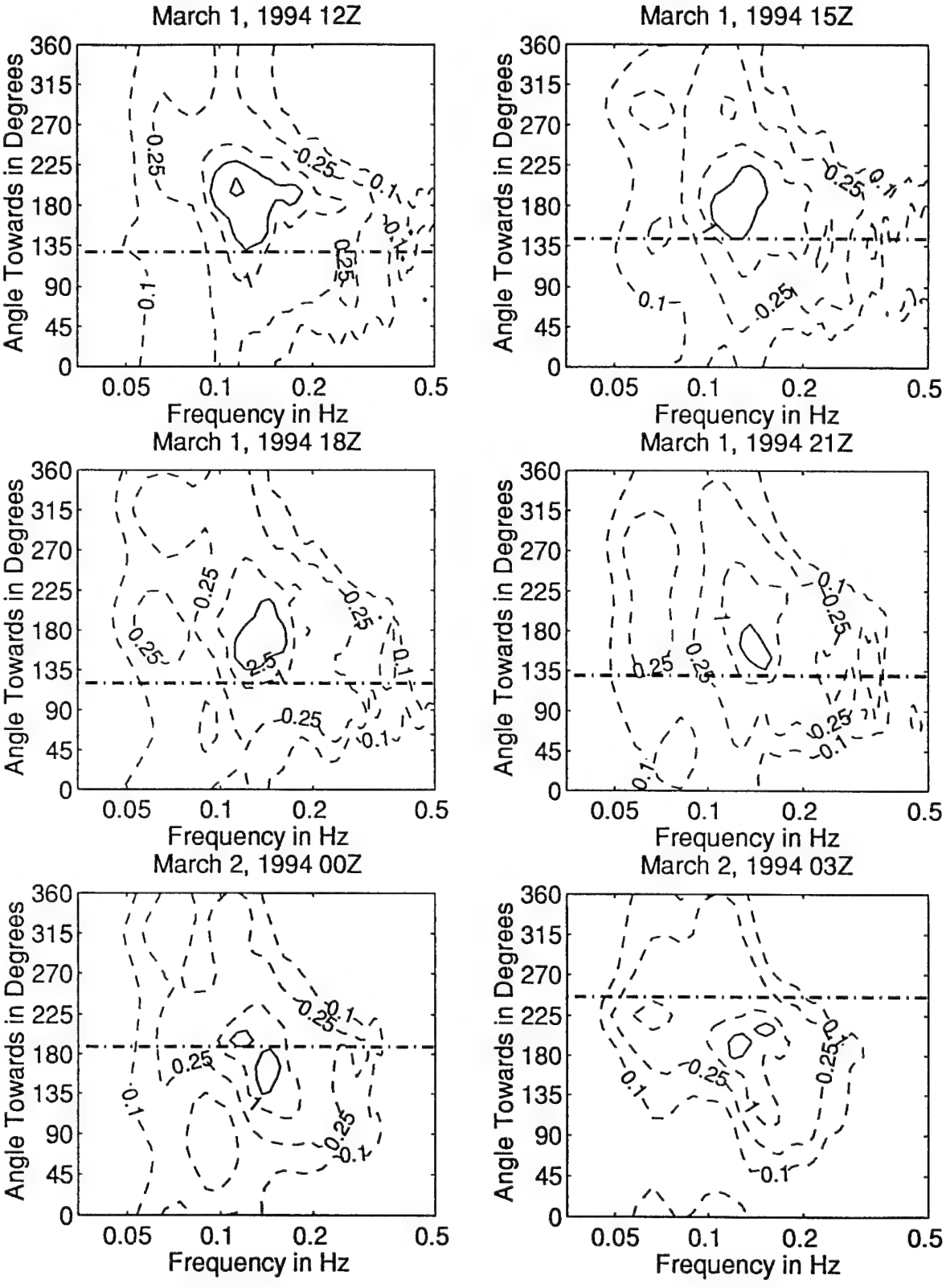

Figure 3.4.112: Directional wave spectra, computed using maximum entropy method. Contours of spectral density as a function of direction. Contours are 0.1, 0.25, 1 (dashed), 2.5, 10, 25, 100, and 250 (solid). Wind direction is shown by thick dashed line.

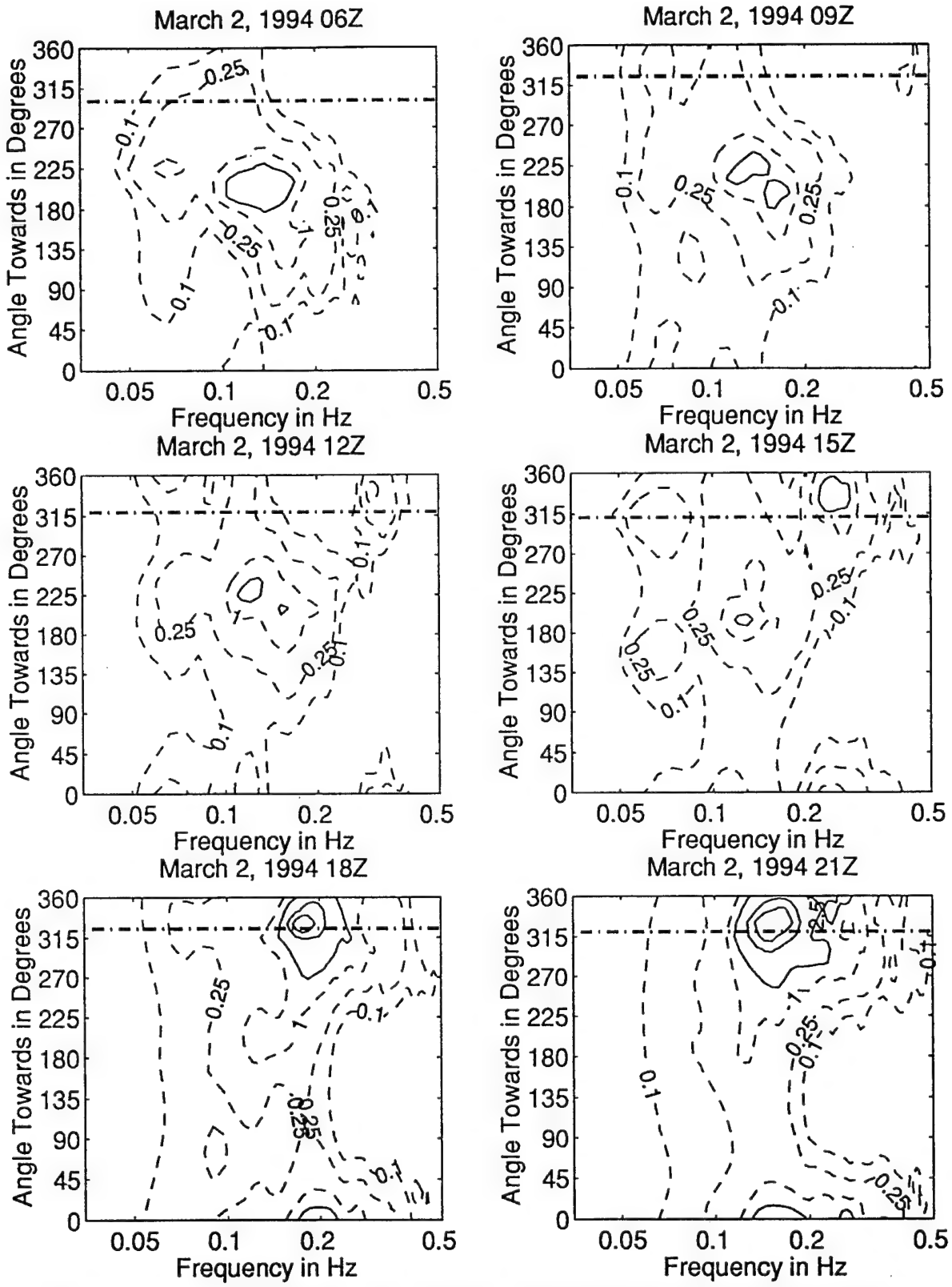

Figure 3.4.113: Directional wave spectra, computed using maximum entropy method. Contours of spectral density as a function of direction. Contours are 0.1, 0.25, 1 (dashed), 2.5, 10, 25, 100, and 250 (solid). Wind direction is shown by thick dashed line.

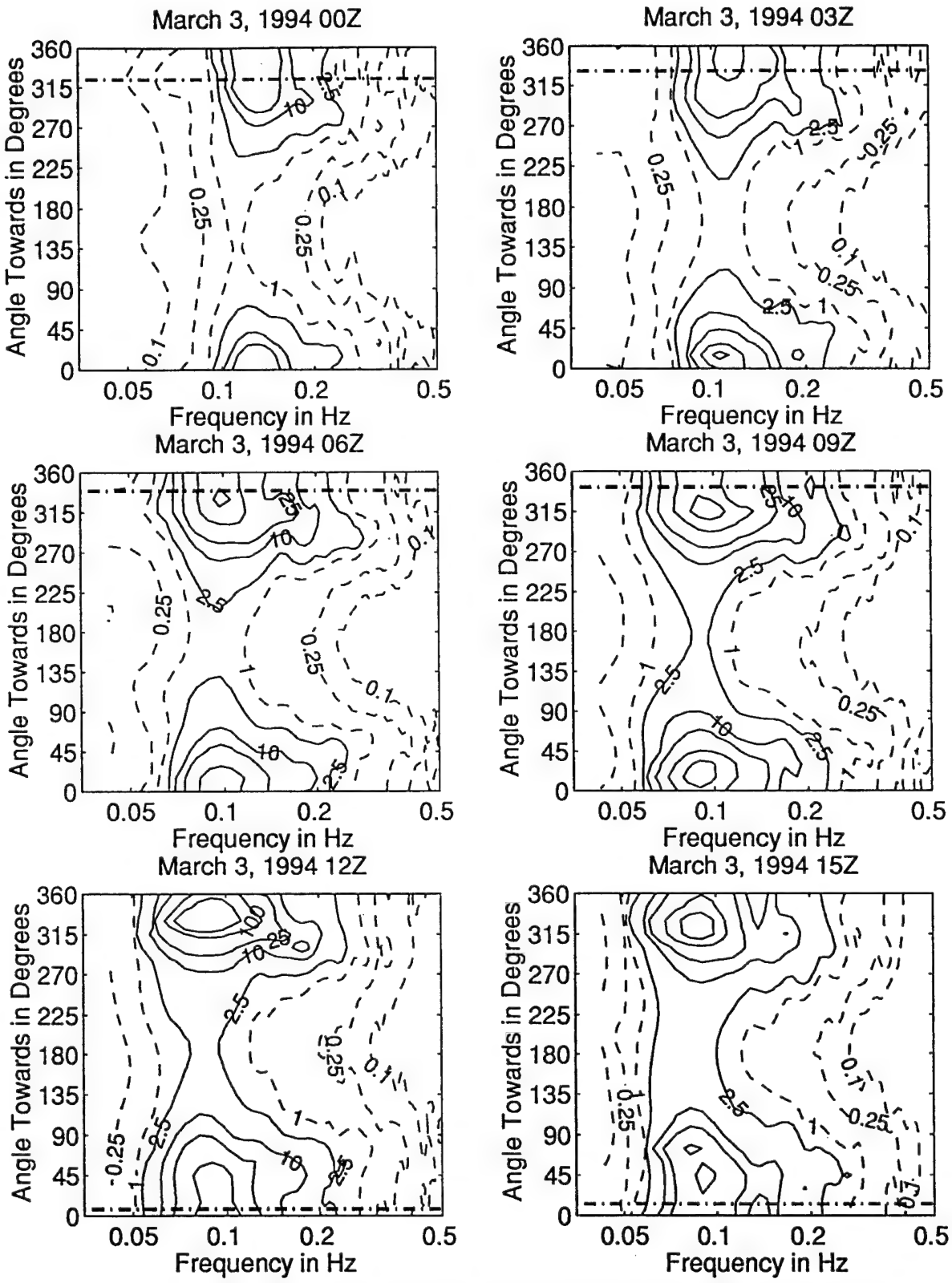

Figure 3.4.114: Directional wave spectra, computed using maximum entropy method. Contours of spectral density as a function of direction. Contours are 0.1, 0.25, 1 (dashed), 2.5, 10, 25, 100, and 250 (solid). Wind direction is shown by thick dashed line.

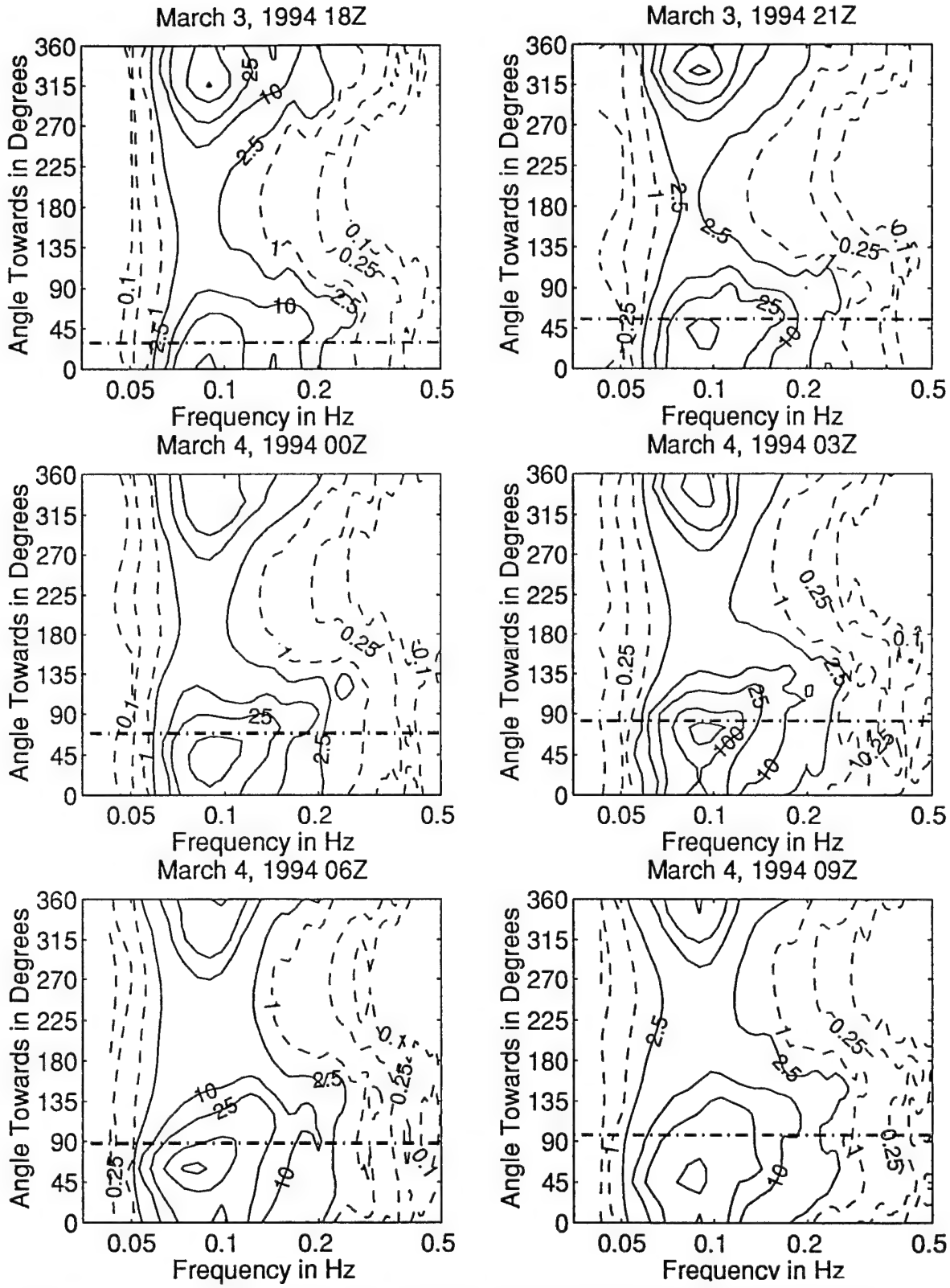

Figure 3.4.115: Directional wave spectra, computed using maximum entropy method. Contours of spectral density as a function of direction. Contours are 0.1, 0.25, 1 (dashed), 2.5, 10, 25, 100, and 250 (solid). Wind direction is shown by thick dashed line.

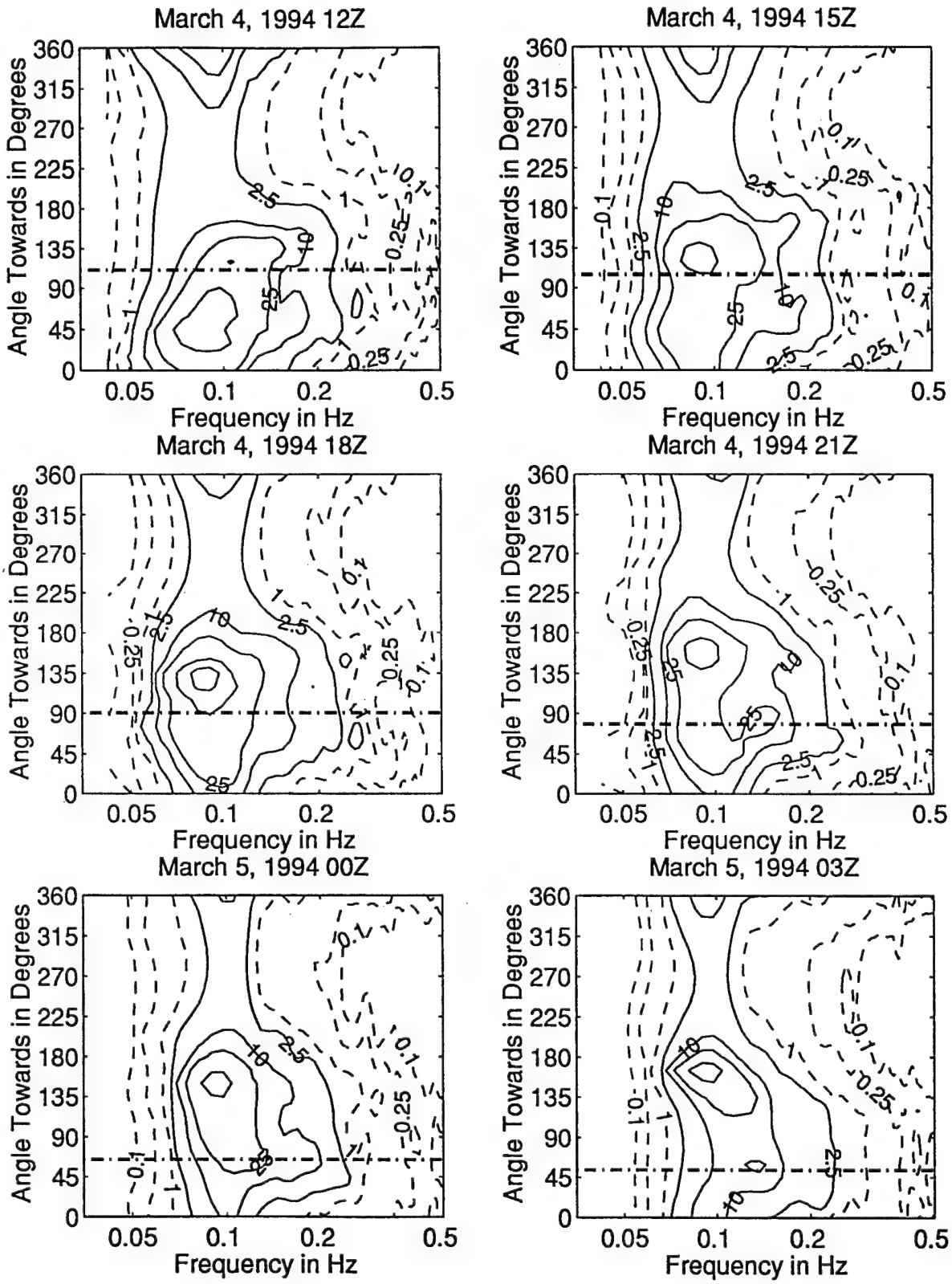

Figure 3.4.116: Directional wave spectra, computed using maximum entropy method. Contours of spectral density as a function of direction. Contours are 0.1, 0.25, 1 (dashed), 2.5, 10, 25, 100, and 250 (solid). Wind direction is shown by thick dashed line.

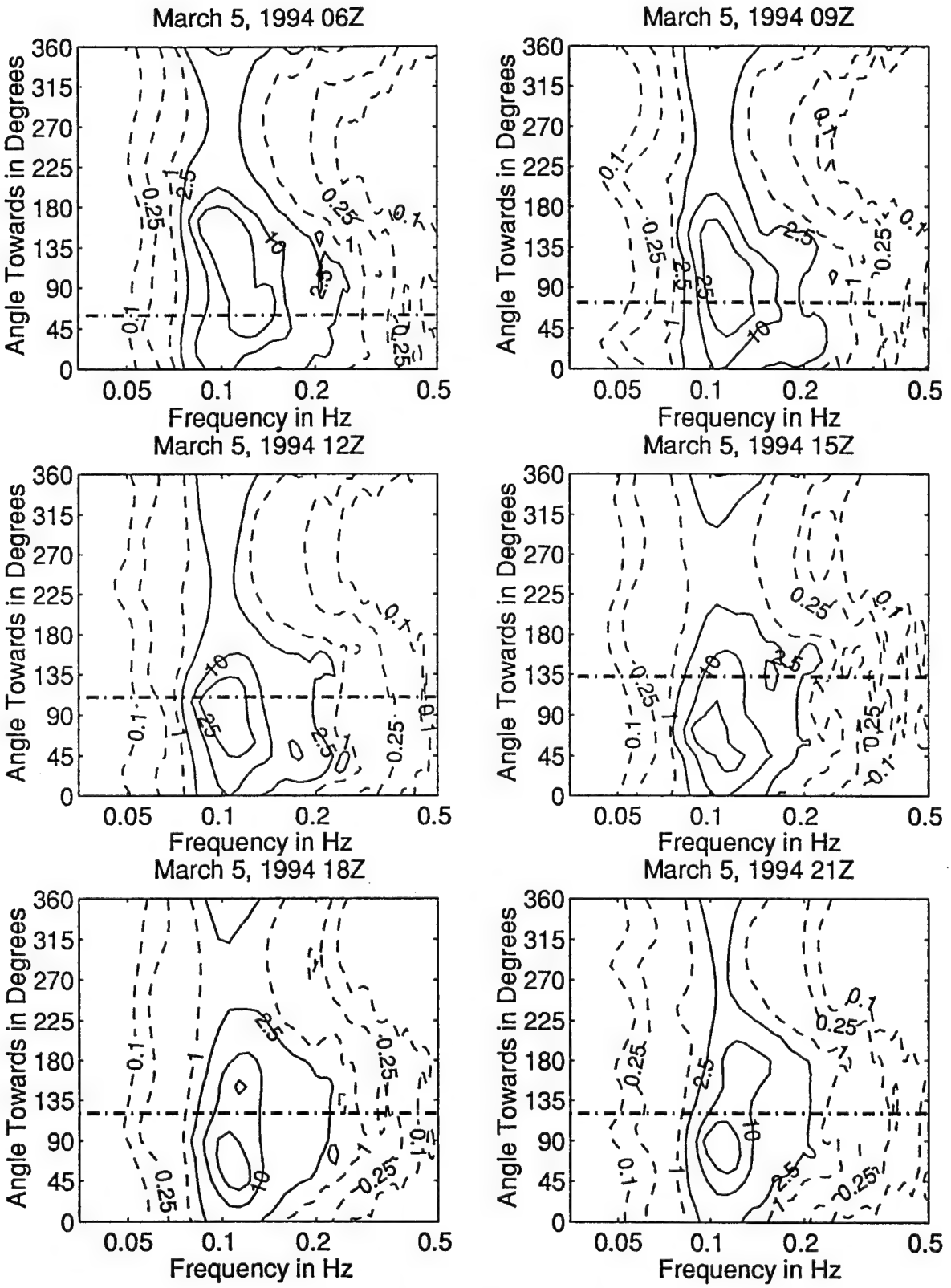

Figure 3.4.117: Directional wave spectra, computed using maximum entropy method. Contours of spectral density as a function of direction. Contours are 0.1, 0.25, 1 (dashed), 2.5, 10, 25, 100, and 250 (solid). Wind direction is shown by thick dashed line.

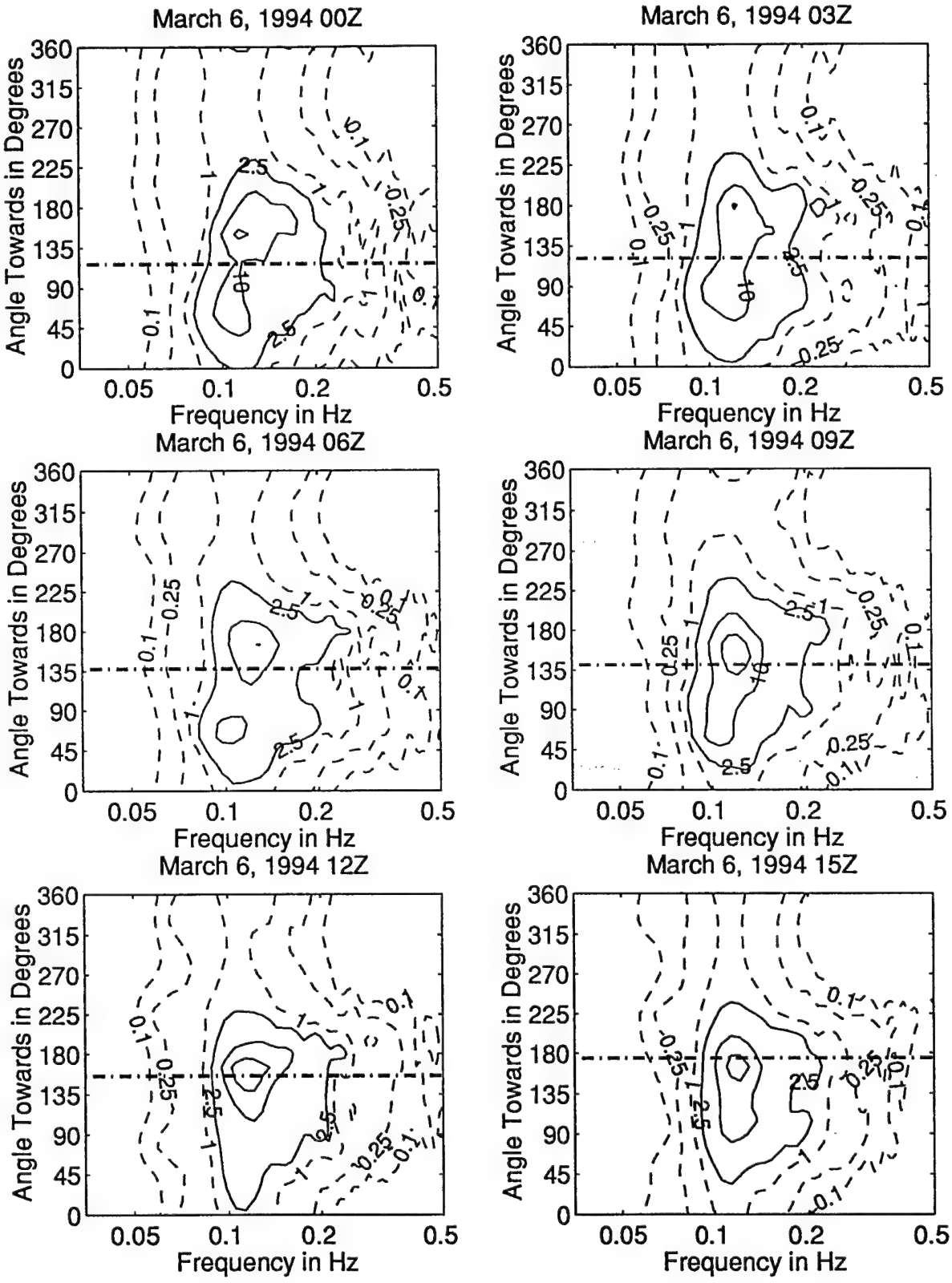

Figure 3.4.118: Directional wave spectra, computed using maximum entropy method. Contours of spectral density as a function of direction. Contours are 0.1, 0.25, 1 (dashed), 2.5, 10, 25, 100, and 250 (solid). Wind direction is shown by thick dashed line.

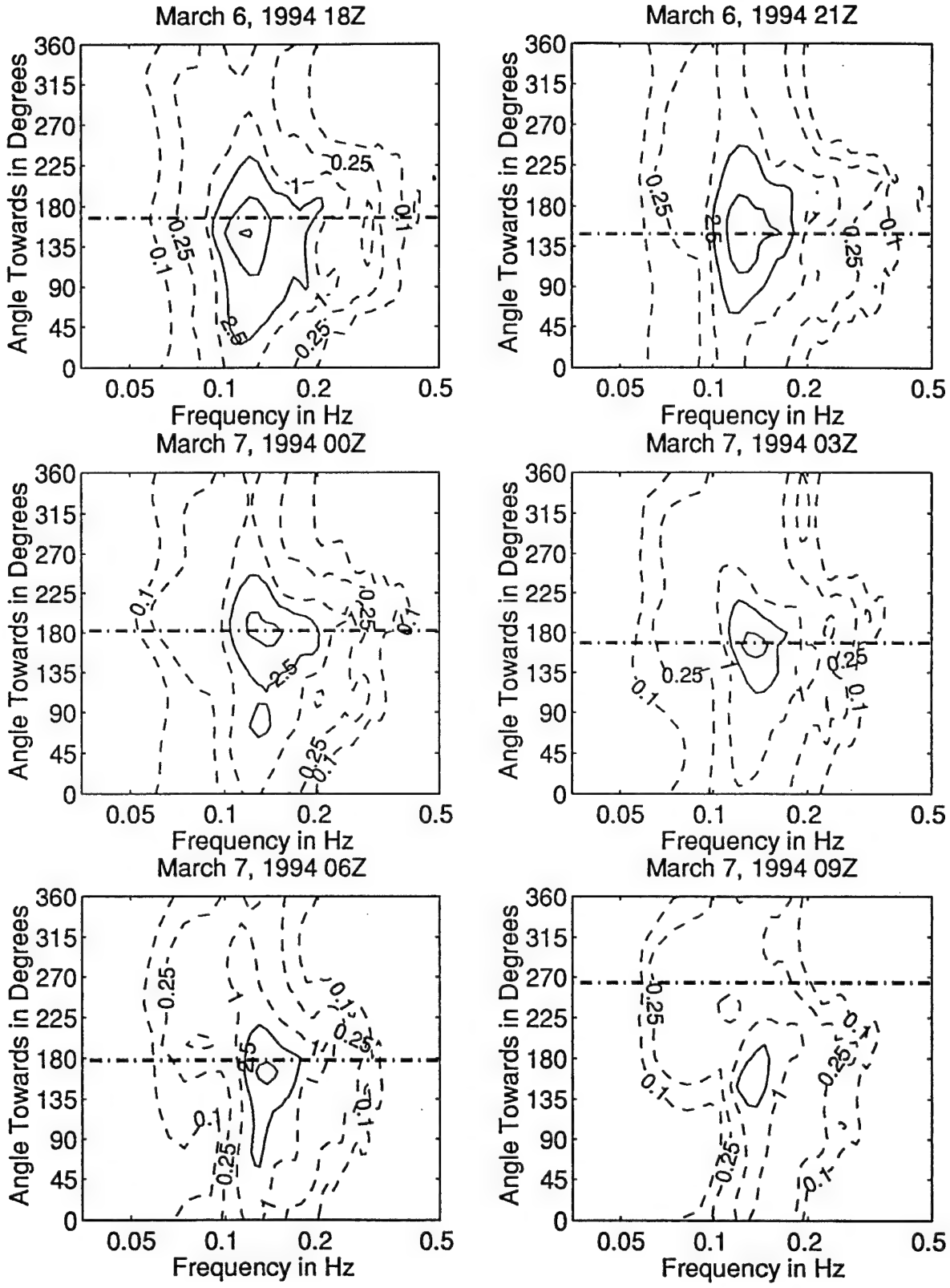

Figure 3.4.119: Directional wave spectra, computed using maximum entropy method. Contours of spectral density as a function of direction. Contours are 0.1, 0.25, 1 (dashed), 2.5, 10, 25, 100, and 250 (solid). Wind direction is shown by thick dashed line.

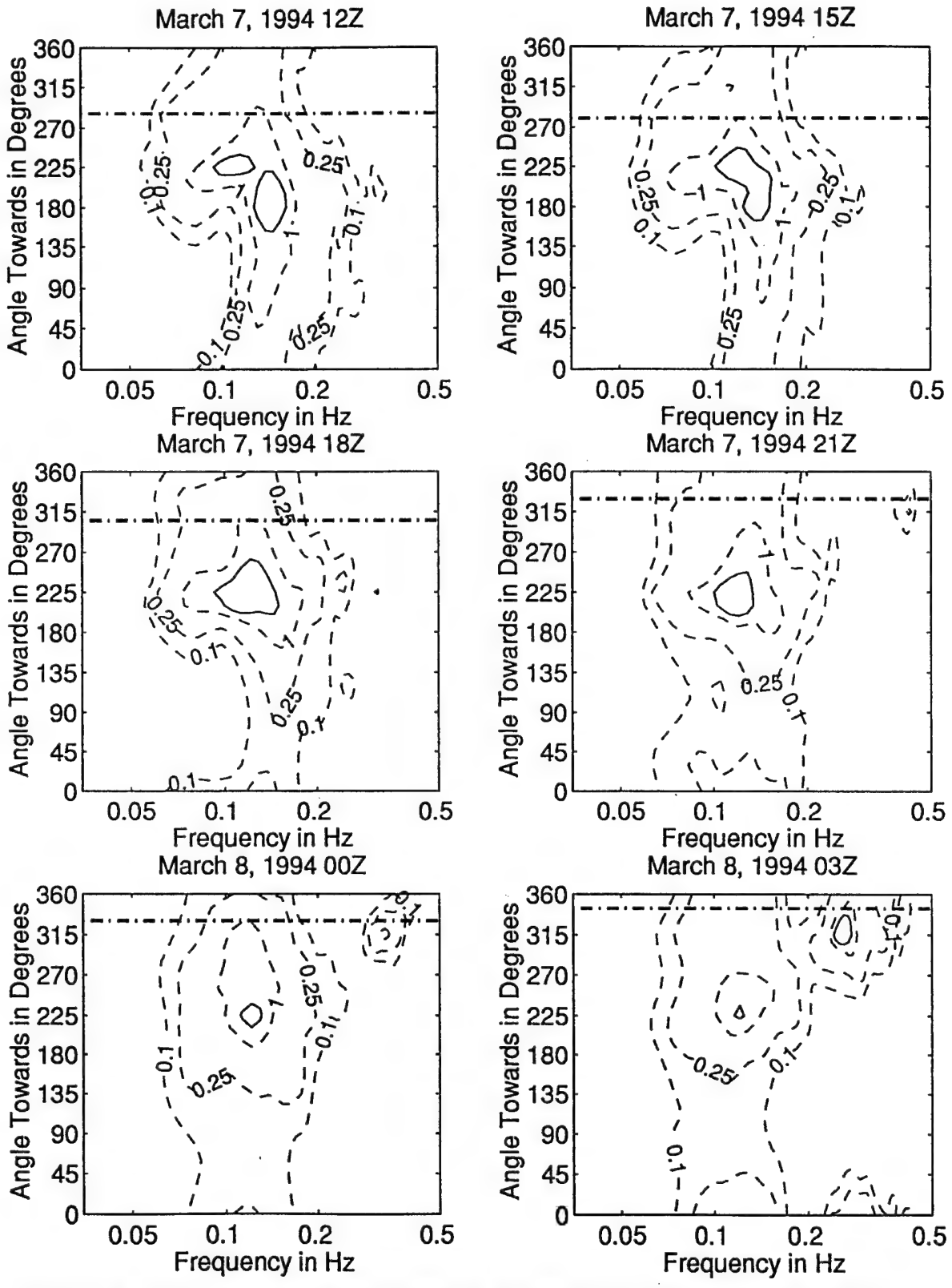

Figure 3.4.120: Directional wave spectra, computed using maximum entropy method. Contours of spectral density as a function of direction. Contours are 0.1, 0.25, 1 (dashed), 2.5, 10, 25, 100, and 250 (solid). Wind direction is shown by thick dashed line.

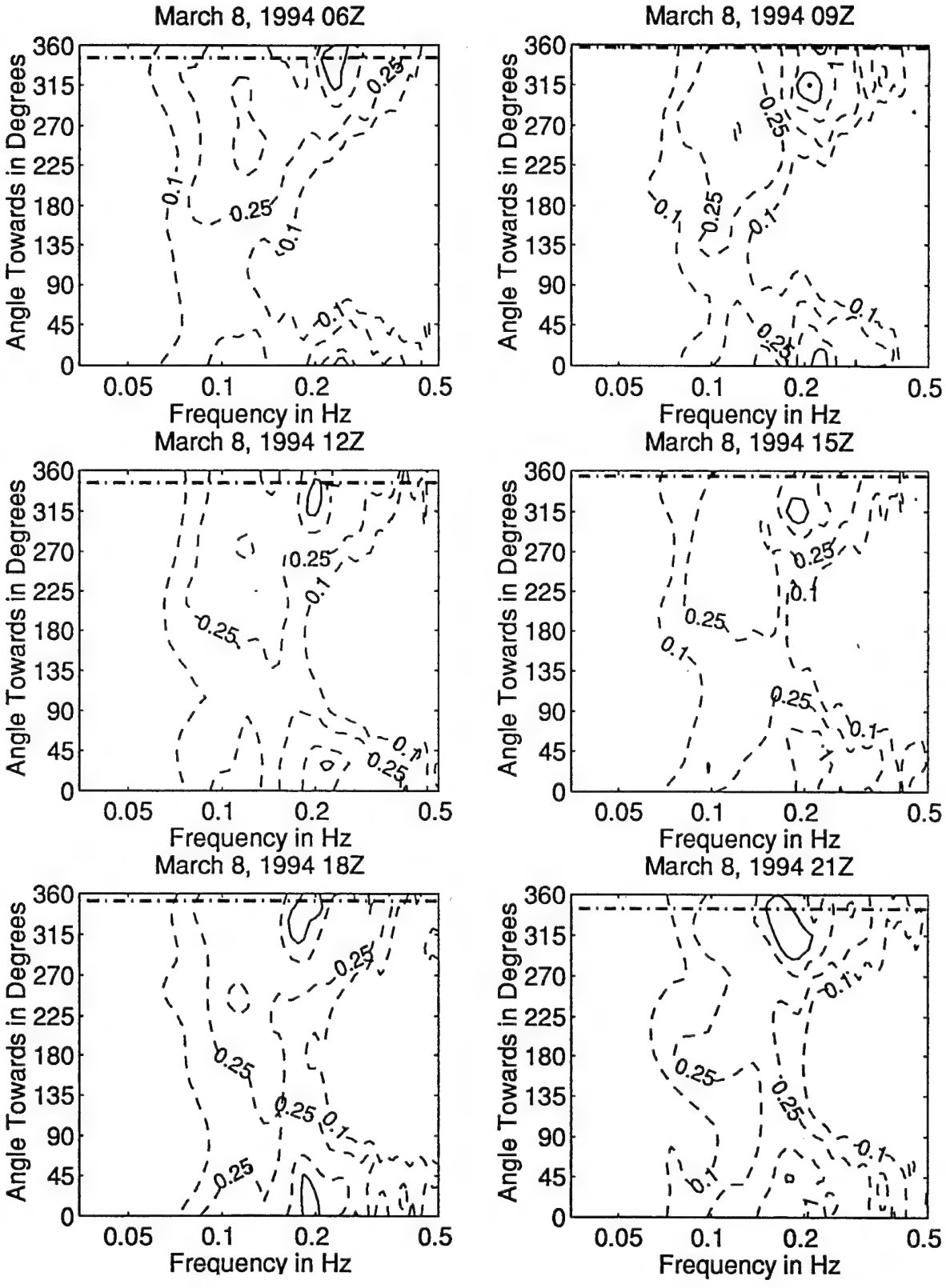

Figure 3.4.121: Directional wave spectra, computed using maximum entropy method. Contours of spectral density as a function of direction. Contours are 0.1, 0.25, 1 (dashed), 2.5, 10, 25, 100, and 250 (solid). Wind direction is shown by thick dashed line.

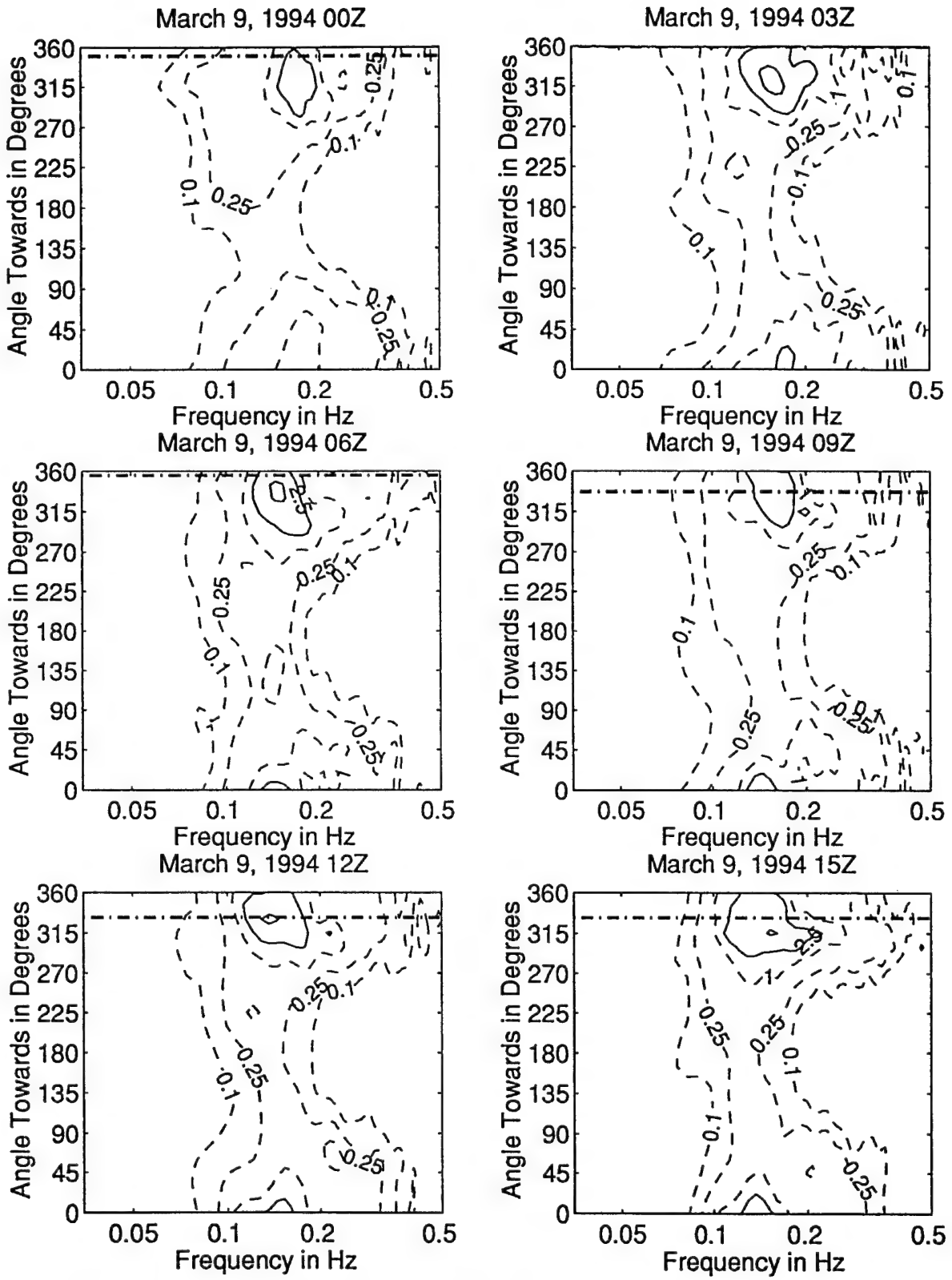

Figure 3.4.122: Directional wave spectra, computed using maximum entropy method. Contours of spectral density as a function of direction. Contours are 0.1, 0.25, 1 (dashed), 2.5, 10, 25, 100, and 250 (solid). Wind direction is shown by thick dashed line.

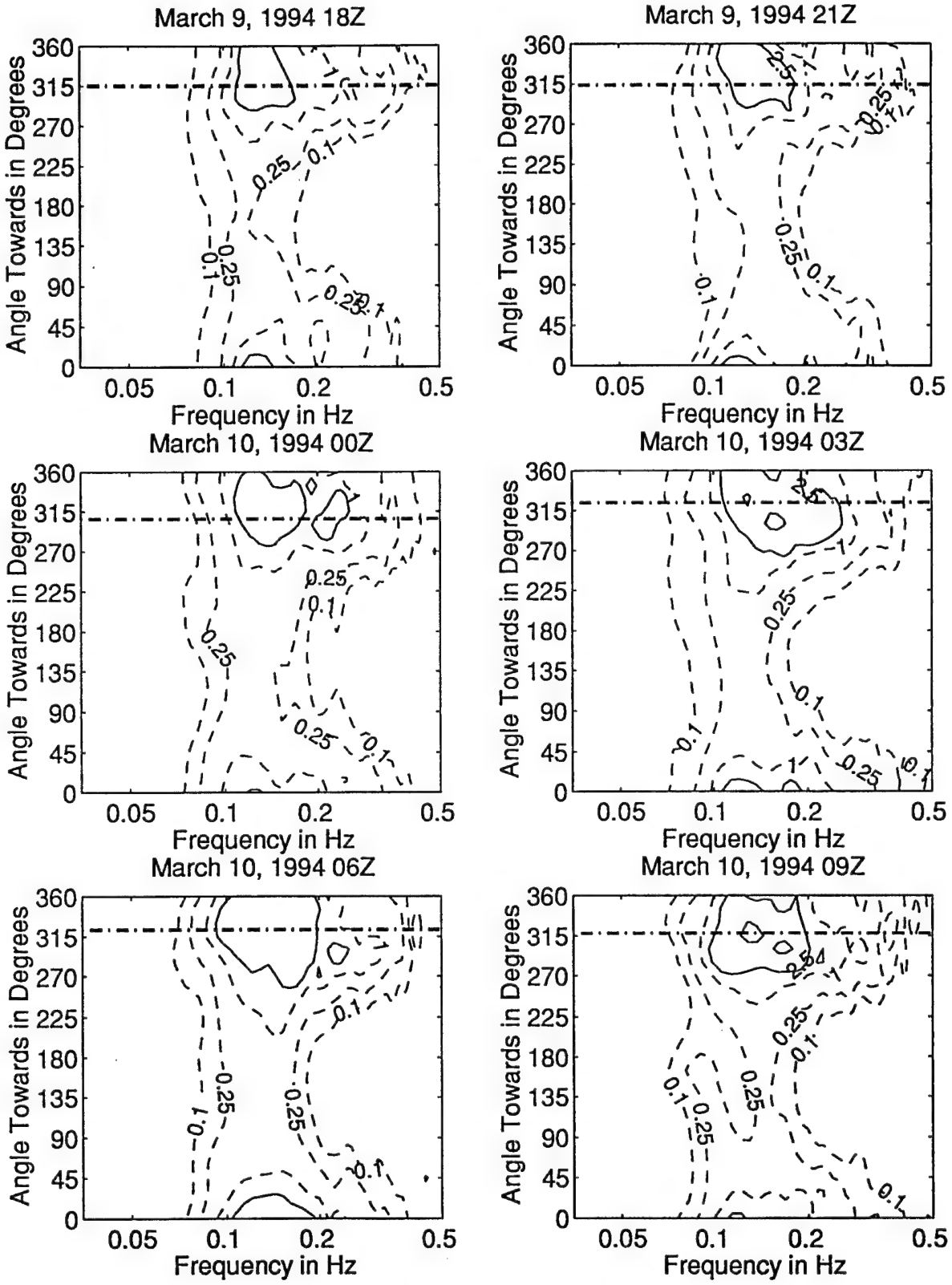

Figure 3.4.123: Directional wave spectra, computed using maximum entropy method. Contours of spectral density as a function of direction. Contours are 0.1, 0.25, 1 (dashed), 2.5, 10, 25, 100, and 250 (solid). Wind direction is shown by thick dashed line.

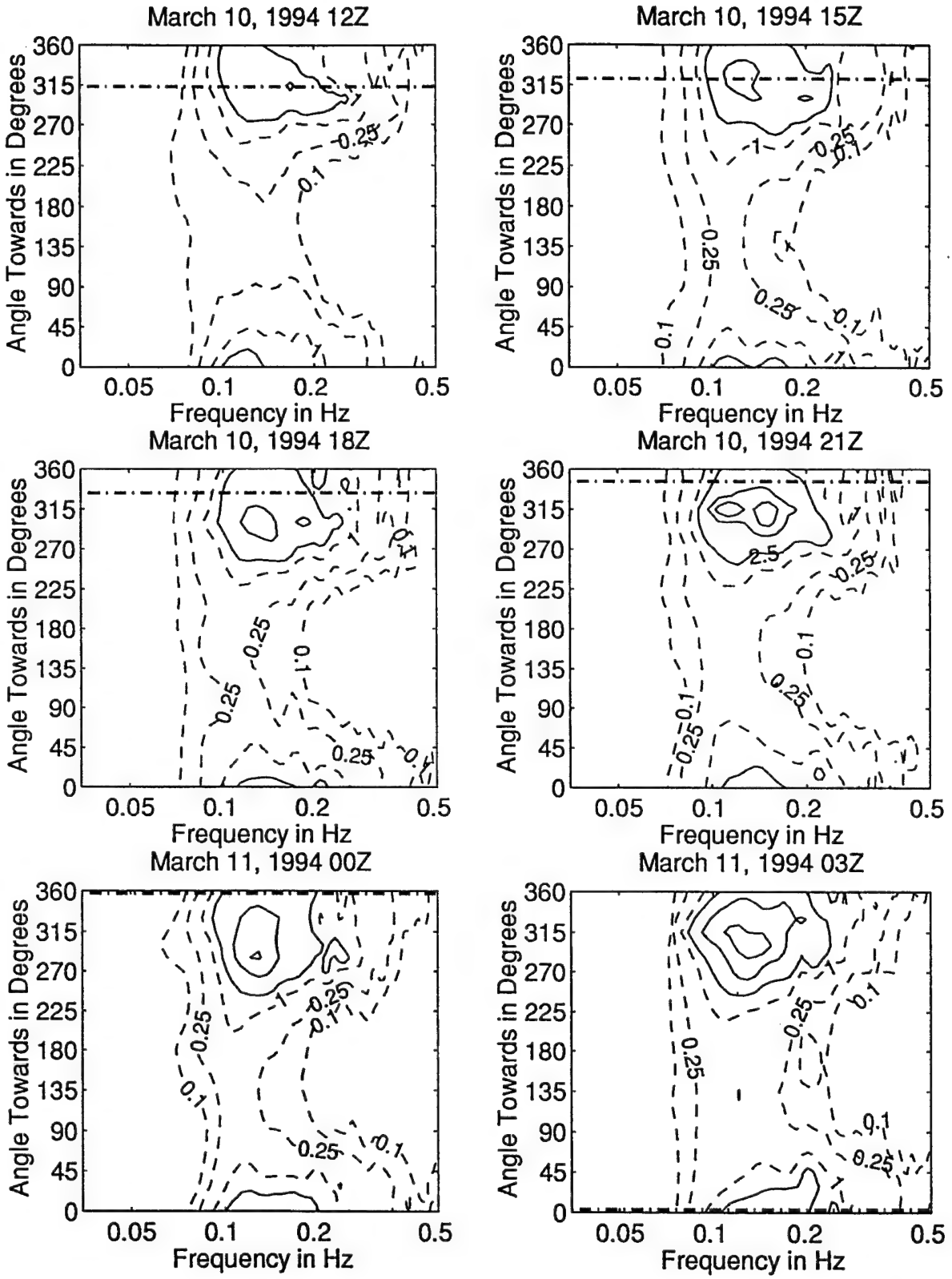

Figure 3.4.124: Directional wave spectra, computed using maximum entropy method. Contours of spectral density as a function of direction. Contours are 0.1, 0.25, 1 (dashed), 2.5, 10, 25, 100, and 250 (solid). Wind direction is shown by thick dashed line.

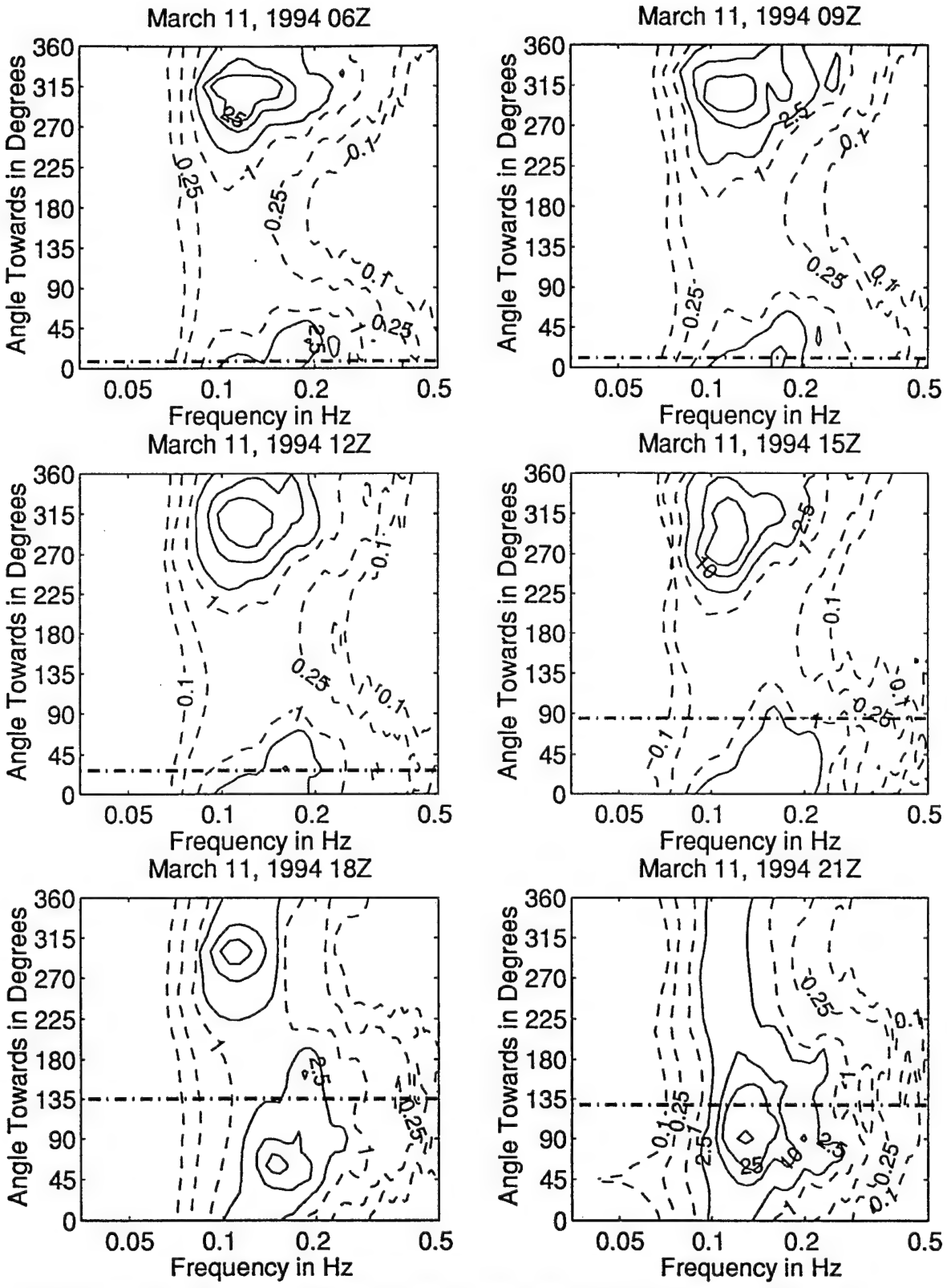

Figure 3.4.125: Directional wave spectra, computed using maximum entropy method. Contours of spectral density as a function of direction. Contours are 0.1, 0.25, 1 (dashed), 2.5, 10, 25, 100, and 250 (solid). Wind direction is shown by thick dashed line.

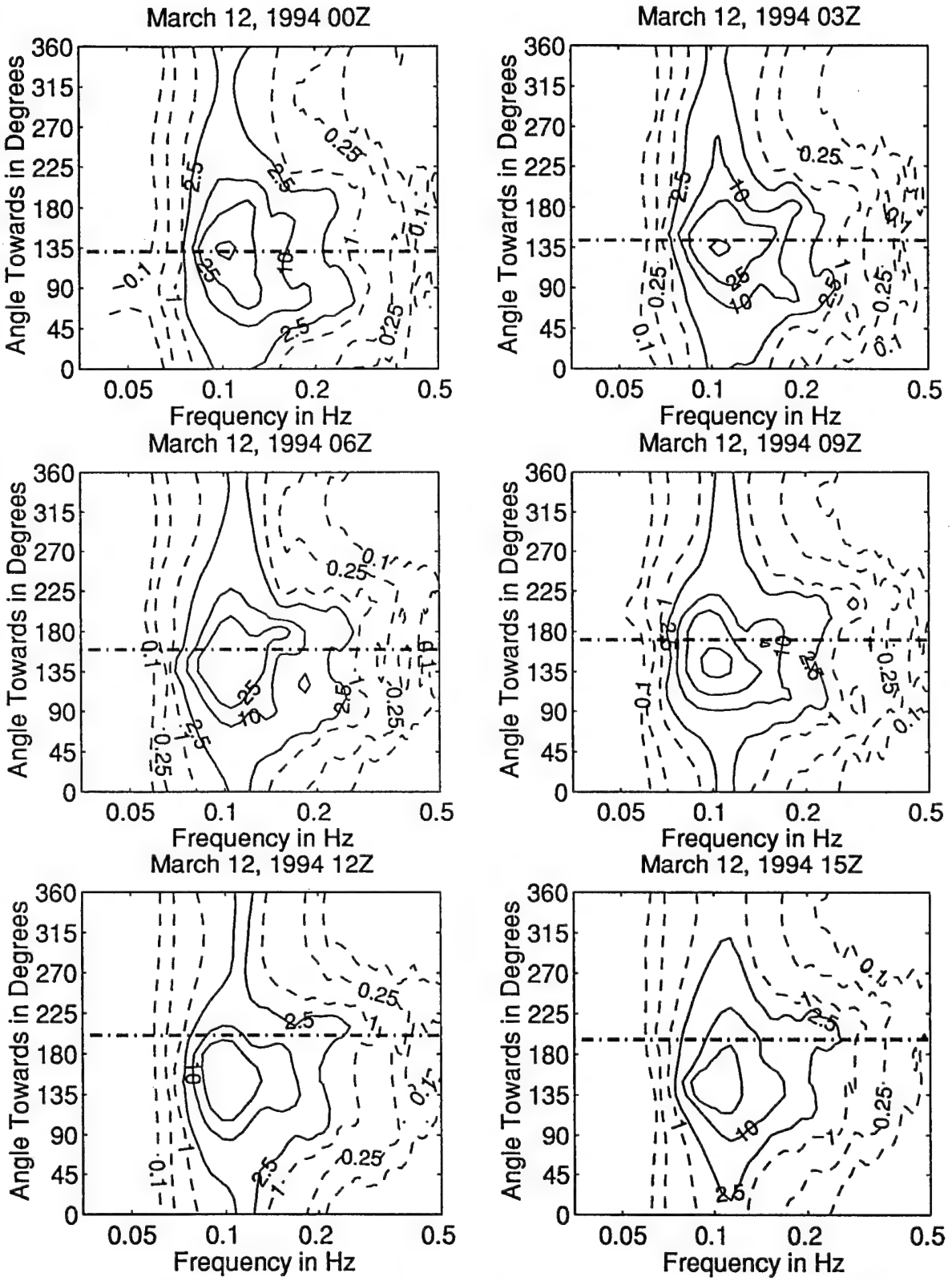

Figure 3.4.126: Directional wave spectra, computed using maximum entropy method. Contours of spectral density as a function of direction. Contours are 0.1, 0.25, 1 (dashed), 2.5, 10, 25, 100, and 250 (solid). Wind direction is shown by thick dashed line.

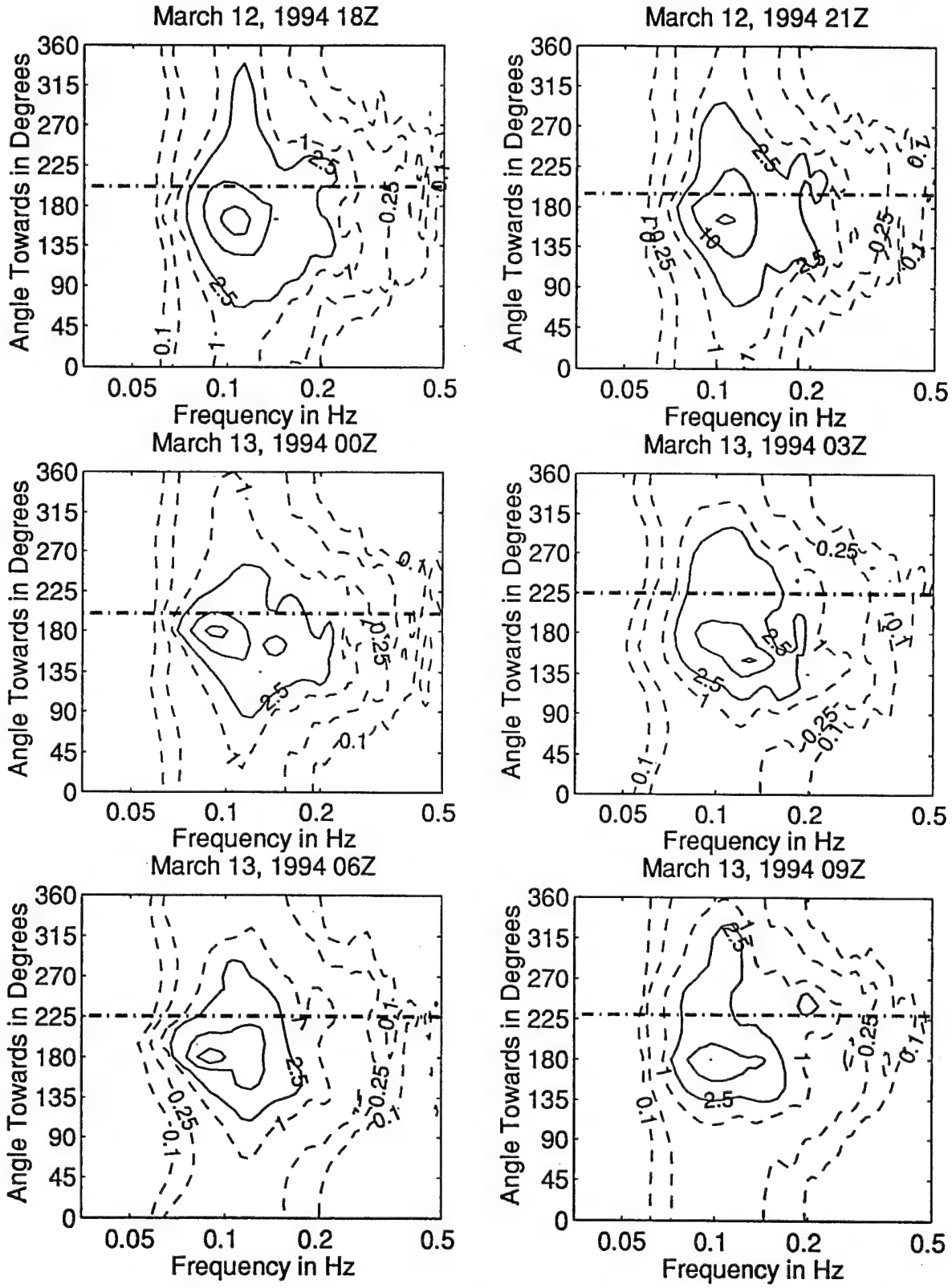

Figure 3.4.127: Directional wave spectra, computed using maximum entropy method. Contours of spectral density as a function of direction. Contours are 0.1, 0.25, 1 (dashed), 2.5, 10, 25, 100, and 250 (solid). Wind direction is shown by thick dashed line.

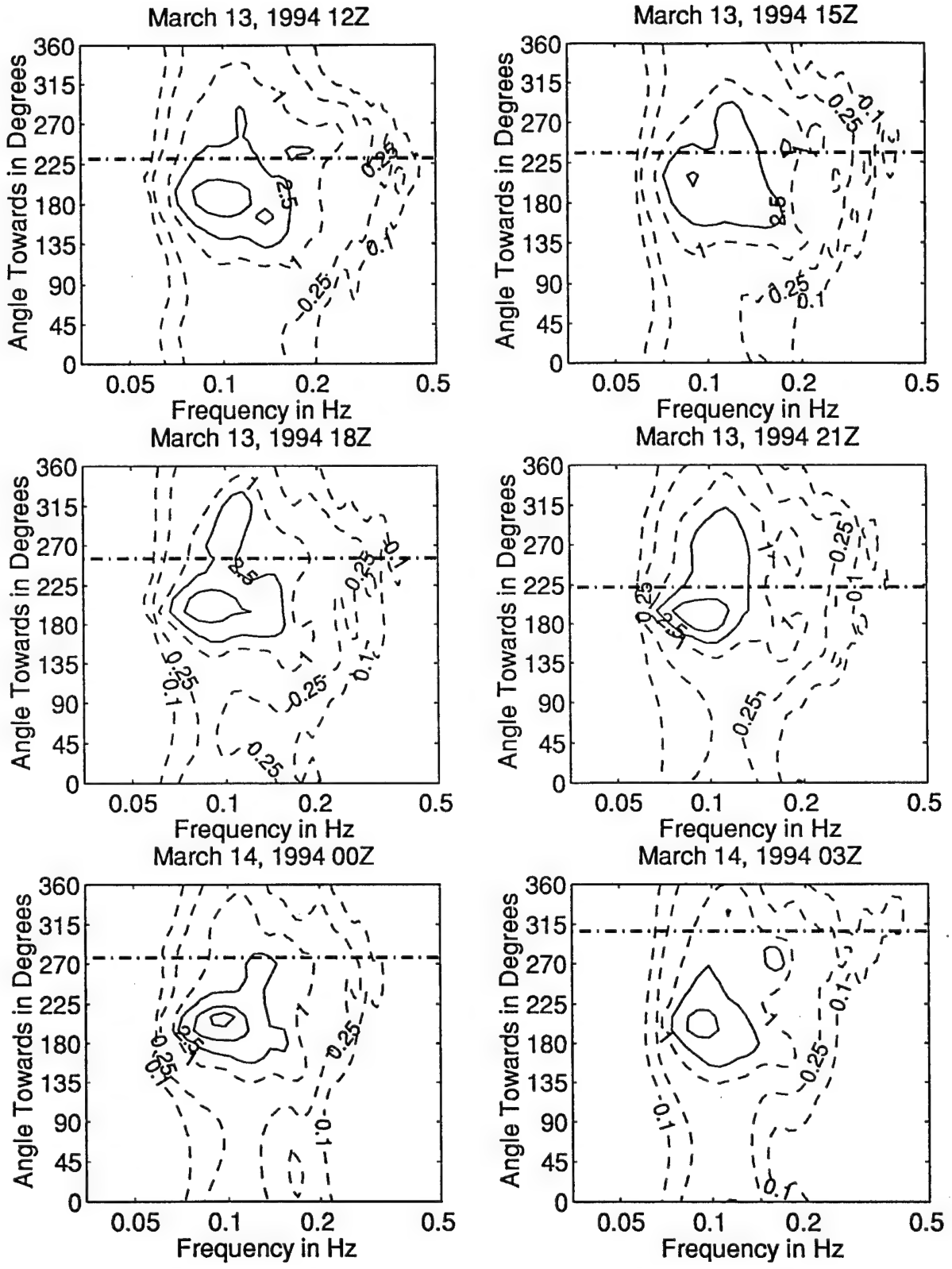

Figure 3.4.128: Directional wave spectra, computed using maximum entropy method. Contours of spectral density as a function of direction. Contours are 0.1, 0.25, 1 (dashed), 2.5, 10, 25, 100, and 250 (solid). Wind direction is shown by thick dashed line.

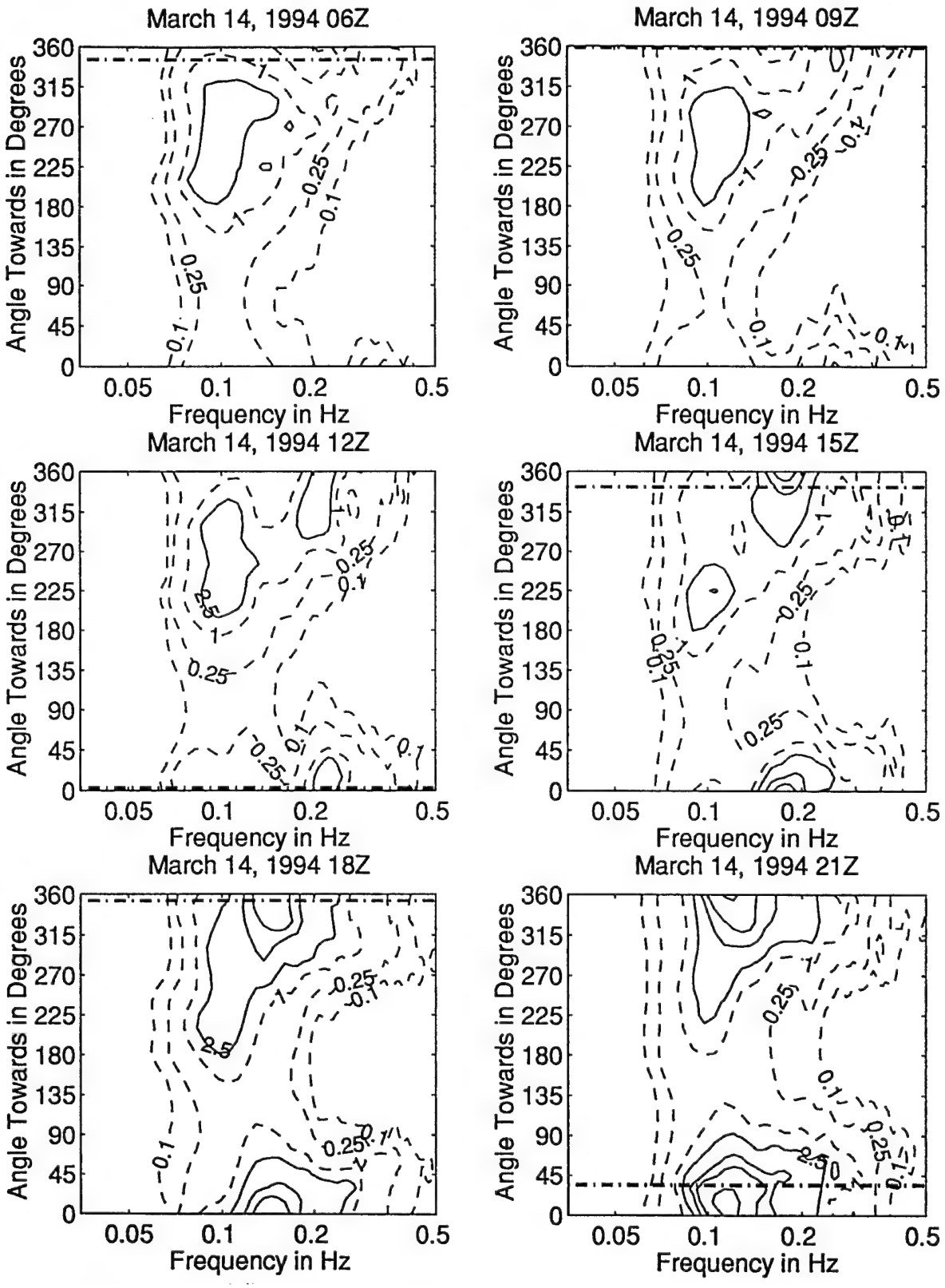

Figure 3.4.129: Directional wave spectra, computed using maximum entropy method. Contours of spectral density as a function of direction. Contours are 0.1, 0.25, 1 (dashed), 2.5, 10, 25, 100, and 250 (solid). Wind direction is shown by thick dashed line.

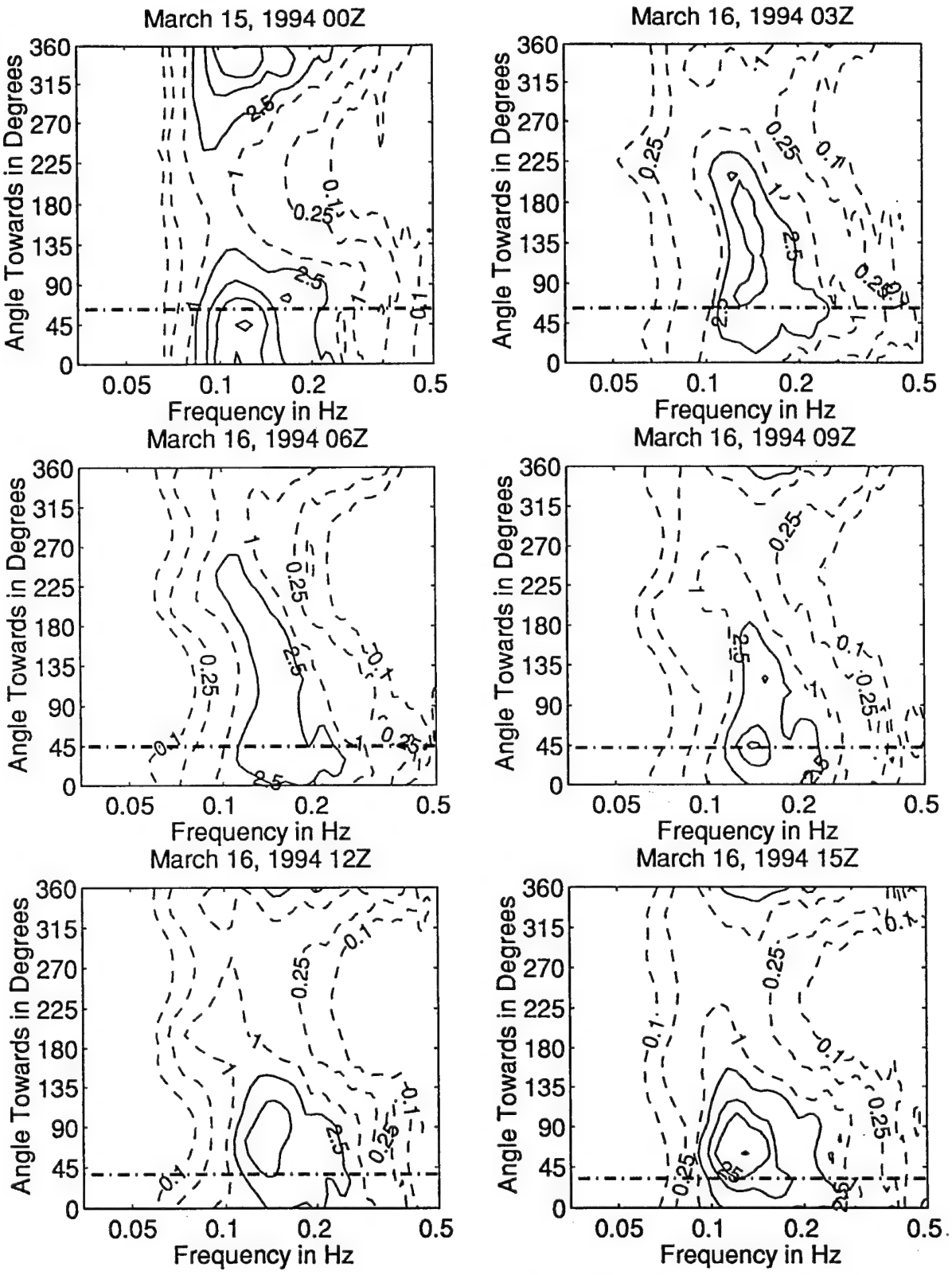

Figure 3.4.130: Directional wave spectra, computed using maximum entropy method. Contours of spectral density as a function of direction. Contours are 0.1, 0.25, 1 (dashed), 2.5, 10, 25, 100, and 250 (solid). Wind direction is shown by thick dashed line.

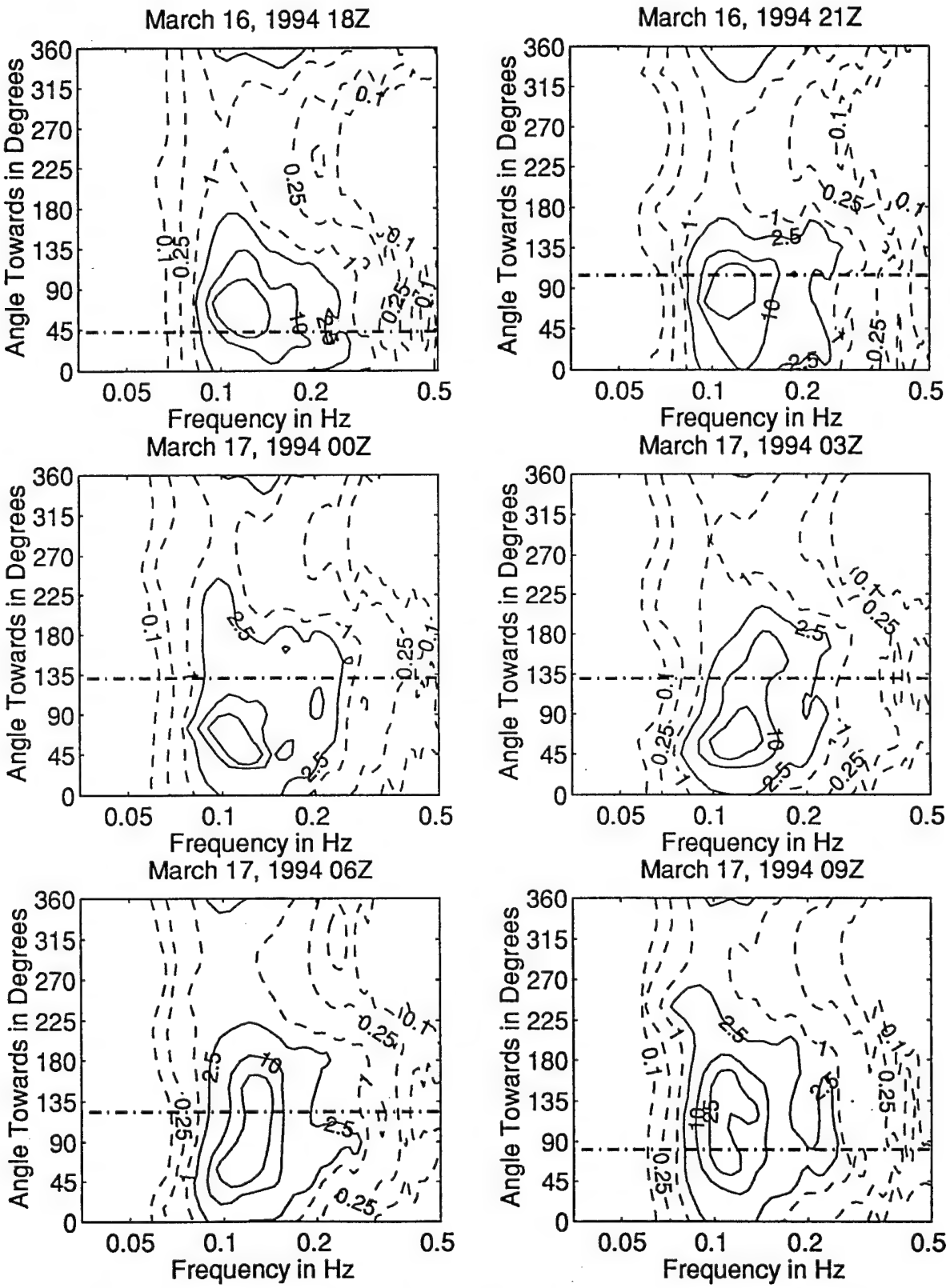

Figure 3.4.131: Directional wave spectra, computed using maximum entropy method. Contours of spectral density as a function of direction. Contours are 0.1, 0.25, 1 (dashed), 2.5, 10, 25, 100, and 250 (solid). Wind direction is shown by thick dashed line.

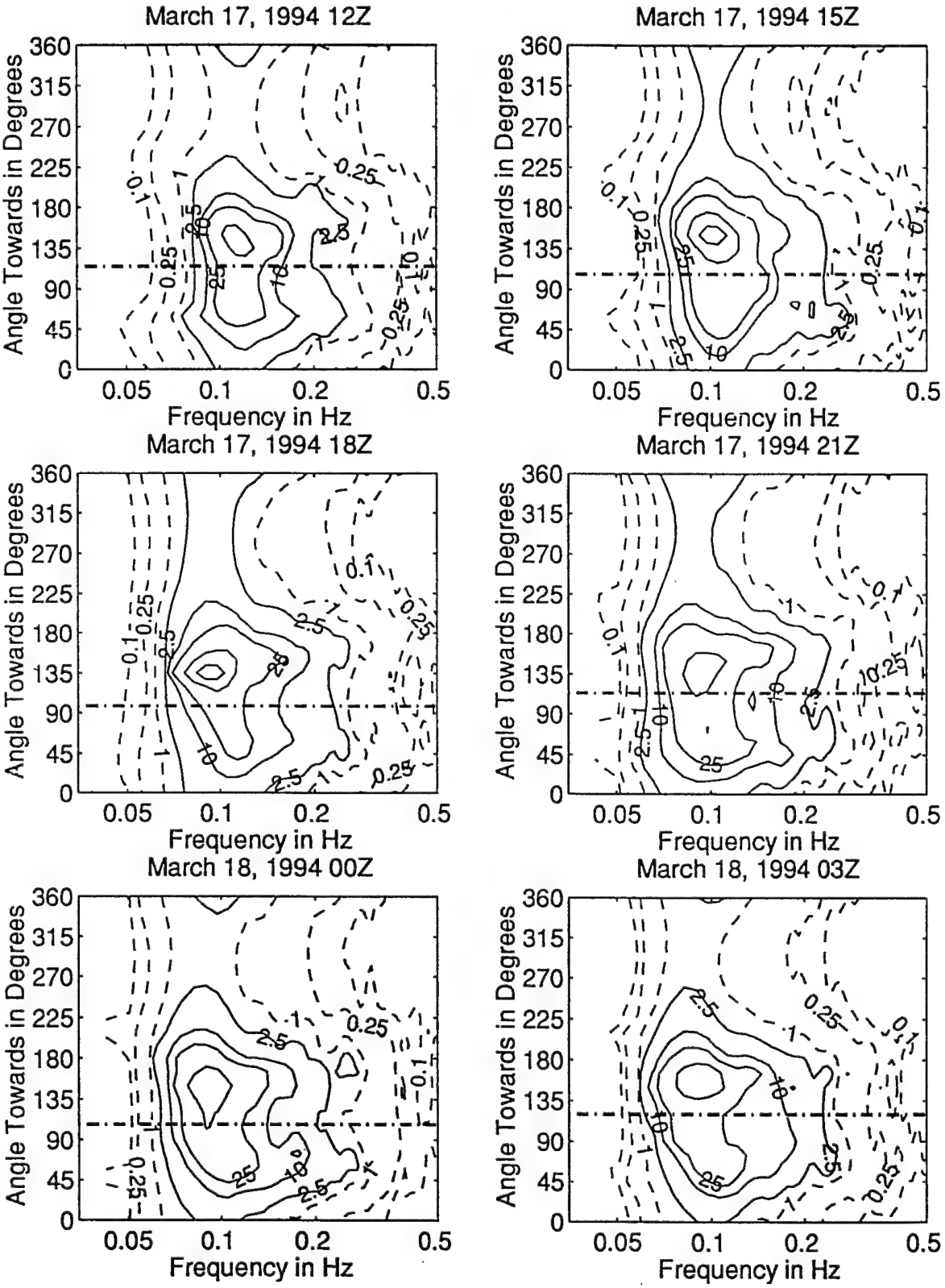

Figure 3.4.132: Directional wave spectra, computed using maximum entropy method. Contours of spectral density as a function of direction. Contours are 0.1, 0.25, 1 (dashed), 2.5, 10, 25, 100, and 250 (solid). Wind direction is shown by thick dashed line.

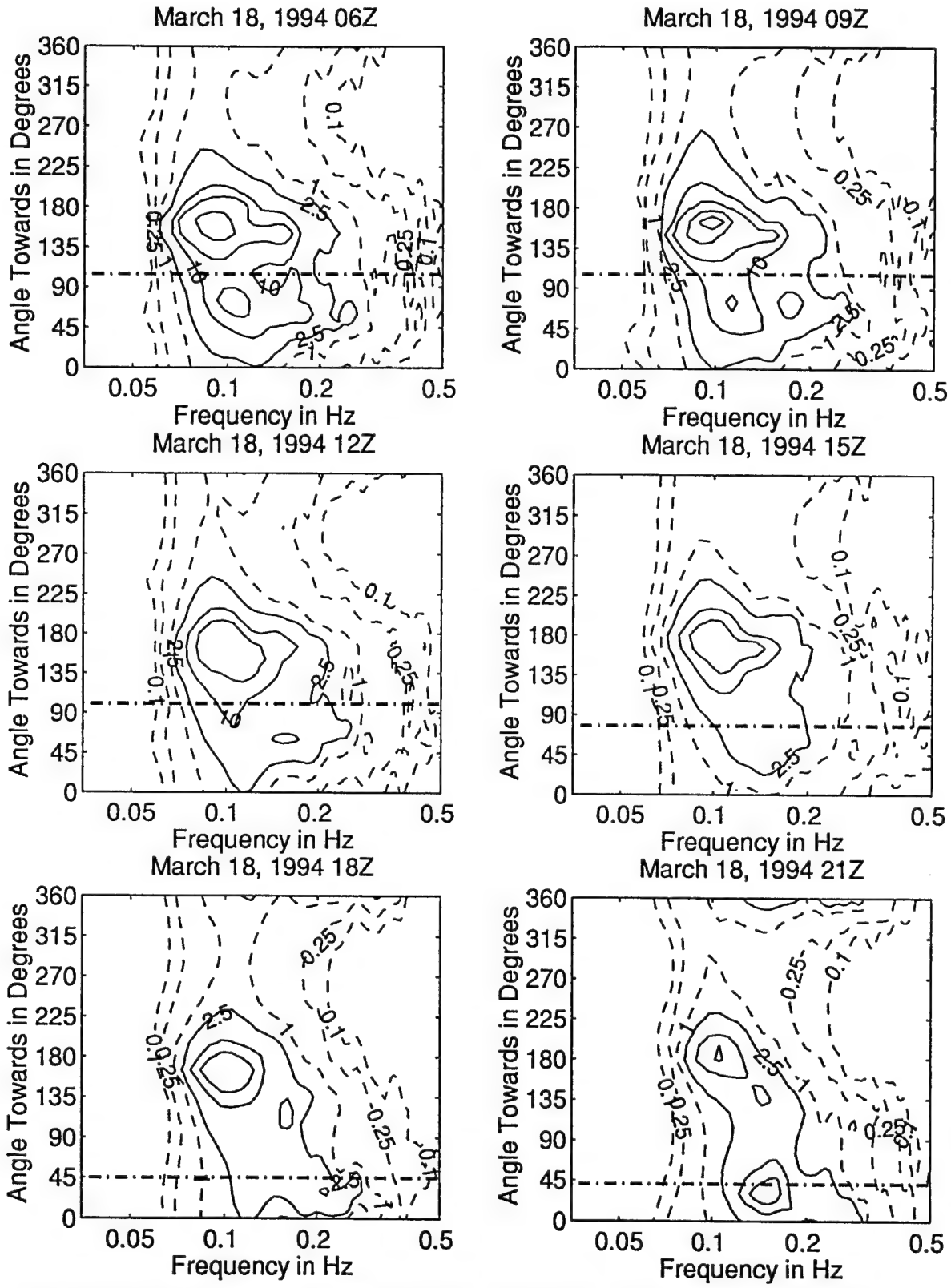

Figure 3.4.133: Directional wave spectra, computed using maximum entropy method. Contours of spectral density as a function of direction. Contours are 0.1, 0.25, 1 (dashed), 2.5, 10, 25, 100, and 250 (solid). Wind direction is shown by thick dashed line.

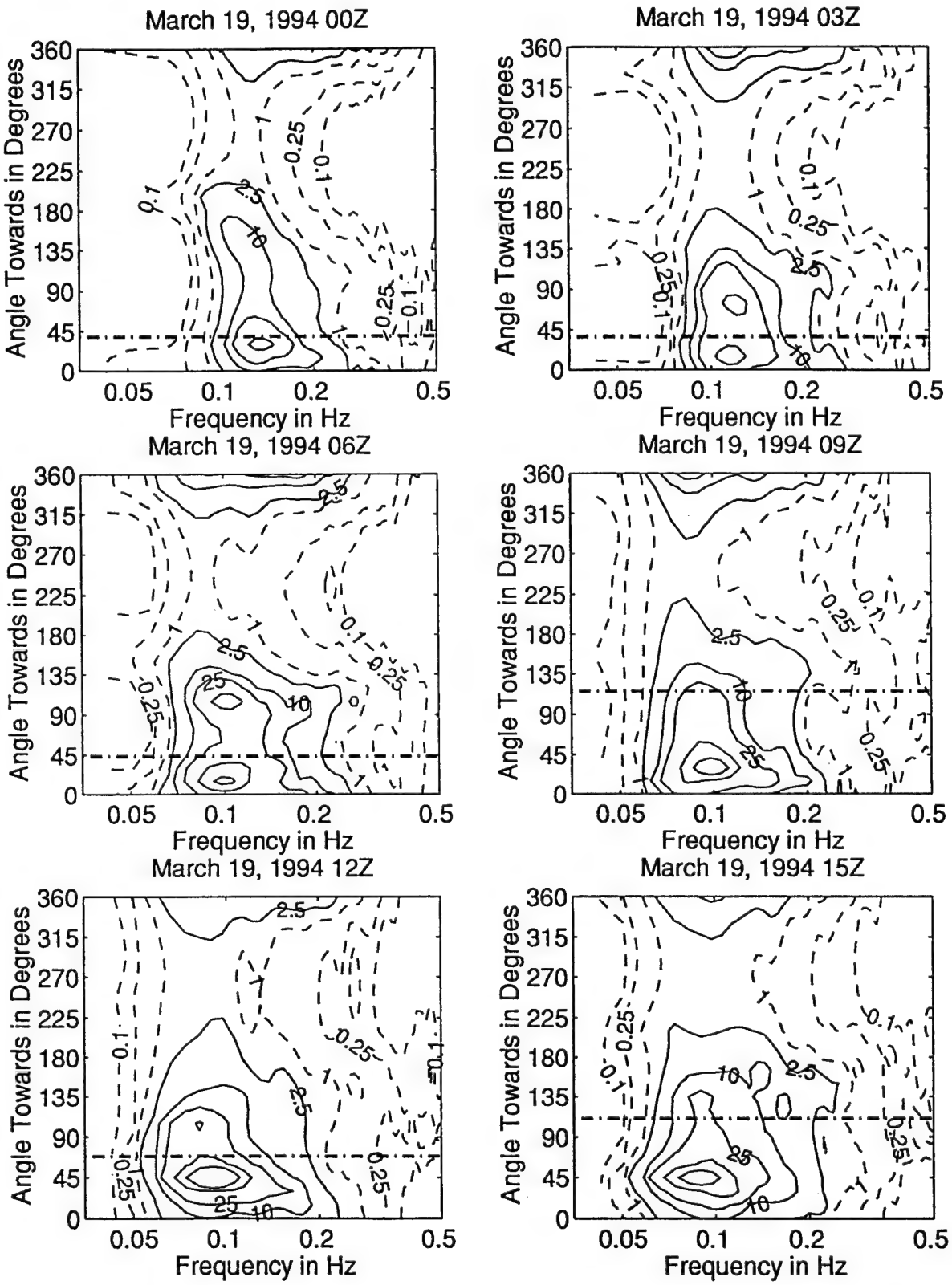

Figure 3.4.134: Directional wave spectra, computed using maximum entropy method. Contours of spectral density as a function of direction. Contours are 0.1, 0.25, 1 (dashed), 2.5, 10, 25, 100, and 250 (solid). Wind direction is shown by thick dashed line.

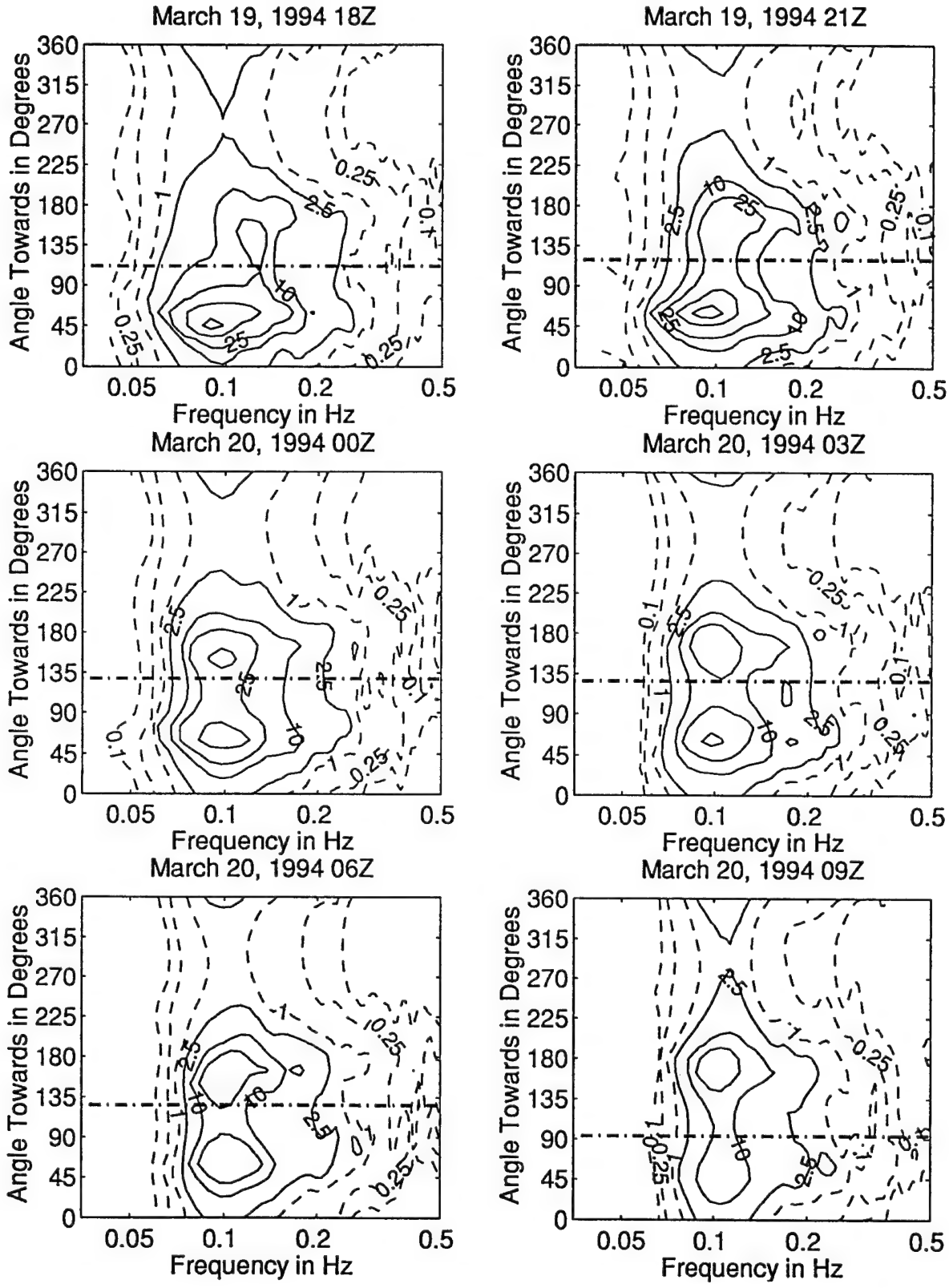

Figure 3.4.135: Directional wave spectra, computed using maximum entropy method. Contours of spectral density as a function of direction. Contours are 0.1, 0.25, 1 (dashed), 2.5, 10, 25, 100, and 250 (solid). Wind direction is shown by thick dashed line.

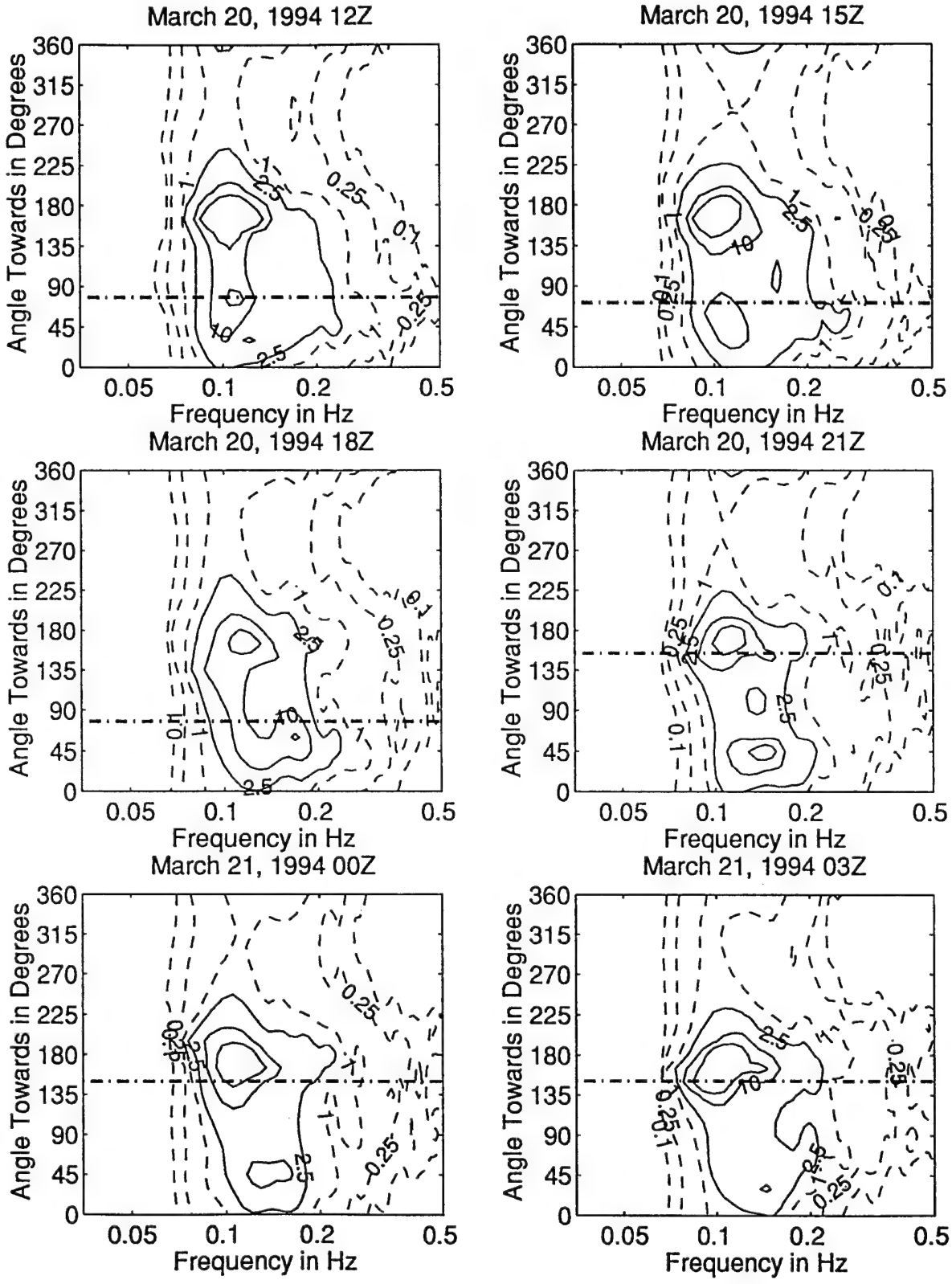

Figure 3.4.136: Directional wave spectra, computed using maximum entropy method. Contours of spectral density as a function of direction. Contours are 0.1, 0.25, 1 (dashed), 2.5, 10, 25, 100, and 250 (solid). Wind direction is shown by thick dashed line.

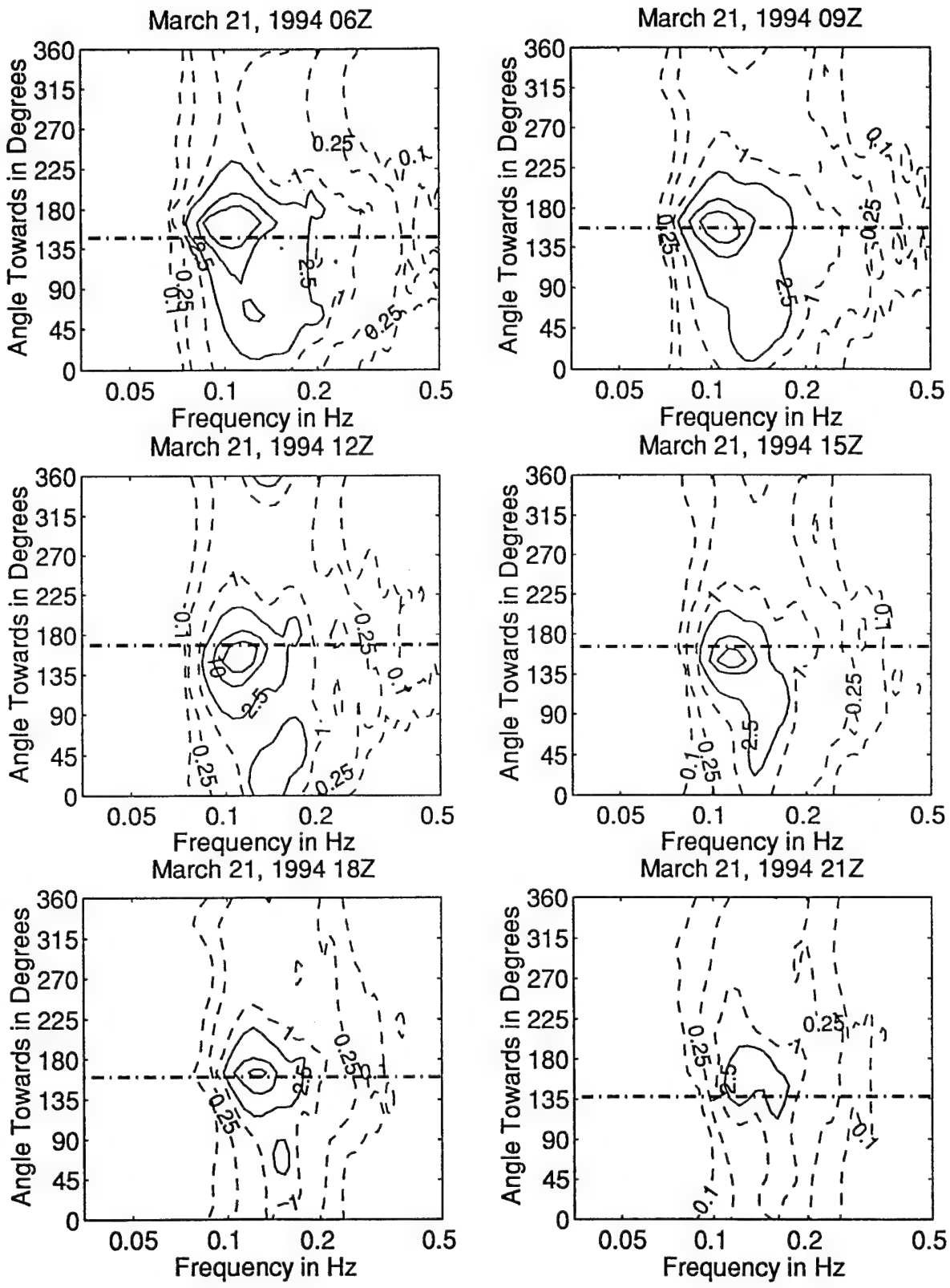

Figure 3.4.137: Directional wave spectra, computed using maximum entropy method. Contours of spectral density as a function of direction. Contours are 0.1, 0.25, 1 (dashed), 2.5, 10, 25, 100, and 250 (solid). Wind direction is shown by thick dashed line.

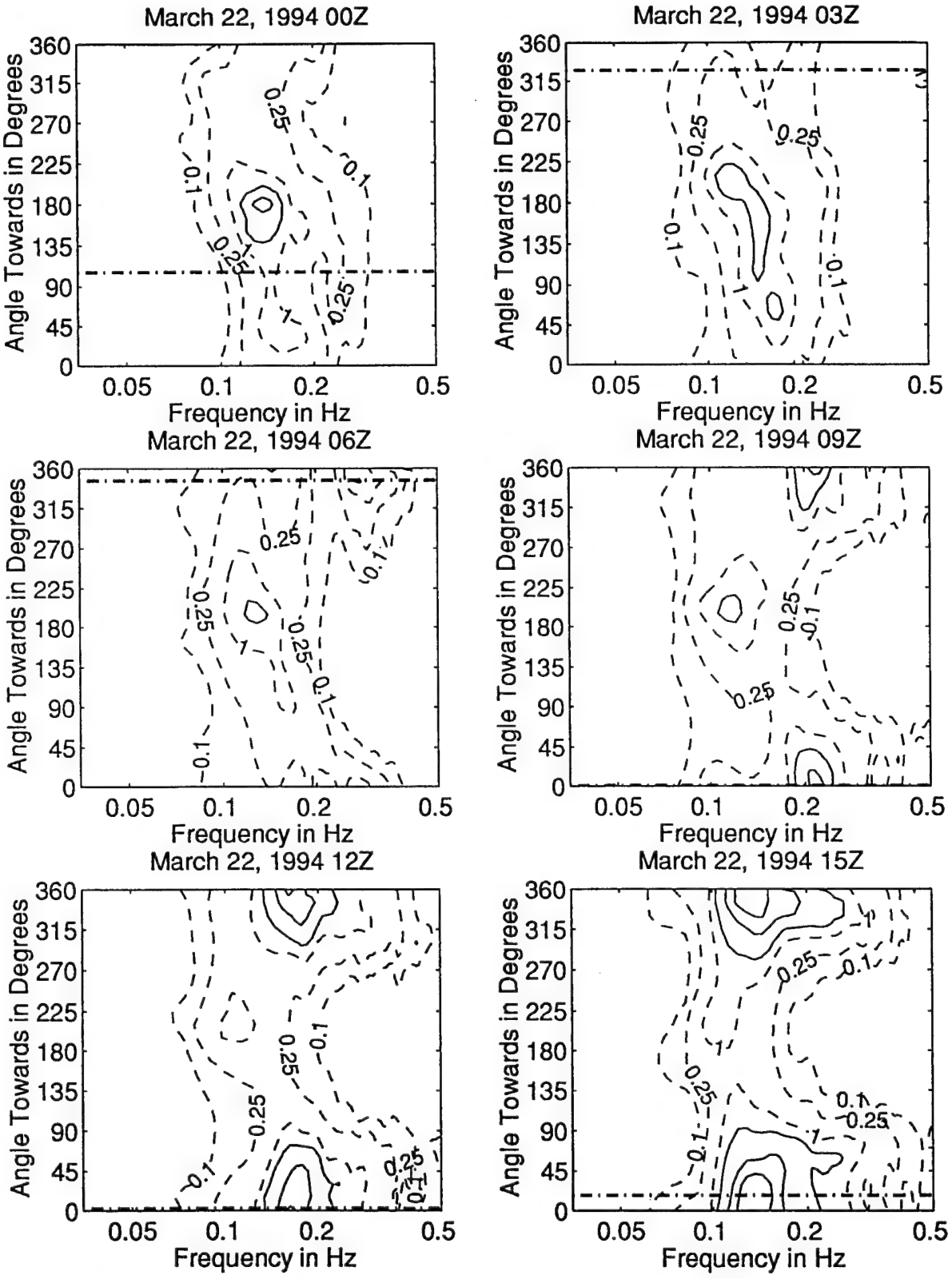

Figure 3.4.138: Directional wave spectra, computed using maximum entropy method. Contours of spectral density as a function of direction. Contours are 0.1, 0.25, 1 (dashed), 2.5, 10, 25, 100, and 250 (solid). Wind direction is shown by thick dashed line.

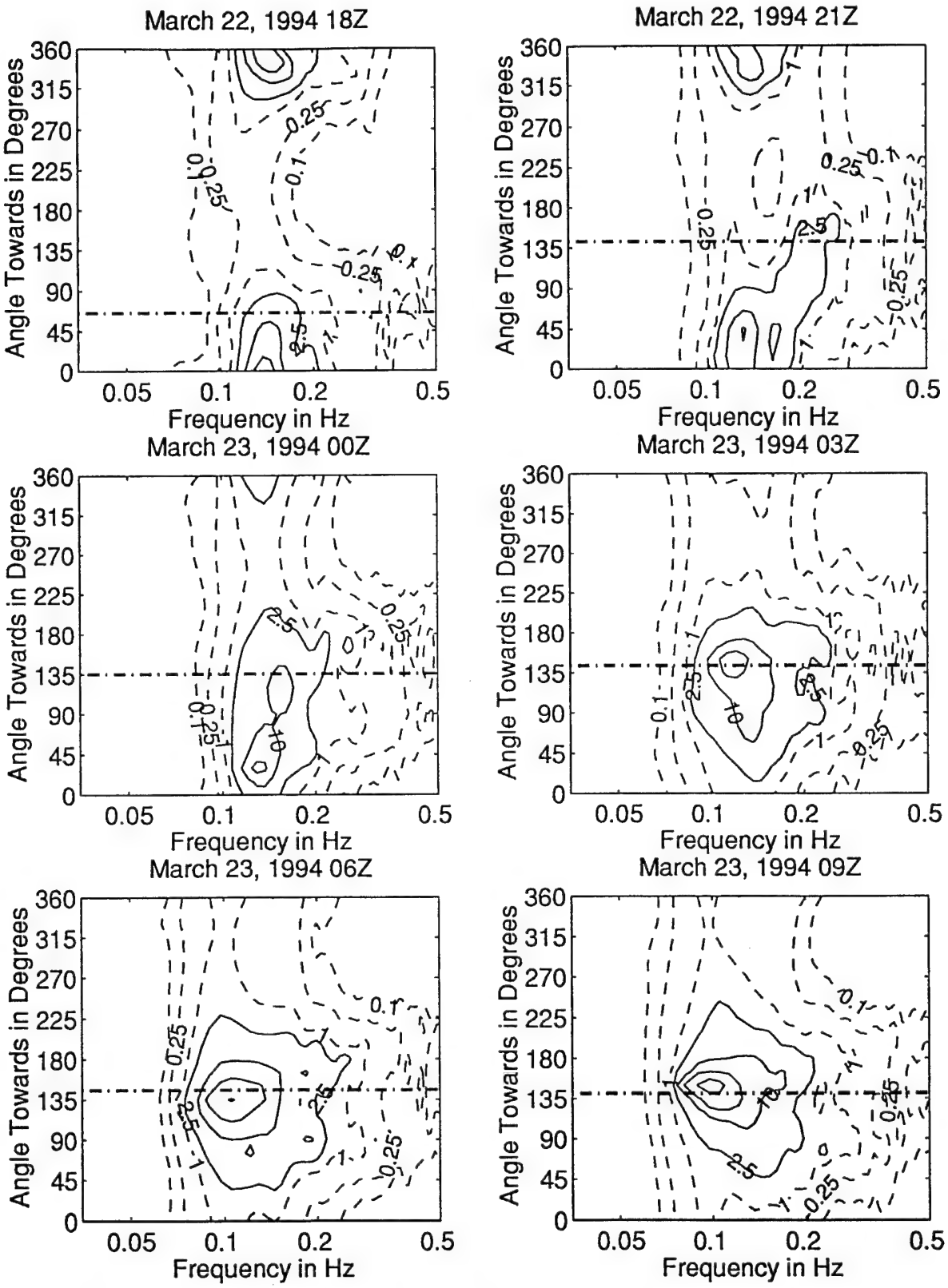

Figure 3.4.139: Directional wave spectra, computed using maximum entropy method. Contours of spectral density as a function of direction. Contours are 0.1, 0.25, 1 (dashed), 2.5, 10, 25, 100, and 250 (solid). Wind direction is shown by thick dashed line.

Appendix 1: Cruise Participants

Deployment Cruise

J. Bouthelette		WHOI
H. DeFerrari	(Chief Scientist)	Miami
T. Gidwitz		WHOI
A. Gnanadesikan		WHOI
S. Hill		IOS
R. Horn		SIO
J. Kemp		WHOI
W. Melville		SIO
M. Rebozo		Miami
W. Saunders		Miami
R. Shear		SIO
E. Terrill		SIO
G. Tupper		WHOI
N. Williams		Miami
B. Way		WHOI

Recovery Cruise

J. Bouthellette		WHOI
A. Gnanadesikan		WHOI
S. Hill		IOS
J. Kemp	(Chief Scientist)	WHOI
M. Rebozo		Miami
E. Terrill		SIO
B. Way		WHOI

Appendix 2: Cruise Chronology

Deployment	Cruise	
8 Dec 93	1800	Leave Dock aboard R/V Knorr.
9 Dec 93	1500	Science meeting.
	1900-2200	Release Testing.
10 Dec 93	1100	Clearing deck for SIO Spar. (WHOI Station No. 957)
	1305	Surface Line in water
	1457	Subsurface Line in water
	2041	Anchor Splash. 33 56.509 N 70 06.426 W PDR Depth 5375m. Steaming up to surface float.
	2150	Surface buoy in water.
	2249	Beginning anchor survey, transducer in water. Wind increasing.
	2358	Finish anchor survey. Anchor at 33 56.62 N 70 06.34W.
11 Dec 93		Hove to. Estimate winds at 30 knots, seas 8-12 ft.
12 Dec 93		Hove to. Estimate winds at 30-40 knots, seas 14 ft.
	1525	Barometric pressure survey within ship shows 1 mb difference between main lab and bridge.
13 Dec 93	1150	Preparing to launch Seatex (WHOI Moored Station 958). Waves still high (15 ft) but wind has dropped.
	1508	Buoy over side. Deploying mooring.
	2216	Anchor splash. 34 03.944N 70 05.425W. PDR Reading 5374m.
	2259	Release on bottom. Beginning survey.
14 Dec 93	0009	Finished survey. Anchor position 34 03.89N 70 05.10W.
	1035	Checking out IMET package.
	1130	Starting Echosounder. System comes up, indicates that it is entering keyboard mode, then fails to do so.

	1445	Begin Discus deployment (WHOI Moored Station 959).
	1727	While changing spools, winch cycles unexpectedly causing us lose end over the side. Begin to recover mooring so as to reset.
	2200	Beginning redeployment of discus.
15 Dec 93	0002	More problems with Lebus winch. Jumps at low speeds.
	0613	Anchor splash, discus mooring 33 52.69N 69 44.97W. PDR Depth 5375m.
	0630	Beginning anchor survey.
	0800	Anchor survey complete 33 52.7N 69 44.83W.
	1400	Miami Acoustics Mooring going over the side.
	1505	Because of 8 foot swells, predictions of increasing swell, and general fatigue, decide to abort Miami Acoustics mooring deployment
16 Dec 93		Hove to. Winds ~35 knots, gusting to 50, seas 18-22 ft.
17 Dec 93		Hove to. Winds ~30 knots. Seas 18-24 ft. (Seatex sees a 39 ft wave on this day).
18 Dec 93	1100	Preparing to launch Miami Acoustics mooring (WHOI Moored Station 960).
	1250	ELSI A over side.
	1321	Source over side.
	2140	Anchor splash, Miami Acoustics mooring 33 59.41N 70 00.13 W. PDR Depth 5372.
	2350	Preparing to deploy ELSI B mooring (WHOI Moored Station 961).
19 Dec 93	0200	Miami Acoustics Mooring comes up on sonabuoy.
	0631	Anchor splash, ELSI B.
	0713	Anchor on bottom. Beginning anchor survey.
	0815	Anchor survey complete 33 54.52N 69 56.20W. Beginning anchor survey for Miami Acoustics Mooring.
	0935	Anchor survey complete. 33 59.05N 70 00.25W. Leaving Site L for Jacksonville, FL.
20 Dec 93		In transit.

21 Dec 93	1600	Arrive Jacksonville, FL.

Moorings at Sea

22 Jan 94		Argos Telemetry lost from SIO Spar as a result of low battery power.
22 Feb 94		New beacon attached to SIO Spar by J. Cotter aboard R/V *Knorr* en route to Barbados.

Recovery Cruise

18 Mar 94	1752	Leave Harbor Branch Oceanographic Inst. aboard R/V *Edwin Link.*
19 Mar 94		Transit
20 Mar 94		Transit
21 Mar 94	1030	Passing SIO Spar. No floats on the surface.
	1148	Taking water samples for O2 concentration.
	1246	Fired ELSI Release on Miami mooring.
	1300	ELSI A aboard.
	1416	Fired release on Miami Acoustics mooring.
	2100	Mooring on deck. Unspooling winch.
22 Mar 94	0200	Finished unspooling winch.
	1100	In sight of Discus. Decide that weather is a little rough (winds about 20 knots) and that we will proceed to ELSI.
	1234	ELSI upper release fired.
	1330	ELSI B aboard after multiple attempts.
	1400	ELSI upper portion recovered. Decide to stop until weather improves.
	1900	Decide to recover bottom of ELSI mooring.
	1933	Release fired.
	2242	Acoustic release aboard.
	2342	Start unspooling and stowing gear.
23 Mar 94	0300	Finished unspooling.

	1100	At discus, weather too rough to recover. Proceeding to Seatex.
	1324	Seatex release fired.
	1357	Cutting surface tether loose.
	1416	Seatex on board. Surface tether has lost most of its floats including polyform sphere. Only 11 of 45 floats remaining. Heavy fouling on buoy. Light damaged on recovery.
	1723	Recovering acoustic release.
	1800-1900	Moving spheres and ELSI to 01 deck.
	2015	By discus, taking intensive observations.
24 Mar 94	1143	Fired release on discus.
	1215	Discus aboard. Pins on Seacat 927 bent badly on recovery.
	1545	Stop to unspool line off winch.
	1729-1808	Bagged VAWR SW sensor.
	1749-1815	Cold bath spike on T-Pods, Seacats.
	1802	Resume spooling line onto winch.
	1912	Acoustic Release aboard. Streaming to SIO Spar.
	2213	Fired release on SIO Spar.
	2330	SIO Spar aboard. Recovering mooring.
25 Mar 94	0345	Acoustic release aboard. Depart for Woods Hole.
26 Mar 94		Transit to Woods Hole
27 Mar 94	0100	Arrive Woods Hole.

Appendix 3: ASREX Antifouling Paint Test

A.3.1: Introduction

The Upper Ocean Processes Group for the past 4 years has used Ameron #635 tributyltin paint for the prevention of bio-fouling on aluminum discus hulls and underwater instrument housing. This antifouling paint has proven to work well in preventing fouling in very temperate waters for up to 6 months immersion. The active antifoulant ingredient, tributyltin, is a state-regulated hazardous material, making it undesirable as well as legally difficult to use for oceanographic applications. The purpose of this test was to find an alternative coating that is as effective and which can be used with less environmental impact.

The ASREX discus surface mooring paint test consisted of a comparison between 3 types of antifouling paint and 1 silicon-based coating applied to several mooring components in the upper 100 meters of the discus mooring. The 3 antifoulant paints tested were Ameron #279 (black), #536 (blue) and Interlux Tri-Lux II (red). The clear silicon polymer tested was Kiss-Cote.

A.3.2: Test samples and coatings

Ameron #279 (black) is a chorinated polymeric antifouling paint suitable for steel. It is a cuprous oxide release ablative. The following mooring components were coated 9 mils dry film thickness.

1. All VMCM fans.
2. Discus bridle legs and discus bridle clamps (Figure A.3.1)

Ameron #635 (blue) is a tributyltin release ablative antifouling suitable for aluminum. The following mooring components were painted with a 9 mils dry film thickness:

1. Approximately 50% underwater surface area of the discus hull bottom (Figure A.3.2)
2. Eight VMCM stings.
3. Upper 11" of the 5 m and 10 m VMCM instrument cases (Figure A.3.3)

Interlux Tri-Lux II is a copper thiocyantate copolymer antifoulant designed to be applied over aluminum. The following mooring components were coated up to 9 mils dry film thickness:

1. Approximately 50% of the underwater surface area of the discus hull bottom (Figure A.3.2).
2. The stainless steel VAWR SST flex tubing.
3. The bottom 11" of the 5 m and 10 m VMCM instrument cases (Figure A.3.3).

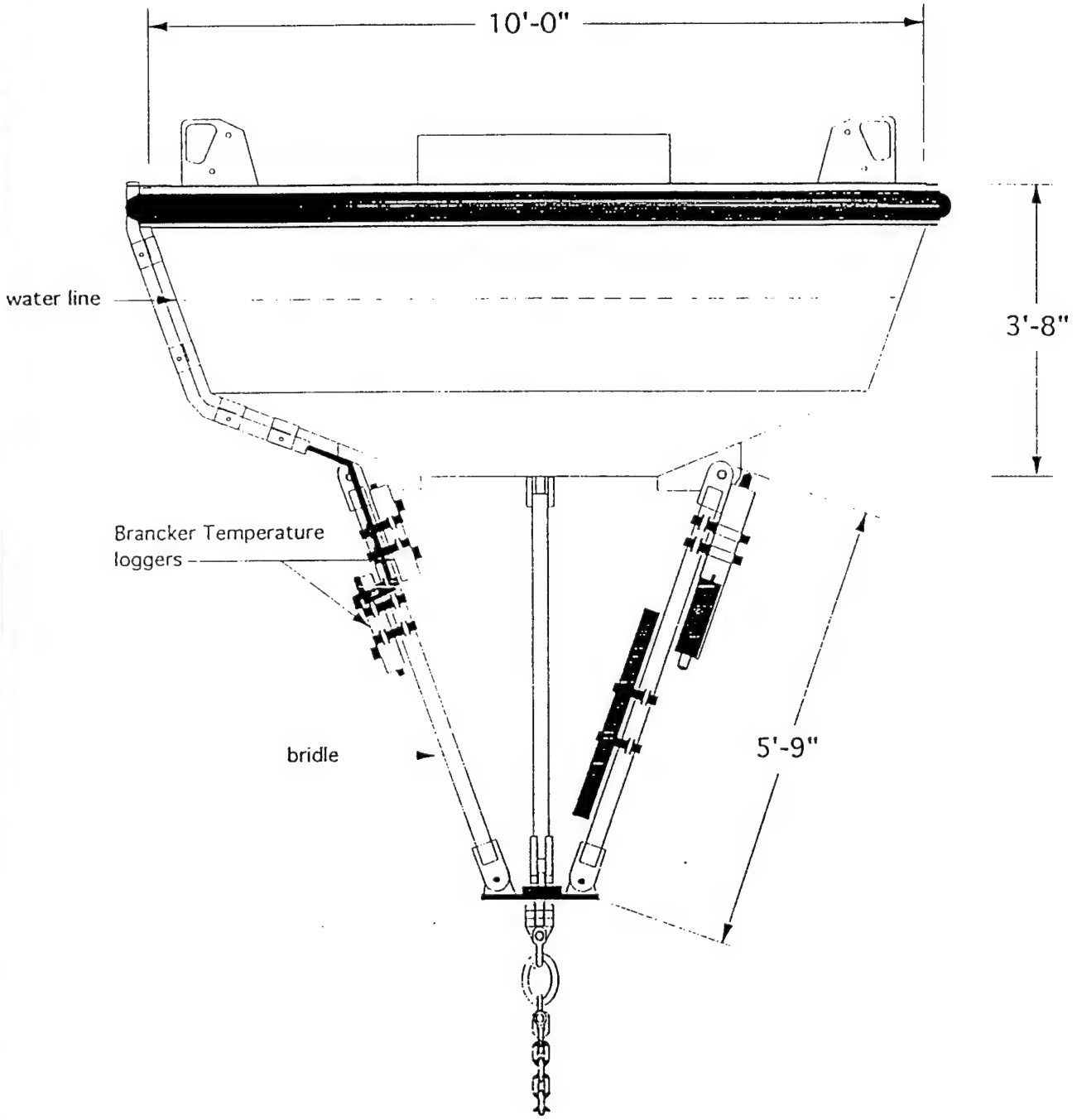

Figure A.3.1: Diagram of the discus hull and bridle profile.

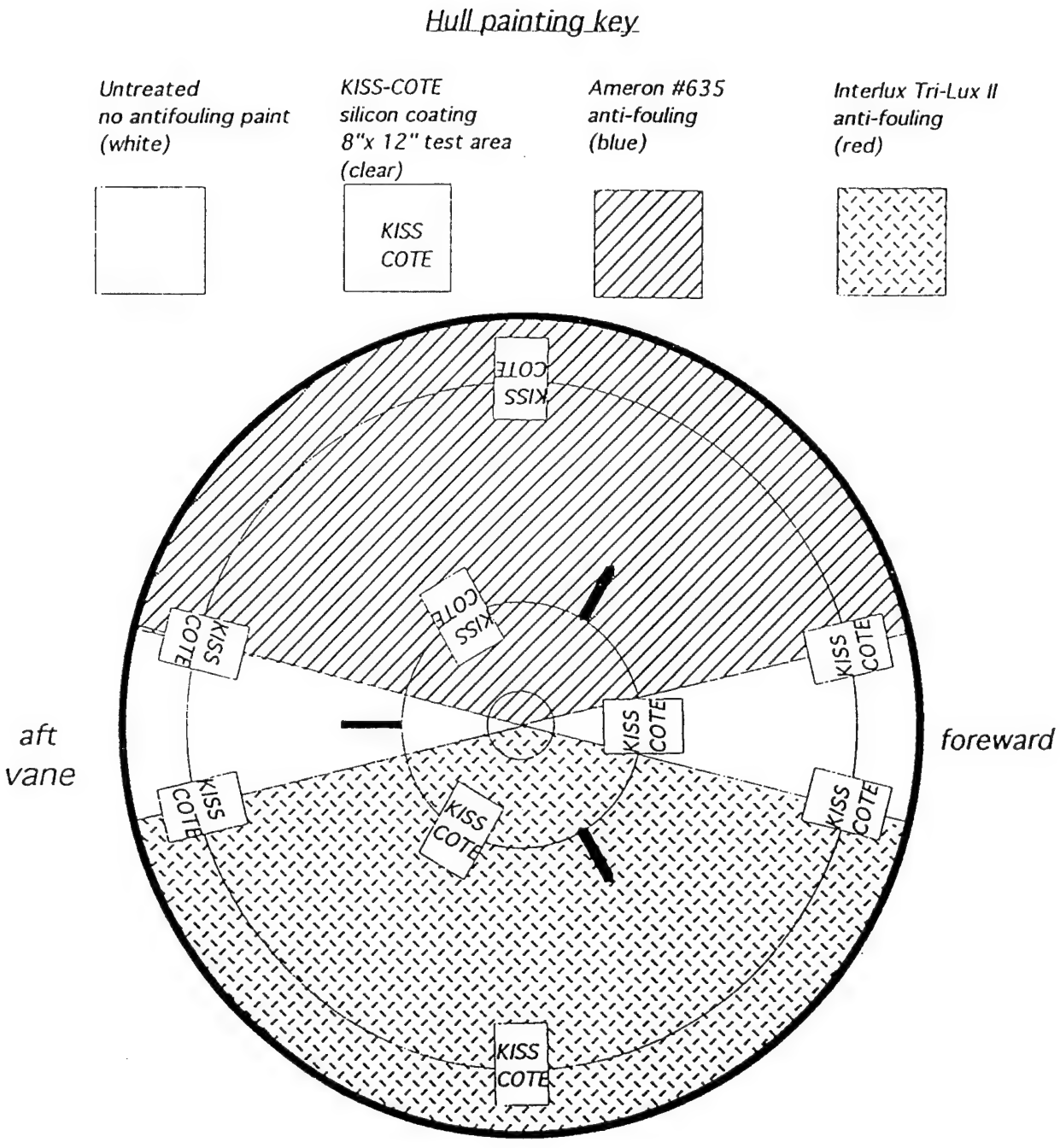

Figure A.3.2: ASREX antifouling paint test. Diagram of hull painting.

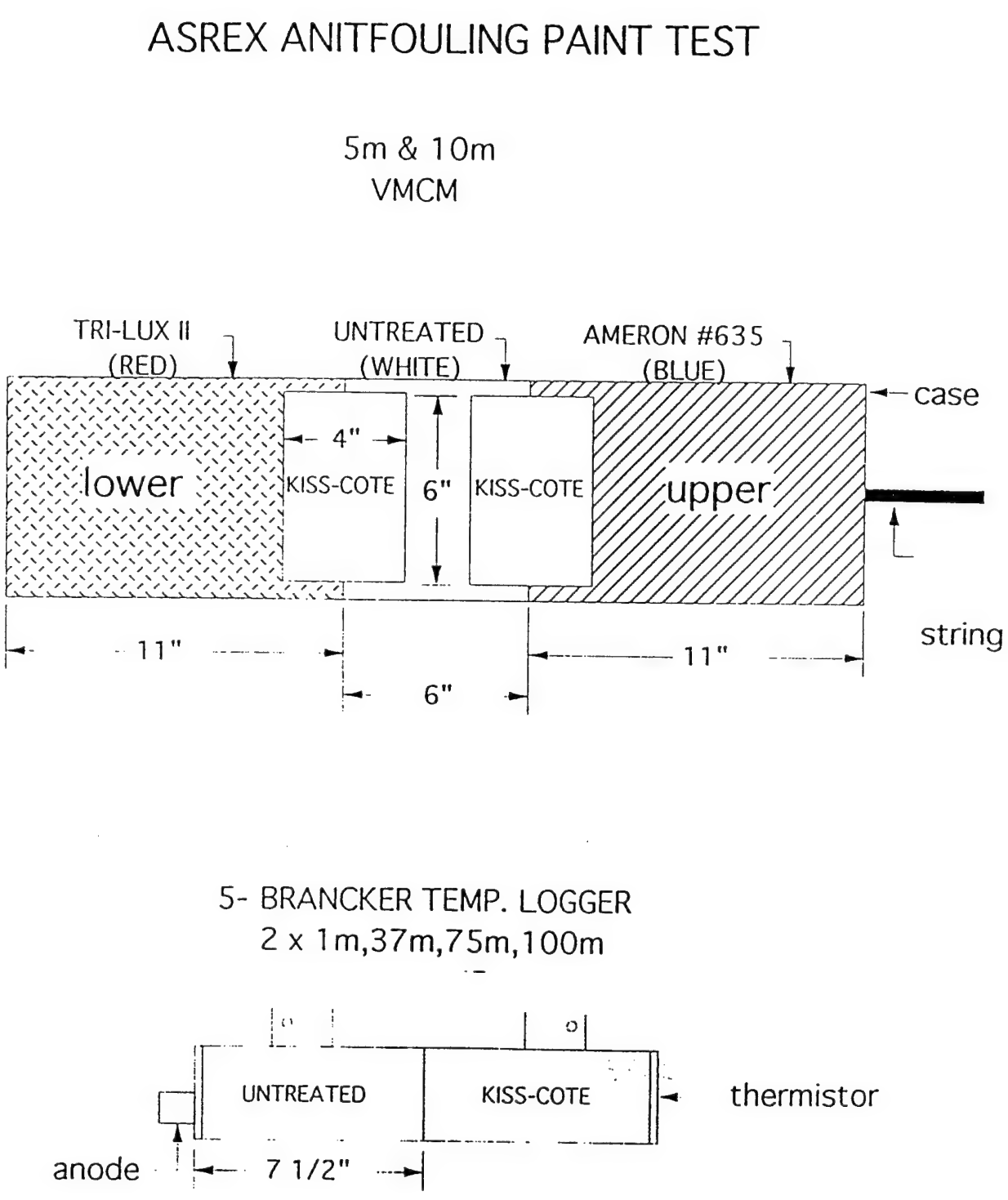

Figure A.3.3: ASREX antifouling paint test. Top: Diagram of how the VMCMs were painted. Bottom: Diagram of how the Brancker T-PODs were painted.

Since the buoy tends to orient into the wind and current, the leading face of the hull tends to be exposed to more scrubbing action from the waves and currents. In order to ensure that the Ameron #635 and Tri-Lux II paints had equal exposure, they were applied on either side of the wind vane axis as is shown in Figure A.3.2. A non-antifouled section, colored white, separated the two. There were 9 test areas measuring 12" by 8" outlined in black on the buoy hull. These sections were coated with a silicon-based polymer, Kiss-Cote. This coating is intended to facilitate the removal of fouling and to extend the antifouling coating effective service life. The test areas were positioned to straddle sections coated with Ameron #635, Trilux II and untreated control surfaces on the buoy hull. The 5 m and 10 m depth VMCM instrument cases were painted in a similar fashion to the discus hull. Eleven inches in from the top and bottom ends of each case were coated with Ameron #635 and Tri-Lux II respectively. An untreated non-antifouled section, colored white, measuring 6" and straddling the midpoint of the case acted as the control for this test. Two Kiss-Cote test patches measuring 6" x 4" were positioned to equally overlay the control and antifouling paints.

The two Brancker TPODs on the bridle, and those at 37.5, 75, and 100 m were coated from the thermistor endcap to the center of the instrument case with Kiss-Cote. The opposite ends of the Branckers were left untreated.

A.3.3: Visual inspection upon recovery

The discus hull's antifouling coating showed varying degrees of fouling. There were two types of fouling, green slime film and gooseneck barnacles, present on the hull. The Ameron #635 had the fewest number of goosenecks, numbering 20 animals over its painted surface. The Tri-Lux II coating had large numbers of barnacles attached hard through the coating, the largest concentration of animals being located around the aft end of the discus bottom. The forward or upwind side of the hull had the least amount of fouling. The forward side of the hull saw a greater degree of wave action, causing the ablative paints to wear and self-polish. The gooseneck barnacles required hand-scraping for removal. The control area on the hull's bottom, which was not antifouled, had the greatest fouling, with large colonies of goosenecks. Present on both coatings was a thin film of slime which washed off easily. The Kiss-Cote patches failed in this test to produce any noticeable difference. The goosenecks which were attached to areas covered with Kiss-Cote, whether antifouled or not, proved to be no easier to remove than barnacles attached to the non-Kiss-Cote surface.

The Ameron #279 which coated the steel bridle legs for the discus had little evidence of fouling. This coating showed a faster ablative wear rate than the Tri-Lux II and Ameron #635. The 9 mils of coating used for this test would not have survived a 6 month deployment.

The VMCM at 5m depth showed a pattern of fouling similar to the discus hull with gooseneck barnacles attached to the Tri-Lux II and control areas, but no fouling on the Ameron #635 coated surface. The VMCM at 10m was clear upon recovery.

The VMCM instrument fans showed no evidence of biofouling. There were, however, areas along the glue joint where the blades and hub intersect where the paint had chipped off. It was concluded that this was due to blade flexure.

The two Brancker TPODs at 1 m depth had goosenecks slime, and grass growth fouling. The Kiss-Cote failed to make these instruments easier to clean. The TPODs at 37 m, 75 m and 100 m were recovered with little sign of fouling.

The coatings were painted onto the discus hull and instrument housings during the period 4–10 December 1993. The mooring was deployed on 14 December 1993 at 33°52N, 69°44 W. The mooring was recovered on 24 March 1994. The average current speed at a depth of 5 m was 28.65 cm/s. The average water temperature was 19.44°C.

A.3.4 Conclusion

Biofouling to the discus hull and instrumentation was minimal below a depth of 10 m. Ameron #635 outperformed the Tri-Lux II in preventing the attachment of gooseneck barnacles. It was noted several days following recovery of the mooring that the Tri-Lux II surface hardness was not as ablative or soft as the Ameron #635 coating. The Tri-Lux II may have developed an oxide film prior to immersion causing a weaker ablative toxic release.

The Ameron #279 worked well. However, due to its high ablative release rate the coating would have failed if the test had been continued up to the standard 6 month deployment. Increasing the mil thickness to around 12 mils would improve the service life for this application.

The 18 Kiss-Cote test patches on the discus hull and sub-surface instrumentation failed to show any appreciable improvement in removal of biofouling. Through discussions with the formulators of Kiss-Cote following the recovery of this mooring, it was concluded that the pre-painted surface on which the Kiss-Cote was applied were too high in profile. This profile allowed the biofouling a greater potential for establishing a physical bond.

Appendix 4: Matlab Code used for computing spectra

```
function [dth,sw,sp,sr,fc,f]=mems1(x)
% mems1.m  Computes the five spectral coefficients from a Seatex wave record
%       using an fft with cosine tapering at the edges and then averaging
%       over nw points. The results are then inserted into a maximum
%       entropy routine of Lygre and Krogstad (JPO 16:2052-2060)
%       Input has form sampno, heave, pitch, roll.
%       Output has format [dth sw f] dth the directional wave
%       spectrum. sw the nondirectional spectrum and
%       f the array of frequencies.
%       Modified 8/21/92 to correct for directional changes
%       due to tilting.


nw=16;
heave=x(:,2);
magvar=-15.9;

fn=((0:1023)*.5)/1024;
Txyi=(.43.^2)./(.43^2-fn.^2+2*i*.1*fn);
Txy=1.0./Txyi;
ht=ones(1,1024);
it=34:1024;
ht(it)=(1.0-1.0./(30.8*fn(it)).^2-sqrt(2)*i*1.0./(30.8*fn(it))).* ...
     (1.0-1.0./(170*fn(it)));

thp=x(:,3)*pi/180.;
thr=x(:,4)*pi/180.;
thc=(x(:,5)+magvar)*pi/180.;

nx=tan(thp);
ny=sin(thr).*(cos(2*thp)./cos(thp))./sqrt(cos(thp).^2-sin(thr).^2);
nn=real((nx+i*ny).*exp(i*thc));
ne=imag((nx+i*ny).*exp(i*thc));

trif(1:128)=sin((0:127)*pi/256).^2;
trif(129:1920)=1.0*ones(size(129:1920));
trif(1921:2048)=trif(128:-1:1);
trif=trif';

ffh=fft(heave.*trif)/sqrt(2048);
ffn=fft(nn.*trif)/sqrt(2048);
ffe=fft(ne.*trif)/sqrt(2048);
ffp=fft(nx);
ffr=fft(ny);

f=zeros(1,1024/nw)';
c11=zeros(1,1024/nw)';
c22=zeros(1,1024/nw)';
c33=zeros(1,1024/nw)';
c23=zeros(1,1024/nw)';
q12=zeros(1,1024/nw)';
```

```
q13=zeros(1,1024/nw)';
sr=zeros(1,1024/nw)';
sp=zeros(1,1024/nw)';


for n=1:64
 for j=1:nw
  j1=(n-1)*nw+j;
  f(n)=f(n)+fn(j1)/nw;
  c11(n)=c11(n)+abs(ffh(j1)*ht(j1)).^2;
  c22(n)=c22(n)+abs(ffn(j1)*Txy(j1)).^2;
  sp(n)=sp(n)+abs(ffp(j1)*Txy(j1)).^2/8;
  sr(n)=sr(n)+abs(ffr(j1)*Txy(j1)).^2/8;
  c33(n)=c33(n)+abs(ffe(j1)*Txy(j1)).^2;
  q12(n)=q12(n)-imag(conj(ffh(j1)*ht(j1))*ffn(j1)*Txy(j1));
  q13(n)=q13(n)-imag(conj(ffh(j1)*ht(j1))*ffe(j1)*Txy(j1));
  c23(n)=c23(n)+real(conj(ffn(j1))*ffe(j1)*abs(Txy(j1)^2));
 end
end

d1=q12./sqrt(c11.*(c22+c33));
d2=q13./sqrt(c11.*(c22+c33));
d3=(c22-c33)./(c22+c33);
d4=2*c23./(c22+c33);

c1=d1+i*d2;
c2=d3+i*d4;

%Convert to oceanographic coordinates

c1=-c1;


fc=[ones(size(c1)) c1 c2];
phi1=(c1-c2.*conj(c1))./(1-abs(c1).^2);
phi2=(c2-c1.*c1)./(1-abs(c1).^2);
for ith=1:25
 theta=15*(ith-1)*pi/180.;
 for j=1:1024/nw
  dth(ith,j)=c11(j)*abs((1-phi1(j)*conj(c1(j))-phi2(j)*conj(c2(j)))/ ...
        (2*pi*(1-phi1(j)*exp(-i*theta)-phi2(j)*exp(-2*i*theta))^2));
  sw(j)=c11(j);
 end
end

% Smooth spectra in frequency space

dth=[(dth(:,1)+dth(:,2))/2 (dth(:,1:62)+2*dth(:,2:63)+dth(:,3:64))/4 (dth(:,63)+dth(:,64))/2];
dth=[(dth(:,1)+dth(:,2))/2 (dth(:,1:62)+2*dth(:,2:63)+dth(:,3:64))/4 (dth(:,63)+dth(:,64))/2];
return
```

DOCUMENT LIBRARY

Distribution List for Technical Report Exchange – May 1995

University of California, San Diego
SIO Library 0175C
9500 Gilman Drive
La Jolla, CA 92093-0175

Hancock Library of Biology & Oceanography
Alan Hancock Laboratory
University of Southern California
University Park
Los Angeles, CA 90089-0371

Gifts & Exchanges
Library
Bedford Institute of Oceanography
P.O. Box 1006
Dartmouth, NS, B2Y 4A2, CANADA

Commander
International Ice Patrol
1082 Shennecossett Road
Groton, CT 06340-6095

NOAA/EDIS Miami Library Center
4301 Rickenbacker Causeway
Miami, FL 33149

Research Library
U.S. Army Corps of Engineers
Waterways Experiment Station
3909 Halls Ferry Road
Vicksburg, MS 39180-6199

Institute of Geophysics
University of Hawaii
Library Room 252
2525 Correa Road
Honolulu, HI 96822

Marine Resources Information Center
Building E38-320
MIT
Cambridge, MA 02139

Library
Lamont-Doherty Geological Observatory
Columbia University
Palisades, NY z10964

Library
Serials Department
Oregon State University
Corvallis, OR 97331

Pell Marine Science Library
University of Rhode Island
Narragansett Bay Campus
Narragansett, RI 02882

Working Collection
Texas A&M University
Dept. of Oceanography
College Station, TX 77843

Fisheries-Oceanography Library
151 Oceanography Teaching Bldg.
University of Washington
Seattle, WA 98195

Library
R.S.M.A.S.
University of Miami
4600 Rickenbacker Causeway
Miami, FL 33149

Maury Oceanographic Library
Naval Oceanographic Office
Building 1003 South
1002 Balch Blvd.
Stennis Space Center, MS, 39522-5001

Library
Institute of Ocean Sciences
P.O. Box 6000
Sidney, B.C. V8L 4B2
CANADA

National Oceanographic Library
Southampton Oceanography Centre
European Way
Southampton SO14 3ZH
UK

The Librarian
CSIRO Marine Laboratories
G.P.O. Box 1538
Hobart, Tasmania
AUSTRALIA 7001

Library
Proudman Oceanographic Laboratory
Bidston Observatory
Birkenhead
Merseyside L43 7 RA
UNITED KINGDOM

IFREMER
Centre de Brest
Service Documentation - Publications
BP 70 29280 PLOUZANE
FRANCE

50272-101

REPORT DOCUMENTATION PAGE	1. REPORT NO. WHOI-96-10	2. UOP 96-01	3. Recipient's Accession No.

4. Title and Subtitle
Meteorological and Oceanographic Measurements during the ASREX III Field Experiment: Cruise and Data Report

5. Report Date
September 1996

6.

7. Author(s) Nancy R. Galbraith, Anand Gnanadesikan, William M. Ostrom, Eugene A. Terray, Bryan S. Way, Neil J. Williams, Steven H. Hill, and Eric Terrill

8. Performing Organization Rept. No.
WHOI-96-10

9. Performing Organization Name and Address

Woods Hole Oceanographic Institution
Woods Hole, Massachusetts 02543

10. Project/Task/Work Unit No.

11. Contract(C) or Grant(G) No.
(C) N00014-91-J-1891
(G) /

12. Sponsoring Organization Name and Address

Office of Naval Research

13. Type of Report & Period Covered
Technical Report

14.

15. Supplementary Notes
This report should be cited as: Woods Hole Oceanog. Inst. Tech. Rept., WHOI-96-10.

16. Abstract (Limit: 200 words)

The Third Acoustic Surface Reverberation Experiment (ASREX III) took place from December 1993 to March 1994 at Site L (34°N, 70°W) in the mid-Atlantic. As part of this experiment, two moorings were deployed to measure the environmental background. A meteorological and oceanographic mooring was deployed to characterize the surface wind stress, buoyancy flux, and the current and temperature structure over the top 500 meters. A Seatex Wavescan™ buoy was deployed to characterize the directional wave spectrum. This report presents results from these moorings. Wind speeds up to 25 m/s were seen, with significant heat losses (up to 1050 W/m^2) when cold continental air moved out over the warm Atlantic. The wave heights ranged up to 8 m, with significant wave heights of several meters persisting for relatively long periods. Wave height and period, nondirectional spectra, directional spectra and a typology of wave events are presented and related to surface forcing.

17. Document Analysis **a. Descriptors**
Meteorology: mid-Atlantic
Oceanography: mid-Atlantic
Moored Instrument Measurements

b. Identifiers/Open-Ended Terms

c. COSATI Field/Group

18. Availability Statement	19. Security Class (This Report)	21. No. of Pages
Approved for public release; distribution unlimited.	UNCLASSIFIED	247
	20. Security Class (This Page)	22. Price

(See ANSI-Z39.18) *See Instructions on Reverse*

OPTIONAL FORM 272 (4-77)
(Formerly NTIS-35)
Department of Commerce